Design of Novel, Heterogeneous Catalysts for Transformation of Bioderived Platform Molecules to Chemicals and Fuels

by

Tarade Komal Pratap
10CC20A26051

A thesis submitted to the
Academy of Scientific & Innovative Research
for the award of the degree of
DOCTOR OF PHILOSOPHY
in
SCIENCE
Under the supervision of

Dr. Sanjay P. Kamble
Dr. Chandrashekhar V. Rode

CSIR-National Chemical Laboratory, Pune

Academy of Scientific and Innovative Research
AcSIR Headquarters, CSIR-HRDC campus,
Sector 19, Kamla NehruNagar, Ghaziabad,
U.P. – 201002, India

September - 2024

Certificate

This is to certify that the work incorporated in this Ph.D. thesis entitled, "*Design of Novel, Heterogeneous Catalysts for Transformation of Bioderived Platform Molecules to Chemicals and Fuels*", submitted by *Tarade Komal Pratap* to the Academy of Scientific and Innovative Research (AcSIR) in fulfillment of the requirements for the award of the Degree of *Doctor of Philosophy in Science*, embodies original research work carried-out by the student. We, further certify that this work has not been submitted to any other University or Institution in part or full for the award of any degree or diploma. Research material(s) obtained from other source(s) and used in this research work has/have been duly acknowledged in the thesis. Image(s), illustration(s), figure(s), table(s) etc., used in the thesis from other source(s), have also been duly cited and acknowledged.

(Signature of Student)	(Signature of Co-Supervisor)	(Signature of Supervisor)
Tarade Komal Pratap	Dr. Chandrashekhar V. Rode	Dr. Sanjay P. Kamble
Date: 22/08/2024	Date: 22/08/2024	Date: 22/08/2024

STATEMENTS OF ACADEMIC INTEGRITY

I Tarade Komal Pratap, a Ph.D. student of the Academy of Scientific and Innovative Research (AcSIR) with Registration No. 10CC20A26051 hereby undertake that, the thesis entitled "Design of Novel, Heterogeneous Catalysts for Transformation of Bioderived Platform Molecules to Chemicals and Fuels" has been prepared by me and that the document reports original work carried out by me and is free of any plagiarism in compliance with the UGC Regulations on *"Promotion of Academic Integrity and Prevention of Plagiarism in Higher Educational Institutions (2018)"* and the CSIR Guidelines for "*Ethics in Research and in Governance (2020)*".

Signature of the Student
Date : 22/ 08/ 2024
Place : Pune

It is hereby certified that the work done by the student, under our supervision, is plagiarism-free in accordance with the UGC Regulations on *"Promotion of Academic Integrity and Prevention of Plagiarism in Higher Educational Institutions (2018)"* and the CSIR Guidelines for "*Ethics in Research and in Governance (2020)*".

Signature of the Co-supervisor
Name : Dr. Chandrashekhar V. Rode
Date : 22/ 08/ 2024
Place : Pune

Signature of the Supervisor
Name : Dr. Sanjay P. Kamble
Date : 22/ 08/ 2024
Place : Pune

Dedicated

To

My Parents & Family

ACKNOWLEDGEMENT

On the occasion of completing my thesis, I would like to extend my heartfelt gratitude to all those who have contributed in various ways to this success story. Your support and encouragement have made this journey an unforgettable experience for me.

First and foremost, I wish to express my sincere gratitude to my research supervisor, ***Dr. Sanjay P. Kamble*** *(Senior Principal Scientist, CSIR-National Chemical Laboratory) and co-supervisor* ***Dr. Chandrashekhar V. Rode*** *(Emeritus Scientist, CSIR-National Chemical Laboratory), for their unwavering guidance, support, enthusiasm, and motivation throughout my research studies. I owe them a great deal. They are both incredibly friendly, caring individuals and fantastic mentors. They have taught me so much and have always encouraged me to think creatively and be open to learning new things. Their receptive attitudes will always remain a source of inspiration for me. I consider myself very fortunate to have been associated with them, as it has given a decisive turn and significant boost to my career and life. I truly feel lucky to have been a part of the* ***SPK*** *and* ***CVR*** *group. I would like to extent my gratitude to* ***Dr. Sunil Bhongale*** *(Senior Technical Officer, CSIR-National Chemical Laboratory) for his constant support and guidance in analytical tools and techniques.*

I would like to express my sincere thanks to Dr. Sunil Joshi, former HOD, and Dr. Chetan Gadgil, current HOD of the CEPD division at CSIR-NCL, for their support during my Ph.D. tenure. I also wish to express my deep gratitude to Dr. Ashwini Kumar Nangia, former Director, and Dr. Ashish Lele, current Director of CSIR-NCL, for allowing me to conduct my research, providing all necessary infrastructural facilities, and permitting me to present this work as a Ph.D. thesis.

I would also like to thank the Doctoral Advisory Committee (DAC) chairperson, Dr. Narendra Kadoo and members, Dr. Manjusha Shelke, Dr. Shafeek A. R. Mulla and Dr. Shashank Gaikwad for evaluating my work and providing valuable suggestions to improve the research.

I am thankful to CEPD office staff Mr. Hasso Raheja, Mr. Palash Kedari and others for their constant cooperation. I thank to current and former chairs of Student Academic Office (SAO). I am also thankful to all SAO staff and others for timely documents evaluation and their cooperation. I specially thank to AcSIR former

coordinators, Dr. Santosh Mhaske and Dr. C. P. Vinod and current coordinator Dr. Benudhar Punji for their cooperative evaluation of AcSIR documents.

I specially thank all the members of Central Analytical Facilities (CAF) such as NMR, XRD, HRMS, TGA, SEM and TEM in CMC groups for their help in obtaining the analytical data. I would like thank to staff of administration, accounts, medical, engineering, library, chemical store, purchase, glass blowing departments of NCL for their cooperation.

I would like to express my deepest gratitude to my Guruji, Dr. Suhas Shinde, for his continuous guidance, attention, and motivation throughout my Ph.D. His keen efforts and willingness to assist were invaluable in making this work possible. I feel truly blessed to have learned research ethics, good laboratory practices, writing and presentation skills from him during my internship period.

This entire work would not be complete without expressing my sincere gratitude to my senior colleagues, Dr. Chetana Patil, Dr. Sachin Sakate, Dr. Aarti Jadhav, Dr. Amol Hengne, Dr. Nishita Lucus, and Dr. Sharda Kondawar, for their help and suggestions. I extend my thanks to my current SPK group lab mates, Mr. Kapil Dhotre, Mr. Narendra Bodawar, Mr. Nishant Markandey, Mr. Abhishek Pathak, Mr. Yash Thombre, Mr. Aashay Bhramhe, Ms. Suvidha Sehravat, Ms. Vishakha Kuthwal, Mr. Mayur Jadhav and Prafulla Gopale, for maintaining a friendly and cordial atmosphere in the lab. A special thanks goes to Ms. Kiran Bandi, Ms. Devanshi Ashok, Ms. Aparna Narkar, Mr. Sachin Sonage, Mr. Mayur Patil, Mr. Atul Dhage, and Mr. Abhinandan Chopada for their encouragement and support. Additionally, I also wish to thank my CVR group lab mates, Dr. Roopa Parate, Dr. Gayatri Kasar, Dr. Dnyanesh Vernekar, Dr. Rajan Pandya, Mr. Anil Patil, and Mrs. Kashmira Deval-Oak. I am grateful to the hardworking and sincere master's trainees, Ms. Jagruti Patil, Atharva Kabade, and Gurunath Patil, for their assistance in accelerating my research work. I would also like to thank Mr. Vikram Mulay and Mr. Ramesh Mandlik, former technicians, for their quick solutions to technical problems. Finally, I am grateful to Mr. Hanmant Mhaske and Mr. Pramod Giri for their assistance in the lab.

My sincere thanks go to my best friends, Mrs. Amruta and Mr. Yogesh Jadhav, who have been one of the greatest assets in my life. Their company has been a joy, and they have been there for me at every stage. I would also like to thank my bestie, Mrs. Seema Sinha-Ghosh, for her lifelong encouragement, support, and motivation.

No words can adequately express my gratitude to my parents, who have always been a source of inspiration and have given me the opportunity to see this beautiful world. I am deeply thankful to my mother, Mrs. Vanita Tarade, and my father, Mr. Pratap Tarade, for believing in my abilities. Without their constant support, encouragement, positive thinking, and inspiration, this dissertation would not have been possible. I would also like to extend my thanks to my elder brother, Mr. Abhijeet Tarade, and my sister-in-law, Mrs. Pratiksha Tarade, for their unwavering support in every situation. Additionally, I am grateful to my elder sister, Mrs. Namrata Tarade-Jadhav, and my brother-in-law, Mr. Rahul Jadhav, for their continuous encouragement. I also thank my cousin brother, Mr. Pratik More, for his unconditional support and encouragement. Lastly, my heartfelt thanks go to my adorable nieces, Adishree and Niharika, whose innocent smiles always make me feel light and happy.

Lastly, I would like to express my sincere gratitude and appreciation to all those whose direct or indirect contributions have been invaluable to this work.

With many thanks,

Komal P. Tarade

CONTENTS

List of Figures

List of Tables

List of Schemes

ABBREVATIONS

2-MeTHF	2-methyltetrahydrofuran
2-MF	2-methylfuran
AcMF	5-(acetoxymethyl)furfural
Al	Aluminium
Al_2O_3	Aluminium oxide
AMPSi	3-aminopropyltriethoxysilane
Aq.	Aqueous
BET	Brunauer-Emmett-Teller
BGB	Bisguaiacol-B
BGE	Bisguaiacol-E
BGF	Bisguaiacol-F
BGP	Bisguaiacol-P
BHMF	bis(hydroxymethyl) furan
BMFP	5,5-bis(5-methylfuran-2-yl)pentan-2-one
BPA	Bisphenol-A
BPCL	Bharat Petroleum Corporation Limited
BTX	Benzene/Toluene/Xylene
CaO	Calcium oxide
$CDCl_3$	Deuterated chloroform
CMF	5-(chloromethyl)furfural
CO	Carbon monoxide
Co	Cobalt
CO_2	Carbon dioxide
DABCO	1,4-diazabicyclo[2.2.2]octane
DBU	1,8-Diazabicyclo[5.4.0]undec-7-ene

DCM	Dichloromethane
DFAc	Difurfurylidene acetone
DFF	2,5-diformyl furan
DMA	N,N-dimethylacetamide
DMAP	N,N-dimethylaminopyridine
DMF	N,N-dimethylformide
DMSO	Dimethyl sulfoxide
DOE	Department of Energy
EMF	5-(ethoxymethyl)furfural
FAc	Furfurylidene acetone
FDCA	2,5-furandicarboxylic acid
Fe_3O_4	Iron oxide
$Fe_3O_4@SiO_2$	Silica coated magnetic nano particles
$FeCl_2$	Iron (II) chloride / ferrous chloride
$FeCl_3$	Iron(III) chloride / ferric chloride
FESEM	Field Emission Scanning Electron Microscopy
FMP	3-(2-furylmethylene)-2,4-pentanedione
FTIR	Fourier Transform Infrared Spectroscopy
FUR	Furfural
GC	Gas Chromatography
GCMS	Gas chromatography–mass spectrometry
GVL	γ-valerolactone
H_2	Hydrogen
H_2O	Water
H_2O_2	Hydrogen peroxide
H_2SO_4	Sulphuric acid
HAA	Hydroxyalkylation-alkylation

HCl	Hydrochloric acid
HDO	Hydrodeoxygenation
HFCA	5-(hydroxymethyl)furan-2-carboxylic acid
HMF	5-(hydroxymethyl)furfural
HMFA	5-hydroxymethylfuranoic acid
HPCL	Hindustan Petroleum Corporation Limited
HPLC	High Performance Liquid Chromatography
HRTEM	High Resolution Transmission Electron Microscopy
IL	Ionic liquid
INA	Isonicotinic acid
IOCL	Indian Oil Corporation Limited
IPA	Isopropyl alcohol
LA	Levulinic acid
$La(OTf)_3$	Lanthanum(III) trifluoromethanesulfonate.
$La–ZrO_2$	Lanthanum Zirconium dioxide
MeOH	Methanol
MgO	Magnesium oxide
MgO	Magnesium oxide
MIBK	Methyl isobutyl ketone
Mn_2O_3	Manganese (III) oxide
MPTMS	3-mercaptopropyl trimethoxysilane
Na_2SO_4	Sodium sulfate
$NaBH_4$	Sodium borohydride
NaOH	Sodium hydroxide
Nb_2O_5	Niobium pentoxide
NH_3	Ammonia
NMP	N-methyl pyrrolidone

NMR	Nuclear Magnetic Resonance
NREL	National Renewable Energy Laboratory
PCC	Pyridinium chlorochromate
$PdCl_2$	Palladium (II) chloride / Palladium dichloride
PEG	Polyethylene glycol
PEO	Polyethylene oxide
PFD	Paraformaldehyde
PHAs	Polyhydroxyalkanoates
Pt	Platinum
p-TSA	*p*-toluene sulfonic acid
Py	Pyridine
Ru/C	Ruthenium on activated carbon
SBNPSA	Silica-bonded-N-propyl sulfamic acid
SiO2	Silicon dioxide
$SnCl_4\,5H_2O$	Tin (IV) chloride pentahydrate
TEM	Transmission Electron Microscopy
TEMPO	2,2,6,6-tetramethylpiperidine-1-oxide
TEOS	Tetraethyl orthosilicate
TGA	Thermogravimetric Analysis
TiO_2	Titanium dioxide
TLC	Thin layer chromatography
TMFP	2,4,4-tris(5-methylfuran-2-yl)pentan-1-ol
TMS	Tetramethylsilane
U. S.	United State
USD	United State Doller
WO_3	Tungsten trioxide
XRD	X-ray diffraction

$Y–ZrO_2$	Yttrium zirconium dioxide
Zn	Zinc
ZrO_2	Zirconium dioxide
ZSM-5	Zeolite Socony Mobil–5

GENERAL REMARKS

1. All the reactions were carried out in a glass apparatus.
2. Speciality chemicals and A. R. Grade dried solvents were procured from authentic suppliers like Sigma-Aldrich (US), Alfa Aesar (US), Loba Chemie and Thomas Baker (India) etc.
3. TLC plates were purchased from Merk and Loba, India.
4. 60-120, 100-200 and 230-400 mesh sized silica was utilized for the column chromatography using ethyl acetate in pet ether as a mobile phase.
5. Conversion of substrates and selectivity of products were calculated by using Thermo Scientific GC (FID detector and a capillary column Stabil wax) and Agilent 7890B GC (FID detector and a capillary column HP5)
6. Conversion of substrates and selectivity of Knoevenagel condensation product were calculated by using Agilent HPLC (column: Chromolith High Resolution RP-18e, detector: UV (254 nm) and mobile phase: millipore water: Methanol (60:40; *v*/*v*) with 0.3 mL/min flow) and for Bisguaiacol (column: Hypersil C18, detector: UV (230 nm) and mobile phase: millipore water: Methanol (45:55; v/v) with 1 mL/min flow).
7. Products were characterized by ^{1}H-NMR and ^{13}C-NMR using CDCl3 (0.01 % TMS) and DMSO-d6 (0.01 % TMS) as solvents on 50 and 200 MHz frequency Bruker instrument.
8. The confirmation of the products was carried out using QP-Ultra 2010 GC-MS Shimadzu instrument on a RTX-5 column using helium as a carrier gas, in EI mode and at ionization source temperature of about 200 ^{o}C.
9. Micromeritics ChemiSorb 2720 sorption analyser instrument used for measuring BET surface area, CO2-TPD and NH3-TPD analysis.
10. Functional group of catalysts and synthesized products were confirmed by FTIR analysis which was performed on spectrometer (Perkin Elmer 2000) in the 4000–400 cm^{-1} wave number range

11. Pyridine-FTIR was done using Harrick Diffuse reflectance praying mantis assembly with temperature controller (30-850 ^{o}C) attached with Perkin Elmer frontier under 150 mL/min flow of nitrogen as a carrier gas.

12. Wide angle X-ray diffraction was recorded on a PANalytical PXRD Model X-Pert PRO-1712, using Ni-filtered CuKα radiation (λ=0.154 nm) as a source (current intensity, 30 mA; voltage, 40 kV) and a Xcelerator detector.

13. High resolution transmission electron spectroscopy (HRTEM) analysis of catalyst was performed on JEOL JEM F200 HR-TEM, with Resolution 0.19 nm and accelerating voltage 20kV-200kV.

14. Field Emission Scanning Electron Microscopy (FESEM) analysis of catalyst was performed on FEI NOVA NANOSEM 450. Resolution: 1nm, Accelerating Voltage: 1kV - 30kV.

Synopsis Report

AcSIR	**Synopsis of the Thesis to be submitted to the Academy of Scientific and Innovative Research for Award of the Degree of Doctor of Philosophy in Sciences/ Engineering**
Name of the Candidate	Tarade Komal Pratap
Degree Enrollment No. &Date	10CC20A26051; Date- 02nd September 2021
Laboratory	CSIR-National Chemical Laboratory, Pune.
Title of the Thesis	Design of Novel, Heterogeneous Catalysts for Transformation of Bioderived Platform Molecules to Chemicals and Fuels
Research Supervisor/ Co-supervisor	Dr. Sanjay P. Kamble Dr. Chandrashekhar V. Rode

1. Introduction

Currently, chemicals and liquid fuels are predominantly produced from crude oil; however, crude oil reserves are expected to diminish in the near future. Additionally, the crude oil refining process emits a significant amount of CO_2, contributing to severe air pollution. Consequently, over the past few decades, scientists and technologists have faced the primary challenge of identifying greener alternatives for energy, fuels, chemicals, and materials. Fortunately, these challenges can be addressed by utilizing lignocellulosic biomass, a sustainable carbon source and green alternative to crude oil [1]. Bioenergy is the largest contributor to global renewable energy, simultaneously providing energy security to billions and stimulating rural development [2]. Biomass feedstock can be harnessed to meet the demands for heat, electricity, and liquid fuel. Lignocellulosic biomass consists of 15-20% lignin (polymeric aromatics), 40-50% cellulose (polymeric C6 sugar), and 25-35% hemicellulose (polymeric C5 sugar). Lignin is a valuable renewable resource for producing useful phenolic building blocks such as guaiacol, vanillin, creosol, and syringol [3]. Cellulose and hemicellulose are the main structural carbohydrate fractions of lignocellulosic biomass, which can be hydrolyzed to produce glucose and xylose, followed by their dehydration to produce 5-hydroxymethylfurfural (HMF) and furfural (FUR), respectively [4,5]. Furfural can be further converted into 2-methylfuran as a major product through hydrogenolysis at 250°C [6]. These platform molecules, with their multiple functional groups, have the

potential to be transformed into new families of useful compounds. Bio-derived platform molecules can be converted into chemicals and fuels through C-C (condensation), C-N (amination), and C-O (etherification and esterification) bond-forming reactions. In this study, we designed and developed various novel organic heterogeneous catalysts, specifically sulfonated acid and amino-functionalized base catalysts, to facilitate the transformation of furfural, 2-methylfuran, and guaiacol into value-added products.

2. Statement of Problem

Owing to diminishing petroleum reserves and environmental problems such as global warming and air pollution it is imperative to utilize biomass resources to produce fuels and chemicals. A substantial growth projected in global oil consumption combined with compelling international situation of crude oil production are the key drivers for exploring alternate sustainable energy sources. The selective conversion of carbon rich biomass to value-added chemicals is the key issue for development of fossil-independent chemical technologies for the production of fuels and chemicals. Furfural and 2-methyl furan are the key starting materials for production of diesel-range long chain alkanes and different fuels components through carbon upgradation by employing various types of C-C bond forming reactions (Knoevenagel/Aldol condensation, Hydroxyalkyalation-alkylation) followed by hydrodeoxygenation. In particular, the Knoevenagel condensation of furfural is not studied much. Knoevenagel condensation between furfural and acetyl acetone was carried out by enzyme (Lipoprotein lipase) catalyst which requires longer reaction time (48h) [7]. Hydrogenation of furan condensation products to obtain cyclic ethers (furan ring saturation) traditionally requires high temperatures (60-170°C) and high hydrogen pressures (40-50 bar) [8,9]. Therefore, there is a need to develop catalysts that can facilitate selective hydrogenation under ambient reaction conditions. Bisphenol-A (BPA) containing materials shows adverse effect on human health. Bisguaiacol-F is a green and sustainable alternative to Bisphenol-A which is synthesized by expensive commodities such as vanilin or vanillyl alcohol and guaiacol. A heterogeneous catalyst is needed for the synthesis of Bisguaiacol-F using an alternative, cost-effective substrate.

3. Objectives of Work

The primary aim of the thesis is to develop and optimize environmentally friendly and cost-efficient strategies for converting biomass-derived molecules into value-added products.

The specific aims are as follows:

- Transformation of bio-derived platform molecules such as furfural, 2-methyl furan (hemicellulose), HMF (cellulose) and guaiacol (lignin) to valuable chemicals and fuel.
- To design, development of various novel organic heterogeneous catalysts specifically sulphonated acids and amino functionalized bases and its details physicochemical characterization.
- To develop suitable analytical techniques (HPLC, GC, TLC) for establishment of concentration of reaction mixture.
- Screening, selection of catalyst as well as optimization of reaction parameters in order to establish optimum reaction conditions.
- To isolation and purification of desired products from reaction crude.

4. Methodology

The novel organic heterogeneous catalysts synthesized in this work were thoroughly characterized using Acid-Base titration, XRD, FT-IR, Py-IR, TGA, SEM, and TEM techniques. The concentration of reaction crude was determined using analytical methods such as GC and HPLC. The products were isolated by column chromatography, and all synthesized products and their structures were characterized and confirmed using advanced analytical and spectroscopic techniques, including high-field NMR (^{1}H and ^{13}C), FTIR, and HRMS.

5. Sample Results

Chapter – 1
General Introduction

Chapter 1 focuses on a general introduction to biomass, the biorefinery process, and bio-derived platform molecules. It provides a detailed review of the literature on the transformation of bio-derived platform molecules into value-added products. This

chapter delves into the fundamentals of catalysis, exploring the different types of catalysts and offering an in-depth review of the literature on catalysts employed in the conversion of bio-derived platform molecules into valuable chemicals and fuels.

Chapter – 2

Magnetic Solid Base Catalyst for Knoevenagel Condensation of Furfural with Acetyl acetone

In this chapter, we presented here a simple and robust Fe_3O_4@SiO_2-Py catalyst system for the Knoevenagel condensation of furfural with acetyl acetone to achieve high yield of FMP (Scheme 1). The condensation product FMP is a unit of C_{10} and could be converted into branched alkanes (Jet fuel) through hydrodeoxygenation process. Novel heterogeneous pyridine immobilized magnetic silica (Fe_3O_4@SiO_2-Py) was found to be an efficient, greener and heterogeneous solid base catalyst for the Knoevenagel condensation of furfural with acetylacetone under optimized reaction conditions. The Knoevenagel condensation product 3-(2-furylmethylene)-2,4-pentanedione (FMP), a jet fuel precursor, was produced in high yield of 85 % with 94 % conversion of furfural at 100 ^oC within a period of 4 h. Structures of organosilica catalysts were confirmed by sophisticated analytical techniques.

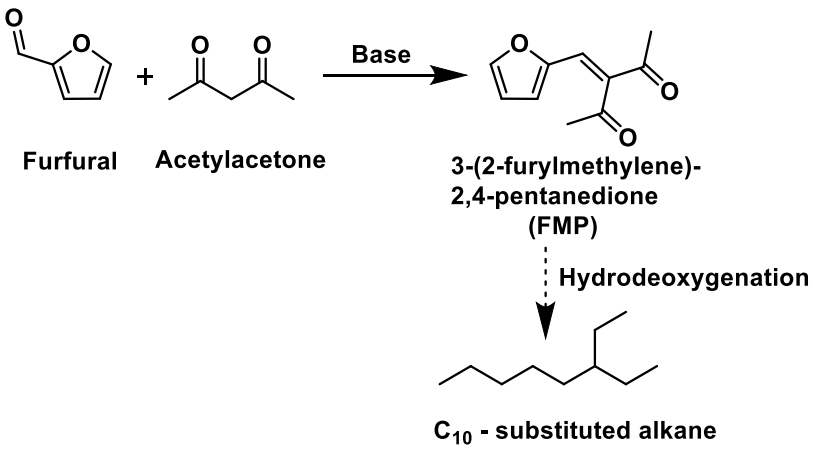

Scheme 1. Synthesis of Jet fuel precursors from furfural and acetyl acetone

Chapter – 3

Condensation of Renewable Aldehydes and 2-Methylfuran to Saturated Cyclic Oxygenates

The saturated cyclic ethers produced from biomass derived aldehydes and 2-methylfural are the potential diesel fuel candidates. The synthesis of saturated cyclic ethers is a two step process which involves acid catalyzed condensation of aldehydes with 2-methylfuran and the subsequent selective furan ring hydrogenation of the condensation products (Scheme 2). Here, we designed a novel recyclable magnetic solid acid catalyst such as $[Fe_3O_4@SiO_2\text{-Pr-Py-H}][2HSO_4^{2-}]$ and employed for the condensation of 2-methylfuran with formaldehyde as model substrates and reaction parameters were optimized. In the first step, a newly designed acidic magnetic solid catalyst $[Fe_3O_4@SiO_2\text{-Pr-Py-H}][2HSO_4^{2-}]$ showed an excellent activity for formaldehyde condensation with 2-methylfuran to give 90% conversion of formaldehyde and 75% isolated yield of the condensation product. This catalyst was successfully explored for a wide variety of aldehydes or ketones for their condensation with 2-methylfuran. Further, several supported noble metal catalysts were screened to in order to find suitable catalyst system for selective furan ring hydrogenation of condensation products. Amongst those, 5% Pd/C was found to be very active and selective for furan ring hydrogenation without formation of ring opened products under very low hydrogen pressure at room temperature in 1,4-dioxane solvent. Among the several supported catalysts, 5% Pd/C gave the highest conversion of 85% with 80% yield of saturated cyclic ether. Prepared catalysts were thoroughly characterized with sophisticated techniques.

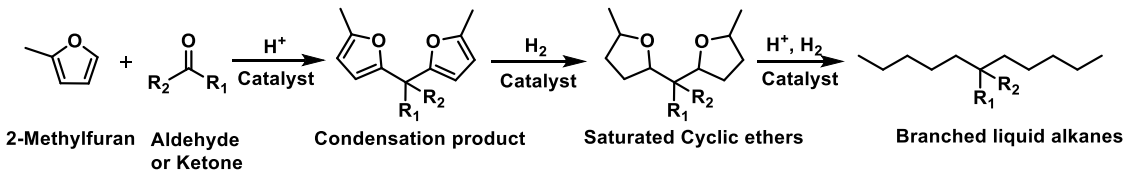

Scheme 2. General scheme for synthesis of saturated cyclic ethers and branched liquid alkanes

Chapter – 4

Conversion of 2-Methylfuran to Diesel Fuel Precursors Catalysed by Solid Acid

Polyfuranic compounds produced after carbon up-gradation of 2-methylfuran by acid catalyzed C-C bond forming reactions when undergo hydro-deoxygenation produce diesel fuel (Scheme 3). Herein, we prepared a simple and novel silica supported sulfonic acid functionalized isonicotinic acid SO_3H-INA@SiO_2 by treating isonicotinic acid with chlorosulphonic acid followed by heterogenization on silica. This heterogeneous solid acid catalyst was explored for the solvent free conversion of 2-methylfuran to diesel fuel precursors of C15 and C20 units via tandem ring opening followed by condensation sequence. Under optimized reaction conditions, SO_3H-INA@SiO_2 was able to convert, 2-methylfuran completely into condensation products such as 5,5-bis(5-methylfuran-2-yl)pentan-2-one (1) and 2,4,4-tris(5-methylfuran-2-yl)pentan-1-ol (2) with 19% and 67% yields, respectively. Superior activity of the prepared catalyst could be attributed for its higher acidity, smaller particle size and high surface area. Structure of the prepared catalyst was confirmed by FT-IR and solid state NMR. In addition, the heterogeneous SO_3H-INA@SiO_2 catalyst is easily separable and reusable several times without losing its activity which is confirmed by catalyst leaching test, recycle study and acid-base titration of used catalyst.

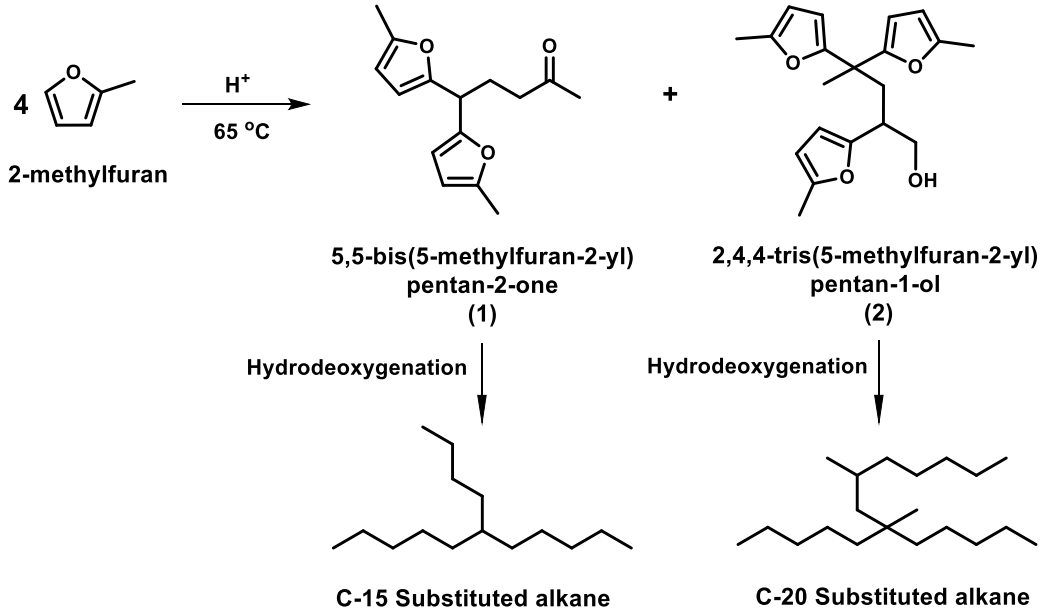

Scheme 3. Synthesis of diesel fuel precursors from 2-methylfuran.

Chapter – 5

Magnetically Separable Brønsted Acid Catalyst for Synthesis of Bisguaiacol-F

Herein, we have systematically synthesized a novel sulfonic acid functionalized, magnetically separable heterogeneous Brønsted acid catalyst, [Fe_3O_4@SiO_2-$(Pr)_3$-N-Bu-SO_3H] [HSO_4^-] and evaluated it for the synthesis of BGF by condensing formaldehyde with two molecules of guaiacol. Our synthesized catalyst facilitates complete conversion of formaldehyde and guaiacol to form regioisomers such as *pp*'-BGF, *mp*'-BGF, and *op*'-BGF with 62%, 15% and 6% selectivity's, respectively. Through meticulous optimization of reaction parameters, time, temperature, reactant molar ratio, and catalyst loading, we have laid the groundwork for a promising and environmentally conscious approach to synthesizing Bisguaiacol-F. The catalyst underwent thorough characterization using Acid-base titration, FT-IR, XRD, TGA and NMR techniques to confirm structure and demonstrate exceptional stability and activityNotably, the catalyst exhibited recyclability over six consecutive runs without any discernible loss in its effectiveness. The catalytic activity was also examined for the condensation of guaiacol with couple of different aldehydes to produce derivatives of Bisguaiacol (Scheme 4).

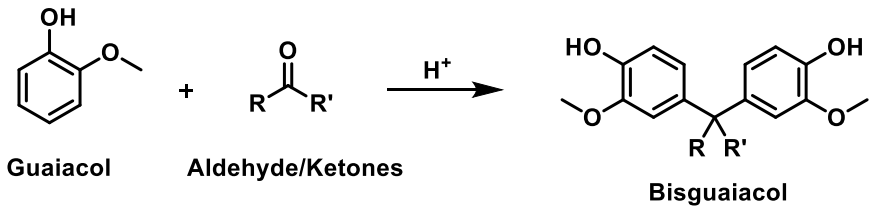

Scheme 4: Synthetic pathway and applications of Bisguaiacol

Chapter – 6

Summary and Future Scope

This chapter provides a comprehensive summary of the current work and provides insights into the potential future directions and applications of this research.

References

1. J. C. Serrano-Ruiz, J. A. Dumesic, *Energy Environ. Sci.,* **2011**, 4, 83−99.
2. P. Pradhan, S. M. Mahajani, A. Arora, *Fuel Processing Technology*, **2018**, 181, 215.
3. M. Kleinert, T. Barth, *Chem. Eng. Technol.*, **2008**, 31, 736–745.
4. G. W. Huber, S. Iborra, A. Corma, *Chem. Rev.*, **2006**, 106, 4044.
5. D. M. Alonso, J. Q. Bond, J. A. Dumesic, *Green Chem*., **2010**, 12, 1493.
6. *a)* K. Zeitsch, *Elsevier Science, Dordrecht,* **2000**, 13, 229-230. *b)* H. Y. Zheng, Y. L. Zhu, B. T. Teng, Z. Q. Bai, C. H. Zhang, H. W. Xiang, Y. W. Li, *J. Mol. Catal.,* **2006**, 246, 18-23.
7. Y. Ding, X. Ni, M. Gu, S. Li, H. Huang, Y. Hu, *Catal. Commun.* **2015**, 64, 101–104.
8. M. Balakrishnan, E. R. Sacia, A. T. Bell, *ChemSusChem*, **2014**, 7, 2796.
9. S. Liu, S. Dutta, W. Zheng, N. S. Gould, Z. Cheng, B. Xu, B. Saha, and D. G. Vlachos, *ChemSusChem*, **2017**, 10, 3225

Chapter – 1

General Introduction

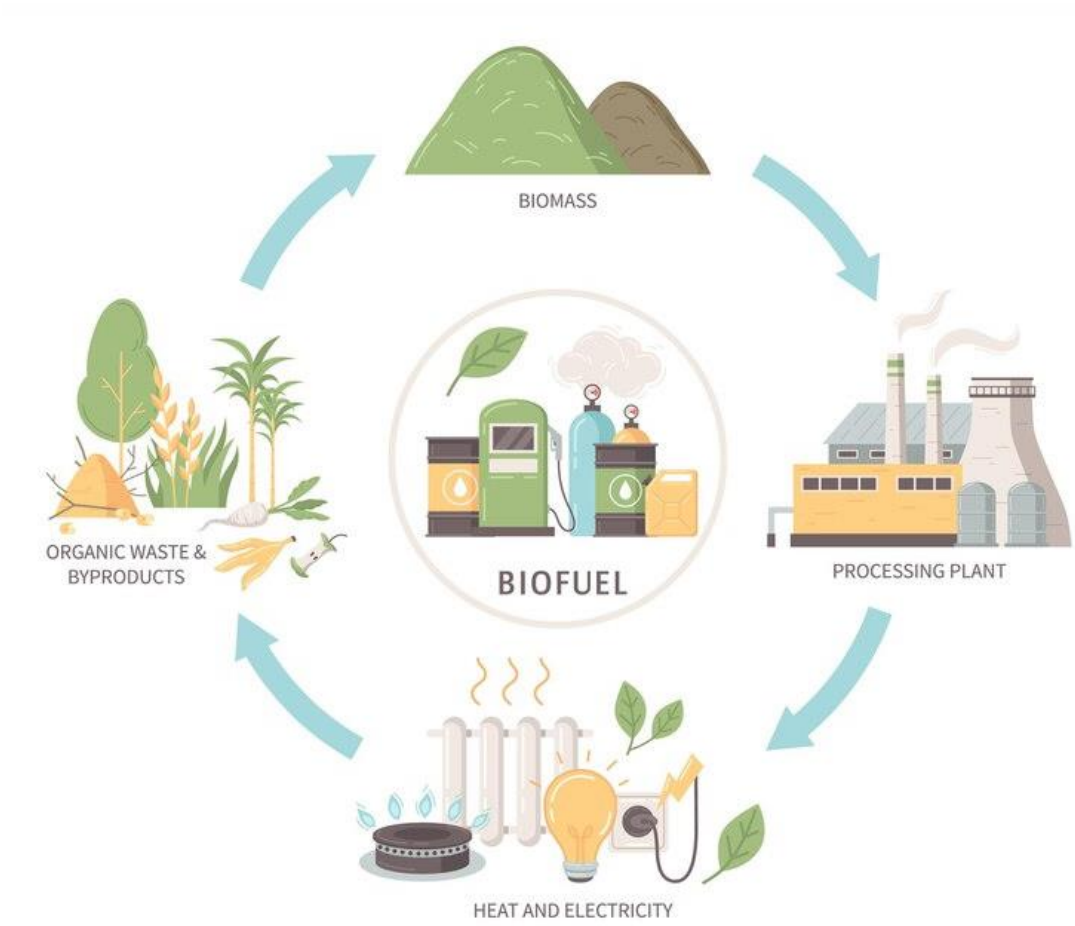

1.1. Biomass

1.1.1. Background

Human beings require energy for day-to-day activities, which can be generated from either renewable or non-renewable sources. Currently, many renewable energy sources, such as solar, wind and hydro power are available for use. However, the majority of our energy supply still comes from non-renewable sources, commonly known as fossil fuels. It is estimated that nearly 90% of the world's energy consumption is derived from fossil fuel resources such as petroleum oil, coal and natural gas. This percentage is even higher in the transportation sector, reaching up to 96% [1]. Petroleum oil, or crude oil, is the most widely used fossil fuel. Crude oil is composed of various organic compounds, including methanol, olefins (e.g., ethylene, propylene, and butadiene), and aromatics (e.g., benzene, toluene, and xylenes), which are collectively known as primary petrochemicals or base chemicals. Through chemical modifications, these base chemicals can be transformed into a wide range of consumer and industrial products, as illustrated in Figure 1.1. [2].

However, it is important to note that the use of fossil fuels for energy generation and the production of chemicals and materials is associated with several significant issues, as outlined below:

- Fossil fuel reserves are limited and the current consumption rate is rapidly increasing due to the high demand from the industrial sector and the development of emerging economies. This trend will inevitably lead to the depletion of these resources within the next few decades [3].
- The consumption of fossil fuels results in net emissions of CO_2 into the atmosphere, which contributes to global warming and has severe impacts on the climate [4].
- The uneven geographical distribution of fossil fuel reserves gives rise to political, economic, and security issues on a global scale [5].

These challenges underscore the need for a transition to more sustainable and environmentally friendly energy sources.

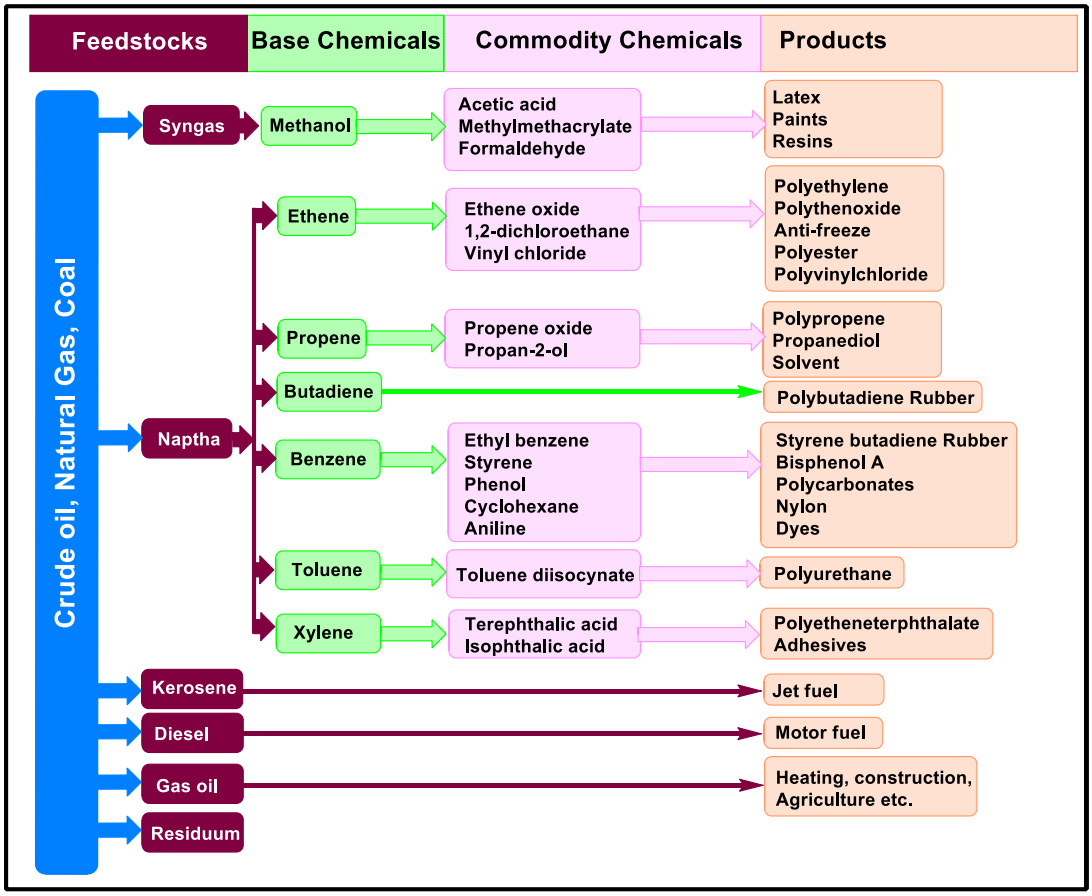

Figure 1.1. Fossil-derived chemical industry

These critical concerns compel us to explore renewable resources for the production of energy and chemicals. In response, aggressive government directives, both in the U.S. [6] and the European Union [7] are encouraging a gradual transition from our current fossil fuel-based economy towards one that is more reliant on renewable energy. The ambitious goal is to produce 20% of fuels and 25% of chemicals from renewable sources by 2030 [8]. Similarly, the Government of India has introduced the National Policy on Biofuels-2018, which aims to increase the use of biofuels in the energy and transportation sectors by promoting their production from domestic feedstocks. The policy targets achieving 20% ethanol blending and 5% biodiesel blending by 2030. Currently, the blending rates stand at approximately 2% for petrol and less than 0.1% for diesel. The growing emphasis on energy security is expected to drive the biomass market in India during the forecast period. Additionally, foreign green energy companies are recognizing opportunities in India's rapidly expanding industrial sector to establish a clean energy ecosystem. New initiatives supporting biomass cogeneration projects are creating incremental opportunities for renewable

energy producers. The biomass market in India is highly competitive, with numerous players operating at local, regional, and international levels. Key players in the Indian biomass market include Emami Agrotech Ltd, Muenzer Bioindustrie GmbH, Universal Biofuel, Aemetis, BIOD Energy (India) Pvt. Ltd., Monopoly Innovations Pvt. Ltd., and Envitec Biogas AG [9]. Ultra-low carbon bioethanol is being produced using Praj's proprietary Enfinity technology, which utilizes lignocellulosic residues such as bagasse, corn cob, rice straw, and wheat straw. This technology has been deployed on a commercial scale, with Praj establishing three commercial-scale plants in collaboration with Fortune 500 companies, including Indian Oil Corporation Limited (IOCL), Hindustan Petroleum Corporation Limited (HPCL), and Bharat Petroleum Corporation Limited (BPCL) [10].

India is a biomass-rich country producing approximately 600-700 million tonnes of agro-waste annually in the form of straw [11]. Indian agriculture accounts for about 8% of the global agricultural domestic product, meeting the needs of 18% of the world's population with only 9% of the world's arable land and 2.3% of the total geographical area [12]. With its strong agricultural base and vast availability of agro-resources, India is well-positioned to generate non-edible biomass that can be explored for power and biofuel production. Currently, the share of biofuel in India's total fuel consumption is very low, primarily limited to a 5% ethanol blending in gasoline which is mandatory in only 10 states. As of now, biodiesel is not available in the Indian fuel market. However, the government has set a target to meet 20% of the country's diesel demand with biodiesel by 2030 (Planning Commission, 2003). Given that the demand for edible oil seeds exceeds domestic production, the government is promoting the use of non-edible oils from sources like Jatropha curcas and Pongamia pinnata as feedstocks for biodiesel production [13]. Considering the primary challenges, it is essential to explore alternative options for fuels, chemicals, and materials. Lignocellulosic biomass presents a sustainable and eco-friendly alternative to fossil resources. Lignocellulose is one of the most abundant organic carbon resources on Earth and is both renewable and reproductive. As such, it has the potential to meet society's needs for energy, chemicals, and materials, offering a promising pathway toward a more sustainable future.

1.1.2. Concept of Biorefinery

The term "biorefinery" is primarily defined as a complex, fully integrated system of sustainable, environmentally friendly, and resource-efficient technologies for

comprehensive material and energy production [14,15]. According to the American National Renewable Energy Laboratory (NREL), a biorefinery is a facility that integrates biomass conversion processes and equipment to produce fuels, power, and chemicals (Figure 1.2) [16]. Meanwhile, the U.S. Department of Energy (DOE) describes a biorefinery as a concept involving the processing of biomass feedstocks to produce a wide range of valuable products, similar to those produced by a petrochemical refinery (Figure 1.3) [17,18]. Biorefineries have been identified as one of the most promising pathways to establish a new domestic bio-based industry [19,20]. Since the inception of the biorefinery concept, several technological advancements have been made, paving the way for more efficient and sustainable production methods.

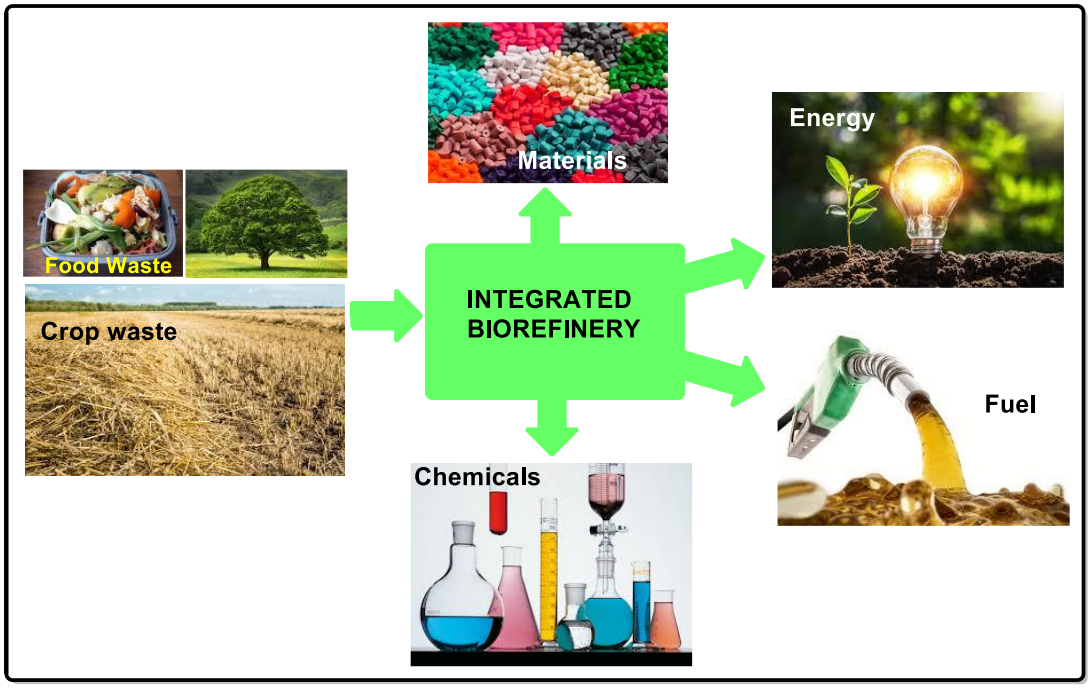

Figure 1.2. The integrated biorefinery as a mixed feedstock source of chemicals, energy, fuels and materials. Reproduced from ref.17.

Biorefineries are categorized into Generation I, II, and III:

Generation I Biorefineries: These facilities use dry milling processes to convert edible grains into ethanol. However, this approach competes directly with the food supply chain. The technology has a limited processing capability, producing a fixed amount of ethanol, which restricts its application to certain specific purposes only [15].

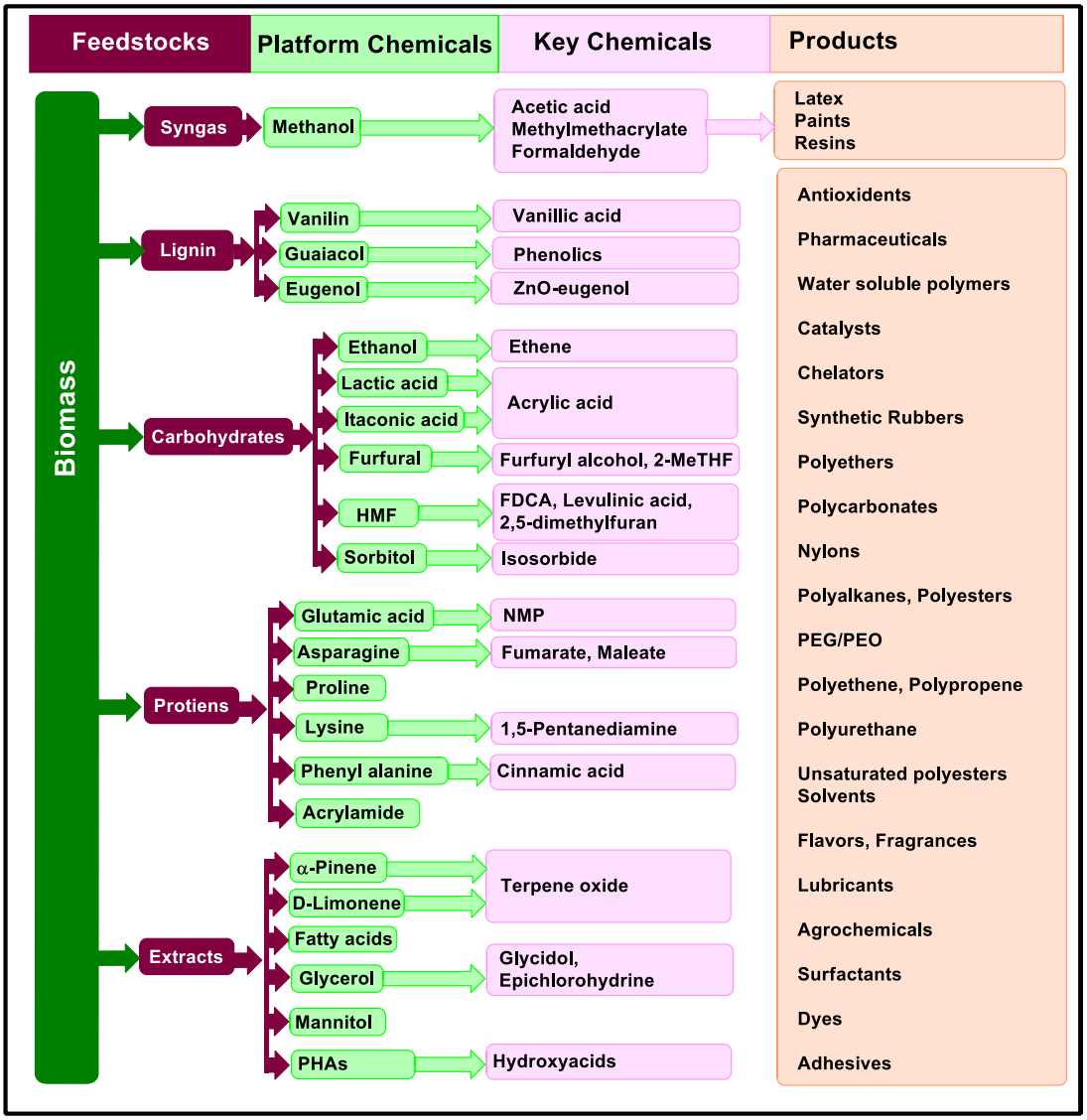

Figure 1.3. Biomass-derived chemical industry. 2-MeTHF: 2-Methyltetrahydrofuran; FDCA: 2,5-furandicarboxylic acid; HMF/CMF: 5-(hydroxymethyl)furfural/5-(chloromethyl)furfural; NMP: N-methyl pyrrolidone; PEG/PEO: Polyethylene glycol/polyethylene oxide; PHAs: Polyhydroxyalkanoids

Generation II Biorefineries: Utilizing wet milling technology, these biorefineries use grain feedstocks and have the capability to produce a diverse range of end products, including starch, high-fructose corn syrup, ethanol, corn oil, corn gluten feed and meal. This versatility allows Generation II biorefineries to integrate industrial product lines with existing agricultural production systems. Examples of industries operating on the Generation II biorefinery model include the NatureWorks PLA facility and Logen.

Generation III Biorefineries: Representing a more advanced stage of biorefinery technology, Generation III biorefineries are designed to utilize agricultural and/or forest waste biomass to generate multiple product streams. Although no Generation III biorefineries have been built yet, they promise to significantly expand the range of products derived from biomass, reducing reliance on edible feedstocks and enhancing sustainability.

1.1.3. Lignocellulosic biomass

In the long term, second-generation bio-renewable feedstocks, primarily derived from lignocellulosic sources are essential to satisfy the demand for renewable carbon. Lignocellulose is the predominant component found in plant and algae biomass with an estimated annual production of approximately 2×10^{11} metric tons [21]. Typically, lignocellulosic biomass consists of about 40-50% cellulose, 20-30% hemicellulose, and 10-25% lignin (Figure 1.4) [22, 23]. This composition makes lignocellulosic biomass a highly abundant and versatile resource for renewable energy and material production.

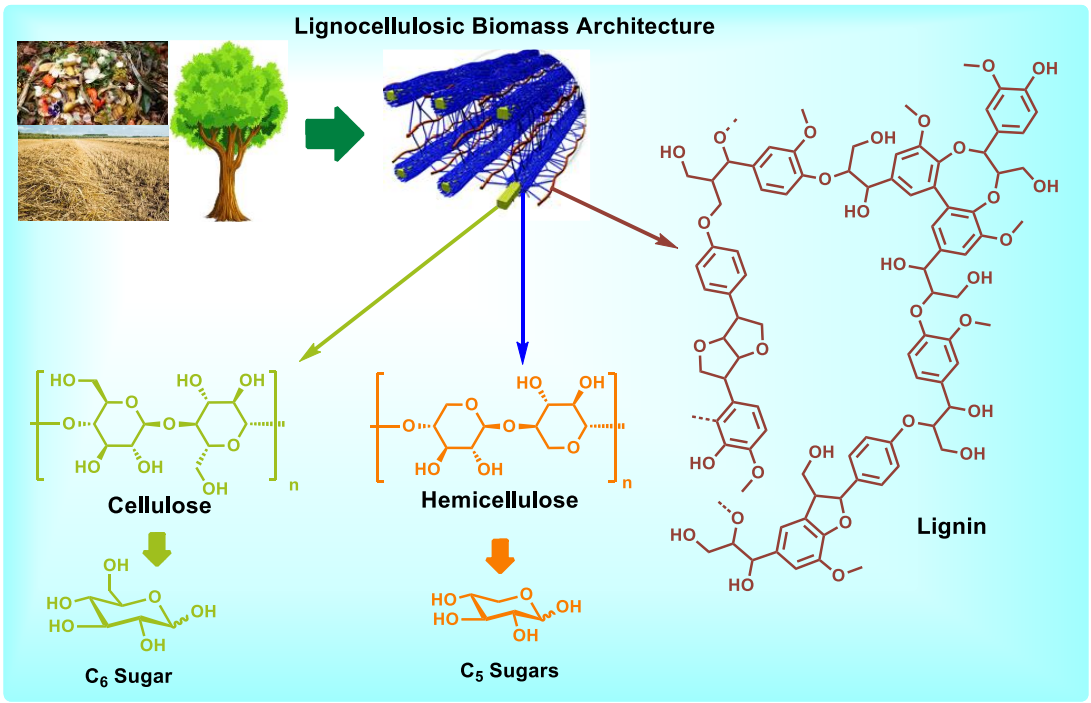

Figure 1.4. Lignocellulose biomass compositions: cellulose, hemicellulose, and lignin

1.1.3.1. Cellulose

Cellulose is composed of D-glucose units linked together by β(1→4)-glycosidic bonds (Figure 1.5). This straight-chain polymer adopts an extended, rigid, rod-like conformation, facilitated by the equatorial orientation of the glucose residues. Cellulose is primarily used in the production of paper and paperboard but smaller quantities are transformed into various derivative products such as cellophane and rayon. The conversion of cellulose from energy crops into biofuels such as cellulosic ethanol is being researched as a potential alternative fuel source. For industrial purposes, cellulose is mainly sourced from wood pulp and cotton [24]. Cellulose is tasteless, odorless, hydrophilic, insoluble in water and most organic solvents, chiral, and biodegradable. It can be broken down into its glucose units through hydrolysis treatment, making it a versatile and valuable resource for various industrial applications.

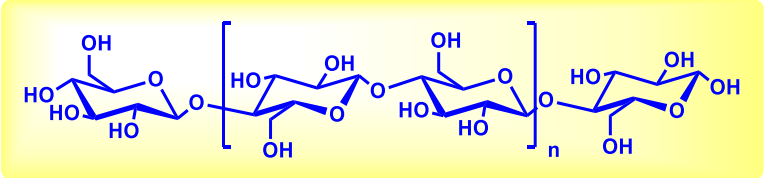

Figure 1.5. Structure of Cellulose

1.1.3.2. Hemicellulose

Hemicellulose, also known as polyose, is a type of heteropolymer (matrix polysaccharide) found alongside cellulose in nearly all plant cell walls such as arabinoxylans [25]. Unlike cellulose, hemicellulose has a random amorphous structure making it less rigid and strong. The average molecular weight of hemicellulose is typically less than 30,000 u. Hemicellulose consists of various polysaccharides including xylan, glucuronoxylan, arabinoxylan, glucomannan, and xyloglucan. These polysaccharides are composed of different sugar monomers such as xylose, mannose, galactose, rhamnose and arabinose. Hemicellulose mainly contains D-pentose sugars and rarely small amounts of L-sugars. In hardwood trees, hemicellulose is predominantly composed of xylan with some glucomannan whereas in softwoods, it is mainly rich in galactoglucomannan with only a small proportion of xylan. Xylan, a polysaccharide made from xylose units (a type of pentose sugar) typically constitutes 10-35% of the total hemicellulose in hardwoods and 10-15% in softwoods. In softwoods, mannose can be the most abundant sugar. Thus,

hemicellulose is a rich source of xylose monomers compared to other sugar monomers (Figure 1.6).

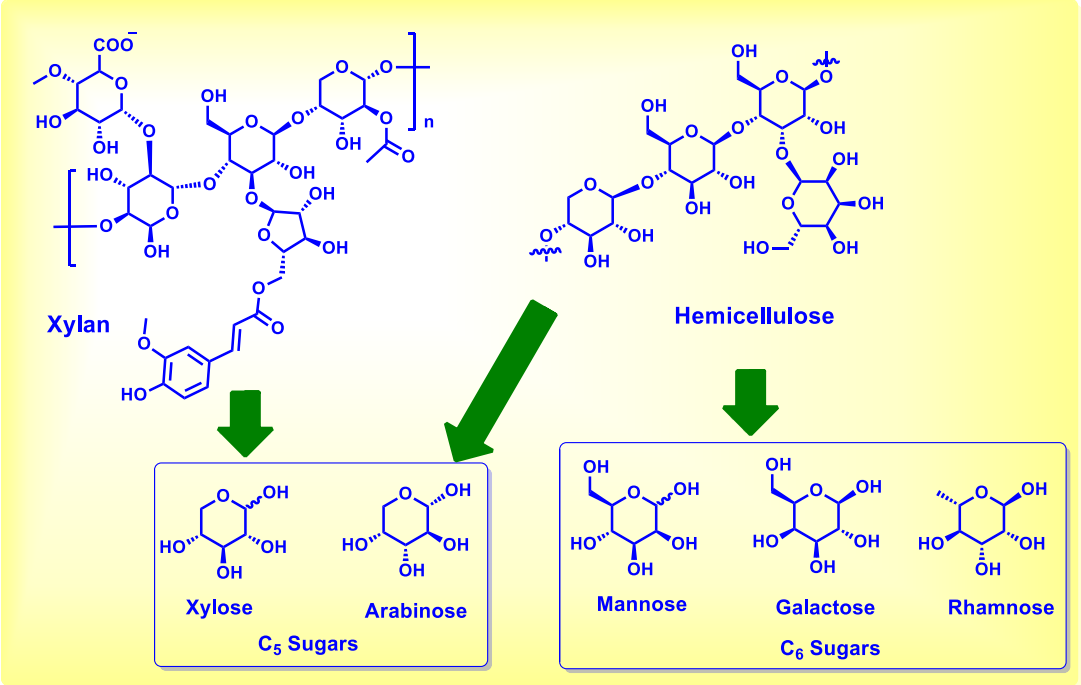

Figure 1.6. C_5 and C_6 sugars derived from hemicellulose and xylan

1.1.3.3. Lignin

Lignin is a class of complex organic polymers that serve as essential structural components in the support tissues of vascular plants and some algae [26]. It is a cross-linked, racemic macromolecule with molecular masses exceeding 10,000 u (Figure 1.7).

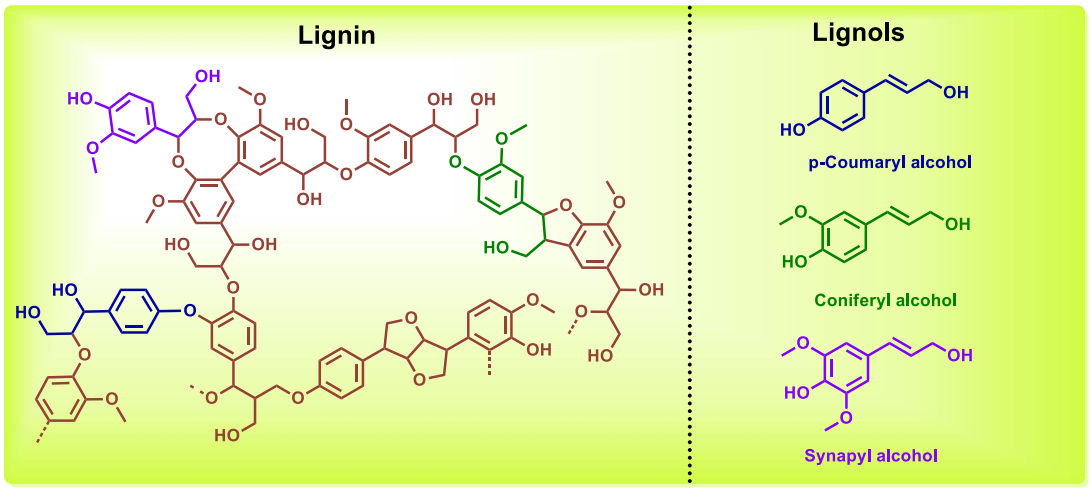

Figure 1.7. C_5 and C_6 sugars derived from hemicellulose and xylan

Lignin is relatively hydrophobic and aromatic in nature. There are three primary monolignol monomers, each with varying degrees of methoxylation: p-coumaryl alcohol, coniferyl alcohol, and sinapyl alcohol [27]. These lignols are integrated into lignin as phenylpropanoids: p-hydroxyphenyl (H), guaiacyl (G), and syringyl (S), respectively [28]. Additionally, all lignins contain small amounts of incomplete or modified monolignols and other monomers are particularly common in non-woody plants [29].

1.1.4. Lignocellulosic derived platform molecules

The U.S. Department of Energy's 2004 report [30] established a foundation for identifying promising bio-based molecules presenting 12 well-known high-value bio-based chemicals as building blocks. These building block chemicals characterized by their multiple functional groups, have the potential to be transformed into a wide array of useful molecules. Later, Bozell and Petersen [31] revisited the DOE's top-10 list from 2004 and proposed a multicriteria analysis to reassess and identify new top bio-based molecules. Their framework evaluated platform chemicals and building blocks based on criteria similar to those used for petrochemical refineries, where olefins, BTX, methane, and CO serve as initial building blocks (base chemicals). In this context, compounds with analogous roles in a biorefinery are referred to as primary building blocks, holding significant importance. According to Bozell and Petersen's criteria, ethanol and succinic acid are exemplary platform chemicals due to their potential as primary building blocks. However, the dominant trend has been to categorize building blocks as platforms. Bomtempo et al. [32] recently proposed a refined definition of platform chemicals. According to this definition, a platform chemical should be an intermediate molecule with a flexible structure that enables the production of a broad range of derivatives, cost-competitive both as a platform molecule and its derivatives support scale-up and economies of scale, integrated within an innovation ecosystem and associated with well-established governance mechanisms. A wide variety of functionalized molecules can be derived from the decomposition of lignocellulose each varying chemically. From these, a team from the Pacific Northwest National Laboratory (PNNL) and the National Renewable Energy Laboratory (NREL) identified a list of 12 chemicals with potential industrial applications. Through an iterative review process, involving over 300 candidates, the team selected a shorter list of 30 potential candidates based on the petrochemical model, chemical data, market information, properties, performance, and previous

industry experience. The reported block chemicals can be produced from sugars through biological and chemical conversions (Figure 1.8).

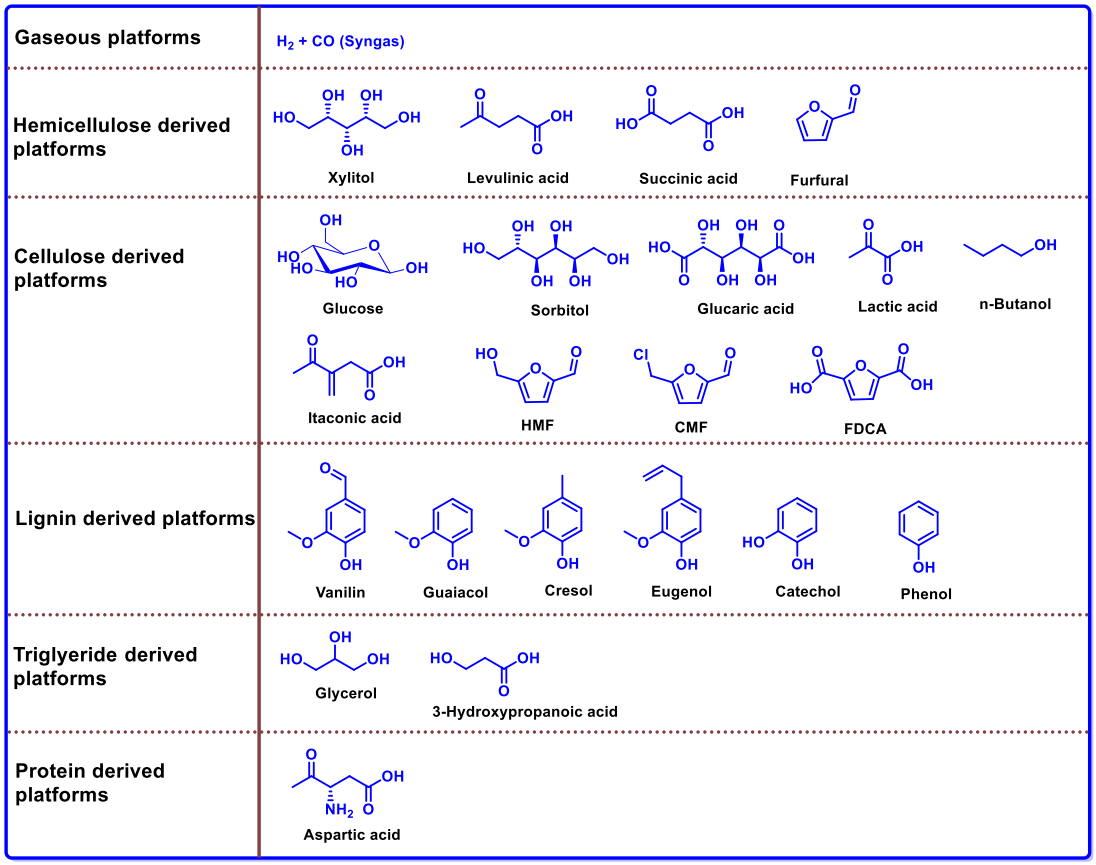

Figure 1.8. Lignocellulose derived initial platform chemicals, CMF: 5-(Chloromethyl)furfural, FDCA: 2,5-furandicarboxylic acid, HMF: 5-(hydroxymethyl)furfural.

These building blocks can be converted into a range of high-value chemicals and materials. Their defining feature is the presence of multiple functional groups, which enables their transformation into diverse families of useful molecules. The broad classification of these 12 sugar-based building blocks includes 1,4-diacids (such as succinic, fumaric, and maleic acids), 2,5-furandicarboxylic acid (FDCA), 3-hydroxypropionic acid, aspartic acid, glucaric acid, glutamic acid, itaconic acid, levulinic acid, 3-hydroxybutyrolactone, glycerol, sorbitol, and xylitol/arabinitol [18, 33-35]. Additionally, a secondary group of building blocks has been identified as promising candidates for commercial applications. This group includes acids such as gluconic, lactic, malonic, propionic, citric, aconitic and xylonic acids as well as acetoin, furfural, levoglucosan, lysine, serine, and threonine. Moving forward, it is recommended to explore high-value products derived from biomass components

such as aromatic compounds, polysaccharides and oils. It is also crucial to evaluate technical challenges in detail, particularly by comparing chemical and biological conversion methods. A general approach to the synthesis of platform chemicals and their downstream products, including fuel additives, is illustrated in Figure 1.9.

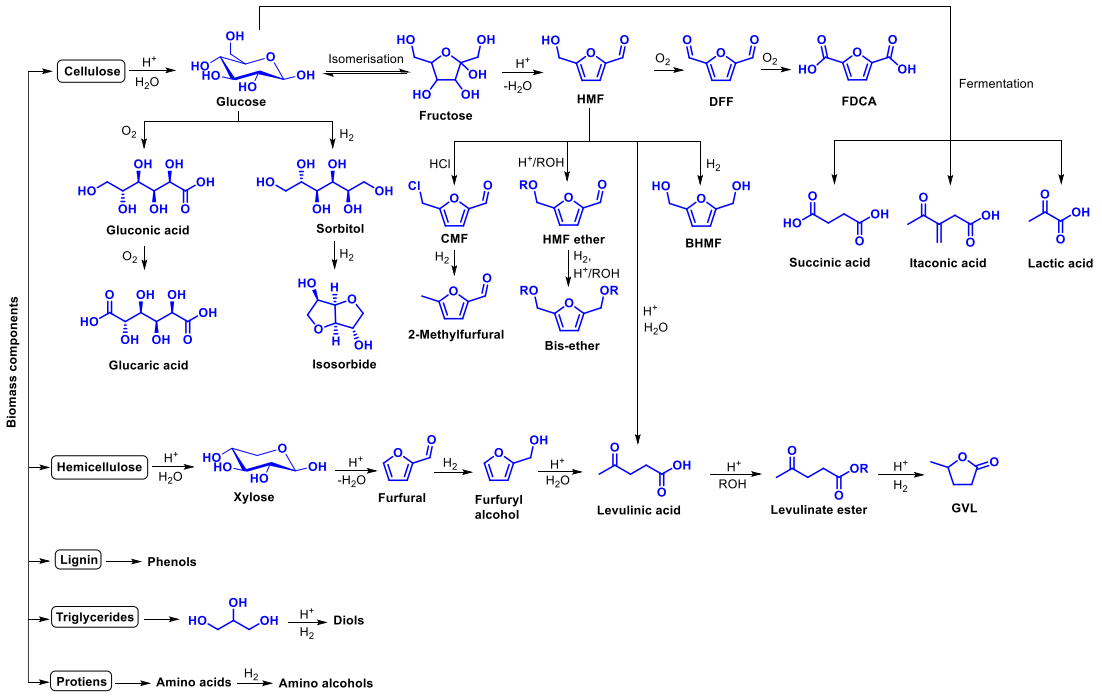

Figure 1.9. A general approach to produce chemicals and fuel additives from biomass. BHMF: bis(hydroxymethyl) furan, CMF: 5-(Chloromethyl)furfural, DFF: 2,5-diformyl furan, FDCA: 2,5-furandicarboxylic acid, GVL: γ-valerolactone, HMF: 5-(hydroxymethyl)furfural.

1.1.4.1. Gaseous platform

Syngas

In the thermal or thermochemical treatment of biomass, synthesis gas (syngas) is produced as a mixture of carbon monoxide (CO) and hydrogen (H_2) [36]. Syngas serves as a valuable starting material for the production of key chemicals such as methanol (MeOH), olefins, alkanes, ethers and ammonia (Figure 1.10). Strategies developed for converting fossil-derived syngas into chemicals can also be applied to bio-derived syngas. However, crude bio-derived syngas requires purification to remove particulates, ash, sulphur compounds, nitrogen compounds and tars [37,38]. Methanol is a major chemical produced from syngas using various copper catalysts at high temperatures and pressures [39]. As a significant platform molecule, methanol can be converted into a wide range of derivative chemicals. Current research is

focused on using syngas in acetogen fermentations to potentially produce ethanol, butanol and 2,3-butanediol [40]. Additionally, the classic Fischer-Tropsch process can be employed with bio-syngas to create biobased drop-ins for diesel, gasoline, olefins, and waxes [39,41]. Another critical application of syngas in biorefineries is in hydroformylation and reduction processes that are highly relevant for platform molecules due to their diverse functionalities.

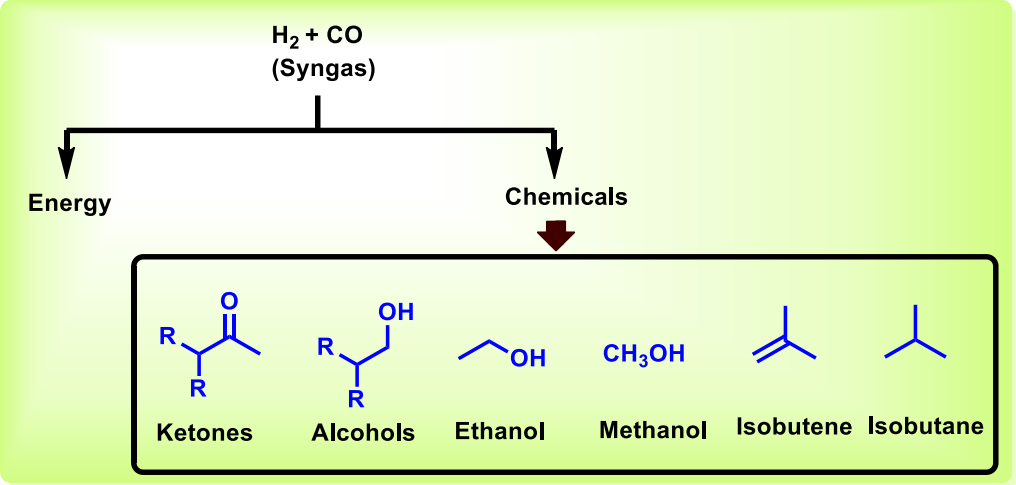

Figure 1.10. Bio-Syngas for C_1 chemistry

1.1.4.2. Hemicellulose derived platform molecules and their valorisation over heterogeneous catalysts

Xylitol

Xylitol is recognized as an artificial sweetener and is used in a variety of products, including medications, dietary supplements, confectioneries, toothpaste and chewing gum [42,43]. It has no effect on blood sugar or insulin levels, as it is absorbed more slowly than table sugar and provides no calories thus, not influencing blood glucose levels [43]. The richest sources of xylitol include plums, strawberries, raspberries, cauliflower, berries, corn husks, oats and mushrooms [44]. Additionally, hardwoods such as birch and beech, wood shavings, cottonseed hulls, nuts, straw, stems, corncobs and sugarcane bagasse which typically contain 20-35% xylan are also significant sources [45]. Xylitol can also be derived from bio-waste materials including birch bark and pulp waste [46]. Industrially, xylitol is produced by the hydrogenation of pure D-xylose using a nickel catalyst under elevated temperatures and pressures [47,48]. Recent studies by Dietrich et al. have reported a method combining phosphotungstic acid and Ru/C catalysts with isopropyl alcohol to convert

hemicellulose to xylitol with high yield [49]. Zhang et al. [50] employed a two-step cascade reaction using a mixture of water and isopropanol as a solvent, H_2SO_4 as an acid catalyst for hydrolysing biomass to D-xylose and Ru/C for hydrogenating D-xylose to xylitol. Isopropanol acts as the hydrogen source for the reduction of xylose to xylitol. Some studies [51-56] suggest that acid catalysts may not be necessary for xylitol production from biomass, as metals such as Ru or Pt can facilitate both hydrolysis and hydrogenation. These metals generate H^+ ions in situ through the dissociative adsorption of H_2 on the catalyst surface which then migrate to Lewis acidic sites, forming protonic acid sites by releasing electrons. Barbaro et al. [57] used a bifunctional ruthenium catalyst supported on resin (Ru@Dowex-H) for the direct and selective conversion of concentrated aqueous solutions of pentoses and hexoses to xylitol. Xylitol serves as a valuable starting material for producing a wide array of chemicals, as illustrated in Figure 1.11.

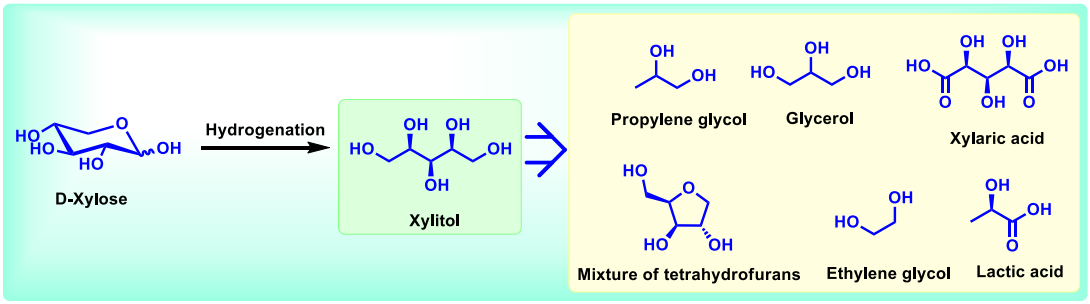

Figure 1.11. Xylitol production and as a platform chemical

Furfural

Furfural is the most commonly produced industrial chemical derived from lignocellulosic biomass with an annual production volume exceeding 200,000 tons [58,59]. Its production relies exclusively on the acid-catalysed conversion of pentosan sugars found in agricultural and forestry residues [60]. The first commercial production of furfural was pioneered by the Quaker Oats Company in 1921 [61]. At that time, Quaker Oats utilized large quantities of oat hulls from oatmeal production, achieving a 50% yield of furfural (based on xylan) by treating the hulls with dilute sulfuric acid and steam pressure [62]. As a versatile platform molecule, furfural can be used to produce various important chemicals through selective hydrogenolysis, reduction, ring opening, and Aldol condensation reactions (Figure 1.12).

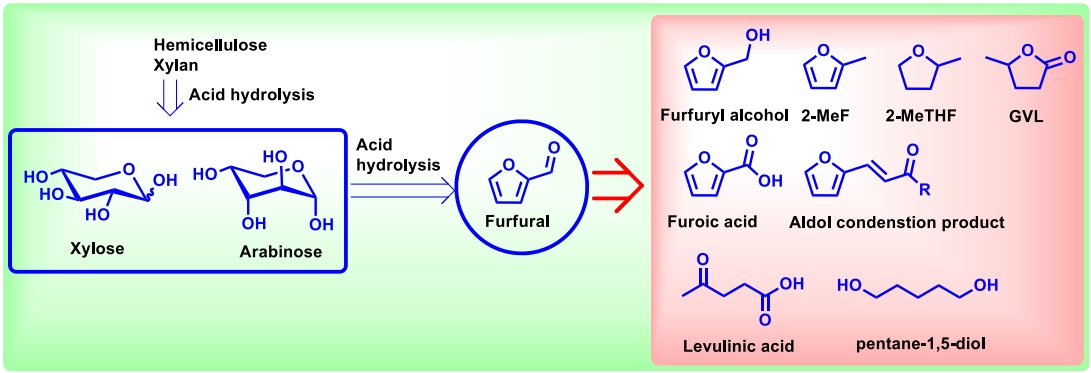

Figure 1.12. Furfural production and as a platform chemical

Furfural was first identified in 1831 by J. W. Döbereiner who noted its aromatic odor reminiscent of almonds. In 1845, G. Fownes isolated and named the substance with the molecular formula $C_5H_4O_2$ as furfural. The bulk production of furfural began after its polymerization properties were discovered. Today, furfural is a unique industrial chemical derived from lignocellulosic biomass with an annual production exceeding 200,000 tonnes [58,59]. Modern furfural production relies exclusively on the acid-catalysed conversion of pentosan sugars from agricultural and forestry residues [60]. Fossil-based technologies for producing furfural are not economically viable and are no longer in use. The primary producers of furfural are South Africa (approximately 20,000 tonnes per year) the Dominican Republic (32,000 tonnes per year) and China (200,000 tonnes per year) which together account for 90% of global production capacity [63]. Since 2000, furfural prices have fluctuated significantly ranging from USD 500 to 1500 per metric ton. However, due to low feedstock costs and increased production capacity in China, there has been a slight price decrease over the past decade. Currently, the market price is around USD 1,000 per tonne, compared to USD 1,740 per tonne in 1990 and USD 1,760 per tonne for furfuryl alcohol. Both the USA and the EU have increased imports of furfural from China to mitigate price differences resulting in a market heavily reliant on Chinese supply [64]. According to a report by Allied Market Research, the global furfural market is projected to reach USD 1,434 million by 2022, up from USD 663 million in 2015 [65]. The first commercial production of furfural was initiated by the Quaker Oats Company in 1921 [61]. The company used large quantities of oat hulls, a byproduct of oatmeal manufacturing and achieved a 50% yield of furfural (based on xylan) by treating the hulls with dilute sulfuric acid and steam pressure [62].

The dehydration of C_5 sugars can produce furfural, a platform chemical with diverse applications, including solvents, resins, and fuel additives [66]. Since xylose is typically available as an aqueous stream, its conversion to furfural in water is preferable. Following the initial discovery, numerous studies have explored the conversion of pentoses, such as xylose into furfural [67]. Research has investigated this conversion in various media and employed Lewis or Brønsted solid acids as catalysts. Formic acid, a co-product of biomass conversion to the C_6 fraction is often involved in these processes. Heterogeneous catalysis combined with efficient catalyst/product separation is crucial for greener and more economically viable industrial processes. An effective strategy involves using a combined solid acid catalyst with both Lewis and Brønsted acidity to facilitate pentose isomerization and conversion. Integrating dual catalysts with a biphasic solvent system can enhance product separation and catalyst recycling. Regarding catalyst activity and selectivity, catalysts with a higher number of Lewis-acid sites generally exhibit greater effectiveness in forming furfural. However, the selectivity of the process is strongly influenced by the presence of Brønsted-acid sites [68].

Furfural conversion to fuels and chemicals

The potential for transforming furfural into fuel components and valuable chemicals is substantial. Over 80 chemicals have been derived directly or indirectly from furfural, establishing it as a versatile top C_5-platform molecule derived from biomass [62]. The global market for furfural is currently estimated at approximately 205 kilotons per year with around 60% allocated to the production of furfuryl alcohol [69]. There is a strong demand for further innovations in the transformation of furfural, aiming to discover new pathways that integrate furfural into the biorefinery product chain.

Through C-C bond forming reaction of furfural

Petroleum-derived jet and diesel fuels typically consist of molecules with carbon chain lengths ranging from C_8 to C_{20}. To produce jet and diesel fuels from biomass, it is essential to form carbon-carbon bonds between biomass-derived molecules. Biomass-derived aromatic aldehydes can undergo condensation reactions, such as Aldol condensation, Pinacol coupling and Hydroxyalkylation-alkylation (Figure 1.13), to generate molecules with C_8 to C_{20} units. These intermediates can be then converted into jet and diesel fuels through hydrodeoxygenation processes.

Table 1.1. Catalysts used for Aldol condensation of furfural with aldehydes/ketones

Catalyst type	Catalyst	Aldehyde/Ketone
Basic oxides	MgO	Acetone [74], Levulinic acid [75]
	CaO	Acetone [74], 2-Pentanone and 2-Heptanone [76]
	La–ZrO_2, Y–ZrO_2, MgO–ZrO_2, MgO–TiO_2, NH_3-functionalised SiO_2	Acetone [74]
	Co–Al spinels	Acetone [77]
	Mg–Al	Acetone [78], MIBK [79], Cyclohexanone [80]
	CaMgAl	MIBK [81]
	Ca–Zr	Acetone [82]
	WO_3–ZrO_2	Acetone [83]
	MgO–ZrO_2	Acetone [84]
	Mg–Zr/graphite	Acetone [85]
	MgO/Na–Y	Acetone [86]
	dolomites	Acetone [87]
Carbocatalyst	chitosan	Acetone [88]
	NaOH-modified chitosan	Levulinic acid [89]
Homogeneous Lewis acid	$SnCl_4$ $5H_2O$	Cyclopentanone [90]
Homogeneous Brønsted base	DBU	Dihydroxyacetone and hydroxyacetone [91]
Acidic resins	Nafion, Amberlyst-15, Amberlyst-36	Cyclopentanone [92]
Acidic Zeolites	H-USY, ZSM-5, H-β	Cyclopentanone [92], Acetone [93]
	Sn-MFI	Acetone [94]
	Sn-beta	Acetone [95]
Acidic oxides	Nb_2O_5	Heptanone [96]
Amphoteric metal oxide	Mn_2O_3	Angelica lactone [97]
	Anatase TiO_2	Acetone [98]
ionic liquid	$[H_3N^+–CH_2–CH_2–OH]$ $[CH_3COO^-]$	Acetoin [99]

Aldol condensation: The Aldol condensation of furfural with acetone is a widely studied reaction producing furfurylidene acetone (4-(2-furyl)-3-buten-2-one, FAc) as a key product. This C_8 monomer can be further reacted with another furfural molecule to yield the C_{13} dimer, difurfurylidene acetone (1,5-bis-(2-furyl)-1,4-pentadien-3-one, DFAc). DFAc is notable for its potential as a precursor to polymers with high thermal and chemical resistance as well as in organo-mineral concretes [70]. FAc, on the other hand, serves as a flavoring agent in the food industry [71]. Aldol condensation is a C-C bond-forming reaction, primarily aimed at increasing the number of carbon atoms

to create fuel molecules [72]. Traditionally, this reaction has been performed using an aqueous NaOH solution as a catalyst [73]. However, the use of heterogeneous solid catalysts is now preferred due to their ease of separation and recyclability. Various catalysts, including basic and acidic oxides, homogeneous acids/bases, carbocatalysts, acidic zeolites, acidic resins, amphoteric oxides and ionic liquids have been explored for the condensation of furfural with aldehydes and ketones (Table 1.1).

***Pinacol coupling*:** Fu et al. demonstrated an advanced C-C bond formation approach where fuel precursors with 10–14 carbons are efficiently obtained through the direct self-coupling of furfural. For this self coupling (Pinacol coupling) of furfural, homogeneous catalysts system containing Zn powder and 10% aq. NaOH solution was used. The obtained fuel precursors have been further hydrodeoxygenated to produce straight chain alkanes [100]. There is scope to develop heterogeneous solid catalyst for this reaction.

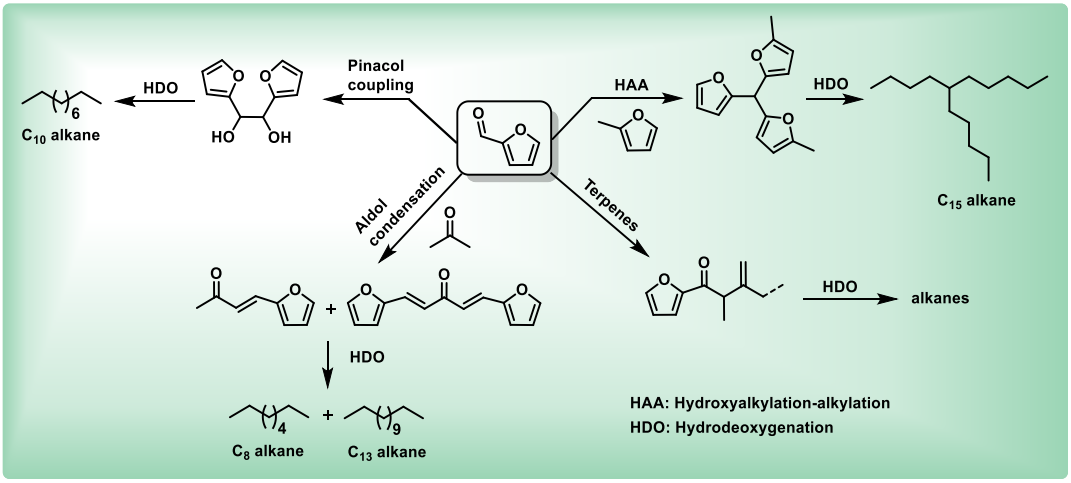

Figure 1.13. C-C bond forming reactions of furfural and subsequent hydrodeoxygenation

***Hydroxyalkylation-alkylation (HAA)*:** It is another approach to upgrade furfural to alkanes. In acid catalyzed hydroxyalkylation-alkylation (HAA) two molecules of 2-methylfuran was condensed with furfural to produce a C_{15} unit of trifurylmethane derivative. Numerous synthetic methods are available for the synthesis of bis- and tris(furyl)alkanes. These methods primarily involve the condensation of 2-methylfuran with carbonyl compounds in the presence of various catalysts, including concentrated H_2SO_4 [101], HCl [102], acidic resins [101, 103, 104], MCM-SO_3H [105], Mo-Zr-MCM-

41 [106], $AuCl_3$ [107], zeolites [108], SiO_2-Pr-S-Pr-SO_3H [109], $Cu(OTf)_2$ [110], I_2 [111], CMH-SO_3H [112], SILC [113], SO_3H-functionalized ILs [114], and TFA-ZrO_2 [115].

C*oupling with Terpenes*: Furfural was reacted with terpenes such as isoprene and myrcene in the presence of a ruthenium catalyst to produce carbon-upgraded coupling products. These products can then undergo hydrodeoxygenation to form alkanes [116].

Through hydrogenation and hydrogenolysis of furfural

Furfural containing aldehyde and aromatic furan ring functionality are susceptible for the hydrogenation and hydrogenolysis. Furfural could produce variety of valuable chemicals and fuel components through hydrogenation and hydrogenolysis (Figure 1.14).

Furfural reduction to furfuryl alcohol: The aldehyde functionality of furfural could be transformed to furfuryl alcohol over noble and non-noble catalysts with or without external hydrogen [88]. Furfuryl alcohol is utilized in the fine chemicals and polymer industries with key applications including the production of thermostatic resins, acid-resistant bricks, corrosion-resistant fiberglass and polymer concrete. It is also used in liquid resins for galvanic baths. Additionally, furfuryl alcohol serves as a crucial intermediate in the synthesis of lysine, vitamin C, lubricants, dispersing agents, plasticizers and tetrahydrofurfuryl alcohol [93,117].

Decarbonylation of furfural to furan derivatives: Decarbonylation furfural provides 2-methylfuran which could be further ring hydrogenate to 2-methyltetrahydrofuran (MeTHF) so that it can be blend into gasoline. The high volatility and carcinogenic nature of furan prevent its direct blending in gasoline. Furfural decarbonylation has been extensively studied using both noble and non-noble heterogeneous catalysts. Non-noble metal oxide catalysts such as Fe, Zn, Mg, Cr, Co, Mo, and Ni are typically employed at temperatures ranging from 300–500°C [91,118]. However, at these high temperatures, furan often decomposes into heavier products, leading to rapid catalyst deactivation. In contrast, despite their higher cost, noble metal catalysts are preferred due to their relatively slower deactivation rates [119].

***Cascade ring opening of furfural to carboxylic acids, esters and lactones*:** Levulinic acid and its ester derivatives are the primary ring open products of the furfural. Levulinate esters are the potential biofuel additives. Traditionally, Levulinic

acid/esters are produced in two different steps and different reactors. In this process, furfural is initially hydrogenated to produce furfuryl alcohol, which is then converted into levulinic acid via acid-catalyzed ring-opening in water. Alternatively, ring-opening of furfuryl alcohol can be carried out in the presence of alcohols to yield alkyl levulinates [120]. However, this two-step process requires costly separation and purification of the furfuryl alcohol intermediate. To streamline this process and enhance efficiency, researchers have developed one-pot methods to convert furfural directly into levulinic acid or its esters. Chen et al. [121] demonstrated a one-pot direct transformation of furfural into alkyl levulinates using a bifunctional Pt/ZrNbPO$_4$ catalyst under hydrogen pressure, thereby avoiding the isolation of furfuryl alcohol. Subsequently, Fang et al. [122] achieved a similar conversion without external hydrogen gas by employing 1.5 wt% Cu/NbP in a cascade reaction with formic acid as both the hydrogen donor and solvent. Bokade et al. [123] introduced an innovative catalytic strategy for the one-pot cascade conversion of furfural to levulinic acid over a bifunctional $H_3PW_{12}O_{40}/SiO_2$ catalyst, using isopropyl alcohol (IPA) as the hydrogen donor and solvent. Alshaikh et al. [124] developed a Dowex-functionalized half-sandwich Ru(II) (η6-p-cymene) complex for catalytic hydrogen transfer reactions with formic acid as the hydrogen donor for furfural hydrogenation. These catalysts demonstrated high activity and selectivity for levulinic acid production and exhibited excellent recyclability. Levulinic acid is among the top-12 promising building blocks identified by the DOE. It serves as a valuable organic intermediate for synthesizing a range of chemicals used in fuel additives, fragrances, solvents, oil additives, pharmaceuticals, and plasticizers [125,126]. Potential derivatives from levulinic acid include levulinate esters, γ-valerolactone, acrylic acid, 1,4-pentanediol, angelica lactone, 2-methyltetrahydrofuran, δ-aminolevulinic acid, nonanone, and pyrrolidones.

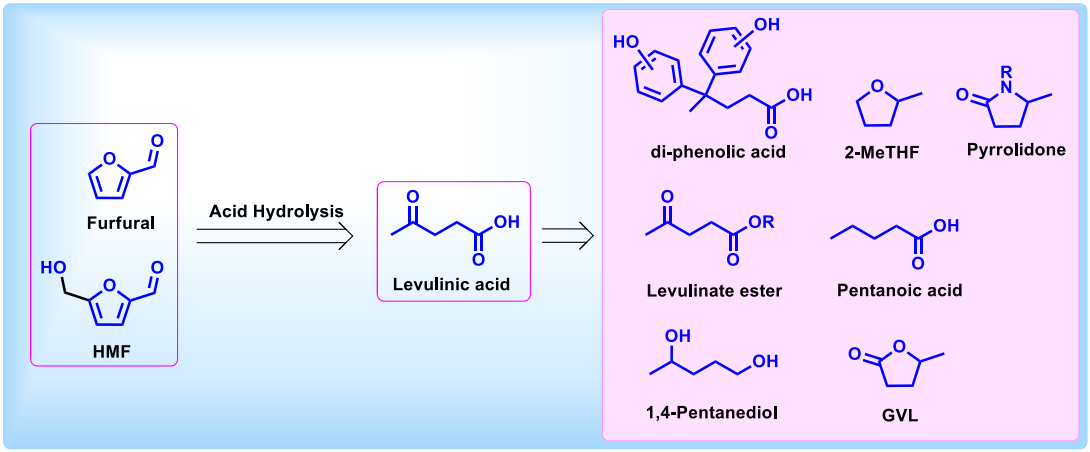

Figure 1.14. Levulinic acid production and as a platform chemical

γ-Valerolactone (γ-GVL) finds diverse applications as a fuel additive [127], food ingredient [128], intermediate in chemical production [129], high-grade alkene fuels [130], nylon synthesis [131] and in niche uses such as cutting oils and brake fluids [132]. It also serves as a renewable solvent for processing lignocellulosic biomass [133-135]. Despite its potential, the commercial use of γ-GVL remains limited due to high production costs. Research on the direct conversion of furfural to γ-GVL primarily focuses on sequential transfer-hydrogenation and hydrolysis reactions catalysed by Lewis and Brønsted acid sites. Notably, Roman-Leshkov et al. [136] achieved this conversion using a combination of Zr-Beta zeolite and Al-MFI catalysts with a secondary alcohol as the hydrogen donor. Tang et al. [137] developed an Hf-Al-USY catalyst with balanced Brønsted and Lewis acidic sites effectively converting furfural to γ-GVL using formic acid. Li et al. [138] utilized a combination of zeolites and Zr-P/SAPO-34 with isopropyl alcohol as the hydrogen donor for this transformation. Winoto *et al*. [139] demonstrated direct conversion with an HPW/Zr-Beta catalyst. Tan *et al*. [140] explored the use of a complex polymeric catalyst, Hf-Organophosphate polymers-p-toluenesulfonic acid, for this process. The presence of Lewis and Brønsted acidic sites as well as surface area and pore volume were key factors in promoting the conversion. Gao et al. [141] used an MCM-41@ZrO_2-Fe_3O_4 magnetic catalyst, where MCM-41 facilitated hydrolysis and ZrO_2 enabled transfer hydrogenation with secondary alcohol. Srinivasa et al. [142] investigated tungstophosphoric acid-Zr-SBA-15, noting its high proportion of Lewis acidic sites due to W addition and strong interaction between the hydrogen donor alcohol and Zr active sites. He et al. [143] explored the Zr-KIT-5 (10) system for the direct conversion of furfural to γ-GVL. García et al. [144] studied the conversion using Zr/Silica spheres, achieving comparable efficiency to zeolite Y-based catalysts.

1.1.4.3. Cellulose-derived platform molecules and their valorisation over heterogeneous catalysts

Glucose

Commercial production of glucose, a starch sugar is typically achieved through enzymatic hydrolysis using glucose amylase or more commonly through acidic hydrolysis [145]. Starch sources include crops such as maize, rice, wheat, cassava, potato, barley, sweet potato, corn husks and sago which are utilized globally [145,146]. Additionally, glucose can be obtained from sucrose which is known as invert sugar comprising an equal mixture of glucose and fructose. Although theoretically possible, the direct acidic hydrolysis of cellulose to glucose is not yet

commercially viable [147]. Glucose is a key starting material for producing valuable derivatives including polyols and furans, as illustrated in Figure 1.15. Gluconic and glucaric acids, oxidation products of glucose have numerous applications in the food and chemical industries [148-151]. D-Glucaric acid, for instance is produced by oxidizing D-glucose or starch with nitric acid [152]. Certain anaerobic bacteria such as those from the genera Clostridium or Acetobacterium, can convert sugars directly to acetic acid without producing ethanol as an intermediate [153]. Pyrolysis of glucose followed by oxidation yields glycolic acid, a critical raw material used in cosmetics, textiles and as an intermediate in organic synthesis. Ethylene glycol, a bulk chemical essential as an automotive coolant and polyester fibre precursor can also be derived from glucose through hydrolytic hydrogenation [154]. Lactic acid, another important carboxylic acid is industrially produced via bacterial fermentation of carbohydrates like sugar and starch [155]. It serves as a monomer for biodegradable polyesters and as a building block for pharmaceuticals, plasticizers and various additives [156,157]. Additionally, glucose undergoes acid hydrolysis to produce levulinic acid.

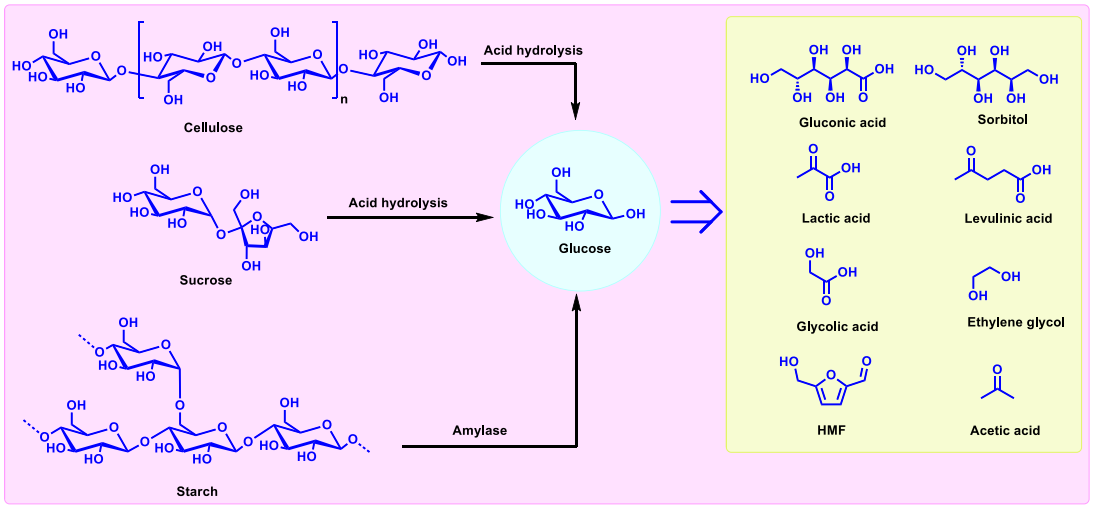

Figure 1.15. Glucose production and as a platform chemical

5-Hydroxymethylfurfural (HMF)

According to the DOE's list of top value-added chemicals from biomass, 5-(Hydroxymethyl)furfural (HMF) is a leading building-block chemical [30]. HMF naturally occurs in honey, vegetables, coffee and other beverages though in small quantities [158]. Its current market price ranges from $500 to $1500 per kilogram, which is about three times higher than that of many fossil-based bulk chemicals. The most effective method for HMF production involves a multistep acid-catalyzed

dehydration of hexoses with a preference for fructose, glucose and cellulose from the C_6 fraction of biomass. The process typically starts with the isomerization of glucose to fructose using enzymes, Lewis acids or base catalysts (Figure 1.16) followed by the dehydration of fructose to HMF.

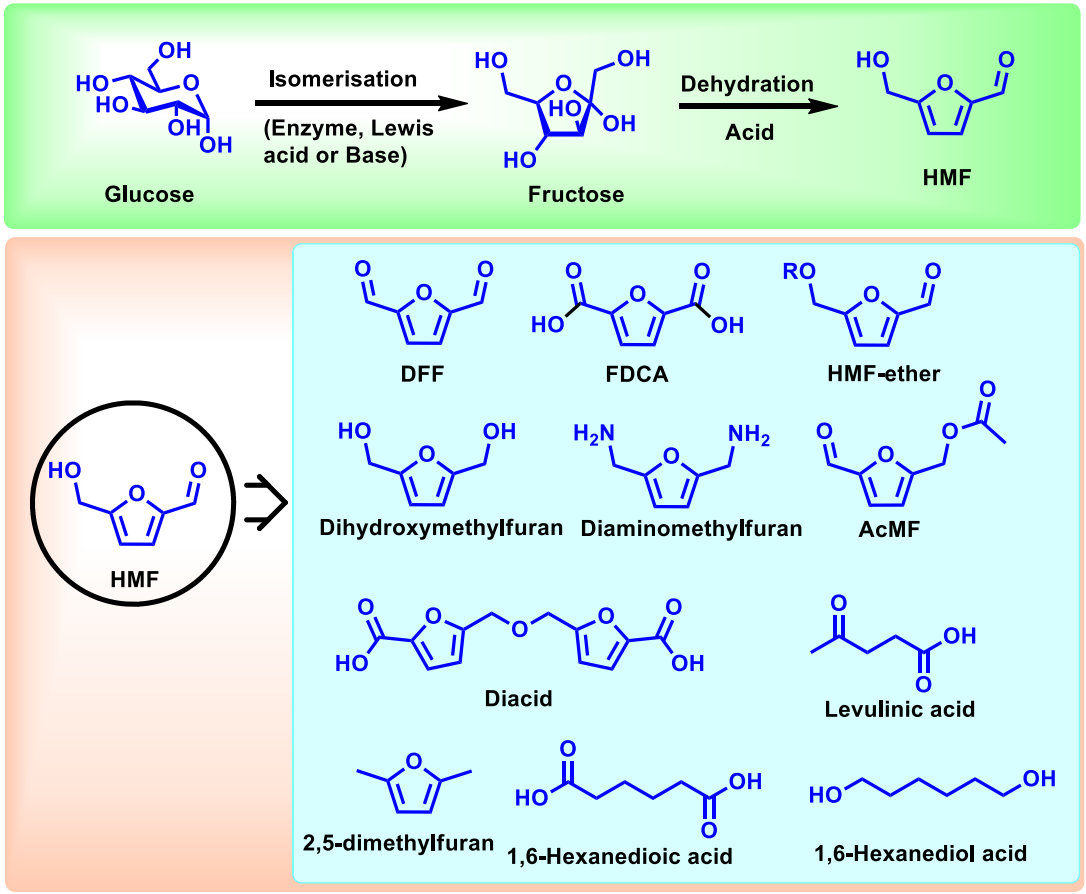

Figure 1.16. HMF production and as a platform chemical

Various methods have been explored for HMF production from mono- and polysaccharides including pre-treated biomass, using homogeneous mineral acids, Brønsted acidic ionic liquids (ILs), Lewis acidic metal halides and recyclable heterogeneous catalysts in both pure organic and aqueous solvents [159-162]. The choice of solvent is crucial, as it affects the yield, purity and ease of separation of HMF impacting the economic and environmental viability of the process. Despite advancements in HMF production chemistry and separation technologies, most research over the past decade has focused on maximizing carbohydrate conversions in high-boiling-point organic solvents such as dimethylsulfoxide (DMSO), N,N-dimethylformamide (DMF), N,N-dimethylacetamide (DMA), methyl isobutyl ketone

(MIBK) and ILs. DMSO, in particular, has been extensively studied with various catalytic systems for converting mono-, di-, polysaccharides and cellulose into HMF. HMF's unique chemical structure featuring aldehyde groups at the C-2 position and a hydroxymethyl group at the C-5 position, has spurred significant interest in its use as a starting material for synthesizing commodity chemicals. Often referred to as a "sleeping giant," HMF bridges carbohydrate chemistry with mineral oil-based industrial chemistry [163]. It is already utilized in resin production [164] but its potential as an intermediate for creating a range of 2,5-disubstituted furan derivatives remains largely untapped. These derivatives can be used to produce fine chemicals, pharmaceuticals, polymers (including polyesters, polyamides and polyurethanes) solvents and liquid transportation fuels [69,165,166]. HMF can be transformed into a variety of valuable compounds through different reactions (Figure 1.16). Oxidation yields 5-hydroxymethyl furoic acid, 2,5-furandicarboxaldehyde and FDCA. Hydrogenation produces hydroxymethyltetrahydrofurfural, 2,5-dihydroxymethyl furan, and 2,5-dihydroxymethyl tetrahydrofuran. Aldol condensation generates C_7-C_{15} liquid alkanes while hydrolysis results in levulinic and formic acids. Despite its broad application potential, HMF is not yet produced on an industrial scale due to high production costs [167-169].

HMF to fuels and chemicals

Through C-C bond forming reaction of HMF

Like furfural, HMF also possesses an aldehyde functionality which serves as a reactive site for C-C bond formation reactions aimed at extending the carbon chain. Notably, HMF undergoes C-C bond forming reactions such as Aldol condensation [160], Furoin condensation [161, 162], Hydroxyalkyaltion-alkylation [102,109], coupling with isoprene [116] and Baylis–Hillman reaction [170] were reported in the literature and briefly elaborated below and represented in Figure 1.17.

Aldol condensation: Aldol condensation is a pivotal C-C bond formation reaction for HMF, crucial for synthesizing fuel precursors, fine chemicals, plasticizers, and fragrances [160]. In this regard, various heterogeneous solid base catalysts have been investigated for the Aldol condensation of HMF with aldehydes and ketones [160].

Hydroxyalkyaltion-alkylation of HMF: In 2014, Balakrishnan et al. reported the use of a sulfonic acid-functionalized solid acid catalyst for the HAA of 2-methylfuran with HMF producing polyfuranic compounds [109]. That same year, the same authors also

demonstrated a hydrodeoxygenation method for synthesizing similar polyfuranic compounds [102].

Furoin condensation: The Furoin condensation of the HMF successfully achieved by coupling two molecules of HMF using organocatalyst followed by hydrodeoxygenation to get linear C_{10}–C_{12} alkanes with a narrow distribution of alkanes [161-162].

Coupling with isoprene: HMF which contains both aldehyde and alcohol functionalities was reacted with isoprene in the presence of a ruthenium catalyst, resulting in a double coupling product isolated with a yield of 48% [116]. In 2010, Huber et al. conducted a Baylis–Hillman reaction between HMF and methyl acrylate using aqueous NMe_3 and DABCO, achieving a high yield of the coupling product [91]. Later, in 2015, Y. Queneau et al. investigated various bio-derived solvents for this reaction, also using DABCO as a catalyst [170].

In the C-C bond forming reactions of HMF, majority of heterogeneous catalysts development was focused on Aldol condensation and Hydroxyalkyaltion-alkylation reactions. However, it is surprising to know that heterogeneous catalysts were not been explored for Furoin condensation, Baylis–Hillman reaction and coupling with isoprene. It is an open opportunity for chemist and technologist to develop heterogeneous catalysts for these reactions.

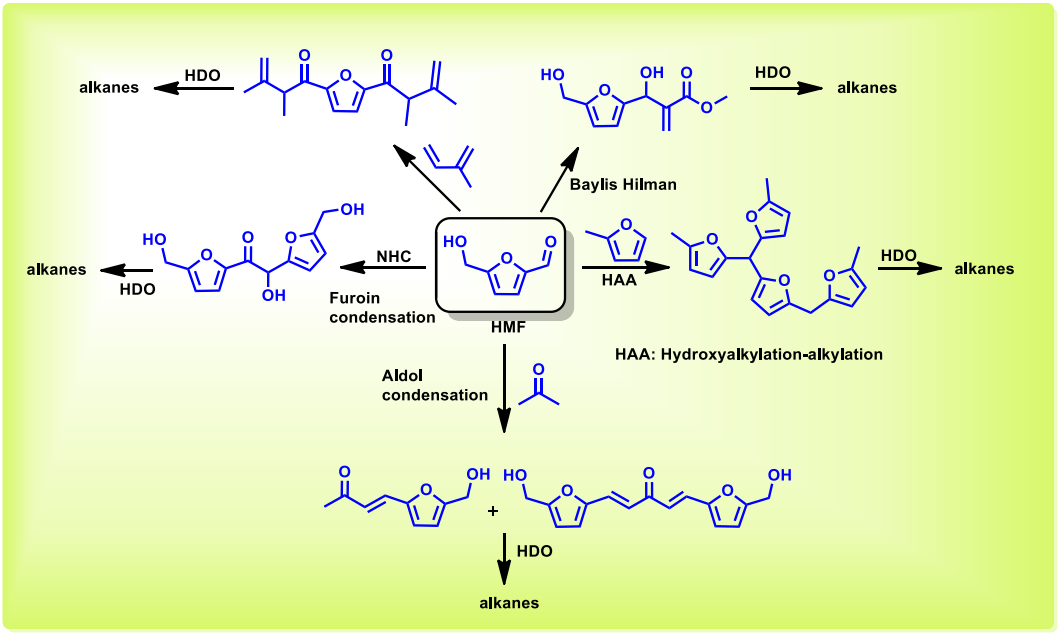

Figure 1.17. C-C bond forming reaction options for HMF

Through hydrogenation and hydrogenolysis HMF

Hydrogenation of HMF produces important polymer precursors and fuel components which is elaborated below (Figure 1.18).

2,5-Bis(hydroxymethyl)furan (BHMF) is utilized as a monomer for producing heat-insulating materials [171], resins and crown ethers [172]. Additionally, BHMF serves as a valuable diol for synthesizing shape-memory and self-healing polymers as well as for producing 1,6-hexanediol, an important polymer precursor [173]. Commercially, BHMF is derived from HMF through the Cannizzaro reaction [174]. However, this reaction also produces 5-hydroxymethylfuranoic acid (HMFA) in equimolar amounts, complicating subsequent separation processes. To address this, selective hydrogenation of HMF to BHMF while minimizing HMFA formation is necessary. Researchers have explored noble metal catalysts such as Pt/MCM-41 [175] and Ru/Co_3O_4 [176], as well as non-noble metal catalysts like Cu–ZnO [177], $ZrO(OH)_2$ [178], and Fe_3O_4@HAP [179] with either external hydrogen or transfer hydrogenation. However, the selective production of BHMF via a direct or integrated approach from carbohydrates using heterogeneous catalysts remains underexplored.

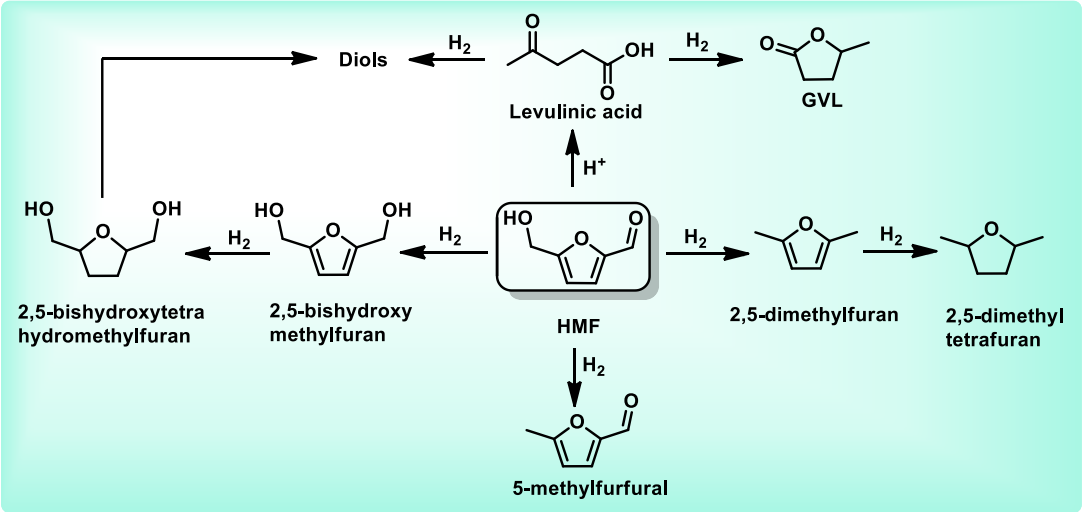

Figure 1.18. Hydrogenation and hydrogenolysis of furfural

2,5-Dimethylfuran (DMF) has garnered significant interest due to its advantageous properties including an almost ideal boiling point (92–94°C), high energy density (30 kJ cm^{-3}) and an impressive research octane number (RON = 119) [180]. Additionally, DMF is immiscible with water and blends more easily with gasoline compared to ethanol. The primary method for producing DMF involves the hydrogenolysis of 5-

(hydroxymethyl)furfural using precious metal-based catalysts such as Cu/Fe nanomorph [181], CuRu/C [180,182], Ru/Co_3O_4 [183], Ru/CoFe-LDO [184], Ru–Na–Y [185], Pt–Co/C [186], and Pd/C [187]. Researchers have also explored the direct conversion of fructose to DMF using various acid and metal catalyst combinations, including Amberlyst-15 + Ru–Sn/ZnO [188], $ZnCl_2$ + Pd/C [189], 'HY + Cu/ZnO/Al_2O_3 [190], and '$AlCl_3$/H_2SO_4/H_3PO_4 + Ru/C' [191]. Notably, Insyani et al. [192] achieved the direct conversion of fructose and glucose to DMF using a bifunctional catalyst, Pd/UiO-66@SGO.

Through oxidation of HMF

2,5-Diformyl furan (DFF): The selective oxidation of the hydroxyl group in HMF to produce 2,5-diformylfuran (DFF) has garnered significant interest due to its versatile applications as a monomer for furan-based biopolymers and as an intermediate for pharmaceuticals, antifungal agents, and ligands [193]. Traditional methods for synthesizing DFF from HMF have utilized classical oxidants such as $BaMnO_4$ [194], pyridinium chlorochromate (PCC) [195], NaOCl [196], and 2,2,6,6-tetramethylpiperidine-1-oxide (TEMPO), as well as free radicals with co-oxidants and metal/bromide systems (Co/Mn/Br) [197]. Recent research has focused on the oxidation of pure HMF using molecular oxygen with both homogeneous and heterogeneous metal catalysts. Various homogeneous catalysts containing metals such as vanadium [168,198-200], cobalt [201], ruthenium [202], copper [203], manganese [204] and molybdenum [205] have been explored. While these catalysts achieve relatively high yields of DFF, they are often expensive, toxic and challenging to remove [206]. Consequently, several heterogeneous recyclable catalysts have been developed to address these issues [207]. Despite these advancements, the production of DFF from pure HMF remains an economically and energy-intensive process.

Furan dicarboxylic acid (FDCA): Furan dicarboxylic acid (FDCA) is listed as one of the top-12 value-added chemicals from biomass by the DOE [50]. The most important application of FDCA is that, it can serve as a polymer building block for the production of biobased polymers such as polyamides, polyesters and polyurethanes [208,209]. FDCA can be viewed to replace the petrochemical-derived terephthalic acid for the synthesis of biobased polyesters. Polyethylene furoate is the esterification product of ethane-1,2-diol and FDCA demonstrates similar properties to the petroleum-based polyethylene terephthalate. FDCA has also been found to be useful in organic synthesis, pharmacology and metal organic framework materials [210, 211]. FDCA

can be formed by catalytic oxidation of HMF and oxidative-dehydration of carbohydrates. FDCA is produced through the oxidation of HMF which has been reported for a number noble and non-noble metal based heterogeneous catalyst systems such as supported gold [125, 212-215], supported palladium [215,216] and supported platinum [126, 215, 217]. Parate et al. used *Klebsiella oxytoca* NCIM 2694 bacteria strain for biocatalytic oxidation of 5-HMF to FDCA [218]. The below presented Figure 1.19 describes some of the potential utility of FDCA.

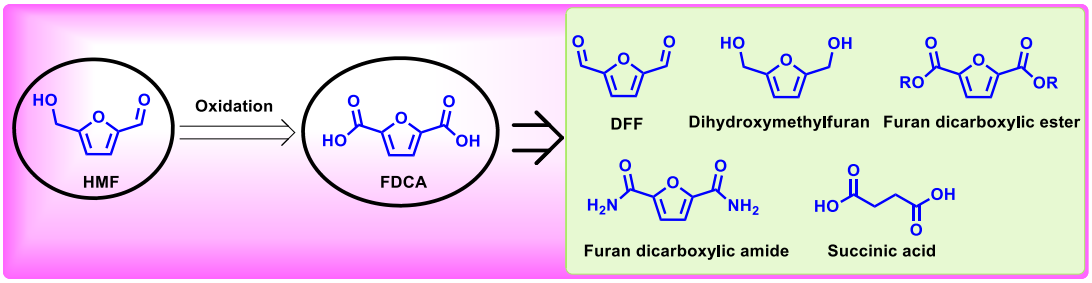

Figure 1.19. 2,5-Furandicarboxylic acid (FDCA) production and as a platform chemical.

Through etherification of HMF

Among the various derivatives of 5-(alkoxymethyl)furfural, 5-(ethoxymethyl)furfural (EMF) has garnered significant attention due to its excellent chemical properties. EMF boasts a high energy density of 8.7 kWh/L, comparable to gasoline (8.8 kWh/L) and nearly as high as diesel (9.7 kWh/L) and substantially higher than ethanol (6.1 kWh/L) [219]. When blended with commercial diesel and tested in engines, EMF demonstrated positive results, significantly reducing dust (fine particulates) and lowering SOx emissions [220]. Furthermore, EMF is widely used as a flavour and aroma additive in wines and beers due to its low toxicity [221]. Interestingly, ethers of HMF derived from branched alcohols such as 5-(tert-butoxymethyl)furfural (t-BMF), exhibit superior blending properties compared to those derived from linear alcohols. For instance, up to 40 vol.% of t-BMF remains fully soluble in commercial diesel without issues of mixing or flocculation. The preparation of t-BMF involves reacting HMF with tert-butanol in the presence of montmorillonite K10 and zeolite HY [222].

A significant challenge with 5-(alkoxymethyl)furfural is its aldehyde functionality which compromises the molecule's stability. Therefore, it is advantageous to first hydrogenate the aldehyde group to an alcohol [223] and then perform etherification to produce the more stable 2,5-bis(alkoxymethyl)furan [224]. The two ether linkages

in 2,5-bis(alkoxymethyl)furan enhance its miscibility in commercial diesel and lower its crystallization temperature compared to 5-(alkoxymethyl)furfural [225]. The synthesis of 2,5-bis(alkoxymethyl)furan from HMF has been explored by several researchers. For instance, in 2014, Jae et al. [226] employed a combination of Pt (a noble metal) and acid catalysts with external H_2. However, the high cost and non-renewable nature of external H_2, along with challenges in its safe transportation, storage and handling, limit its widespread use. Other studies have utilized zeolite [227,228] and combinations of Zr-Mont + $ZrO(OH)_2$ [229] catalysts for producing 2,5-bis(alkoxymethyl)furan from HMF through transfer hydrogenation and etherification using secondary alcohols.

Through esterification of HMF

One of the ester derivatives of HMF, 5-(acetoxymethyl)furfural (AcMF), is a versatile compound with a range of applications, including as a fuel blending agent, additive for bulk chemicals, monomer for polymer synthesis, natural surfactant and fungicide [230-236]. Additionally, AcMF serves as a key building block in the development of therapeutic agents for osteoporosis and inhibitors of protein tyrosine phosphatase 1B (PTP1B) [237]. Notably, AcMF has an energy content of approximately 8.7 kWh/L, comparable to gasoline (8.8 kWh/L) and higher than ethanol (6.1 kWh/L) [232,233], making it a promising candidate for use as a fuel blending agent. Furthermore, AcMF is more stable than HMF, offering advantages such as hydrophobicity, reduced reactivity and easier isolation from aqueous mixtures. These properties potentially make AcMF more useful than HMF. Unlike HMF, which exhibits weak cytotoxicity and mutagenicity, AcMF is neither cytotoxic nor mutagenic [238].

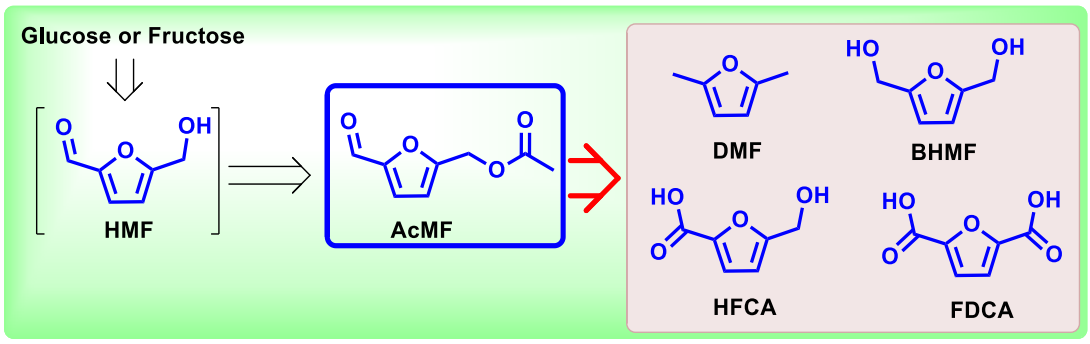

Figure 1.20. Conversion of 5-(acetoxymethyl)furfural (AcMF) into useful furans. BHMF: 2,5-bis(hydroxymethyl)furan; FDCA: 2,5-furandicarboxylic acid; HFCA: 5-(hydroxymethyl)furan-2-carboxylic acid; DMF: 2,5-dimethylfuran.

AcMF can be synthesized from 5-(chloromethyl)furfural (CMF) through a substitution reaction with acetic acid or alkyl ammonium acetate salts in the presence of a weak inorganic or organic base [239]. Alternatively, AcMF can be produced from HMF by reacting it with acetic acid in the presence of a weak inorganic base or using a lipase enzyme [240]. Several patents describe methods for direct preparation of AcMF from carbohydrates using acetic acid or ionic liquids [241, 242]. AcMF can be further converted into valuable building blocks such as FDCA, BHMF, and HFCA [238], or into liquid fuel 2,5-dimethylfuran [231] (Figure 1.20).

1.1.4.4. Lignin-derived platform molecules and their valorisation over heterogeneous catalysts

Despite advancements in engineered lignin structures and tailored pre-treatment methods, some lignin fractions from a bio-refinery may not be suitable for material applications but can still be valuable for conversion into fuels and chemicals (Figure 1.21).

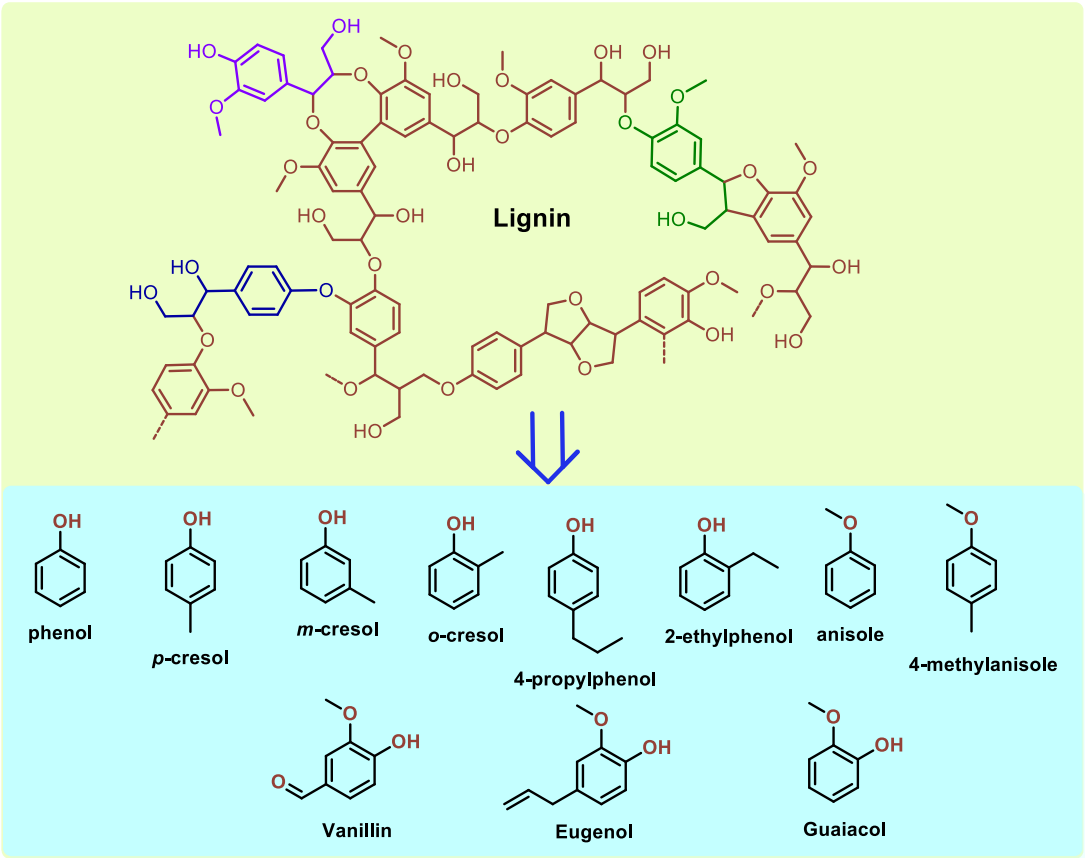

Figure 1.21. Lignin derived phenolics

Understanding and manipulating lignin from its role in plant cell walls to its extraction and processing into value-added products is crucial. This approach not only enhances our knowledge of complex biological structures but also ensures that the valorization of lignin does not come at the expense of effectively utilizing other biopolymers, such as cellulose and hemicellulose.

Guaiacol

Guaiacol is a naturally occurring yellowish aromatic oil extracted from guaiacum or wood creosote. It serves as a precursor to various flavourings including eugenol [243] and vanillin [244]. In the chemical industry, guaiacol is a key raw material for synthesizing a range of value-added chemicals, such as spices (vanillin, veratraldehyde, and eugenol) [245, 246], pesticides [247], and drugs (eugenol, potassium guaiacolsulfonate, guaifenesin, berberine, and isoprenaline) [248-250], as well as plant growth regulators (e.g., 2-methoxy-5-nitrophenol sodium salt). The annual demand for guaifenesin, vanillin and eugenol is substantial at 37,000, 16,000, and 7,300 tons per year, respectively [251-254]. This high demand underscores the importance of guaiacol. However, current guaiacol production relies predominantly on the costly methylation of catechol, a downstream chemical derived from fossil resources using reagents such as methanol and methyl chloride [255]. Shen *et al*. [256] demonstrated successful selective production of guaiacol from lignin using a homogeneous $La(OTf)_3$ catalyst. However, achieving selective guaiacol production from lignin using heterogeneous catalysts remains a challenging task.

The conversion chemistry of guaiacol as a platform molecule is illustrated in Figure 1.22. Research indicates that the large pore diameter and high surface area of catalysts significantly enhance catechol selectivity [257-259]. Zhang et al. [260] demonstrated that varying the Si/Al ratio in ZSM-5 catalysts affects catechol yield, with an Si/Al ratio of 25 yielding the highest catechol production. Similarly, Nimmanwudipong et al. [261] found that guaiacol conversion over HY Zeolite produced more catechol compared to Pt/γ-Al_2O_3.

Several studies have focused on the partial or complete deoxygenation of guaiacol to produce chemicals such as phenol, cyclohexane, anisole and benzene [262-264]. Various heterogeneous catalyst systems have been reported for the full deoxygenation of guaiacol to benzene with high selectivity, including Ni-Al_2O_3-based catalysts [262], β-Mo_2C [264], and MoWC [265].

Vanillin was first synthesized from eugenol, a compound found in clove oil in 1875, less than 20 years after its identification and isolation. For decades, vanillin was commercially produced from eugenol. However, starting in the 1920s, production shifted to using lignin-containing “brown liquor,” a byproduct of the sulphite process for making wood pulp. Despite its use of waste materials, this lignin-based process fell out of favour due to environmental concerns. Today, most vanillin is produced from the petrochemical raw material guaiacol. Several methods exist for synthesizing vanillin from guaiacol. For instance, Corbet et al. [266] achieved selective formylation of guaiacol at the para position to produce vanillin though they employed homogeneous catalysts for this process. Ren et al. [267] used a Reimer–Tiemann reaction involving guaiacol and chloroform in the presence of zeolites, resulting in vanillin as the major product with high selectivity.

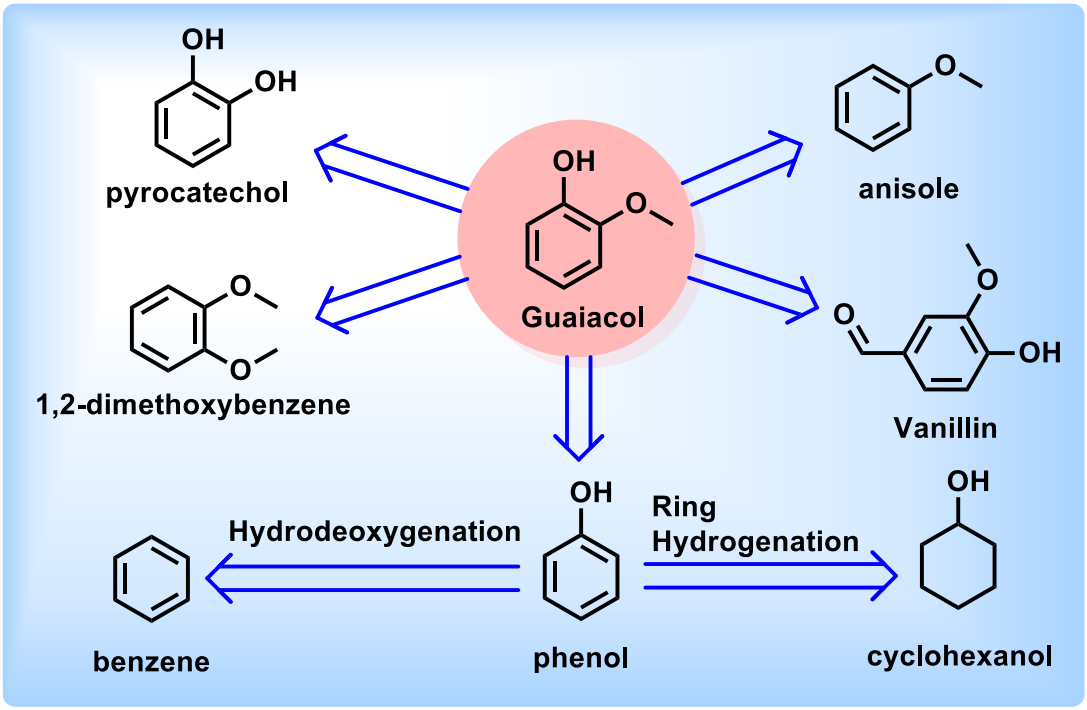

Figure 1.22. Guaiacol as a platform molecule

Vanillin

Vanillin is the most widely available pure monoaromatic phenol produced at an industrial scale from lignin [34]. Approximately 20,000 tons of vanillin are produced annually with around 15% (about 3,000 tons) derived from lignin [268, 269]. Vanillin holds significant potential as a renewable aromatic building block serving as a

precursor for various compounds through hydrogenation, oxidation, reductive amination and hydrogenolysis reactions (Figure 1.23).

The conversion of vanillin presents challenges due to numerous side reactions that yield various hydrogenated products. Among these products, vanillyl alcohol is particularly valuable due to its high commercial worth and extensive use in the pharmaceutical industry [270]. Despite its importance, there are limited studies focused on the hydrogenation of vanillin to vanillyl alcohol, primarily due to the complexity of managing these side reactions.

2-Methoxy-4-methylphenol (MMP) is a key intermediate used in medicine and perfume typically produced via the hydrodeoxygenation (HDO) of vanillin. Nie et al. [271] reported that with N-doped carbon-supported Pd as the catalyst and formic acid as the hydrogen donor, both the conversion of vanillin and the selectivity for MMP exceeded 90%. Nickel-based amorphous alloy catalysts have gained considerable attention for their cost-effectiveness, straightforward preparation and outstanding performance in the HDO reaction of vanillin [272-274].

Vanillic acid obtained through the selective oxidation of vanillin, is valuable for its diverse chemical, biological and medicinal applications as well as its use in the food and fragrance industries [275-277]. Rautiainen *et al*. [278] demonstrated the selective oxidation of vanillin to vanillic acid using gold nanoparticle catalysts.

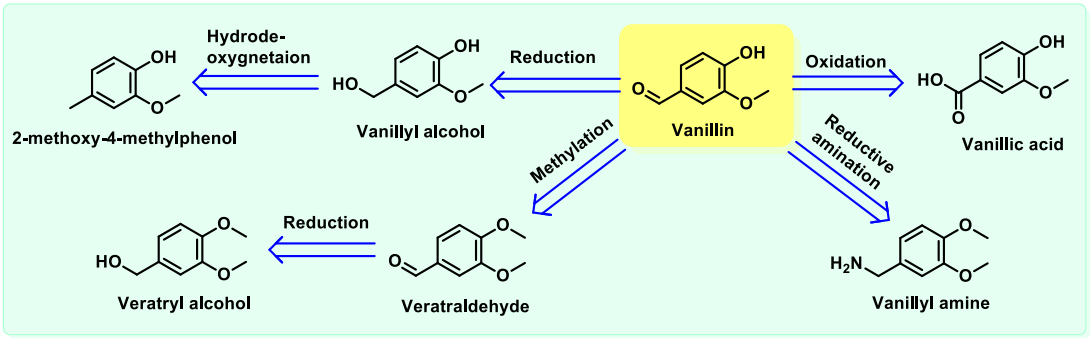

Figure 1.23. Vanillin as a platform molecule

1.2. Catalysis

1.2.1. Catalysis Background

The concept of “catalysis” was first introduced by chemist Elizabeth Fulhame in her 1794 book where she documented her oxidation-reduction experiments. In 1811, Russian chemist Gottlieb Kirchhoff conducted the first study of a chemical reaction in organic chemistry that utilized a catalyst. Later, in 1835 J. J. Berzelius defined the term “catalyst” as a chemical substance that increases the rate of a chemical reaction without being consumed in the process. Catalysts can exist in solid, liquid or gaseous forms. Key characteristics of catalysts include:

- A catalyst does not initiate a chemical reaction.
- A catalyst is not consumed during the reaction.
- Catalysts interact with reactants to form intermediates, facilitating the production of the final product and can be regenerated after the process.

The subject catalysis has been extensively studied and broadly divided into three types such as “Bio, Homogeneous and Heterogeneous Catalysis” which are briefly discussed below.

1.2.1.1. Biocatalysis

Biocatalysts, which are essentially enzymes or complex naturally occurring protein molecules catalysed reactions within living cells. Proteins are fundamentally composed of amino acids linked by peptide bonds which define an enzyme’s structure. Typically, a cleft in the protein's morphology surrounded by an array of amino acids serves as the enzyme's active site. Enzymes utilize four types of interactions to bind with their substrates: electrostatic interactions, hydrogen bonding, Van der Waals forces and hydrophobic interactions [279,280]. The specific arrangement of amino acids in the active site makes enzymes highly efficient and selective biocatalysts. Biocatalysts are commercially significant, particularly in the pharmaceutical, flavouring/fragrance and food industries [280]. Enzymes can function in both aqueous and organic solvents and some resin-bound enzymes can be recycled multiple times without losing activity. However, enzymes are often heat sensitive; excessive heating can denature the weak bonds that maintain their functional shape, thus destroying the enzyme’s active site [280,281].

1.2.1.2. Homogeneous Catalysis

When the catalyst and reactants are in the same state of matter, it is referred to as homogeneous catalysis. The primary advantage of homogeneous catalysis is that all of the catalyst's active sites are accessible to the reactant, resulting in greater activity. However, homogeneous catalysts have several drawbacks including difficulty in separation from the reaction mixture, environmental concerns, safety issues and high costs. As a result, some homogeneous catalytic processes may not be commercially viable [282].

1.2.1.3. Heterogeneous Catalysis

In heterogeneous catalysis, the reacting substances and the catalyst are in different states of matter. The catalytic reaction occurs at the interface between the reaction mixture and the catalyst surface (either outer or inner) where reactants are temporarily adsorbed. Transient bonds connect the reactant molecules to the catalyst surface at the active site where the reaction takes place. The product then desorbs from the catalyst surface due to the weak nature of these transient bonds [279]. Heterogeneous catalysts have extensive commercial applications including the production of inorganic chemicals, petrochemically-derived compounds and novel 'green' technologies [283,284] such as fuel cells [285,286] and biotechnology [287-289]. A comparison of heterogeneous and homogeneous catalysis is provided in Table 1.2.

Table 1.2. Comparison of Heterogeneous and Homogeneous Catalysis

Homogeneous Catalysis	**Heterogeneous Catalysis**
Same phase as the reaction medium	Different phase as the reaction medium
Catalyst separation is difficult	Easy separation of the catalyst
Expensive and difficult to recycle	Cost effective as it can be readily regenerated and recycled
High selectivity	Low selectivity
Works under low reaction temperature	Works under high reaction temperature
Easy modification of the catalyst	Relatively difficult modification of the catalyst
Short life and requires extensive purification step	Long life and less purification step
Environmentally non-friendly	Environmentally Friendly
Some are unsafe to handle therefore special care required	Safe to handle
Some are unstable at ambient conditions	Stable at ambient as well as severe conditions

Mechanistic Aspects of Heterogeneous Catalysis

In heterogeneous catalysis, the reactants are usually gases or liquids, while the catalyst is often solid. Because the reaction occurs at the surface of the solid catalyst this process is also known as surface catalysis. These catalysts offer a large surface area for interactions. To understand the mechanistic action of the catalyst, it's important to know that the process involves several steps. Initially, the reactants must diffuse from the fluid phase to the solid surface. This is followed by three key steps: adsorption, surface reaction, and desorption. Figure 1.24 illustrates the hydrogenation of ethene on a solid catalyst, providing a schematic representation of the general mechanism of heterogeneous catalytic reactions.

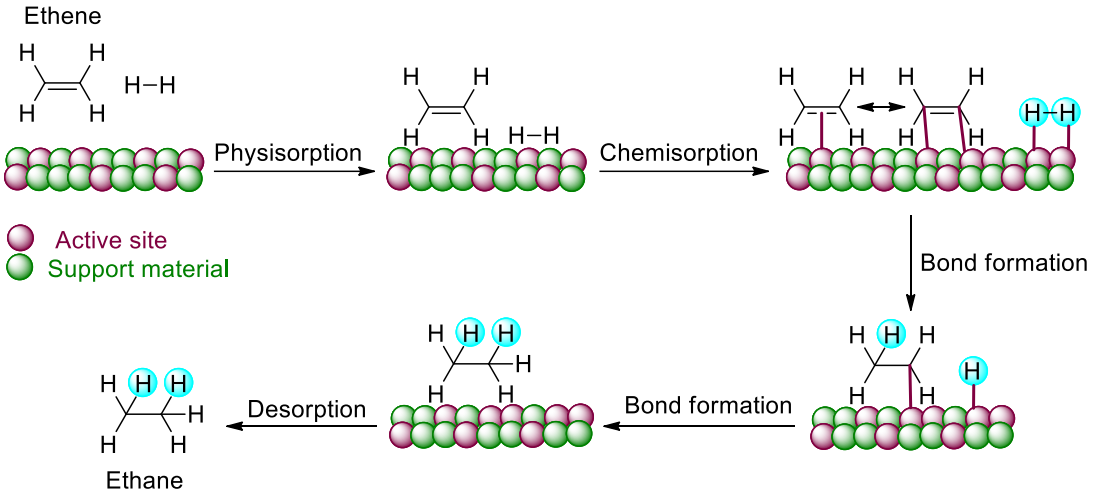

Figure 1.24. Mechanism for the hydrogenation of ethene on a solid catalyst

In the porous heterogeneous catalysis, the reaction takes place at the surface inside the pores of the catalysts. Overall process mechanism is almost similar to the surface catalysis. The reactant is first transported with fluid phase into the pores and then it is followed by three consecutive steps such as adsorption, surface reaction and desorption. Reaction progress in the porous heterogeneous catalysis is represented in Figure 1.25. Zeolites, MCM-41, montmorillonite etc, are some examples of solid catalysts having porous architecture.

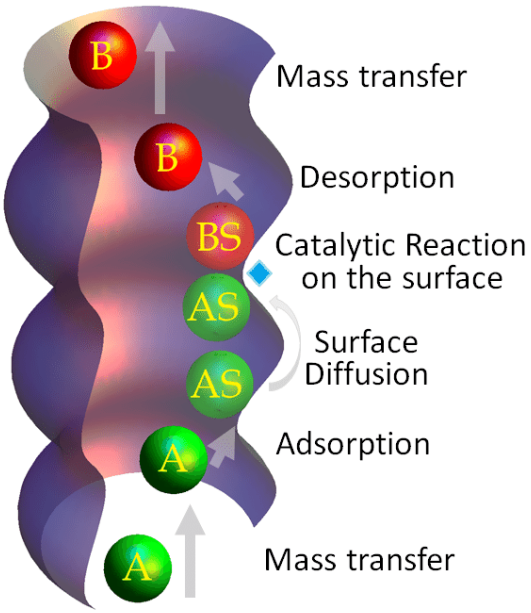

Figure 1.25. Different steps of the heterogeneous catalysis inside the pore. Adopted from ref. [290]

In general, heterogeneous catalysts can be broadly divided into inorganic and organic solids which are briefly discussed below.

Inorganic Solid Catalysts

The inorganic solid catalyst is often a conjunction of an active phase and support material. Active phase is usually a metal nanoparticle, a metal complex, acidic or basic site. Support materials are usually metal oxide(s), aluminosilicates or carbon. Support materials are commonly used to stabilize active phase. In order to understand more about catalyst supports it is briefly discussed below.

Supports for Inorganic solid catalysts

The primary purpose of using a support material is to achieve an optimal distribution of the catalytically active component often precious or non-precious metals by providing a larger active surface area. Additionally, the support material stabilizes the active component and protects it from particle growth [291]. The characteristics of support materials such as reactivity, surface area and pore size distribution significantly impact the overall activity of solid catalysts. For metal-based solid catalysts the support material is crucial for controlling the metal particle size, charge, and morphology which in turn generates specific active sites at the metal-support boundary [292]. This can lead to variations in the catalytic properties of the metal nanoparticles. Therefore, understanding the essential physicochemical properties

and characteristics of a support material is vital. These properties and characteristics are detailed in Tables 1.3 and 1.4.

Table 1.3. Physical and chemical properties of support materials [293]

Chemical properties	**Physical properties**
Stable under reaction and regeneration conditions	Optimised bulk density
High specific activity/selectivity	High active surface area
Unreactive to unwanted reactions	Mechanical strength
Protects the catalyst from sintering	Optimises catalyst porosity
Minimises catalytic poisoning	Optimises metal crystal and particle size

Table 1.4. List of supports and their characteristics [294]

Support	**Properties**	**General Applications**
Carbon	surface area up to 1000 m^2g^{-1} unstable in oxide environment	hydrogenation
Zeolites	Highly defined pore system shape selective	bifunctional catalysts
Silica Alumina	surface area up to 800 m^2g^{-1} medium strong acid sites	dehydrogenation; bifunctional catalysts
Al_2O_3	surface area up to 400 m^2g^{-1} thermally stable	catalyst for three-way converters; steam reforming
TiO_2	surface area up to 150 m^2g^{-1} limited thermal stability	selective catalytic reduction
MgO	surface area up to 200 m^2g^{-1}	steam reforming

A variety of catalyst supports are available with the most commonly used being alumina, silica, titania, magnesia, cupric oxide, nickel oxide, zeolites, silica-alumina and various carbon materials such as charcoal and activated carbon [15]. Support materials can be synthesized in different morphologies including spheres, granules, extrudates, cylinders and powders. The choice of support morphology depends on the type of reaction and reactor being used aiming for optimal performance and cost efficiency [16]. The primary catalyst metal phase should be evenly dispersed over the support to ensure stability of the metal nanoparticles [295,296]. Porous support materials facilitate high dispersion of nanoparticles and enhance electron transfer leading to improved catalytic activity [297-299]. However, the support material can also exert structural effects known as textural and active phase-linked effects [299]. Thus, an ideal support material should have specific characteristics such as surface area, porosity, dispersion, activity and selectivity [297,300]. The pore size and morphology of the support material are critical for enhancing the performance and stability of heterogeneous catalysts [301,302].

Immobilized organic solid catalysts

Preparing immobilized organic solid catalysts typically requires additional effort which increases both the complexity of synthesis and the overall cost. However, its heterogeneous nature is more advantageous. Generally, catalytically active organic species are immobilized on either inorganic supports like mesoporous silica or onto polymer matrixes.

Immobilization methods of organic species

Various immobilization methods have been reported for attaching organic groups or metal complexes to solid supports [303]. Covalent attachment is the most commonly used strategy. Other techniques such as adsorption and entrapment are also frequently employed. The different methods for immobilizing organic species are briefly discussed below.

Covalent binding: The covalent binding method establishes a robust attachment between functional groups and solid supports. Compared to non-covalent interactions, catalysts prepared using this method can operate under a broader range of reaction conditions and reduce the risk of catalyst leaching. Different strategies have been developed for covalently attaching active species to solid surfaces, depending on the type of support. Silicas and organic polymers are the two most commonly used supports for catalyst immobilization [304]. For silica materials [305], two primary methods are widely discussed: post-grafting and co-condensation (direct synthesis). The post-grafting method (Figure 1.26) involves modifying the silica surface through silylation, a chemical reaction between surface silanols and alkoxy- or chloro-organosilanes. This method attaches organic groups or ligands with defined structures to the solid surface, minimizing potential side reactions and undesirable chemical species. In contrast, the co-condensation method prepares catalysts by sol-gel co-condensation of siloxanes and the desired organosiloxanes often with structure-directing agents. While the post-grafting method typically results in materials with more precisely defined structures the co-condensation method produces materials with a more uniform surface coverage of functional groups. For polymeric materials, similar strategies are employed: copolymerization of monomers, co-monomers, and crosslinking agents (direct synthesis) or the attachment of functional groups to anchor points in pre-formed resins (post-grafting).

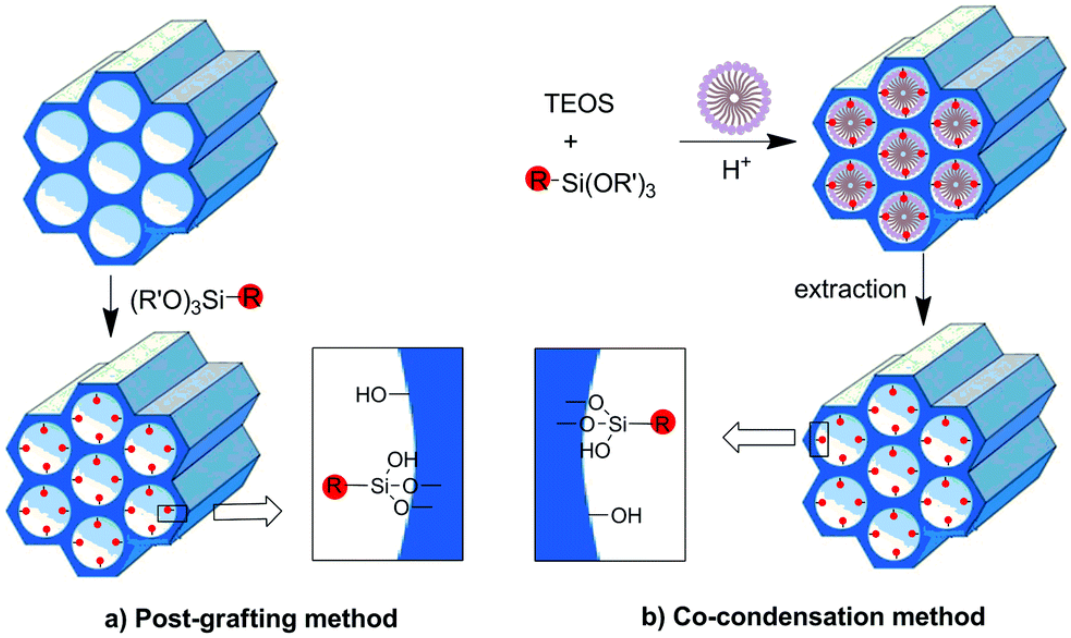

Figure 1.26. Post-grafting and co-condensation method in mesostructured silica materials. This image is adopted from [306]

Adsorption: Adsorption is another commonly used immobilization technique for catalytically active species. This method involves contacting preformed solids with organic species allowing the catalytic species to bond to the surface via physisorption, typically a weak interaction or chemisorption, which includes stronger interactions such as anionic or cationic bonding or metal-ligand interactions. The adsorption method is relatively easier than covalent binding as it does not require modifications to the organic ligands for immobilization. However, catalysts prepared by adsorption are often limited to specific reaction solvents and temperatures, and the catalytic species may partially leach into the reaction solution.

Entrapment: A distinctive example of the entrapment method is the "ship-in-a-bottle" technique. In this approach, catalysts are assembled and then entrapped within the cage-like pores of porous materials such as zeolites or MCM-41. The dimensions of the metal complexes or organic groups are typically larger than the pore openings to prevent the diffusion of active species out of the pores. However, this method often limits the diffusion of reactants and products and restricts interactions between substrates and active sites, which makes it less widely applicable.

Support materials for immobilization of organic solid catalysts

Silicas and polymeric matrices are commonly used as supports for organic catalyst immobilization. Using materials with defined and ordered structures is advantageous, as it ensures an even distribution of active sites and provides a uniform local environment around the active species. Materials with high surface areas and large pore sizes enhance the accessibility of these active sites. Additionally, support materials should be inert during the immobilization process and stable during catalytic reactions. Several commonly used materials for catalyst immobilization are discussed below.

Silica materials: Silica materials possess many of the desired properties for catalyst supports and have been extensively used in the preparation of immobilized catalysts. They offer excellent thermal stability can withstand a wide range of pressures and are generally stable in most chemical reactions. Silicas have high surface areas and a high density of surface silanols which readily react with organosilanes for catalyst immobilization. However, the disordered nature of amorphous silicas complicates the characterization of catalysts and the analysis of catalytic performance. Additionally, achieving a uniform distribution of active sites is challenging due to the wide range of pore sizes in amorphous silicas. The rapid development of mesoporous silicas in the 1990s introduced a series of ordered silica materials with unprecedented control over porosity and extremely high surface areas. MCM (Mobile Crystalline Material) and SBA (Santa Barbara mesoporous silica material) are two prominent examples of mesoporous silicas.

Magnetic nanoparticles: Another interesting material worth mentioning is the magnetic nanoparticles [307,308]. When the nanoparticle size is below a critical value, which is typically around 10-20 nm and varies with the material, each nanoparticle becomes a single magnetic domain and shows super paramagnetic behaviour when the temperature is above the blocking temperature. In this case, every nanoparticle behaves like a giant paramagnetic atom with a quick response to the applied magnetic field. Another notable material is magnetic nanoparticles. When the size of these nanoparticles falls below a critical threshold, typically around 10-20 nm, each nanoparticle becomes a single magnetic domain and exhibits superparamagnetic behaviour above the blocking temperature. In this state, each nanoparticle acts like a giant paramagnetic atom, responding rapidly to an applied magnetic field with

negligible remanence (residual magnetization in the absence of a magnetic field) and coercivity (the field required to demagnetize the material).

These unique properties make magnetic nanoparticles highly attractive for various applications, including catalysis. The advantages of using magnetic nanoparticles for immobilized catalysts include:

- **Easy Recovery:** Catalysts can be recovered using an external magnetic field, providing a more energy-efficient separation method compared to traditional filtration and centrifugation.
- **High Surface Area:** Nanoparticles offer high external surface areas.
- **Reduced Internal Diffusion Issues:** Active sites are distributed on the outer surface, reducing problems with internal diffusion.
- **High Dispersion:** The small particle size ensures the nanoparticles are highly dispersible in solvents, facilitating easy access to active sites.

However, synthesizing pure metal nanoparticles can be challenging due to their tendency to oxidize in air. Various methods, including co-precipitation, thermal decomposition, microemulsion and hydrothermal synthesis are used to produce magnetic nanoparticles.

Inorganic-polymer composites: Inorganic-polymer composites represent a unique category of organic-inorganic hybrid materials. The polymer component can be used to attach active sites serve as the catalytic species or be part of the catalytic species. Various inorganic particles, such as metals (Au, Fe, Al), metal oxides (Al_2O_3, TiO_2), non-metal oxides (SiO_2), and other materials (SiC) [309], have been employed in these composites. Compared to purely polymeric resins, inorganic-polymer composites generally exhibit less dramatic shrinking or swelling in solvents due to the structural rigidity provided by the inorganic supports [310]. They also offer improved thermal and mechanical properties, better long-term stability, high catalyst loadings, and enhanced flexibility and accessibility of active sites [311-313]. Two common approaches for covalently functionalizing inorganic materials with polymers are "grafting from" and "grafting to" [314-316]. The "grafting from" method involves initially immobilizing initiators on the surface of the inorganic materials followed by surface-initiated polymerization. This method can produce composites with high grafting density but requires strict control over initiator concentrations and monomer amounts to achieve the desired materials. In contrast, the "grafting to" method involves

attaching pre-formed polymers to functional groups on the solid surface through appropriate chemical reactions. This method allows for the use of polymers with known molecular weights and structures simplifying the synthesis process. However, a key limitation is that the initially grafted polymers can sterically hinder the attachment of additional polymer chains, resulting in relatively low polymer loadings. Although the preparation, characterization, processing techniques and various properties of inorganic-polymer composites have been extensively studied their applications in catalysis are still limited [311-313, 317-326]. This suggests that further research is needed to develop catalysts supported by inorganic-polymer composites.

Illustrations of immobilized organic catalysts

Some common and representative examples of immobilized organic catalysts and their applications are briefly discussed below.

Immobilized Lewis base catalysts

4-(dimethylamino)-pyridine (DMAP) immobilized onto silica and polymer matrix (Figure 2.4) have been widely used as base catalyst in organic transformations such as condensation reactions, hydrolysis of esters [327,328] and esterification of carboxylic acids [329-332].

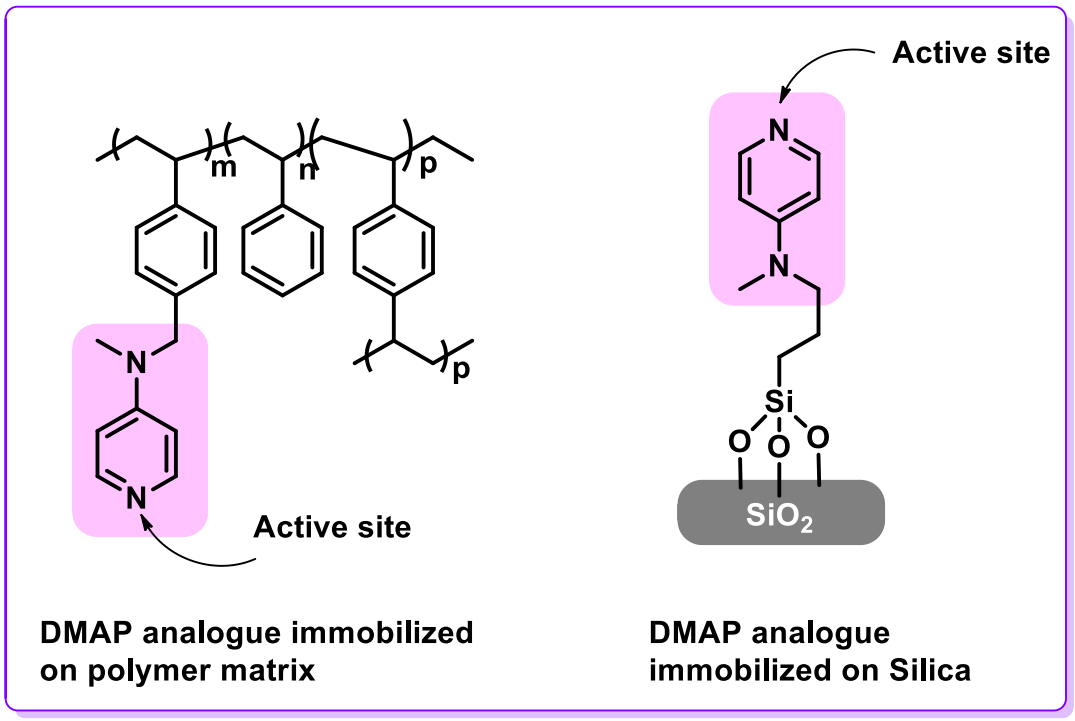

Figure 1.27. Immobilized DMAP analogue as a Lewis base

Immobilized Brønsted acid catalysts

In the last decade of the 20th century, Van Rijn et al. [333] proposed three approaches for covalently attaching 3-mercaptopropyltrimethoxysilane (MPTMS) to the surfaces of MCM and HMS (Hybrid Mesoporous Silica). The first two approaches involved grafting and co-condensation followed by the oxidation of the thiol group to a sulfonic acid group using H_2O_2. The third approach was in-situ thiol oxidation (see Figures 1.28a, 1.28b, 1.28c). Shaker et al. [334] reported the synthesis of propyl sulfonic silica with a magnetic core-shell structure. This solid acid catalyst was prepared via the co-condensation of tetraethyl orthosilicate (TEOS) and 1,2-bis(triethoxysilyl)methane (BTEM) around magnetic nanoparticles followed by grafting MPTMS onto the silica and oxidizing the thiol group to a sulfonic acid. The catalyst, depicted in Figure 1.28d, was tested for the esterification of carboxylic acids with alcohols to explore its potential use in biodiesel production. This magnetic nano-catalyst demonstrated excellent performance in terms of efficiency, selectivity, recovery and reusability.

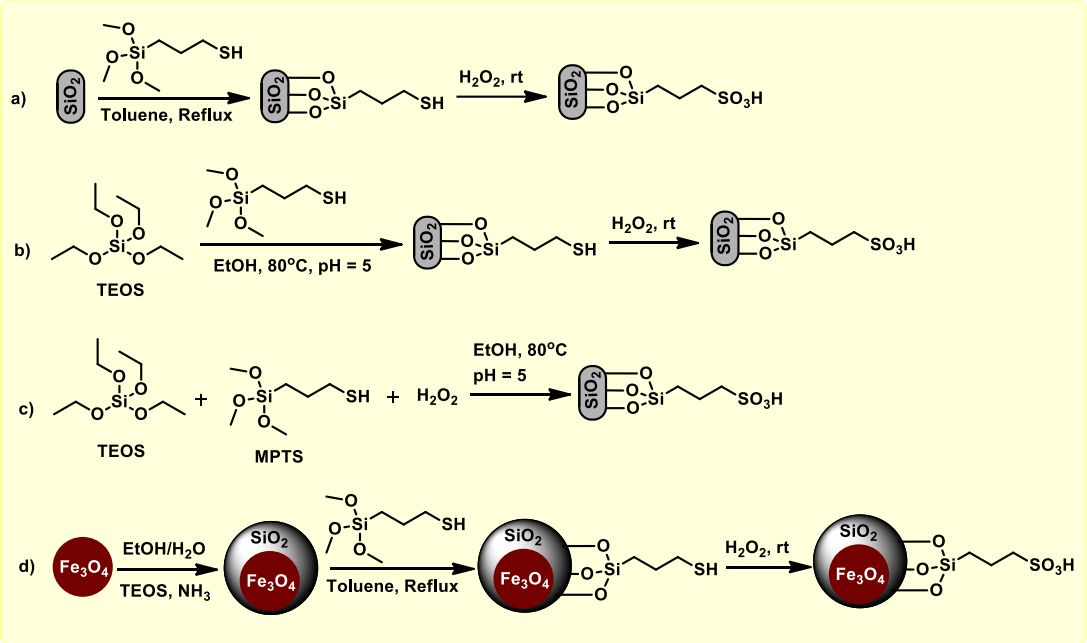

Figure 1.28. Synthesis of propyl sulfonic silica

Nikman et al. [335,336] reported the direct sulfonation of mercaptopropyl silica using chlorosulfonic acid to introduce -S-SO_3H functionality (Figure 1.29a). They also produced another sulfonic acid catalyst with an extended chain and -O-SO_3H functionality using a similar approach (Figure 1.29a). Moradi et al. [337] developed a magnetic silica catalyst with -S-SO_3H functionality and tested it in the synthesis of heterocycles (Figure 1.29b).

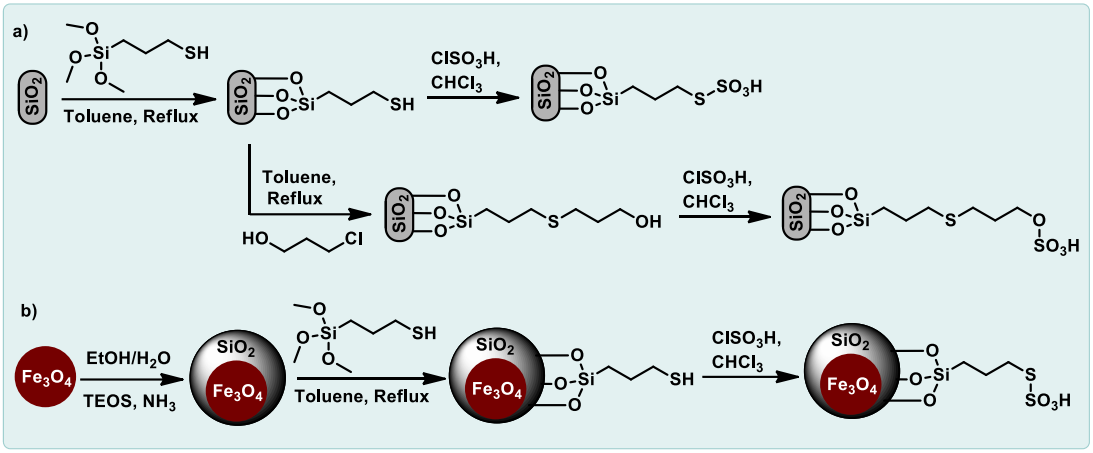

Figure 1.29. Synthetic approaches for thioether containing catalysts

Cyclic sulphate esters such as propane or butane sultones have also been extensively used as precursors for -SO_3H functionalized catalysts. Bell et al. [338] prepared a silica-bound alkyl sulfonic acid catalyst by reacting mercaptopropyl silane with propane sultone followed by heterogenization with silica and acidification. This catalyst was employed for the condensation of 2-methylfuran with various aldehydes or ketones. Similar catalysts were prepared by Safaei et al. [339] and used for multicomponent reactions in the synthesis of heterocycles (Figure 1.30).

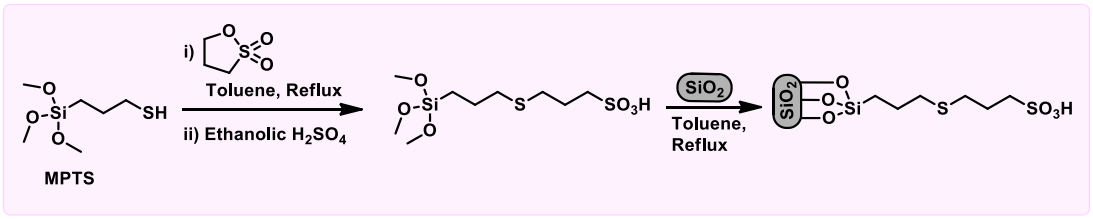

Figure 1.30. Synthetic approaches for Thioether containing catalysts

Ng et al. [340] adopted a similar approach by reacting aminopropylsilica with butane sultone and the resulting catalyst was tested for microwave assisted Friedel–Crafts butylation of hydroquinone (Figure 1.31a). Jetti et al. [341] reported the preparation of silica-bonded-N-propyl sulfamic acid (SBNPSA) by sulfonating the amino group with chlorosulphonic acid. This catalyst was tested in organic heterocyclic chemistry [342,343], transesterification of soybean oil with methanol [344] and acetylation of aromatic alcohols and amines [345,346] (Figure 1.31b-1.31e).

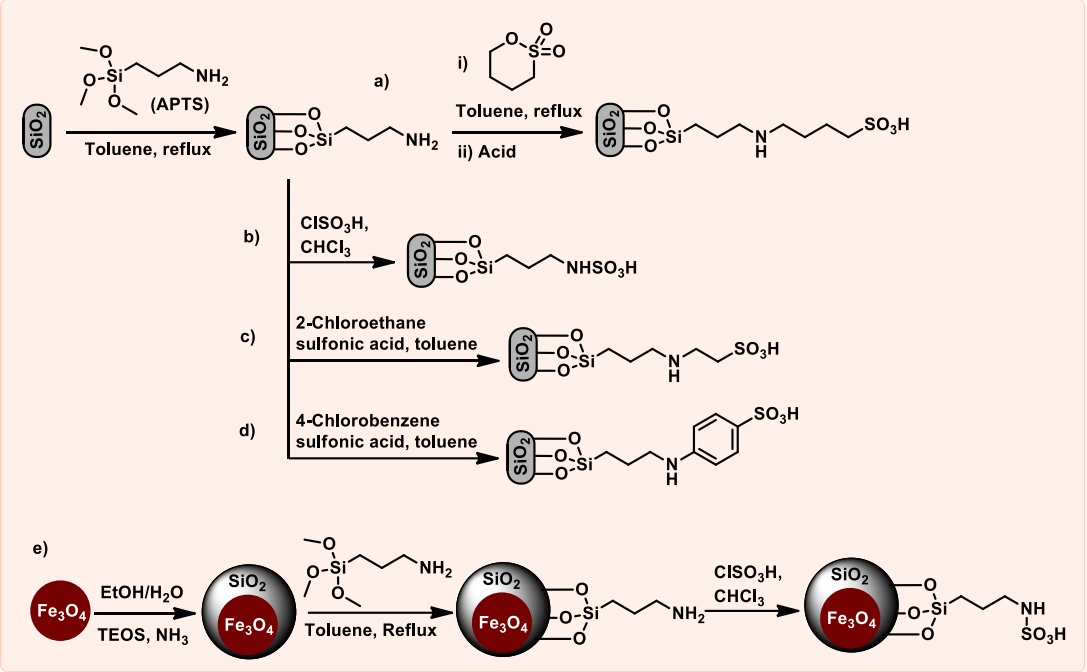

Figure 1.31. Synthetic approaches for amine containing Brønsted acid catalysts

Lindlar et al. [347] synthesized arene sulphonic MCM-41 using a multistep approach. They grafted phenyl groups to the silica surface through either gas-phase or liquid-phase reactions with the latter proving more effective due to a higher number of functional groups. The phenyl silica was then acidified by sulfonation with chlorosuphuric acid. To prevent further sulfonation of free silanol groups, these groups were protected with capping agents such as trimethoxymethylsilane (Figure 1.32a). Similar magnetic silica catalysts were prepared by Mobaraki et al. [348] and investigated for one-pot synthesis of amino nitriles via the Strecker reaction of aldehydes and amines (Figure 1.32b).

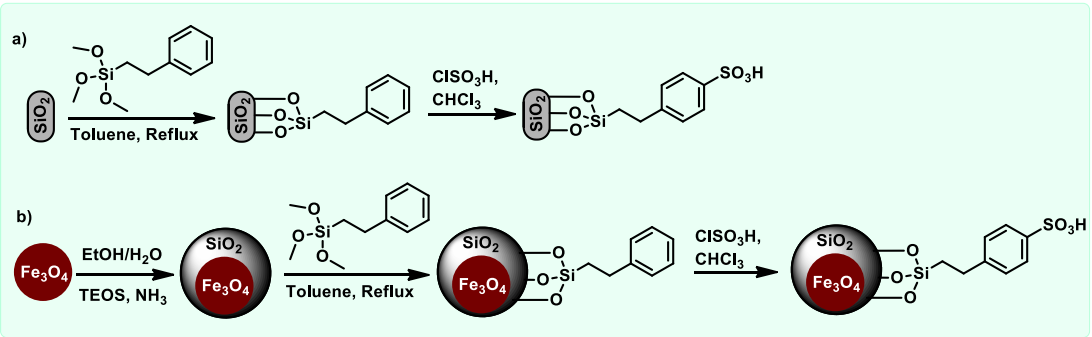

Figure 1.32. Synthetic approaches for amine containing Brønsted acid catalysts

Silica-supported imidazolium-based acidic Supported Ionic Liquid Catalysts (SILCs) have also been extensively studied for acid-responsive reactions. For example, Sidhpuria et al. [349] prepared a 1-methylimidazolium-based catalyst and used it for the dehydration of fructose to produce 5-hydroxymethylfurfural (Figure 1.33a). Park et al. [350] synthesized allylimidazolium-based Brønsted acid ionic liquids with triflate ([ASBI][TfO]) and sulphate ([ASBI][HSO_4]) anions and their Lewis acid derivatives ([ASCBI][TfO]) and ([ASCBI][HSO_4]) were covalently immobilized on silica via thiol (-SH) functional groups. These catalysts were tested for the esterification of glycerol with acetic acid and demonstrated high selectivity for Diacetin (DAG) and Triacetins (TAG) compared to other established heterogeneous acid catalysts, with excellent recyclability (Figure 1.33b). Li et al. [113] employed the same catalyst for the condensation of 2-methylfuran with formalin.

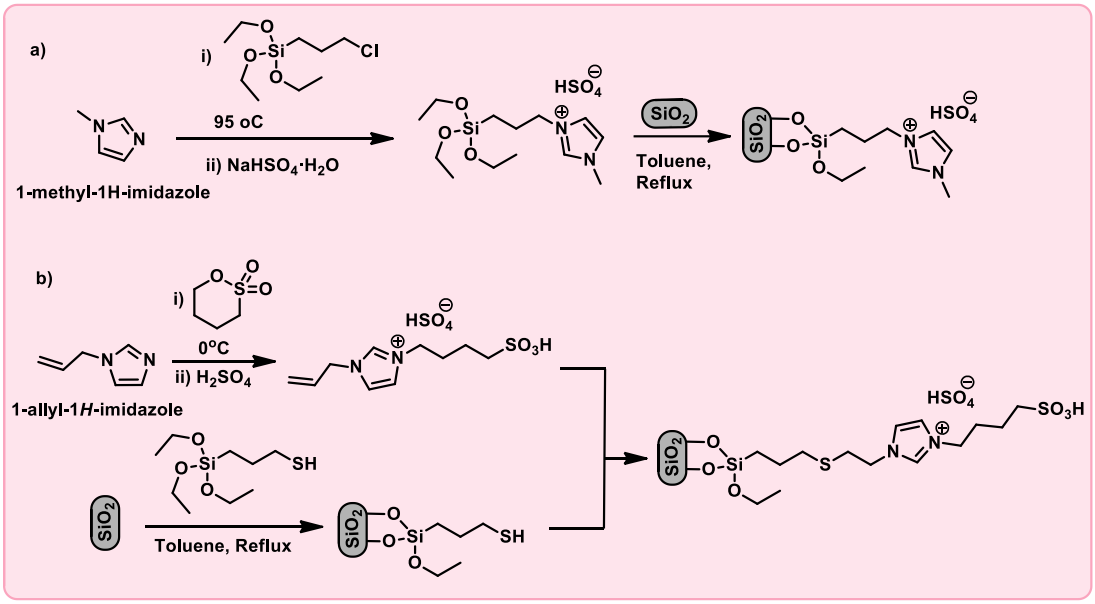

Figure 1.33. Synthetic approaches for imidazolium containing Brønsted acid catalysts

SO_3H-functionalized polymeric materials have also been explored for acid-responsive reactions. For instance, Brønsted acidic polymeric materials such as DVB-[C_3vim][X] and poly(VMPS)-X were tested for the dehydration-etherification of fructose to produce 5-ethoxymethylfurfural (Figure 1.34a) [351]. Long et al. evaluated silica-supported poly(styrene sulfonic acid) for the hydrolysis of ethyl lactate (Figure 1.34b) [313]. Xu et al. prepared a polymeric catalyst and tested it for acid-catalyzed hydrolysis of esters (Figure 1.34c) [352]. Senapak et al. [353] reported a similar acid-ionic polymer bearing imidazolium trifluoromethanesulfonate ([PS-Im][OTf]) as an

efficient catalyst in a one-pot, three-component Mannich reaction of aldehydes, amines and ketones (Figure 1.34d).

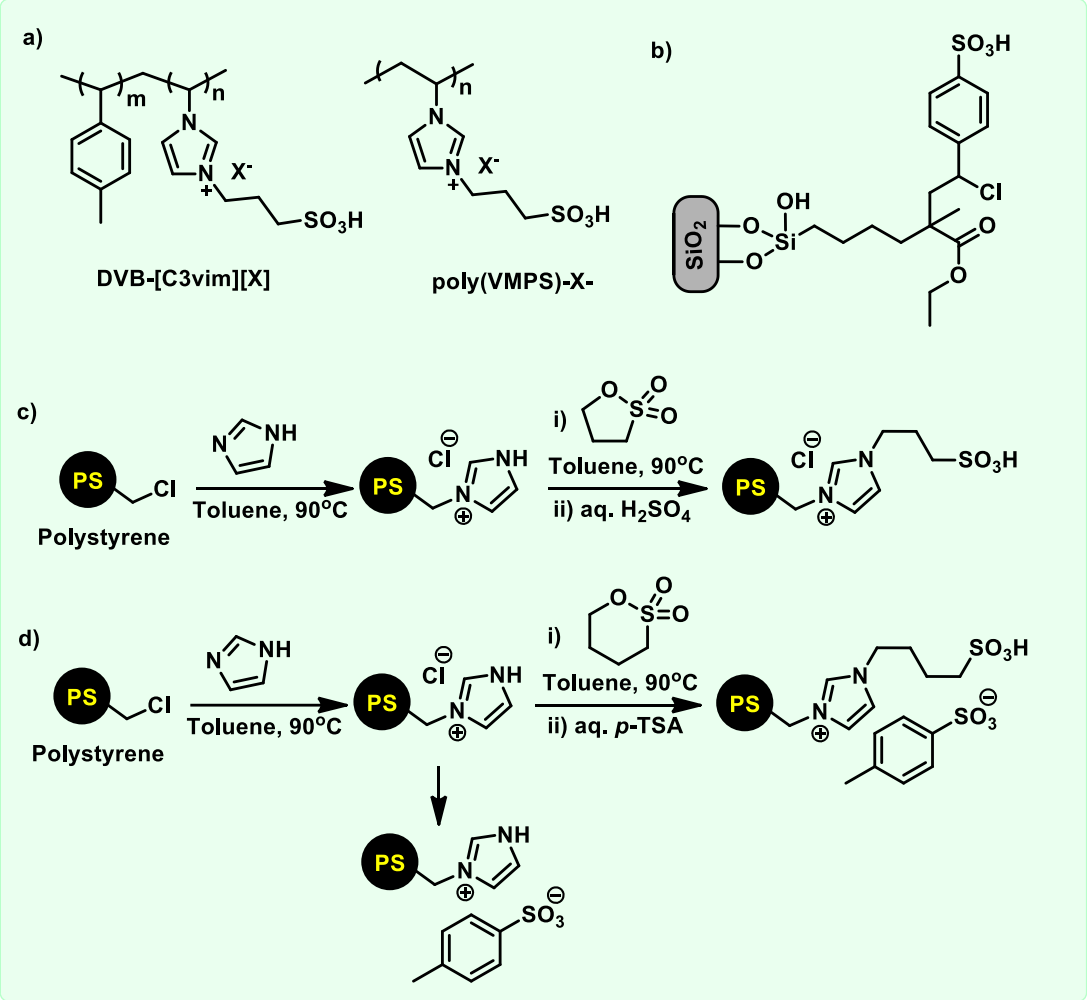

Figure 1.34. SO_3H-Functionalized organic polymeric materials

1.3. Scope of the thesis

Biomass is a globally available, renewable and natural carbon resource used for producing chemicals and fuels. Conserving carbon from biomass waste to create value-added chemicals is crucial for developing fossil-free chemical technologies for manufacturing transportation fuels, additives and other carbon-based products. Biomass-derived platform molecules, with their multiple reactive functional groups are ideal for transformation into valuable products. The aldehyde functionality enables the formation of long-chain alkanes through C-C bond-forming reactions with acid or base catalysts. The alcohol functionality supports the production of ethers and esters also facilitated by acid or base catalysts. Furthermore, the aromatic ring in these molecules

allows for the generation of saturated ring products using metal catalysts. In summary, bio-derived platform molecules are pivotal in various reactions, including C-C and C-O bond formation, hydrogenation, and hydrogenolysis. The required catalysts for these processes are detailed in the table below.

Table 1.5. Broad class of reactions involved in valorisation of biomass derived platform molecules

Sr. No.	Reaction type	Type of catalysts required
1	C-C bond forming reaction	acid or base catalysts
2	C-O bond forming reactions	acid and base catalysts
3	Hydrogenation reaction	noble or non-noble metal catalysts
4	Hydrogenolysis reaction	noble or non-noble metal catalysts along with acid catalysts

Generally, homogeneous catalysts are much active and easy to prepare but they are usually expensive, difficult to separate from reaction mass, difficult to reuse and difficult to handle. The downsides of homogeneous catalyst are making it a secondary choice. On the other hand, heterogeneous catalyst has several advantages as it is easy to separate from reaction mass, recyclable, easy to handle, stable, works under extreme reaction conditions etc. Considering the advantages of heterogeneous catalysts and its wide exploration in chemical transformations, it is becoming always a first choice of the chemists and technologist.

Although, numerous catalyst systems have been developed for the valorisation of biomass, development of novel heterogeneous catalysts and testing/utilizing them for conversion of platform molecules is still in demand. Based on the problem statement, path forward and our technical expertise we have broadly established our objectives enlisted below in order to utilization/valorisation of selected lignocellulose derived platform molecules.

- Inspiring from the catalysts systems presented in section 1.2 of the current chapter we have designed novel immobilized organic catalysts having active Brønsted acids and Lewis bases. Novel immobilized organic catalysts were synthesized from unique starting organic molecules and their structural modifications to generate active acids or bases followed by heterogenized on silica/magnetic silica.
- Structural designing, synthesis procedures of novel immobilized organic catalysts and its evaluation for conversion of some biomass derived platform molecules to fuel and chemicals is presented in details in next chapters.

- To thoroughly characterise the developed catalyst by using sophisticated analytical testing tools such as FTIR, TEM, SEM, XRD, XPS, TGA, NMR etc.
- To test the novel heterogeneous acid or base catalysts for C-C bond forming reactions of selected platform molecules to produce carbon upgraded products which could be further converted to fuels or chemicals.
- To test the novel heterogeneous acid catalysts for production building blocks/ intermediates which could be further utilized to make polymers, pharmaceuticals or other valuable products.

1.4. Organisation of the thesis

Chapter 1 provides an introduction of Biomass, concept of Biorefinery, Biomass derived platform molecules and catalytic conversions of biomass derived platforms to fuel, fuel precursors, chemicals and materials. This chapter also provides a brief explanation of catalysis, explores the different types of catalysts, and discusses the synthesis of immobilized organic catalysts.

Chapter 2 provides details for synthesis of novel magnetically immobilized organic Lewis base catalyst and its application for Knoevenagel condensation of furfural with acetyl acetone. Magnetic nature of this catalyst allows us to effortlessly separate it from reaction mixture using an external magnetic field. This feature not only minimizes handling losses but also ensures sustained catalyst activity over multiple cycles without significant decrease in its activity.

Chapter 3 provides details for synthesis of another novel magnetically immobilized organic Brønsted acid catalyst and its application for production of saturated cyclic oxygenates as potential fuel candidates. The synthesis of saturated cyclic ethers involves a two-step process, first the acid-catalyzed condensation of aldehydes with 2-methylfuran, followed by the selective hydrogenation of the furan ring in the condensation products.

Chapter 4 provides details for synthesis of a simple and novel silica supported sulfonic acid functionalized isonicotinic acid SO_3H-INA@SiO_2 and explored for the solvent free conversion of 2-methylfuran to polyfuranic compounds (fuel precursors) of C_{15} and C_{20} units. These polyfuranic compounds can further undergo hydrodeoxygenation to produce a diesel fuel.

Chapter 5 provides details for synthesis of one more novel magnetically immobilized organic Brønsted acid catalyst and its application for production of Bisguaiacol-F (BGF) and its derivatives. Astonishingly, our synthesized catalyst facilitates complete conversion of aqueous formaldehyde and guaiacol to form regioisomers such as *pp*'-BGF, *mp*'-BGF and *op*'-BGF with remarkable selectivity. Materials containing BPA are well known for serious health concerns hence, being outlawed in many countries. In order to mitigate this threat, Bisguaiacol-F (BGF) has emerged as safer and more sustainable alternative to Bisphenol-A.

Chapter 6 lists the overall summary of the present work and comments on the future scope.

1.5. References

[1] D. A. Simonetti, J. A. Dumesic, *ChemSusChem* **2008**, *1*, 725–331.

[2] https://www.lenntech.com/greenhouse-effect/fossilfuels.htm#ixzz8N4X8Qz7 R

[3] D. Y Goswami, F. Kreith 2007. *Global energy system. In Handbook of Energy Efficiency and Renewable Energy, ed. F Kreith, DY Goswami*, *1*, 1–24.

[4] Intergov. Panel Climate Change (IPCC). 2007. http://www.aaas.org/news/press_room/climate_change/media/fourth_spm2feb07.pdf

[5] BP Stat. Rev. World Energy. **2009**. http://www.bp.com/productlanding.do?categoryId=6929&contentId=704462

[6] President Bush State Union Address. White House. **2007**. http://usgovinfo.about.com/b/2007/01/23/bush-delivers-his-seventh-state-of-the-union-address.html

[7] Directive 2003/30/EC Eur. Union Parliam., *Off. J. Eur. Union*. **2003**. http://ec.europa.eu/energy/res/legislation/doc/biofuels/en_final.pdf

[8] http://www.brdisolutions.com/pdfs/FinalBiomassRoadmap.pdf

[9] https://www.transparencymarketresearch.com/india-biomass-market.html

[10] https://www.praj.net/wp-content/uploads/2023/08/BIOREFINERY-A-Way-Forward-towards-Energy-Transition-Mr-Ghanshyam-Deshpandes-article-in-Sampada-Aug-2023.pdf

[11] http://www.thehindubusinessline.com/opinion/biomass-the-forgottenoption/ article5029373.

[12] http://www.icar.org.in/files/ICAR-Vision-2030.pdf

[13] http://www.eai.in/ref/ae/bio/tf/biomass_tf.html

[14] P.M. Sanders, E. Scott, R. Weusthuis, H. Mooibroek, *Macromol. Biosci*. **2007**, *7*, 105-117.

[15] O. Cavalett, T. L. Junqueira, O.S.D. Marina, D.F.J. Charles, E.M. Paulo, P.C. Marcelo, C.J.F. Henrique, F.C. Terezinha, M.F. Rubens, E.V.R. Carlos, B. Antonio, *Clean Technol. Environ. Policy*, **2012**, *14*, 399-410.

[16] E. S. Lipinsky, *Science*, **1981**, *212*, 1465-1471.

[17] Y. Chisti, *Biotechnol. Adv*. **2007**, *25*, 294-306.

[18] A. Aden, M. Ruth, K. Ibsen, J. Jechura, K. Neeves, J. Sheehan, B. Wallace, L. Montague, A. Slayton, J. Lukas, *National Renewable Energy Laboratory, Golden*, CO, NREL/TP-510-32438, **2002**.

[19] T. L. Donaldson, O. L. Culberson, *Energy*, **1984** *9* 693-707.

[20] J. P. Kaiser, K. W. Hanselmann, *Experientia*, **1982**, *38*, 167-176.

[21] M. E. Zakrzewska, E. Bogel-Łukasik, R. Bogel-Łukasik, *Chem. Rev.*, **2010**, *111*, 397–417.

[22] P. Kumar, D. Barrett, M. M. J. Delwiche, P. Stroeve, *Ind. Eng. Chem. Res.*, **2009**, *48*, 3713-3729.

[23] S. Malherbe, T. E. Cloete, *Rev. Environ. Sci. Biotechn.*, **2002**, *1*, 105-114.

[24] K. Freudenberg, A. C. Nash (eds.) *Constitution and Biosynthesis of Lignin. Berlin: Springer-Verlag*, **1968.**

[25] W. Boerjan, J. Ralph, M. Baucher, *Annu. Rev. Plant Biol*. **2003**, *54*, 519–549.

[26] a) J. P. Lange, *Biofuels Bioprod. Bioref*. **2007**, *1*, 39–48; b) X. Yan, O. R. Inderwildi, D. A. King, *Energy Environ. Sci*. **2010**, *3*, 190–197; c) B. D. Solomon, N. Y. Ann. *Acad. Sci*. **2010**, *1185*, 119–134.

[27] C. M. Cai, T. Zhang, R. Kumar, C. E. Wyman, *J. Chem. Technol. Biotechnol.* **2014**, *89*, 2-10.

[28] A. D. Kulkarni, H. M. Modak, S. J. Jadhav, R. Khan, *J. Sci. Ind. Res*. **1989**, *47*, 335−339.

[29] Global 5-Hydroxymethylfurfural (CAS 67-47-0) Market by Manufacturers, Countries, Type and Application, Forecast to **2022**. www.1marketresearch.com

[30] T. Werpy, G. Petersen, A. Aden, J. Bozell, J. Holladay, J. White, A. Manheim, D. Eliot, L. Lasure, S. Jones, *U. S. DoE Report. Pacific Northwest National Laboratory/U.S. Department of Energy, Oak Ridge*, **2004**, *1*.

[31] J. J. Bozell, R. Petersen, *Green Chem*. **2010**, *12*, *4*, 539-554.

[32] J. V. Bomtempo, F.C. Alves, F.A. Oroski, *Faraday Discuss*. **2017**, *202* 213-225.

[33] K. Weissermel, H.J. *Arpe, Ind. Org. Chem., 4th ed., Wiley-VCH, Weinheim*, **2003.**

[34] J. J. Bozell, J. E. Holladay, D. Johnson, J. F. White, Top Value Added Chemicals from Biomass, PNNL, 2007, 2, 16983.

[35] T. Jenkins, *Biofuels, Bioprod. Biorefin*. **2008**, *2*, 133-143.

[36] M. M. Wright, R.C. Brown, *Biofuels Bioprod. Bior. Biofpr*, **2007**, *1*, 1, 49-56.

[37] P.J. Woolcock, R.C. Brown, *Biomass Bioenergy*, **2013**, *52*, 54-84.

[38] Ø. Borg, N. Hammera, B. C. Enger, R. Myrstad, O. A. Lindvåg, S. Eri, T. H. Skagseth, E. Ryttera, *J. Catal*., **2011**, *279*, 1, 163-173.

[39] P. L. Spath, D. C. Dayton, National Renewable Energy Laboratory, Golden, CO, USA, **2003**. NREL/TP-510-34929.

[40] J. Daniell, M. Kopke, S. D. Simpson, *Energies*, **2012**, *5*, 12, 5372-5417.

[41] K. Okabe, K. Murata, M. Nakanishi, T. Ogi, M. Nurunnabi, Y. Liu, *Catal. Lett*. **2009**, *128* 171-176.

[42] B. Reusens, Remacle, claude, in: B. Reusens (Ed.), Woodhead Publishing, Cambridge, **2004**, ISBN 978-1-85573-725-9, 202.

[43] Artificial Sweeteners and Other Sugar Substitutes, Mayo Clinic, August 20, **2015**.

[44] G. A. Evrendilek. Sugar alcohols (polyols), in: T. Varzakas, A Labropoulos., & S. Anestis, (Eds.), Sweeteners: *Nutritional Aspects, Applications, and Production Technology*, **2012**, 45-78.

[45] L. Hyvönen, P. Koivistoinen, F. Voirol, Advances in food research. *Academic Press*, **1982**, *28*, 373-403.

[46] https://www.grandviewresearch.com/industry–analysis/xylitol–market.

[47] T. B. Granström, K. Izumori, M. Leisola, *Appl. Microbiol. Biotechnol*. **2007**, *74*, 273-276.

[48] H. Ojamo, M. Penttila, H. Heikkila, J. Uusitalo, M. Ilmen, M.L. Sarkki, M.L. Vehkomaki, U.S. Patent, 7, 482, 144 B2.

[49] K. Dietrich, C. Hernandez-Mejia, P. Verschuren, G. Rothenberg, N. Raveendran Shiju, *Org. Proc. Res. Dev*., **2017**, *21*, 165-170.

[50] G. Yi, Y. Zhang. *ChemSusChem*, **2012**, 5, (8), 1383-1387.

[51] L. S. Ribeiro, J. J. Órfão, M. F. Pereira, *Green Process Synth*, **2017**, *6* (3), 265-272.

[52] L. S. Ribeiro, J. J. Delgado, J. J. de Melo Órfão, M. F. R. Pereira. *RSC Adv*., **2016**, *6*, (97), 95320-95327.

[53] M. Tudorache, S. M. Coman, V. I. Parvulescu., A. Tiwari, & S. Titinchi, (Eds.), *Advanced Catalytic Materials*, **2015**, 313-352.

[54] A. Yamaguchi, O. Sato, N. Mimura, M. Shirai. *Catal. Today*, **2016**, 265, 199-202.

[55] L. S. Ribeiro, J. J. Órfão, M. F. R. Pereira. *Bioresour. Technol*., **2017**, *244*, 1173-1177.

[56] X. Li, T. Guo, Q. Xia, X. Liu, Y. Wang. *ACS Sustainable Chem. Eng*., **2018**, *6* (3) 4390-4399.

[57] P. Barbaro, F. Liguori, C. Moreno-Marrodan. *Green Chem*., **2016**, *18* (10), 2935-2940.

[58] R.H. Kottke, Kirk-Othmer Encyclopedia of Chemical Technology, Wiley Inter science, New York, 2004.

[59] B. Kamm, P. R. Gruber, M. Kamm, Biorefineries-Industrial Processes and Products, Wiley-VCH, Weinheim, 2006.

[60] A.S. Mamman, J. M. Lee, Y. C. Kim, I. T. Hwang, N. J. Park, Y. K. Hwang, J. S. Chang, J. S. Hwang, *Biofuels. Biofuels, Bioprod. Biorefin*. **2008**, *2*, 438-454.

[61] K. J. Zeitsch, The Chemistry and Technology of Furfural and its Many by Products, Elsevier, Amsterdam, **2000**.

[62] J. P. Lange, E. van der Heide, J. van Buijtenen, R. Price, *ChemSusChem*, **2012** *5*, 150-166.

[63] G. Machado, S. Leon, F. Santos, R. R. Lourega, J. Dullius, M. E. Mollmann, P. Eichler, *Natural Resoures*, **2016**, 7, 115−129.

[64] http://www.marketwatch.com/(accessed June 12, 2017).

[65] H. J. Brownlee, C. S. Miner, *Ind. Eng. Chem*. **1948**, *40*, 201–204.

[66] R. D. Sproull, P. R. Bienkowski, G. T. Tsao, *Biotechnol. Bioeng. Symp*., **1985**, *15*, 561–577.

[67] W. Yang, P. Li, D. Bo, H. Chang, X. Wang, T. Zhu, *Bioresour. Technol*. **2013**, *133*, 361−369.

[68] R. Weingarten, G. A. Tompsett, W. C. Conner, G. W Huber, *J. Catal*., **2011**, *279*, 174−182.

[69] G. W. Huber, J. N. Chheda, C. J. Barrett, J. A. Dumesic, *Science*, **2005**, *308*, 1446–1450.

[70] a) D. A. Isacescu, I. Gavat, C. Stoicescu, C. Vass, I. Petrus, *Rev. Roum. Chim*., **1965**, *10*, 219–231; b) A. A. Patel, S. R. Patel, *Eur. Polym. J*., **1983**, *19*, 231–234.

[71] N. Fakhfakh, P. Cognet, M. Cabassud, Y. Lucchese, M. D. de Los Rios, *Chem. Eng. Process*., **2008**, *47*, 349–362.

[72] a) H. Olcay, A. V. Subrahmanyam, R. Xing, J. Lajoie, J. A. Dumesic, G. W. Huber, *Energy Environ. Sci*., **2013**, *6*, 205–216; b) R. M. West, Z. Y. Liu, M. Peter, C. A. Gartner, J. A. Dumesic, *J. Mol. Catal. A: Chem*., **2008**, *296*, 18–27; c) J. N. Chheda, J. A. Dumesic, *Catal. Today*, **2007**,*123*, 59–70; d) J. A. Dumesic, G. W. Huber, J. N. Chheda, C. J. Barrett, US pat., 7671246, 2010.

[73] a) D. A. Isacescu, I. Gavat, C. Stoicescu, C. Vass, I. Petrus, *Rev. Roum. Chim*., **1965**, *10*, 219–231 b) A. A. Patel, S. R. Patel, *Eur. Polym. J*., **1983**, 19, 231–234. c) D. A. Isacescu, F. Avramescu, *Rev. Roum. Chim*., **1978**, *23*, 661–665.

[74] J. N. Chheda, J. A. Dumesic, *Catal. Today*, **2007**,*123*, 59–70.

[75] G. Liang, A. Wang, X. Zhao, N. Lei, T. Zhang, *Green Chem*., **2016**, *18*, 3430–3438.

[76] J. Yang, N. Li, S. Li, W. Wang, L. Li, A. Wang, X. Wang, Y. Cong, T. Zhang, *Green Chem*., **2014**, *16*, 4879–4884.

[77] a) W. J. Xu, X. H. Liu, J. W. Ren, H. H. Liu, Y. C. Ma, Y. Q. Wang, G. Z. Lu, *Microporous Mesoporous Mater*., **2011**, *142*, 251–257; b) W. J. Xu, X. H. Liu, J. W. Ren, P. Zhang, Y. Q. Wang, Y. L. Guo, Y. Guo, G. Z. Lu, *Catal. Commun*., **2010**, *11*, 721–726.

[78] L. Hora, V. Kelbichova, O. Kikhtyanin, O. Bortnovskiy, D. Kubicka, *Catal. Today*, **2013**, *223*, 138–147.

[79] J. Yang, N. Li, G. Li, W. Wang, A. Wang, X. Wang, Y. Cong and T. Zhang, *ChemSusChem*, **2013**, *6*, 1149–1152.

[80] O. Kikhtyanin, D. Kadlec, R. Velvarsk´a and D. Kubiˇcka, *ChemCatChem*, **2018**, *10*, 1464–1475.

[81] S. Shinde, K. Tarade, G. Mitra, C. Rode, *ChemistrySelec*t, **2020**, *5*, 392–400.

[82] L. Faba, E. Diaz, S. Ordonez, *Catal. Today*, **2011**, *164*, 451–456.

[83] W. Dedsuksophon, K. Faungnawakij, V. Champreda, N. Laosiripojana, *Bioresour. Technol*., **2011**, *102*, 2040–2046.

[84] a) L. Faba, E. Diaz, S. Ordonez, *Appl. Catal., B*, **2012**, *113*, 201–211; b) I. Sadaba, M. Ojeda, R. Mariscal, R. Richards, M. L. Granados, *ChemPhysChem*, **2012**, *13*, 3282–3292.

[85] L. Faba, E. Diaz, S. Ordonez, *ChemSusChem*, **2013**, *6*, 463–473.

[86] X.-M. Huang, Q. Zhang, T.-J. Wang, Q.-Y. Liu, L.-L. Ma, Q. Zhang, *J. Fuel Chem. Technol*., **2012**, *40*, 973–978.

[87] R. E. O'Neill, L. Vanoye, C. De Bellefon, F. Aiouache, *Appl. Catal., B: Environ*., **2014**, *144*, 46–56.

[88] H. Kayser, C. R. Muller, C. A. Garcia-Gonzalez, I. Smirnova, W. Leitner, P. Domınguez de Marıa, *Appl. Catal., A*, **2012**, 445–446, 180–186.

[89] X. Zhao, S. Li, Y. Hu, X. Zhang, L. Chen, C. Wang, L. Ma and Q. Zhang, *Chem. Eng. J*., **2022**, 428, 131368.

[90] Y. Liu, Y. Wang, Y. Cao, X. Chen, Q. Yu, Z. Wang and Z. Yuan, *ACS Sustainable Chem. Eng*., **2020**, *8*, 6949–6955.

[91] A. V. Subrahmanyam, S. Thayumanavan, G. W. Huber, *ChemSusChem*, **2010**, *3*, 1158–1161.

[92] W. Wang, X. Ji, H. Ge, Z. Li, G. Tian, X. Shao and Q. Zhang, *RSC Adv*., **2017**, *7*, 16901–16907.

[93] O. Kikhtyanin, V. Kelbichov´a, D. Vitvarov´a, M. Kubu, D. Kubicka, *Catal. Today*, **2014**, *227*, 154–162.

[94] W. Li, M. Su, T. Zhang, Q. Ma, W. Fan, *Fuel*, **2019**, *237*, 1281–1290.

[95] M. Su, W. Li, T. Zhang, H. Xin, S. Li, W. Fan, L. Ma, *Catal. Sci. Technol*., **2017**, *7*, 3555–3561.

[96] Y. Jing, Y. Xin, Y. Guo, X. Liu and Y. Wang, *Chin. J. Catal*., **2019**, *40*, 1168–1177.

[97] J. Xu, N. Li, X. Yang, G. Li, A. Wang, Y. Cong, X. Wang, T. Zhang, *ACS Catal*., **2017**, *7*, 5880–5886.

[98] D. Nguyen Thanh, O. Kikhtyanin, R. Ramos, M. Kothari, P. Ulbrich, T. Munshi, D. Kubiˇcka, *Catal. Today*, **2016**, *277*, 97–107.

[99] C. Zhu, T. Shen, D. Liu, J. Wu, Y. Chen, L. Wang, K. Guo, H. Ying and P. Ouyang, *Green Chem*., **2016**, *18*, 2165–2174.

[100] Y. B. Huang, Z. Yang, J. J. Dai, Q. X. Guo, Y. Fu, *RSC Adv*., **2012**, *2*,11211–11214.

[101] A. Corma, O. D. Torre, M. Renz, N. Villandier, *Angew. Chem., Int. Ed*., **2011**, *50*, 2375.

[102] M. Balakrishnan, E. R. Sacia, A. T. Bell, *ChemSusChem*, **2014**, *7*, 2796-2800.

[103] G. Li, A. N. Li, A. S. Li, A. A. Wang, A. Y. Cong, A. X. Wanga, T. Zhang, *Chem. Commun*., **2013**, *49*, 5727-5729.

[104] (a) W. H. Brown, W. N. French, *Can. J. Chem*., **1958**, *36*, 537; (b) W. H. Brown, B. J. Hutchinson, *Can. J. Chem*., **1978**, *56*, 617; c) A. Riad, Z. Mouloungui, M. Delmas, A. Gaset, *Synth. Commun*., **1989**, *19*, 3169.

[105] W. M. VanRhijn, D. E. DeVos, B. F. Sels, W. D. Bossaert, P. A. Jacobs, *Chem. Commun*., **1998**, 317-318.

[106] T. Li, S. I. Cheng, J. F. Lee, L. Y. Jang, *J. Mol. Catal. A: Chem*., **2003**, *198*, 139.

[107] a) A. S. K. Hashmi, L. Schwarz, P. Rubenbauer, M. C. Blanco, *Adv. Synth. Catal*., **2006**, *348*, 705; (b) V. Nair, K. G. Abhilash and N. Vidya, *Org. Lett*., **2005**, *7*, 5857.

[108] F. Algarraa, A. Corma, H. Garciaa and J. Primoa, *Appl. Catal., A*, **1995**, *128*, 119.

[109] A.S. Mamman, J. M. Lee, Y. C. Kim, I. T. Hwang, N. J. Park, Y. K. Hwang, J. S. Chang, J. S. Hwang, *Biofuels. Bioprod. Biorefin*. **2008**, *2*, 438-454.

[110] M. Muthyala, V. K. Rao, A. Kumar, *Chin. J. Chem*., **2011**, *29*, 1483-1488.

[111] J. Jaratjaroonphong, S. Tuengpanya, R. Saeeng, S. Udompong and K. Srisook, *Eur. J. Med. Chem*., **2014**, *83*, 561-568.

[112] I. Ogino, Y. Suzuki, S. R. Mukai, *ACS Catal*., **2015**, *5*, 4951.

[113] H. Li, S. Saravanamurugan, S. Yang, A. Riisager, *ACS Sustainable Chem. Eng*. **2015**, *3*, 12, 3274–3280.

[114] S. H. Shinde, C. V. Rode, *Green Chem*., **2017**, *19*, 4804–4810.

[115] C. Zhu, T. Shen, D. Liu, J. Wu, Y. Chen, L. Wang, K. Guo, H. Ying, P. Ouyang, *Green Chem*., **2016**, *18*, 2165-2174.

[116] C. M. Nicklaus, A. J. Minnaard, B. L. Feringa, J. G. de Vries, *ChemSusChem*, **2013**, *6*, 1631–1635.

[117] O. Kikhtyanin, P. Chlubna, T. Jindrova, D. Kubicka, *Dalton Trans*., **2014**, *43*, 10628–10641.

[118] J. A. Dumesic, G. W. Huber, J. N. Chheda, C. J. Barrett, WO2007103858A2, **2007**

[119] A. S. Amarasekara, T. B. Singh, E. Larkin, M. A. Hasan, H. J. Fan, *Ind. Crops Prod*., **2015**, *65*, 546–549.

[120] a) G. M. Gonzalez Maldonado, R. S. Assary, J. Dumesic, L. A. Curtiss, *Energy Environ. Sci*., **2012**, *5*, 6981–6989; b) J. A. Dumesic, D. M. Alonso, E. I. Gurbuz, S. G. Wettstein, US 8399688, **2013**.

[121] B. Chen, F. Li, Z. Huang, T. Lu, Y. Yuan, G. Yuan, *ChemSusChem*, **2014**, *7*, 202–209]

[122] C. Fang, Y. Liu, W. Wu, H. Li, Z. Wang, W. Zhao, T. Yang, S. Yang, *Waste and Biomass Valorization*, **2019**, *10*, 1141-1150.

[123] K. Y. Nandiwale, M. Vishwakarma, S. Rathod, I. Simakova, V. V. Bokade, *Energy Fuels*, **2021**, *35*, 1, 539–545.

[124] H. Alshaikh, *J. Polym. Res*. **2021**, *28*, 127.

[125] Y. Wang, K. Yu, D. Lei, W. Si, Y. Feng, L.-L. Lou, S. Liu, *ACS Sustainable Chem. Eng.* **2016**, *4*, 4752−4761.

[126] Z. Gui, W. Cao, S. Saravanamurugan, A. Riisager, L. Chen, Z. Qi, *ChemCatChem*, **2016**, *8*, 3636–3643.

[127] T. Horvath, H. Mehdi, V. Fabos, L. Boda, L. T. Mika, *Green Chem*. **2008**, *10*, 238–242.

[128] B. L. Oser, S. Carson, M. Oser, *Food Cosmet. Toxicol*., **1965**, *3*, 563–569.

[129] D. Cerniauskaite, J. Rousseau, A. Sackus, P. Rollin, A. Tatibouet, *Eur. J. Org. Chem*. **2011**, 2293–2300.

[130] J. Q. Bond, D. M. Alonso, D. Wang, R. M. West, J. A. Dumesic, *Science,* **2010**, *327*, 1110–1114.

[131] J. P. Lange, J. Z. Vestering, R. J. Haan, *Chem. Commun*. **2007**, 3488–3490.

[132] A. P. Dunlop, J. W. Madden, (Quaker Oats Co.), US 2786852, **1957**.

[133] P. G. Jessop, *Green Chem*. **2011**, *13*, 1391–1398.

[134] D. M. Alonso, S. G. Wettstein, J. A. Dumesic, *Green Chem*., **2013**, 15, 584–595.

[135] D. Fegyverneki, L. Orha, G. Lang, I. T. Horvath, *Tetrahedron*, **2010**, *66*, 1078–1081.

[136] L. Bui, H. Luo, W. R. Gunther, Y. Roma´n-Leshkov, *Angew. Chem., Int. Ed*., **2013**, *52*, 8022–8025.

[137] B. Tang, S. Li, W. Song, Y. Li, E. Yang, *Sustain Energy Fuels*, **2021**, *5*, 4724-4735.

[138] Li W, Li M, Liu H, Jia W, Yu X, Wang S, *Molecular Catal*. **2021**, *506*, 111538.

[139] H. P. Winoto, Z. A. Fikri, J. M. Ha, Y. K. Park, H. Lee, D. J. Suh, *Appl Catal B Environ*. **2019**, *241*, 588-597.

[140] J. Tan, Y. Liu, M. Li, H. Li, S. Yang, *Sustain Energy Fuels*, **2022**, *6*, 484-501.

[141] X. Gao, X. Yu, L. Peng, L. He, J. Zhang, *Fuel*, **2021**, 300, 120996.

[142] B. S. Rao, D. D. Lakshmi, P. K. Kumari, N. Lingaiah, *Sustain Energy Fuels*. **2021**, *5*, 3719-3728.

[143] J. He, H. Li, Y. Xu, S. Yang, *Renew Energy*, **2020**, *146*, 359-370.

[144] A. García, P. J. Miguel, A. Ventimiglia, N. Dimitratos, B. Solsona, *Fuel*, **2022**, *324*, 124549.

[145] P.J. Fellows, Food Processing Technology, Woodhead Publishing, **2016**, ISBN 978-0-081-00523-1, *197*.

[146] F. W. Schenck, Ullmann's Encyclopedia of Industrial Chemistry, Wiley-VCH, Weinheim, **2006**.

[147] A. J. Vroemen, M. Beverini, Enzymatic Production of Gluconic Acid or Its Salts, US5, 897, **1999**, 995A.

[148] S. Anastassiadis, H. J. Rehm, *Appl. Microbiol. Biotechnol*., **2006**, *73* (3) 541-548.

[149] R. Sumitra, F. Pierre, A. Pandey, L. Christian, *Food Technol. Biotechnol*., **2006**, *44* (2) 185-195.

[150] S. Anastassiadis, I. G. Morgunov, *Recent Pat. Biotechnol*. **2007**, *1*, 167-180.

[151] R. J. Bose, T. L. Hullar, B. A. Lewis, F. Smith, *J. Org. Chem*., **1961**, *26* 1300-1301.

[152] Y. Noriyuki, K. Satoru, Y. Makoto, P. Peter, W. Steve, *Appl. Catal. Gen*., **2001**, *221*, 253-265.

[153] D. J. Loder, U.S. Patent 2, **1939**, 152, 852A.

[154] N. Ashammakhi, P. Rokkanen, *Biomaterials*, **1997**, *18*, 3-9.

[155] G. Zhao, M. Zheng, J. Zhang, A. Wang, T. Zhang, *Ind. Eng. Chem. Res*., **2013**, *52* (28) 9566-9572.

[156] H. Benninga, Of Chemists and Chemistry, *Springer*, **1990**, 11, ISBN 9780792306252, 0792306252.

[157] K.F. Dietrich, W. Ebertz, Ullmann's Encyclopedia of Industrial Chemistry, Wiley-VCH, Weinheim, **2005**.

[158] A. D. Kulkarni, H. M. Modak, S. J. Jadhav, R. Khan, *J. Sci. Ind. Res*., **1989**, *47*, 335-339.

[159] A. Chinnappan, A. H. Jadhav, W.-J. Chung, H. Kim, *Ind. Crops Prod*., **2015**, *76*, 12-17.

[160] K. Pupovac, R. Palkovits, *ChemSusChem*, **2013**, *6*, 2103–2110.

[161] D. Liu, Y. Zhang, E. Y. X. Chen, *Green Chem*., **2012**, *14*, 2738–2746.

[162] D. Liu, E. Y. X. Chen, *ChemSusChem*, **2013**, *22*, 2236-2239.

[163] F.W. Lichtenthaler, E. Cuny, D. Martin, S. Ronninger, F.W. Lichtenthaler (Ed.), Carbohydrates as Organic Raw Materials, VCH Publishers, Weinheim/New York, **1991**, 214.

[164] H. Koch, J. Pein, *Polym. Bull*., **1985**, *13*, 525-532.

[165] J. O. Metzger, *Angew. Chem. Int. Ed*., **2006**, *45*, 696-698.

[166] E. L. Kunkes, D. A. Simonetti, R. M. West, J. C. Serrano-Ruiz, C. A. Gartner, J. A. Dumesic, *Science*, **2008**, *322*, 417-421.

[167] A. Boisen, T. B. Christensen, W. Fu, Y. Y. Gorbanev, T. S. Hansen, J. S. Jensen, S. K. Klitgaard, S. Pedersen, A. Riisager, T. Ståhlberg, J. M. Woodley, *Chem. Eng. Res. Des*., **2009**, *87*, 1318-1327.

[168] C. Moreau, M. N. Belgacem, A. Gandini, *Top. Catal*., **2004**, *27*, 11-30.

[169] B. M. F. Kuster, *Starch*, **1990**, 42, 314-321.

[170] J. N. Tan, M. Ahmara, Y. Queneau, *RSC Adv*., **2015**, *5*, 69238-69242.

[171] H. Cai, C. Li, A. Wang, T. Zhang, *Catal. Today*, **2014**, *234*, 59–65.

[172] J. M. Timko, D. J. Cram, *J. Am. Chem. Soc*., **1974**, *96*, 7159–7160.

[173] C. Zeng, H. Seino, J. Ren, K. Hatanaka, N. Yoshie, *Macromolecules*, **2013**, *46*, 1794–1802.

[174] S. Subbiah, S. P. Simeonov, J. M. S. S. Esperanca, L. P. N. Rebelo, C. A. M. Afonso, *Green Chem*., **2013**, *159*, 2849–2853.

[175] M. Chatterjee, T. Ishizaka, H. Kawanami, *Green Chem*., **2014**, *16*, 4734–4739.

[176] T. Wang, J. Zhang, W. Xie, Y. Tang, D. Guo, Y. Ni, *Catalysts*, **2017**, *7*, 92-99.

[177] Y. Zhu, X. Kong, H. Zheng, G. Ding, Y. Zhu, Y.W. Li, *Catal. Sci. Technol*., **2015**, *5*, 4208–4217.

[178] W. Hao, W. Li, X. Tang, X. Zeng, Y. Sun, S. Liu, L. Lin, *Green Chem*., **2016**, *18*, 1080-1088.

[179] F. Wang, Z. Zhang, *ACS Sustainable Chem. Eng*., **2017**, *5*, 942−947.

[180] Y. Roman-Leshkov, C. J. Barrett, Z. Y. Liu, J. A. Dumesic, *Nature*, **2007**, 447, 982–985.

[181] B. S. Solanki, C. V. Rode, *Green Chem*., **2019**, *21*, 6390-6406.

[182] J. B. Binder, R. T. Raines, *J. Am. Chem. Soc*., **2009**, *131*, 1979–1985.

[183] Y. Zu, P. Yang, J. Wang, X. Liu, J. Ren, G. Lu, Y. Wang, *Appl. Catal. B: Environ*., **2014**, *146*, 244–248.

[184] Q. Li, P. Man, L. Yuan, P. Zhang, Y. Li, S. Ai, *Molecular Catalysis*, **2017**, *431*, 32–38.

[185] A. S. Nagpure, N. Lucas, S. V. Chilukuri, *ACS Sustainable Chem. Eng*., **2015**, *3*, 2909–2916.

[186] G. H. Wang, J. Hilgert, F. H. Richter, F. Wang, H. J. Bongard, B. Spliethoff, C. Weidenthaler, F. Schüth, *Nat. Mater*., **2014**, *13*, 293–300.

[187] a) T. Thananatthanachon, T. B. Rauchfuss, *Angew. Chem., Int. Ed*., **2010**, 49, 6616–6618; b) M. Chidambaram, A. T. Bell, *Green Chem*., **2010**, *12*, 1253–1262.

[188] P. P. Upare, D. W. Hwang, Y. K. Hwang, U. H. Lee, D. Y. Hong, J. S. Chang, *Green Chem*., **2015**, *17*, 3310–3313.

[189] B. Saha, C. M. Bohn, M. M. Abu-Omar, *ChemSusChem*, **2014**, *7*, 3095–3101.

[190] X. Xiang, J. Cui, G. Ding, H. Zheng, Y. Zhu, Y. Li, *ACS Sustainable Chem. Eng*., **2016**, *4*, 4506–4510.

[191] Z. Wei, J. Lou, Z. Li, Y. Liu, *Catal. Sci. Technol*., **2016**, *6*, 6217–6225.

[192] R. Insyani, D. Verma, S. Min Kim, J. Kim, *Green Chem*., **2017**, *19*, 2482–2490.

[193] A. S. Amarasekara, D. Green, L. D. Williams, *Eur. Polym. J*., **2009**, *45*, 595–598.

[194] F. W. Lichtenthaler, *Acc. Chem. Res*., **2002**, *35*, 728−737.

[195] T. Shimo, S. Ueda, T. Suishu, K. Somekawa, *J. Heterocycl. Chem*., **1995**, *32*, 727−730.

[196] A. S. Amarasekara, D. Green, E. McMillan, *Catal. Commun*., **2008**, *9*, 286−288.

[197] a) W. Partenheimer, V. V. Grushin, *Adv. Synth. Catal*., **2001**, *343*, 102–111. b) G. A. Halliday, R. J. Young, V. V. Grushin, *Org. Lett*., **2003**, *5*, 2003–2005.

[198] C. Carlini, P. Patrono, A. M. R. Galletti, G. Sbrana, V. Zima, *Appl. Catal. A*, **2005**, *289*, 197–204.

[199] O. Casanova, A. Corma, S. Iborra, *Top. Catal*., **2009**, *52*, 304–314.

[200] J. Ma, Z. Du, J. Xu, Q. Chu, Y. Pang, *ChemSusChem*, **2011**, *4*, 51–54.

[201] Y. Wang, B. Liu, K. Huang, Z. Zhang, *Ind. Eng. Chem. Res*., **2014**, *53*, 1313−1319.

[202] J. Nie, J. Xie, H. Liu, *J. Catal*., **2013**, *301*, 83−91.

[203] T. S. Hansen, I. Sádaba, E. J. García -Suárez, A. Riisager, *Appl. Catal. A*, **2013**, *456*, 44−50.

[204] B. Liu, Z. Zhang, K. Lv, K. Deng, H. Duan, *Appl. Catal. A*, **2014**, *472*, 64−71.

[205] R. Liu, J. Chen, L. Chen, Y. Guo, J. Zhong, *ChemPlusChem*, **2014**, *79*, 1448−1454.

[206] D. R. Dreyer, H.-P. Jia, C. W. Bielawski, *Angew. Chem. Int. Ed*., **2010**, *49*, 6813−6816.

[207] S. H. Shinde, C. V. Rode, *Biomass, Biofuels, Biochemicals*, **2020**, 95-133.

[208] S. Rajendran, R. Raghunathan, I. Hevus, R. Krishnan, A. Ugrinov, M.P. Sibi, D.C. Webster, J. Sivaguru, *Angew. Chem. Int. Ed*., **2015**, *54*, 1159-1163.

[209] C. H. R. M. Wilsens, N. J. M. Wullems, E. Gubbels, Y. F. Yao, S. Rastogi, B. A. Noordover, *Polym. Chem*., **2015**, *6*, 2707-2716.

[210] S. S. Nagarkar, A. K. Chaudhari, S. K. Ghosh, *Cryst. Growth Des*., **2012**, *12*, 572-576.

[211] M. Rose, D. Weber, B. V. Lotsch, R. K. Kremer, R. Goddard, R. Palkovits, *Microporous Mesoporous Mater*., **2013**, *181*, 217-221.

[212] O. Casanova, S. Iborra, A. Corma, *ChemSusChem*, **2009**, *2*, 1138–1144.

[213] Y. Y. Gorbanev, S. K. Klitgaard, J. M. Woodley, C. H. Christensen, A. Riisager, *ChemSusChem*, **2009**, *2*, 672–675.

[214] T. Pasini, M. Piccinini, M. Blosi, R. Bonelli, S. Albonetti, N. Dimitratos, J. A. Lopez-Sanchez, M. Sankar, Q. He, C. J. Kiely, G. J. Hutchings, F. Cavani, *Green Chem*., **2011**, *13*, 2091–2099.

[215] B. Saha, S. Dutta, M. M. Abu-Omar, *Catal. Sci. Technol*., **2012**, *2*, 79–81.

[216] S. E. Davis, L. R. Houk, E. C. Tamargo, A. K. Datye, R. J. Davis, *Catal. Today*, **2011**, *160*, 55–60.

[217] Z. Miao, T. Wu, J. Li, T. Yi, Y. Zhang, X. Yang, *RSC Adv*., **2015**, *5*, 19823–19829.

[218] R. D. Parate, M. S. Dharne, C. V. Rode, *Biomass Bioenergy*, **2022**, *161*, 106474.

[219] M. Mascal, E. B. Nikitin, *Angew. Chem., Int. Ed*. **2008**, *47*, 7924-7926.

[220] G. J. M. Gruter, F. Dautzenberg, U.S. Patent Appl. 2011/0082304A1, **2011**.

[221] H. O. Silva, P. G. de Pinho, B. P. Machado, T. Hogg, J. C. Marques, J. S. Camara, F. Albuquerque, A. C. S. Ferreira, *J. Agric. Food Chem*., **2008**, *56*, 11989-11996.

[222] G. J. M. Gruter, US 2010/0218416 A1, **2010**.

[223] E. J. Ras, S. Maisuls, P. Haesakkers, G. J. Gruter, G. Rothenberg, *Adv. Synth. Catal*., **2009**, *351*, 3175–3185.

[224] M. Balakrishnan, E. R. Sacia, A. T. Bell, *Green Chem*., **2012**, *14*, 1626–1634.

[225] G. J. M. Gruter, US8277521B2, **2012**.

[226] J. Jae, E. Mahmoud, R. F. Lobo, D. G. Vlachos, *ChemCatChem*, **2014**, *6*, 508–513.

[227] J. D. Lewis, S. V. de Vyver, A. J. Crisci, W. R. Gunther, V. K. Michaelis, R. G. Griffin, Y. Roman-Leshkov, *ChemSusChem*, **2014**, *7*, 2255–2265.

[228] J. Luo, J. Yu, R. J. Gorte, E. Mahmoud, D. G. Vlachos, M. A. Smith, *Catal. Sci. Technol*., **2014**, *4*, 3074–3081.

[229] S.H. Shinde, C. V. Rode, *ChemSusChem*, **2017**, *10*, 4090-4101.

[230] P. Maki-Arvela, E. Salminen, T. Riitonen, P. Virtanen, N. Kumar, J. P. Mikkola, *Int. J. Chem. Eng*., **2012**, ID674761.

[231] T. Thananatthanachon, T. B. Rauchfuss, *Angew. Chem*., **2010**, *122*, 6766-6768.

[232] G. J. M. Gruter, US2010/0212218, **2010**.

[233] A. J. Sanborn, US2009/0156841, **2009**.

[234] M. Mascal, US2009/ 0234142, **2009**.

[235] M. K. Jogia, V. Vakamoce, R. T. Weavers, *Aust. J. Chem*. **1985**, *38*, 1009-1016.

[236] A. C. Cope, US3079449, **1963**.

[237] H.-L. Dai, Q. Shen, J.-B. Zheng, J.-Y. Li, R. Wen, J. Li, *Lett. Org. Chem*., **2011**, *8*, 526-530.

[238] E.-S. Kang, Y.-W. Hong, D. W. Chae, B. Kim, B. Kim, Y. J. Kim, J. K. Cho, Y. G. Kim, *ChemSusChem,* **2015**, *8*, 1179-1188.

[239] a) J. K. Kim, S. W. Kim, K. O. Oh, S. Y. Ko, J. Y. Kim, B. E. Lee, B. T. Kim, Y. S. Lee, Y. K. Min, N. K. Park, Oscotec Inc.; Korea research institute of chemical technology, WO 2004/037804, **2004**; b) J. K. Kim, S. W. Kim, K. O. Oh, J. Y. Kim, B. E. Lee, B. T. Kim, Y. S. Lee, Y. K. Min, N. K. Park, US 2008/ 0221205, **2008**; c) J. B. Zheng, J. Li, R. Wen, J. Y. Li, H. L. Dai, Q. Shen, CN 101775008 A 20100714, **2010**.

[240] M. Krystof, M. Perez-Sanchez, P. Dominguez de Maria, *ChemSusChem*, **2013**, *6*, 630-634.

[241] a) G. J. M. Gruter, F. Dautzenberg, Avantium International B.V., WO 2007/104514, **2007**; b) G. J. M. Gruter, L. E. Manzer, A. S. V. De Sousa Dias, F. Dautzenberg, J. Purmova, Furanix Technologies B.V., WO 2009/030512, **2009**; c) G. J. M. Gruter, F. Dautzenberg, Furanix Technologies B.V., US 2009/131690, **2009**; d) G. J. M. Gruter, L. E. Manzer, Furanix Technologies B.V., US 2010/0058650, **2010**; e) G. J. M. Gruter, Furanix Technologies B.V. US 2010/0083565, **2010**; f) G. J. M. Gruter, L. E. Manzer, Furanix Technologies B.V., US 2010/ 0218415, **2010**.

[242] S. Shinde, K. Deval, R. Chikate, C. Rode, *ChemistrySelect*, **2018**, *3*, 8771-8779.

[243] C. F. H. Allen, J. W. Gates Jr., "o-Eugenol", *Organic Syntheses.; Collective*, **1955**, *3*, 418.

[244] L. J. Esposito, K. Formanek, G. Kientz, F. Mauger, V. Maureaux, G. Robert, F. Truchet, KirkeOthmer Encyclopedia of Chemical Technology, fourth ed., John Wiley & Sons, New York, NY, **1997**, *24*, 812-825.

[245] K. Li, J. W. Frost, *J. Am. Chem. Soc*., **1998**, *120*, 10545–10546.

[246] L. J. Esposito, K. Formanek, G. Kientz, F. Mauger, V. Maureaux, G. Robert, F. Truchet, Van Nostrand's Encyclopedia of Chemistry, ed. G.D. Considine, John Wiley & Sons, Ltd., **2005**, 1.

[247] L. Yang, W. Zhou, K. Seshan, Y. Li, *J. Mol. Catal. A: Chem*., **2013**, 368–369, 61–65.

[248] N. Mahé, B. Nicolaï, M. Barrio, M.-A. Perrin, B. Do, J.-L. Tamarit, R. Céolin, I. B. Rietveld, *Cryst. Growth Des*., **2013**, *13*, 3028–3035.

[249] A. A. Khalil, U. U. Rahman, M. R. Khan, A. Sahar, T. Mehmood, M. Khan, *RSC Adv*., **2017**, *7*, 32669–32681.

[250] S. L. Bhanawase, G. D. Yadav, *Catal. Today*, **2017**, *291*, 213–222.

[251] P. C. Rodrigues Pinto, E. A. Borges da Silva, A. E. Rodrigues, Biomass Conversion: The Interface of Biotechnology, Chemistry and Materials Science, ed. C. Baskar, S. Baskar and R. S. Dhillon, Springer Berlin Heidelberg, Berlin, Heidelberg, **2012**, 381.

[252] https://www.factmr.com/report/513/eugenol-market.

[253] https://www.marketresearchhub.com/report/global-guaifenesin-api-sales-market-report-2018-report.%20html.

[254] P. J. Deuss, M. Scott, F. Tran, N. J. Westwood, J. G. de Vries, K. Barta, *J. Am. Chem. Soc*., **2015**, *137*, 7456–7467.

[255] R. Bal, M. Tada, T. Sasaki, Y. Iwasawa, *Angew. Chem., Int. Ed*., **2006**, *45*, 448–452.

[256] X. Shen, Q. Meng, Q. Mei, H. Liu, J. Yan, J. Song, D. Tan, B. Chen, Z. Zhang, G. Yang, B. Han, *Chem. Sci*, **2020**, *11*, 1347-1352.

[257] M.M. Ambursa, P. Sudarsanam, L.H. Voon, S.B.A. Hamid, S.K. Bhargava, *Fuel Process. Technol*., **2017**, *162*, 87-97.

[258] S. Qiu, Y. Xu, Y. Weng, L. Ma, T. Wang, *Catalysts*, **2016**, *6* (9), 134.

[259] S. B. A. Hamid, M. M. Ambursa, P. Sudarsanam, L. H. Voon, S. K. Bhargava, *Catal. Commun*., **2017**, *94*, 18-22.

[260] H. Zhang, Y. Wang, S. Shao, R. Xiao, *Sci. Rep*., **2016**, *6* (1), 37513.

[261] T. Nimmanwudipong, R. C. Runnebaum, D. E. Block, B. C. Gates, *Energy Fuels*, **2011**, *25*, 3417-3427.

[262] R. F. Nunes, D. Costa, A. M. Ferraria, A. M. Botelho do Rego, F. Ribeiro, A. Martins, A. Fernandes, *Molecules*, **2023**, *28*, 2245.

[263] H. Yang, X. Zhu, H.W. Amini, B. Fachri, M. Ahmadi, G.H. ten Brink, P.J. Deuss, H.J. Heeres, *Appl. Catal. A Gen*. **2023**, *654*, 119062.

[264] F. G. Baddour, V. A. Witte, C. P. Nash, M. B. Griffin, D. A. Ruddy, J. A. Schaidle, *ACS Sustain. Chem. Eng*. **2017**, *5*, 11433–11439.

[265] C.-C. Tran, O. Mohan, A. Banerjee, S. H. Mushrif, S. Kaliaguine, *Energy Fuel*, **2020**, *34*, 16265–16273.

[266] M. Corbet, P. Metivier, F. Decampo, US20150119606A1.

[267] S. Ren, Z. Wu, Q. Guo, B. Shen, *Catal. Lett.*, **2015**, *145*, 712–714.

[268] M. M. Bomgardner, *Chem. Eng. News*, **2014**, *92*, 14.

[269] E. Borges da Silva, M. Zabkova, J. Araújo, C. Cateto, M. Barreiro, M. Belgacem, A. E. Rodrigues, *Chem. Eng. Res. Des*., **2009**, *87*, 1276-1292.

[270] F. Liguori, C. Moreno-Marrodan, P. Barbaro, *Chem. Soci. Rev*., **2020**, *49*, 6329-6363.

[271] R. Nie, X. Peng, H. Zhang, X. Yu, X. Lu, D. Zhou, Q. Xia, *Catal. Sci. Technol*., **2017**, *7*, 627-634.

[272] A. Jia, X. Yao, L. Feng, Z. Ma, F. Li, Y. Wang, *Eur. J. Inorg. Chem*., **2020**, *13*, 1184-1191.

[273] W. Wang, Y. Yang, H. Luo, W. Liu, *React. Kinet., Mech. Catal*., **2010**, *101*, 105-115.

[274] M. Duan, Q. Cheng, M. Wang, Y. Wang, *RSC Adv*., **2021**, *11*, 10996-11003.

[275] D. Sachdev, A. Dubey, B. G. Mishra, S. Kannan, *Catal Commun*, **2008**, *9*, 391-394.

[276] M. Fache, E. Darroman, V. Besse, R. Auvergne, S. Caillol, B. Boutevin, *Green Chem*, **2014**, *16*, 1987-1998.

[277] M. Gitzinger, C. Kemmer, D. A. Fluri, M. Daoud El-Baba, W. Weber, M. Fussenegger, *Nucl Acids Res*, **2011**, *40*(5), 37.

[278] S. Rautiainen, J. Chen, M. Vehkama¨ki, T. Repo, *Top Catal*., **2016**, *59*, 1138–1142.

[279] I. Chorkendorff, J. W. Niemantsverdriet*, Concepts of Modern Catalysis and Kinetics, John Wiley & Sons, **2003**,* 696.

[280] G. Rothenberg*, Catalysis : concepts and green applications, Wiley-VCH, Weinheim ; Chichester,* **2008.**

[281] M. Bowker*, The Basis and Applications of Heterogeneous Catalysis, Oxford University Press, New York,* **1998***.*

[282] D. J. Cole-hamilton*, Science,* **2003***, 299,* 1702–1706*.*

[283] S. Chassaing, V. Bénéteau, P. Pale, Curr. Opin. *Green Sustain. Chem*., **2018**, *10*, 35–39.

[284] S. P. Gabriele Centi, *Catal. Today*, **2003**, *77*, 287–297.

[285] F. Sanchez, D. Motta, A. Roldan, C. Hammond, A. Villa, N. Dimitratos, *Top. Catal.*, **2018**, *61*, 1–13.

[286] K. Wei, X. Wang, R. A. Budiman, J. Kang, B. Lin, F. Zhou, Y. Ling, *J. Mater. Sci.*, **2018**, *53*, 1–19*.*

[287] G. W. Huber, J. W. Shabaker, J. Dumesic, *Science*, **2003**, *300*, 2075–2078.

[288] S. Varadarajan, D. J. Miller, *Biotechnol. Prog*, **1999**, *15*, 845–854.

[289] A. L. de Lima, C. M. Ronconi, C. J. A. Mota, *Catal. Sci. Technol.*, **2016**, *6*, 2877–2891.

[290] I. Santamaría-Holek, S. I. Hernández, C. García-Alcántara, A. Ledesma-Durán, *Catalysts*, **2019**, *9*, 281.

[291] E. Marceau, X. Carrier, M. Che, O. Clause, Handbook of Heterogeneous Catalysis ed. J. W. G. Ertl, H. Knozinger, F. Schuth, **2008**, 467–484.

[292] Z. Qu, W. Huang, S. Zhou, H. Zheng, X. Liu, M. Cheng and X. Bao, *J. Catal*., **2005**, *234*, 33–36.

[293] F. K. E. M. Holt, G.J. Kelly, Reactor Design for Chemical Engineers, ed. J. M. W. and M. B. King, **1999**, 276–300.

[294] O. Deutschmann, H. Knözinger, K. Kochloefl, T. Turek, *Heterogeneous Catalysis and Solid Catalysts*, **2009.**

[295] B. Uysal, B. S. Oksal, *Res. Chem. Intermed.*, **2015**, *41*, 3893–3911.

[296] N. Shibasaki-Kitakawa, H. Honda, H. Kuribayashi, T. Toda, T. Fukumura, T. Yonemoto, *Bioresour. Technol*., **2007**, *98*, 416–421.

[297] S. Bagheri, N. Muhd Julkapli, S. Bee Abd Hamid, *ScientificWorldJournal,* **2014**, 727496–727517.

[298] J. M. Planeix, N. Coustel, B. Coq, V. Brotons, P. S. Kumbhar, R. Dutartre, P. Geneste, P. Bernier, P. M. Ajayan, *J. Power Sources*, **1994**, *116*, 7935–7936.

[299] P. D. Kent, J. E. Mondloch, R. G. Finke, *J. Am. Chem. Soc*., **2014**, *136*, 1930–1941.

[300] E. Guibal, *Prog. Polym. Sci.*, **2005**, *30*, 71–109.

[301] N. Masoud, B. Donoeva, P. E. de Jongh, *Appl. Catal. A Gen.*, **2018**, *561*, 150–157.

[302] S. De, S. Dutta, B. Saha, *Catal. Sci. Technol*., **2016**, *6*, 7364–7385.

[303] P. McMorn, G. J. Hutchings, *Chem. Soc. Rev*. **2004**, *33*, 108-122.

[304] C. W. Jones, M. W. McKittrick, J. V. Nguyen, K. Yu, *Top Catal*. **2005**, *34*, 67-76.

[305] J. A. Melero, R. V. Grieken, G. Morales, *Chem. Rev.* **2006**, *106*, 3790

[306] T. Cheng, Q. Zhao, D. Zhang, G. Liu, *Green Chem*., **2015**, *17*, 2100-2122.

[307] S. Laurent, D. Forge, M. Port, A. Roch, C. Robic, L. Vander Elst, R. N. Muller, *Chem. Rev.* **2008**, *108*, 2064-2110.

[308] A. Lu, E. L. Salabas, F. Schüth, *Angew. Chem. Int. Ed*. **2007**, *46*, 1222-1244.

[309] F. Hussain, M. Hojjati, M. Okamoto, R. J. Gorga, *Compos. Mater.* **2006**, *40*, 1511.

[310] M. Hughes, P. Miranda, D. Nielsen, E. Rosenberg, R. Gobetto, A. Viale, S. Burton, *Macromol. Symp*. **2006**, *235*, 161.

[311] C. S. Gill, W. Long, C. W. Jones, *Catal. Lett.* **2009**, *131*, 425-431.

[312] C. S. Gill, K. Venkatasubbaiah, N. T. S. Phan, M. Weck, C. W. Jones, *Chem. Eur. J.* **2008**, *14*, 7306-7313.

[313] W. Long, C. W. Jones, *ACS Catalysis*, **2011**, *1*, 674-681.

[314] J. N. Coleman, U. Khan, Y. K. Gun'ko, *Adv. Mater*. **2006**, *18*, *689*. 2-4.

[315] P. Liu, *Eur. Polym. J*. **2005**, *41*, 2693-2703.

[316] R. Guillet-Nicolas, L. Marcoux, F. Kleitz, *New J. Chem*., **2010**, *34*, 355-366.

[317] M. Choi, F. Kleitz, D. Liu, H. Y. Lee, W.S. Ahn, R. J. Ryoo, *Am. Chem. Soc.* **2005**, *127*, 1924-1932.

[318] B. I. N. Zhao, X. Jiang, D. Li, X. Jiang, T. G. O. Lenick, B. Li, C. Y. Li, *J. Polym. Sci.*, *Part A: Polym. Chem.* **2008**, *46*, 3438-3446.

[319] X. Jiang, B. Wang, C. Y. Li, B. I. N. Zhao, *J. Polym. Sci., Part A: Polym. Chem*. **2009**, *47*, 2853-2870.

[320] F. Costantini, W. P. Bula, R. Salvio, J. Huskens, H. J. G. E.Gardeniers, D. N. Reinhoudt, W. Verboom, *J. Am. Chem. Soc.* **2009**, *131*, 1650-1651.

[321] F. Costantini, E. M. Benetti, R. M. Tiggelaar, H. J. G. E. Gardeniers, D. N. Reinhoudt, J. Huskens, G. J. Vancso, W. Verboom, *Chem. Eur. J.* **2010**, *16*, 12406-12411.

[322] C. Li, J. Yang, P. Wang, J. Liu, Q. Yang, *Micropor. Mesopor. Mater*. **2009**, *123*, 228-233.

[323] A. Martín, G. Morales, F. Martínez, R. van Grieken, L. Cao, M. Kruk, *J. Mater. Chem.* **2010**, *20*, 8026-8035.

[324] T. Okayasu, K. Saito, H. Nishide, M. T. W. Hearn, *Chem. Commun*. **2009**, 4708-4710.

[325] T. Okayasu, K. Saito, H. Nishide, M. T. W. Hearn, *Green Chem*. **2010**, *12*, 1981-1989.

[326] Y. Jiang, Q. J. Gao, *Am. Chem. Soc.* **2006**, *128*, 716.

[327] E. J. Delaney, L. E. Wood, I. M. Klotz, *J. Am. Chem. Soc.* **1982**, *104*, 799-807.

[328] M. A. Hierl, E. P. Gamson, I. M. Klotz, *J. Am. Chem. Soc*. **1979**, *101*, 6020-6022.

[329] S. Shinkai, H. Tsuji, Y. Hara, O. Manabe, *Bull. Chem. Soc. Jpn*. **1981**, *54*, 631.

[330] M. Tomoi, Y. Akada, H. Kakiuchi, *Makromol. Chem. Rapid Commun.* **1982**, 3, 537.

[331] F. M. Menger, D. J. McCann, *J. Org. Chem*. **1985**, *50*, 3928-3930.

[332] A. Deratani, G. D. Darling, D. Horak, J. M. Frechet, *J. Macromolecules*, **1987**, *20*, 767-772.

[333] W. M. Van Rhijn, D. E. De Vos, B. F. Sels, W. D. Bossaert, *Chem. Commun.* **1998**, 317–318.

[334] M. Shaker, D. Elhamifar, *Front. Energy Res*. **2020**, *8*, 78.

[335] K. Niknam, D. Saberi, M.N. Sefat, *Tetrahedron Lett*. **2009**, *50*, 4058–4062.

[336] K. Niknam, D. Saberi, *Appl. Catal. A Gen*. **2009**, *366*, 220–225.

[337] S. Moradi, M.A. Zolfigol, M. Zarei, D. A. Alonso, A. Khoshnood, A. Tajally, *Appl. Organomet. Chem.* **2017**, *32*, 4043-4061

[338] M. Balakrishnan, E. R. Sacia, A. T. Bell, *ChemSusChem*, **2014**, *7*, 1078-1085.

[339] S. Safaei, I. Mohammadpoor-Baltork, A. R. Khosropour, M. Moghadam, S. Tangestaninejad, V. Mirkhani, *J. Iran. Chem. Soc*. **2017**, *14*, 1583–1589.

[340] E.-P. Ng, S. N. M. Subari, O. Marie, R. R. Mukti, J.-C. Juan, *Appl. Catal. A Gen.* **2013**, *450*, 34–41.

[341] S. R. Jetti, A. Bhatewara, T. Kadre, S. Jain, *Chin. Chem. Lett.* **2014**, *25*, 469–473.

[342] A. Ghorbani-Choghamarani, F. Ghorbani, Z. Yousofvand, G. Azadi, *J. Porous Mater.* **2015**, *22*, 665–673.

[343] A. Gharib, N. N. Pesyan, B. R. H. Khorasani, M. Roshani, J. W. Scheeren, *Bulg. Chem. Commun*. **2013**, *45*, 371–378.

[344] W. Xie, D. Yang, *Bioresour. Technol*. **2011**, *102*, 9818–9822.

[345] K. Niknam, D. Saberi, *Tetrahedron Lett.* **2009**, *50*, 5210–5214.

[346] H. A. Beejapur, V. La Parola, L. F. Liotta, M. L. Testa, *ChemistrySelect,* **2017**, *2*, 4934–4941.

[347] B. Lindlar, M. Lüchinger, A. Röthlisberger, M. Haouas, G. Pirngruber, A. Kogelbauer, R. Prins, *J. Mater. Chem.* **2002**, *12*, 528–533.

[348] A. Mobaraki, B. Movassagh, B. Karimi, *ACS Comb. Sci*. **2014**, *16*, 352–358.

[349] K. B. Sidhpuria, A. L. Daniel-da-Silva, T. Trindadea, J. A. P. Coutinho, *Green Chem*. **2011**,*13*, 340-349.

[350] Y. B. Park, P. Kasinathan, *J. Thermodyn Catal*, *13, 2*, 1000293.

[351] H. Li, Q. Zhang, S. Yang, *International Journal of Chemical Engineering*, **2014**, *12*, 1-7.

[352] Z. Xu, H. Wan, J. Miao, M. Han, C. Yang, G. Guan, *J. Mol. Cat. A: Chem.*, **2010**, *332*, 152-157.

[353] W. Senapak, R. Saeeng, U. Sirion, *RSC Adv*., **2017**, *7*, 30380.

Chapter – 2

Magnetic Solid Base Catalyst for Knoevenagel Condensation of Furfural with Acetyl acetone

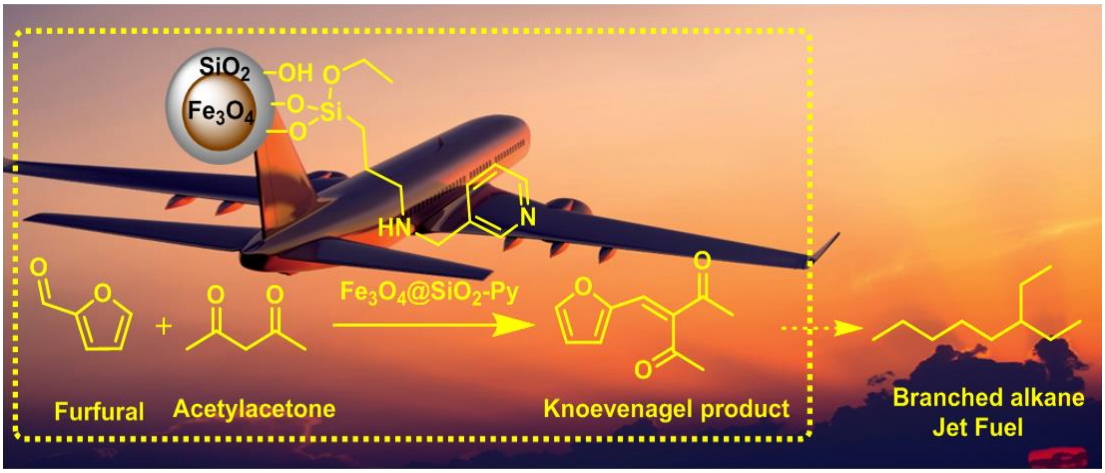

The Knoevenagel condensation is a valuable synthetic organic reaction for forming C-C bonds between carbonyl functionalities and active methylene compounds. The resulting α, β-unsaturated products serve as key intermediates in the synthesis of fine chemicals, pharmaceuticals, cosmetics, and products for the food and agrochemical industries. In this study, a novel heterogeneous catalyst, pyridine-immobilized magnetic silica (Fe_3O_4@SiO_2-Py) was developed and evaluated for the Knoevenagel condensation of furfural with acetylacetone. This catalyst demonstrated high efficiency under optimized reaction conditions. The Knoevenagel condensation product, 3-(2-furylmethylene)-2,4-pentanedione (FMP), a precursor for jet fuel, was produced in a high yield of 85% with a 94% conversion of furfural at 100°C within 4 hours. The Fe_3O_4@SiO_2-Py catalyst exhibited excellent stability and recyclability, maintaining its initial activity over multiple cycles. Comprehensive characterization of the catalyst was performed using FTIR, NMR, XRD and TEM techniques.

Komal Tarade, Suhas Shinde, Sachin Sakate and Chandrashekhar Rode, **Catalysis Communication,** 2019, 124, 81-85

2.1. Introduction

Currently, chemicals and liquid fuels are primarily produced from crude oil. However, crude oil sources are on the verge of depletion in the near future. Moreover, the refining of crude oil results in the release of significant amounts of CO_2, contributing to severe air pollution. Fortunately, these challenges can be addressed by utilizing lignocellulosic biomass as a sustainable carbon source and a green alternative to crude oil [1]. Furfural, a critical platform molecule, is produced through the hydrolysis and dehydration of xylan found in lignocellulosic biomass. Diesel-range long-chain alkanes can be synthesized from furfural via acid or base-catalysed C–C bond formation followed by hydrodeoxygenation [2,3]. In this context, carbon upgrading of furfural can be achieved through reactions such as aldol and Knoevenagel condensations [4,5], Baylis−Hillman coupling reactions [6,7] and the HAA reaction [8–10]. These upgraded products are carbon-rich and can be further converted into liquid hydrocarbons through ring-opening, dehydration, and hydrodeoxygenation processes [11,12].

2.2. Literature Survey

The Knoevenagel condensation of furfural with acetylacetone has not been extensively studied. For example, Ding et al. demonstrated an enzyme-catalysed Knoevenagel condensation between furfural and acetylacetone using lipoprotein lipase at 35°C. However, this catalytic system required a lengthy reaction time of 48 hours and resulted in a moderate yield of 76% in dimethyl sulfoxide solvent [13]. More recently, Appaturi et al. developed an alanine-functionalized MCM-41 catalyst for the Knoevenagel condensation of furfural with acetylacetone. This catalyst system achieved 100% selectivity for α,β-unsaturated products with a 92% conversion of furfural under solvent-free conditions and a short reaction time of 30 minutes [5]. Additionally, various organic–inorganic hybrid materials containing nitrogen-based functionalities, such as pyridine-functionalized porous polymers [14], DABCO-based ionic liquids [15], primary amine-functionalized MCM-41 [16,17] and organic polymers [18] have been successfully employed for the Knoevenagel condensation of active methylene compounds with aldehydes.

2.3. Scope of the Present Work

With the above background we report here a novel magnetically separable silica immobilised pyridine (Fe_3O_4@SiO_2-Py) (Scheme 3.2) as an effective solid base catalyst that shows excellent performance for the Knoevenagel condensation of

furfural with acetyl acetone (Scheme 2.1). Fe_3O_4@SiO_2-Py catalyst showed the highest furfural conversion of 94% with 85% yield of condensation product at 100 °C in the absence of any solvent. Magnetic nature of this catalyst allows us to effortlessly separate it from reaction mixture using an external magnetic field. This feature not only minimizes handling losses but also ensures sustained catalyst activity over multiple cycles without significant decrease in its activity.

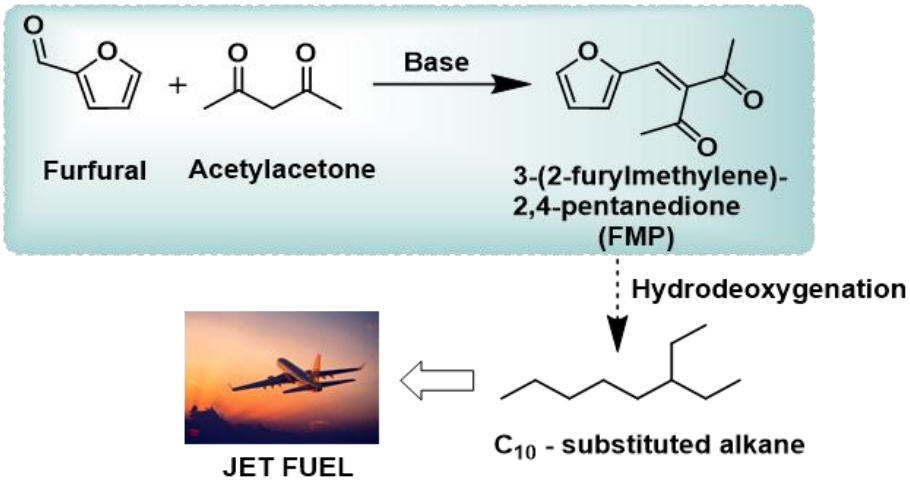

Scheme 2.1. Synthesis of Jet fuel precursors from furfural and acetyl acetone

2.4. Experimental Section

2.4.1. Materials

Furfural, N,N-dimethylaminopyridine, furfurylamine, DBU, 4-hydroxypyridine, 3-pyridinecarbaldehyde, 3-aminopropyltriethoxysilane, tetraethyl orthosilicate, $FeCl_2$ and $FeCl_3$ were purchased from Sigma Aldrich. Sodium hydroxide, triethylamine, zinc oxide, calcium oxide and aq. ammonia (10% *w/v*) were obtained from Thomas-Baker. Acetylacetone was sourced from Merck, India. Methanol, toluene, pyridine, dichloromethane, ethyl acetate, petroleum ether and silica gel (230–400 mesh) were purchased from Chem Labs, India.

2.4.2. Catalyst synthesis

2.4.2.1. Preparation of 3-aminopropylsilica

To a solution of 3-aminopropyltriethoxysilane (3.5 g) in toluene: pyridine (1:1, 20 mL), SiO_2 (2 g, 230–400 mesh) was added. The resulting mixture was refluxed for 24 hours under a nitrogen atmosphere. After the reaction, the mixture was filtered and the

residue was washed sequentially with toluene (20 mL × 1) and dichloromethane (20 mL × 1). The residue was then dried in an oven for 24 hours, yielding 4.8 g of an off-white powder.

2.4.2.2. Preparation of silica-pyridine (SiO_2-Py)

Step 1: 1-(pyridin-3-yl)-N-(3-(triethoxysilyl)propyl)methanimine
A mixture of 1.8 g of 3-aminopropyltriethoxysilane (AMPSi), 3-pyridinecarbaldehyde (0.877 g) and dichloromethane (25 mL) was heated at 50°C with continuous stirring for 24 h. The solvent was then evaporated under vacuum using a rotary evaporator, yielding a colourless oil (2.5 g).

Step 2: 1-(pyridin-3-yl)-N-(3-(triethoxysilyl)propyl)methanimine-silica
To a solution of 1-(pyridin-3-yl)-N-(3-(triethoxysilyl)propyl)methanimine (2.5 g) in toluene (20 mL), SiO_2 (1.7 g, 230–400 mesh) was added lot wise. The resulting heterogeneous mixture was refluxed with stirring for 24 hours under a nitrogen atmosphere. Then, mixture was filtered and residue was washed with toluene (20 mL × 1) and dichloromethane (20 mL × 1). The obtained residue was dried in an oven for 24 h to afford off white powder (4.0 g) of desired product.

Step 3: N-(pyridin-3-ylmethyl)propylamino-silica [19]
A mixture of 1-(pyridin-3-yl)-N-(3-(triethoxysilyl)propyl)methaniminesilica (3.5 g) and methanol (25 mL) was cooled to 0 °C and $NaBH_4$ (0.619 g) was added lot wise under stirring. The reaction mixture was then allowed to warm to room temperature and stirred for an additional 24 hours. The solvent was evaporated to dryness, yielding an off-white powder (3.2 g).

2.4.2.3. Synthesis of nano-magnetite particles (Fe_3O_4)

A solution of $FeCl_2$ (5.4 g) and $FeCl_3$ (2 g) in aqueous hydrochloric acid (2 M, 25 mL) was sonicated at room temperature until the salts completely dissolved. To this solution, an aqueous ammonia solution (25% *w*/*v*, 40 mL) was added slowly under argon atmosphere followed by stirring for 30 minutes. The resulting Fe_3O_4 nanoparticles were separated using an external magnet then washed with deionized water (3 × 50 mL) and ethanol (3 × 50 mL). The nanoparticles were subsequently dried under vacuum (Scheme 2.2).

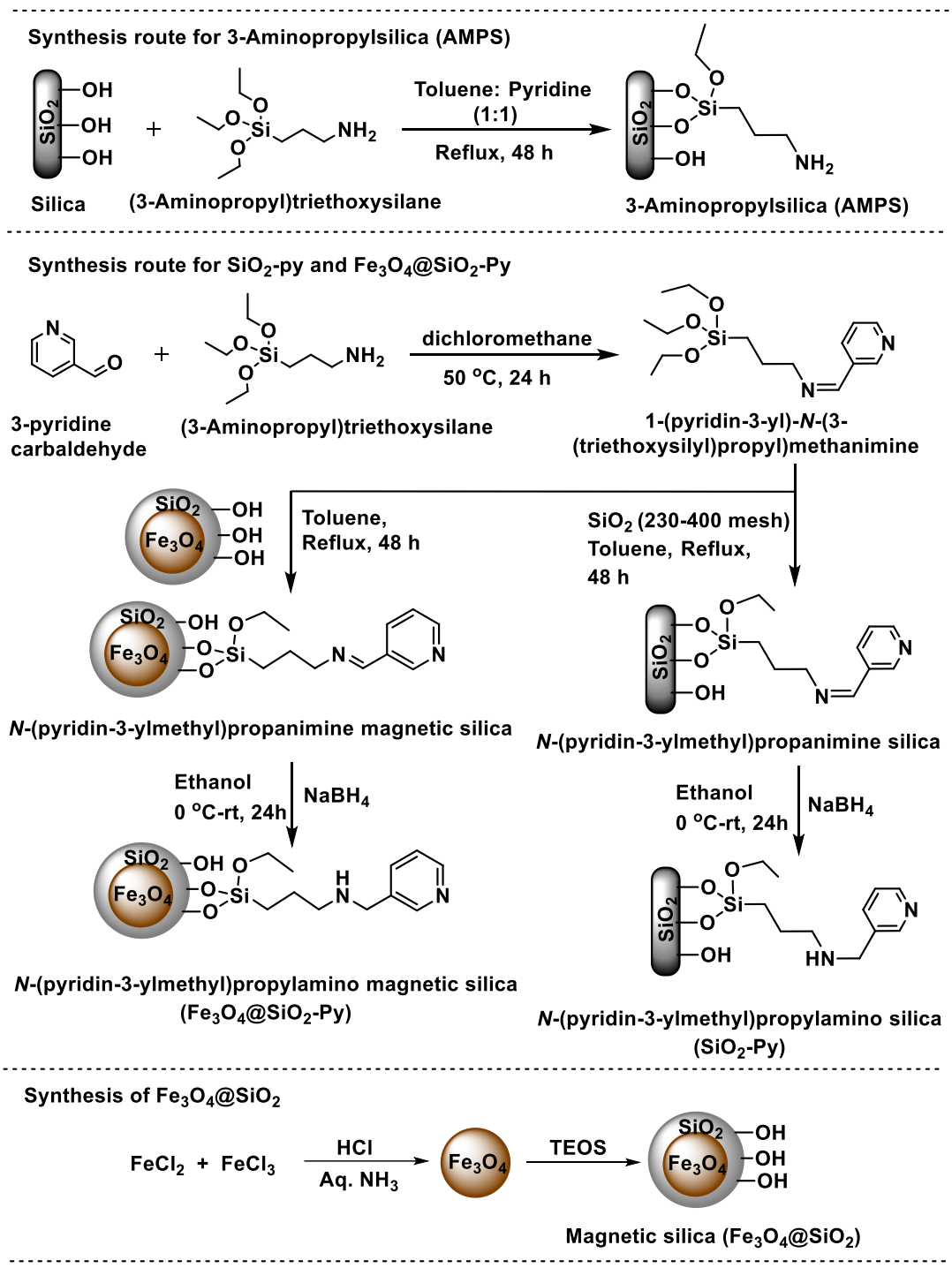

Scheme 2.2. Synthesis routes for 3-Aminopropylsilica, Fe_3O_4@SiO_2-Py and SiO_2-Py and Fe_3O_4@SiO_2

2.4.2.4. Synthesis of silica-coated magnetite nanoparticles (Fe_3O_4@SiO_2)

The synthesized Fe_3O_4 nanoparticles were suspended in a mixture of 35 mL ethanol and 6 mL deionized water. The resulting heterogeneous mixture was sonicated for 15

minutes. After sonication, 1.5 mL of tetraethyl orthosilicate (TEOS) was slowly added, and the mixture was sonicated for an additional 10 minutes. Subsequently, aqueous ammonia (10% w/v, 1.4 mL) was slowly added under stirring, and the mixture was heated to 40°C for 12 hours. The iron oxide nanoparticles coated with a thin layer of silica (Fe_3O_4@SiO_2) were then separated using an external magnet, washed three times with ethanol (3 × 50 mL), and dried under vacuum.

2.4.2.5. Preparation of Fe_3O_4@SiO_2-Py

To a solution of 1-(pyridin-3-yl)-N-(3-(triethoxysilyl)propyl)methanimine (2.5 g) in toluene (20 mL), Fe_3O_4@SiO_2 (10 g) was gradually added. The resulting mixture was refluxed for 24 hours under a nitrogen atmosphere and then filtered. The residue was washed with toluene (20 mL × 1) and dichloromethane (20 mL × 1) and then dried in an oven for 24 hours, yielding 4.0 g of an off-white powder of 1-(pyridin-3-yl)-N-(3-(triethoxysilyl)propyl)methanimine magnetic silica. Subsequently, a mixture of 1-(pyridin-3-yl)-N-(3-(triethoxysilyl)propyl)methanimine magnetic silica (4.0 g) and methanol (25 mL) was cooled to 0°C, and $NaBH_4$ (0.69 g) was gradually added. The resultant mixture was stirred at room temperature for 24 hours, and the solvent was evaporated to yield 3.6 g of off-white powder, identified as Fe_3O_4@SiO_2-Py.

2.4.3. Catalyst test

A mixture of furfural (0.192 g, 2 mmol), acetylacetone (0.2 g, 2 mmol), and Fe_3O_4@SiO_2-Py (0.1 g) was stirred at 100 °C for 4 hours. After the reaction, the catalyst was separated using an external magnet and the resultant mixture was diluted with ethyl acetate (20 mL × 1). The mixture was then washed sequentially with water (20 mL × 1) and brine solution (20 mL × 1). The organic layer was separated, dried over sodium sulphate, and evaporated under reduced pressure. The resulting crude oil was purified by column chromatography with an ethyl acetate: petroleum ether (2:98; v/v) eluent to yield a yellowish-brown liquid. The catalyst was recovered using an external magnet, and after decanting the reaction mass, the catalyst was washed with ethyl acetate and reused for subsequent reactions.

2.4.4. Analysis of reaction crude

Thin-layer chromatography (TLC) was performed on Merck 5554 aluminum-backed silica plates and compounds were visualized under UV light (254 nm). Pure products were characterized and confirmed by ^{1}H-NMR and ^{13}C-NMR using $CDCl_3$ (0.01%, TMS) as the solvent on a 200 MHz Bruker instrument.

An analytical method based on High-Performance Liquid Chromatography (HPLC) was developed and validated to monitor the synthesis of the Knoevenagel condensation product 3-(2-furylmethylene)-2,4-pentanedione (FMP) from furfural and acetylacetone using Fe_3O_4@SiO_2-Py as the catalyst. The conversion of furfural and yield of the condensation product were calculated using an Agilent HPLC system (column: Chromolith High Resolution RP-18e, detector: UV at 254 nm, mobile phase: Millipore water (60:40; v/v) with a flow rate of 0.3 mL/min). System calibration was performed by using external standard method. The standard solutions (having concentrations of 5 levels each) for furfural and FMP were prepared by dissolving requisite amounts of individual standards in methanol (solvent) using 10 mL of volumetric flasks. The data on concentrations of analytical standards and the peak areas is shown in Figure 2.1 and 2.2 (which was used for system calibration).

The samples for analysis withdrawn from reaction mixture were diluted in methanol (solvent) in such a way that their estimated concentrations will fall in a specified calibrated range of respective standards, namely furfural and FMP. The concentrations (ppm values) for furfural and FMP in a particular reaction sample were determined by putting corresponding peak areas in the linear equation, $y=mx+c$ of a particular component. The weight% concentrations were determined by applying dilution factor that was applicable for a particular set of reaction samples.

.

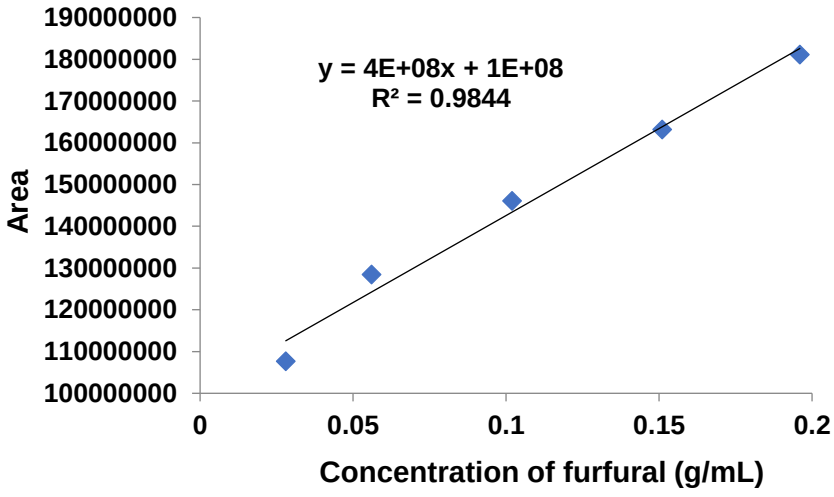

Figure 2.1. Calibration curve for furfural

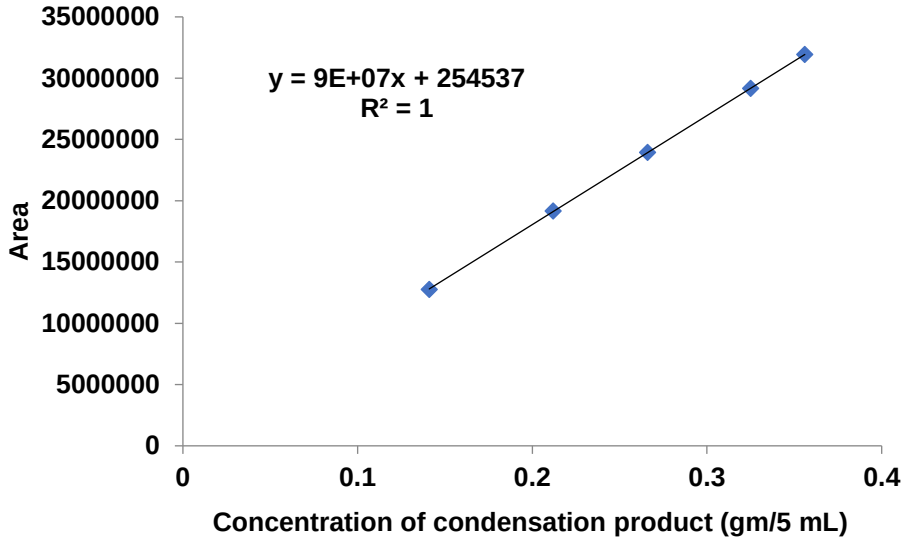

Figure 2.2. Calibration curve for condensation product

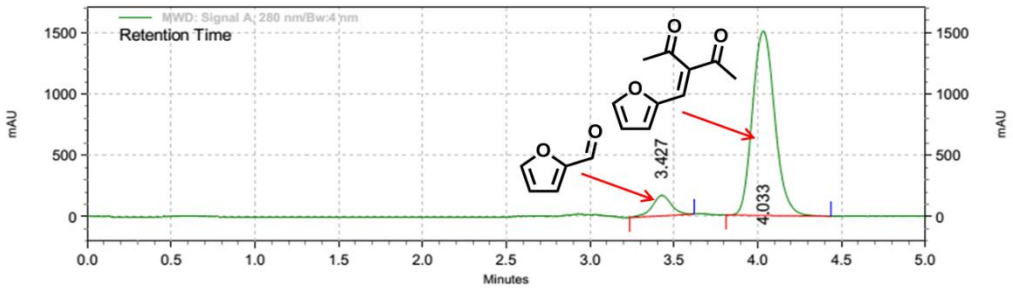

MWD: Signal A,
280 nm/Bw:4 nm
Results

Retention Time	Area	Area %	Height	Height %
3.427	2775816	8.69	350219	9.99
4.033	29151896	91.31	3154036	90.01
Totals	31927712	100.00	3504255	100.00

Figure 2.3. Representative chromatogram depicting separation of furfural and FMP

The conversion of furfural and yield or selectivity of condensation products were calculated using following equations.

$$\text{Conversion of furfural (\%)} = \frac{\text{Initial moles of furfural - Moles of furfural remained}}{\text{Initial moles of furfural}} \times 100 \quad \text{(I)}$$

$$\text{Yield of Knoevenagel product (\%)} = \frac{\text{Moles of product formed}}{\text{Initial moles of furfural}} \times 100 \quad \text{(II)}$$

$$\text{Selectivity of Knoevenagel product (\%)} = \frac{\text{Moles of product formed}}{\text{Moles of furfural reacted}} \times \text{Stoitiometric ratio of moles of furfural to condensation product} \times 100 \quad \text{(III)}$$

2.5. Results and Discussion

2.5.1. Catalyst characterization

2.5.1.1. BET surface analysis

The surface area of the catalyst materials was determined using nitrogen adsorption experiments conducted on a Micromeritics ChemiSorb 2720 sorption analyzer. In a representative experiment, a U-shaped, flow-through quartz sample tube was filled with 0.05 g of the catalyst. The catalyst was initially pre-treated in helium (30 cm^3/min) at 100 °C for 2 hours. Subsequently, nitrogen gas was passed through the U-shaped tube at a flow rate of 30 cm^3/min and a temperature of 50 °C for 30 minutes. The sample was then flushed with helium at the same flow rate and temperature for 1 hour. The temperature-programmed desorption of nitrogen was measured in the range of 50 to 200 °C with a heating rate of 10 °C/min. The desorbed nitrogen concentration was recorded using a gold-plated filament thermal conductivity detector. The surface area of the Fe_3O_4@SiO_2-Py catalyst was found to be 138 m^2/g.

2.5.1.2. Fourier transform infrared spectroscopy (FTIR)

The structures of the organosilica catalysts were confirmed by FTIR analysis performed on a Perkin Elmer 2000 spectrometer in the 4000–400 cm^{-1} wave number range (Figure 2.4). For the Fe_3O_4@SiO_2-Py catalyst, intense peaks observed between 580 cm^{-1} and 630 cm^{-1} were attributed to the stretching vibration mode of metal–oxygen (Fe-O) bonds in the crystalline lattice of Fe_3O_4. A band at 1647 cm^{-1} was assigned to the –C=N– group of the pyridine moiety, while a band at 3375 cm^{-1} was attributed to hydroxyl functionality. The FTIR patterns of Fe_3O_4@SiO_2-Py and SiO_2-Py were almost identical, except for the Fe_3O_4 pattern. Aminopropylsilica showed bands at 1020 cm^{-1} and 1472 cm^{-1} corresponding to Si-O-Si and $–NH_2$ functionalities, respectively.

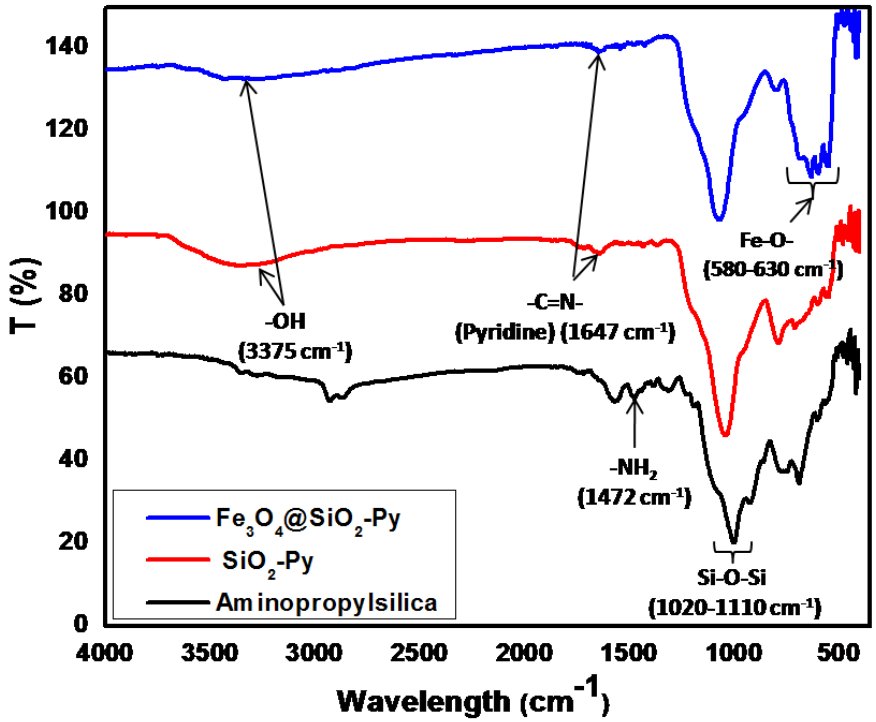

Figure 2.4. FTIR of 3-Aminopropylsilica, Py-SiO_2 and Fe_3O_4@SiO_2-Py catalysts

2.5.1.3. Solid state NMR

To confirm the structure of the catalyst, solid-state ^{13}C NMR was performed on a Bruker instrument at 75 MHz. The solid state ^{13}C NMR of SiO_2-Py catalyst is presented below (Figure 2.5).

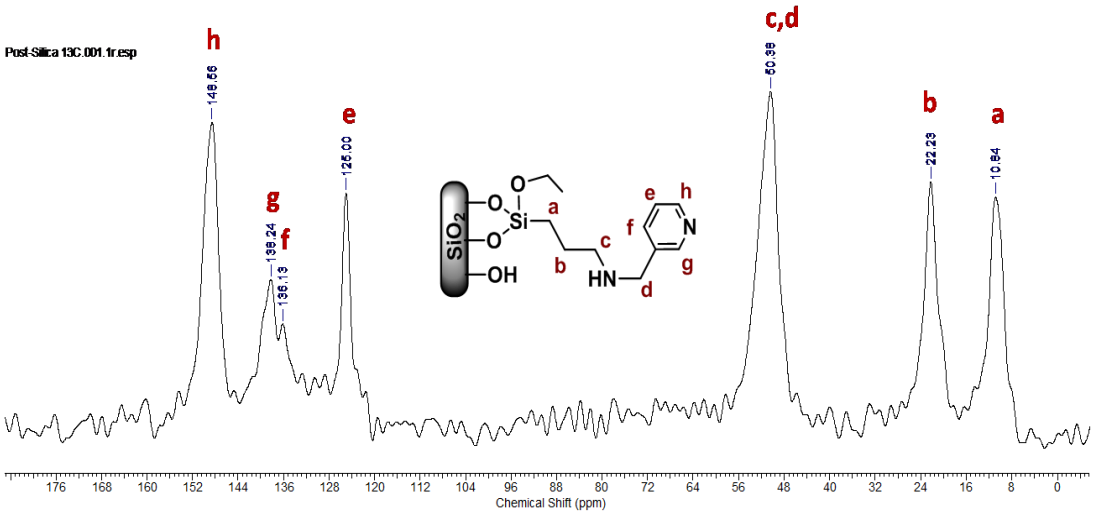

Figure 2.5. Solid state 13C NMR of SiO_2-Py

In the solid state ^{13}C NMR of SiO_2-Py catalyst, three well resolved lines at 10.53, 22.23, 50.38 ppm were observed, which were assigned to $–CH_2–$ groups indicated as **a**, **b**, (**c** and **d**) respectively on NMR spectrum. The peaks at 125, 136.13, 138.24 and 148.56 ppm are assigned to –CH– groups of pyridine with carbon atoms numbered as **e**, **f**, **g** and **h**, respectively.

2.5.1.4. X-ray diffraction (XRD)

Wide-angle X-ray diffraction was recorded using a PANalytical PXRD Model X-Pert PRO-1712, equipped with a Ni-filtered CuKα radiation source (λ = 0.154 nm), a current intensity of 30 mA, and a voltage of 40 kV, along with an Xcelerator detector. To confirm the presence of Fe_3O_4 phases, XRD pattern of Fe_3O_4@SiO_2-Py was compared with the standard Fe_3O_4 (Figure 2.6). A series of characteristic peaks at $2\theta = 31.32^o$, 36.60^o, 43.36^o, 54.00^o, 58.54^o and 62.28^o which corresponds to the indices (220), (311), (4 0 0), (4 2 2), (5 1 1) and (4 4 0) were observed in the Fe_3O_4@SiO_2-Py sample which are in well accordance with the inverse cubic spinel phase of Fe_3O_4 (JCPDS 85–1436).

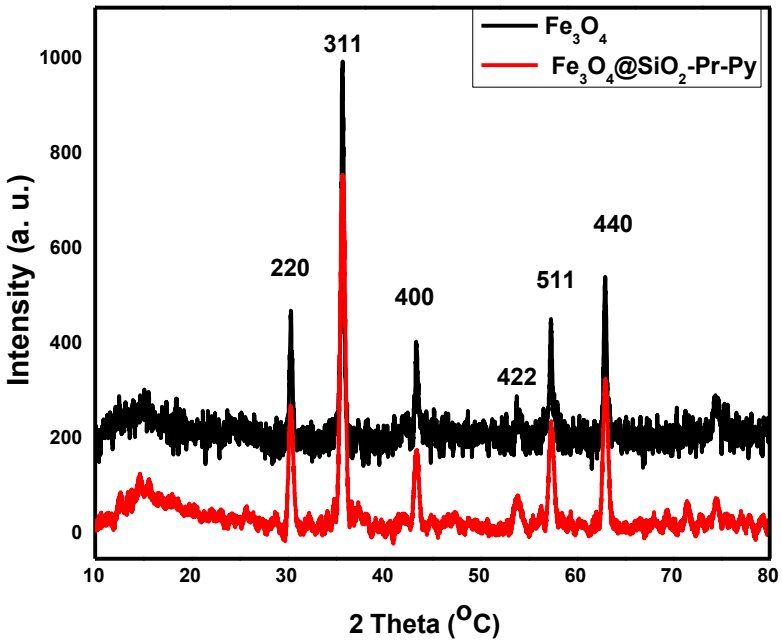

Figure 2.6. XRD patterns of Fe_3O_4 and Fe_3O_4@SiO_2-Py

2.5.1.5. High resolution transmission electron spectroscopy (HR-TEM)

High resolution transmission electron spectroscopy (HRTEM) analysis of fresh and reused catalysts was performed on JEOL JEM F200 HRTEM instrument, with resolution 0.19 nm and accelerating voltage 20kV-200kV.

The morphology and particle sizes of $Fe_3O_4@SiO_2$, $Fe_3O_4@SiO_2$-Py, and $Fe_3O_4@SiO_2$-Py (reused) were investigated using TEM analysis (Figure 2.7). The results indicated that $Fe_3O_4@SiO_2$-Py, $Fe_3O_4@SiO_2$-Py, and $Fe_3O_4@SiO_2$-Py (reused) exhibited similar morphology (hexagonal shape) with average particle sizes of 36, 40, and 41 nm, respectively. Figure 2.7 clearly shows that Fe_3O_4 nanoclusters were successfully coated with a thin layer of SiO_2, resulting in a core/shell structure of $Fe_3O_4@SiO_2$ NPs. The morphology and particle size of $Fe_3O_4@SiO_2$-Py were retained even after reuse, demonstrating the stability of the catalyst (Figure 2.7).

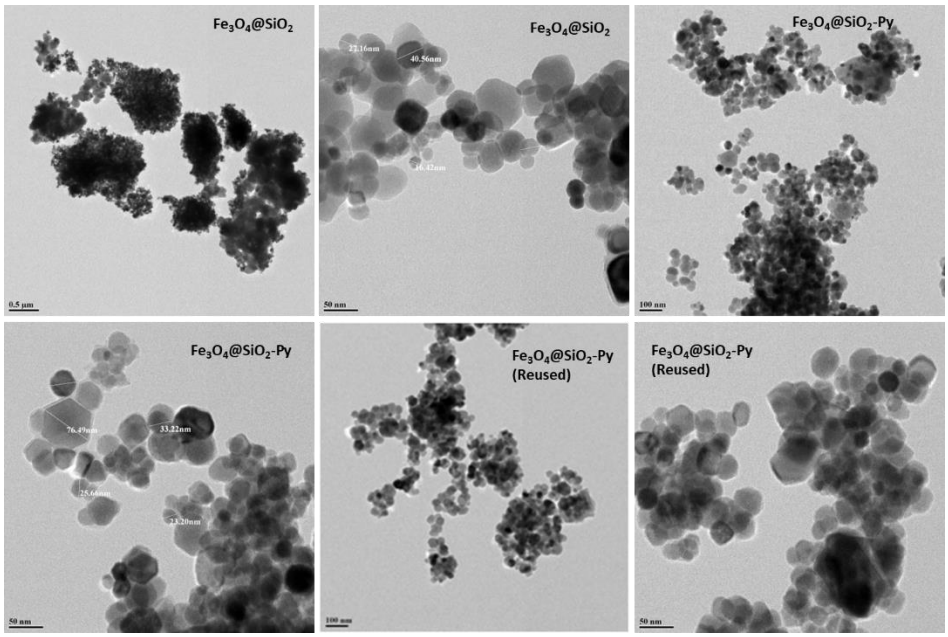

Figure 2.7. HR-TEM images of $Fe_3O_4@SiO_2$, $Fe_3O_4@SiO_2$-Py and $Fe_3O_4@SiO_2$-Py (reused).

2.5.2. Catalyst screening for Knoevenagel condensation of furfural with acetylacetone

The Knoevenagel condensation reaction is usually facilitated by basic catalysts. In this work, several basic catalysts were tested for the Knoevenagel condensation of furfural with acetylacetone (Table 2.1). Initially, furfural was treated with acetylacetone in presence of sodium hydroxide a homogeneous solid base at 80 °C for 4 h to give

the Knoevenagel product (FMP) in 78% yield with 95% conversion of furfural (Table 2.1, entry 1). Indeed, use of homogeneous base catalyst is generally unattractive due to its downsides such as non-reusable, hazardous waste generation and it also need to be neutralized with strong homogeneous acids which ultimately increases the process operations. Therefore, easily recoverable and environmentally compatible solid bases are usually most preferred. In this direction, we performed Knoevenagel condensation over series of solid bases. For instance, with heterogeneous solid base such as hydrotalcite having Mg/Al ratio as 3, FMP was formed in 31% yield with only 56% conversion of furfural under optimized reaction conditions (Table 2.1, entry 2). With CaO, FMP was obtained in 41% yield with a 67% conversion of furfural (Table 2.1, entry 3). With ZnO-400 catalyst, FMP obtained was in 29% yield with lower conversion (41%) of furfural (Table 2.1, entry 4). Although, the basic metal oxides gave 100% selectivity to FMP but the yield was low to moderate due to lower conversion of furfural. Generally, the Knoevenagel condensation is more prone over amine containing organic bases (Lewis bases). In presence of catalytic amount of tertiary amine such as triethylamine, 79% yield of FMP was achieved with 89% conversion of furfural (Table 2.1, entry 5). Biomass derived furfurylamine also used as a Lewis base catalyst, which showed similar activity as of triethylamine (Table 2.1, entry 6). Further, when reaction was performed with N,N-dimethylaminopyridine (DMAP) the FMP was produced in 77% yield (Table 2.1, entry 7). In presence of amine containing bicyclic catalysts such as 1,8-Diazabicyclo[5.4.0]undec-7-ene (DBU) catalyst, the FMP was formed in 78% yield (Table 2.1, entry 8). With 4-hydroxypyridine, furfural was consumed up to 95% and 83% yield of FMP was achieved (Table 2.1, entry 9). Amine functionalized homogeneous bases gave good yield and 99% selectivity to the FMP with almost 90% conversion of furfural. However, homogeneous bases are not only non-recyclable but they are soluble in organic solvents hence, they could contaminate the product. Interestingly, these catalysts (functionalized organic amines) can be heterogenized by anchoring on silica or magnetic materials. For instance, 3-Aminopropylsilica was used for this reaction however a moderate yield (76%) of FMP with 99% selectivity was noticed with almost 90% conversion of furfural (Table 2.1, entry 10). Pyridine anchored on silica (SiO_2-Py) showed better catalytic performance than 3-Aminopropylsilica. With SiO_2-Py catalyst, 94% conversion of furfural was achieved to obtain 85% yield of FMP (Table 2.1, entry 11). In case of SiO_2-Py catalyst, pyridine moiety is planar and the lone pair of electrons are present perpendicular to the plane of pyridine. Hence, hydrogen from the active methylene group of acetylacetone can be easily approached. On the contrary, in 3-

Aminopropylsilica, there is a distorted tetrahedral structure which creates some hinderance for the reactant as compared to pyridine. Due to these reasons SiO_2-Py showed better activity than 3-Aminopropylsilica. Fe_3O_4@SiO_2-Py catalyst showed similar activity to that of SiO_2-Py (Table 2.1, entry 12). Use of magnetic catalyst (Fe_3O_4@SiO_2-Py) is advantageous over SiO_2-Py because, the former can be easily separated with the help of external magnate. While, in case of SiO-Py, catalyst recovery needs to be done by filtration which is associated with handling losses.

Table 2.1. Catalyst screening for Knoevenagel condensation of furfural with acetylacetone [a]

Entry	Catalyst	Loading	T [ºC]	Conv.[b] [%]	Yield[b] [%]	Sel.[b] [%]
1	NaOH	10 mol%	80	95	78	92
2	Hydrotalcite	0.1 g	100	56	31	100
3	CaO	0.1 g	100	67	41	100
4	ZnO-400	0.1 g	100	41	29	100
5	Triethylamine	10 mol%	100	89	79	99
6	Furfurylamine	10 mol%	100	90	80	99
7	DMAP	10 mol%	100	85	77	98
8	DBU	10 mol%	100	87	78	99
9	4-Hydroxypyridine	10 mol%	100	95	83	99
10	3-Aminopropylsilica	0.1 g	100	81	76	99
11	SiO_2-Py	0.1 g	100	94	85	100
12	Fe_3O_4@SiO_2-Py	0.1 g	100	94	85	100

[a] Reaction condition: Furfural (0.196 g, 2 mmol), catalyst, acetylacetone (0.2 g, 2 mmol), 4 h. [b] Yields are determined using HPLC.

2.5.3. Reaction optimization

2.5.3.1. Effect of temperature

To determine the optimum reaction temperature, the reaction was performed at temperatures ranging from 80 to 100 °C, with all other parameters kept constant. It was noticed that, the yield of **FMP** was increased gradually with rise in temperature from 80 to 100 °C. At 100 °C, yield of **FMP** was noted as 86% which is highest as compared to the results obtained at lower temperatures. Further increase in temperature to 110 °C, the yield of FMP was not improved (Figure 2.8).

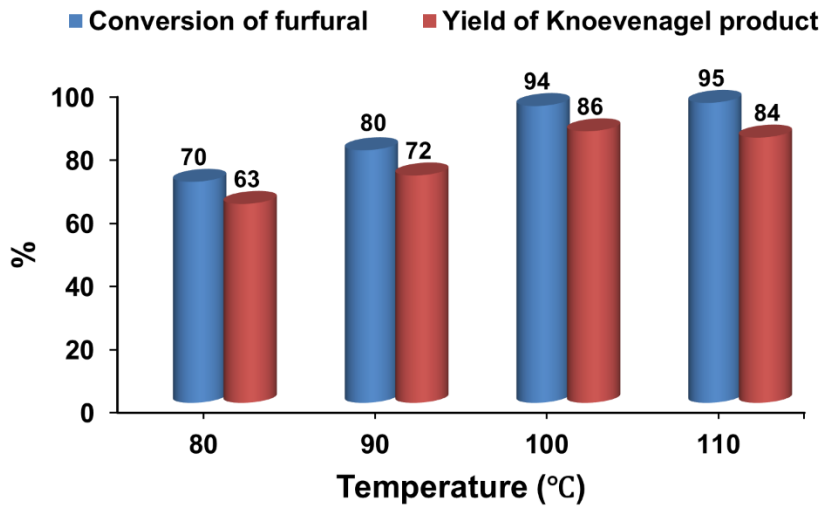

Figure 2.8. Effect of temperature. Reaction conditions: Furfural (0.192 g, 2 mmol), acetyl acetone (0.2 g, 2 mmol), Fe_3O_4@SiO_2-Py (0.1 g), 4 h.

2.5.3.2. Effect of time

The progress of the reaction with time was monitored from 0 h to 4.5h and obtained results are plotted which is presented in Figure 2.9.

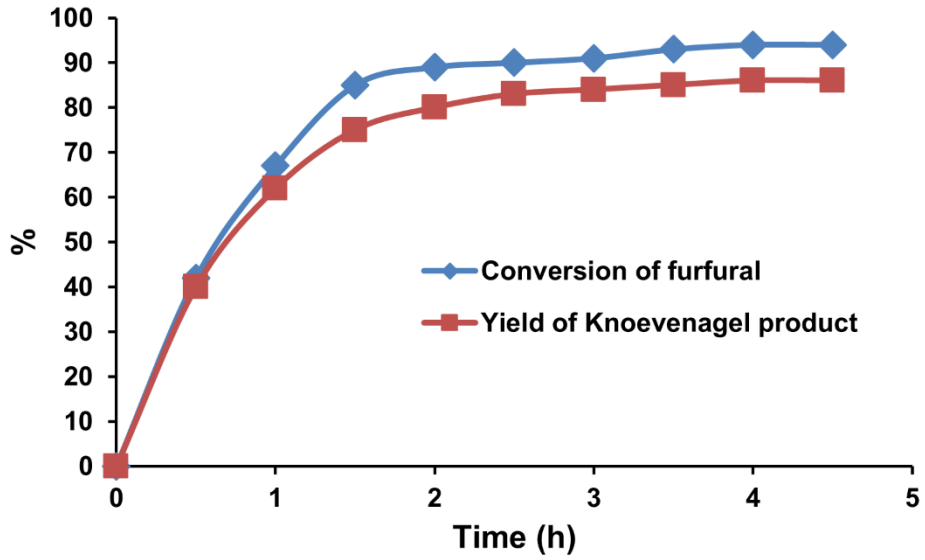

Figure 2.9. Effect of time. Reaction conditions: Furfural (0.192 g, 2 mmol), acetylacetone (0.2 g, 2 mmol), Fe_3O_4@SiO_2-Py (0.1 g), 100 ^oC 0-5 h.

The progress of the reaction with time was monitored from 0 h to 4.5h and obtained results are plotted which is presented in Figure 3.9. Initially reaction progress was pretty fast as in just 1.5 h, up to 85% furfural conversion and 78% yield of FMP was noted. After that conversion of furfural and the yield of FMP was slowly increased. Maximum conversion of furfural and yield of FMP were achieved by the end of the 4th hour. Extending reaction beyond 4 h did not show any improvement in the conversion of furfural as well as yield of **FMP** as reaction must have reached to the equilibrium (Figure 2.9).

2.5.3.3. Effect of catalyst amount

For solid catalysts, determining the optimal amount needed for maximum conversion and yield is crucial. The effect of catalyst amount, ranging from 0.05 to 0.15 g, was investigated (Figure 2.10). With 0.05 g of Fe_3O_4@SiO_2-Py the yield of **FMP** was only 61% while, increasing the catalyst amount to 0.075 g, resulted in enhancement of FMP (79%) yield due to increase in active sites. With 0.1 g of Fe_3O_4@SiO_2-Py the yield of **FMP** was highest as 85%. The lower catalyst amount gave lower yield obviously due to insufficient active site. However, with catalyst amount of 0.15 g the yield of FMP was comparable with that of 0.1 g.

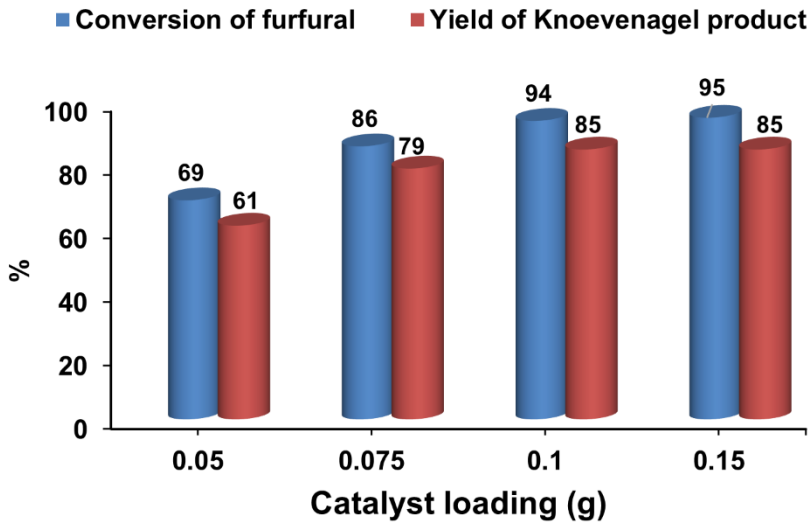

Figure 2.10. Effect of catalyst amount. Reaction conditions: Furfural (0.192 g, 2 mmol), acetylacetone (0.2 g, 2 mmol), Fe_3O_4@SiO_2-Py (0.05 - 0.15 g), 100 ^oC, 4 h.

2.5.3.4. Recycle study

The stability of Fe_3O_4@SiO_2-Py was evaluated by performing recycle runs (Figure 2.11). It was found that the catalytic activity of Fe_3O_4@SiO_2-Py was very much consistent even after being used for six times. After each run, the reaction mixture was decanted, the catalyst was washed with ethyl acetate and then reused for the next cycle.

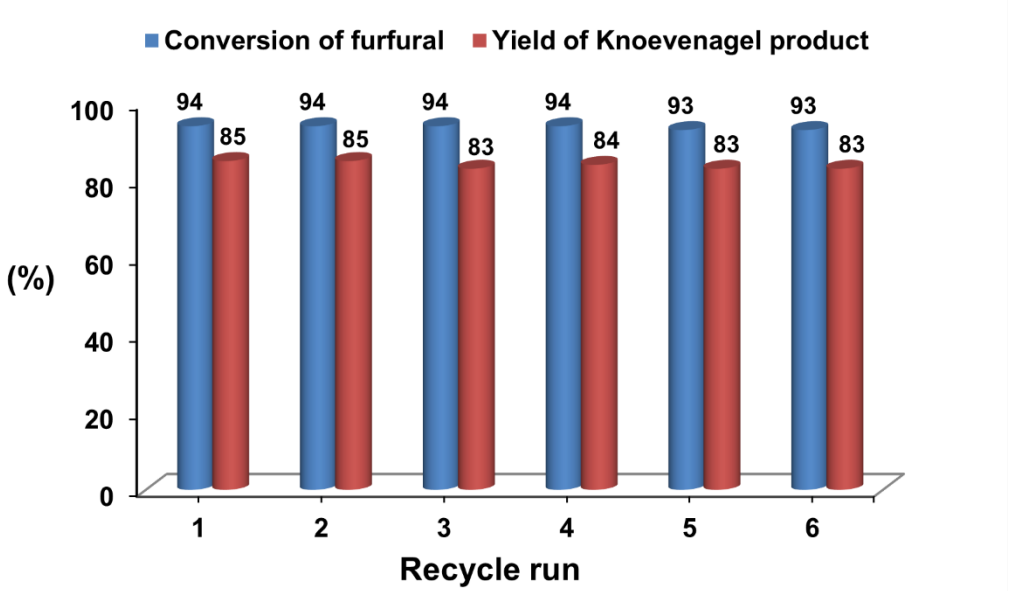

Figure 2.11. Recycling of Fe_3O_4@SiO_2-Py. Reaction conditions: Furfural (0.192 g, 2 mmol), acetyl acetone (0.2 g, 2 mmol), Fe_3O_4@SiO_2-Py (0.1 g), 100 ^oC, 4 h.

2.6. Reaction Mechanism

Reaction mechanism of Knoevenagel reaction involves three steps such as proton abstraction from α-carbon of active methylene compound then condensation followed by dehydration. Acetyl acetone has active methylene group which generally has acidic protons due to adjacent electron withdrawing groups. A Lewis base abstracts the hydrogen from active methylene group to generate nucleophilic carbonian. The active nucleophilic carbon ion immediately attacks on electropositive carbonyl carbon of furfural to form β-oxonium diketone which subsequently gets protonated from pyridinium ion (conjugated Lewis acid of pyridine) to form β-hydroxyketone. Then again Lewis base abstracts the hydrogen from active methylene group of β-hydroxyketone and immediately removed –OH from β-carbon of β-hydroxyketone to form α,β-unsaturated ketone that is **FMP**. A conjugated Lewis acid (pyridinium ion) formed was then converted back to Lewis base (pyridine) and it enters into next cycle

of Knoevenagel condensation. A proposed reaction mechanism is presented below in Figure 2.12.

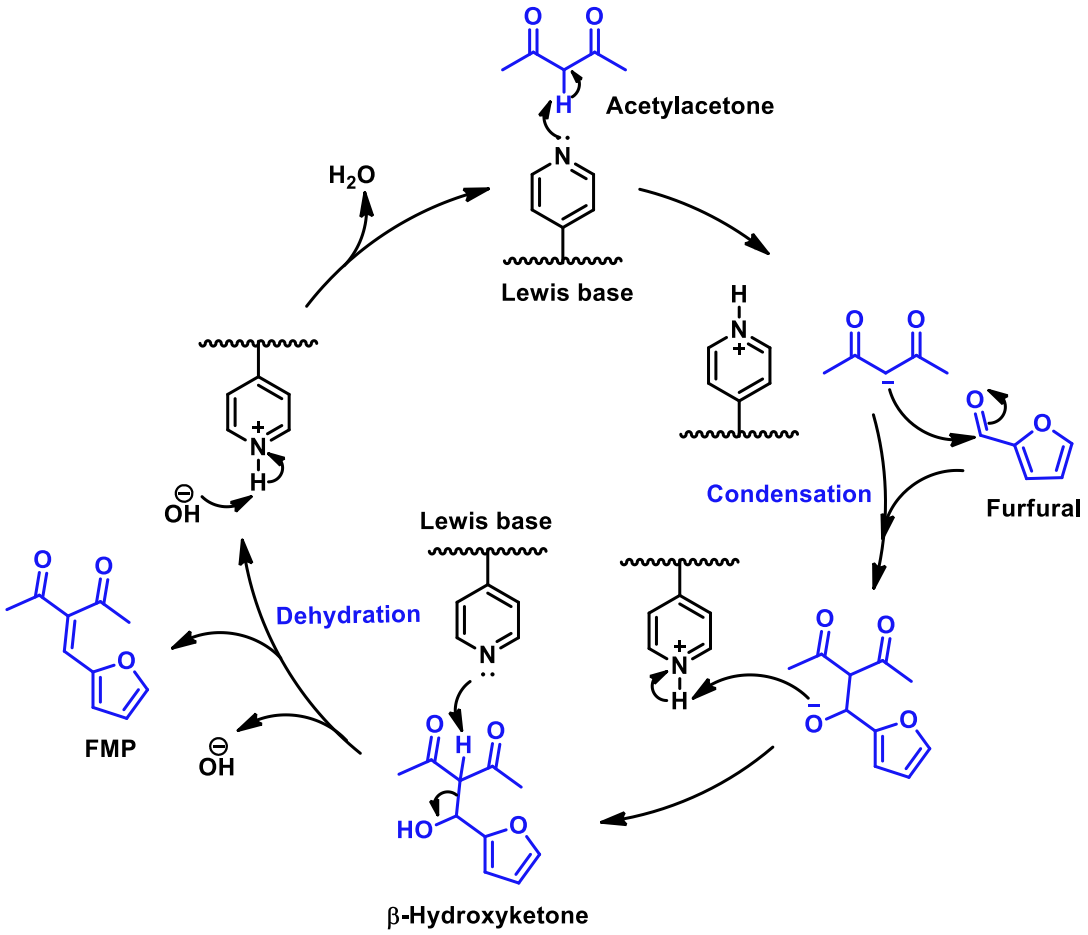

Figure 2.12. Proposed reaction pathway for Knoevenagel condensation

2.7. Conclusions

In this chapter, we have synthesized a novel, simple and robust Fe_3O_4@SiO_2-Py catalyst having active Lewis base site. The performance of this catalyst is evaluated for solvent free Knoevenagel condensation of biomass derived furfural with acetyl acetone. As compared to basic metal oxides and homogeneous Lewis bases our catalyst showed superior activity due to unique structural features. In our catalyst has pendant pyridine moiety which is generally planar and the lone pair of electrons are present perpendicular to the plane of pyridine due to this hydrogen from the active methylene group of acetylacetone can be easily approached. Under optimized reaction conditions and in presence of our catalyst, **FMP** produced in 85% yield after 95% conversion of furfural. Interestingly, the condensation product **FMP** is a unit of

C_{10} and could be converted into branched alkanes (Jet fuel) through hydrodeoxygenation process. With its magnetic properties, the Fe_3O_4@SiO_2-Py catalyst can be effortlessly separated using an external magnetic field and reused multiple times for subsequent condensation reactions. This feature not only minimizes handling losses but also ensures sustained catalyst activity over multiple cycles.

2.8. References

[1] J. C. Serrano-Ruiz, J. A. Dumesic, *Energy Environ. Sci*., **2011** *4*, 83–99.

[2] J. P. Lange, E. van der Heide, J. van Buijtenen, R. Price, *ChemSusChem,* **2012**, *5*, 150–166.

[3] W. Dabelstein, A. Reglitzky, A. Schutze, K. Reders, Automotive fuels, Ullmann's Encyclopedia of Industrial Chemistry, *Wiley-VCH, Weinheim*, **2000**.

[4] G. Liang, A. Wang, X. Zhao, N. Lei, T. Zhang, *Green Chem*. **2016**, *18*, 3430–3438.

[5] J. N. Appaturi, M. Selvaraj, S. B. A. Hamid, *Microporous Mesoporous Mater*., **2018**, *260*, 260–269.

[6] A. V. Subrahmanyam, S. Thayumanavan, G. W. Huber, *ChemSusChem*, **2010**, 3, 1158–1161.

[7] C. M. Nicklaus, A. J. Minnaard, B. L. Feringa, J.G. de Vries, *ChemSusChem*, **2013**, *6*, 1631–1635.

[8] A. Corma, O. de la Torre, M. Renz, N. Villandier, *Angew. Chem. Int. Ed*., **2011**, *50*, 2375–2378.

[9] M. Balakrishnan, E. R. Sacia, A. T. Bell, *ChemSusChem*, **2014**, *7*, 1078–1085.

[10] S. H. Shinde, C. V. Rode, *Green Chem*. **2017**, *19*, 4804–4810.

[11] G. W. Huber, J. N. Chheda, C. J. Barrett, J. A. Dumesic, *Science*, **2005**, *308*, 1446–1450.

[12] K. S. Arias, M. J. Climent, A. Corma, S. Iborra, *Energy Environ. Sci*., **2015**, *8* 317–331.

[13] P. Oliveira, A. Machado, A. M. Ramos, I. Fonseca, F. M. B. Fernandes, A. M. B. D. Rego, J. Vital, *Microporous Mesoporous Mater*., **2009**, *120*, 432–440.

[14] Y. L. Zhang, S. Liu, S. Y. Liu, F. J. Liu, H. Y. Zhang, Y. Y. He, F. S. Xiao, *Catal. Commun*., **2011**, *12*, 1212–1217.

[15] D. Z. Xu, Y. Liu, S. Shi, Y. M. Wang, *Green Chem*., **2010**, *12*, 514–517.

[16] J. Mondal, A. Modak, A. Bhaumik, *J. Mol. Catal. A Chem*., **2011**, *335*, 236–241.

[17] K. M. Parida, D. Rath, *J. Mol. Catal. A Chem*., **2009**, *310*, 93–100.

[18] A. Modak, J. Mondal, A. Bhaumik, *Appl. Catal. A General*, **2013**, *459*, 41–51.

[19] O. C. Navarro, A. Corma, S. I. Chornet, *Top. Catal*., **2009**, *52*, 304–314.

2.9. NMR data of synthesized compound

2.9.1. 3-(2-furylmethylene)-2,4-pentanedione (FMP): Yellowish brown liquid

^{1}H NMR (200 MHz, $CDCl_3$, 0.01%, TMS, δ ppm): 2.38 (s, 3 H) 2.45 (s, 3 H) 6.52 (dd, *J*=3.54, 1.77 Hz, 1 H) 6.78 (d, *J*=3.54 Hz, 1 H) 7.16 (s, 1 H) 7.55 (s, 1 H).

^{13}C NMR (50 MHz, $CDCl_3$, 0.01%, TMS, δ ppm): 26.16, 31.49, 112.97, 118.30, 124.96, 138.38, 146.55, 148.87, 195.81, 204.39.

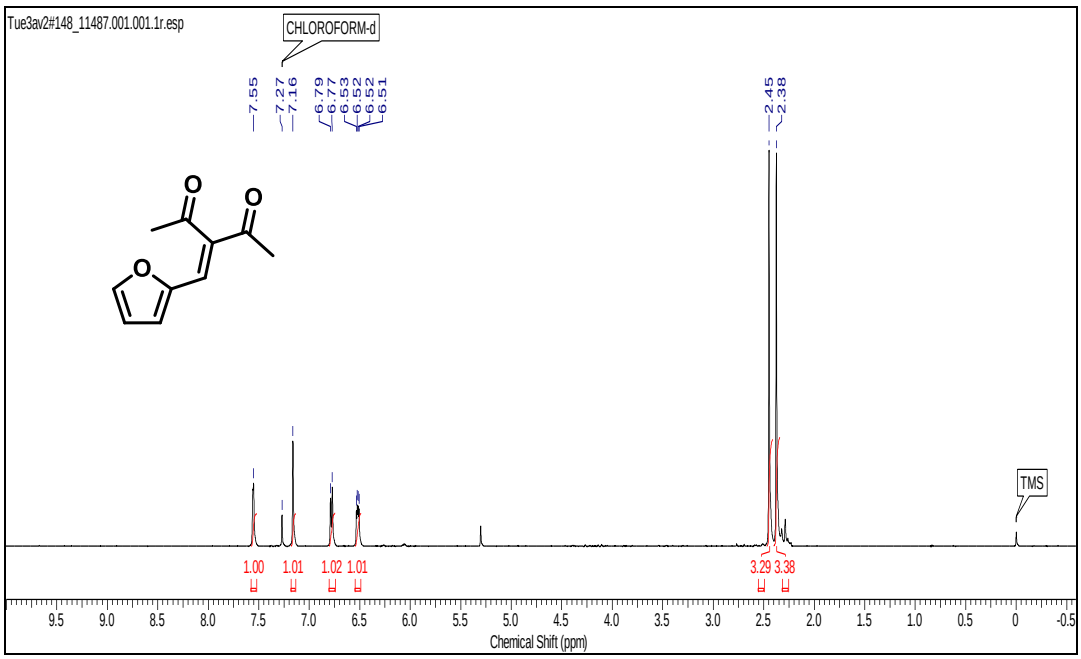

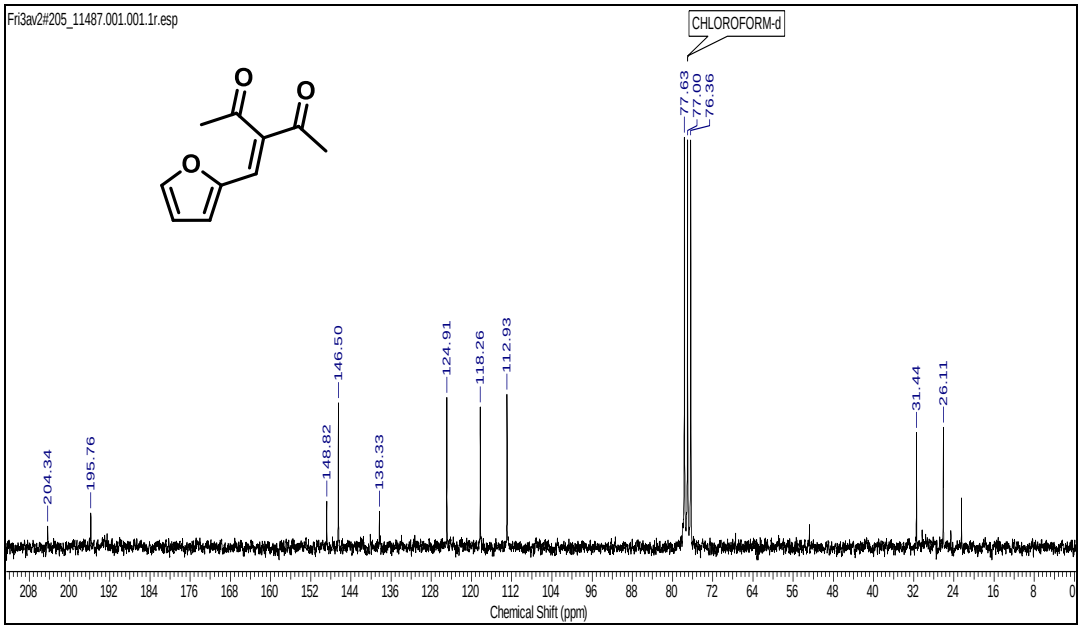

2.9.2. 1-(pyridin-3-yl)-N-(3-(triethoxysilyl)propyl)methanimine: Colourless oil

^{1}H NMR (200 MHz, $CDCl_3$, 0.01%, TMS, δ ppm): 0.64-0.72 (q, 2 H) 1.18-1.27 (m, 8 H) 1.80-1.89 (m, 2 H) 3.48-3.89 (m, 7 H) 7.30-7.38 (m, 1 H) 8.09-8.17 (m, 2 H) 8.62-8.66 (m, 1 H) 8.85-9.09 (m, 1 H).

^{13}C NMR (50 MHz, $CDCl_3$, 0.01%, TMS, δ ppm): 7.97, 18.20, 24.08, 58.30, 64.30, 123.5, 124, 131.7, 134.3, 135.71, 150.02, 151.17, 151.99, 154.66, 157.99.

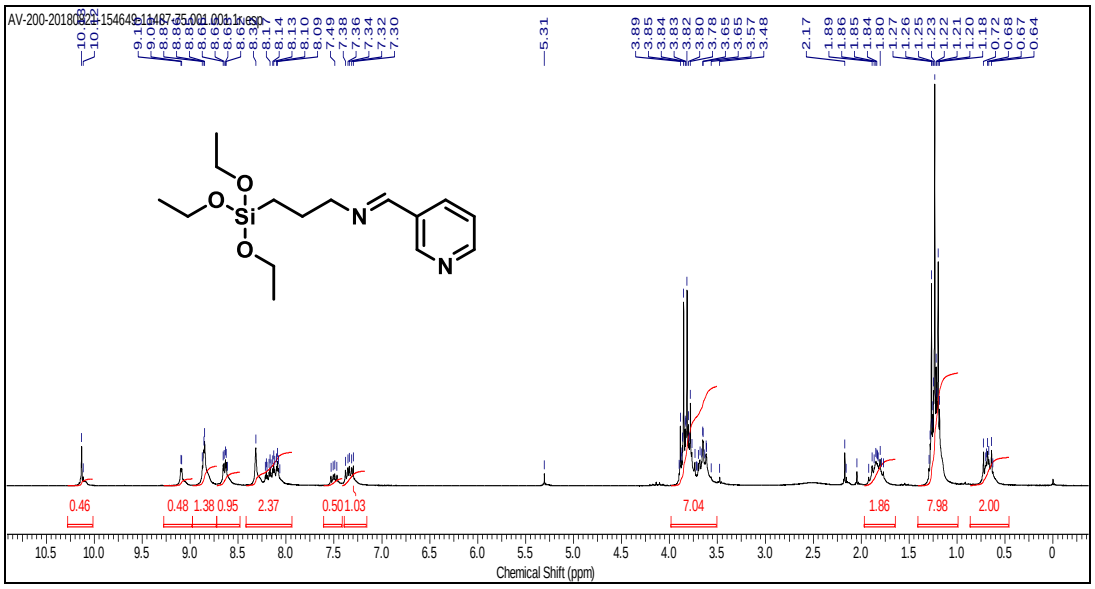

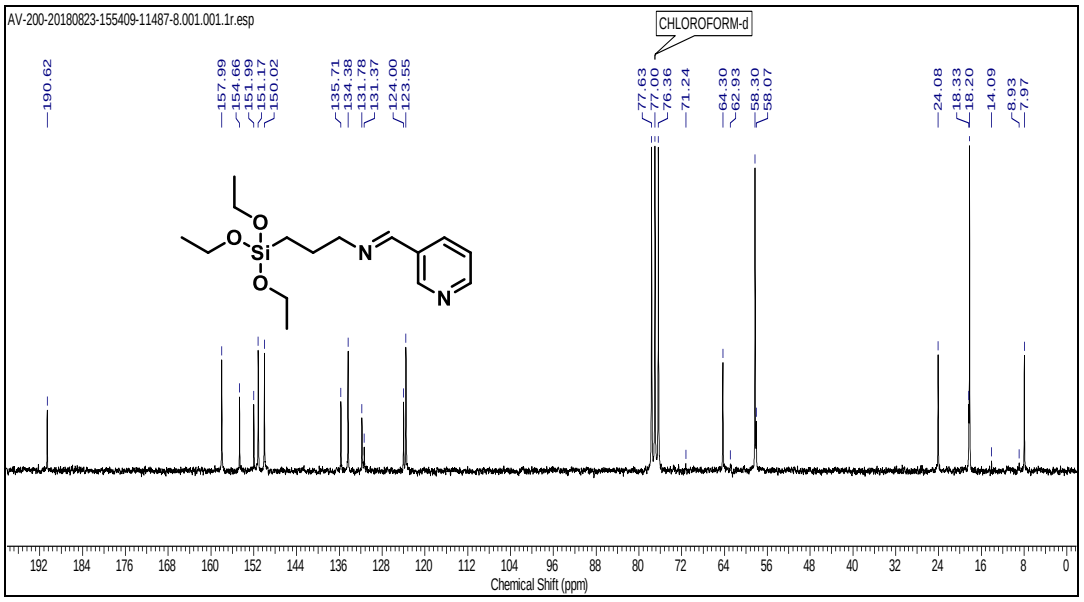

Chapter - 3

Condensation of Renewable Aldehydes and 2-Methylfuran to Saturated Cyclic Oxygenates

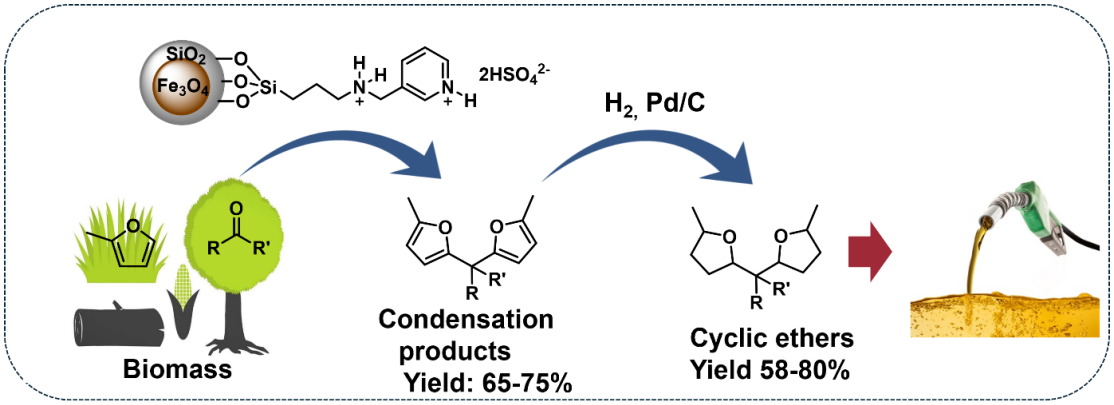

Saturated cyclic ethers produced from biomass-derived aldehydes and 2-methylfuran have significant potential as diesel fuel candidates. The synthesis of these saturated cyclic ethers involves a two-step process: acid-catalysed condensation of aldehydes with 2-methylfuran followed by selective furan ring hydrogenation of the condensation products. In this study, we developed a novel recyclable magnetic solid acid catalyst, $[Fe_3O_4@SiO_2\text{-}Pr\text{-}Py\text{-}H][2HSO_4^{2-}]$ and employed it for the condensation of 2-methylfuran with formaldehyde as model substrates, optimizing the reaction parameters systematically. Under the optimized conditions, condensation of 2-methylfuran with various aldehydes was also successfully achieved with excellent yields. Additionally, several supported noble metal catalysts were screened to identify a suitable system for the selective hydrogenation of the furan ring in the condensation products. Among these, the in-house prepared 5% Pd/C catalyst proved to be highly active and selective for furan ring hydrogenation, effectively avoiding the formation of ring-opened products even under very low hydrogen pressure at room temperature. The prepared catalysts were thoroughly characterized using advanced techniques.

Komal Tarade, Suhas Shinde and Chandrashekhar Rode, **Fuel Processing Technology**, 2020, 197, 106191.

3.1. Introduction

Given the diminishing petroleum reserves and the pressing environmental issues such as global warming and air pollution, utilizing biomass resources for fuel and chemical production has become imperative [1]. A substantial growth projected in global oil consumption sector combined with compelling international situation of crude oil production are the key drivers for exploring alternate sustainable energy sources. Bioenergy stands as the largest contributor to global renewable energy, providing energy security to billions while stimulating rural development [2]. Among several options, biomass is currently the leading source of carbon-based renewable energy worldwide. In principle, biomass feedstock can be harnessed to meet the demands of heat, electricity and liquid fuel. Among these, heat has been traditionally obtained to the extent of 60% from biomass mainly for cooking application in major part of the world [3]. There have been several biomass co-firing plants commissioned to produce electricity and heat [4]. However, burning of biomass is a kind of its underutilization when a practical potential of its conversion to liquid fuel like products is exists [5]. Considering this fact, several countries have set a target of deriving 10-20% of transportation fuels from biomass feedstock during next decade or so [6]. Cellulose and hemicellulose, the primary structural carbohydrates in lignocellulosic biomass, are hydrolysed to produce glucose and xylose. These sugars are then dehydrated to yield 5-hydroxymethylfurfural (HMF) and furfural (FUR), respectively [7,8]. Both 5-HMF and furfural are the key starting materials for production of fuel components through carbon upgradation by employing various types of C-C bond forming reactions. Hydroxyalkylation-alkylation is one such reaction involving acid catalysed condensation of 2-methylfuran with the aldehydes, ketones or alcohols.

3.2. Literature Survey

Furan condensation reaction has been reported using several types of reagents / catalysts e.g. conc. H_2SO_4 [9], HCl [10], acidic resins [9-14], MCM-SO_3H [15], Mo-Zr-MCM-41 [16], $AuCl_3$ [17-19], Sn^{+4}-K-10 [19], zeolites [20], SiO_2-Pr-S-Pr-SO_3H [21], $Cu(OTf)_2$ [22], I_2 [23], CMH-SO_3H [24], SILC [25], TFA-ZrO_2 [26], ionic liquids [27], Sn-Mont [28] etc. The furan condensation products thus obtained can be then hydrodeoxygenated to produce hydrocarbons (Scheme 1). Corma et al. have reported the use of physical mixture of Pt/C and Pt/TiO_2 at 400 °C and 5 MPa hydrogen pressure for 1 h [9]. Recently, Liu et al. showed that hydrodeoxygenation of condensation products over Ir-ReO_x/SiO_2 could provide high selectivity of the desired alkanes at lower temperature of 170 °C [29]. Notably, Balakrishnan et al. found that

complete hydrodeoxygenation of furan condensation products to alkanes requires 55–60% more hydrogen compared to hydrogenation for producing cyclic ethers (furan ring saturation) that meet most diesel specifications. They found that, almost complete selectivity with 95% yield of cyclic ethers, without formation of ring open products could be achieved by using Pd/IL(PF6)-SiO_2 catalyst [10]. Several Ni, Pt, Pd, Ir and Rh metal supported on different acidic supports have been designed and used for the selective production of alkanes from bio-derived platform molecules [30-39].

3.3. Scope of the Present Work

In this study, we present a recyclable magnetic catalyst for the hydroxyalkylation-alkylation of 2-methylfuran with aldehydes to produce a diverse range of furan condensation products. It has been also demonstrated that these condensation products could be successfully hydrogenated to cyclic ethers over in-house prepared 5%Pd/C under very mild conditions of pressure and room temperature.

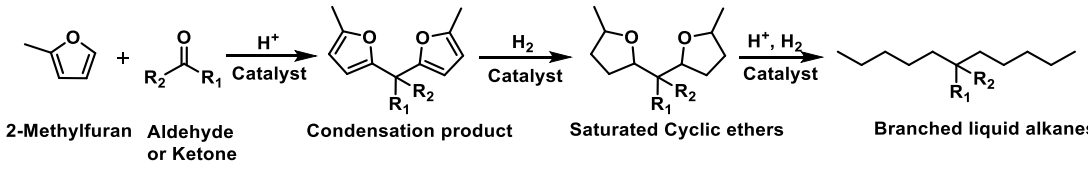

Scheme 3.1. General scheme for synthesis of saturated cyclic ethers and branched liquid alkanes

3.4. Experimental Section

3.4.1. Materials

Furfural, benzaldehyde, 37% (*w*/*v*) aqueous formaldehyde, acetone, amberlyst-15, amberlyte IR-120, 3-pyridinecarbaldehyde, 3-aminopropyltriethoxysilane, tetraethyl orthosilicate, $FeCl_2$, $FeCl_3$ and palladium chloride and carbon black were purchased from Sigma-Aldrich, India. 2-Methylfuran was obtained from TCI, India. Sodium hydroxide, sulphuric acid, methanol, acetonitrile, 1,4-dioxane, ethyl acetate, petroleum ether, toluene and silica gel (100-200 mesh) were acquired from Chem Labs, India. $NaBH_4$ received from Thomas Bakers, India. Commercial 5% Pd/C was obtained from Aldrich chemical company. Ethanol obtained from Changshu Hongsheng Fine Chemicals.

3.4.2. Catalyst Preparation

3.4.2.1. Synthesis of magnetic solid acid [Fe_3O_4@SiO_2-Py-Pr-H][$2HSO_4^{2-}$]

Process for a stepwise synthesis of magnetic solid acid [Fe_3O_4@SiO_2-Py-Pr-H][$2HSO_4^{2-}$] catalyst is presented below.

Preparation of nano-magnetic (Fe_3O_4)

A solution of $FeCl_2$ (5.4 g) and $FeCl_3$ (2 g) in aqueous hydrochloric acid (2 M, 25 mL) was sonicated at room temperature until both salts were completely dissolved. To this homogeneous solution, aqueous ammonia (25% w/v, 40 mL) was added dropwise under an argon atmosphere and stirred for 30 minutes. The Fe_3O_4 nanoparticles were separated using an external magnet, washed with deionized water (3 × 50 mL) and ethanol (3 × 50 mL), and then dried under vacuum.

Preparation of Fe_3O_4@SiO_2

The prepared Fe_3O_4 nanoparticles were suspended in a mixture of 35 mL of ethanol and 6 mL of deionized water and sonicated for 15 minutes. To this solution, 1.5 mL of tetraethyl orthosilicate (TEOS) was added slowly and sonicated for an additional 10 minutes. Aqueous ammonia (10% w/v, 1.4 mL) was then added slowly while stirring, and the mixture was heated at 40°C for 12 hours. The iron oxide nanoparticles on silica (Fe_3O_4@SiO_2) were separated using an external magnet, washed three times with ethanol (50 mL), and dried under vacuum.

Preparation of [Fe_3O_4@SiO_2-Pr-Py-H][$2HSO_4^{2-}$]

Step 1: Preparation of 1-(pyridin-3-yl)-N-(3-(triethoxysilyl)propyl)methanimine

A mixture of 1.8 g of 3-aminopropyltriethoxysilane (AMPSi), 3-pyridinecarbaldehyde (0.877 g) and dichloromethane (25 mL) was stirred at 50 ^oC for 24 h and then the reaction mixture was evaporated on rotary evaporator to afford colorless oil (2.5 g).

Step 2: Preparation of 1-(pyridin-3-yl)-N-(3-(triethoxysilyl)propyl) methaniminemagnetic-silica

To a solution of 1-(pyridin-3-yl)-N-(3-(triethoxysilyl)propyl)methanimine (2.5 g) in toluene (20 mL), Fe_3O_4@SiO_2 (1.7 g, 230-400 mesh) was added in portions. The mixture was refluxed for 24 hours under an N_2 atmosphere, then cooled to room temperature and filtered. The residue was washed with toluene (20 mL × 1) and dichloromethane (20 mL × 1) and dried in an oven for 24 hours to yield an brown coloured powder (4.0 g).

Step 3: (N-(pyridin-3-ylmethyl)propylaminomagnetic-silica) [39]

A mixture of 1-(pyridin-3-yl)-N-(3-(triethoxysilyl)propyl)methaniminemagnetic-silica (3.5 g) and methanol (25 mL) was cooled to 0 ^{o}C and then $NaBH_4$ (0.619 g) was added lot-wise. The mixture was stirred at room temperature for 24 hours, then evaporated using a rotary evaporator to yield an brown coloured powder (3.2 g).

Step 4: N-(pyridin-3-ylmethyl)propylaminomagneticacidic-silica [Fe_3O_4@SiO_2-Py-Pr-H][$2HSO_4^{2-}$]

N-(pyridin-3-ylmethyl)propylaminomagnetic-silica (0.5 g) was treated with 15% v/v H_2SO_4 in ethanol (5 mL) at room temperature for 24 hours and then dried under vacuum.

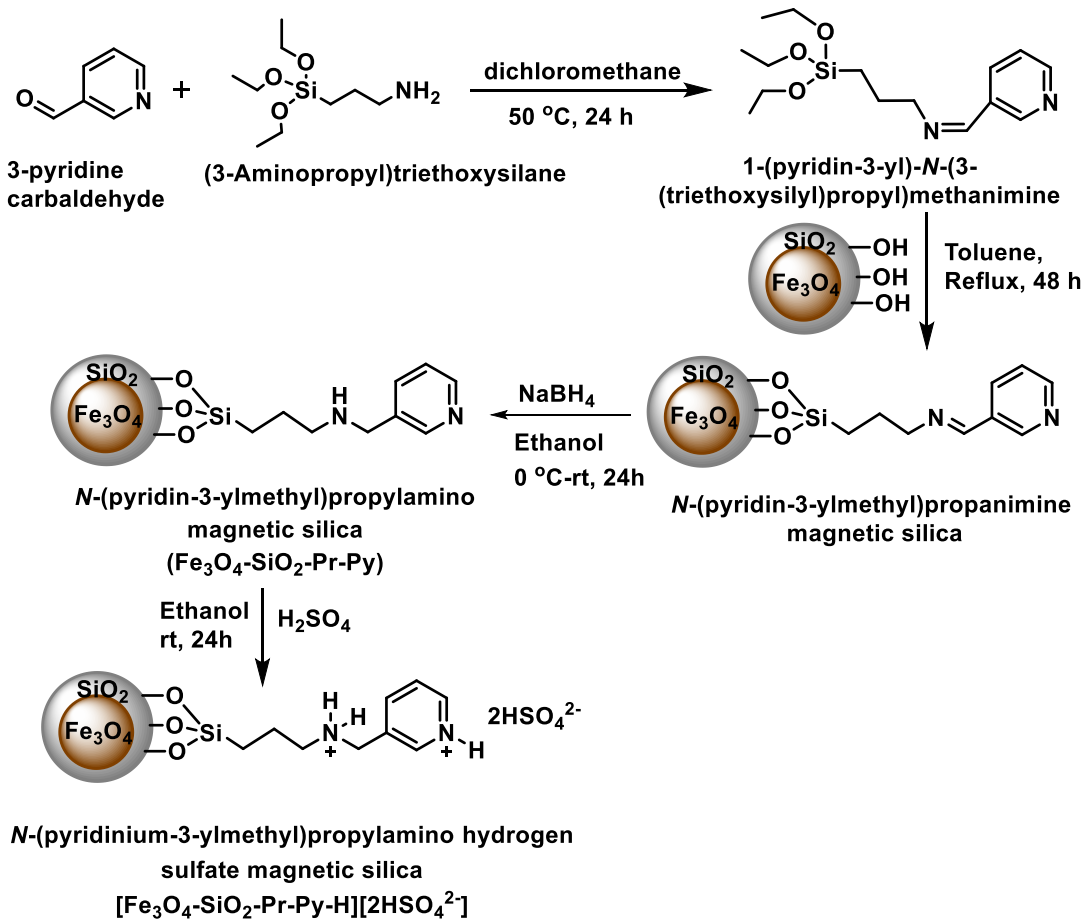

Scheme 3.2. Synthesis of [Fe_3O_4-SiO_2-Pr-Py-H][$2HSO_4^{2-}$]

3.4.2.2. Preparation of supported Pd catalysts

Carbon-supported catalysts with varying Pd loadings were prepared according to a previously reported procedure [40]. Typically, 33 mg of $PdCl_2$ was dissolved in 50 mL of aqueous hydrochloric acid and stirred for 30 minutes. A slurry of 0.99 g of activated carbon in water was then added slowly with constant stirring and kept for 2 hours. The pH of the reaction mixture was adjusted to 7-8 using aqueous 10 M NaOH and the mixture was further stirred for 30 minutes. $NaBH_4$ (1 g) was added in portions and stirring continued for 30 minutes. The resulting solid catalyst was filtered, washed several times with distilled water and dried in an oven at 100°C. A similar procedure was used to prepare catalysts with 1-5% palladium loadings on different supports.

3.4.3. Determination of catalyst acidity

Sodium chloride aqueous solution (0.05 mol L^{-1}, 30 mL) was added to the $[Fe_3O_4@SiO_2\text{-}Pr\text{-}Py\text{-}H][2HSO_4^{2-}]$ catalyst (0.250 g). The mixture was stirred for 60 minutes at room temperature under ultrasonic conditions. After centrifugal separation, the supernatant was titrated with a sodium hydroxide aqueous solution (0.05 mol L^{-1}) using phenolphthalein as an indicator [41, 42]. The total acidity of $[Fe_3O_4@SiO_2\text{-}Pr\text{-}Py\text{-}H][2HSO_4^{2-}]$ was found to be 0.027 M. Acidity of $[Fe_3O_4@SiO_2\text{-}Pr\text{-}Py\text{-}H][2HSO_4]^{2-}$ sample after 3rd reuse determined was 0.026 M. By using similar method, acidity of other sulfonic acid functionalized solid acid catalysts was estimated and presented in Table 3.1.

3.4.4. Condensation of 2-methylfuran with aldehydes

A mixture of an aldehyde (2 mmol), 2-methylfuran (4 mmol) and an acidic catalyst (0.1 g for solid acid or 10 mol% for liquid acid) was stirred for 3 hours at 65°C. For liquid acids, the reaction was neutralized with a saturated sodium bicarbonate solution, and the resulting mixture was extracted with ethyl acetate (20 mL × 1), followed by washes with water (20 mL × 1) and brine (20 mL × 1). For solid acid catalysts, the catalyst was separated by filtration or using an external magnet (for magnetic catalysts), and the filtrate was diluted with ethyl acetate (20 mL × 1), then washed with water (20 mL × 1) and brine (20 mL × 1). The organic layer was dried over sodium sulphate and evaporated under reduced pressure. The obtained crude oil was purified by column chromatography using petroleum ether as the eluent.

3.4.5. Hydrogenation of condensation products

A mixture of the condensation product (0.2 g) dissolved in a solvent (20 mL) was added to a round-bottom flask containing the supported Pd catalyst (0.05 g). The mixture was stirred at room temperature under a hydrogen atmosphere using a bladder for 10 hours. The reaction mixture was then filtered to separate the catalyst, and the filtrate was evaporated under reduced pressure to obtain the desired product. For gram-scale hydrogenation, the reaction was performed in a 300 mL Parr reactor. Typically, 2.0 g of the condensation product was dissolved in 140 mL of solvent and charged into the Parr reactor containing 5% w/w Pd/C (0.610 g). The mixture was stirred at 800 rpm under a hydrogen pressure of 50 psi. After 10 hours, the reaction mixture was filtered and the filtrate was extracted with ethyl acetate (200 mL × 2) and washed with water (100 mL × 1). The organic layer was dried over anhydrous Na_2SO_4 and concentrated under reduced pressure. The filtered moist catalyst was stored in a bottle and can be reused after calcination and activation.

3.4.6. Analysis of the reaction products

Thin-layer chromatography was performed using Merck 5554 aluminum-backed silica plates, and compounds were visualized under UV light (254 nm). The conversion of reactants and selectivity of products were calculated using GC with a flame ionization detector and a capillary column (FFAP). Pure products were characterized and confirmed by ^{1}H NMR and ^{13}C NMR (50 MHz) using CDCl3 (0.01%, TMS) as a solvent on a 200 MHz Bruker instrument (4.6). Products were also confirmed using a QP-Ultra 2010 GC-MS Shimadzu instrument with an RTX-5 column, helium as the carrier gas, electrospray ionization mode, and an ionization source temperature of 200°C.

3.5. Results and Discussion

3.5.1. Catalyst characterization

3.5.1.1. X-ray diffraction (XRD)

X-ray diffraction (XRD) analysis of magnetic organosilica catalysts $Fe_3O_4@SiO_2$, [$Fe_3O_4@SiO_2$-Pr-Py], and [$Fe_3O_4@SiO_2$-Pr-Py-H][$2HSO_4^{2-}$], both before and after the reaction, revealed diffraction peaks at 2θ = 30.32°, 35.80°, 43.36°, 53.88°, 57.54°, and 63.26°. These peaks correspond to the indices (220), (311), (400), (422), (511), and (440) of Fe_3O_4 (Figure 3.1a). The XRD patterns of all the catalysts were similar due to the common $Fe_3O_4@SiO_2$ backbone. The XRD patterns for prepared 1-5% w/w

Pd/C and commercial 5% w/w Pd/C catalysts are shown in Figure 3.1b. Broad diffraction peaks at 2θ = 25° and 43.5° exhibited the carbon structure of the support, with decreased intensity of these peaks upon Pd loading. Pd-supported catalysts

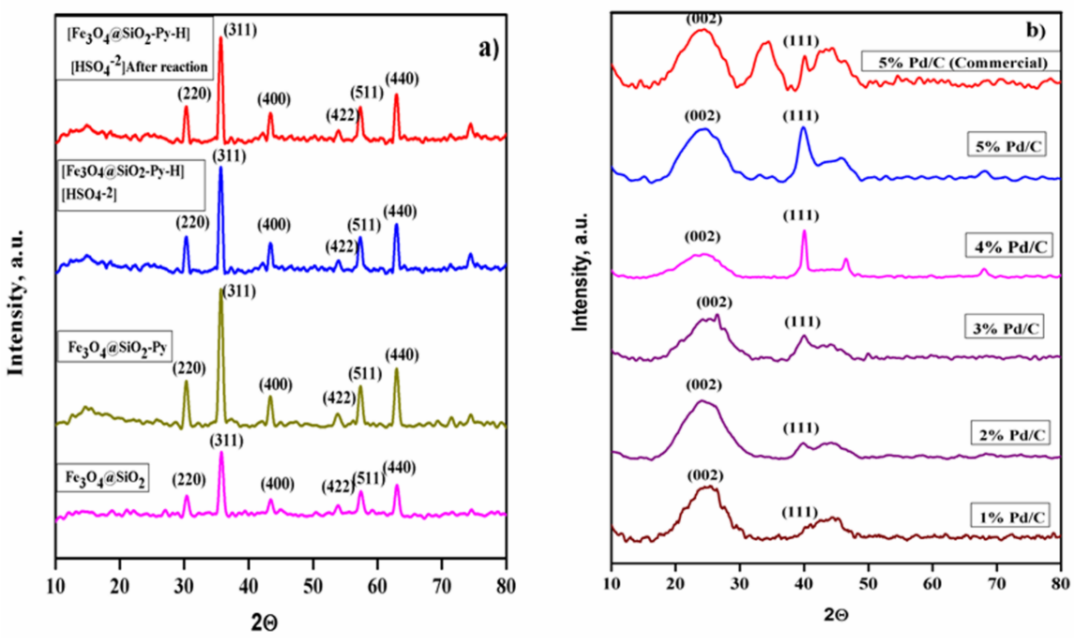

Figure 3.1. a) XRD Patterns of magnetic samples and b) carbon supported 1-5%w/w palladium samples.

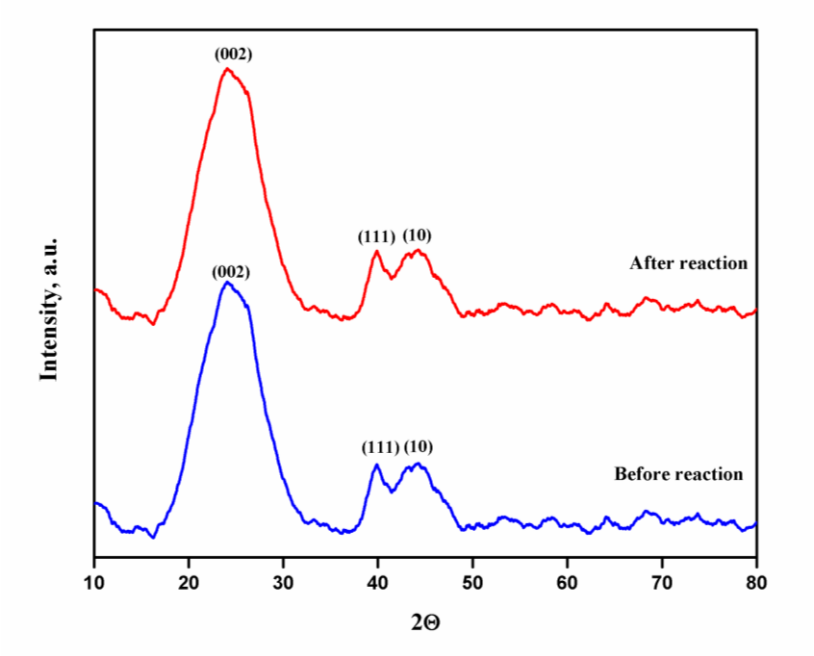

Figure 3.2. XRD of 5% Pd/C catalyst before and after reaction

displayed peaks at 2θ = 40.1°, 68.1°, and 82.4°, attributed to the (111), (220), and (311) planes of the face-centered cubic structure of Pd (JCPDS card no. 46-1043). A broad peak at 2θ = 24.37° and a sharp peak at 2θ = 39.93° corresponded to (002) and (111) planes of carbon and palladium, respectively, while a broad peak at 2θ = 44.23° related to the (100) plane due to turbostratic carbon. An increase in the intensity of the (111) peak with higher palladium loading suggested the spherical nature of Pd nanoparticles.

The XRD pattern of the both spent catalysts [Fe_3O_4@SiO_2-Pr-Py-H][$2HSO_4^{2-}$] and Pd/C after subsequent reuse runs are given in Figure 3.1 and 3.2 respectively. Even after 3 reuses of the catalyst, no any change in the XRD pattern of [Fe_3O_4@SiO_2-Pr-Py-H][$2HSO_4^{2-}$] was noticed this confirmed the excellent stability of catalyst [Figure. 3.1a]. The XRD pattern of spent Pd/C catalyst does not showed any change in characteristics peak positions, confirms the robustness of catalyst even after catalyst reuse runs [Figure 3.2].

3.5.1.2. Fourier transform infrared spectroscopy (FTIR)

The FT-IR spectrum of the magnetic organosilica catalyst [Fe_3O_4@SiO_2-Pr-Py-H][$2HSO_4^{2-}$] is shown in Figure 3.3a. Intense peaks between 580 cm^{-1} and 630 cm^{-1} were assigned to the Fe-O bond stretching vibrations in Fe_3O_4. A band at 1635 cm^{-1} was attributed to the –C=N– stretching of the pyridine moiety and a band at 3375 cm^{-1} indicated hydroxyl functionality.

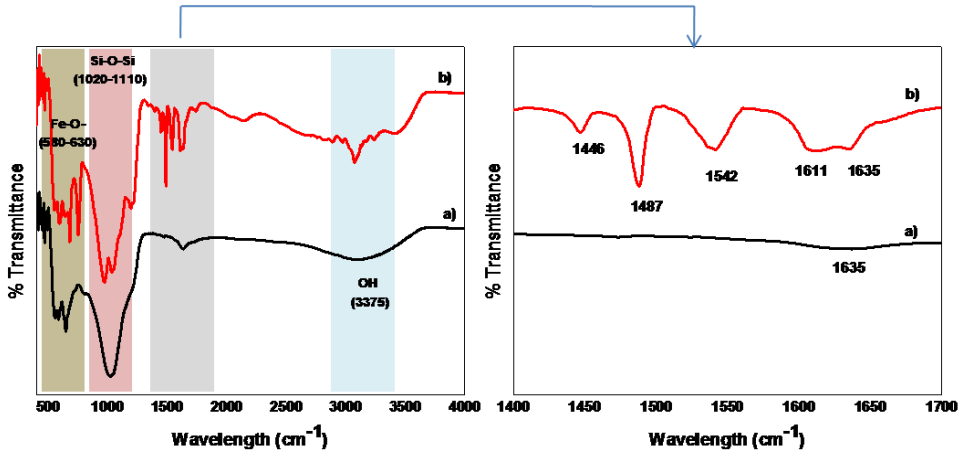

Figure 3.3. a) FTIR and b) FTIR after pyridine adsorption of [Fe_3O_4@SiO_2-Pr-Py-H][$2HSO_4^{2-}$]

To identify and confirm the type of acid sites in [Fe_3O_4@SiO_2-Pr-Py-H][$2HSO_4^{2-}$] pyridine was adsorbed on the catalyst surface, and the FT-IR spectrum was recorded. A band at 1446 cm^{-1} was attributed to Lewis acid sites on Fe_3O_4 nanoparticles not coated with silica, while a band at 1542 cm^{-1} was assigned to Brønsted acid sites from $–NH_2$, Py-H, and HSO_4 species (Figure 3.3b). FT-IR analysis confirmed the stability of both fresh and used [Fe_3O_4@SiO_2-Pr-Py-H][$2HSO_4^{2-}$] catalysts, with peak positions remaining consistent between fresh and used samples (Figure 3.4).

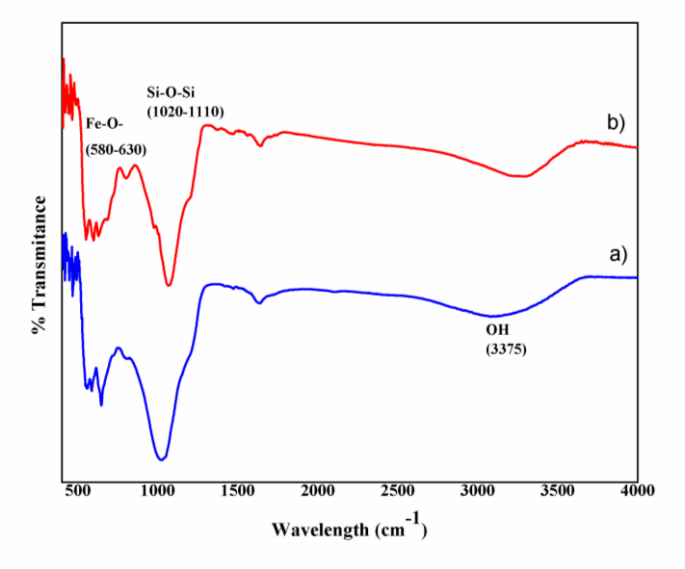

Figure 3.4. FTIR of [Fe_3O_4@SiO_2-Pr-Py-H][$2HSO_4^{2-}$] a) before reaction and b) after reaction.

3.5.1.3. High resolution transmission electron spectroscopy (HR-TEM)

Morphology and particle sizes of commercial, in house prepared and reused 5% *w*/*w* Pd/C were compared by HR-TEM analysis. From HR-TEM images of these catalysts, it was observed that distribution of palladium nano particles was uniform. Average particle size of commercial and the prepared 5% *w*/*w* Pd/C was 6.73 nm and 7.6 nm, respectively (Figures 3.5 a, b). No major change in morphology of 5% *w*/*w* Pd/C was observed after its reuse (Figure 3.5e). From the HR-TEM images of these catalysts, homogeneous dispersion of palladium nano particles was observed in both fresh and used catalyst.

In the [Fe_3O_4@SiO_2-Pr-Py-H][$2HSO_4^{2-}$] sample, almost hexagonal geometry with an average particle size of 39.39 nm was observed (Figure 3.5c). HR-TEM images demonstrated that most Fe_3O_4 nanoclusters were successfully coated with a thin layer of SiO_2, resulting in a core/shell structure of Fe_3O_4@SiO_2 NPs (Figure 3.5d). After

reuse of [Fe_3O_4@SiO_2-Pr-Py-H][$2HSO_4^{2-}$] catalyst its morphology was found to be the same as that of the fresh sample (Figure 3.5f). The used catalyst has hexagonal shape with average particle size.

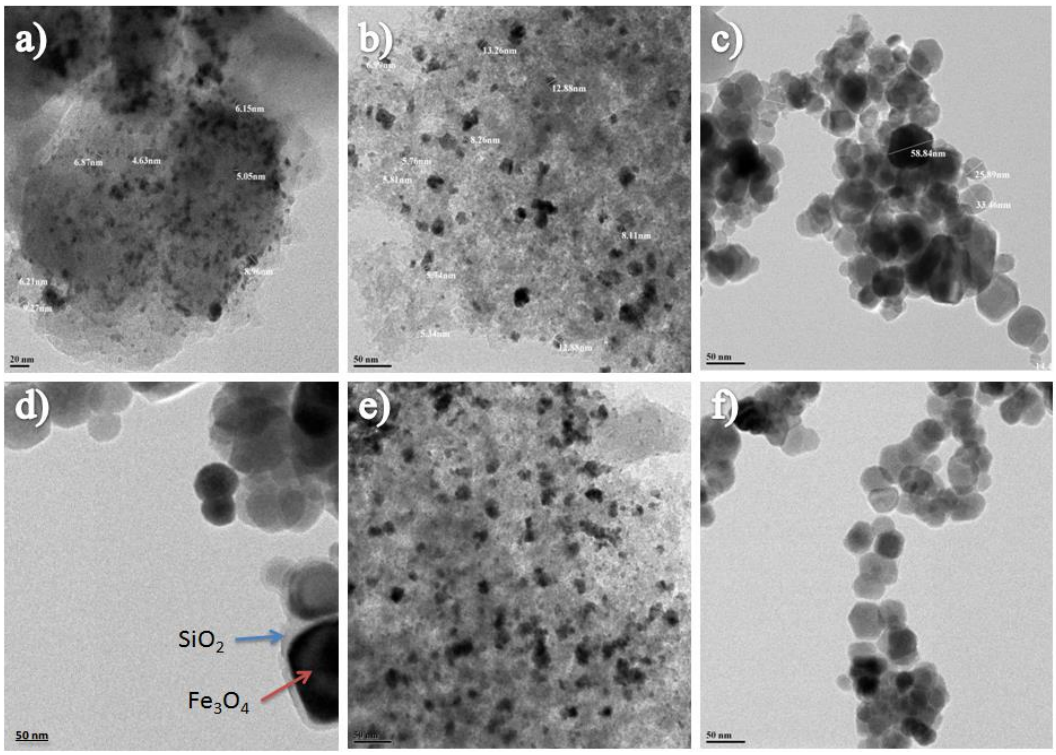

Figure 3.5. HR-TEM images of 5% w/w Pd/C (Commercial), 5% w/w Pd/C (Prepared), 5% w/w Pd/C (Prepared) 3rd reuse, [Fe_3O_4@SiO_2-Pr-Py-H][$2HSO_4^{2-}$] and [Fe_3O_4@SiO_2-Pr-Py-H][$2HSO_4^{2-}$].

3.5.1.4. Solid state NMR

The structure of [Fe_3O_4@SiO_2-Pr-Py-H][$2HSO_4^{2-}$] catalyst was confirmed by taking solid state ^{13}C NMR of its non-magnetic and not acidic counterpart SiO_2-Pr-Py. In SiO_2-Pr-Py sample three well resolved peak at 10.53, 22.23, 50.38 ppm were observed, which were assigned to aliphatic -CH_2- groups. The bands at 125, 136.13, 138.24 and 148.56 ppm are assigned to –CH- groups of pyridine [Figure 2.5, Chapter 2] [43].

3.5.2. Condensation of formaldehyde with 2-methylfuran

Table 3.1. Catalyst screening for condensation of formaldehyde with 2-methylfuran [a]

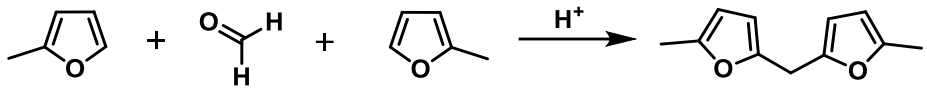

2-methylfuran + formaldehyde + 2-methylfuran → bis(5-methylfuran-2-yl)methane **1**

Entry	Catalyst	Acidity [mol/g]	Conv. Of 2-methyl furan [%]	Conv. of HCHO [c] [%]	Yield of 1 [d] [%]	Carbon balance [%]
1[b]	H_2SO_4	---	95	92	74 (66)	74
2	Amberlyst-15	0.016	92	89	83 (74)	83
3	Amberlyte IR-120	0.014	90	87	82 (72)	82
4	Sn-Mont	---	62	60	67 (56)	67
5	Zr-Mont	---	59	58	60 (52)	60
6	$[Fe_3O_4@SiO_2$-Pr-Py-H] $[HSO_4^{2-}]$	0.027	93	90	86 (75)	86
7	SO_4^{2-} / SiO_2	0.013	71	70	74 (66)	74
8	SO_4^{2-} / $Fe_3O_4@SiO_2$	0.019	73	72	79 (69)	79

[a] Reaction conditions: Formaldehyde (0.162 mL, 2 mmol), 2-methylfuran (0.328 g, 4 mmol), catalyst (0.1g), 65 °C, 3h. [b] 10 mol% of H_2SO_4 was used. [c] Determined by using GC. [d] Yields are reported by GC and values in parenthesis represent isolated yields after workup and column chromatography. Selectivity of 1 is 100% for all the catalysts.

Several acid catalysts were screened for the condensation of aqueous formaldehyde with 2-methylfuran, as summarized in Table 3.1. The reaction with H_2SO_4 (10 mol%) at 65°C for 3 hours yielded 74% of the condensation product 1 with 92% formaldehyde conversion (Table 3.1, entry 1). Amberlyst-15 provided 89% conversion of formaldehyde with 83% yield of product 1 (Table 3.1, entry 2). Further, condensation reaction was performed over Amberlyte IR-120, to give 82% yield of **1** with 87% conversion of formaldehyde (Table 3.1, entry 3). Sn and Zr supported on montmorillonite catalysts gave 60% and 58% conversion of furfural with 67% and 60% yield of **1**, respectively (Table 3.1, entries 4 and 5). Our novel magnetic solid acid $[Fe_3O_4@SiO_2$-Pr-Py-H][$2HSO_4^{2-}$] catalyst showed the highest conversion of both formaldehyde and 2-methyl furan (90% and 93 %, respectively) with 86% yield of **1** (Table 3.1, entry 6). Sulphated silica and sulphated magnetic silica showed almost 70% conversion of formaldehyde with >74% yield (Table 3.1, entries 7 and 8). Table 3.1 also shows the Carbon balance, which was highest (86%) for the best catalyst i.e. $[Fe_3O_4@SiO_2$-Pr-Py-H][$2HSO_4^{2-}$]. The acidity of all the solid acid catalysts used in this

work is presented in Table 3.1. It was observed that [Fe_3O_4@SiO_2-Pr-Py-H][$2HSO_4^{2-}$] catalyst possessed the maximum acidity of 0.027M which contributed to its excellent activity towards the condensation reaction.

Turn over number (TON) and turn over frequency (TOF) of catalysts

The turnover number (k cat) is defined as the limiting number of chemical conversions of substrate molecules per second that a single active site will execute.

In catalytic chemical conversion, Turn over number (TON) and Turn over frequency (TOF) usually determined when conversion of limiting reagent is below 50% as in the initial time of the reaction the catalyst exist in most active state.

Turn over number of heterogeneous catalysts can be calculated by using following equation,

Turn over number (TON) = (Number of mols of reactant consumed/ number of moles of active sites in the catalyst)

And

Turn over frequency (TOF) of heterogeneous catalysts can be calculated by using following equation,

Turn over frequency (TOF) = (Turn over number/ time)

For our catalysts [Fe_3O_4@SiO_2-Pr-Py-H] [HSO_4^{2-}], the conversion of formaldehyde after 1h was 49%. Initial moles of formaldehyde used in the reaction is 0.002 moles.

Moles of formaldehyde consumed = 0.002 moles x (49/100) = 0.00098 moles

Amount of catalysts used in the reaction was 0.1 g.

Acidity of this catalyst is 0.027 moles/g, which means 1 g of catalyst contains 0.027 moles of acid sites.

Moles of active site in the catalyst = [0.1 g x 0.027 moles]/ 1g = 0.0027 moles

Turn over number (TON) = (Number of mols of reactant consumed/ number of moles of active sites in the catalyst) = 0.00098 moles/ 0.0027 moles = 0.3629

Turn over frequency (TOF) = (Turn over number/ time) = 0.3629/ 60 min = 0.00604 min^{-1}

The turn over number (TON) and turn over frequency (TOF) of other sulfonic acid-functionalized solid acid catalysts was also calculated using a similar equation, the results presented in Table 3.2.

Table 3.2. Catalysts acidity, turn over number (TON) and turn over frequency (TOF)

Entry	Catalyst	Acidity [mol/g]	Conv. of HCHO [%]	TON	TOF [min $^{-1}$]
1	H_2SO_4	---	---		
2	Amberlyst-15	0.016	44	0.55	0.00916
3	Amberlyte IR-120	0.014	41	05857	0.00976
4	Sn-Mont	---	---		
5	Zr-Mont	---	---		
6	[Fe_3O_4@SiO_2-Pr-Py-H] [HSO_4^{2-}]	0.027	49	0.3629	0.00604
7	SO_4^{2-} / SiO_2	0.013	32	0.4923	0.00820
8	SO_4^{2-} / Fe_3O_4@SiO_2	0.019	37	0.3894	0.00649
For each catalysts conversion measured after 60 min					

3.5.3. Catalyst screening for hydrogenation

Various supported noble metal catalysts were evaluated for the hydrogenation of condensation product 1. Initially, 1% *w*/*w* Pd/C was used for hydrogenation of condensation product **1**, to give 45% conversion and 40% yield of the ring hydrogenation product **2** (cyclic ether) along with 4.2% semi hydrogenation product **2'** (Table 3.3, entry 1). With increasing Pd loading from 1 to 5%, the conversion of **1** also increased gradually from 45% to 91% with an increase in the yield of cyclic ether from 40 to 87% (Table 3.3, entries 2-5). The 5% w/w Pd/Al_2O_3 catalyst achieved 80%conversion with a 74% yield of cyclic ether (Table 3.3, entry 6). The 5% Ru/C catalyst provided 47% yield of cyclic ether with 56% conversion of the condensation product (Table 3.3, entry 7). With 5% *w*/*w* Ru/Al_2O_3, slightly better conversion of starting material and yield of product was observed than 5% *w*/*w* Ru/C (Table 3.3, entry 8). The lowest conversion and the product yield of 41% and 35%, respectively was obtained over 5% *w*/*w* Pt/C catalyst (Table 3.3, entry 9). The commercial 5% *w*/*w* Pd/C gave 87% conversion of condensation product with 82% yield of cyclic ether,

which was comparable with that shown by the prepared 5% *w*/*w* Pd/C catalyst (Table 3.3, entry 10).

Table 3.3. Catalyst screening for hydrogenation of condensation product [a]

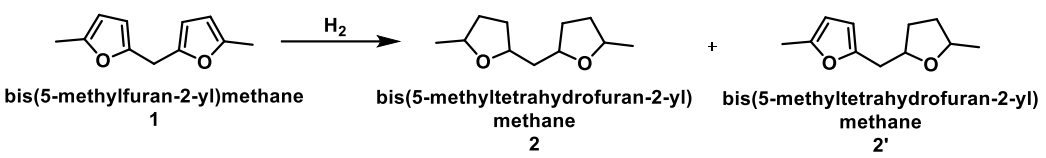

Entry	Catalyst	Conv. of 1 [b] [%]	Yield [c] [%]		Selectivity of [%]		Carbon balance [%]
			2	2'	2	2'	
1	1% Pd/C	45	40 (35)	4.2	88	12	44.2
2	2% Pd/C	54	49 (43)	4.8	91	09	43.8
3	3% Pd/C	66	62 (52)	3.9	94	06	65.9
4	4% Pd/C	78	73 (68)	5	93	07	82
5	5% Pd/C	91	87 (81)	4	96	05	91
6	5% Pd/Al_2O_3	80	74 (68)	6	92	08	80
7	5% Ru/C	56	47 (31)	7.5	84	16	54.5
8	5% Ru/Al_2O_3	67	55 (41)	12	82	18	67
9	5% Pt/C	41	35 (29)	6.1	85	15	41.1
10	5% Pd/C (Commercial)	87	82 (76)	5.2	94	06	87.2

[a] Reaction conditions: Condensation Product-**1** (0.2 g, 0.826 mmol), catalyst (0.050 g), 1,4-Dioxane (5 mL), room temperature, H_2 (bladder pressure), 10 h. [b] Conversion determined by GC. [c] Yields are reported by GC and values in parenthesis represent isolated yields after workup and column chromatography.

3.5.4. Solvent screening for the hydrogenation reaction

The activity of 5% *w*/*w* Pd/C catalyst was studied for the ring hydrogenation of condensation product in various organic solvents at room temperature for 10 h (Table 3.4). Under the optimized reaction conditions in isopropyl alcohol, an 85% yield of ring hydrogenation product **2** was achieved (Table 3.4, entry 1). In methanol, the yield was 76% (Table 3.4, entry 2), while, in presence of acetonitrile, 71% yield of **2** was achieved (Table 3.4, entry 3). With, 1,4-dioxane highest yield of 90% for cyclic ether **2** was obtained (Table 3.4, entry 4). In Chloroform and dichloromethane solvents lower

yield of cyclic ether **2** was observed (Table 3.4, entries 5 and 6). Due to its superior performance, 1,4-dioxane was selected as the ideal solvent for further experiments.

Table 3.4. Solvent screening for hydrogenation of condensation product [a]

Entry	Solvent	Yield of 2 [%][b]
1	Isopropyl alcohol	85 (76)
2	Methanol	76 (65)
3	Acetonitrile	71 (62)
4	1,4-Dioxane	90 (81)
5	Chloroform	63 (55)
6	Dichloromethane	79 (69)

[a]Reaction conditions: Condensation product (0.2 g, 0.826 mmol), 5% *w*/*w* Pd/C (0.035 g, 0.016 mmol), solvent (5 mL), H_2 (bladder pressure), room temperature, 10 h. [b] Yields are reported by GC and values in parenthesis represent isolated yields after workup and column chromatography.

3.5.4. Substrate scope for the synthesis of cyclic ethers

Encouraged by the successful two step synthesis of cyclic ether from 2-methylfuran and formaldehyde, the scope of this protocol was further explored for the synthesis of Pd/C catalyst to achieve 69% yield of the ring saturated product **4** (Table 3.5, entry 1). Condensation product **5** was obtained in 74% yield from acetaldehyde and 2-methylfuran after 85% conversion of acetaldehyde. Subsequent hydrogenation of **5**, selectively gave product **6** in 70% yield (Table 3.5, entry 2). The condensation of acetone with 2-methylfuran produced condensation product 7 in 65% yield after 72% conversion of acetone. Further, hydrogenation of **7**, provided ring saturated product **8** with 58% yield (Table 3.5, entry 3). The condensation of benzaldehyde with provided 72% yield of **9** after 80% conversion of benzaldehyde. Under optimized reaction 72% yield of **9** after 80% conversion of benzaldehyde. Under optimized reaction conditions hydrogenation of **9** was performed, furan rings were successfully hydrogenated but benzene ring was left as it is, resulting in product **10** with a 65% yield (Table 3.5, entry 4).

Table 3.5. Substrate screening for synthesis of cyclic ethers

Entry	Substrate	Condensation Product, 1 [Yield, %]	Hydrogenation Product, 2 [Yield, %]
1	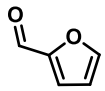	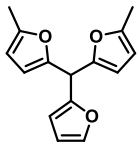 3 73 %	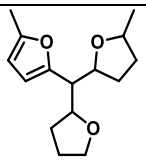 4 69 %
2	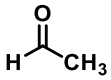	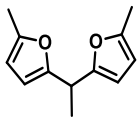 5 74 %	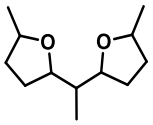 6 70 %
3		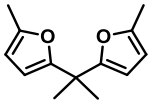 7 65 %	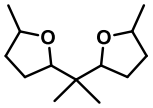 8 58 %
4	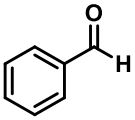	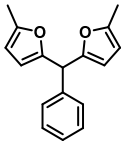 9 72 %	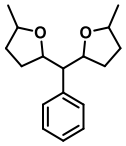 10 65 %

Reaction conditions: Step 1**-** 2-methylfuan (4 mmol), aldehyde or ketone (2 mmol), $[Fe_3O_4@SiO_2\text{-}Pr\text{-}Py\text{-}H][2HSO_4^{2-}]$ (0.1 g), 65 ^oC, 3 h. Step 2**-** Condensation product (0.2 g), 5% *w*/*w* Pd/C (0.050 g), Room temperature, 1,4-Dioxane (5 mL), H_2 (bladder pressure), 10 h. Isolated yields after workup and column chromatography purification are reported.

3.5.6. Plausible reaction pathway

The proposed reaction pathway for the formation of bis(5-methyltetrahydrofuran-2-yl)methane from formaldehyde and 2-methylfuran is presented in Figure 3.6. Initially, the protonation of formaldehyde is catalyzed by the Brønsted acid sites of $[Fe_3O_4@SiO_2\text{-}Py\text{-}H]$ $[2HSO_4^{2-}]$ catalyst followed by its reaction with 2-methylfuran to form (5-methylfuran-2-yl)methanol, which was further reacted with the second molecule of 2-methylfuran to produce the condensation product **1**. Product **1** then

serves as the starting material for hydrogenation over 5% Pd/C, where initially one furan ring is hydrogenated, followed by hydrogenation of the second ring to produce cyclic ether **2**.

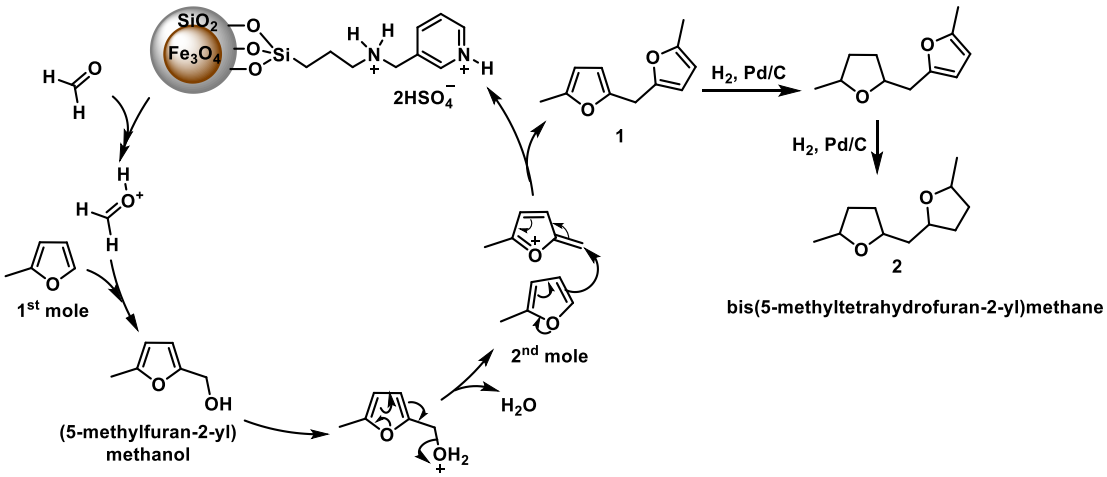

Figure 3.6. Plausible reaction mechanism for condensation and hydrogenation steps

3.5.7. Recycle study

3.5.7.1. Recycling of [Fe_3O_4@SiO_2-Pr-Py-H][$2HSO_4^{2-}$]

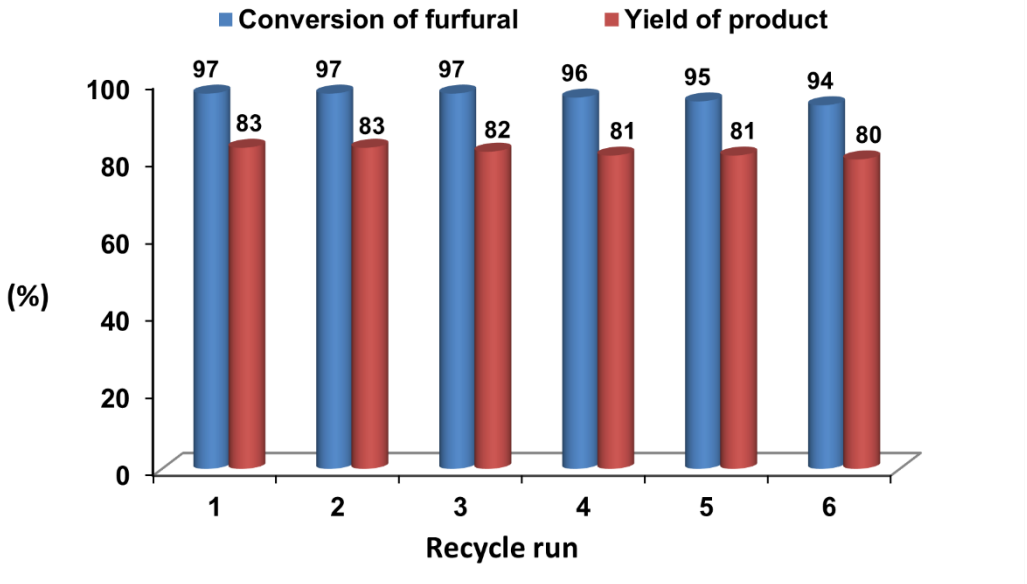

Figure 3.7. Recycling of [Fe_3O_4@SiO_2-Py-H] [$2HSO_4^{2-}$], Reaction Conditions: Formaldehyde (0.162 mL, 2 mmol), 2-methylfuran (0.328 g, 4 mmol), catalyst (0.1 g), 65 ^oC, 3h.

To evaluate the stability of [Fe_3O_4@SiO_2-Py-H] [$2HSO_4^{2-}$], the catalyst was separated using an external magnetic field after the first reaction, washed with ethyl acetate and reused for subsequent runs. The catalyst's stability was assessed through several recycling cycles (Figure 3.7). The catalytic activity remained consistent after five uses. During the sixth reuse, the activity slightly decreased, yielding 77% of the condensation product 1 with 86% formaldehyde conversion. The catalyst's acidity remained nearly the same (0.026 M) after the third reuse, confirming its stability under reaction conditions.

3.5.7.2. Recycling of 5% Pd/C

The stability of the hydrogenation catalyst, 5% Pd/C, was also evaluated through recycle runs (Figure 3.8). After each reaction, the catalyst was filtered, washed with distilled water, dried, and reused. The 5% Pd/C catalyst demonstrated excellent stability, with consistent activity up to the fourth reuse. A slight decrease in activity was observed during the fourth reuse, likely due to handling losses.

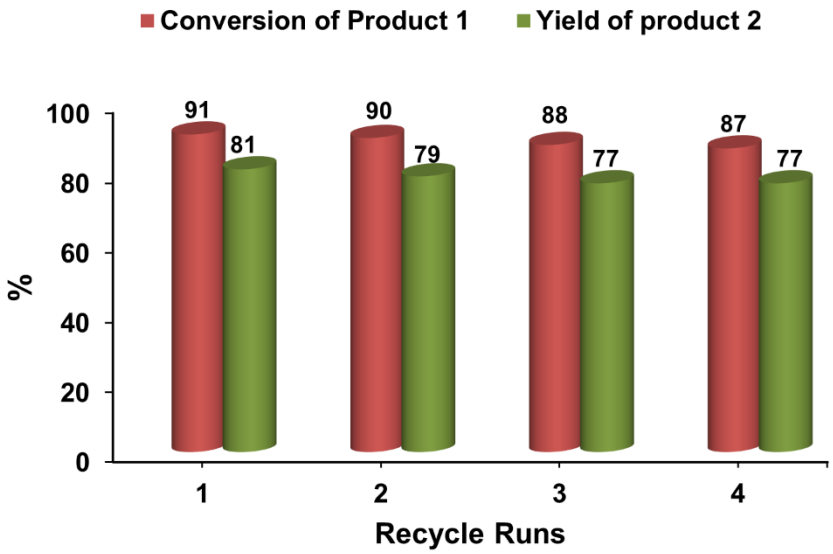

Figure 3.8. Recycling of 5% Pd/C, Condensation Product-1 (0.2 g, 0.826 mmol), catalyst (0.050 g), 1,4-Dioxane (5 mL), room temperature, H_2 (bladder pressure), 10 h.

3.5.8. Carbon balance calculation

Carbon present in reactants for 1 mol of reactants

HCOH [1 mol] :

30.03 MW = **12 g carbon** + 16 g oxygen + 2 g of hydrogen

2-methylfuran [C_5H_6O] [1 mol] :

82.1 = [60 g carbon + 6 g hydrogen + 16 g of oxygen]

Total reactant carbon= 12 + 60 = 72 g

For 1 mol [30 g] of formaldehyde has 12 g carbon

Thus, for 2 mmol [0.060 g] of formaldehyde has 0.024 g carbon

For 1 mol [82.1 g] of 2-methyfuran 60 g carbon

Thus, for 4 mmol [0.328 g] of 2-methyfuran is 0.239 g of carbon

Total carbon in reactants = 0.012 g [formaldehyde carbon] + 0.239 g [2-methyfuran carbon] = 0.251 g

Carbon in product: condensation product 1 [$C_{11}H_{12}O_2$] [MW=176]

For 1 mol of product

176 g product contains = 132 g of carbon + 12 g of hydrogen + 32 g of oxygen

2 mmol of HCHO + 4 mmol of 2-methylfuran = 2 mmol of product

From 0.264 g carbon of reactants we must get 0.264 g of carbon in product then it will be 100% C balance.

GC yields are considered for carbon balance calculation

100% yield of product is 0.352 g of product which contains 0.264 g carbon

Thus, for Entry 1. H_2SO_4 [Yield: 74%] product quantity is 0.260 g which contains 0.195 g carbon

Thus, 0.264 g of carbon is 100% carbon balance

Thus, for 0.195 g will be 73.86%

For other entries it will be same as above calculation.

3.6. Conclusions

A two-step reaction protocol involving condensation and hydrogenation has been established for the synthesis of cyclic ethers as potential fuel additives from 2-methylfutran and aldehydes or ketones. In the first step, a newly designed acidic magnetic solid catalyst [Fe_3O_4@SiO_2-Pr-Py-H][$2HSO_4^{2-}$] showed an excellent activity for formaldehyde condensation with 2-methylfuran to give 90% conversion of formaldehyde and 75% isolated yield of the condensation product. The magnetic nature of the catalyst allowed its easy separation from reaction mixture. This catalyst was successfully explored for a wide variety of aldehydes or ketones for their condensation with 2-methylfuran. In the second step, hydrogenation of the

condensation products was performed. Among the several supported catalysts, 5% *w*/*w* Pd/C gave the highest conversion of 85% with 80% yield of saturated cyclic ether at ambient hydrogen pressure conditions in 1,4-dioxane solvent. Hydrogenation of several other condensation products was also successfully catalysed by the prepared 5% *w*/*w* Pd/C catalyst.

3.7. References

[1] T. Zhao, Y. Zhang, G. Zhao, X. Chen, L. Han, W. Xiao, *Fuel Process. Technol*., **2018**, *180*, 14-22.

[2] P. Pradhan, S. M. Mahajani, A. Arora, *Fuel Process. Technol*., **2018**, *181*, 215-232.

[3] IPCC, Renewable Energy Sources and Climate Change Mitigation, **2012**.

[4] E. Agbor, X. Zhang, A. Kumar, *Renewable Sustainable Energy Rev*., **2014**, *40*, 930–943.

[5] A. Shrotri, H. Kobayashi, A. Fukuoka, *Advances in Catalysis*, **2017**, *60*, 59-123.

[6] M. Guo, W. Song, J. Buhain, *Renewable Sustainable Energy Rev*., **2015**, *42*, 712–725.

[7] G. W. Huber, S. Iborra, A. Corma, *Chem. Rev*. **2006**, *106*, 4044-4098.

[8] D. M. Alonso, J. Q. Bond, J. A. Dumesic, *Green Chem*. **2010**, *12*, 1493-1513.

[9] A. Corma, O. D. Torre, M. Renz, N. Villandier, *Angew. Chem., Int. Ed*., **2011**, *50*, 2375-2378.

[10] M. Balakrishnan, E. R. Sacia, A. T. Bell, *ChemSusChem*, **2014**, 7, 2796-2800.

[11] G. Li, A. N. Li, A. S. Li, A. A. Wang, A. Y. Cong, A. X. Wanga, T. Zhang, *Chem. Commun*., **2013**, *49*, 5727.

[12] W. H. Brown, W. N. French, *Can. J. Chem*., **1958**, *36*, 537

[13] W. H. Brown and B. J. Hutchinson, *Can. J. Chem*., **1978**, 56, 617.

[14] A. Riad, Z. Mouloungui, M. Delmas, A. Gaset, *Synth. Commun*., **1989**, *19*, 3169-3173.

[15] W. M. Van Rhijn, D. E. DeVos, B. F. Sels, W. D. Bossaert, P. A. Jacobs, *Chem. Commun*., **1998**, *3*, 317-318.

[16] T. Li, S. I. Cheng, J. F. Lee, L. Y. Jang, *J. Mol. Catal. A: Chem*., **2003**, *198*, 139.

[17] A. S. K. Hashmi, L. Schwarz, P. Rubenbauer, M. C. Blanco, *Adv. Synth. Catal*., **2006**, *348*, 705-708.

[18] V. Nair, K. G. Abhilash, N. Vidya, *Org. Lett*., **2005**, *7*, 5857-5859.

[19] Z. Wang, H. Li, W. Zhao, S. Yang, *J. Ind. and Engg. Chem*, **2018**, *66*, 325.

[20] F. Algarraa, A. Corma, H. Garciaa, J. Primoa, *Appl. Catal., A*, **1995**, *128*, 119.

[21] M. Balakrishnan, E. R. Sacia, A. T. Bell, *ChemSusChem*, **2014**, *7*, 1078-1085.

[22] M. Muthyala, V. K. Rao, A. Kumar, *Chin. J. Chem.*, **2011**, *29*, 1483-1488.

[23] J. Jaratjaroonphong, S. Tuengpanya, R. Saeeng, S. Udompong, K. Srisook, *Eur. J. Med. Chem.*, **2014**, *83*, 561-568.

[24] I. Ogino, Y. Suzuki, S. R. Mukai, *ACS Catal.*, **2015**, *5*, 4951-4958.

[25] H. Li, S. Saravanamurugan, S. Yang, A. Riisager, *ACS Sustain. Chem. Eng.*, **2015**, *3*, 3274-3280.

[26] C. Zhu, T. Shen, D. Liu, J. Wu, Y. Chen, L. Wang, K. Guo, H. Ying, P. Ouyang, *Green Chem.*, **2016**, *18*, 2165-2174.

[27] S. H. Shinde, C. V. Rode, *Green Chem.*, **2017**, *19*, 4804-4810.

[28] S. H. Shinde, C. V. Rode, *ChemistrySelect*, **2018**, *3*, 4039-4046.

[29] S. Liu, S. Dutta, W. Zheng, N. S. Gould, Z. Cheng, B. Xu, B. Saha, D. G. Vlachos, *ChemSusChem*, **2017**, *10*, 3225-3234.

[30] Y. Nakagawa, S. Liu, M. Tamura, K. Tomishige, *ChemSusChem*, **2015**, *8*, 1114-1132.

[31] S. Liu, M. Tamura, Y. Nakagawa, K. Tomishige, *ACS Sustain. Chem & Engg*, **2014**, *2*, 1819-1827.

[32] S. Liu, Y. Okuyama, M.Tomura, Y. Nakagawa, A. Imai, K. Tomishige, *Green Chem*, **2016**, *18*, 165-175

[33] S. Liu, Y. Amada, M. Tamura, Y. Nakagawa, K. Tomshige, *Green Chem*, **2014**, *16*, 617-624.

[34] Y. Nakagawa, M. Tamura, K. Tomishige, *Journal of the Japan Petroleum Institute*, **2017**, *60*, 1-9.

[35] Y. Nakagawa, K. Takada, M. Tamura, K. Tomishige, *ACS Catal*. **2014**, *4*, 2718-2726.

[36] Y. Nakagawa, K. Tomishige, *Catal. Commun*. **2010**, *12*, 154-156.

[37] S. Lui, Y. Okuyama, M. Tamura, Y. Nakagawa, A. Imai, K. Tomishige, *ChemSusChem*, **2015**, *8*, 628.

[38] Y. Nakagawa, M. Tamura, K. Tomishige, *Fuel Process. Technol*., **2019**, *193*, 404-422.

[39] O. C. Navarro, A. Corma, S. I. Chornet, *Top Catal*., **2009**, *52*, 304-314.

[40] N. S. Date, N. S. Biradar, R. C. Chikate, C.V. Rode, *ChemistrySelect*, **2017**, 2, 24-32.

[41] S. Suganuma, K. Nakajima, M. Kitano, D. Yamaguchi, H. Kato, S. Hayashi, M. Hara, *J. Am. Chem. Soc.*, **2008**, *130*, (38), 12787-12793.

[42] R. S. Thombal, A. R. Jadhav, V. H Jadhav, *RSC Adv*., **2015**, *5* (17), 12981-12986.

[43] K. Tarade, S. Shinde, S. Sakate, C. Rode, *Catal. Commun*., **2019**, *124*, 81-85

3.8. NMR spectroscopic data of synthesized compounds

5,5'-(furan-2-ylmethylene)bis(2-methylfuran)

^{1}H NMR (200 MHz, $CDCl_3$, 0.01%, TMS, δ ppm): 2.15 - 2.21 (m, 6 H) 5.43 (s, 1 H) 5.91 (dt, *J*=2.04, 0.96 Hz, 2 H) 5.99 (d, *J*=2.98 Hz, 2 H) 6.12 (dt, *J*=3.20, 0.77 Hz, 1 H) 6.33 (dd, *J*=3.20, 1.87 Hz, 1 H) 7.37 (dd, *J*=1.82, 0.83 Hz, 1 H)

^{13}C NMR (50 MHz, $CDCl_3$, 0.01%, TMS, δ ppm): 12.94, 30.25, 38.43, 105.58, 106.42, 107.25, 109.64, 141.18, 149.69, 150.89, 151.95.

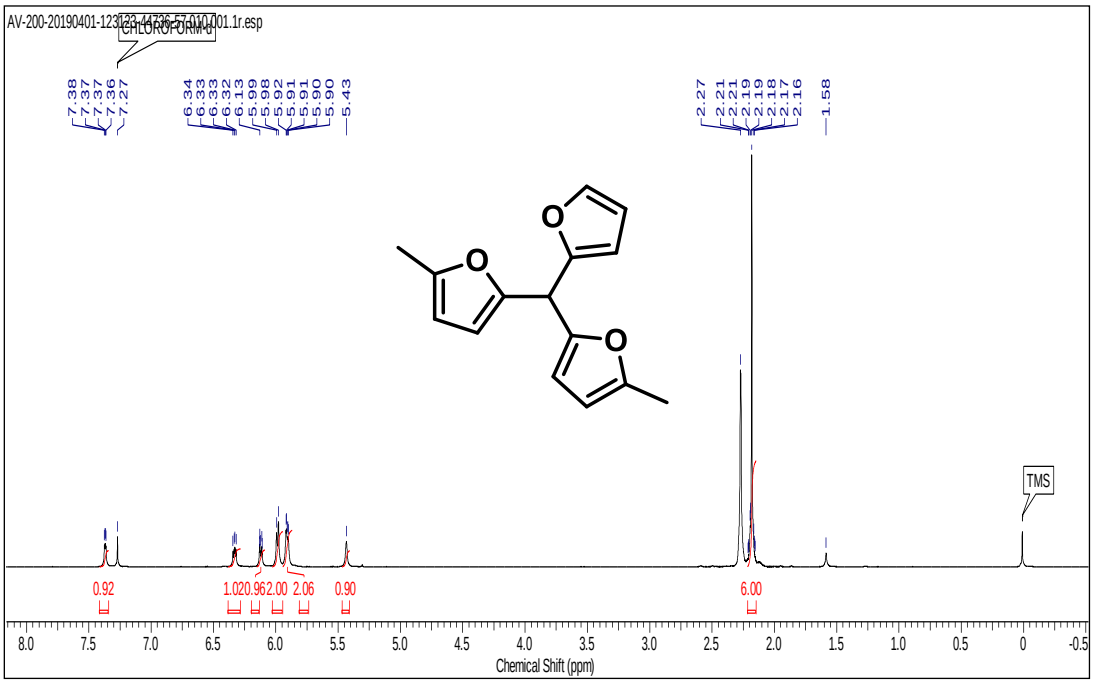

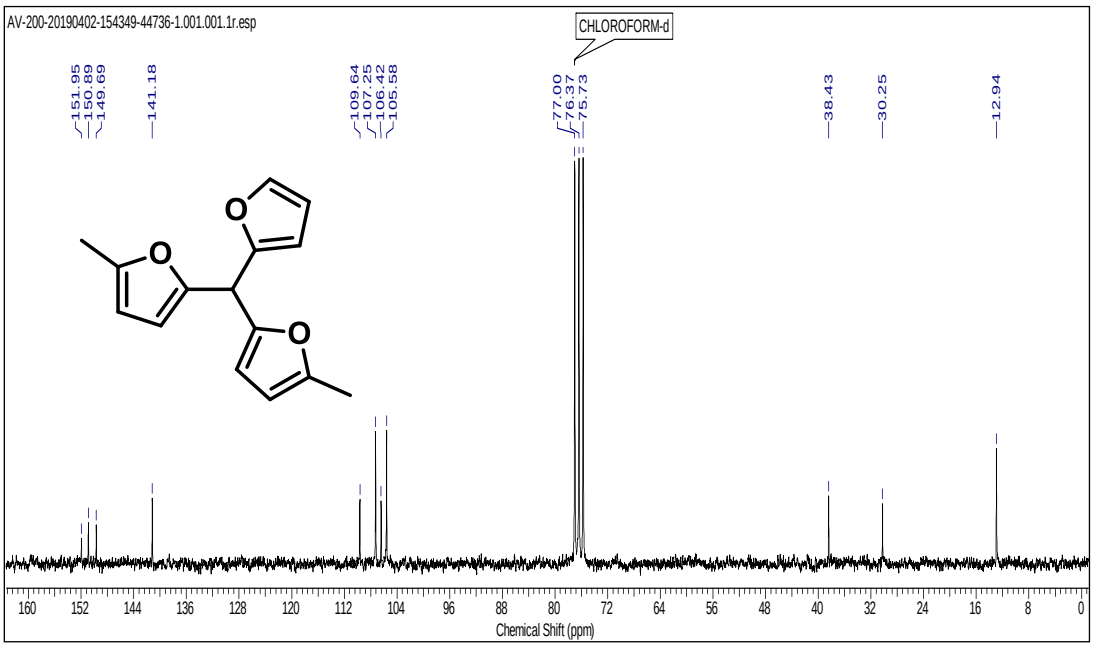

2-methyl-5-((5-methyltetrahydrofuran-2-yl)(tetrahydrofuran-2-yl)methyl)furan

^{1}H NMR (200 MHz, $CDCl_3$, 0.01%, TMS, δ ppm): 1.06 - 1.35 (m, 5 H) 1.63 - 2.04 (m, 7 H) 2.26 (s, 3 H) 3.61 - 4.08 (m, 3 H) 4.08 - 4.31 (m, 2 H) 4.36 (br. s., 1 H) 5.79 - 6.18 (m, 2 H)

^{13}C NMR (101 MHz, $CDCl_3$, 0.01%, TMS, δ ppm): 13.50, 13.58, 20.84, 21.16, 25.44, 25.84, 28.31, 29.04, 29.23, 29.98, 30.41, 32.82, 33.01, 33.13, 49.10, 49.18, 49.34, 49.45, 49.66, 50.18, 67.12, 67.51, 67.96, 68.20, 74.38, 74.51, 77.77, 77.85, 77.96, 77.97, 78.90, 78.97, 105.74, 105.95, 106.04, 106.19, 107.94, 108.02, 108.19, 108.32, 150.13, 151.75, 151.89. (Note: Isomeric products might be present due to two chiral centres)

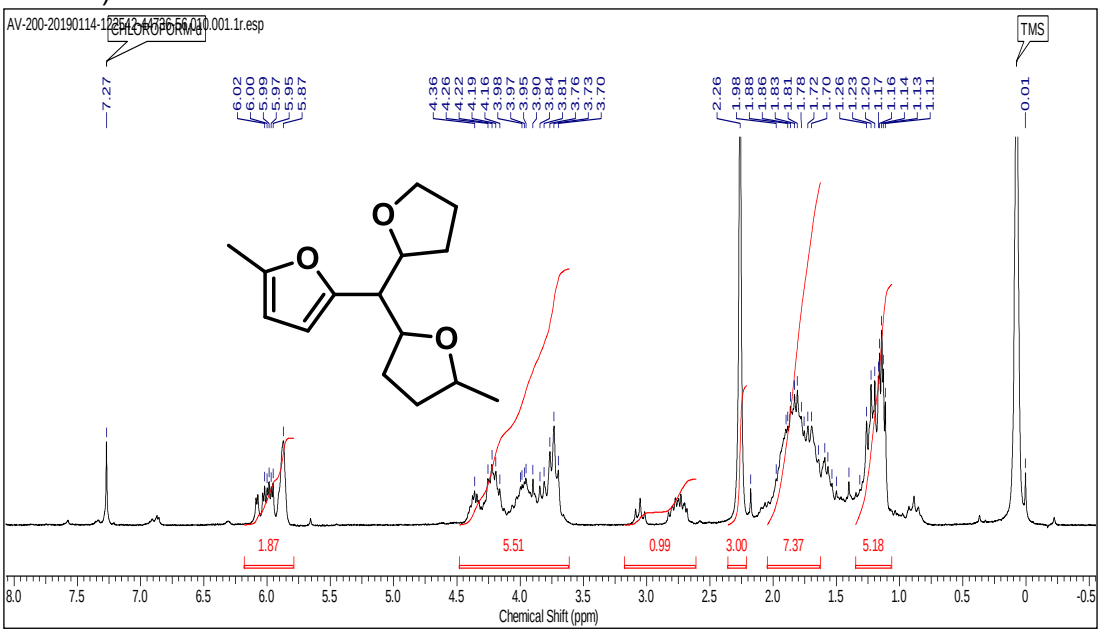

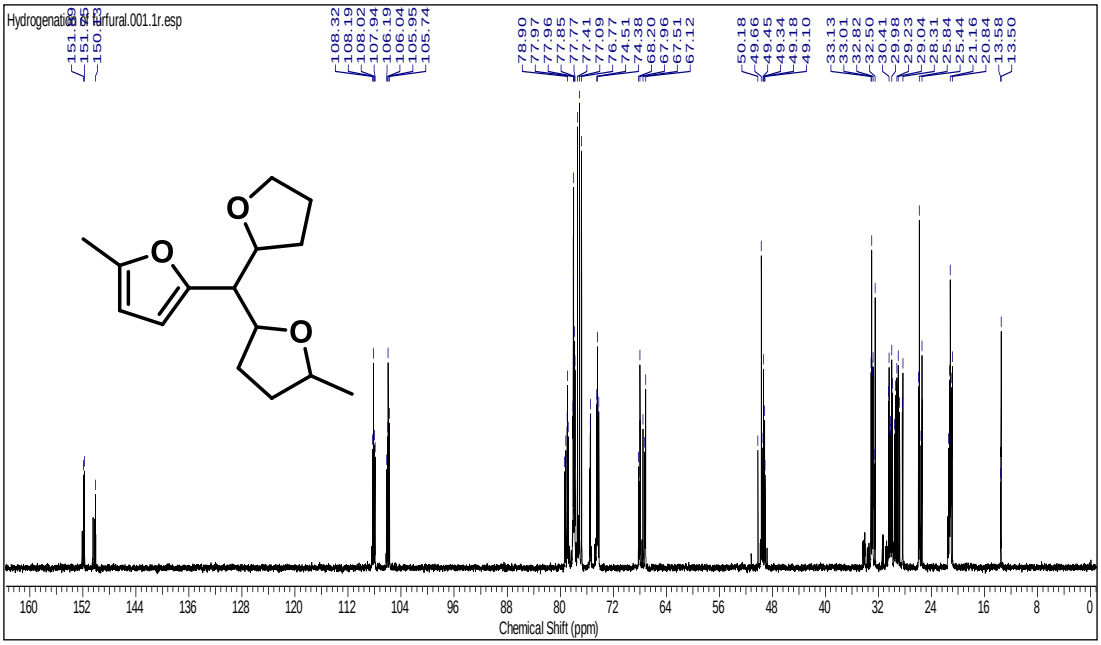

bis(5-methylfuran-2-yl)methane

^{1}H NMR (200 MHz, $CDCl_3$, 0.01%, TMS, δ ppm): 2.27 (s, 6 H) 3.91 (s, 2 H) 5.83 - 5.92 (m, 2 H) 5.96 (d, *J*=2.87 Hz, 2 H)

^{13}C NMR (50 MHz, $CDCl_3$, 0.01%, TMS, δ ppm): 13.51 (s, 1 C) 27.50 (s, 1 C) 76.37 (s, 1 C) 77.63 (s, 1 C) 106.09 (s, 1 C) 106.90 (s, 1 C) 149.99 (s, 1 C) 150.94 (s, 1 C)

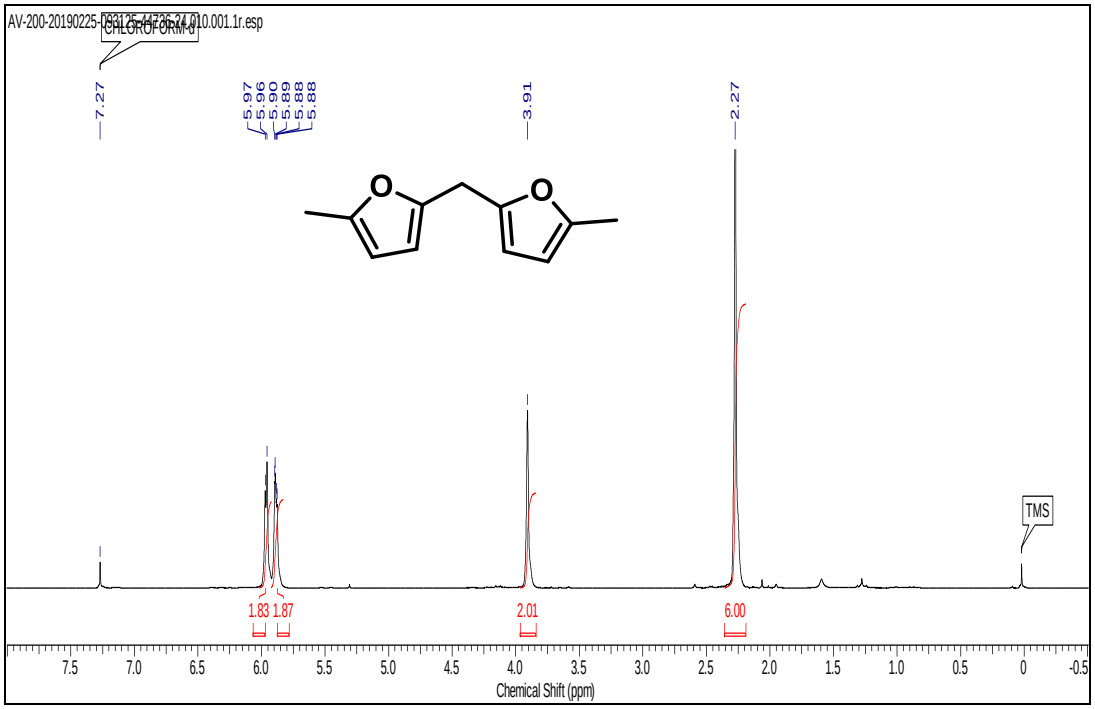

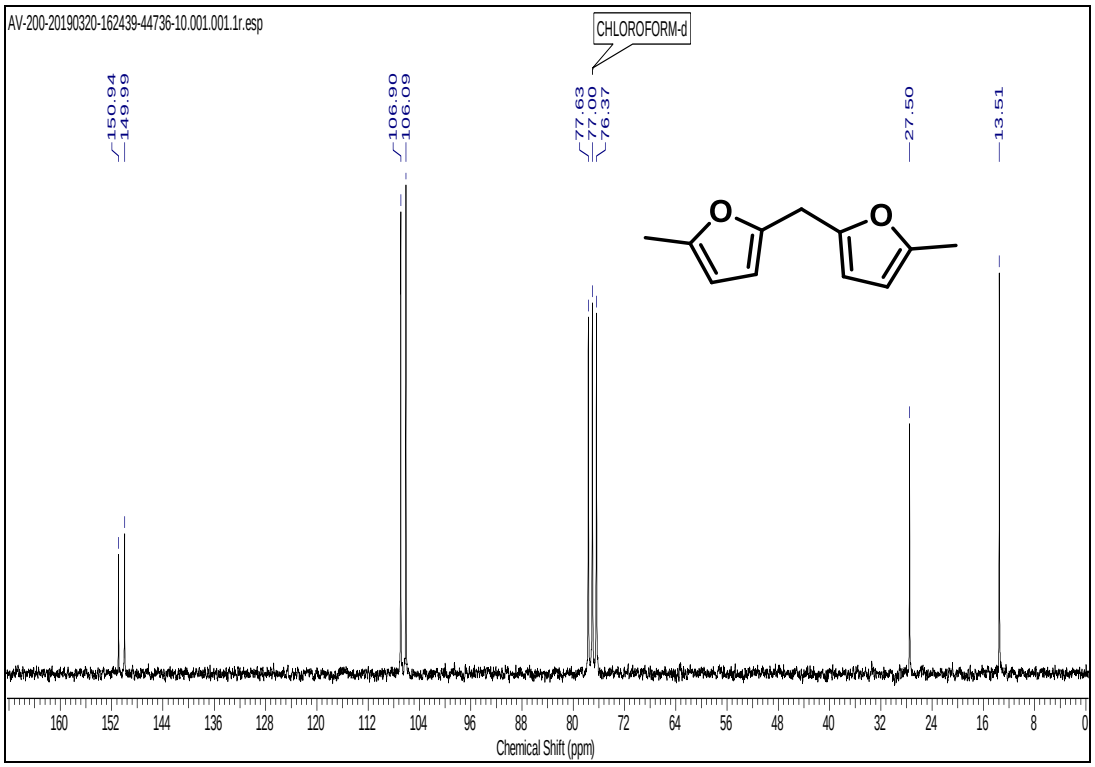

bis(5-methyltetrahydrofuran-2-yl)methane

^{1}H NMR (200 MHz, $CDCl_3$, 0.01%, TMS, δ ppm): 1.11 - 1.30 (m, 6 H) 1.36 - 1.81 (m, 5 H) 1.81 - 2.21 (m, 6 H) 3.78 - 4.32 (m, 4 H)

^{13}C NMR (50 MHz, $CDCl_3$, 0.01%, TMS, δ ppm) 14.12, 20.96, 21.41, 31.31, 31.87, 32.43, 32.70, 32.88, 33.79, 42.21, 42.44, 42.90, 43.07, 53.35, 60.30, 74.30, 75.07, 75.96, 76.25

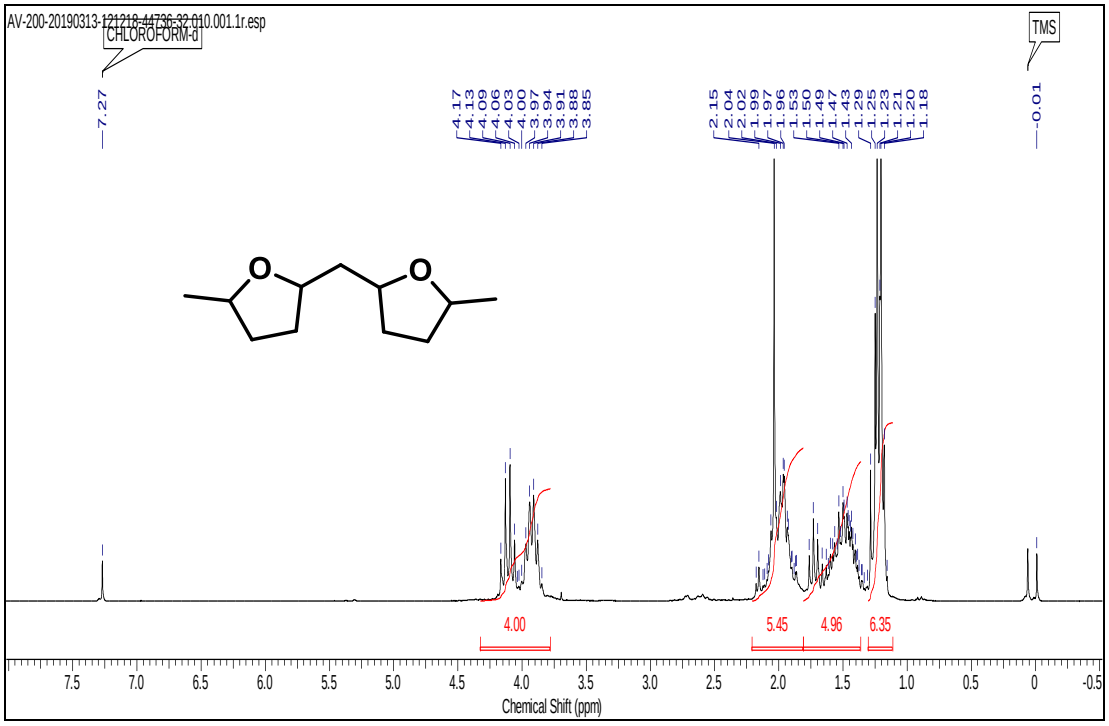

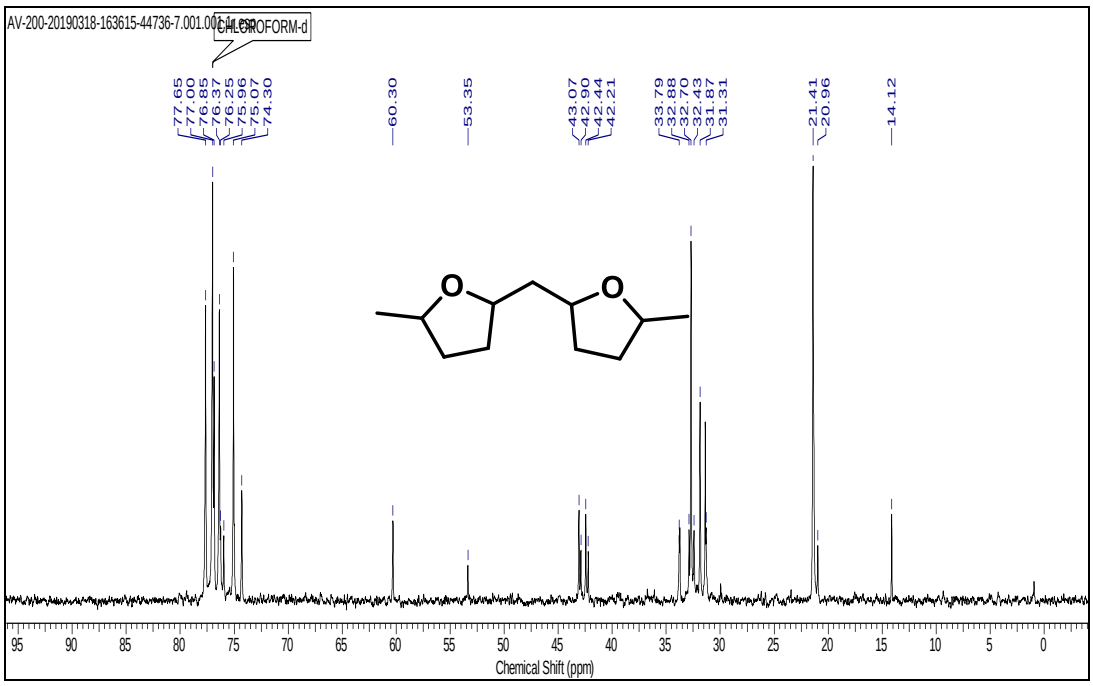

5,5'-(propane-2,2-diyl)bis(2-methylfuran)

^{1}H NMR (200 MHz, $CDCl_3$, 0.01%, TMS, δ ppm): 1.61 (s, 6 H) 2.22 - 2.28 (m, 6 H) 5.82 - 5.96 (m, 4 H)

^{13}C NMR (50 MHz, $CDCl_3$, 0.01%, TMS, δ ppm): 13.57 (s, 1 C) 26.45 (s, 1 C) 37.18 (s, 1 C) 76.36 (s, 1 C) 77.63 (s, 1 C) 104.49 (s, 1 C) 105.68 (s, 1 C) 150.51 (s, 1 C) 158.59 (s, 1 C)

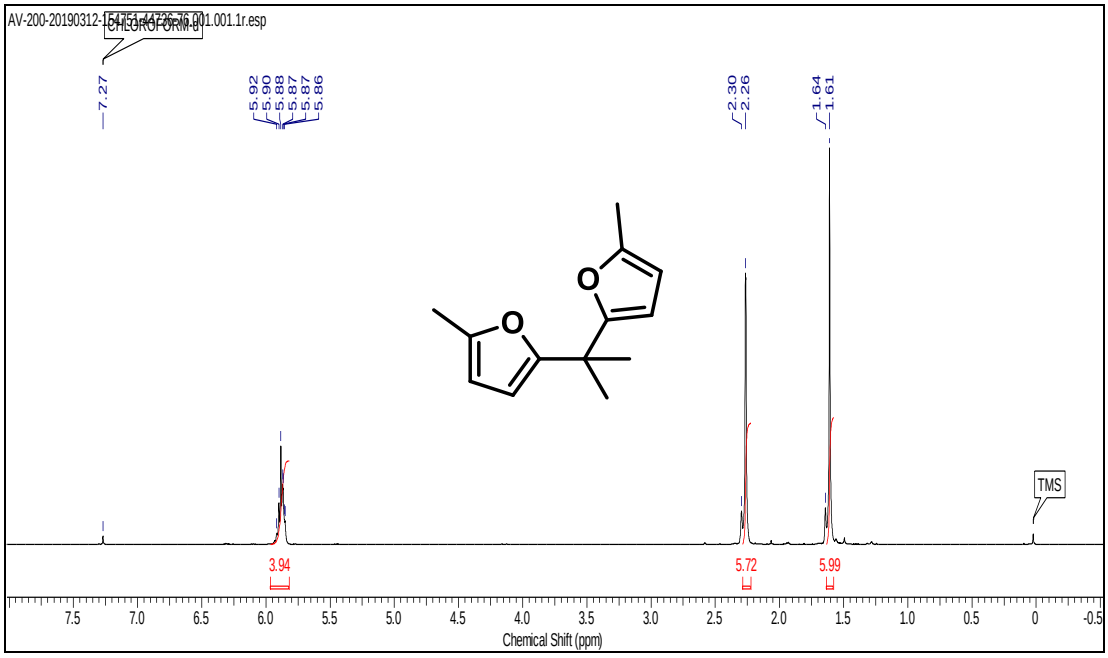

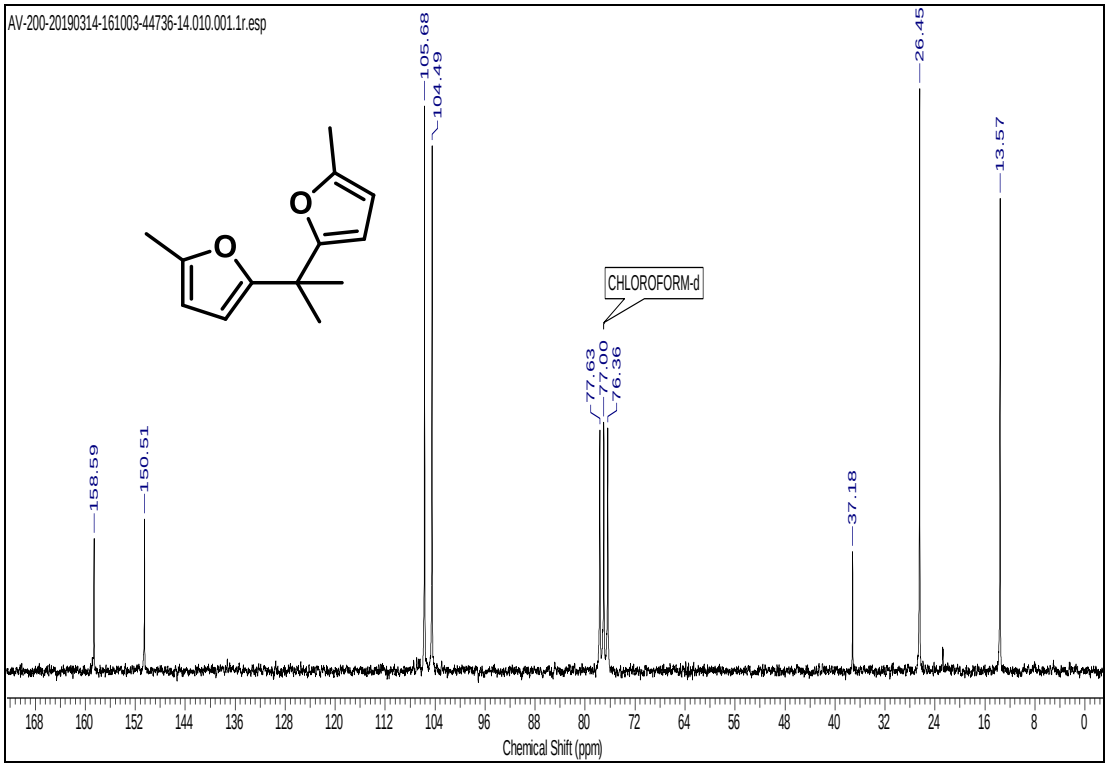

5,5'-(propane-2,2-diyl)bis(2-methyltetrahydrofuran)

^{1}H NMR (200 MHz, $CDCl_3$, 0.01%, TMS, δ ppm): 0.76 (s, 5 H) 0.81 - 0.98 (m, 2 H) 1.02 - 1.21 (m, 6 H) 1.21 - 1.44 (m, 2 H) 1.50 - 2.01 (m, 6 H) 3.63 - 4.07 (m, 4 H)

^{13}C NMR (101 MHz, $CDCl_3$, 0.01%, TMS, δ ppm): 17.00, 17.24, 18.18, 18.76, 20.77, 20.83, 25.58, 25.71, 32.49, 32.53, 32.72, 32.76, 38.51, 38.72, 74.10, 74.24, 74.27, 83.12, 84.12.

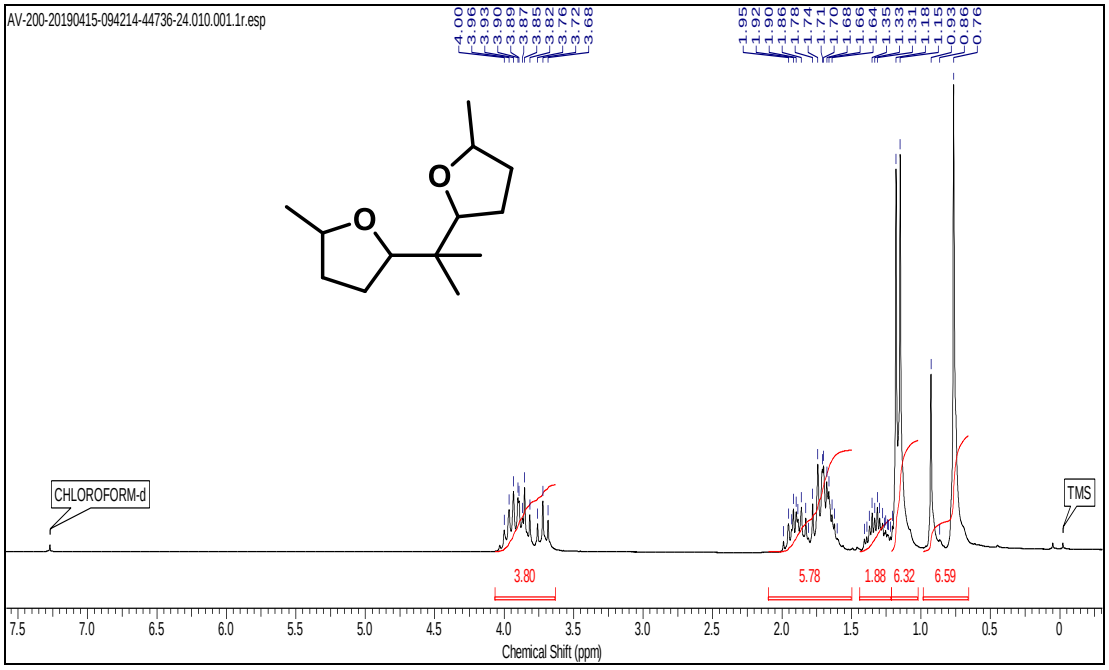

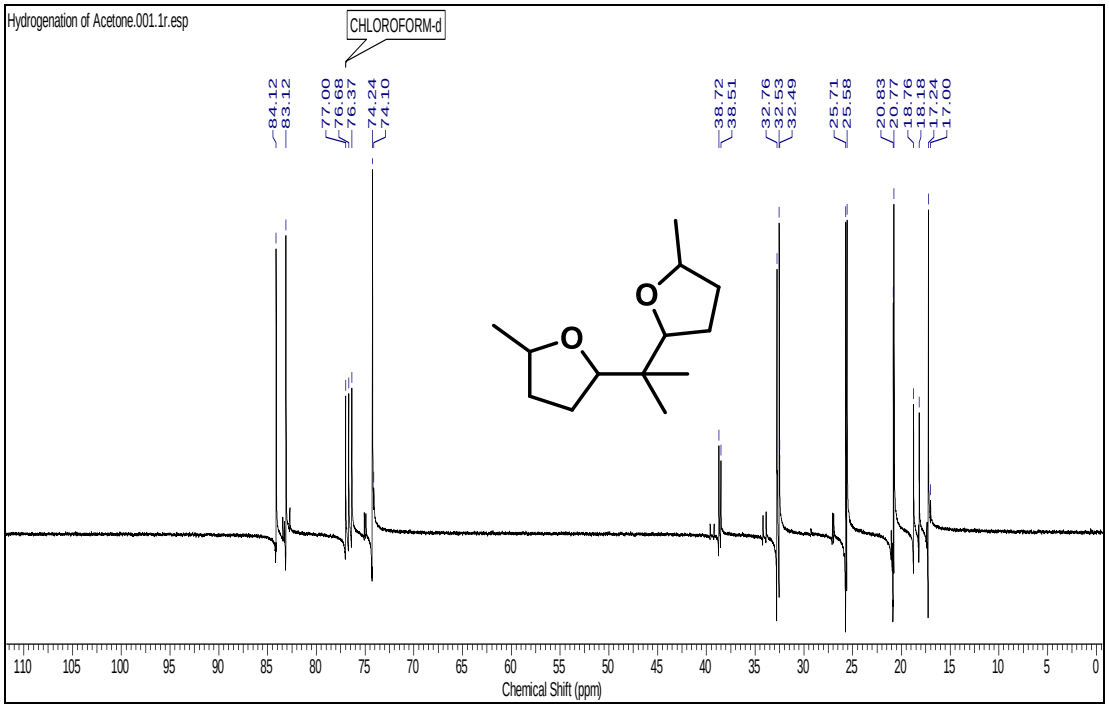

5,5'-(phenylmethylene)bis(2-methylfuran)

^{1}H NMR (200 MHz, $CDCl_3$, 0.01%, TMS, δ ppm): 1.40 - 1.72 (m, 1 H) 2.10 - 2.50 (m, 6 H) 5.33 (s, 1 H) 5.62 - 6.10 (m, 4 H) 7.10 - 7.43 (m, 5 H)

^{13}C NMR (50 MHz, $CDCl_3$, 0.01%, TMS, δ ppm): 12.96, 44.46, 105.39, 107.50, 126.28, 127.75, 139.37, 150.78, 152.19

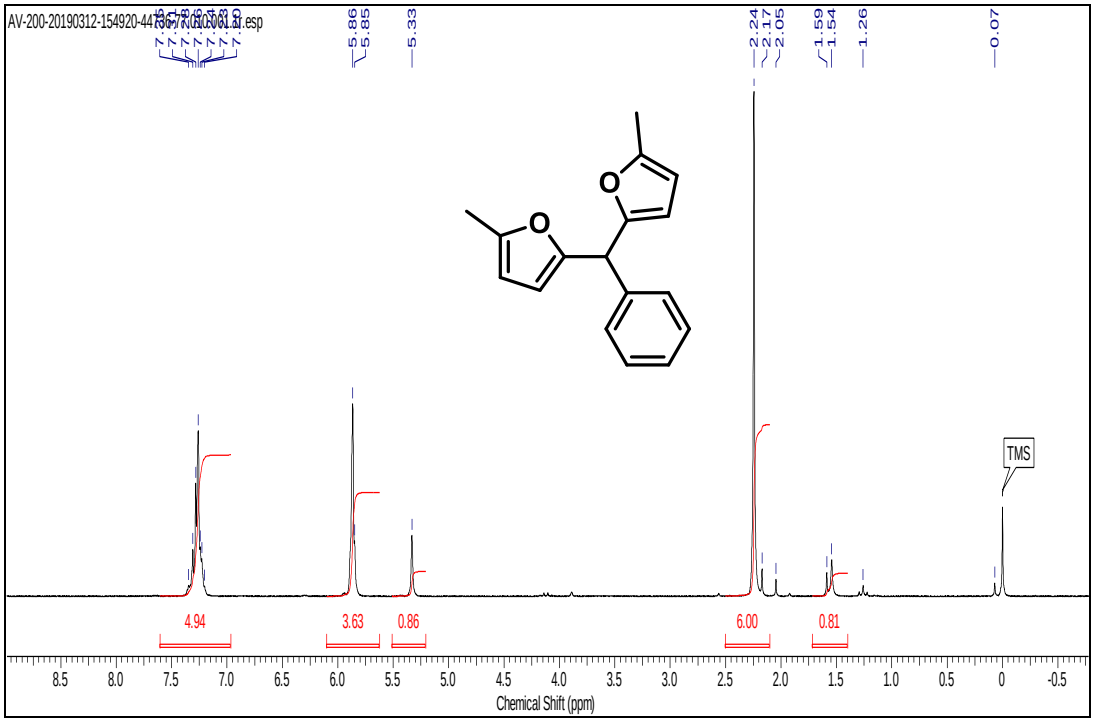

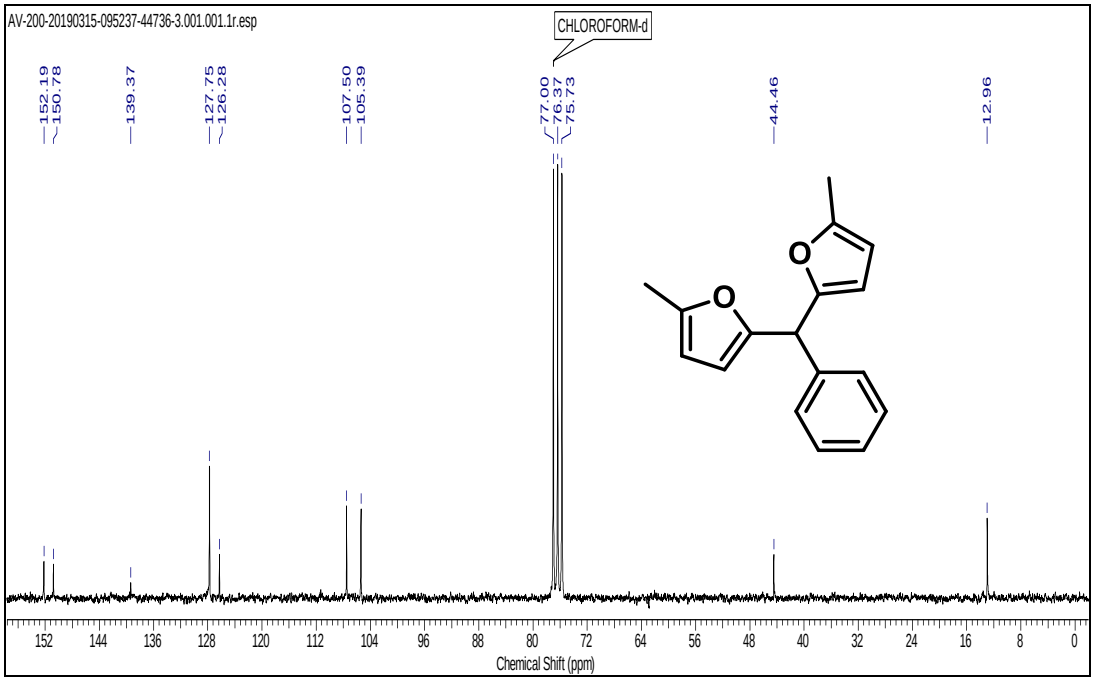

5,5'-(phenylmethylene)bis(2-methyltetrahydrofuran)

^{1}H NMR (200 MHz, $CDCl_3$, 0.01%, TMS, δ ppm): 0.95 - 1.29 (m, 8 H) 1.50 - 2.10 (m, 6 H) 2.75 - 3.26 (m, 1 H) 3.77 - 4.18 (m, 2 H) 4.18 - 4.65 (m, 2 H) 7.11 - 7.40 (m, 5 H)

^{13}C NMR (50 MHz, $CDCl_3$, 0.01%, TMS, δ ppm): 20.72, 21.16, 21.58, 29.07, 30.78, 32.61, 32.79, 54.87, 56.48, 75.36, 75.55, 79.75, 79.89, 126.23, 126.47, 127.50, 129.90, 130.37, 139.89.

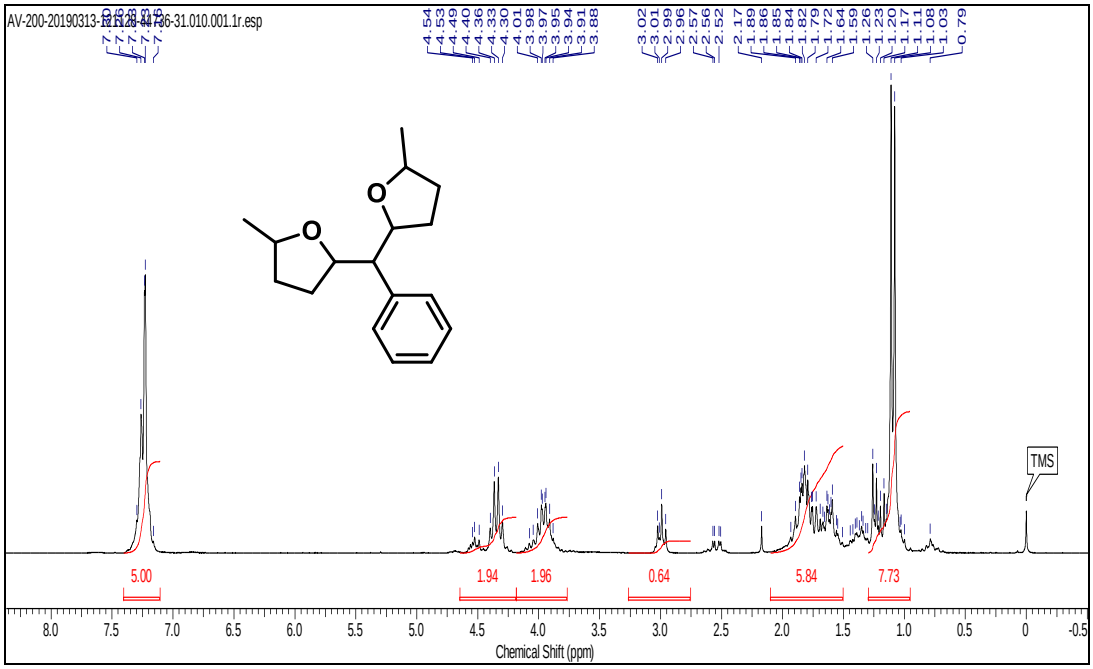

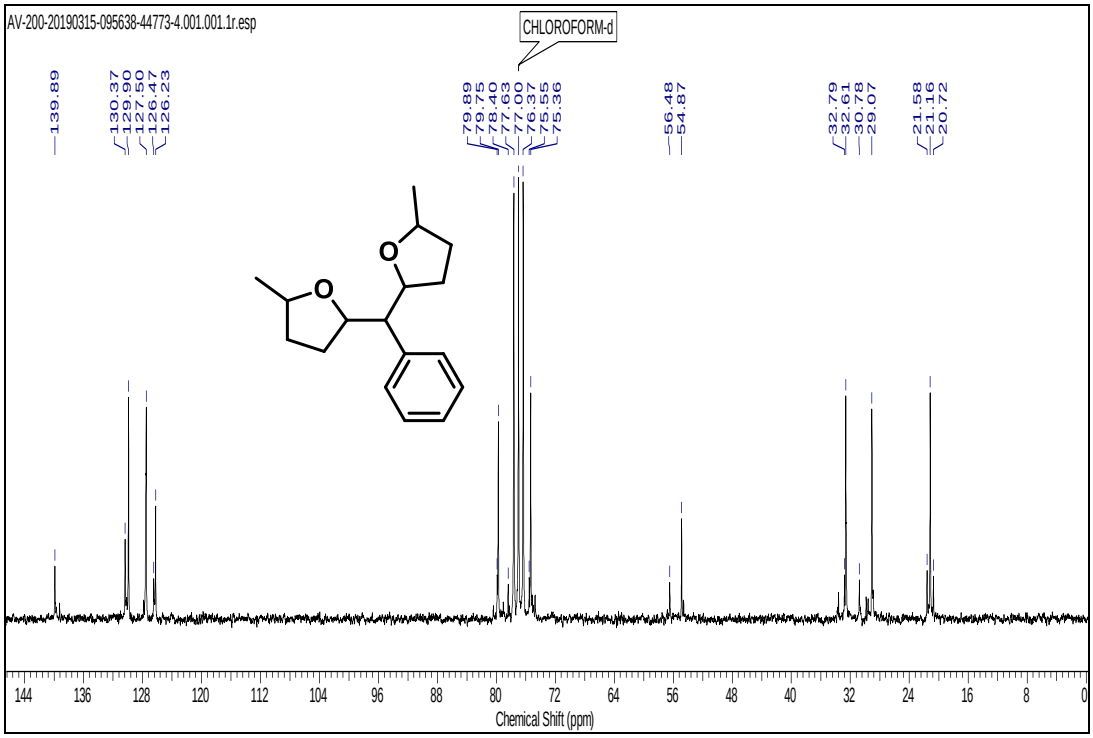

5,5'-(ethane-1,1-diyl)bis(2-methylfuran)

^{1}H NMR (200 MHz, $CDCl_3$, 0.01%, TMS, δ ppm): 1.54 (d, *J*=7.17 Hz, 3 H) 2.25 (s, 6 H) 4.09 (d, *J*=7.17 Hz, 1 H) 5.68 - 6.03 (m, 4 H)

^{13}C NMR (50 MHz, $CDCl_3$, 0.01%, TMS, δ ppm): 13.53, 18.20, 33.13, 105.38, 105.85, 150.67, 155.06.

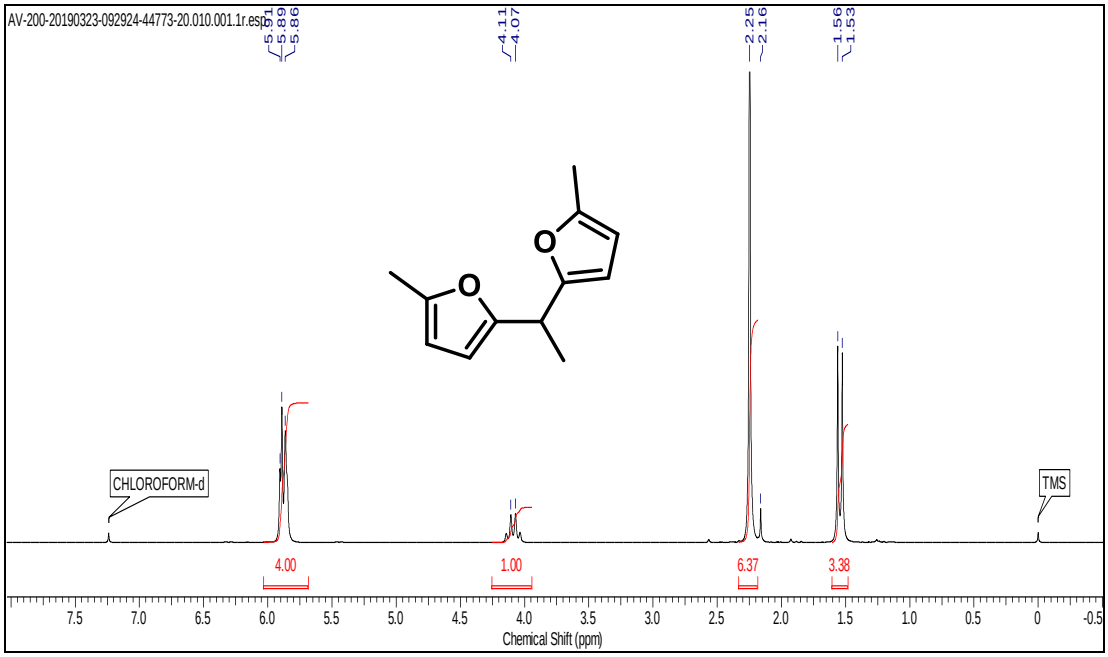

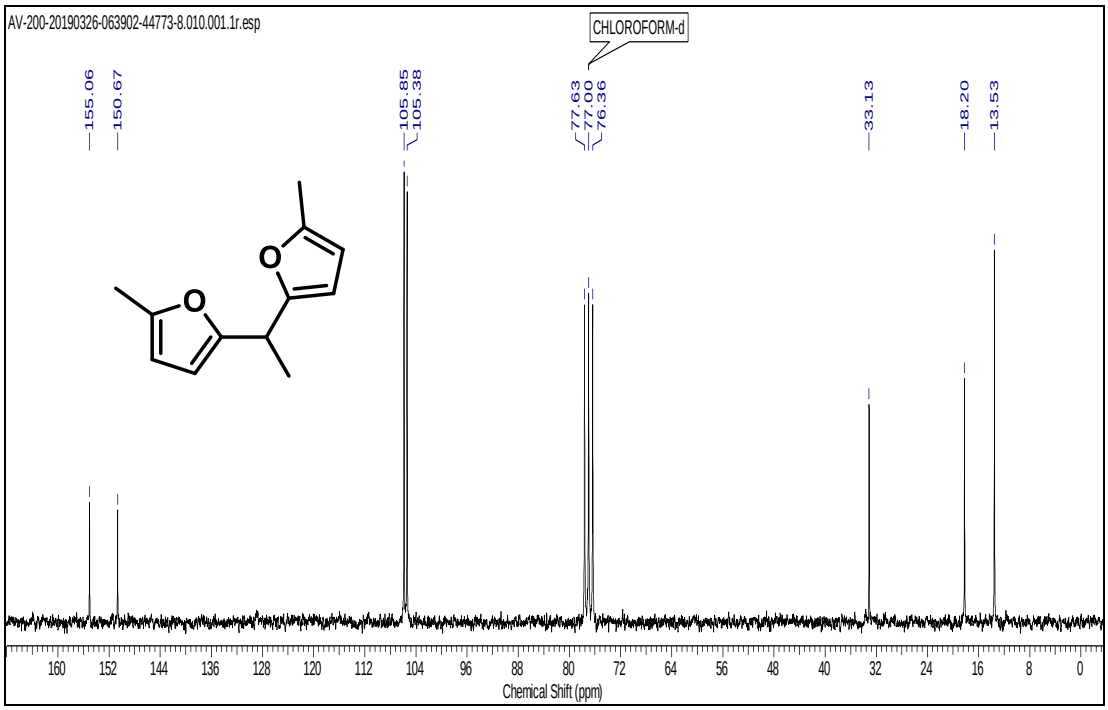

5,5'-(ethane-1,1-diyl)bis(2-methyltetrahydrofuran)

^{1}H NMR (200 MHz, $CDCl_3$, 0.01%, TMS, δ ppm): 0.74 - 0.94 (m, 3 H) 0.94 - 1.08 (m, 1 H) 1.21 (dd, *J*=6.06, 1.32 Hz, 6 H) 1.32 - 1.51 (m, 2 H) 1.51 - 1.78 (m, 3 H) 1.78 - 2.13 (m, 5 H) 3.66 - 4.17 (m, 4 H)

^{13}C NMR (50 MHz $CDCl_3$, 0.01%, TMS, δ ppm): 10.02, 21.03, 21.18, 21.32, 27.42, 28.95, 29.28, 29.47, 32.91, 33.23, 34.24, 42.92, 74.80, 74.94, 76.37, 77.00, 79.95, 80.82, 80.98, 81.38.

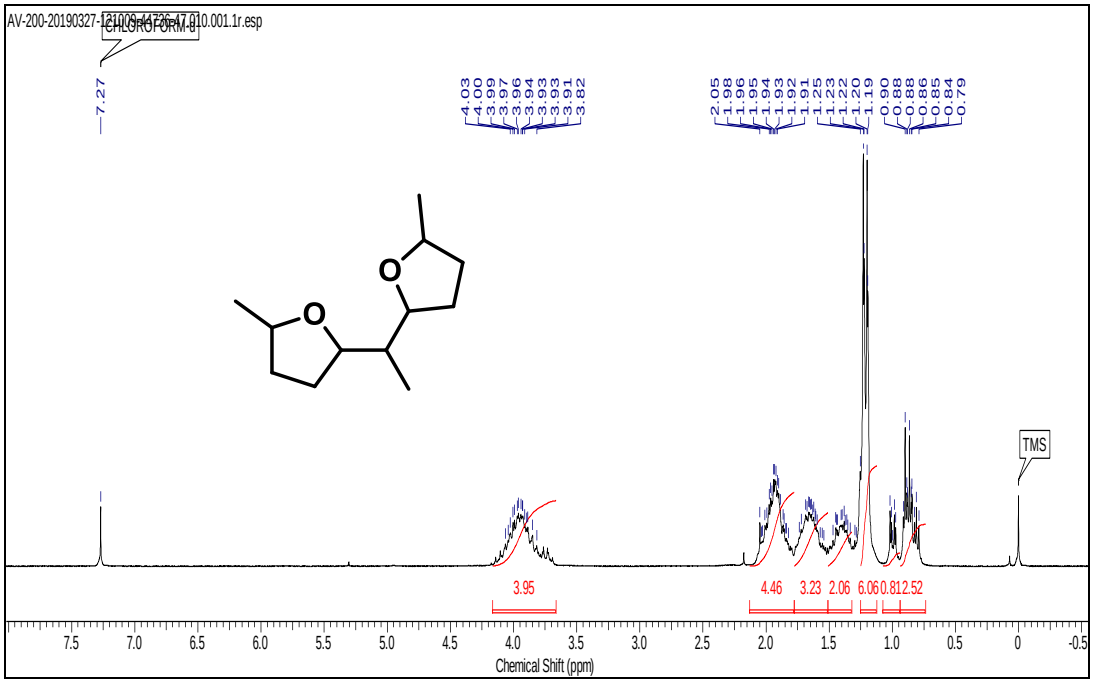

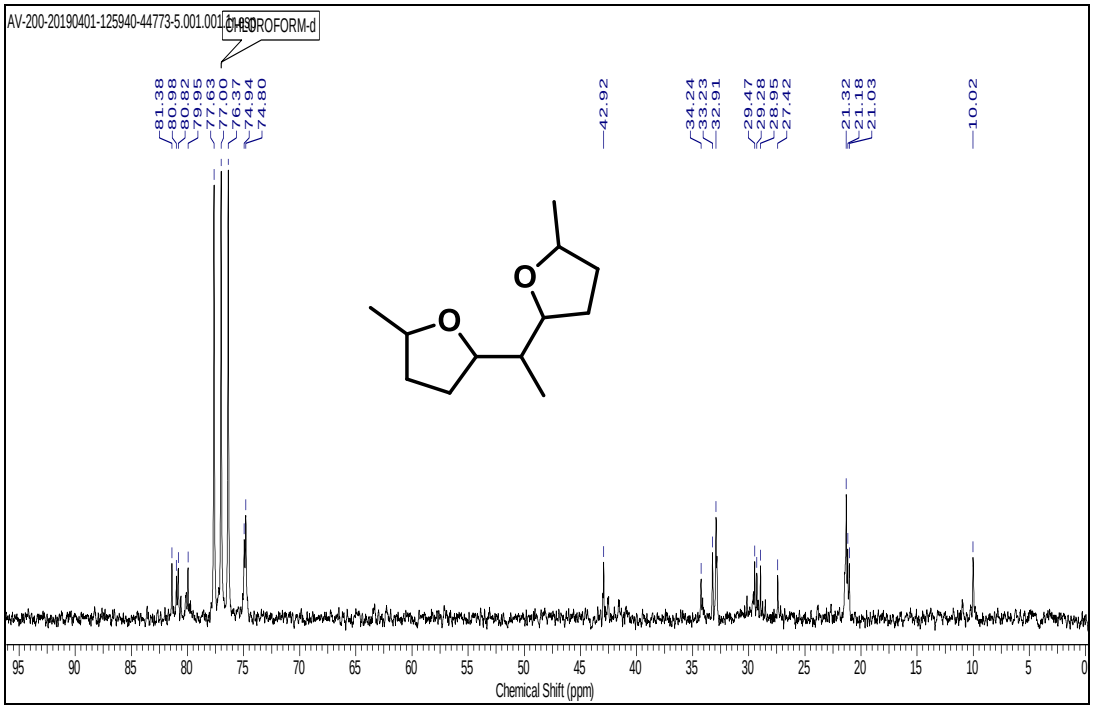

Chapter - 4

Conversion of 2-Methylfuran to Diesel Fuel Precursors Catalysed by Solid Acid

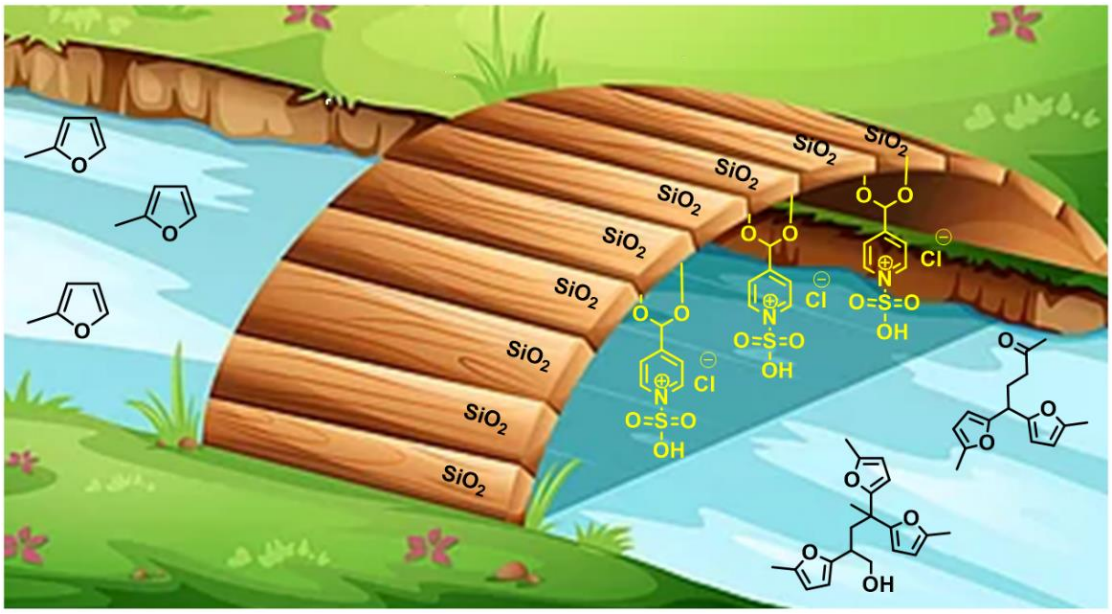

Polyfuranic compounds produced from 2-methylfuran could undergo hydro-deoxygenation to produce diesel fuel *via* tandem ring opening followed by condensation sequence. In this study, we developed a novel and straightforward silica-supported sulfonic acid functionalized isonicotinic acid catalyst, denoted as SO_3H-INA@SiO_2, and we evaluated the efficiency of SO_3H-INA@SiO_2 in the solvent-free transformation of 2-methylfuran into polyfuranic compounds containing C_{15} and C_{20} units. Under optimized reaction conditions, SO_3H-INA@SiO_2 effectively converted 2-methylfuran completely into polyfuranic compounds, specifically 5,5-bis(5-methylfuran-2-yl)pentan-2-one (**1**) and 2,4,4-tris(5-methylfuran-2-yl)pentan-1-ol (**2**), with yields of 19% and 67%, respectively. The heterogeneous SO_3H-INA@SiO_2 catalyst was successfully recycled up to six consecutive runs without loss of its activity. The SO_3H-INA@SiO_2 catalyst offered superior activity as compared to the commercially available -SO_3H functionalized resins. Superior activity of the prepared catalyst could be attributed for its higher acidity, smaller particle size and high surface area. Structure of the prepared catalyst was confirmed by FTIR and solid-state NMR. Total acidity of the prepared catalyst was determined by acid-base titration.

Komal Tarade, Sanjay Kamble and Chandrashekhar Rode, **Catalysis Letters**, 2023, 154, 1511-1520

4.1. Introduction

Energy and chemicals produced across the globe almost entirely rely on fossil resources. Nevertheless, these resources are exhausting much faster than expected and would be extinct in near future due to their expeditious consumption in transportation and industrial sectors. At the same time, formation of fossil-based resources requires millions of years through natural anaerobic decomposition of buried organisms [1]. In addition to that, during refining of fossil resources huge amount of carbon dioxide (CO_2) is being continuously thrown out into the environment which not only enhances global warming but also known to inflict serious health issues to living organisms [2]. This presents a significant challenge for scientists and technologists to seek greener alternatives for energy, fuels, chemicals and materials. Recently, biomass has gained attention as a sustainable substitute for fossil resources due to its renewability and widespread availability as a source of organic carbon. Indeed, abundantly available lignocellulosic biomass has complex structure comprising cellulose, hemicellulose and polymeric aromatics (lignin). Cellulose (polymeric C_6 sugars) and hemicellulose (polymeric C_5 sugars) are very tightly bound with lignin thus, separation of these three components is of utmost importance. After pre-treatment of lignocellulosic biomass, a hemicellulosic part decomposes into C_5 (e.g. xylose and arabinose) and C_6 sugars (e.g. mannose, galactose and rhamnose) [1]. The C_5 sugars (xylose and arabinose) present in agricultural and forest residues can be dehydrated in presence of an acid to form furfural [3]. Furfural is the most valuable industrial chemical whose current production volume is more than 200,000 tons/year [4,5]. Furfural can be further converted into 2-methylfuran as a major product by hydrogenolysis at 250 ^oC [6,7]. 2-Methylfuran features an electron-rich aromatic ring and undergoes selective electrophilic substitution at the C4 position when acid catalysts are present [8]. 2-Methylfuran is hydrophobic in nature which allows its easy separation from water at room temperature, thus it can be used as a product extraction solvent [9].

4.2. Literature Survey

Hydroxyalkylation-alkylation of 2-methylfuran with aldehydes/ketones/active alcohols have been well studied as these products have wide range of industrial applications [10]. These products can be processed for the production of bio-fuels *via* hydrodeoxygenation (HDO) reaction [11]. In this context, numerous catalytic systems were investigated for hydroxyalkylation-alkylation of 2-methylfuran which includes conc. H_2SO_4, acidic resins [8,12,13], sulfonic acid functionalized silica [14-19],

carbocatalysts [20,21], ionic liquids [10], supported phosphotungstic acid [22], Mo-Zr-MCM-41 [23], $AuCl_3$ [24,25], zeolites [26], $Cu(OTf)_2$ [27], TFA-ZrO_2 [28], and molecular iodine [29]. In 2011, Corma et al. [8] reported for the first time, the tandem conversion of sylvan (aqueous 2-methylfuran) to produce diesel fuel precursor of C_{15} unit using sulfonic acid functionalized solids (e.g. Amberlyst-15, PTSA) and liquid acids (e.g. conc. H_2SO_4). In 2015, the similar cascade reaction sequence was attempted by Yati et al. over Amberlyst-15, in which they found that addition of water promotes the formation of diesel precursors of C_{15} unit while without water, diesel precursors of C_{20} unit can be selectively produced [30]. However, they observed that without water, conversion of 2-methyfuran reached maximum up to 37% and addition of water leads to lowering of conversion. In 2018, Gebresillase et al. [31]. A sulfonic acid functionalized silica, such as KCC1SO_3H, was reported for the selective tandem conversion of 2-methylfuran to a C_{15} diesel fuel precursor by conducting the reaction at 80°C over an extended period of 48 hours

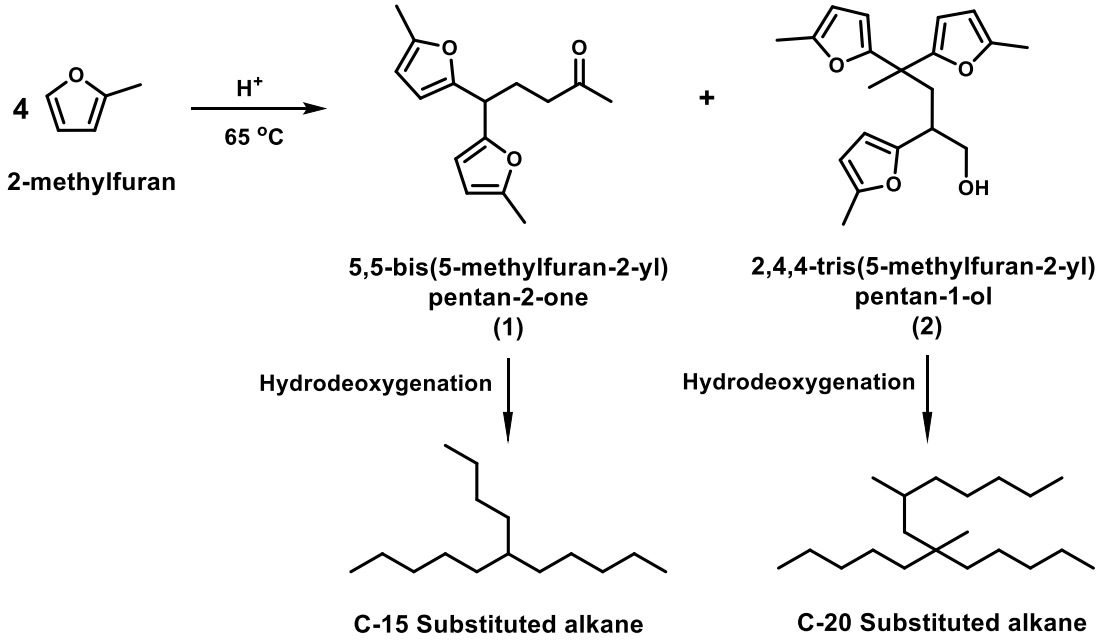

Scheme 4.1. Synthesis of diesel fuel precursors from 2-methylfuran.

4.3. Scope of the Present Work

In continuation of our recent work on new -SO_3H functionalized heterogeneous catalysts systems [18], we further developed SO_3H-INA@SiO_2 as a simple, novel and highly active heterogeneous acid catalyst and we investigated the use of SO_3H-INA@SiO_2 for the tandem, solvent-free conversion of 2-methylfuran into precursors for kerosene-diesel range products (C_{15} to C_{20}) (Scheme 4.1). The catalyst achieved

nearly complete conversion of 2-methylfuran resulting in high yields of diesel fuel precursors with C_{15} and C_{20} units. The study also thoroughly examined the effects of reaction parameters, including catalyst loading and reaction time, on the conversion efficiency of 2-methylfuran have been studied in detail.

4.4. Experimental Section

4.4.1. Materials

Chemicals such as 2-methylfuran, 3-pyridinecarboxylic acid, conc. H_2SO_4, para-toluenesulfonic acid and chlorosulfonic acid were obtained from Sigma-Aldrich, India. Commercial sulphonic acid functionalized resins, such as Amberlyst-15, Amberlyte IR-120, Thermax resin, Dowex 50WX8, and Lanxess K11311S, were also acquired from Sigma-Aldrich, India. Solvents like ethanol, ethyl acetate, petroleum ether, and silica gel (230-400 mesh) were purchased from Chem Labs, India. The catalysts Sn-Mont and Zr-Mont were synthesized following the established procedures. [32, 33].

4.4.2. Catalyst preparation

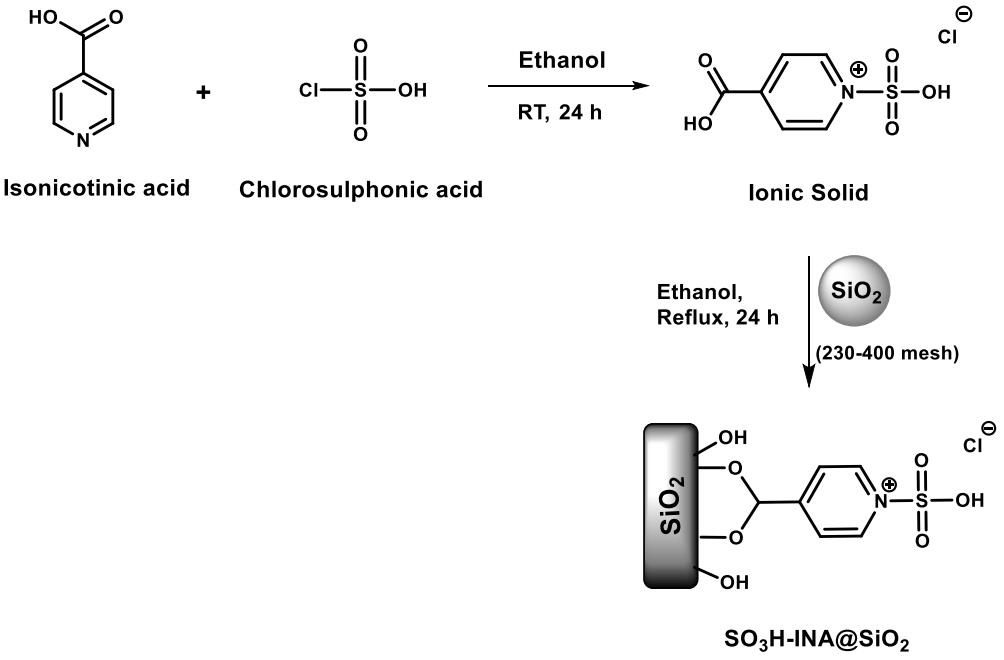

Scheme 4.2. Synthesis of SO_3H-INA@SiO_2

4.4.2.1. Synthesis of ionic solid, SO_3H-INA

To a solution of chlorosulphonic acid (1.8 mL) in ethanol (25 mL), 3-pyridine carboxylic acid (2 g) was added at room temperature under continuous stirring for 24 h. Following

this, the solvent was removed from the reaction mixture using a rotary evaporator, yielding a white solid (3 g).

4.4.2.2. Synthesis of silica supported ionic solid SO_3H-INA@SiO_2

To a stirred solution of ionic solid, SO_3H-INA (1g) dissolved in ethanol (25 mL), silica gel (1 g, 230-400 mesh) was added portion wise and then resultant mixture was refluxed for 24 h. The mixture was then cooled to room temperature, filtered and washed with ethyl acetate (20 mL × 3). It was subsequently dried on a rotary evaporator at 45°C for 2-3 hours to obtain a white powder (Scheme 4.2). The surface area and particle size of SO_3H-INA@SiO_2 was observed to be 523 m^2/g and 48 µm, respectively.

4.4.3. Determination of catalyst acidity

Aqueous solution of sodium chloride (0.05 mol/g, 30 mL) was added to the SO_3H-INA@SiO_2 catalyst (0.250 g) and the resultant mixture was stirred for 1h at room temperature under ultrasonic conditions. After centrifugation, the supernatant solution was titrated against aqueous solution of sodium hydroxide (0.05 mol/g) using phenolphthalein indicator [34, 35] giving total acidity as 0.031 mol/g. Acidity of SO_3H-INA@SiO_2 catalyst after reuse was determined to be 0.030 mol/g. Total acidity of other sulphonic acid functionalized solid acid catalysts was also estimated by similar acid-base titration method and the results are shown in Table 4.1.

4.4.4. Catalyst test

A mixture of 2-methylfuran (1 g, 0.012 mol) and SO_3H-INA@SiO_2 (0.1 g, 10% w/w relative to 2-methylfuran) was stirred at 65°C for 7 hours. The catalyst was then separated by filtration, and the filtrate was diluted with ethyl acetate (20 mL). The diluted reaction mixture was washed with water (20 mL × 1) and brine solution (20 mL × 1). The organic layer was dried over anhydrous sodium sulphate and concentrated using a rotary evaporator to obtain crude oil, which was then subjected to column chromatography. 5,5-Bis(5-methylfuran-2-yl)pentan-2-one **(1)** was eluted with 100% petroleum ether, while 2,4,4-tris(5-methylfuran-2-yl)pentan-1-ol **(2)** was eluted with a mixture of ethyl acetate and petroleum ether (2:98; *v/v*). The eluted fractions were evaporated to remove solvents, yielding a greenish-yellow liquid for **1** and a yellowish-brown liquid for **2**. After the reaction, the catalyst was washed with ethyl acetate (10 mL × 1) and dried in an oven at 45°C for 3-4 hours before reuse.

4.4.5. Analysis of the reaction products

The primary analysis of the reaction crude was conducted using thin-layer chromatography on Merck 5554 aluminum-backed silica plates, with compounds visualized under UV light (254 nm) and stained with phosphomolybdic acid. Pure products were characterized and confirmed by ^{1}H NMR and ^{13}C NMR (500 MHz) in DMSO-d6 (0.01%, TMS) using a 200 MHz Bruker instrument (see Supporting Information). Additionally, the products were verified using a QP-Ultra 2010 GC-MS Shimadzu instrument with an RTX-5 column, helium as the carrier gas, electrospray ionization mode, and an ionization source temperature of 200°C.

An analytical method based on Gas Chromatography (GC) was developed and validated to monitor the synthesis of the condensation products 5,5-bis(5-methylfuran-2-yl)pentan-2-one (**BMFP**) and 2,4,4-tris(5-methylfuran-2-yl)pentan-1-ol (**TMFP**) from 2-methylfuran using an SO_3H-INA@SiO_2 catalyst. The conversion of 2-methylfuran and the selectivity of the products were determined using an Agilent 7890B Gas Chromatograph with a flame ionization detector and an HP-5 column.

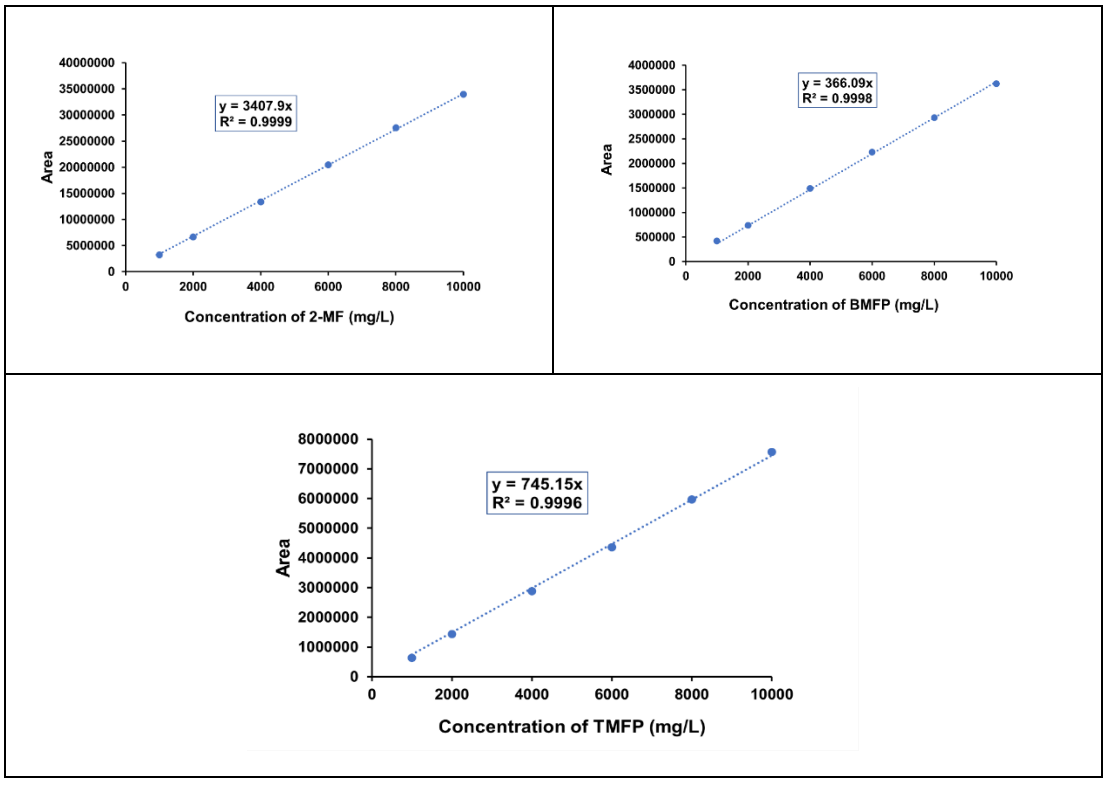

Figure 4.1. Calibration curves for 2-methylfuran, product 1 (**BMFP**) and 2 (**TMFP**)

System calibration was performed using the external standard method. Standard solutions (ranging from 1000 to 10000 ppm) for 2-methylfuran, **BMFP** (product 1), and **TMFP** (product 2) were prepared by dissolving the required amounts of each standard in methanol (solvent) using 10 mL volumetric flasks. The data on the concentrations of analytical standards and peak areas is shown in Figure 4.1, which was used for system calibration.

The samples for analysis, withdrawn from the reaction mixture were diluted in methanol (solvent) to ensure that their estimated concentrations would fall within the specified calibrated range of the respective standards: 2-methylfuran, **BMFP**, and **TMFP**. The concentrations (in ppm) for the reactant and products in a particular reaction sample were determined by substituting the corresponding peak areas into the linear equation, $y=mx+c$ (with $c=0$), for each component. The weight% concentrations were then calculated by applying the appropriate dilution factor for the specific set of reaction samples.

GC chromatograph of reaction mixture

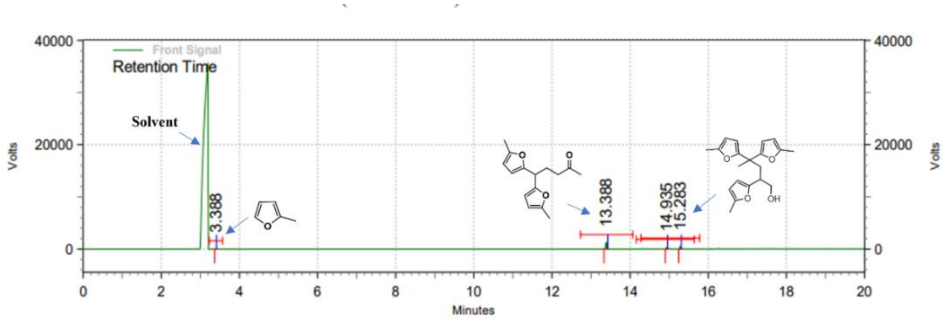

Front Signal
Results

	Retention Time	Area	Area %	Height	Height %
2-MF	3.388	198036	0.90	180606	1.18
1	13.388	13915830	63.09	9177472	59.78
Unidentified	14.935	2651154	12.02	2071653	13.49
2	15.283	5291101	23.99	3923524	25.55
Totals		22056121	100.00	15353255	100.00

Figure 4.2. GC Chromatograph of reaction crude by using resins

The self-condensation reaction of 2-methylfuran was carried out using commercially available acidic resins alongside our synthesized sulfonic functionalized solid acid

catalyst. Notably, the use of the commercial acid resins demonstrated selectivity towards product 1 (**BMFP**) (Figure 4.2). In contrast, our synthesized SO_3H-INA@SiO_2 catalyst exhibited selectivity towards product 2 (**TMFP**) (Figure 4.3), attributed to its higher concentration of Brønsted acid sites, smaller particle size and high surface area.

Reaction performed with SO_3H-INA@SiO_2 catalyst

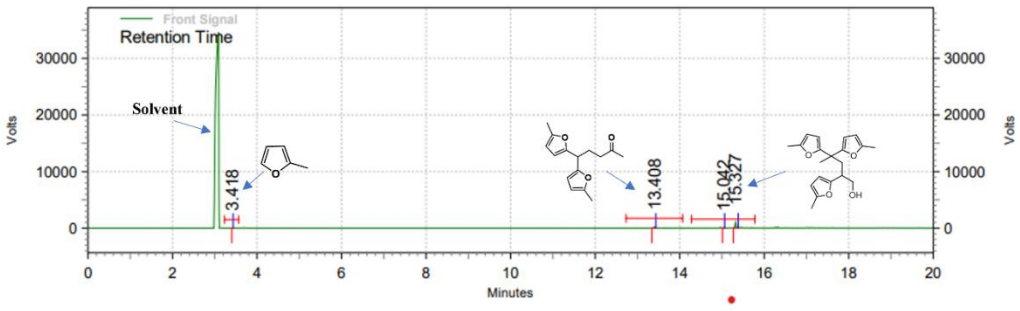

Front Signal
Results

	Retention Time	Area	Area %	Height	Height %
2-MF	3.418	74076	0.45	76247	0.74
1	13.408	3023727	18.52	1741515	16.99
Unidentified	15.042	582628	3.57	498111	4.86
2	15.327	12643515	77.45	7932878	77.40
Totals		16323946	100.00	10248751	100.00

Figure 4.3. GC Chromatograph of reaction crude by using SO_3H-INA@SiO_2

4.5. Results and Discussion

4.5.1. Catalyst characterization

4.5.1.1. Fourier transform infrared spectroscopy (FTIR)

Functional groups present in isonicotinic acid, SiO_2, SO_3H-INA and SO_3H-INA@SiO_2 were observed by using FTIR analysis (Figure 4.4). Characteristic band for C=O bond stretching was observed at 1700 cm^{-1} for isonicotinic acid (Figure 4.4a). For SO_3H-INA, bands observed at 1090-1300, 1600, 1700 and 2700-3100 cm^{-1} were attributed for S=O, C=N, C=O and -OH (SO_3H group), respectively (Figure 4.4b). In case of SiO_2, a broad band observed in the range between 950-1290 cm^{-1} could be attributed to -Si-O-Si bond stretching (Figure 4.4c). In case of SO_3H-INA@SiO_2 bands observed at 1090-1300, 1600, 1700 and 2700-3100 cm^{-1} were attributed for S=O, C=N, C=O

and -OH (SO_3H group), respectively (Figure 4.4d). Similar FTIR pattern was observed for reused SO_3H-INA@SiO_2 suggesting that reused catalyst has retained its structural features (Figure 4.4e). All the characteristic bands present in SO_3H-INA were observed in SO_3H-INA@SiO_2 which suggests that SO_3H-INA species is successfully heterogenized on SiO_2 [36].

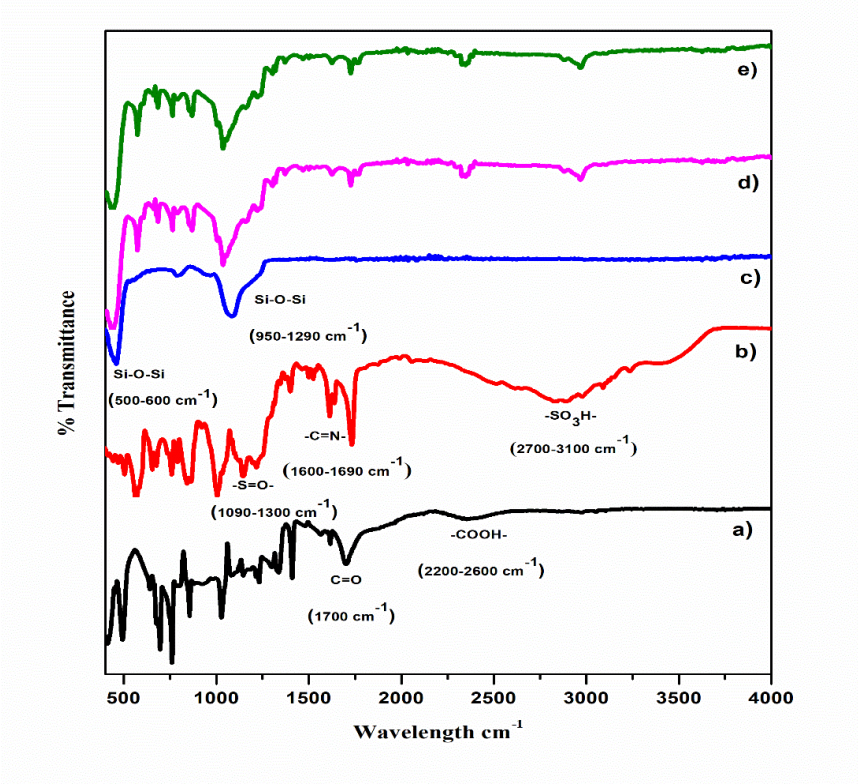

Figure 4.4. FT-IR analysis of a) isonicotinic acid b) SO_3H-INA c) SiO_2 d) SO_3H-INA@SiO_2 and e) SO_3H-INA@SiO_2 (reused) catalysts.

4.5.1.2. Thermogravimetric analysis (TGA)

A thermo gravimetric analysis of fresh and reused SO_3H-INA@SiO_2 catalysts is presented in Figure 4.5. For the fresh catalyst, a 7% weight loss was observed up to 100°C, attributed to the loss of physically adsorbed water. In contrast, the reused catalyst showed only 2-3% weight loss up to 100°C, as it had been dried at 45°C under vacuum in an oven after recovery from the reaction mixture. After that gradual weight loss up to 46% and 52% was observed up to 400 °C for fresh and reused catalysts, respectively which could be attributed to the thermal decomposition of SO_3H-isonicotinic acid moiety of the catalyst. It has been reported that organic groups usually to desorb in TGA at temperatures above 260 °C [37]. Based on the TGA

results, it can be concluded that the SO_3H-INA group is effectively supported on the silica.

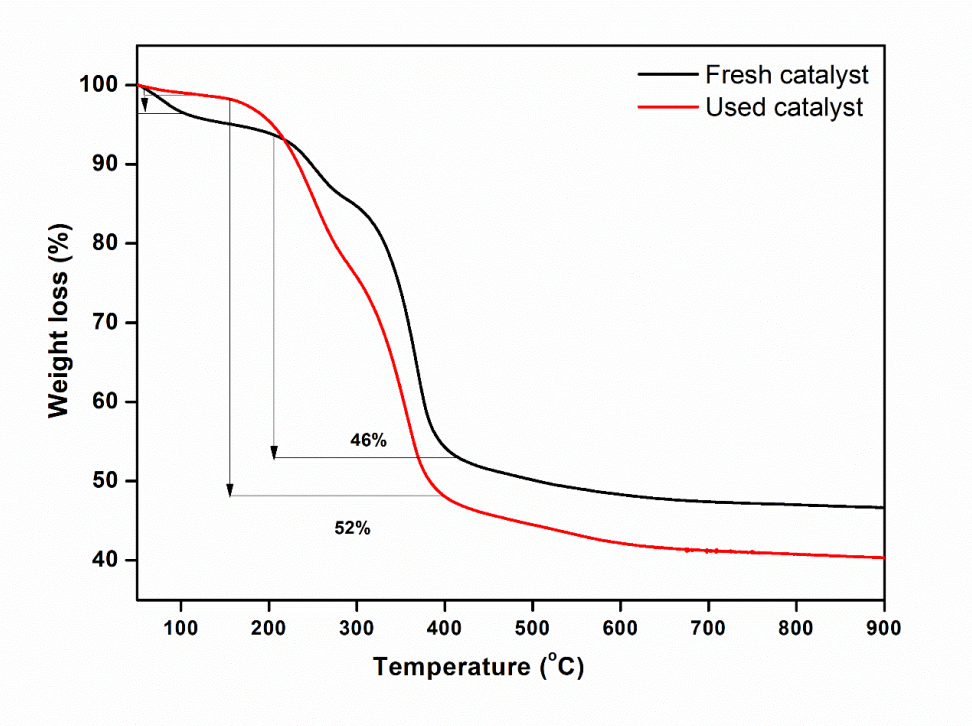

Figure 4.5. TGA analysis of fresh and used SO_3H-INA@SiO_2 catalyst

4.5.1.3. Solid state NMR

The structure of SO_3H-INA@SiO_2 catalyst was confirmed by solid state ^{13}C NMR (Figure 4.6). A peak observed at 162.08 ppm is attributed to carbonyl carbon of carboxylic acid. A peak at 145.63 ppm is responsible for the two chemically equivalent =CH- groups which are meta to carboxylic acid group. A peak at 144.95 ppm must be a quaternary carbon where carboxylic acid is attached. A couple of peaks noticed at 128.75 and 126.81 ppm are two =CH- ortho to carboxylic acid group. The presence of a similar peak in both the fresh and used SO_3H-INA@SiO_2 catalyst indicates that the catalyst structure is retained after use (Figure 4.7).

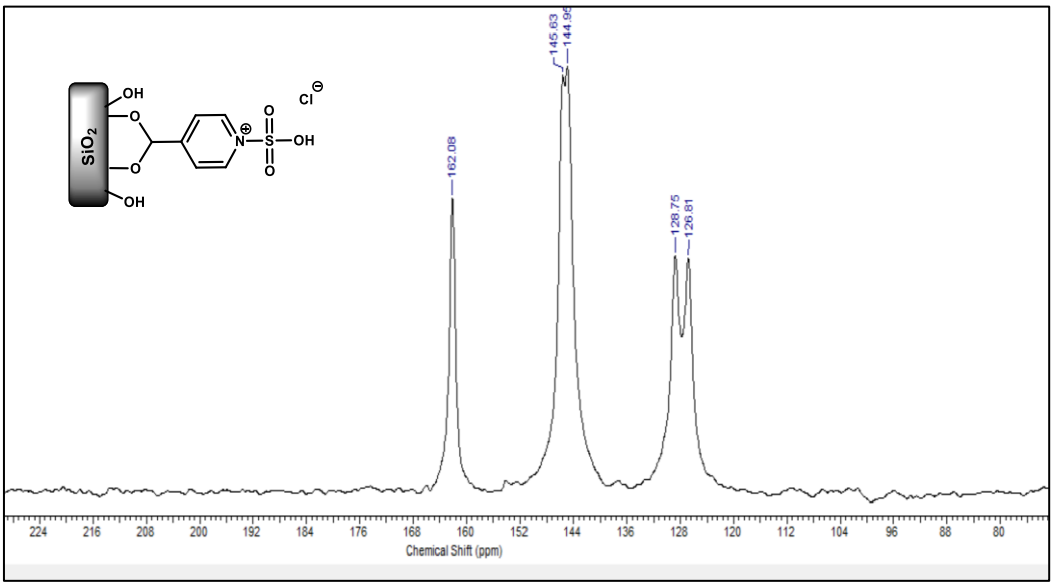

Figure 4.6. Solid state NMR of fresh SO_3H-INA@SiO_2 catalyst

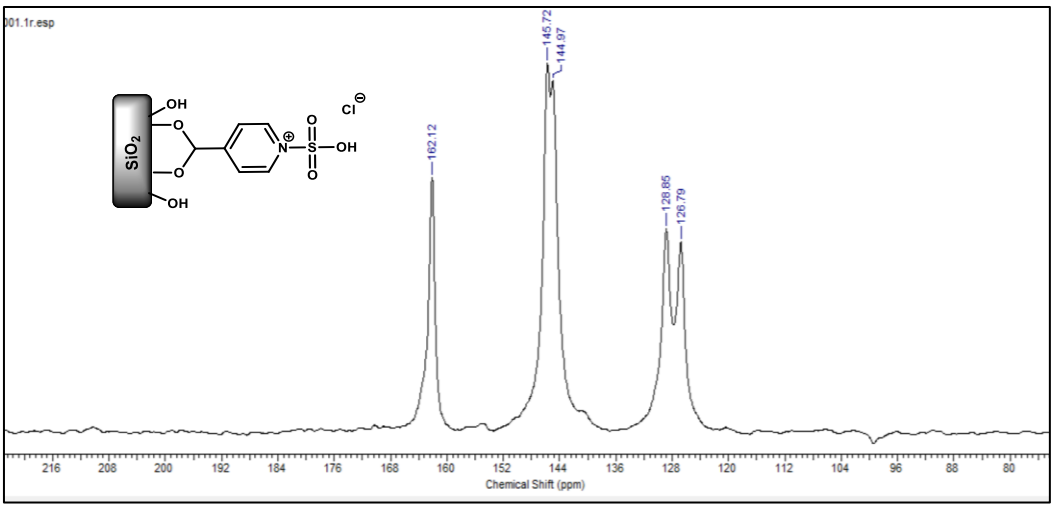

Figure 4.7. Solid state NMR of used SO_3H-INA@SiO_2 catalyst

4.5.2. Catalyst screening for conversion of 2-methylfuran to diesel fuel precursors

The conversion of 2-methylfuran to diesel fuel precursors (C_{15} and C_{20} unit) is aided by Brønsted acid catalysts. Therefore, several Brønsted acid catalysts were screened for self-condensation of 2-methylfuran. When aqueous solution of conc. H_2SO_4 (10 mol %) was used for the condensation reaction, 97% conversion of 2-methylfuran was noticed with 65% and 32% selectivity to products **1** and **2**, respectively (Table 4.1, Entry 1). The para toluene sulfonic acid (*p*-TSA) catalyst showed 92% conversion of 2-methylfuran with 69% selectivity to product **1** and 28% selectivity to product **2** (Table 4.1, Entry 2). Amberlyst-15 resin offered 95% conversion of 2-methylfuran with 68% and 28% selectivity to product **1** and **2**, respectively (Table 4.1, Entry 3). The Amberlyte IR-120 showed somewhat less conversion (90%) of 2-methylfuran, with 62% selectivity to product **1** and 31% selectivity to product **2** (Table 4.1, Entry 4). Dowex-500 offered 93% conversion of 2-methylfuran with 70% and 25% selectivity to product **1** and **2**, respectively (Table 4.1, Entry 5). Self-Condensation reaction was further performed with Lanxess K11311S resin which showed 96% conversion of 2-methylfuran with 63% selectivity to product **1** and 32% selectivity to product **2** (Table 4.1, Entry 6). The Thermax resin used for this reaction offered 67% selectivity to product **1** and 27% selectivity to product **2** with 95% conversion of 2-methylfuran (Table 4.1, Entry 7). Astonishingly, selectivity pattern of products has been reversed when our synthesized ionic solid, [SO_3H-INA] was used which offered the highest conversion (99%) of 2-methyfuran with 20% selectivity to product **1** and 72% selectivity to product **2** (Table 4.1, Entry 8). Heterogeneous SO_3H-INA@SiO_2 catalyst also offered the same conversion with 21% selectivity to product **1** and 74% selectivity to product **2** (Table 4.1, Entry 9). As compared to -SO_3H functionalized catalysts (entries 1-7), SO_3H-INA and SO_3H-INA@SiO_2 showed high selectivity towards product **2** that could be ascribed for their higher acidity. A heterogeneous Lewis-Brønsted acid catalyst such as Zr-Mont showed lower conversion (60%) of 2-methylfuran with 10%,75% and 15% selectivity to products **1**, **2** and unidentified product, respectively (Table 4.1, Entry 10). Sn-Mont (Lewis-Brønsted acid) gave 9%, 73% and 18% selectivity to product **1**, **2** and unidentified product, respectively with 35% conversion of 2-methylfuran (Table 4.1, Entry 11). Lewis acid sites present in Zr-Mont and Sn-Mont catalysts might have responsible for the increased formation unidentified product.

Table 4.1. Catalyst screening for conversion of 2-methylfuran to diesel fuel precursors [a]

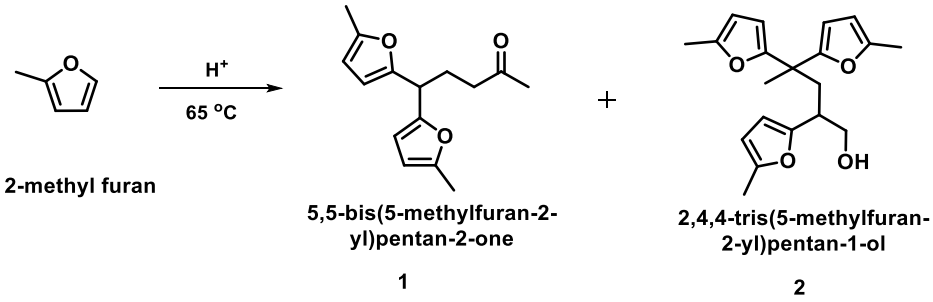

Entry	Catalyst	Acidity [mol/g]	2-methylfuran conversion [%][d]	Selectivity [%][e]		
				1	2	Unidentified product
1[b]	Conc. H_2SO_4	---	97	65	32	03
2[c]	*p*-TSA	---	92	69	28	03
3	Amberlyst-15	0.019	95	68	28	04
4	Amberlyte IR-120	0.016	90	62	31	07
5	Dowex-50WX8 resin	0.018	93	70	25	05
6	Lanxess K11311S resin	0.018	96	63	32	05
7	Thermax resin	0.019	95	67	27	06
8	SO_3H-INA	0.046	99	20	72	08
9	SO_3H-INA@SiO_2	0.031	99	21	74	05
10	Zr-Mont	---	60	10	75	15
11	Sn-Mont	---	35	9	73	18

[a] Reaction conditions: 2-methylfuran (1 g, 0.012 mol), catalyst (0.1 g), 65 °C, 7h. [b,c] 10 mol% of catalyst was used. [d,e] Conversion of 2-methylfuran and products selectivity was determined by using GC.

Turn over number (TON) and turn over frequency (TOF) of catalysts

Turn over number of heterogeneous catalysts can be calculated by using following equation,

Turn over number (TON) = (Number of moles of reactant consumed/ number of moles of active sites in the catalyst)

And

Turn over frequency (TOF) of heterogeneous catalysts can be calculated by using following equation,

Turn over frequency (TOF) = (Turn over number/ time)

For our catalysts [SO_3H-INA@SiO_2], the conversion of 2-methyfuran after 1h was 40%. Initial moles of 2-methyfuran used in the reaction is 0.012 moles.

Moles of 2-methyfuran consumed = 0.012 moles x (40/100) = 0.0048 moles

Amount of catalysts used in the reaction was 0.1 g.

Acidity of this catalyst is 0.031 moles/g, which means 1 g of catalyst contains 0.031 moles of acid sites.

Moles of active site in the catalyst = [0.1 g x 0.031 moles]/ 1g = 0.0031 moles

Turn over number (TON) = (Number of mols of reactant consumed/ number of moles of active sites in the catalyst) = 0.0048 moles/ 0.0031 moles = 1.548

Turn over frequency (TOF) = (Turn over number/ time) = 1.548/ 60 min = 0.025 min^{-1}

The turn over number (TON) and turn over frequency (TOF) of other sulfonic acid-functionalized solid acid catalysts was also calculated using a similar equation, the results presented in Table 4.2.

Table 4.2. Catalyst acidity, turn over number (TON) and turn over frequency (TOF)

Entry	Catalyst	Acidity [mol/g]	2-methylfuran conversion [%]	TON	TOF [min^{-1}]
1	Conc. H_2SO_4	---	---	---	---
2	*p*-TSA	---	---	---	---
3	Amberlyst-15	0.019	35	2.21	0.0368
4	Amberlyte IR-120	0.016	32	2.37	0.0395
5	Dowex-50WX8 resin	0.018	28	1.86	0.0311
6	Lanxess K11311S resin	0.018	39	2.60	0.0433
7	Thermax resin	0.019	38	2.40	0.040
8	SO_3H-INA	0.046	48	1.25	0.020
9	SO_3H-INA@SiO_2	0.031	40	1.54	0.025
10	Zr-Mont	---	---	---	---
11	Sn-Mont	---	---	---	---
For each catalysts conversion measured after 60 min					

4.5.3. Effect of variation in ionic solid SO_3H-INA (%w/w) loading on silica

During catalyst screening study, 50% w/w SO_3H-INA loaded on silica was used as an optimized catalyst system which offered 99% conversion of 2-methylfuran. In order to justify the selection of optimized catalyst system, lower %w/w loading of ionic solid SO_3H-INA on silica were also tested for transformation of 2-methylfuran to diesel fuel precursors (Figure 4.8). With 10% w/w SO_3H-INA loaded on silica, lower conversion (65%) of 2-methylfuran was observed which was result of insufficient active sites. It was observed that as %w/w loading of ionic solid on silica increased from 20 to 50% w/w, the conversion of 2-methylfuran and yield of products **1** and **2** gradually increased. With 50% w/w SO_3H-INA loaded on silica, maximum 99% conversion of 2-methylfuran with 21% selectivity to product **1** and 74% selectivity to product **2** was observed. Therefore, for further experiments, 50% w/w SO_3H-INA loaded on silica was used as the optimized catalyst.

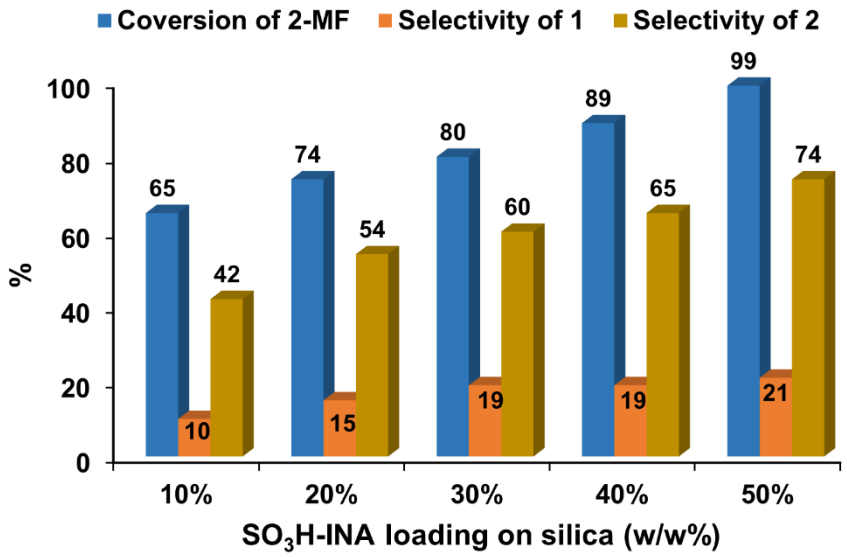

Figure 4.8. Effect of ionic solid SO_3H-INA (10-50% w/w) loading on silica on conversion of 2-methylfuran. Reaction conditions: 2-methylfuran (1 g, 0.012 mol), 10-50%w/w SO_3H-INA@SiO_2 (0.1 g), 65 ^oC, 7h.

4.5.4. Effect of reaction time

To determine the optimized reaction time to reach complete conversion of 2-methylfuran, reaction samples were withdrawn after every one hour and analyzed by GC. Effect of reaction time on reaction profile is presented in Figure 4.9. Both the conversion of 2-methylfuran and the selectivity for the products increased with longer reaction times. The maximum conversion of 2-methylfuran (99%) was achieved after 7 hours, with selectivity of 21% for product **1** and 74% for product **2**. No further variation in the conversion of 2-methylfuran or the selectivity for products **1** and **2** was observed when the reaction was extended to 8 hours.

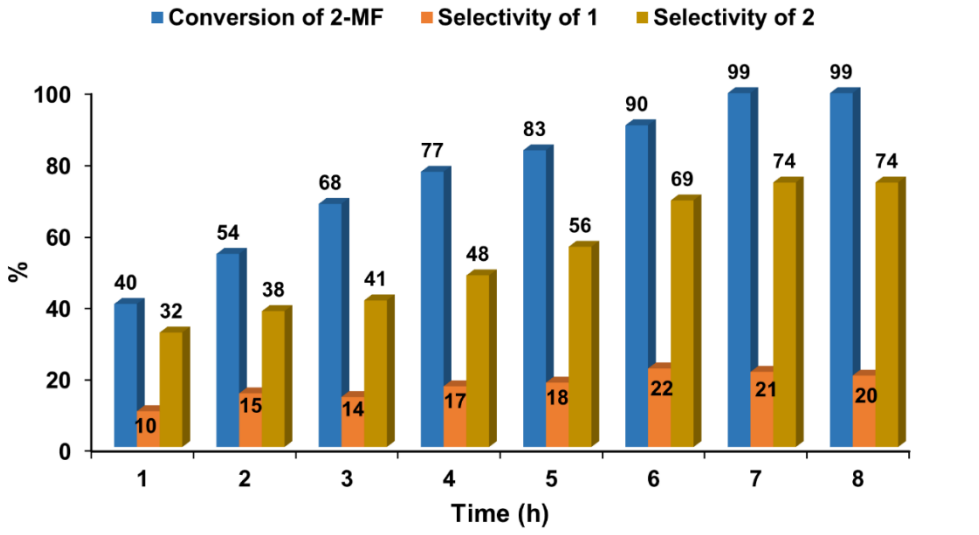

Figure 4.9. Effect of reaction time on conversion of 2-methylfuran. Reaction conditions: 2-methylfuran (1 g, 0.012 mol), SO_3H-INA@SiO_2 (0.1 g), 65 ^oC, 1-8 h.

4.5.5. Effect of catalyst amount

To find out the optimum catalyst amount needed to reach maximum conversion of 2-methylfuran, the effect of catalyst amount in the range between 5-15% w/w with respect to 2-methylfuran was studied (Figure 4.10). With 5%w/w of catalyst, 2-methylfuran conversion reached to 70% with 10% selectivity to product **1** and 58% selectivity to product **2**. When the amount of catalyst was increased to 10% w/w, conversion of 2-methylfuran increased to 99% with 18% and 70% selectivity to products **1** and **2**, respectively. More than 10% w/w catalyst amount didn't affect the conversion of 2-methylfuran and product distribution. From this study, it is revealed

that maximum 10% w/w catalyst amount is required to reach the maximum conversion of 2-methylfuran.

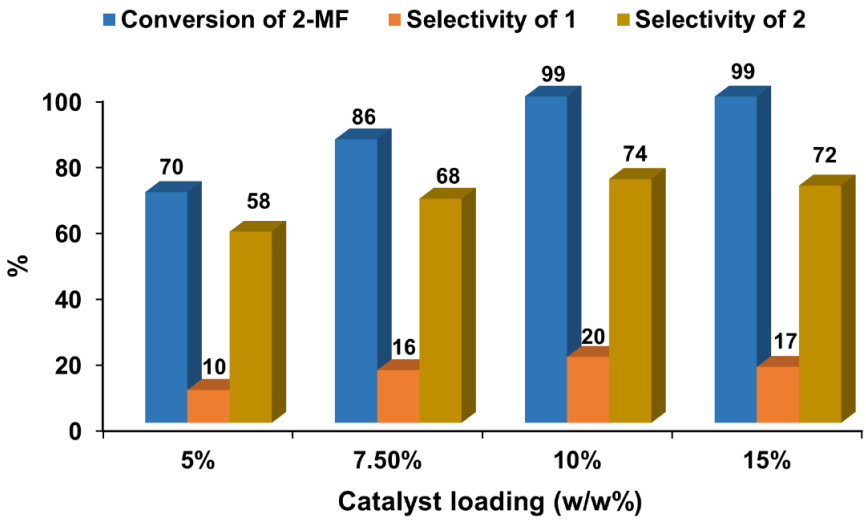

Figure 4.10. Effect of catalyst amount on conversion of 2-methylfuran. Reaction conditions: 2-methylfuran (1 g, 0.012 mol), SO_3H-INA@SiO_2 (5-15% w/w), 65 ^oC, 7h.

5.5.6. Effect of water content

In 2015, Yati et al. [28] investigated the conversion of 2-methylfuran to diesel fuel precursors using Amberlyst-15 catalyst. According to their investigation, product **1** (C_{15} unit) can be selectively formed if the reaction is performed in presence of water. On the other hand, they observed that in absence of water product **2** can be selectively produced. To explore the effect of water on product distribution, water was added in amounts ranging from 0-15% w/w (Figure 4.11). In the initial experiment without addition of water, 2-methylfuran (0.5% w/w initial moisture content) conversion was 99% with 21% selectivity to product **1** and 74% selectivity to product **2**. As extra water was added from 4-15%, conversion of 2-methylfuran gradually decreased to 68% and selectivity to products **1** and **2** also significantly decreased due to enhanced formation of unidentified by-product. Addition of water to the reaction not only reduced the conversion of 2-methylfuran but also altered the selectivity pattern of both the products. After addition of water selectivity to product **1** was increased as compared to product **2** which aligns with the findings of Yati et al. [28].

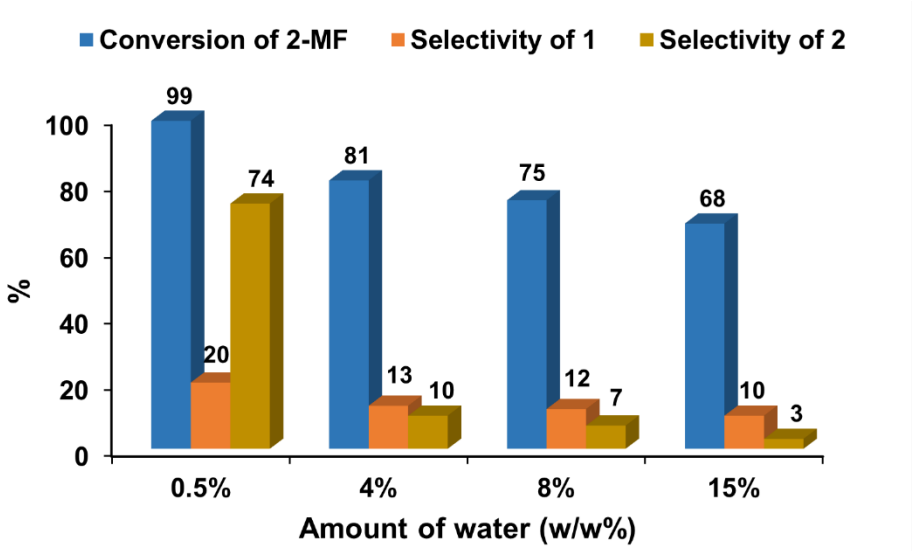

Figure 4.11. Effect of water content on conversion of 2-methylfuran Reaction conditions: 2-methylfuran (1 g, 0.012 mol), SO_3H-INA@SiO_2 (0.1 g), 65 ^oC, 7h.

4.5.7. Catalyst leaching test

The stability of the catalyst can be examined by leaching test experiment which was performed by following standard procedure.

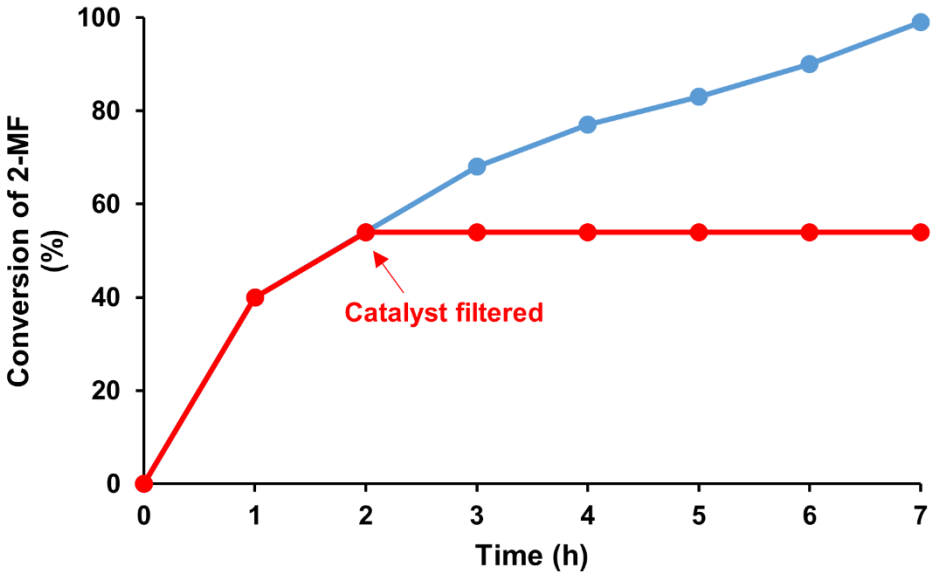

Figure 4.12. Catalyst leaching test. Reaction conditions: 2-methylfuran (1g, 0.012 mol), SO_3H-INA@SiO_2 (0.1g), 65 ^oC, 7h.

A reaction mixture containing 2-methylfuran (1 g, 0.012 mol) and SO_3H-INA@SiO_2 (0.1 g) was heated at 65 ^oC for 2 h to reach certain conversion (54%) of the 2-methylfuran. The reaction mixture was then rapidly cooled to room temperature and filtered to separate the catalyst. The filtrate was then recharged into the reaction vessel and heated at 65 ^oC up to 7 h. It was noticed that there was no further conversion of 2-methylfuran after catalyst separation which confirms that there is no leaching or loss of active sites of the catalyst in reaction mixture. The results are shown in Figure 4.12.

4.5.8. Recycle study of SO_3H-INA@SiO_2

The stability and reusability of the SO_3H-INA@SiO_2 catalyst were assessed through a recycling study. For each recycling experiment, the catalyst was separated from the reaction mixture by simple filtration after each run. The separated catalyst was then washed with ethyl acetate and reused directly for the subsequent run. The stability of SO_3H-INA@SiO_2 was evaluated by performing several recycle runs (Figure 4.13). It was found that, the catalytic activity of SO_3H-INA@SiO_2 was very much consistent after being used for five times. However, during the 6th reuse, the activity of catalyst was slightly reduced, which could be attributed due to partial blockage of the catalyst's active sites from product deposition.

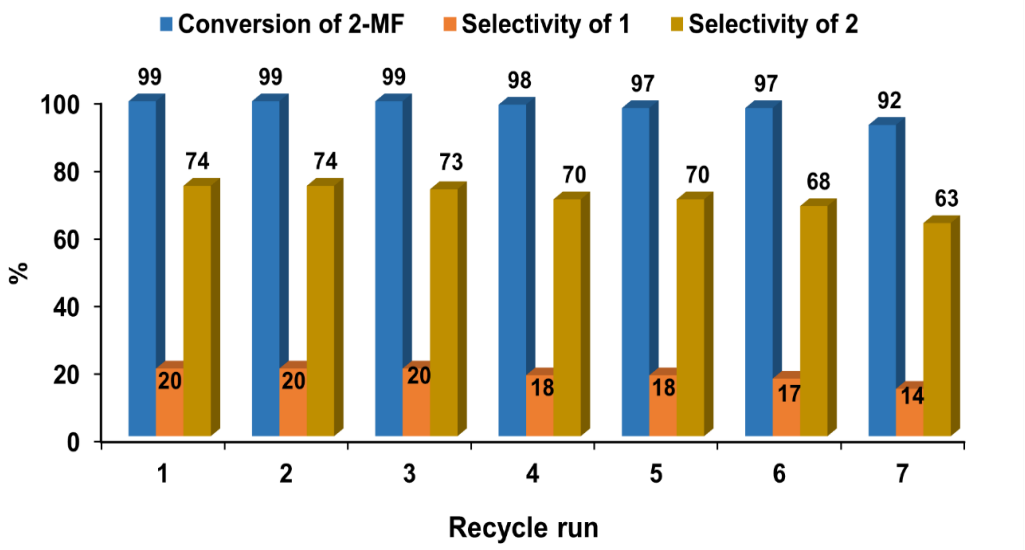

Figure 4.13. Recycle study of SO_3H-INA@SiO_2. Reaction conditions: 2-methylfuran (1 g, 0.012 mol), SO_3H-INA@SiO_2 (0.1 g), 65 ^oC, 7h.

4.6. Plausible reaction pathway

Mechanistic pathway for the formation of product **1** from 2-methylfuran in presence acid catalyst is proposed in Figure 4.14. In presence of an acid catalyst, the molecule of 2-methylfuran is protonated which then undergoes ring opening to form 4-oxopentanal. The protonation takes place at C_3 carbon so as to form a stable tertiary carbocation which can be further attacked by water molecule to open the ring. Then electrophilic carbonyl carbon of the aldehyde group of 4-oxapentanal is attacked by second molecule of 2-methylfuran to form a tertiary alcohol. Then tertiary alcohol gets protonated and immediately removes water leaving behind a stable secondary carbocation. The third molecule of 2-methyfuran is then added to that stable carbocation to form product **1** [28].

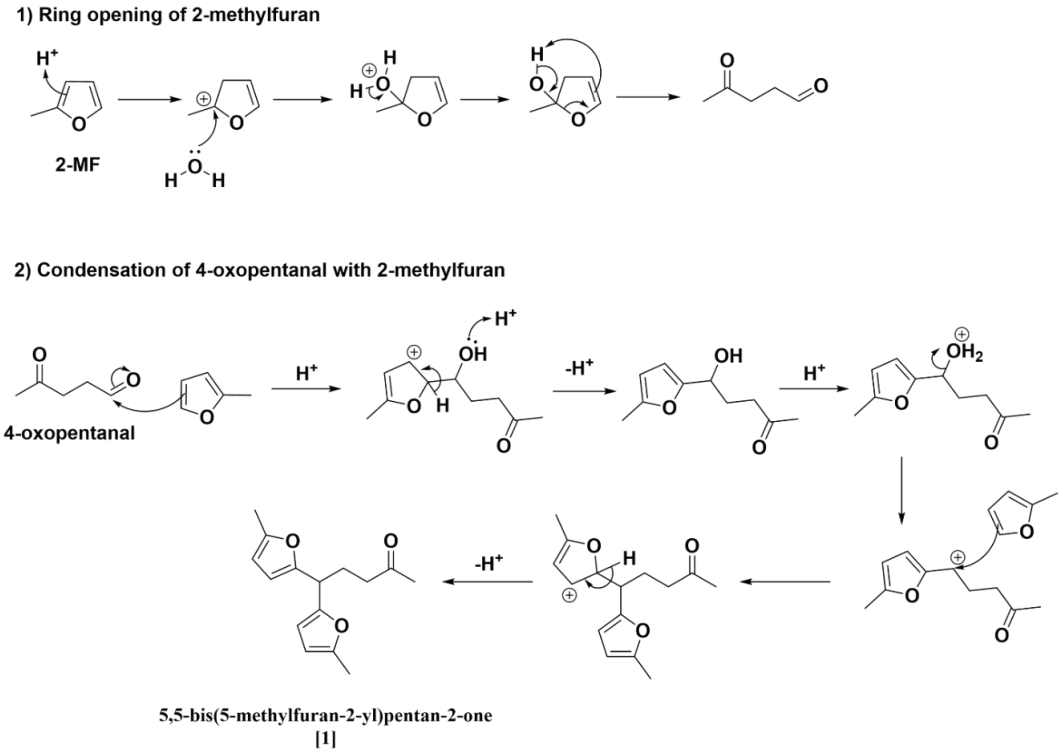

Figure 4.14. Plausible reaction mechanism for condensation of 2-methylfuran to product **1**.

Formation of product **2** from 2-methylfuran in presence acid catalyst is proposed in Figure 4.15. Under acidic condition, 2-methylfuran protonated at C_2 to form carbocation at C_3 allows nucleophilic addition of second molecule of 2-methylfuran at C_3 to form another carbocation which is stabilized by removal of proton to form an intermediate-I. A stable tertiary carbocation formed after protonation of dihydrofuran

ring to which nucleophilic addition of third molecules takes place followed by proton elimination to form intermediate-II. Tetrahydrofuran ring opening takes place after protonation which allows to form stable tertiary carbocation. Then tertiary carbocation undergoes nucleophilic addition by fourth molecule of 2-methyfuran to form product **2**.

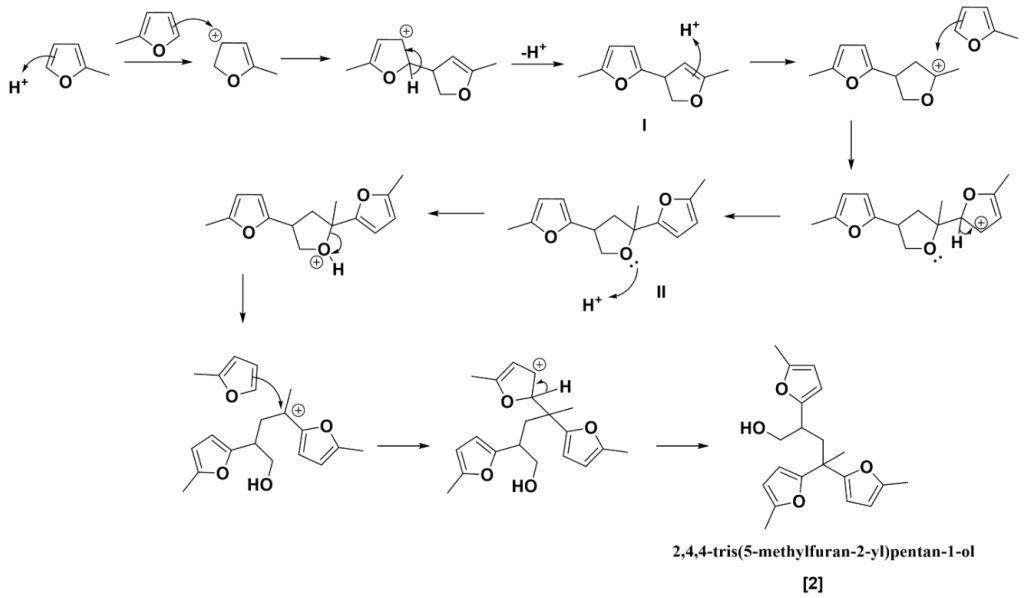

Figure 4.15. Plausible reaction mechanism for condensation of 2-methylfuran to product **2**.

4.7. Carbon balance calculation

Carbon present in reactant for 1mol of reactants

2-methylfuran [C_5H_6O] [1 mol]

82.1 = [60 g carbon + 6 g hydrogen +16 g of oxygen]

Total reactant carbon= 60 g

For 1 mol [82.1 g] of 2-methyfuran 60 g carbon

Thus for 12 mmol [1 g] of 2-methyfuran is 0.730 g of carbon

Total carbon in reactants = 0.730 g

Carbon in products:

Condensation product 1 [$C_{15}H_{18}O_3$] [MW: 246]

For 1 mol of product

246 g product contains = 180 g of carbon + 18 g of hydrogen + 48 g of oxygen

12 mmol of 2-methylfuran = 3 mmol of product

From 1 g of 2-methyl furan = 1 g of product should form

Thus, theoretical yield of product is 1 g

GC yields are considered for carbon balance calculation.

Thus, for SO_3H-INA@SiO_2 [Yield: 21%] product quantity is 0.210 g

246 g of product contains 180 g of carbon,

Therefore, 0.210 g of product contains 0.153 g carbon.

Condensation product 2 [$C_{20}H_{24}O_4$] [MW: 328]

For 1 mol of product

328 g product contains = 240 g of carbon + 24 g of hydrogen + 64 g of oxygen

12 mmol of 2-methylfuran = 4 mmol of product

From 1 g of 2-methylfuran = 1 g of product should form

Thus, theoretical yield of product is 1 g

GC yields are considered for carbon balance calculation

Thus, for SO_3H-INA@SiO_2 [Yield: 73%] product quantity is 0.730 g

328 g of product contains 240 g of carbon,

Therefore, 0.730 g of product contains 0.534 g carbon.

Total carbon in unreacted 2-methylfuran [C_5H_6O] [MW: 82.1]

For 1mol [82.1 g] of 2-methyfuran 60 g carbon

Thus for 12 mmol [1 g] of 2-methyfuran is 0.730 g of carbon

Total carbon in reactants = 0.730 g

For SO_3H-INA@SiO_2 catalyst conversion of 2-methyl furan is 99%.

Thus, 1% 2-methylfuran is unreacted.

1% of 1 g of reactant in 0.01 g.

Therefore, unreacted moles of reactant is 0.00012.

82.1 g of product contains 60 g of carbon.

Therefore, 0.010 g of reactant contains 0.0073 g of carbon.

The total carbon balance is calculated as follows [38]:

$$\text{Carbon balance}(\%) = \frac{\text{Total Carbon in (Product 1 + Product 2 + unreacted reactant)}}{\text{Total carbon in initial reactant}} \times 100$$

$$\text{Carbon balance}(\%) = \frac{(0.153 + 0.534 + 0.0073)}{0.730} \times 100$$

The total carbon balance of reaction = **95.10 %**

The carbon balance of reaction performed with catalysts (showed in Table-1) was calculated by same way and presented in Table- 4.3.

Table 4.3. Carbon balance of condensation reaction with various catalysts [a]

Entry	Catalyst	Conversion [%][b]	Yield [%][c]		Carbon balance of reaction [%]
			1	2	
1	Conc. H_2SO_4	97	63	31	96.96
2	p-TSA	92	63	25	95.89
3	Amberlyst-15	95	64	26	95.06
4	Amberlyte IR-120	90	56	28	93.97
5	Dowex-50WX8 resin	93	65	23	95.06
6	Lanxess K11311S resin	96	60	30	94.10
7	Thermax resin	95	63	25	92.87
8	SO_3H-INA	99	19	71	91.13
9	SO_3H-INA@SiO_2	99	21	73	95.10
10	Zr-Mont	60	06	45	90.95
11	Sn-Mont	35	03	25	93.00

[a] Reaction conditions: 2-methylfuran (1 g, 0.012 mmol), catalyst (0.1g), 65 °C, 7h. [b] Conversion of 2-methyl furan and [c] Yield of products was determined by using GC.

4.8. Conclusions

In summary, a simple, novel heterogeneous solid acid catalyst SO_3H-INA@SiO_2 was developed to explore solvent free conversion of bio-derived 2-methylfuran to diesel fuel precursors of C_{15} and C_{20} units. Catalytic activity of several -SO_3H functionalized acid catalysts were compared with our developed SO_3H-INA@SiO_2 catalyst, the later showed much more superior activity, due to its higher concentration of Brønsted acid sites, smaller particle size and high surface area. The SO_3H-INA@SiO_2 catalyst offered the highest conversion (99%) of 2-methylfuran with 21% selectivity to product **1** and 74% selectivity to product **2**. In addition, the heterogeneous, SO_3H-INA@SiO_2 catalyst is easily separable and reusable several times without losing its activity which is confirmed by catalyst leaching test, recycle study and acid-base titration of used

catalyst. This work can inspire researchers to develop multifunctional catalysts to convert 2-methylfuran directly to diesel fuel.

4.9. References

[1] S. H. Shinde, A. Hengne, C. V. Rode, *Biomass, Biofuels, Biochemicals*, **2020**, 1-31.

[2] J. Kirkinen, T. Palosuo, K. Holmgren, I. Savolainen, *Environ Manage*, **2008**, *42*, 458–469

[3] A. S. Mamman, J. M. Lee, Y. C. Kim, I. T. Hwang, N. J. Park, Y. K. Hwang, J. S. Chang, J. S. Hwang, *Biofuels, Bioprod. Biorefin.*, **2008**, *2*, 438-454.

[4] R. H. Kottke, *Wiley Inter science*, New York, **2004**.

[5] B. Kamm, P. R. Gruber, M. Kamm, *Wiley-VCH, Weinheim,* **2006**.

[6] K. Zeitsch, *Elsevier Science, Dordrecht*, **2000**, *13*, 229-230.

[7] H. Y. Zheng, Y. L. Zhu, B. T. Teng, Z. Q. Bai, C. H. Zhang, H. W. Xiang, Y. W. Li, *J. Mol. Catal*., **2006**, *246*, 18-23.

[8] A. Corma, O. D. Torre, M. Renz, N. Villandier, *Angew. Chem*., **2011**, *50*, 2375-2378.

[9] A. Gandini, M. N. Belgacem, *Prog. Polym. Sci*., **1997**, *22*, 1203–1379.

[10] S. H. Shinde, C. V. Rode, *Green Chem*. **2017**, *19*, 4804.

[11] M. Balakrishnan, E. R. Sacia, A. T. Bell, *ChemSusChem*., **2014**, *7*, 2796.

[12] G. Li, N. Li, X. Wang, X. Sheng, S. Li, A. Wang, Y. Cong, X. Wang, T. Zhang, *Energy Fuels*, **2014**, *28*, 5112–5118.

[13] E. Ramírez, R. Soto, R. Bringué, M. Iborra, J. Tejero, *Ind. Eng. Chem. Res*., **2020**, *59*, 20676–20685.

[14] W. M. VanRhijn, D. E. DeVos, B. F. Sels, W. D. Bossaert, P. A. Jacobs, *Chem. Commun*., **1998**, 317.

[15] M. Balakrishnan, E. R. Sacia, A. T. Bell, *ChemSusChem*, **2014**, *7*, 1078.

[16] I. Ogino, Y. Suzuki, S. R. Mukai, *ACS Catal*. **2015**, *5*, 4951.

[17] H. Li, S. Saravanamurugan, S. Yang, A. Riisager, *ACS Sustainable Chem. Eng*., **2015**, *3*, 3274.

[18] K. Tarade, S. Shinde, C. Rode, *Fuel Process. Technol*., **2020**, *197,* 106191.

[19] M. N. Gebresillase, J. GilSeo, *Applied Catalysis A: General*, **2021**, *628*, 118421.

[20] L. J. Konwar, A. Samikannu, P. Mäki-Arvela, J. P. Mikkola, *Catal. Sci. Technol*., **2018**, *8*, 2449-2459.

[21] H. Li, Q. Deng, X. Cao, J. Zheng, Y. Zhong, P. Zhang, J. Wang, Z. Zeng, S. Deng *Applied Catalysis A: General*, **2019**, *580*, 178-185.

[22] J. SunKwon, H. Choo, J. W. Choi, J. Jae, D. J. Suh, K. Y. Lee, J. M. Ha, *Applied Catalysis A: General*, **2019**, *570*, 238-244.

[23] T. Li, S. I. Cheng, J. F. Lee, L. Y. Jang, *J. Mol. Catal. A: Chem*., **2003**, *198*, 139.

[24] A. S. K. Hashmi, L. Schwarz, P. Rubenbauer, M. C. Blanco, *Adv. Synth. Catal*., **2006**, *348,* 705.

[25] V. Nair, K. G. Abhilash, N. Vidya, *Org. Lett*., **2005**, *7*, 5857.

[26] F. Algarraa, A. Corma, H. Garciaa, J. Primoa, *Appl. Catal. A*., **1995**, *128*, 119.

[27] M. Muthyala, V. K. Rao, A. Kumar, *Chin. J. Chem*., **2011**, *29*, 1483.

[28] C. Zhu, T. Shen, D. Liu, J. Wu, Y. Chen, L. Wang, K. Guo, H. Ying, P. Ouyang, *Green Chem.*, **2016**, *18*, 2165.

[29] J. Jaratjaroonphong, S. Tuengpanya, R. Saeeng, S. Udompong, K. Srisook, *Eur. J. Med. Chem.*, **2014**, *83*, 561.

[30] I. Yati, M. Yeom, J. W. Choi, H. Choo, D. J. Suh, J. M. Ha, *Applied Catalysis, A: General*, **2015**, *495*, 200-205.

[31] M. N. Gebresillase, R. Shavi, J. G. Seo, *Green Chem*., **2018**, *20*, 5133-5146.

[32] S. Shinde, C. Rode, *Catal. Commun*., **2017**, *88*, 77-80.

[33] S. Shinde, C. Rode, *ChemSusChem*, **2017**, *10*, 4090-4101.

[34] S. Suganuma, K. Nakajima, M. Kitano, D. Yamaguchi, H. Kato, S. Hayashi, M. Hara, *J. Am. Chem. Soc*., **2008**, *130*, 12787.

[35] R. S. Thombal, A. R. Jadhav, V. H. Jadhav, *RSC Adv*., **2015**, *5*, 12981.

[36] A. Khazaei, M. Tavasoli, A. R. Moosavi-Zara, *Res Chem Intermed*. **2018**, *44*, 5893-5910.

[37] A. Ghorbani-Choghamarani, G. Azadi, *RSC Adv*., **2015**, *5*, 9752-9758.

[38] G. Wenze, Z. Zheng, H. Jasper, J. H. Hero, Y. Jun, *Chemical Engineering Journal*, **2021**, *409*, 128182.

4.10. NMR data of synthesized compounds

4.10.1. NMR of synthesized compounds

5,5-bis(5-methylfuran-2-yl)pentan-2-one (BMFP)- Greenish yellow liquid

^{1}H NMR (500 MHz, DMSO-d6, 0.01%, TMS, δ ppm): 2.03 (s, 3 H), 2.20 (s, 6 H), 2.30-2.40 (m, 2 H), 2.45-2.55 (t, 2 H), 3.95 (t, 1 H), 5.95-5.96 (d, 2 H), 6.00-6.01 (d, 2 H).

^{13}C NMR (500 MHz, DMSO-d6, 0.01%, TMS, δ ppm): 13.74, 26.68, 30.25, 37.73, 40.80, 106.71, 106.96, 150.68, 153.39, 208.22.

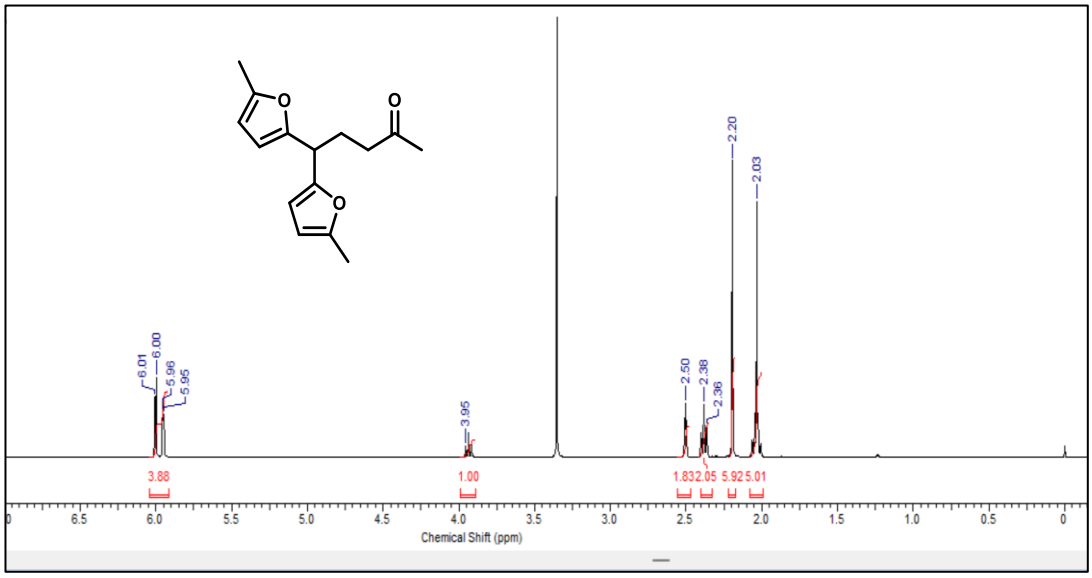

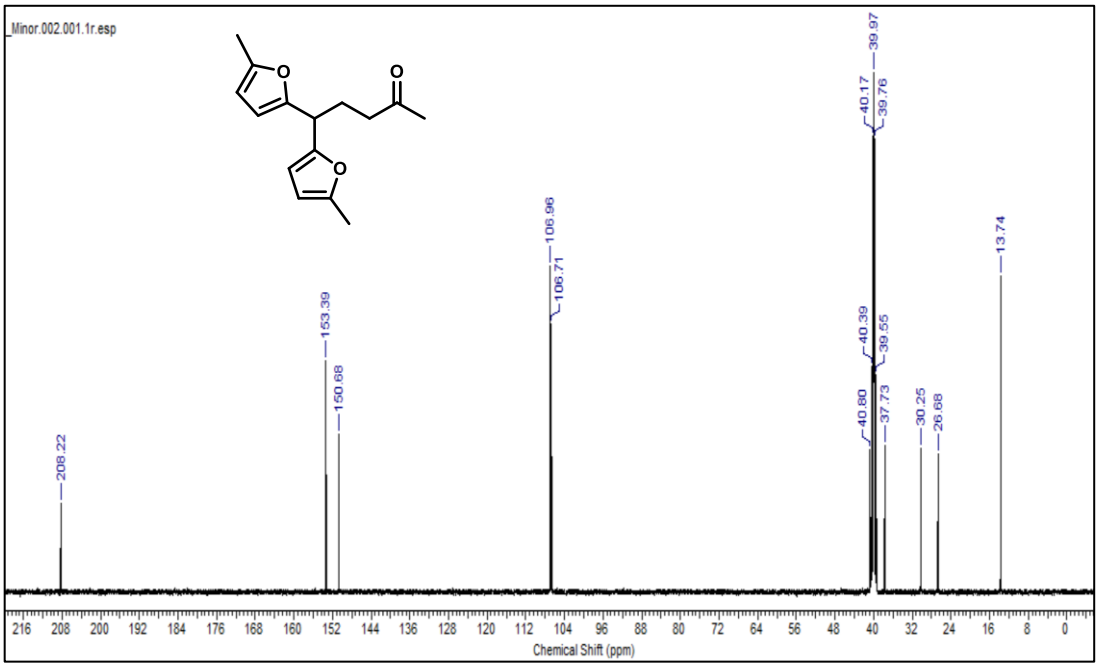

2,4,4-tris(5-methylfuran-2-yl)pentan-1-ol (TMFP) – Yellowish brown liquid

^{1}H NMR (400 MHz, $CDCl_3$, 0.01%, TMS, δ ppm): 1.48 (s, 3 H), 2.19 (s, 3 H), 2.22-2.23 (S, 6 H), 2.29 (m, 1 H), 2.35-2.40 (m, 1 H), 2.75-2.85 (m, 1 H), 3.45-3.85 (m, 1 H), 5.80-5.82 (d, 2 H), 5.83-5.84 (m, 3 H), 5.92-5.93 (d, 1 H).

^{12}C NMR (400 MHz, $CDCl_3$, 0.01%, TMS, δ ppm): 13.56, 23.29, 38.49, 38.75, 40.76, 65.88, 105.42, 105.71, 105.85, 105.92, 106.29, 107.15, 150.51, 150.73, 150.79, 154.23, 156.61, 157.37.

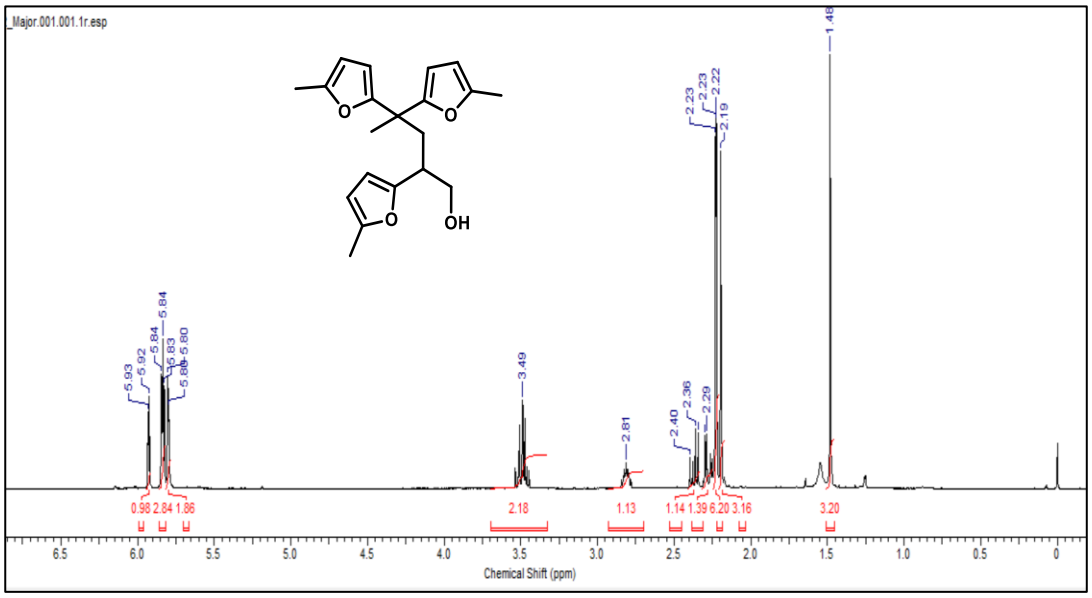

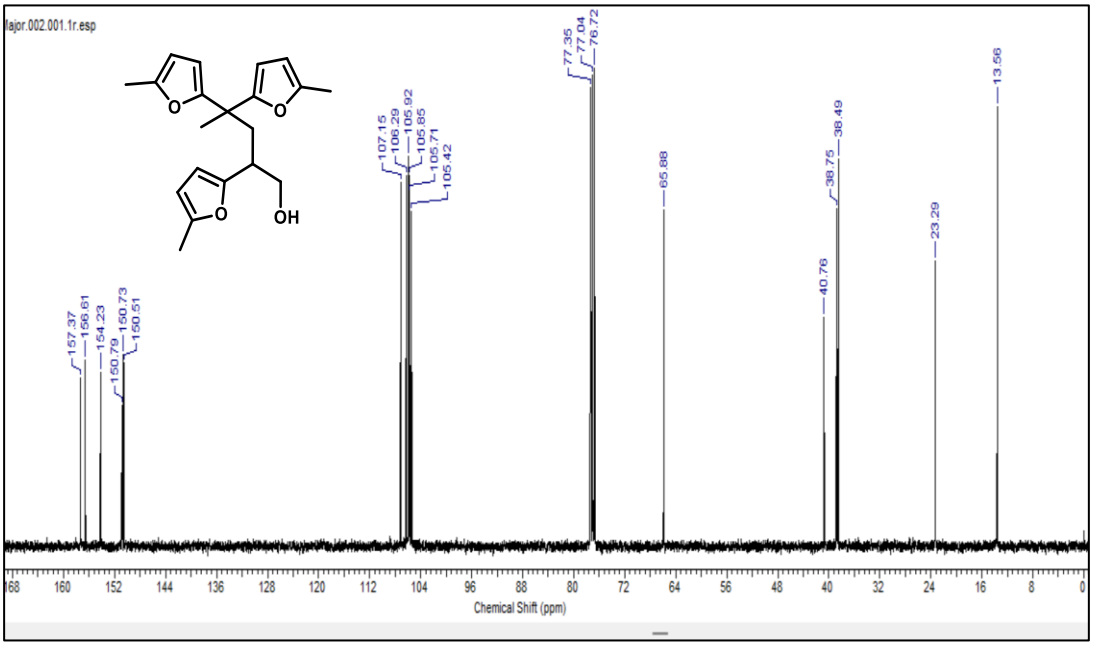

4.10.2. SO_3H-INA – White solid

^{13}C NMR (400 MHz, $CDCl_3$, 0.01%, TMS, δ ppm): 126.91, 144.16, 146.28, 164.35.

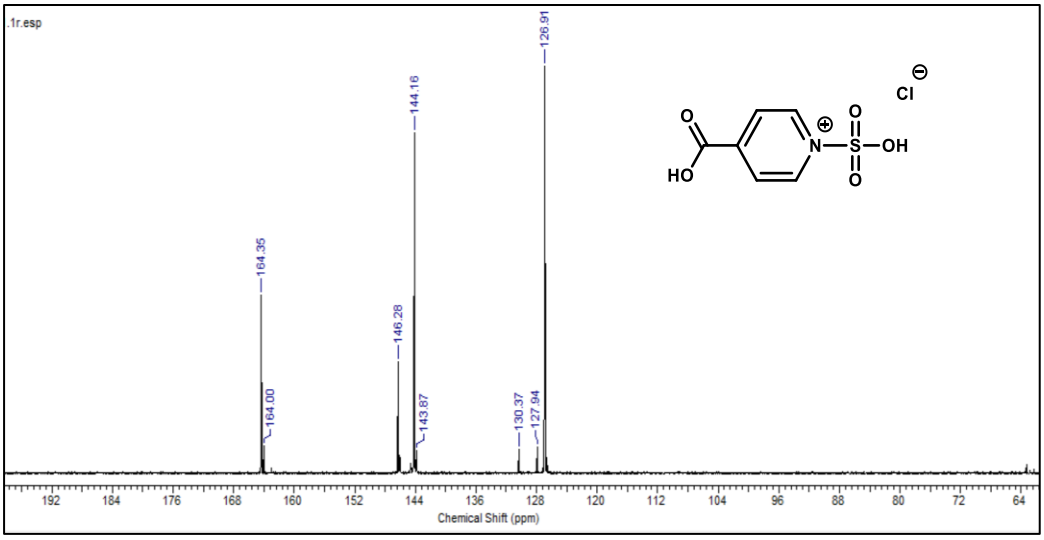

Chapter – 5

Magnetically Separable Brønsted Acid Catalyst for Synthesis of Bisguaiacol-F

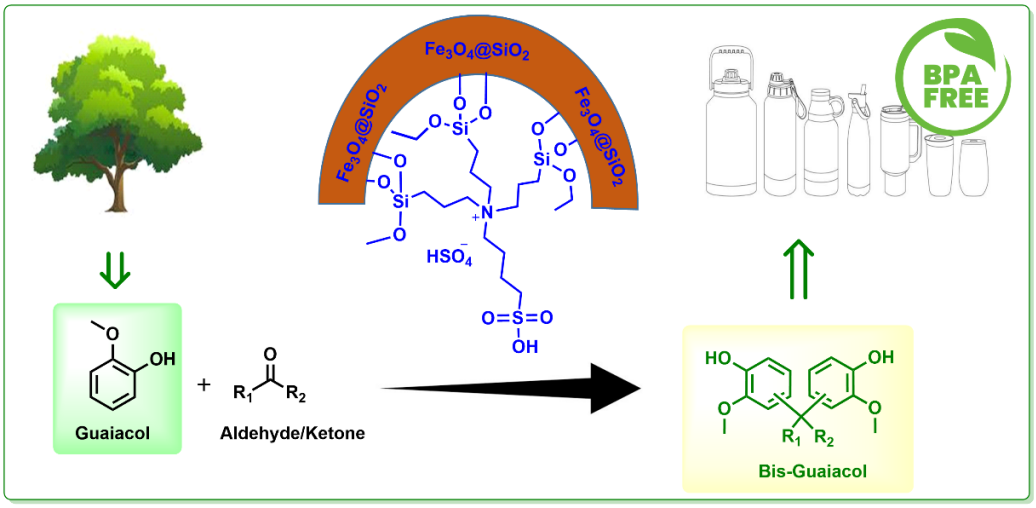

Polycarbonates, epoxy resins and plastics are commercially produced from Bisphenol-A (BPA). However, materials containing BPA are well known for serious health concerns hence, being outlawed in many countries. In order to mitigate this threat, Bisguaiacol-F (BGF) has emerged as safer and more sustainable alternative to Bisphenol-A. Herein, we have systematically synthesized a novel sulfonic acid functionalized, magnetically separable heterogeneous Brønsted acid catalyst, [Fe_3O_4@SiO_2-$(Pr)_3$-N-Bu-SO_3H] [HSO_4^-] and successfully applied for the synthesis of BGF by condensing aqueous formaldehyde with two molecules of guaiacol. The major challenge for this reaction was to avoid excess use of guaiacol and to attain complete conversion of both the starting materials. Astonishingly, our synthesized catalyst facilitates complete conversion of aqueous formaldehyde and guaiacol to form regio-isomers such as *pp*'-BGF, *mp*'-BGF and *op*'-BGF with 62%, 15% and 6% selectivity, respectively. The superior catalytic activity of our novel magnetically separable heterogeneous catalyst in terms of starting material conversion and product distribution could be attributed to its unique structural feature. It has pendant –SO_3H group which is attached to a long butyl chain making it easily accessible in the reaction. The catalytic activity was also examined for the condensation of guaiacol with couple of different aldehydes to produce derivatives of Bisguaiacol.

Komal Tarade, Chandrashekhar Rode and Sanjay Kamble, **New Journal of Chemistry**, (Under revision)

5.1. Introduction

Worldwide commonly used polycarbonates, epoxy resins and plastics are manufactured from Bisphenol-A (BPA) in various industries. These materials exhibit optical transparency and boast excellent mechanical and electrical properties [1]. Additionally, polycarbonates are resistant to heat and water, free from any taste or odor, impermeable to oils, fats, and bacteria, and physiologically inert. Bisphenol-A based plastics are very hard, clean and tough therefore, these are used to make water bottles and sports equipment. BPA containing epoxy resins are used in the manufacture of food and beverage cans, water pipeline etc. [2]. As a result of this, global demand of Bisphenol-A has increased tremendously, the Bisphenol A market is projected to grow from 8.18 million tons in 2024 to 11.23 million tons by 2029 [3]. However, Bisphenol-A is outlawed in baby bottles and other food packaging materials as it is harmful to children and pregnant women. Bisphenol-A plays a vital role in disrupting our normal hormones like estrogen and also shows adverse effect on endocrine system. Endocrine mediated toxicity causes diabetes, obesity, reproductive disorders, birth defects, breast cancer and chronic respiratory diseases etc. [4]. Due to serious health concerns associated with the utilization of Bisphenol-A based materials, search for safe alternative sources becomes a necessity. In order to mitigate this threat, Bisguaiacol-F (BGF) has emerged as a safer and more sustainable alternative to Bisphenol-A [2]. Bisguaiacol-F (BGF) is synthesized through the acid-catalyzed condensation of lignin-derived compounds, such as vanillyl alcohol or vanillin, with guaiacol. Vanillin, vanillyl alcohol and guaiacol are lignin-derived molecules utilized in the synthesis of a wide range of chemicals and building blocks [2, 5-8]. Lignocellulose is composed of cellulose, hemicellulose and lignin [9-11]. Lignin is one of the most abundant materials on Earth with an estimated annual production in the millions of metric tons [11-13]. However, currently lignin is mainly utilized as a fuel for the purpose of heat generation in the paper and pulp industry [12,14]. Indeed, lignin is a highly valuable renewable resource for producing essential phenolic building blocks, including guaiacol, vanillin, creosol and syringol [12]. These lignin-derived substituted phenols present viable alternatives to petrochemical-based phenolics in polymer synthesis [7-9, 15-21]. Notably, wood-tar creosote, an industrially available and cost-effective phenolic mixture (priced at $1000–3000 per metric ton), is also derived from lignin. Wood-tar creosote is obtained by distilling wood tar which is produced during the carbonization of beech wood or pine trees. Its primary constituents are guaiacol (2-methoxyphenol) and creosol (2-methoxy-4-methylphenol) [22,23]. During Bisguaiacol-F synthesis several regio-isomers such as

pp'-BGF, *mp*'-BGF and *op*'-BGF are being produced which have lower estrogenic activity than Bisphenol-A (BPA) [24]. In addition to that, Bisguaiacol-F has wide range of applications which includes the production of biomedical devices, household products, automation components, fuel cell membranes, food packaging materials, printed circuit boards and water treatment membranes etc. (Scheme 1). Apart from that, Bisguaiacol-F can be converted to branched cyclic lubricants *via* hydrodeoxygenation process [25].

5.2. Literature Survey

Typically, Bisguaiacol-F is synthesized by electrophilic aromatic condensation of vanillyl alcohol or vanillin with guaiacol in presence of mineral acid such as H_2SO_4 [2, 26] and sulphonic acid functionalized resins like Amberlyst-15 [5] and Dowex [8]. However, raw materials such as vanillin, vanillyl alcohol and guaiacol are expensive commodities, further aggravated by the use of stoichiometric excess guaiacol in the condensation reaction. The subsequent removal of excess guaiacol by vacuum distillation significantly escalates energy consumption and time [5]. The serious issues associated with synthesis of Bisguaiacol-F opened up an opportunity to find cheap alternative for vanillin and vanillyl alcohol. In this regard, efforts were made in the past to synthesize thermosetting polymer (Guaiacol Novolac) directly by condensation of guaiacol with paraformaldehyde without isolation of Bisguaiacol-F using non-reusable homogeneous acids such as HCl [27] and *p*-Toluene sulphonic acid monohydrate [28].

5.3. Scope of Present Work

In order to have sustainable and economical route for Bisguaiacol-F in our process, guaiacol was condensed with cheapest raw material such as 37% aq. formaldehyde in presence of reusable solid acid catalyst (Scheme 6.1). In this reaction process, first molecule of guaiacol reacts with aq. formaldehyde to form vanillyl alcohol which further reacts with the second molecule of guaiacol to produce Bisguaiacol-F [26,29]. For this reaction, we designed and synthesized a novel -SO_3H functionalized magnetically separable solid acid catalyst [Fe_3O_4@SiO_2-$(Pr)_3$-N-Bu-SO_3H] [HSO_4^-] and further explored it for this reaction. In this work, reaction parameters such as time, temperature, catalyst loading and molar ratio were also meticulously optimized. [Fe_3O_4@SiO_2-$(Pr)_3$-N-Bu-SO_3H] [HSO_4^-] catalyst gave complete conversion of aq. formaldehyde and guaiacol under optimized reaction conditions. The catalytic activity was also explored for the condensation of guaiacol with couple of different aldehydes to produces derivatives of BGF.

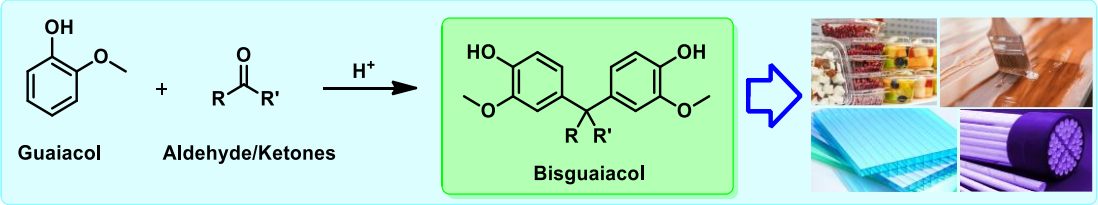

Scheme 5.1. Synthetic pathway and applications of Bisguaiacol

5.4. Experimental Section

5.4.1. Materials

Guaiacol, 37% aqueous formaldehyde, acetaldehyde, propionaldehyde, butyraldehyde, $FeCl_2$ and $FeCl_3$ purchased from Loba Chemie. 3-Aminopropyltriethoxysilane, 3-chloropropyltrimethoxysilane, ethylene diamine, 1,4-butane sultone, triethylamine, tetraethyl orthosilicate and resins such as Amberlyst-15, Amberlyte IR-120, Dowex-50WX8 were obtained from Sigma-Aldrich, India. Solvents such as methanol, acetonitrile, ethanol, toluene, ethyl acetate and petroleum ether, and silica gel (230-400 mesh) were purchased from Chem Labs, India.

5.4.2. Catalyst preparation

5.4.2.1. Preparation of $[(EtO)_3(MeO)_6Si\text{-}(Pr)_3\text{-}N\text{-}Bu\text{-}SO_3^-]$

Step 1: $[(EtO)_3(MeO)_6Si\text{-}(Pr)_3\text{-}N]$ (3-(triethoxysilyl)-N,N-bis(3-(trimethoxysilyl) propyl) propan-1-amine):

A mixture of 3-aminopropyl triethoxysilane (3 g, 0.0135 mole), 3-chloropropyl trimethoxysilane (5.38 g, 0.0271 mole) and ethylene diamine (3.24 g, 0.0540 mole) was stirred at 115 °C for 96 h. After the reaction mixture was cooled to room temperature, 100 mL of pentane was added with stirring. The mixture was then filtered to remove the salt, and the filtrate was evaporated and dried using a rotary evaporator for 1 hour, yielding a pale-yellow viscous liquid (7 g) [30]. ^1H NMR (400 MHz, $CDCl_3$, 0.01% TMS, δ ppm) 0.65 (m, 6H) 1.23 (m, 9H), 1.60 (m, 6H), 2.62 (m, 6H), 3.40 (s, 2H), 3.56 (s, 16H), 3.82 (m, 6H). ^{13}C NMR (400 MHz, $CDCl_3$, 0.01% TMS, δ ppm) 18.20, 18.38, 23.11, 26.99, 41.74, 44.91, 49.27, 49.65, 50.18, 50.30, 50.34, 50.40, 52.43, 58.24, 58.31, 58.38 (Section 5.8.3.1).

Step 2: $[(EtO)_3(MeO)_6Si\text{-}(Pr)_3\text{-}N\text{-}Bu\text{-}SO_3^-]$ (4-((3-(triethoxysilyl) propyl) bis(3-(trimethoxysilyl) propyl) ammonio) butane-1-sulfonate):

To a solution of (3-(triethoxysilyl)-N,N-bis(3-(trimethoxysilyl)propyl)propan-1-amine) (4 g, 0.0073 moles) in 10 mL of acetonitrile was prepared, to which 1,4-butane sultone (1 g, 0.0073 moles) was added dropwise under continuous stirring. The mixture was stirred at room temperature for 10 hours, then dried using a rotary evaporator. This process yielded a colorless oil of the desired product (4.86 g). ^{1}H NMR (400 MHz, $CDCl_3$, 0.01% TMS, δ ppm) 0.66 (m, 6H), 1.22 (m, 9H), 1.61 (m, 8H), 1.86 (m, 2H), 2.26(m, 2H), 3.17 (m, 3H), 3.43 (s, 5H), 3.56 (s, 18H), 3.82 (m, 6H). ^{13}C NMR (400 MHz, $CDCl_3$, 0.01% TMS, δ ppm) 6.63, 7.04, 7.46, 18.25, 18.40, 22.82, 23.57, 41.49, 48.23, 50.11, 50.43, 50.49, 51.96, 52.29, 57.85, 58.40, 58.46, 73.95 (Section 6.8.3.1).

5.4.2.2. Preparation of $[SiO_2\text{-}(Pr)_3\text{-}N\text{-}Bu\text{-}SO_3H]$ $[HSO_4^-]$

Step 1: $[SiO_2\text{-}(Pr)_3\text{-}N\text{-}Bu\text{-}SO_3^-]$ (4-((3-(triethoxysilyl) propyl) bis(3-(trimethoxysilyl) propyl) ammonio) butane-1-sulfonate) silica:

To a solution of (4-((3-(triethoxysilyl)propyl)bis(3-(trimethoxysilyl) propyl)ammonio) butane-1-sulfonate) (3 g) in 100 mL of toluene was prepared, to which SiO2 (3 g, 230-300 mesh) was gradually added under continuous stirring. The resulting mixture was refluxed at 110 °C for 48 hours. After cooling to room temperature, the mixture was filtered, and the residue was washed with toluene and dried in an oven. This process yielded a white solid material (5.5 g).

Step 2: $[SiO_2\text{-}(Pr)_3\text{-}N\text{-}Bu\text{-}SO_3H]$ $[HSO_4^-]$ (4-((3-(triethoxysilyl) propyl) bis(3-(trimethoxysilyl)propyl) ammonio) butane-1-sulfonate) acidic silica:

Conc. H_2SO_4 was diluted in 20 mL of ethanol and placed in an ice bath. To this chilled acidic solution, (4-((3-(triethoxysilyl)propyl)bis(3-(trimethoxysilyl)propyl) ammonio) butane-1-sulfonate) silica (2 g) was gradually added under continuous stirring. After 1 hour, the ice bath was removed, and the mixture was stirred for an additional 3 hours. The mixture was then dried using a rotary evaporator, resulting in a white solid of the desired catalyst.

5.4.2.3. Preparation of $[Fe_3O_4@SiO_2\text{-}(Pr)_3\text{-}N\text{-}Bu\text{-}SO_3H]$ $[HSO_4^-]$

Step 1: Synthesis of magnetic nano particles (Fe_3O_4)

A solution of $FeCl_2$ (5.4 g) and $FeCl_3$ (2 g) in 25 mL of 2M HCl was sonicated at room temperature for 30 minutes. A 25% aqueous ammonia solution (40 mL) was then added dropwise to the mixture, which was stirred for an additional 30 minutes. The resulting magnetic particles were separated using an external magnet. These particles were washed three times with deionized water and ethanol.

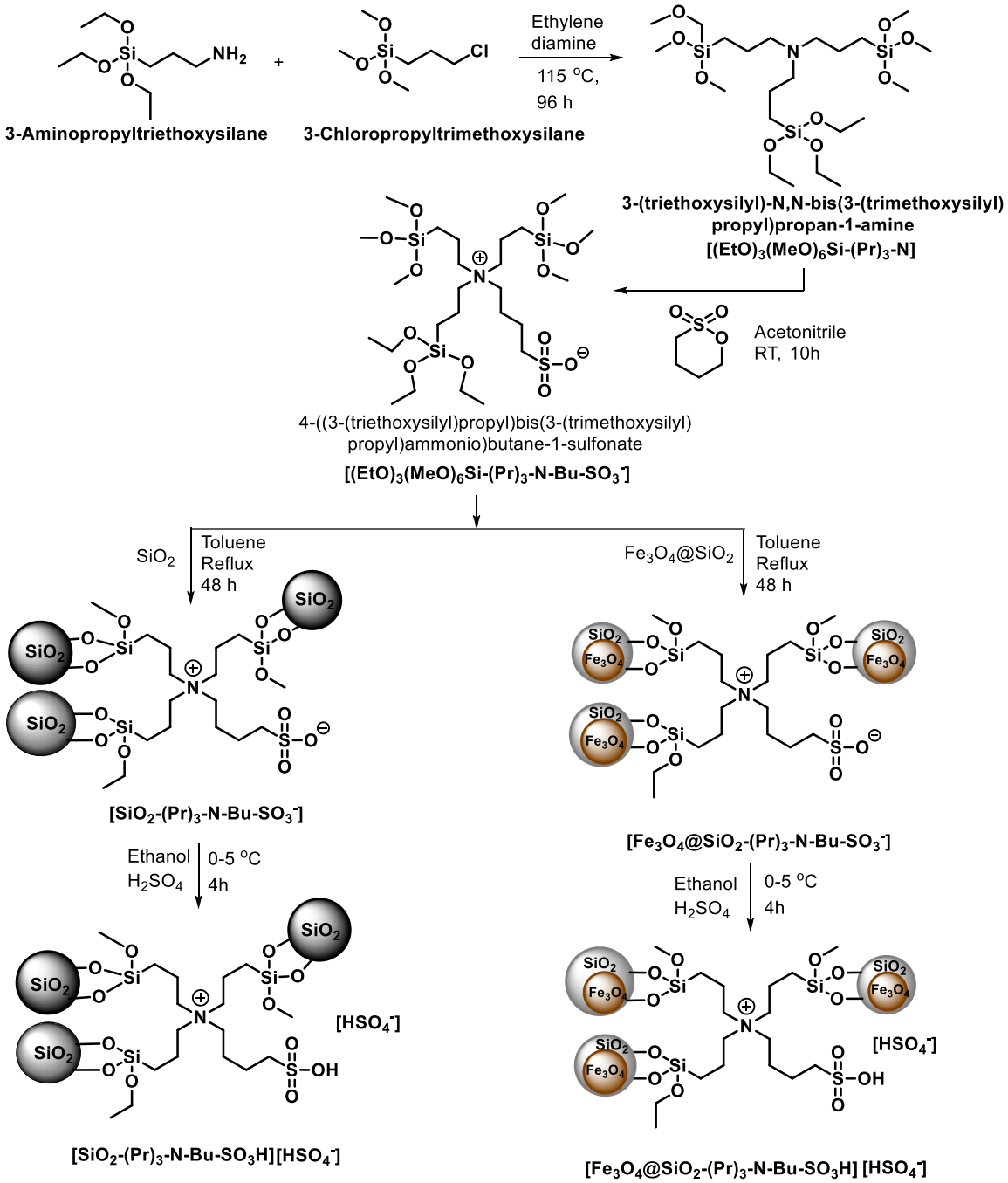

Scheme 5.2. Synthesis of [SiO_2-$(Pr)_3$-N-Bu-SO_3H] [HSO_4^-] and [Fe_3O_4@SiO_2-$(Pr)_3$-N-Bu-SO_3H] [HSO_4^-] catalysts.

Step 2: Synthesis of silica coated magnetic nano particles (Fe_3O_4@SiO_2)

The synthesized Fe_3O_4 nanoparticles (4 g) were suspended in 80 mL of ethanol and 12 mL of deionized water and sonicated for 15 minutes at room temperature. Tetraethyl orthosilicate (7.62 mL) was then added to the solution, which was kept

under sonication for an additional 10 minutes. Next, aqueous ammonia (3 mL) was added dropwise with continuous stirring. The mixture was then heated to 40 °C and stirred continuously for 12 hours. The silica-coated magnetic nanoparticles were separated using an external magnet and washed with ethanol (3 × 50 mL).

Step 3: [Fe_3O_4@SiO_2-$(Pr)_3$-N-Bu-SO_3^-] (4-((3-(triethoxysilyl)propyl)bis(3-(trimethoxysilyl) propyl)ammonio) butane-1-sulfonate) magnetic silica:

To a solution of (4-((3-(triethoxysilyl)propyl)bis(3-(trimethoxysilyl)propyl) ammonio) butane-1-sulfonate) (3 g) in 100 mL of toluene, Fe_3O_4@SiO_2 (3 g) was gradually added under continuous stirring. The mixture was refluxed at 110 °C for 48 hours. After cooling to room temperature, the mixture was filtered and the residue was washed with toluene and dried in an oven. A brown, solid, amorphous material was obtained (5.8 g).

Step 4: [Fe_3O_4@SiO_2-$(Pr)_3$-N-Bu-SO_3H] [HSO_4^-] (4-((3-(triethoxysilyl)propyl)bis(3-(trimethoxysilyl)propyl) ammonio) butane-1-sulfonate) magnetic acidic silica

Conc. H_2SO_4 was diluted in 20 mL of ethanol and placed in an ice bath. To this acidic solution, (4-((3-(triethoxysilyl)propyl)bis(3-(trimethoxysilyl)propyl)ammonio)butane-1-sulfonate) magnetic silica (2 g) was gradually added under continuous stirring. After 1 hour, the ice bath was removed, and the mixture was stirred for an additional 3 hours before being dried using a rotary evaporator, yielding a brown solid of the desired catalyst. The acidity of the resulting [Fe_3O_4@SiO_2-$(Pr)_3$-N-Bu-SO_3H] [HSO_4^-] catalyst was determined to be 0.021 mol/g by acid-base titration [31,32] (Table 6.1). The stepwise sequence of the catalyst synthesis is illustrated in Scheme 5.2.

5.4.2.4. Synthesis of [SO_3H-INA] [Cl]

The detail catalyst synthesis procedure is already presented in 4.4.2.1., Chapter 4 [33].

5.4.2.5. Synthesis of [SO_3H-INA@SiO_2] [Cl]

The detail catalyst synthesis procedure is already presented in 4.4.2.2., Chapter 4 [33].

5.4.2.6. Synthesis of *p*-toluene sulphonic acid–paraformaldehyde (*p*TSA-PFD)

The solid acid catalyst, *p*-TSA-PFD, was synthesized through the polymerization of *p*-toluene sulfonic acid (*p*-TSA) and paraformaldehyde (PFD) in the presence of sulfuric acid, following the method described by Patil et al. [34]. In a round bottom

flask equipped with a reflux condenser and magnetic stirrer, *p*-TSA (5 g) and H_2SO_4 (0.2 g) were combined. The mixture was heated within the range of 100-110 ºC until the *p*-TSA completely melted. Subsequently, paraformaldehyde (2 g) was promptly added to the solution, and the reaction mixture was maintained at 100-110 ºC for 8 hours. Following this, the temperature was raised to 130 ºC and held for an additional 24 hours to yield a black solid. The resulting solid was then filtered and washed with hot water until all SO_4^{2-} was completely removed. The catalyst was then oven-dried at 120 ºC overnight, followed by calcination at 185 ºC for 6 hours. The resulting catalyst was designated as *p*-TSA-PFD.

5.4.2.7. Synthesis of $[(Et)_3\text{-N-Bu-}SO_3H]$ $[HSO_4^-]$

The ionic liquid $[(Et)_3\text{-N-Bu-}SO_3H]$ $[HSO_4^-]$ was synthesized following a method reported by Shinde et al. [35]. Initially, triethylamine (1.01 g, 0.01 mol) and 1,4-butanesultone (1.36 g, 1.02 mL, 0.01 mol) were stirred at 40 °C for 24 hours. The resulting white solid zwitterion was washed three times with toluene to remove any unreacted material and then dried under vacuum. A stoichiometric amount of concentrated sulfuric acid (0.01 mol) was then added dropwise to the zwitterion. The mixture was stirred at 40 °C for 2–3 days until it liquefied, forming the ionic liquid. The ionic liquid was repeatedly washed with toluene and diethyl ether to eliminate any remaining unreacted material and then dried under vacuum.

5.4.3. Condensation of guaiacol with 37% aq. formaldehyde

A mixture of guaiacol (2 g, 0.016 mole), 37% aq. formaldehyde (1.2 g, 0.016 mole), acetonitrile (1 mL) and acid catalyst (0.3 g solid acid catalyst) or (10 mol% liquid acid catalyst) was stirred for 6 h at 90 °C in a round bottom flask. After that, reaction mixture containing homogeneous catalyst (liquid acid) was neutralized by dilute aqueous solution of sodium bicarbonate. While, the reaction mixture containing the solid acid catalyst was filtered to separate the catalyst. The neutralized reaction mixture (for the homogeneous catalyst system) or the filtrate (for the heterogeneous catalyst system) was then extracted with ethyl acetate. The organic layer was washed with water and brine solution. Separated organic layers were combined and dried over anhydrous sodium sulphate and evaporated on rotary evaporator to get crude product which contains a mixture of regioisomers of BGF which were separated by column chromatography using petroleum ether and ethyl acetate mixture as an eluent. Separated regioisomers were characterized by spectroscopic techniques and spectroscopic data is presented in section 5.8.

5.4.4. Analysis of reaction products

Thin layer chromatography was conducted using Merck 5554 aluminum-backed silica plates. The plates were visualized under UV light (254 nm) and stained with phosphomolybdic acid for preliminary analysis of the reaction crude. The percentage conversion of guaiacol and aq. formaldehyde was determined from chromatograms obtained in Shimadzu GC 2014 equipped with Stabil wax column and Flame Ionization detector. Percentage selectivity of Bisguaiacol-F regioisomers was calculated from chromatograms obtained in Agilent High Performance Liquid Chromatography (column: Hypersil C18, detector: UV (230 nm) and mobile phase: millipore water: Methanol (45:55; v/v) with 1 mL/min flow). The pure products were characterized and confirmed using ^{1}H NMR and ^{13}C NMR (50 MHz) in DMSO-d6 (0.01%, TMS) solvent on a 500 MHz Bruker instrument. Additionally, the isolated products were verified using a LABINDIA MR-VIS melting point apparatus.

5.4.5. Determination of catalyst acidity

An aqueous solution of sodium chloride (0.05 mol/g, 30 mL) was added to the [Fe_3O_4 @SiO_2-$(Pr)_3$-N-Bu-SO_3H] [HSO_4^-] catalyst (0.250 g), and the mixture was stirred for 1 hour at room temperature under ultrasonic conditions. After centrifugation, the supernatant was titrated with an aqueous sodium hydroxide solution (0.05 mol/g) using phenolphthalein as an indicator, a total acidity of 0.021 mol/g [31,32]. Upon reuse, the acidity of the [Fe_3O_4@SiO_2-$(Pr)_3$-N-Bu-SO_3H] [HSO_4^-] catalyst was determined to be 0.020 mol/g. The total acidity of other sulfonic acid-functionalized solid acid catalysts was also estimated using a similar acid-base titration method, with the results presented in Table 5.2.

5.5. Results and Discussion

5.5.1. Catalyst characterization

5.5.1.1. Fourier transform infrared spectroscopy (FTIR)

A) [Fe_3O_4@SiO_2-$(Pr)_3$-N-Bu-SO_3H] [HSO_4^-] catalyst

Functional groups present in the catalysts were investigated by FT-IR analysis (Figure 5.1). FT-IR of the samples of [$(EtO)_3(MeO)_6$Si-$(Pr)_3$-N] and [$(EtO)_3(MeO)_6$Si-$(Pr)_3$-N-Bu-SO_3^-] showed bands due to stretching vibration mode of Si-O-Si at 1020-1110 cm^{-1} and bending mode by a band located around 750-800 cm^{-1}. The band between 1090-1300 cm^{-1} was attributed to the -S=O bond, providing a clear indication of its presence within the chemical structure. The C-H stretching vibration in the O-CH_3 group occurs within the spectral range of 2800-2860 cm^{-1}. The band observed at 2700-3100 cm^{-1}

could be attributed to -OH functionality present in -SO_3H group. The intense bands between 580 cm^{-1} and 630 cm^{-1} were assigned to the stretching vibrations of metal-oxygen (Fe-O) bonds in the crystalline lattice of Fe_3O_4. The functional groups present in $[(EtO)_3(MeO)_6Si\text{-}(Pr)_3\text{-}N]$ and $[(EtO)_3(MeO)_6\text{-}(Pr)_3\text{-}N\text{-}Bu\text{-}SO_3^-]$ are similar to those in $[Fe_3O_4@SiO_2\text{-}(Pr)_3\text{-}N\text{-}Bu\text{-}SO_3H]$ $[HSO_4^-]$, indicating successful heterogenization by $Fe_3O_4@SiO_2$. Fresh and used $[Fe_3O_4@SiO_2\text{-}(Pr)_3\text{-}N\text{-}Bu\text{-}SO_3H]$ $[HSO_4^-]$ catalysts showed similar bands in FTIR indicating that structure remained unchanged.

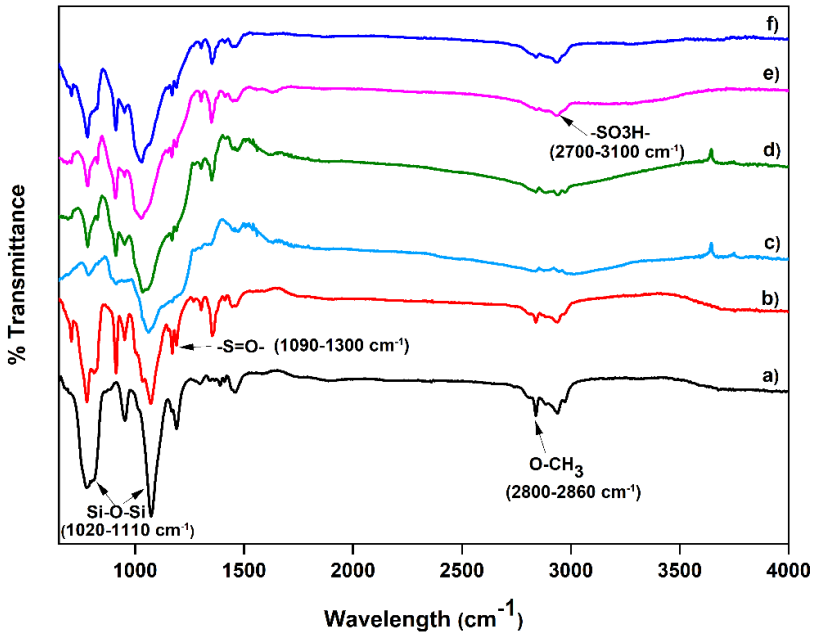

Figure 5.1. FT-IR of a) $[(EtO)_3(MeO)_6Si\text{-}(Pr)_3\text{-}N]$, b) $[(EtO)_3(MeO)_6\text{-}(Pr)_3\text{-}N\text{-}Bu\text{-}SO_3\text{-}]$, c) $[Fe_3O_4@SiO_2]$, d) $[Fe_3O_4@SiO_2\text{-}(Pr)_3\text{-}N\text{-}Bu\text{-}SO_3^-]$ e) fresh $[Fe_3O_4@SiO_2\text{-}(Pr)_3\text{-}N\text{-}Bu\text{-}SO_3H]$ $[HSO_4^-]$ and f) used $[Fe_3O_4@SiO_2\text{-}(Pr)_3\text{-}N\text{-}Bu\text{-}SO_3H]$ $[HSO_4^-]$.

To reveal and confirm the acid sites within $[Fe_3O_4@SiO_2\text{-}(Pr)_3\text{-}N\text{-}Bu\text{-}SO_3H]$ $[HSO_4^-]$, pyridine was adsorbed onto the catalyst surface and the resulting FT-IR spectrum was meticulously analyzed [Figure 5.2]. A distinct band at 1472 cm^{-1} clearly indicated the presence of Lewis acid sites residing on the Fe_3O_4 nanoparticles. Meanwhile, A band at 1542 cm^{-1} confirmed the presence of Brønsted acid sites, attributed to Py-H and HSO4 species. Fresh and used $[Fe_3O_4@SiO_2\text{-}(Pr)_3\text{-}N\text{-}Bu\text{-}SO_3H]$ $[HSO_4^-]$ catalysts showed similar patterns in Py-FTIR indicating that active acid sites remained intact even after the reaction.

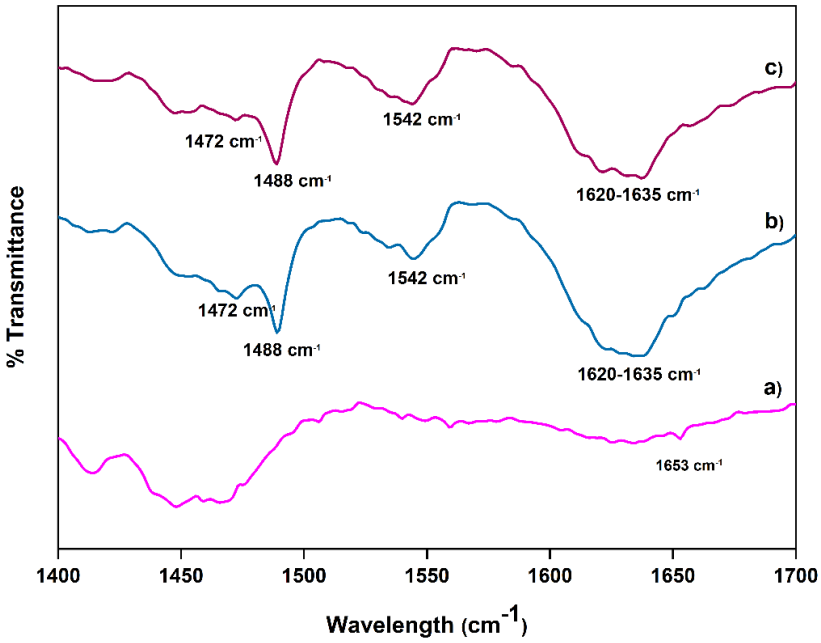

Figure 5.2. Pyridine-IR: a) $[Fe_3O_4@SiO_2\text{-}(Pr)_3\text{-}N\text{-}Bu\text{-}SO_3H]$ $[HSO_4^-]$ before pyridine adsorption, b) fresh $[Fe_3O_4@SiO_2\text{-}(Pr)_3\text{-}N\text{-}Bu\text{-}SO_3H]$ $[HSO_4^-]$ after pyridine adsorption and c) used $[Fe_3O_4@SiO_2\text{-}(Pr)_3\text{-}N\text{-}Bu\text{-}SO_3H]$ $[HSO_4^-]$ after pyridine adsorption.

B) $[SiO_2\text{-}(Pr)_3\text{-}N\text{-}Bu\text{-}SO_3H]$ $[HSO_4^-]$ catalyst

Functional groups present in the catalysts were investigated by FT-IR analysis (Figure 5.3). FT-IR analysis of $[(EtO)_3(MeO)_6Si\text{-}(Pr)_3\text{-}N]$ and $[(EtO)_3(MeO)_6Si\text{-}(Pr)_3\text{-}N\text{-}Bu\text{-}SO_3^-]$ compound showed stretching vibration mode of Si-O-Si at 1020-1110 cm^{-1} and bending mode located around 750-800 cm^{-1}. The peak between 1090-1300 cm^{-1} attributes to the -S=O bond, providing a clear indication of its presence within the chemical structure. The C-H stretching vibration in the $O\text{-}CH_3$ group occurs within the spectral range of 2800-2860 cm^{-1}. The band observed at 2700-3100 cm^{-1} attributes -OH functionality present in $-SO_3H$ group. The functional groups present in $[(EtO)_3(MeO)_6Si\text{-}(Pr)_3\text{-}N]$ and $[(EtO)_3(MeO)_6\text{-}(Pr)_3\text{-}N\text{-}Bu\text{-}SO_3^-]$ are similar to those in $[SiO_2\text{-}(Pr)_3\text{-}N\text{-}Bu\text{-}SO_3H][HSO_4^-]$, indicating successful heterogenization by SiO_2.

To identify and confirm the acid sites within $[SiO_2\text{-}(Pr)_3\text{-}N\text{-}Bu\text{-}SO_3H][HSO_4^-]$, pyridine was adsorbed onto the catalyst surface and the resulting FT-IR spectrum was meticulously analyzed. A distinct band at 1546 cm^{-1} was confirmed the existence of Brønsted acid sites due to Py-H and HSO_4 species (Figure 5.4). Here pyridine IR of used $[SiO_2\text{-}(Pr)_3\text{-}N\text{-}Bu\text{-}SO_3H][HSO_4^-]$ catalyst showed less intense peak at 1546 cm^{-1} which indicates a reduction in the number of acidic sites after the recycling process.

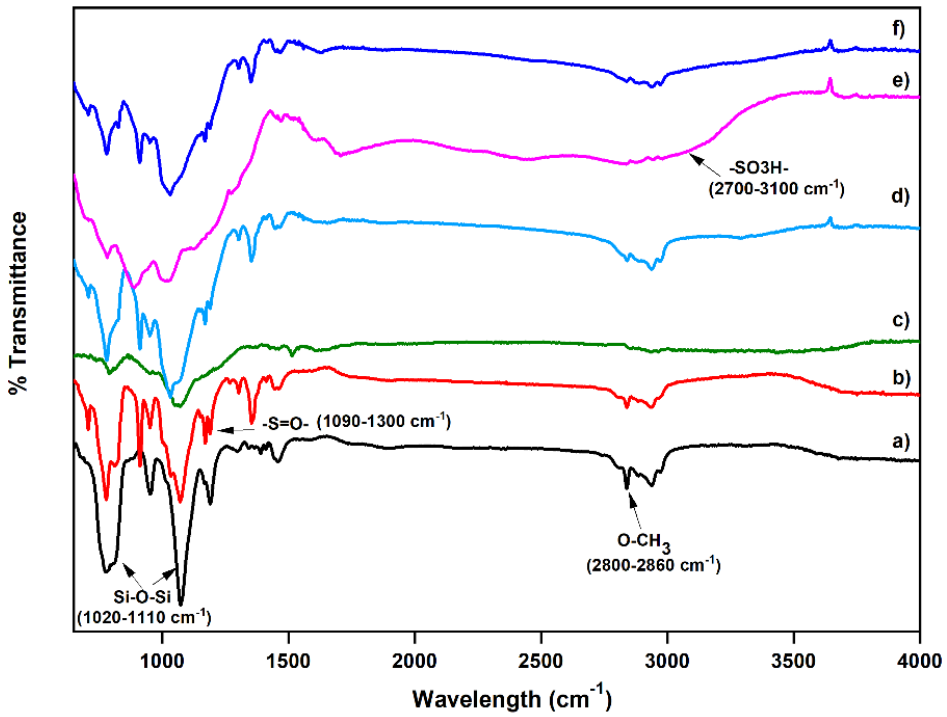

Figure 5.3. FT-IR of a) $[(EtO)_3(MeO)_6Si\text{-}(Pr)_3\text{-}N]$, b) $[(EtO)_3(MeO)_6Si\text{-}(Pr)_3\text{-}N\text{-}Bu\text{-}SO_3^-]$, c) SiO_2, d) $[SiO_2\text{-}(Pr)_3\text{-}N\text{-}Bu\text{-}SO_3^-]$ e) fresh $[SiO_2\text{-}(Pr)_3\text{-}N\text{-}Bu\text{-}SO_3H]$ $[HSO_4^-]$ and f) used $[SiO_2\text{-}(Pr)_3\text{-}N\text{-}Bu\text{-}SO_3H][HSO_4^-]$

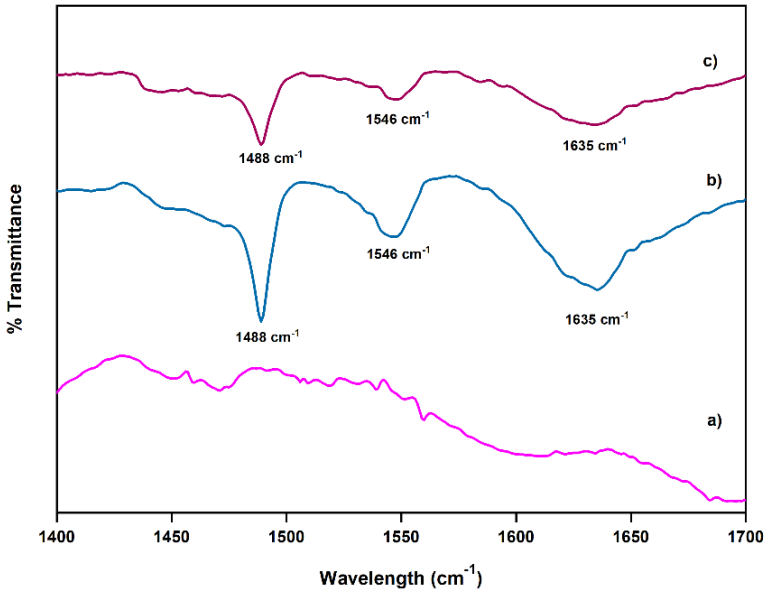

Figure 5.4. Pyridine-IR: a) $[SiO_2\text{-}(Pr)_3\text{-}N\text{-}Bu\text{-}SO_3H][HSO_4^-]$ before pyridine adsorption, b) fresh $[SiO_2\text{-}(Pr)_3\text{-}N\text{-}Bu\text{-}SO_3H][HSO_4^-]$ after pyridine adsorption and c) used $[SiO_2\text{-}(Pr)_3\text{-}N\text{-}Bu\text{-}SO_3H][HSO_4^-]$ after pyridine adsorption.

5.5.1.2. Thermogravimetric analysis (TGA)

A thermogravimetric analysis of fresh and reused $[Fe_3O_4@SiO_2\text{-}(Pr)_3\text{-}N\text{-}Bu\text{-}SO_3H][HSO_4^-]$ catalyst is presented in Figure 5.5.

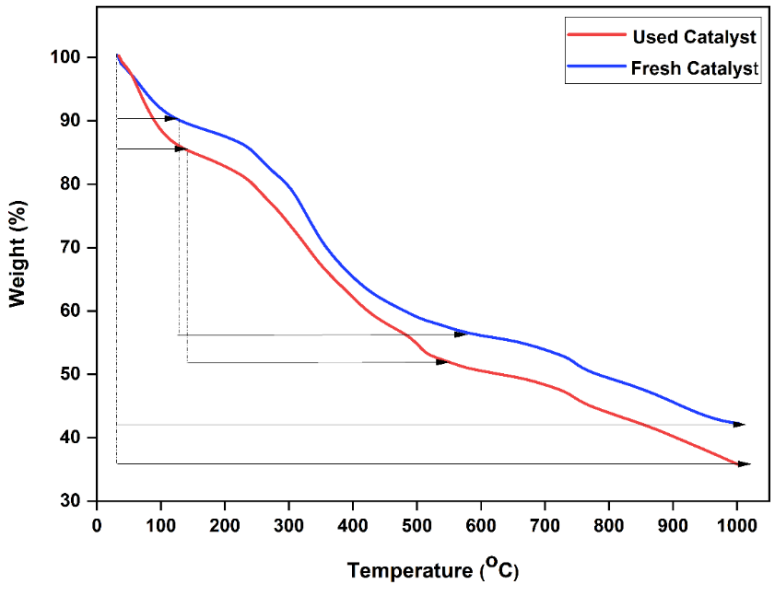

Figure 5.5. Thermogravimetric (TGA) analysis of fresh and used $[Fe_3O_4@SiO_2\text{-}(Pr)_3\text{-}N\text{-}Bu\text{-}SO_3H][HSO_4^-]$ catalyst.

At 100 °C, both fresh and reused catalysts exhibited a weight loss of 10% and 14%, respectively, attributed to desorption of physically adsorbed water. Subsequently, a gradual weight loss was observed up to 500 °C, reaching 43% in the fresh catalyst and 48% in the reused catalyst which could be attributed for decomposition of organic moiety present in the catalysts. It has been reported that organic groups typically desorb in TGA at temperatures above 260 °C [36]. Around 45% weight loss suggesting that, the whole catalyst system contains 45% w/w "$(Pr)_3$-N-Bu-SO_3H" (organic part) and 55% w/w "Fe_3O_4@SiO_2" (Inorganic part). At 1000 °C, both the fresh and reused catalysts exhibited the highest weight loss, reaching 58% and 65%, respectively.

5.5.1.3. X-ray diffraction (XRD)

Silica coated magnetic nanoparticles [Fe_3O_4@SiO_2] and organosilica catalyst [Fe_3O_4@SiO_2-$(Pr)_3$-N-Bu-SO_3H] [HSO_4^-] were characterized by X-ray diffraction technique (Figure 5.6).

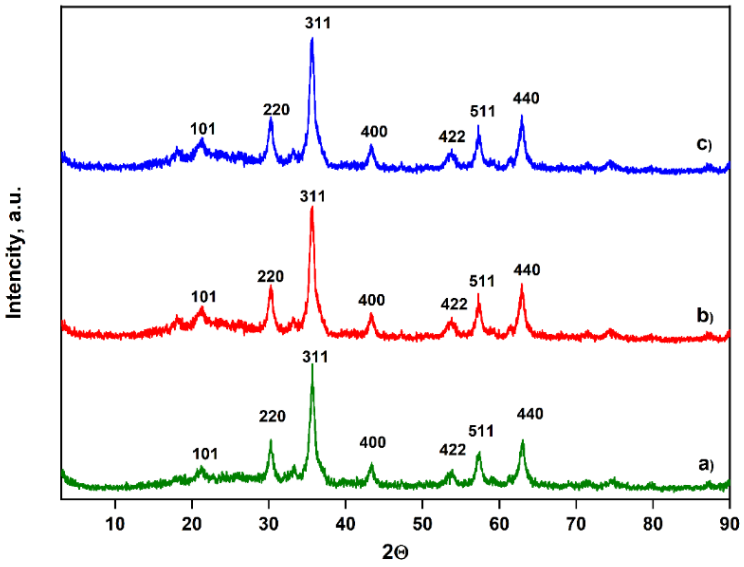

Figure 5.6. X-ray diffraction (XRD) analysis of a) [Fe_3O_4@SiO_2], b) fresh [Fe_3O_4@SiO_2-$(Pr)_3$-N-Bu-SO_3H] [HSO_4^-] and c) used [Fe_3O_4@SiO_2-$(Pr)_3$-N-Bu-SO_3H] [HSO_4^-] catalyst.

The XRD pattern shows a broad band centered at 2θ = 21.26º corresponding to indices (101) that confirmed the presence of silica (SiO_2). The peaks observed at 2θ = 30.19º, 35.60º, 43.47º, 53.87º, 57.28º and 63.01º corresponded to indices (220), (311), (400), (422), (511) and (440) of Fe_3O_4 species present in [Fe_3O_4@SiO_2-$(Pr)_3$-

N-Bu-SO_3H] [HSO_4^-] similar to [Fe_3O_4@SiO_2]. The identical X-ray diffraction pattern was obtained due to common backbone of [Fe_3O_4@SiO_2] particles. The X-ray diffraction pattern validates the successful binding of silica-coated magnetic nanoparticles and the presence of $(Pr)_3$-N-Bu-SO_3H.

5.5.1.4. Field emission scanning electron microscopy (FE-SEM)

The surface morphology and particle size of fresh and reused [Fe_3O_4@SiO_2-$(Pr)_3$-N-Bu-SO_3H] [HSO_4^-] catalyst was determined by FE-SEM analysis (Figure 5.7). The fresh [Fe_3O_4@SiO_2-$(Pr)_3$-N-Bu-SO_3H] [HSO_4^-] catalyst shows spherical particles with average particle size of 26 nm (Figure 5.7c) and used [Fe_3O_4@SiO_2-$(Pr)_3$-N-Bu-SO_3H] [HSO_4^-] catalyst shows particle 28 nm (Figure 5.7f) which indicates that there is no change in morphology of the catalyst after use.

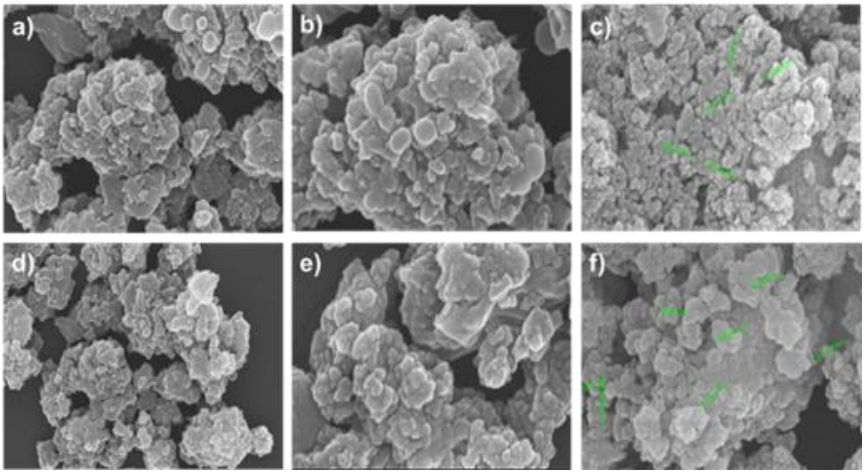

Figure 5.7. FE-SEM images of [Fe_3O_4@SiO_2-$(Pr)_3$-N-Bu-SO_3H] [HSO_4^-] (a, b, c) and used [Fe_3O_4@SiO_2-$(Pr)_3$-N-Bu-SO_3H] [HSO_4^-] (d, e, f).

5.5.1.5. High-resolution transmission electron microscopy (HR-TEM)

An internal morphology and particle size distribution of the synthesized [Fe_3O_4@SiO_2-$(Pr)_3$-N-Bu-SO_3H] [HSO_4^-] catalyst was determined by HR-TEM analysis (Figure 5.8). TEM images of both the fresh and used catalyst samples revealed an almost similar spherical geometry, with an average particle size of 10.69 nm (Figure 5.8c). Notably, the TEM images clearly depicted that the majority of Fe_3O_4 nanoclusters were effectively coated with a thin layer of SiO_2, resulting in a distinctive core/shell structure of Fe_3O_4@SiO_2 nanoparticles (Figure 5.8b). Upon characterization of the used

catalyst through HR-TEM, it was observed that the core-shell [37] structure of Fe_3O_4@SiO_2 remained intact (Figures 5.8e and 5.8f).

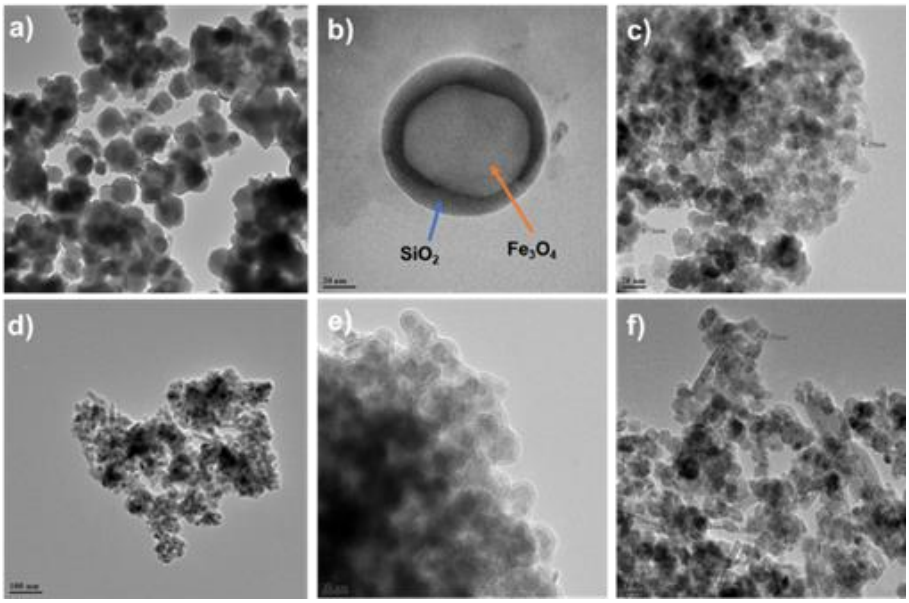

Figure 5.8. HR-TEM images of fresh [Fe_3O_4@SiO_2-$(Pr)_3$-N-Bu-SO_3H] [HSO_4^-] (a, b, c, d) and used [Fe_3O_4@SiO_2-$(Pr)_3$-N-Bu-SO_3H] [HSO_4^-] (e, f).

5.5.2. Characterization of Bigsuaiacol-F product

5.5.2.1. Identification of Bisguaiacol-F products

pp'-Bisguaiacol-F (*pp*'-BGF) was obtained as white coloured needle shaped crystals with melting point as 100 ℃ (Figure 5.9a). ^{1}H NMR (500 MHz, DMSO-*d*6, 0.01% TMS) 3.65 (s, 6H; OCH_3), 3.70 (s, 2H; CH_2), 6.55 (d, 2H; *o*-ArH), 6.65 (dd, 2H; *m*-ArH), 6.75 (d, 2H; *o*-ArH) and 8.75 ppm (s, 2H; *p*-ArOH). 13C NMR (500 MHz, DMSO-*d*6, 0.01% TMS) 40.38, 55.99, 113.22, 115.75, 121.17, 133.12, 144.99 and 147.82. FT-IR bands were observed at $\bar{\upsilon}_{max}$ = 3427 (O–H), 2850-3000 (aliph. C–H), 1606 (C=C), 1509 (-C-C), 1120-1300 (C–O) and 700-900 cm^{-1} (=C–H) (Figure 5.10).

mp'-Bisguaiacol-F (*mp*'-BGF) was obtained as white coloured amorphous powder with melting point as 118 ℃ (Figure 5.9b). ^{1}H NMR (500 MHz, DMSO-*d*6, 0.01%, TMS) 3.34 (s, 2H; CH_2), 3.66 (s, 3H; *m*-OCH_3), 3.71 (s, 3H; *p*-OCH_3), 6.65 (dd, 1H; *m*-ArH), 6.67 (d, 1H, *o*-ArH), 6.76 (dd, 1H; *m*-ArH), 6.74 (d, 1H; *o*-ArH), 6.56 (d, *o*-ArH) and 6.58 ppm (d, 1H; *o*-ArH). 8.78 (s, 1H; *p*-ArOH), 8.67 (s, 1H; *m*-ArOH). ^{13}C NMR (500 MHz, DMSO-*d*6, 0.01% TMS) 40.41, 56.04, 112.74, 113.32, 115.79, 116.41, 121.21, 133.12, 145.04, 147.85 and 146.80. FT-IR showed bands at $\bar{\upsilon}_{max}$ =

3435 (O–H), 2825-3000 (aliph. C–H), 1606 (C=C), 1504 (-C-C), 1104-1300 (C–O) and 700-900 cm^{-1} (=C–H) (Figure 5.10).

op'-Bisguaiacol-F (*op*'-BGF) was obtained as white coloured spherical crystals with melting point as 105 ℃ (Figure 5.9c). ^{1}H NMR (500 MHz, DMSO-*d*6, 0.01%, TMS) 3.75 (s, 3H; *m*-OCH_3), 3.77 (s, 3H; *m*-OCH_3), 3.70 (s, 2H; CH_2), 6.52–6.69 ppm (m, 5H; ArH), 6.77 (d, 1H; *o*-ArH). 8.64 (s, 1H; *p*-ArOH), 8.47 (s, 1H; *o*-ArOH). ^{13}C NMR (500 MHz, DMSO-*d*6, 0.01% TMS) 40.61, 56.2, 110.05, 113.54, 115.67, 119.02, 121.30, 122.57, 128.56, 132.49, 144.17, 144.96, 147.73 and 147.84. FT-IR of the product showed bands at $\bar{\upsilon}_{max}$ = 3444 (O–H), 2813-3000 (aliph. C–H), 1611 (C=C), 1513 (-C-C), 1100-1300 (C–O) and 700-900 cm^{-1} (=C–H) (Figure 5.10).

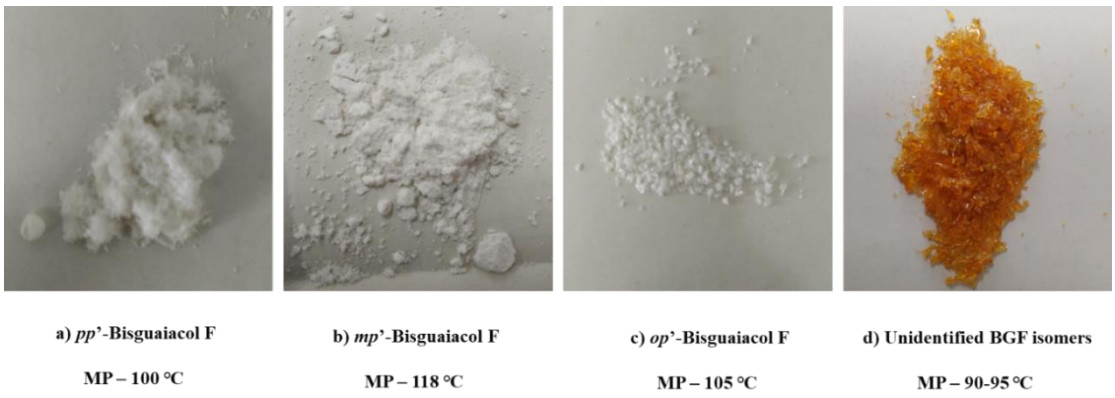

Figure 5.9. Images of isolated regioisomers of Bisguaiacol-F

5.5.2.2. Fourier transform infrared spectroscopy (FTIR) of synthesized Bisguaiacol derivatives

Functional groups present in Bisguaiacol derivatives like *pp'*-BGF, *mp'*-BGF, *op'*-BGF, BGE, BGP and BGB were observed by using FTIR analysis (Figure 5.10). A broad band for aromatic O-H bond stretching was observed at 3300-3700 cm^{-1}. The bands observed at 2825-3042, 1600-1680, 1440-1550 and 1100-1300 cm^{-1} were attributed stretching frequency for C-H, C=C, C-C, and C-O, respectively (Figure 5.10). In aromatic hydrocarbon =C-H bond bending is observed around 700-900 cm^{-1}.

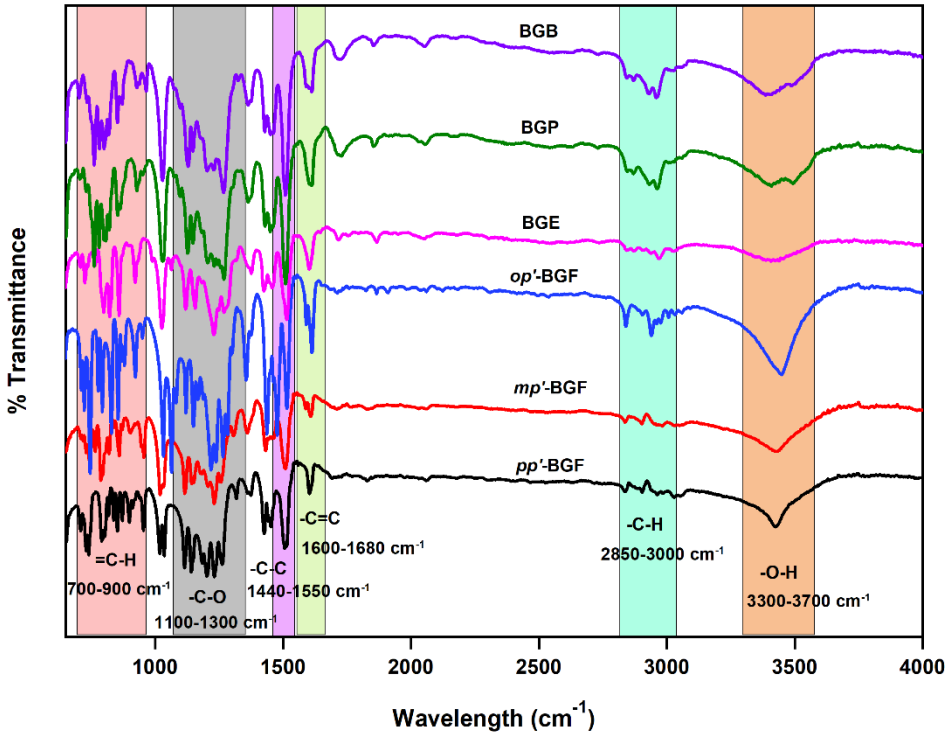

Figure 5.10. FTIR of synthesized Bisguaiacol derivatives

5.5.3. Catalyst screening for condensation of guaiacol with aq. formaldehyde

Condensation of guaiacol with aq. formaldehyde is promoted by an acid catalyst to produce several regioisomers of BGF. Consequently, several acid catalysts were examined under specific reaction conditions and compared their catalytic activity with our novel heterogeneous catalyst [Fe_3O_4@SiO_2-$(Pr)_3$-N-Bu-SO_3H] [HSO_4^-] for the condensation of guaiacol with aqueous formaldehyde (Table 5.1). Initially, homogeneous H_2SO_4 (10 mol%) was used for this model condensation reaction which showed 96% conversion of guaiacol and complete conversion of formaldehyde with regioisomers selectivity of 37%, 14% and 7% to *pp*'-BGF, *mp*'-BGF and *op*'-BGF, respectively (Entry 1, Table 5.1). The Amberlyst-15 offered 79% conversion of guaiacol and 85% conversion of formaldehyde with 62%, 18% and 5% selectivity to *pp*'-BGF, *mp*'-BGF and *op*'-BGF, respectively (Entry 2, Table 5.1). Further, condensation reaction was performed in presence of Amberlyte IR-120 resin, that offered 71% conversion of guaiacol and 92% conversion of formaldehyde with regioisomer's selectivity of 56%, 16% and 6% to *pp*'-BGF, *mp*'-BGF and *op*'-BGF, respectively (Entry 3, Table 5.1). Dowex-50WX8 resin showed very less conversion of guaiacol (21%) and conversion of formaldehyde (63%) with regioisomer's

selectivity of 60%, 18% and 5% to *pp*'-BGF, *mp*'-BGF and *op*'-BGF, respectively (Entry 4, Table 5.1). Polysulphonic acid such as *p*-toluene sulphonic acid paraformaldehyde (*p*TSA-PFD) [34] catalyst was prepared according to procedure reported in the literature and it was also tested for this model condensation reaction which offered 64% conversion of guaiacol and 83% conversion of formaldehyde with regioisomer's selectivity of 55%, 16% and 6% to *pp*'-BGF, *mp*'-BGF and *op*'-BGF, respectively (Entry 5, Table 5.1) A heterogeneous Lewis-Brønsted acid catalyst such as Sn-Mont [38] was also evaluated for the synthesis of Bisguaiacol-F but it gave moderate conversion of guaiacol as well as formaldehyde with regioisomer's selectivity of 53%, 16% and 5% to *pp*'-BGF, *mp*'-BGF and *op*'-BGF, respectively (Entry 6, Table 5.1). Our previously reported ionic solid acid ([SO_3H-INA][Cl]) [33] was also used for condensation of guaiacol with formaldehyde which gave 80% conversion of guaiacol and 95% conversion of formaldehyde with regioisomer's selectivity of 59%, 13% and 4% to *pp*'-BGF, *mp*'-BGF and *op*'-BGF, respectively (Entry 7, Table 5.1). Another of our previously reported heterogeneous silica supported isonicotinic acid catalyst [SO_3H-INA@SiO_2] [Cl] [33] gave 48% conversion of guaiacol and 52% conversion of formaldehyde with regioisomer's selectivity of 60%, 13% and 5% to *pp*'-BGF, *mp*'-BGF and *op*'-BGF, respectively (Entry 8, Table 5.1). Sulphonated silica catalyst (SO_4^{2-}/SiO_2) offered 57% conversion of guaiacol and 69% conversion of formaldehyde with regioisomer's selectivity of 59%, 15% and 9% to *pp*'-BGF, *mp*'-BGF and *op*'-BGF, respectively (Entry 9, Table 5.1). The use of sulphonic acid functionalized SBA-15 catalyst showed 51% conversion of guaiacol and 58% conversion of formaldehyde with regioisomer's selectivity of 58%, 14% and 6% to *pp*'-BGF, *mp*'-BGF and *op*'-BGF, respectively (Entry 10, Table 5.1). The sulphonated ionic liquid [$(Et)_3$-N-Bu-SO_3H] [HSO_4^-] [35] was prepared using a method described in the literature. and explored for this reaction which gave 90% conversion of guaiacol and 94% conversion of formaldehyde with regioisomer's selectivity 61%, 15% and 5% to *pp*'-BGF, *mp*'-BGF and *op*'-BGF, respectively (Entry 11, Table 5.1). Our newly designed heterogeneous [SiO_2-$(Pr)_3$-N-Bu-SO_3H][HSO_4^-] catalyst offered highest conversion of guaiacol (99%) and formaldehyde (100%) with regioisomer's selectivity of 62%, 15% and 6% to *pp*'-BGF, *mp*'-BGF and *op*'-BGF, respectively (Entry 12, Table 5.1). Magnetically separable heterogeneous catalyst [Fe_3O_4@SiO_2-$(Pr)_3$-N-Bu-SO_3H] [HSO_4^-] showed similar activity to that of [SiO_2-$(Pr)_3$-N-Bu-SO_3H] [HSO_4^-] (Entry 13, Table 5.1). The use of the magnetically separable catalyst [Fe_3O_4@SiO_2-$(Pr)_3$-N-Bu-SO_3H] [HSO_4^-] offered distinct advantages over the silica-based catalyst [SiO_2-$(Pr)_3$-N-Bu-SO_3H] [HSO_4^-] due to its magnetic properties, the catalyst can be

effortlessly separated from the reaction mixture using an external magnet. In contrast, the silica catalyst requires filtration for separation, resulting in handling loss.

Table 5.1. Catalyst screening for condensation of guaiacol with aqueous formaldehyde

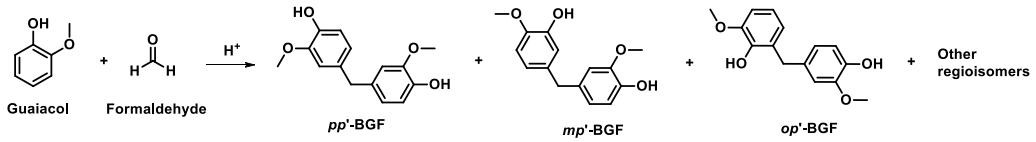

Sr. No.	Catalyst	Conversion [%][b]		Selectivity to BGF regioisomers [%][c]			
		Guaiacol	HCHO	*pp*'	*mp*'	*op*'	Unidentified isomer
1	H_2SO_4[a]	96	100	37	14	07	42
2	Amberlyst-15	79	85	62	18	05	15
3	Amerlyte IR-120	71	92	56	16	06	22
4	Dowex-50WX8 resin	21	63	60	18	05	17
5	*p*-TSA-PFD	64	83	55	16	06	23
6	Sn-Mont	30	23	53	16	05	26
7	[SO_3H-INA][Cl]	80	95	59	13	04	24
8	[SO_3H-INA@SiO_2] [Cl]	48	52	60	13	05	22
9	SO_4^{2-}/SiO_2	57	69	59	15	05	21
10	SO_3H@SBA-15	51	58	58	14	06	22
11	[$(Et)_3$-N-Bu-SO_3H] [HSO_4^-]	99	100	60	15	05	20
12	[SiO_2-$(Pr)_3$-N-Bu-SO_3H] [HSO_4^-]	98	100	62	15	06	17
13	[Fe_3O_4@SiO_2-$(Pr)_3$-N-Bu-SO_3H] [HSO_4^-]	99	100	62	15	06	17

Reaction conditions: Guaiacol (2 g, 0.016 mol), 37% aq. formaldehyde (1.2 g, 0.016), (Acetonitrile, 1 mL), solid acid catalyst (0.3 g, 15 w/w% of guaiacol), 90 °C, 6h. [a]10 mol% of H_2SO_4 was used. [b]Conversion of Guaiacol and formaldehyde was determined by using GC. [c]Selectivity of products was determined by HPLC.

The main challenge in this reaction was to minimize the excess use of guaiacol and to attain complete conversion of both the starting materials. Astonishingly, our catalyst system was able to achieve this objective and avoided tedious separation of

unconsumed guaiacol. The superior catalytic activity of our novel magnetically separable heterogeneous catalyst in terms of starting material conversion and product distribution could be attributed for the easy access of acid sites as $–SO_3H$ group is attached to a long butyl chain. This can be evidenced by comparing it's activity with the sulphonated ionic liquid $[(Et)_3\text{-N-Bu-}SO_3H][HSO_4^-]$ (Entry 11, Table 5.1). For every catalyst tested, along with *pp*', *mp*' and *op*'-BGF an unidentified BGF regioisomer was also noticed. The unidentified regioisomer's molecular formula was confirmed by LCMS (See 5.8.2), however we were not able to recognize its structure because of complex NMR. Due to very low Rf difference, it was become challenging task to isolate the purified sample of unidentified regioisomer. However, it is delighting to know that mixture of all the BGF regioisomers can be processed as it is meant for the production of polymers [27,28].

Turn over number (TON) and turn over frequency (TOF) of catalysts

Turn over number of heterogeneous catalysts can be calculated by using following equation,

Turn over number (TON) = (Number of mols of reactant consumed/ number of moles of active sites in the catalyst)

And

Turn over frequency (TOF) of heterogeneous catalysts can be calculated by using following equation,

Turn over frequency (TOF) = (Turn over number/ time)

For our catalysts $[Fe_3O_4@SiO_2(Pr)_3\text{-N-Bu-}SO_3H]$ $[HSO_4^-]$, the conversion of guaiacol after 1h was 32%. Initial moles of guaiacols used in the reaction is 0.016 moles.

Moles of guaiacols consumed = 0.016 moles x (32/100) = 0.00512 moles

Amount of catalysts used in the reaction was 0.3 g.

Acidity of this catalyst is 0.021 moles/g, which means 1 g of catalyst contains 0.021 moles of acid sites.

Moles of active site in the catalyst = [0.3 g x 0.021 moles]/ 1g = 0.0063 moles

Turn over number (TON) = (Number of mols of reactant consumed/ number of moles of active sites in the catalyst) = 0.00512 moles/ 0.0063 moles = 0.812

Turn over frequency (TOF) = (Turn over number/ time) = 0.812/ 60 min

$= 0.0135\ min^{-1}$

The turn over number (TON) and turn over frequency (TOF) of other sulfonic acid-functionalized solid acid catalysts was also calculated using a similar equation, the results presented in Table 5.2.

Table 5.2. Catalyst acidity, turn over number (TON) and turn over frequency (TOF)

Sr. No.	Catalyst	Acidity (mol/g)	Conversion of Guaiacol [%]	TON	TOF [min^{-1}]
1	H_2SO_4 [a]	--	--	--	--
2	Amberlyst-15	0.019	39	1.54	0.0257
3	Amerlyte IR-120	0.016	40	1.33	0.022
4	Dowex-50WX8 resin	0.018	41	1.36	0.022
5	*p*-TSA-PFD	--	--	--	--
6	Sn-Mont	--	--	--	--
7	[SO_3H-INA][Cl]	0.046	45	1.5	0.025
8	[SO_3HINA@SiO_2][Cl]	0.031	41	1.36	0.022
9	SO_4^{2-} /SiO_2	0.013	21	0.7	0.0116
10	SO_3H@SBA-15	0.017	24	0.8	0.0133
11	$(Et)_3$-N-BuSO_3H][HSO_4^-]	--	--	--	--
12	[SiO_2-$(Pr)_3$-N-BuSO_3H] [HSO_4^-]	0.020	32	0.853	0.0142
13	[Fe_3O_4@$SiO_2(Pr)_3$-N-Bu-SO_3H] [HSO_4^-]	0.021	32	0.812	0.0135
14	Used [Fe_3O_4@$SiO_2(Pr)_3$-N-Bu-SO_3H] [HSO_4^-]	0.021	31	0.787	0.0131
For each catalysts conversion measured after 60 min					

5.5.4. Solvent screening for condensation of guaiacol with aq. formaldehyde

Several randomly selected solvents were screened for condensation reaction of guaiacol and aq. formaldehyde with optimized reaction conditions. Initially, methanol was used for condensation reaction but, lower conversion of guaiacol (51%) was noticed. It is well known that in hydroxy methylation reaction between guaiacol and formaldehyde when methanol used as solvent, it resists guaiacol to convert into further products due to competition between methanol and formaldehyde on the active sites (Entry 1, Table 5.3) [26]. The same thing was also observed with ethanol, there was also very less conversion (44%) of guaiacol (Entry 2, Table 5.3). While in presence of 1,4-dioxane 90% conversion of guaiacol and 50% conversion of formaldehyde were noticed (Entry 3, Table 5.3). In presence of polar aprotic solvents

such as acetonitrile, highest conversion of guaiacol (99%) with complete conversion of formaldehyde was observed (Entry 4, Table 5.3). The use of water lowered the conversion of guaiacol and formaldehyde this is due to lower solubility of guaiacol (Entry 5, Table 5.3). Use of isopropyl alcohol gave only moderate conversion of guaiacol and formaldehyde (Entry 6, Table 5.3). Isopropyl alcohol do not/less involve in the reaction with formaldehyde as product of this reaction would be sterically hindered (high energy molecule) due to branched structure of isopropyl alcohol. As a result of this reaction of guaiacol with formaldehyde in isopropyl alcohol gave better yield as compared to the reaction in methanol and ethanol.

Table 5.3. Solvent screening for condensation of guaiacol with aq. formaldehyde

Sr. No.	Solvent	Conversion [%][a]		Selectivity of BGF regioisomers [b] [%]			
		Guaiacol	HCHO	*pp'*	*mp'*	*op'*	Unidentified isomer
1	Methanol	51	96	52	21	13	14
2	Ethanol	44	77	52	19	09	20
3	1,4-dioxane	90	50	45	10	07	38
4	Acetonitrile	99	100	62	15	06	17
5	Water	38	40	42	08	06	44
6	Isopropyl alcohol	80	81	47	14	08	31

Reaction conditions: Guaiacol (2 g, 0.016 mol), 37% aq. formaldehyde (1.2 g, 0.016), solvent (1 mL), $[Fe_3O_4@SiO_2\text{-}(Pr)_3\text{-}N\text{-}Bu\text{-}SO_3H]$ $[HSO_4^-]$ (0.3 g, 15 w/w% of guaiacol), 90 °C, 6h. [a] Conversion of Guaiacol and 37% aq. formaldehyde was determined by using GC, [b]selectivity of products was determined by HPLC.

5.5.5. Reaction optimization

5.5.5.1. Effect of reaction temperature

The conversion of guaiacol and formaldehyde steadily escalates as the temperature rises from 40 to 90 °C (Figure 5.11). At 40 °C guaiacol and formaldehyde showed lowest conversions. When reaction was performed at 60 °C conversion of both the reactants improved and reached up to 70% of guaiacol and 79% of formaldehyde. At 80 °C conversion of guaiacol reached up to 85% and that of formaldehyde reached up to 90%. At 90 °C, guaiacol demonstrated a remarkable 99% conversion, while formaldehyde conversion reached up to 100%. Elevating the temperature further to 100 °C, conversion and selectivity patterns were unchanged. Notably, temperature above 100 °C exerted no discernible influence on product distribution. In presence

our catalyst at 90 °C reaction reached to equilibrium thus, this temperature emerged as an optimal reaction temperature for the condensation of guaiacol and formaldehyde.

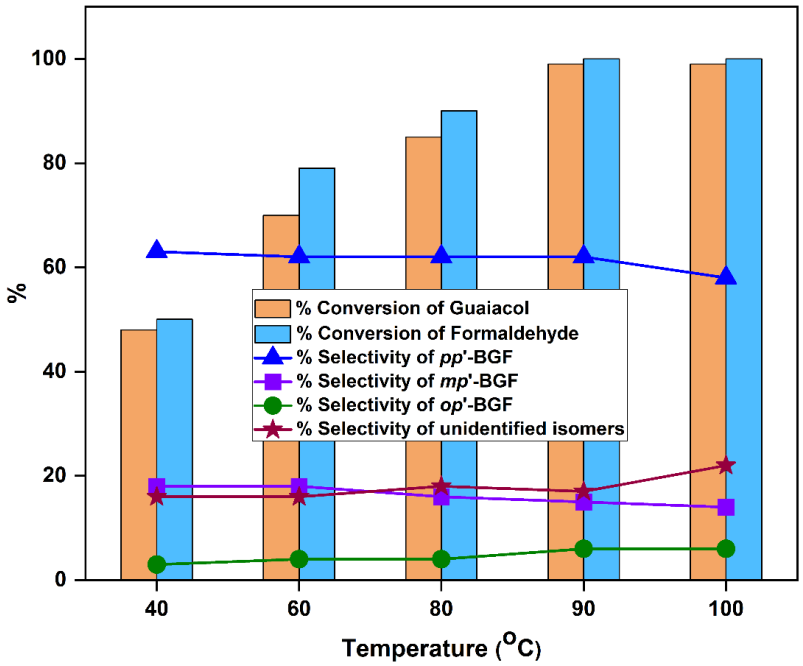

Figure 5.11. Effect of reaction temperature. Reaction conditions: Guaiacol (2 g, 0.016 mol), 37% aq. formaldehyde (1.2 g, 0.016 mol), $[Fe_3O_4@SiO_2\text{-}(Pr)_3\text{-}N\text{-}Bu\text{-}SO_3H][HSO_4^-]$ (0.3 g), Acetonitrile (1 mL), 40-90 °C, 6h.

5.5.5.2. Effect of reaction time

To investigate the reaction's behaviour over time, we conducted the experiment for a duration of 7 hours, with samples withdrawn at hourly intervals. As the reaction time progressed, the conversion of guaiacol and formaldehyde exhibited a steady increase. However, after the 6th hour, no further enhancements in the conversion of either reactant or in the selectivity pattern of products were noticed which suggests that reaction reached to equilibrium after 6th hour (Figure 5.12).

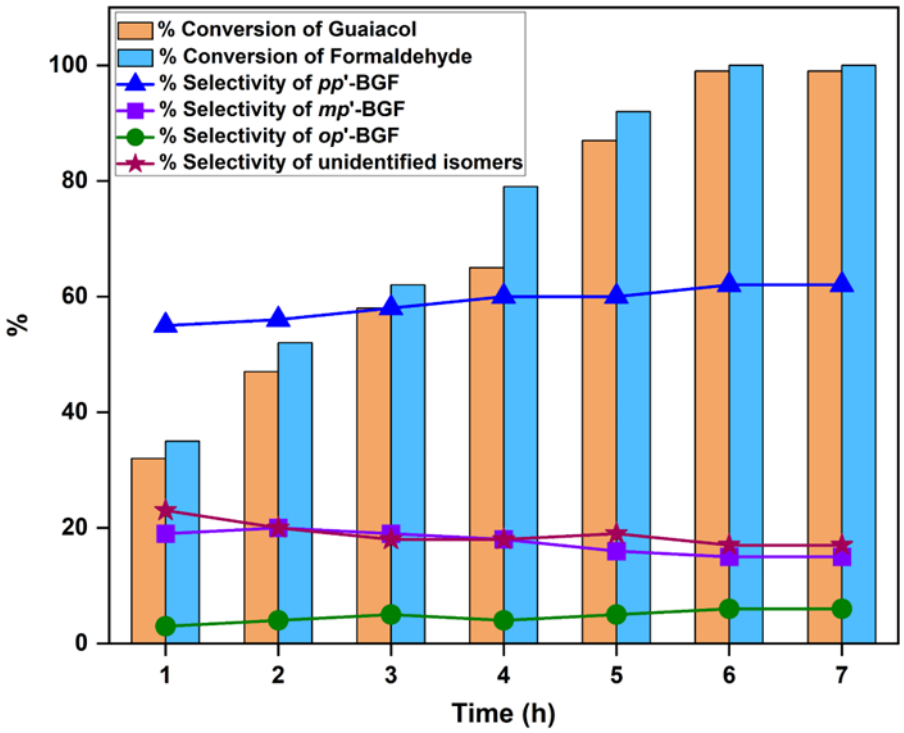

Figure 5.12. Effect of reaction time. Reaction conditions: Guaiacol (2 g, 0.016 mol), 37% aq. formaldehyde (1.2 g, 0.016 mol), [Fe_3O_4@SiO_2-$(Pr)_3$-N-Bu-SO_3H] [HSO_4^-] (0.3 g), Acetonitrile (1 mL), 90 ^oC.

5.5.5.3. Effect of molar ratio of guaiacol to aq. formaldehyde

The reaction was executed using the stoichiometrically required molar ratio of guaiacol to aqueous formaldehyde, set at 1:0.5 respectively. Surprisingly, while formaldehyde achieved complete conversion, guaiacol only attained a 44% conversion. Consequently, the molar ratio of guaiacol to aqueous formaldehyde varied between 1:0.5 and 1:2 for the synthesis of Bisguaiacol-F. Remarkably, it was observed that a guaiacol to aqueous formaldehyde ratio of 1:1 resulted as optimum molar ratio, yielding the highest conversion of guaiacol (99%) and formaldehyde (100%) and also enhancing productivity (Figure 5.13). As the guaiacol to aqueous formaldehyde molar ratio increased to 1:2, a decrease in conversion rates was observed, with only 54% conversion of guaiacol and 49% conversion of formaldehyde achieved. Thus, the 1:1 molar ratio of guaiacol to aqueous formaldehyde stands out as the optimal condition for the reaction. As formaldehyde used in this reaction already have 63% *w/w* water, thus use of more aqueous formaldehyde would leads to

increase water content in the reaction which may hamper the overall reactivity of reactants by reducing solubility of guaiacol. This was evidenced, when reaction was performed in water as a solvent (Entry 5, Table 5.3).

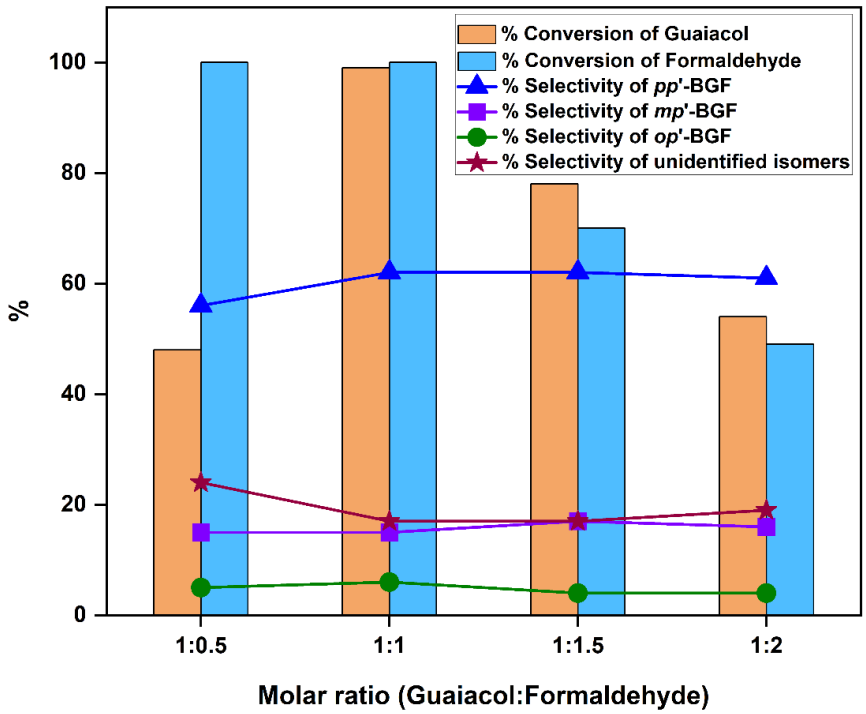

Figure 5.13. Effect of reactant molar ratio. Reaction condition: Guaiacol (1 mole equivalent), 37% aq. formaldehyde (0.5-2 mole equivalent), $[Fe_3O_4@SiO_2\text{-}(Pr)_3\text{-}N\text{-}Bu\text{-}SO_3H]$ $[HSO_4^-]$ (0.3 g), Acetonitrile (1 mL), 90 ^oC, 6h.

5.5.5.4. Effect of catalyst loading

To explore the appropriate quantity of catalyst required for the condensation reaction of guaiacol with aqueous formaldehyde, the catalyst amount was varied between 5% and 20% *w*/*w* with respect to guaiacol. Starting with a 5% *w*/*w* catalyst loading, guaiacol reached to a 40% conversion, while formaldehyde conversion reached 47%. Upon increasing the catalyst amount to 10% *w*/*w*, conversion rates were significantly improved. Further increasing the catalyst loading to 15% *w*/*w* resulted in complete conversion of formaldehyde and 99% conversion of guaiacol. However, employing excess catalyst (20% *w*/*w*) did not seen any improvement in conversion of guaiacol

or selectivity pattern of Bisguaiacol-F (Figure 5.14). Therefore, 15% *w/w* catalyst loading considered as optimized and used same for further experiments.

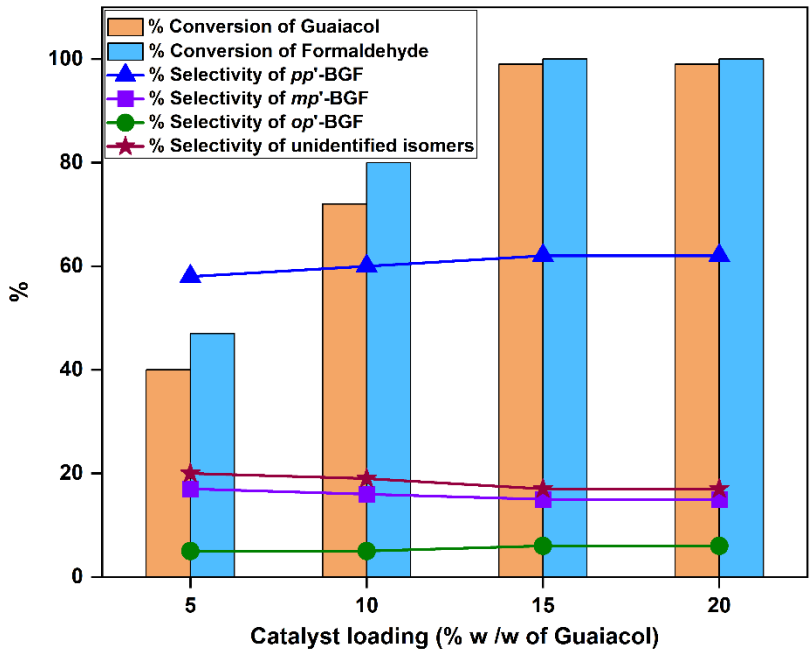

Figure 5.14. Effect of catalyst loading. Reaction condition: Guaiacol (2 g, 0.016 mol), 37% aq. formaldehyde (1.2 g, 0.016 mol), $[Fe_3O_4@SiO_2\text{-}(Pr)_3\text{-}N\text{-}Bu\text{-}SO_3H]$ $[HSO_4^-]$ (5-20% w/w of Guaiacol), Acetonitrile (1 mL), 90 ^oC, 6h.

5.5.6. Catalyst recycle study

To study the stability and reproducibility of a synthesized magnetically separable catalyst, we have conducted a catalyst recycle study (Figure 5.15). After the first run, catalyst was separated from the reaction mixture by applying an external magnetic field to the reaction vessel while allowing the decantation of the reaction mixture. The catalyst was then washed with ethyl acetate and dried using a rotary evaporator. In the same flask, fresh reactants were added, and the reaction was repeated. Due to the magnetically separable nature of the catalyst, no physical loss of catalyst occurred. Remarkably, over six consecutive runs, the catalyst maintained the consistent activity levels, demonstrating its robustness and reliability. After 6^{th} run, the catalyst exhibited slight reduced in conversion of guaiacol and formaldehyde that could be due to minor blocking of acidic sites.

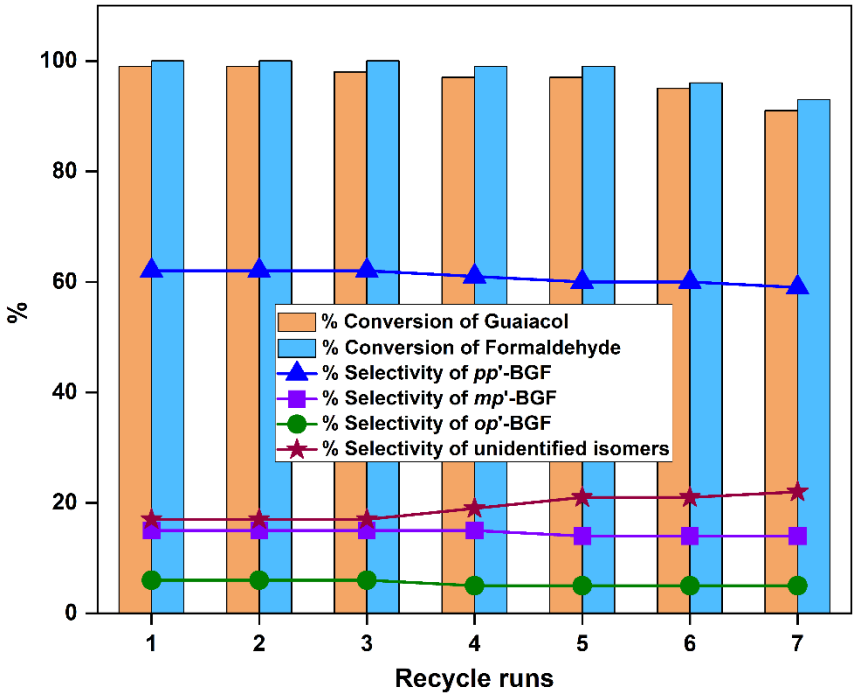

Figure 5.15. Catalyst recycle study. Reaction condition: Guaiacol (2 g, 0.016 mol), 37% aq. formaldehyde (1.2 g, 0.016 mol), $[Fe_3O_4@SiO_2\text{-}(Pr)_3\text{-}N\text{-}Bu\text{-}SO_3H]$ $[HSO_4^-]$ (0.3 g), Acetonitrile (1 mL), temperature, 90 ^oC, reaction time, 6h.

5.5.7. Substrate scope

After successful synthesis of Bisguaiacol-F by condensation reaction of guaiacol with aqueous formaldehyde, the scope of this protocol was explored for further synthesis of couple of Bisguaiacol derivatives. Various aldehydes, such as acetaldehyde, n-propionaldehyde and n-butyraldehyde were employed in the condensation reaction with guaiacol. Guaiacol condensed with acetaldehyde in presence of $[Fe_3O_4@SiO_2\text{-}(Pr)_3\text{-}N\text{-}Bu\text{-}SO_3H]$ $[HSO_4^-]$ catalyst offered 85% conversion of guaiacol with 98% selectivity of *pp*'-Bisguaiacol-E (Entry 1, Table 5.4) with minor amount of unidentified products. The condensation reaction of guaiacol with n-propionaldehyde showed 65% conversion of guaiacol and 100% selectivity of *pp*'-Bisguaiacol-P (Entry 2, Table 5.4). Astonishingly, we didn't notice the formation of other regioisomer's of Bisguaicol-P (Figure 5.18). Condensation of guaiacol with n-butyraldehyde gave bit lower conversion for guaiacol (78%) and lower selectivity (73%) towards Bisguaiacol-B (Entry 3. Table 5.4). After reaction condensation crude products were analyzed by HPLC (5.8.1) followed by purification by column chromatography and identification by

NMR (5.8.3). As anticipated, this catalyst shows remarkable activity and found successful for the synthesis of Bisguaiacol derivatives in descent yields.

Table 5.4. Substrate screening for Bisguaiacol derivatives

Sr. No.	Substrate	Product	Guaiacol conversion [%]	Selectivity [%]
1	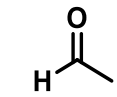 Acetaldehyde	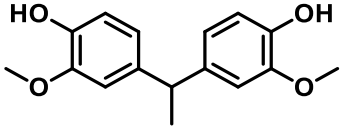 Bisguaiacol-E	85	98
2	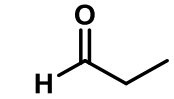 Propionaldehyde	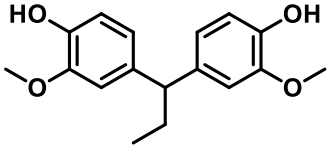 Bisguaiacol-P	65	100
3	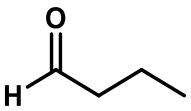 Butyraldehyde	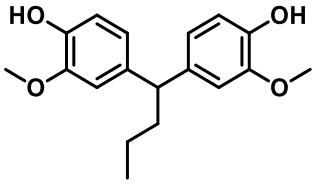 Bisguaiacol-B	78	73

Reaction conditions: Guaiacol (2 g, 0.016 mol), aldehyde (0.016 mol), (Acetonitrile, 1 mL), $[Fe_3O_4@SiO_2\text{-}(Pr)_3\text{-}N\text{-}Bu\text{-}SO_3H]$ $[HSO_4^-]$ (0.3g, 15 w/w% of guaiacol), 90 °C, 6h. Conversion of Guaiacol and selectivity of products was determined by HPLC.

5.6. Reaction Mechanism

A mechanistic scheme for formation of different isomers of Bisguaiacol-F is presented below. In the process of Bisguaiacol-F formation, two molecules of guaiacol are reacted with the one molecules of formaldehyde. The –OH and $–OCH_3$ groups present on guaiacol are electron donating groups, both these groups are positioned as ortho to each other, thus all remaining four carbons are electron rich centres due to delocalisation of electrons from –OH and $–OCH_3$ groups.

In the mechanistic flow of the *p,p'*-Bisguaiacol-F, guaiacol resonates by delocalisation of electrons from –OH group to create electron rich centre at para position corresponds to –OH group. Formaldehyde protonates in presence of acid to form oxonium ion which has electrophilic carbon attached to oxygen atom. The electron

rich guaiacol with its nucleophilic centre attacks on electron deficient centre of formaldehyde to *p*-hydroxymethylguaiacol. Then *p*-hydroxymethylguaiacol protonates with the acid to form electrophilic benzylic species. Then electron rich second molecule of guaiacol attacks on electrophilic benzylic species followed by aromatisation to form *p,p'*-Bisguaiacol-F (Figure 5.16)

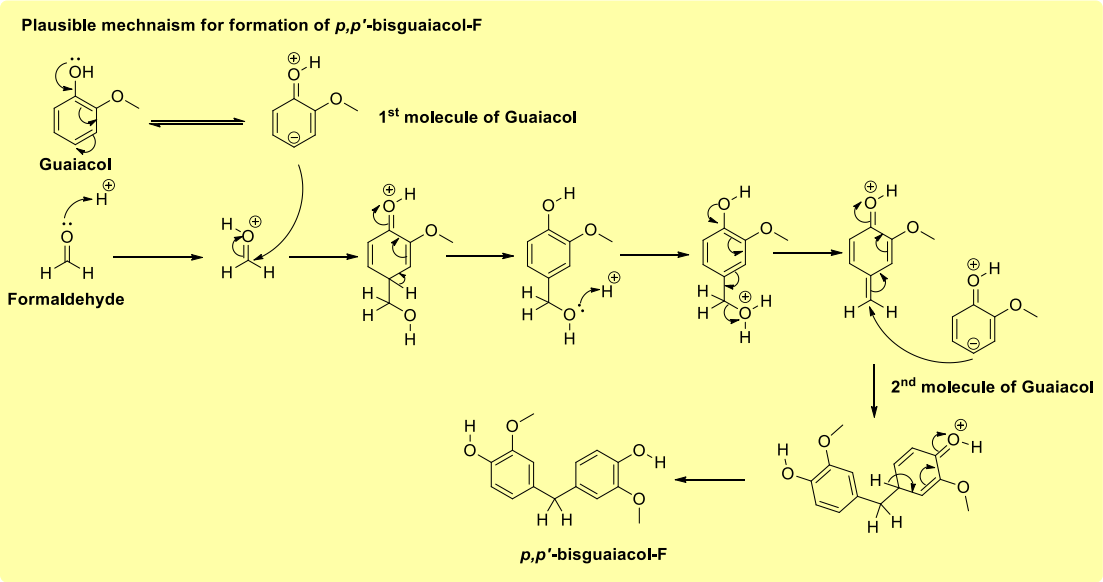

Figure 5.16. Plausible reaction mechanism for synthesis of pp'-Bisguaiacol-F.

In the mechanistic flow of the m,*p'*-Bisguaiacol-F, formation of *p*-hydroxymethylguaiacol is similar to discussed above. Then *p*-hydroxymethylguaiacol protonates with the acid to form electrophilic benzylic species. Then second molecules of guaiacol resonates by delocalisation of electrons from $–OCH_3$ group to create electron rich centre at para position corresponds to $–OCH_3$ group. Then electron rich second molecule of guaiacol attacks on electrophilic benzylic species followed by aromatisation to form m,*p'*-Bisguaiacol-F (Figure 5.17).

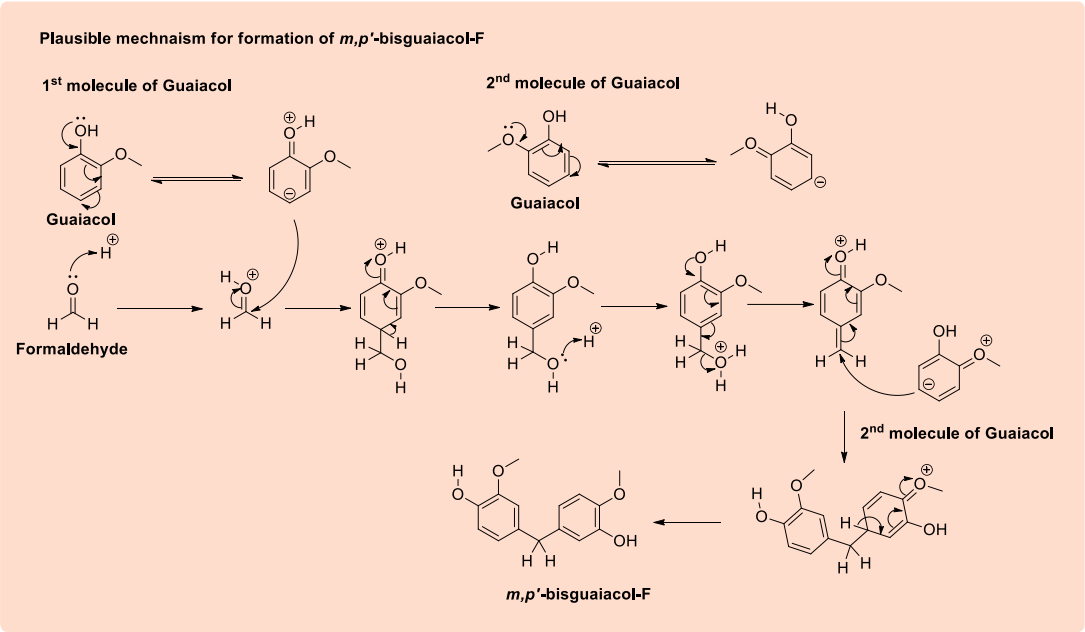

Figure 5.17. Plausible reaction mechanism for synthesis of mp'-Bisguaiacol-F.

In the mechanistic flow of the o,*p'*-Bisguaiacol-F, formation of *p*-hydroxymethylguaiacol is similar to discussed above. Then *p*-hydroxymethylguaiacol protonates with the acid to form electrophilic benzylic species. Then second molecules of guaiacol resonates by delocalisation of electrons from –OH group to create electron rich centre at ortho position corresponds to –OH group. Then electron rich second molecule of guaiacol attacks on electrophilic benzylic species followed by aromatisation to form o,*p'*-Bisguaiacol-F (Figure 5.18)

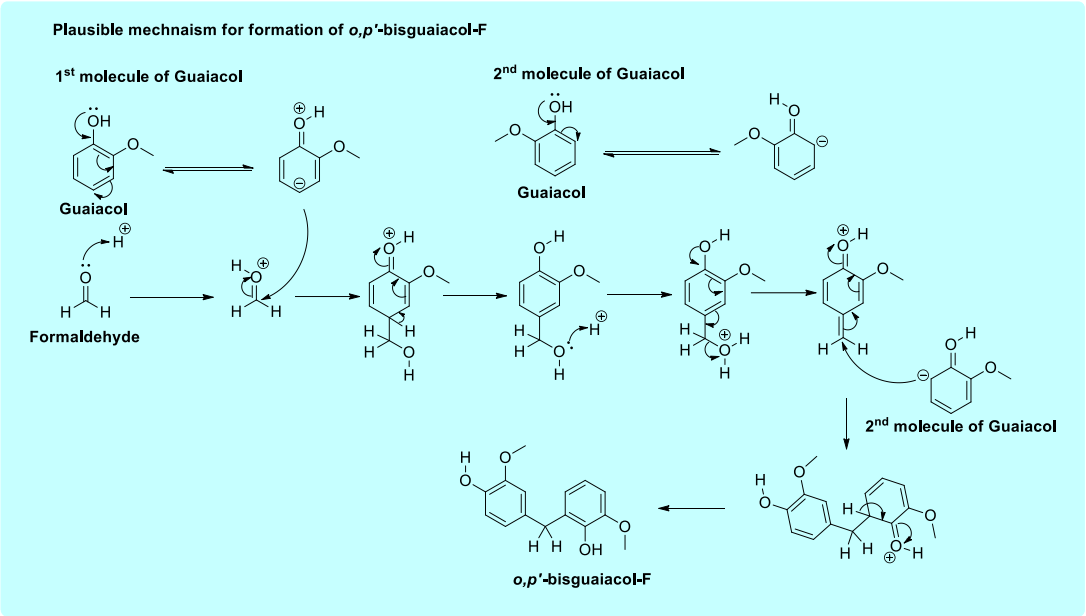

Figure 5.18. Plausible reaction mechanism for synthesis of op'-Bisguaiacol-F.

5.7. Conclusions

Successful synthesis of Bisguaiacol-F and its derivatives could be achieved using a bio-derived guaiacol condensation with different aldehydes in presence of a magnetically separable catalyst. A robust and novel heterogeneous acid catalyst, [Fe_3O_4@SiO_2-$(Pr)_3$-N-Bu-SO_3H] [HSO_4^-], has proven to be highly effective in facilitating 99% conversion of guaiacol and complete conversion of aqueous formaldehyde with excellent products yield. Stoichiometric use of guaiacol and its complete conversion over our catalyst avoided an energy intensive operation to recover excess guaiacol. A remarkable regioisomers selectivity of 62%, 15% and 6% to *pp*'-BGF, *mp*'-BGF and *op*'-BGF, respectively was achieved. For every catalyst tested, along with *pp*', *mp*' and *op*'-BGF and unidentified BGF regioisomer was also noticed. However, it is interesting to know that, a mixture of BGF regioisomers can be processed for the production of polymers [27,28]. The superior catalytic activity of our novel magnetically separable heterogeneous catalyst could be attributed to the easy access of acid sites, since –SO_3H group is like a pendant which is attached to a long butyl chain. With its magnetic properties, the [Fe_3O_4@SiO_2-$(Pr)_3$-N-Bu-SO_3H] [HSO_4^-] catalyst can be effortlessly separated using an external magnetic field and reused multiple times for subsequent condensation reactions. This feature not only minimizes handling losses but also ensures sustained catalyst activity over multiple cycles. Our work serves as an inspiration for other researchers, highlighting the viability of the bio

route for synthesizing environmentally friendly and health-conscious bulk molecules, which find applications across various industries.

5.7. References

[1] A. S. Trita, L. C. Over, J. Pollini, S. Baader, S. Riegsinger, M. A. R. Meier, L. J. Gooßen, *Green Chem.*, **2017**, *19*, 3051–3060.

[2] T. Periyasamy, S. P. Asrafali, S. Muthusamy, S. Kim, *New J. Chem.*, **2016**, *40*, 9313.

[3] Bisphenol-A Market Size & Share Analysis - Growth Trends & Forecasts (2024 - 2029). Source: https://www.mordorintelligence.com/industry-reports/bisphenol-a-bpa-market

[4] R. Rezg, S. El-Fazaa, N. Gharbi, B. Mornagui, *Environ. Int.* **2014**, *64*, 83−90.

[5] S. Koelewijn, D. Ruijten, L. Trullemans, T. Renders, P. V. Puyvelde, H. Witters, B. F. Sels, *Green Chem.*, **2019**, *21*, 6622.

[6] K. M. Hambleton, J. F. Stanzione, *ACS Omega*, **2021**, *6*, 23855−23861.

[7] K. H. Nicastro, C. J. Kloxin, T. H. Epps, *ACS Sustainable Chem. Eng.* **2018**, *6*, 14812−14819.

[8] E. D. Hernandez, A. W. Bassett, J. M. Sadler, J. J. La Scala, J. F. Stanzione, *ACS Sustainable Chem. Eng.* **2016**, *4*, 4328−4339.

[9] R. Auvergne, S. Caillol G. David, B. Boutevin, J. P. Pascault, *Chem. Rev.*, **2014**, *114*, 1082–1115.

[10] H. Wang, Y. Pu, A. Ragauskas, B. Yang, *Bioresour. Technol.*, **2019**, *271*, 449–461.

[11] F. G. Calvo-Flores, J. A. Dobado, *ChemSusChem,* **2010**, *3*, 1227–1235.

[12] M. Kleinert, T. Barth, *Chem. Eng. Technol.*, **2008**, *31*, 736–745.

[13] M. N. Belgacem, A. Gandini, *Elsevier Science*, **2011**.

[14] D. Stewart, *Ind. Crops Prod*. **2008**, *27*, 202–207.

[15] A. W. Bassett, C. M. Breyta, A. E. Honnig, J. H. Reilly, K. R. Sweet, J. J. La Scala, J. F. Stanzione, *Eur. Polym. J.* **2019**, *111*, 95–103.

[16] M. Fache, R. Auvergne, B. Boutevin, S. Caillol, *Eur. Polym. J.*, **2015**, *67*, 527–538.

[17] M. Fache, E. Darroman, V. Besse, R. Auvergne, S. Caillol, B. Boutevin, *Green Chem*., **2014**, *16*, 1987–1998.

[18] J. S. Mahajan, R. M. O'Dea, J. B. Norris, L. T. J. Korley, T. H. Epps, *ACS Sustainable Chem. Eng.*, **2020**, *8*, 15072–15096.

[19] C. H. Chen, S. H. Tung, R. J. Jeng, M. M. Abu-Omar, C.-H. Lin, *Green Chem*., **2019**, *21*, 4475–4488.

[20] S. Zhao, X. Huang, A. J. Whelton, M. M. Abu-Omar, *ACS Sustainable Chem. Eng*., **2018**, *6*, 7600–7608.

[21] S. Fadlallah, P. S. Roy, G. Garnier, K. Saito, F. Allais, *Green Chem*., **2021**, *23*, 1495–1535.

[22] N. Ogata, T. Bada, *Res. Commun. Chem. Pathol. Pharmacol*., **1989**, *66*, 411-423.

[23] K. G. Lee, S. E. Lee, G. R. Takeoka, J. H. Kim, B. S. Park, *J. Sci. Food Agric.*, **2005**, *85*, 1580–1586.

[24] Y. Peng, K. H. Nicastro, T. H. Epps, W. Changqing, *J. Agric. Food Chem.*, **2018**, *66*, 11775−11783.

[25] E. O. Ebikade, S. Sadula, S. Liu, D. G. Vlachos, *Green Chem.*, **2021**, *23*, 10090.

[26] F. Cavani, M. Corrado, R. Mezzogori, *J. Mol. Catal. A Chem.*, **2002**, *182*, 447–453.

[27] J. J. Lindberg, V. A. Era, H. Sairanen, *Angew. Makromol. Chem*., **1974**, *39*, 159.

[28] M. Enjoji, A. Yamamoto, M. Shibata, *J. Appl. Polym. Sci.*, **2015**, *132*, 41347.

[29] T. Nakamura, H. Kawamoto, S. Saka, *Journal of Wood Chemistry and Technology*, **2007**, *27*, 121–133.

[30] T. P. Nguyen, P. Hesemann, T. M. L. Tranb, J. J. E. Moreaua, *J. Mater. Chem.*, **2010**, *20*, 3910–3917.

[31] S. Suganuma, K. Nakajima, M. Kitano, D. Yamaguchi, H. Kato, S. Hayashi, M. Hara, *J. Am. Chem. Soc.*, **2008**, *130*, 12787.

[32] R. S. Thombal, A. R. Jadhav, V. H. Jadhav, *RSC Adv.*, **2015**, *17*, 12981.

[33] K. P. Tarade, S. P. Kamble, C. V. Rode, *Catal. Letters*, **2023**, *154*, 1511-1520.

[34] C. R. Patil, S. P. Kamble, C. V. Rode, *ChemistrySelect*, **2021**, *6*, 6636.

[35] S. H. Shinde, C. V. Rode, *Green Chem*., **2017**, *19*, 4804–4810.

[36] A. Ghorbani-Choghamarani, G. Azadi, *RSC Adv.*, **2015**, *5*, 9752-9758.

[37] K. Tarade, S. Shinde, C. Rode, *Fuel Process. Technol.*, **2020**, *197*, 106191.

[38] S. Shinde, C. Rode, *Catal. Commun.*, **2017**, *88*, 77–80.

[39] C. V. Rode, M. J. Vaidya, R. Jaganathan, R. V. Chaudhari, *Chem. Eng. Sci.*, **2001**, *56*, 1299.

[40] S. P. Bawane, S. B. Sawant, *Applied Catalysis A: General*, **2005**, *293*, 162–170.

5.8 Spectroscopic Data

5.8.1. HPLC Chromatogram of reaction crude of Bisguaiacol

5.8.1.1. HPLC Chromatogram of reaction crude of Bisguaiacol-F

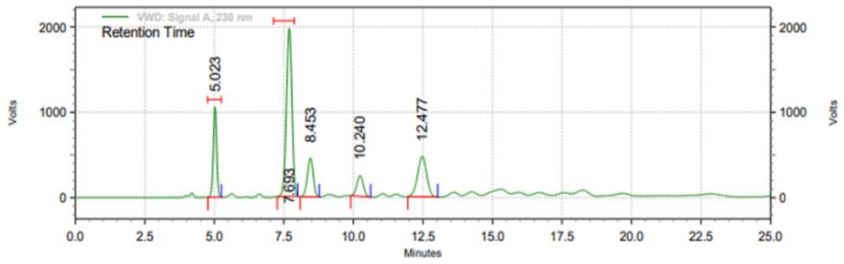

VWD: Signal A, 230 nm Results

	Retention Time	Area	Area %	Height	Height %
Guaiacol	5.023	151058543	15.65	17718455	25.17
pp-BGF	7.693	456778524	47.31	33018780	46.91
mp-BGF	8.453	111888215	11.59	7620875	10.83
op-BGF	10.240	66160663	6.85	4086821	5.81
Unidentified isomer	12.477	179525179	18.60	7936330	11.28
	Totals	965411124	100.00	70381261	100.00

Figure 5.19. HPLC Chromatogram of reaction crude of Bisguaiacol-F

5.8.1.2. HPLC Chromatogram of reaction crude of Bisguaiacol-E

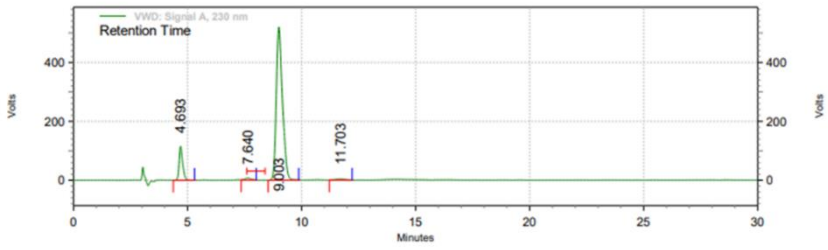

VWD: Signal A, 230 nm Results

	Retention Time	Area	Area %	Height	Height %
Guaiacol	4.693	20690456	11.05	1930824	17.83
Unidentified	7.640	1847613	0.99	110876	1.02
pp-BGE	9.003	162983891	87.01	8717724	80.52
Unidentified	11.703	1786421	0.95	67600	0.62
	Totals	187308381	100.00	10827024	100.00

Figure 5.20. HPLC Chromatogram of reaction crude of Bisguaiacol-E

5.8.1.3 HPLC Chromatogram of reaction crude of Bisguaiacol-P

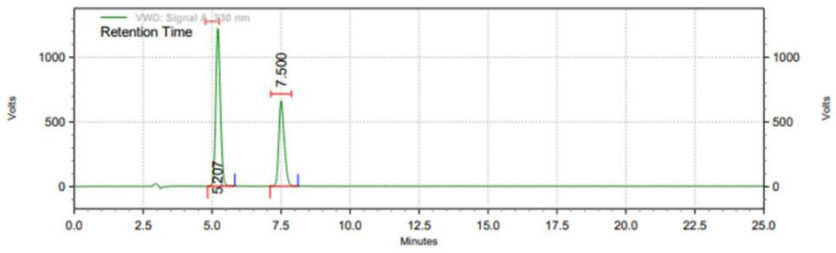

VWD: Signal A, 230 nm Results

Retention Time		Area	Area %	Height	Height %
Guaiacol	5.207	239731126	61.11	20459069	64.93
pp-BGP	7.500	152561962	38.89	11048257	35.07
Totals		392293088	100.00	31507326	100.00

Figure 5.21. HPLC Chromatogram of reaction crude of Bisguaiacol-P

5.8.1.4. HPLC Chromatogram of reaction crude of Bisguaiacol-B

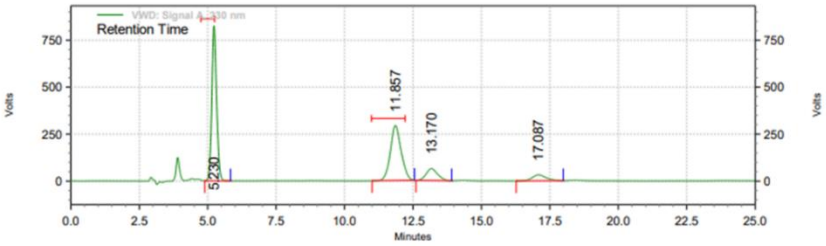

VWD: Signal A, 230 nm Results

Retention Time		Area	Area %	Height	Height %
Guaiacol	5.230	168737246	47.83	13844732	68.04
pp-BGB	11.857	134355199	38.08	4906783	24.11
Unidentified	13.170	31031846	8.80	1068819	5.25
Unidentified	17.087	18659547	5.29	528832	2.60
Totals		352783838	100.00	20349166	100.00

Figure 5.22. HPLC Chromatogram of reaction crude of Bisguaiacol-B

5.8.2. LCMS of regioisomers of Bisguaiacol-F

5.8.2.1. LC-MS spectrum of *pp*'-Bisguaiacol F

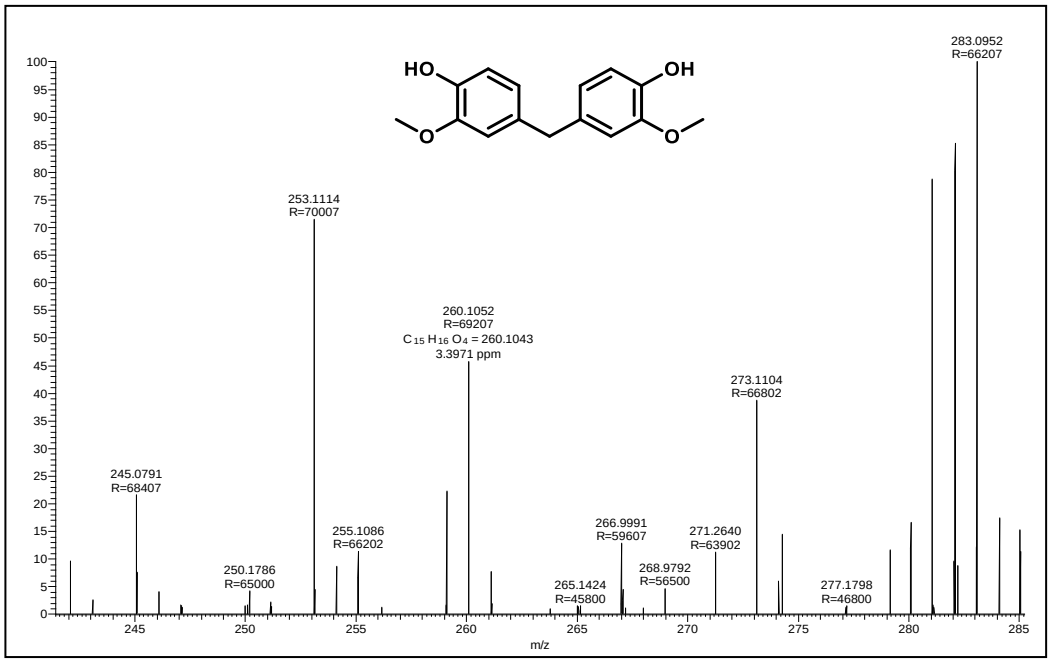

5.8.2.2. LC-MS spectrum of *mp'*-Bisguaiacol F

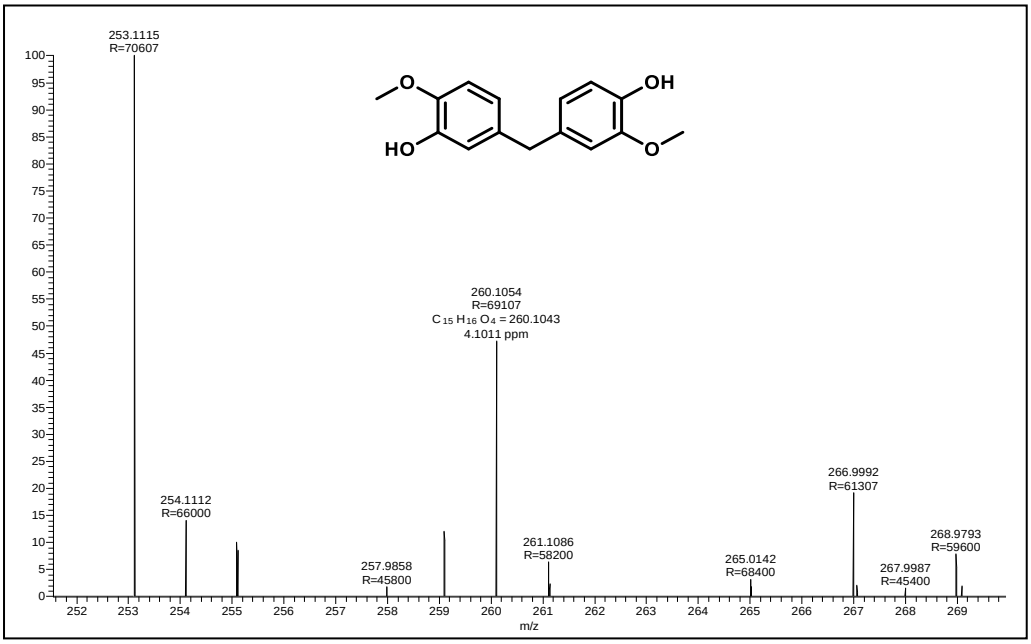

5.8.2.3. LC-MS spectrum of *op*'-Bisguaiacol F

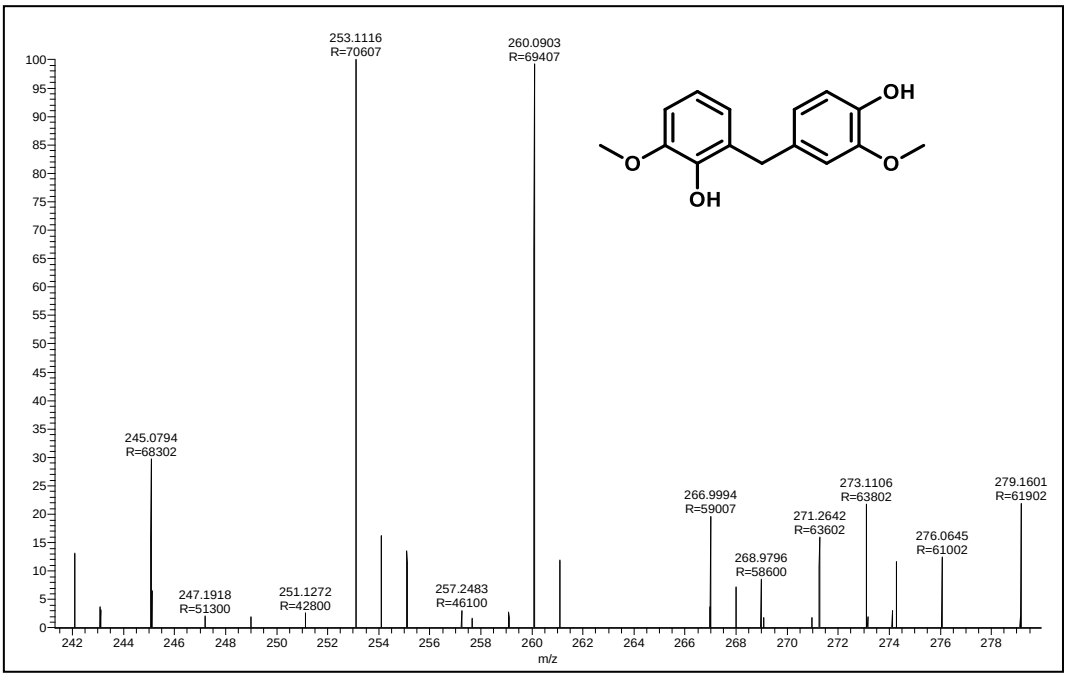

5.8.2.4. LC-MS spectrum of other unidentified isomers

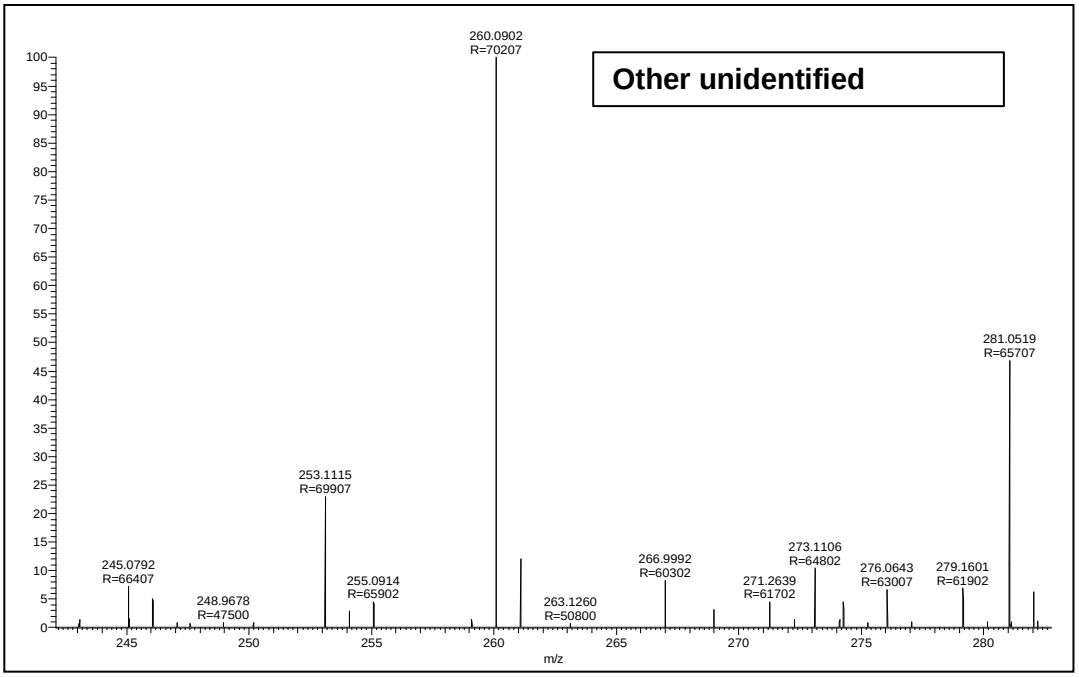

5.8.3. NMR data

5.8.3.1. NMR of catalyst

3-(triethoxysilyl)-N,N-bis(3-(trimethoxysilyl) propyl) propan-1-amine [$(EtO)_3(MeO)_6Si$-$(Pr)_3$-N]

^{1}H NMR (400 MHz, $CDCl_3$, 0.01% TMS, δ ppm): 0.65 (*m*, 6H), 1.23 (*m*, 9H), 1.60 (*m*, 6H), 2.62 (*m*, 6H), 3.40 (*s*, 2H), 3.56 (*s*, 16H), 3.82 (*m*, 6H). **Note:** Since the product is not purified, therefore there are extra protons appeared in NMR that could be attributed for unreacted starting materials such as 3-aminopropyl triethoxysilane, 3-chloropropyl trimethoxysilane and ethylene diamine.

^{13}C NMR (400 MHz, $CDCl_3$, 0.01% TMS, δ ppm): 18.20, 18.38, 23.11, 26.99, 41.74, 44.91, 49.27, 49.65, 50.18, 50.30, 50.34, 50.40, 52.43, 58.24, 58.31, 58.38. **Note:** Since the product is not purified, therefore there are extra carbons appeared in NMR that could be attributed for unreacted starting materials such as 3-aminopropyl triethoxysilane, 3-chloropropyl trimethoxysilane and ethylene diamine.

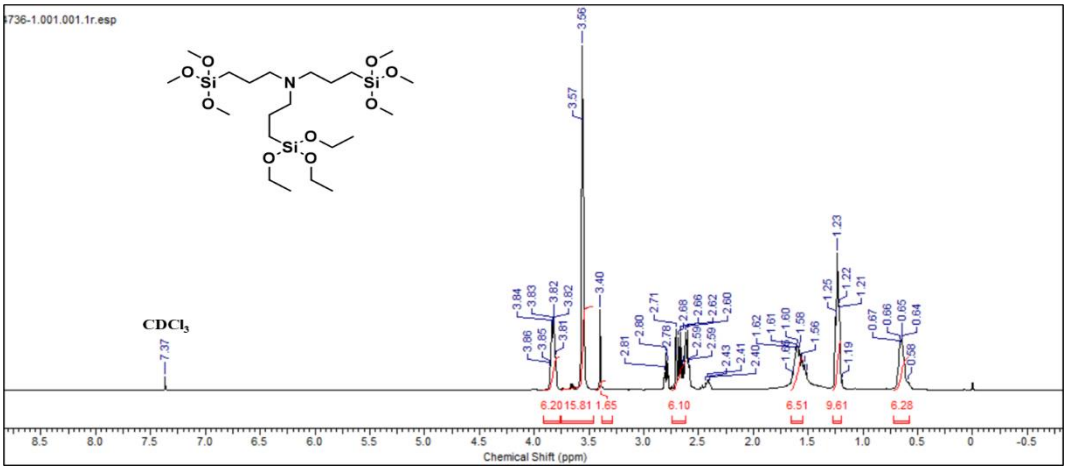

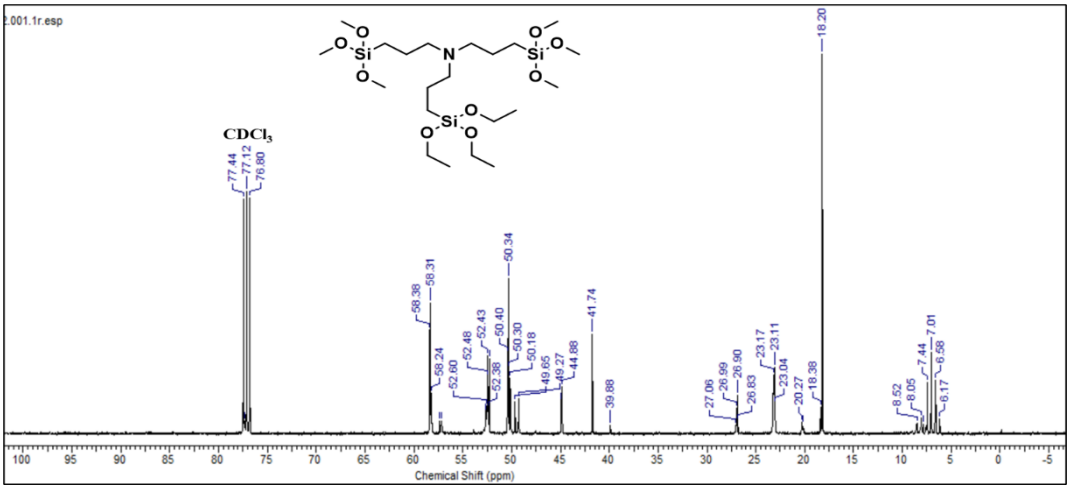

4-((3-(triethoxysilyl) propyl) bis(3-(trimethoxysilyl) propyl) ammonio) butane-1-sulfonate [$(EtO)_3(MeO)_6Si$-$(Pr)_3$-N-Bu-SO_3^-]

^{1}H NMR (400 MHz, $CDCl_3$, 0.01% TMS, δ ppm): 0.66 (*m*, 6H), 1.22 (*m*, 9H), 1.61 (*m*, 8H), 1.86 (*m*, 2H), 2.26 (*m*, 2H), 3.17 (*m*, 3H), 3.43 (*s*, 5H), 3.56 (*s*, 18H), 3.82 (*m*, 6H). **Note:** Since the product is not purified, therefore there are extra protons appeared in NMR that could be attributed for unreacted starting materials such as 3-aminopropyl triethoxysilane, 3-chloropropyl trimethoxysilane, ethylene diamine and 1,4-butanesultone.

^{13}C NMR (400 MHz, $CDCl_3$, 0.01% TMS, δ ppm): 6.63, 7.04, 7.46, 18.25, 18.40, 22.82, 23.57, 41.49, 48.23, 50.11, 50.43, 50.49, 51.96, 52.29, 57.85, 58.40, 58.46, 73.95. **Note:** Since the product is not purified, therefore there are extra protons appeared in NMR that could be attributed for unreacted starting materials such as 3-aminopropyl triethoxysilane, 3-chloropropyl trimethoxysilane, ethylene diamine and 1,4-butanesultone.

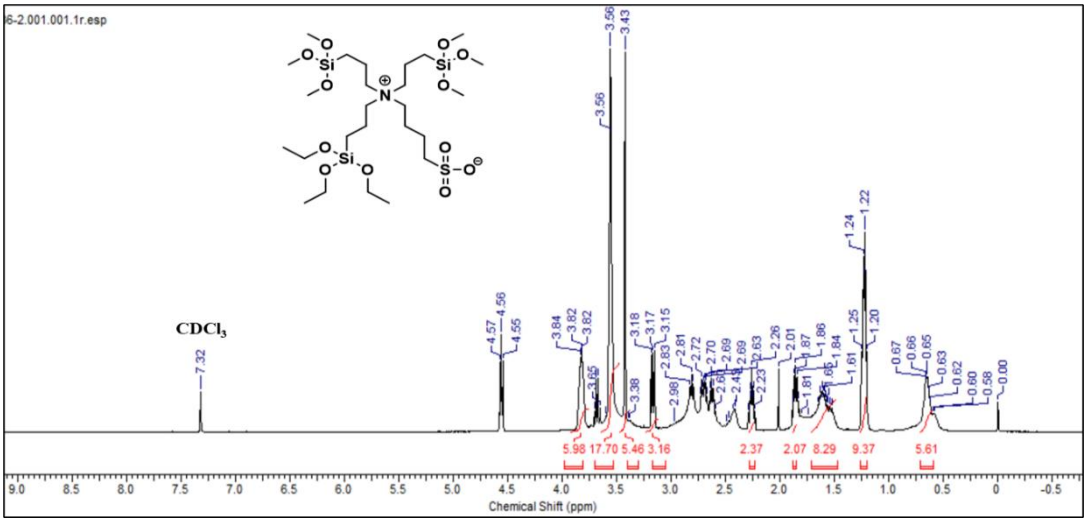

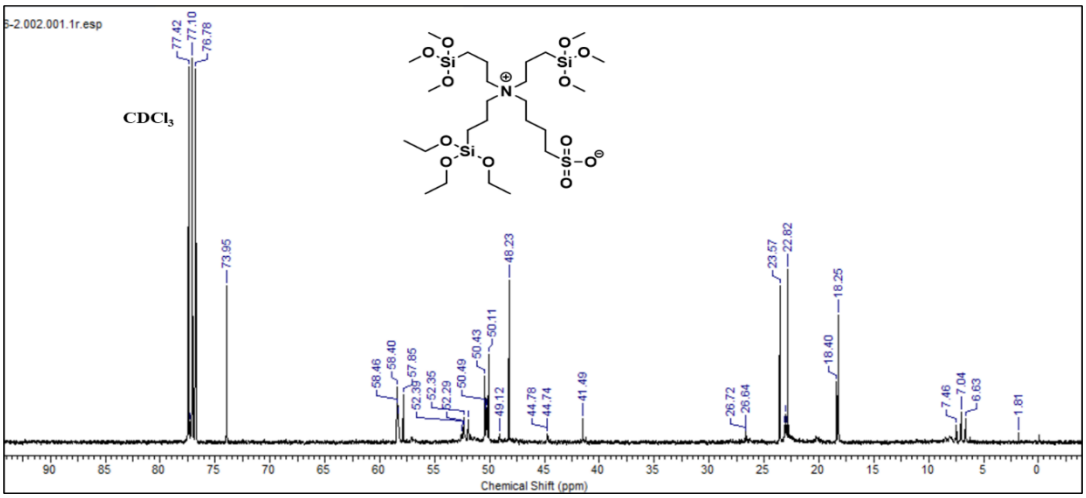

5.8.3.2. NMR of synthesized Bisguaiacol compounds

***pp'*-Bisguaiacol F –** White needle shaped crystals

^{1}H NMR (500 MHz, DMSO-d6, 0.01% TMS, δ ppm): 3.65 (*s*, 6H; –OCH_3), 3.70 (*s*, 2H; CH_2), 6.55 (*d*, 2H; *o*-ArH), 6.65 (*dd*, 2H; *m*-ArH), 6.75 (*d*, 2H; *o*-ArH), 8.75 (*s*, 2H; *p*-ArOH).

^{13}C NMR (500 MHz, DMSO-d6, 0.01% TMS, δ ppm): 40.38, 55.99, 113.22, 115.75, 121.17, 133.12, 144.99, 147.82.

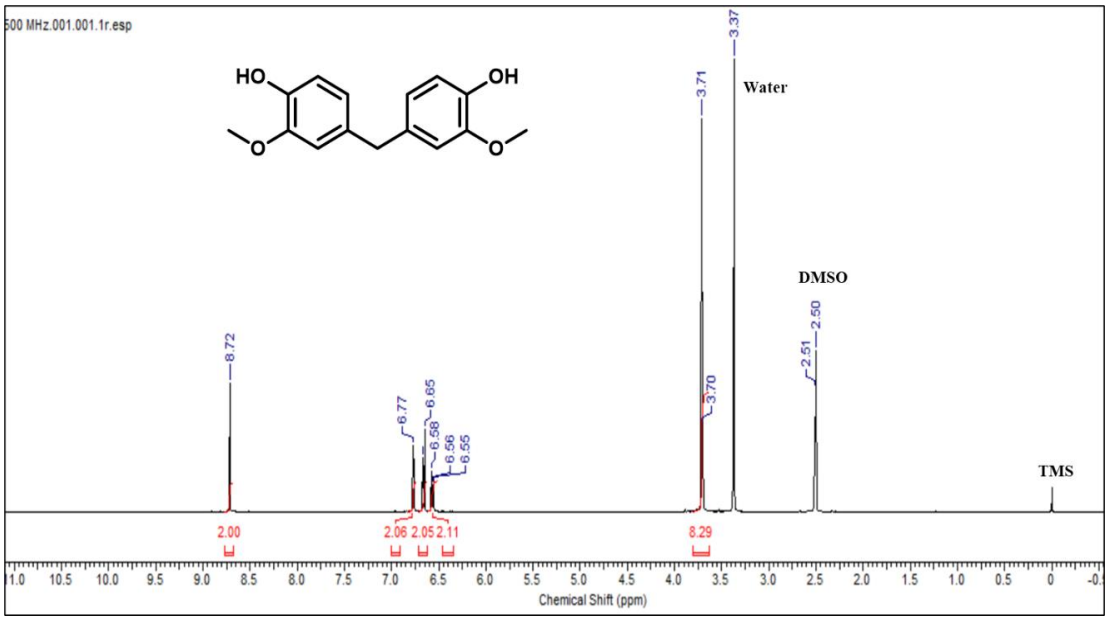

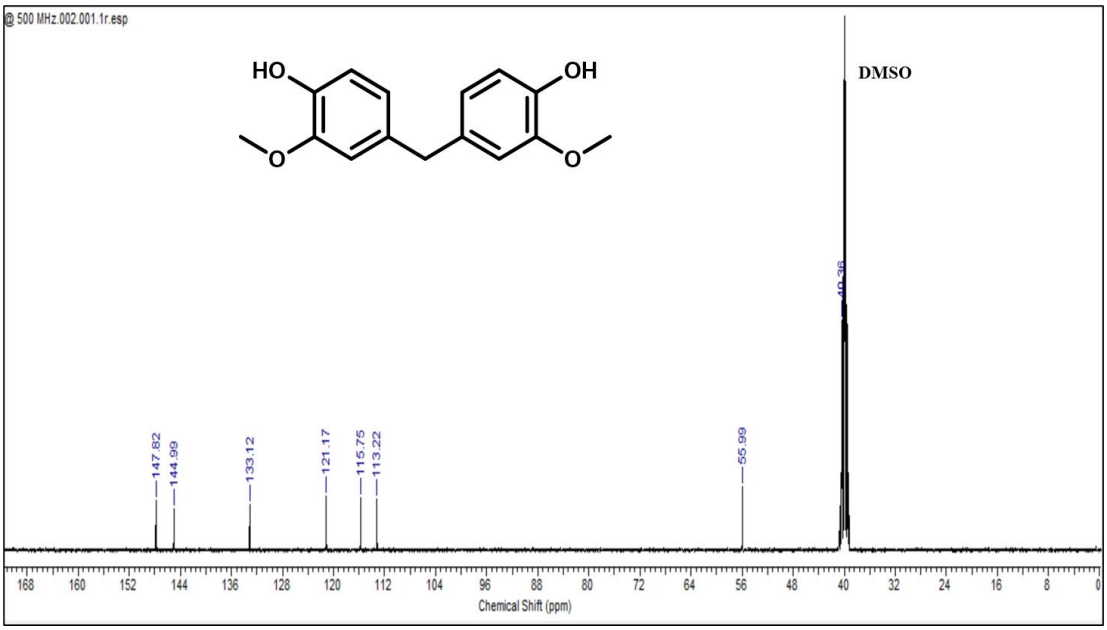

***mp*'- Bisguaiacol F –** White amorphous powder

^{1}H NMR (500 MHz, DMSO-d6, 0.01%, TMS, δ ppm): 3.34 (*s*, 2H; CH_2), 3.66 (s, 3H; *m*-OCH_3), 3.71 (*s*, 3H; *p*-OCH_3), 6.65 (*dd*, 1H; *m*-ArH), 6.67 (*d*, 1H, *o*-ArH), 6.76 (*dd*, 1H; *m*-ArH), 6.74 (*d*, 1H; *o*-ArH), 6.56 (*d*, *o*-ArH) and 6.58 (*d*, 1H; *o*-ArH), 8.78 (*s*, 1H; *p*-ArOH), 8.67 (s, 1H; *m*-ArOH).

^{13}C NMR (500 MHz, DMSO-d6, 0.01% TMS, δ ppm): 40.41, 56.04, 112.74, 113.32, 115.79, 116.41, 121.21, 133.12, 145.04, 147.85, 146.80.

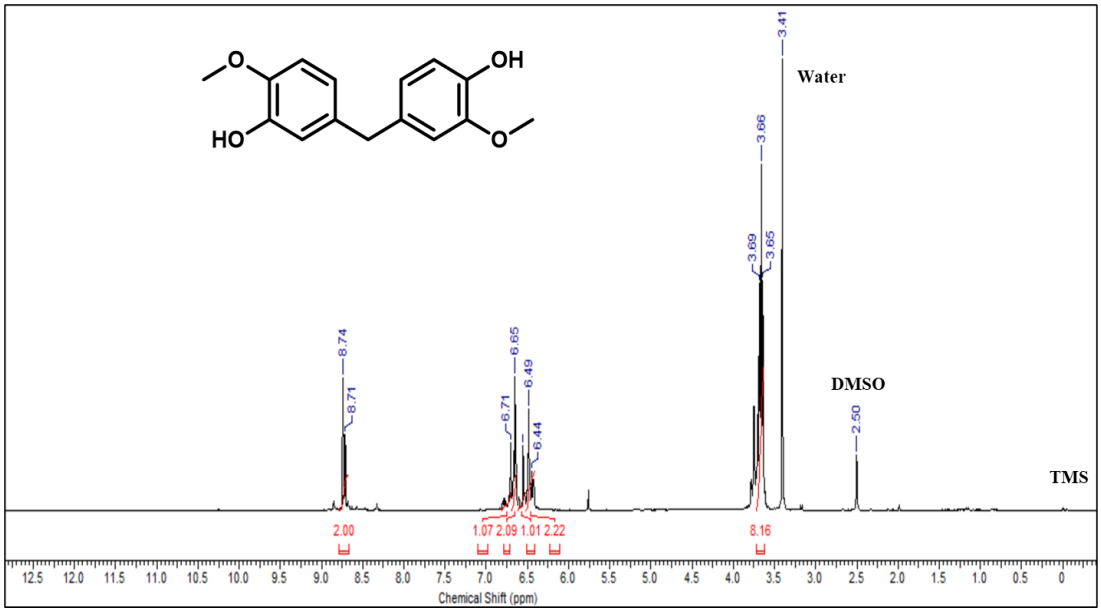

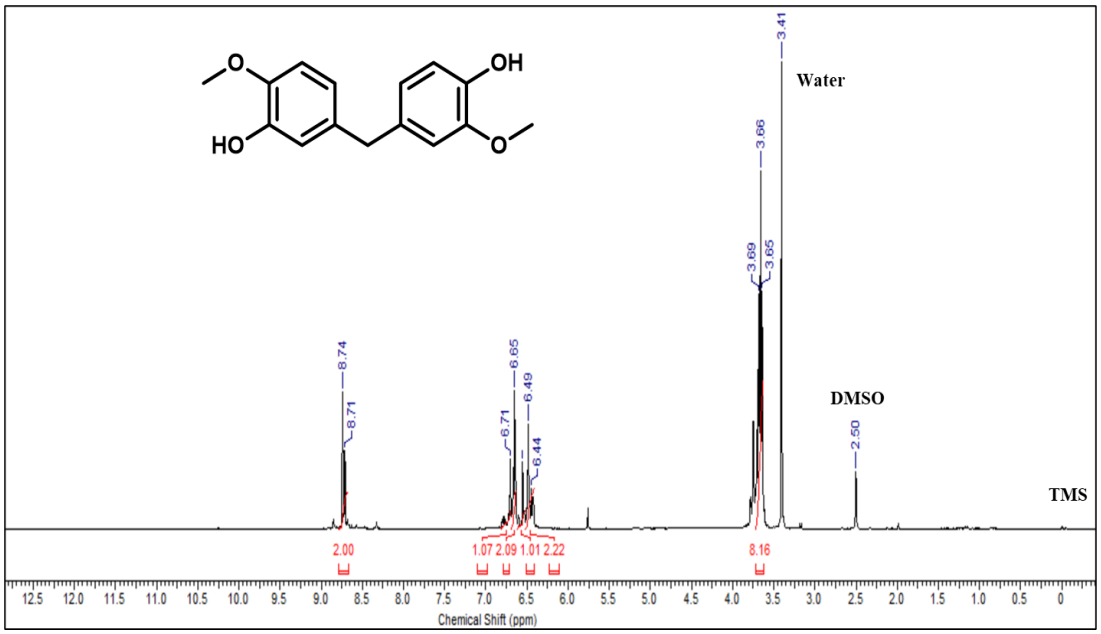

***op'*-Bisguaiacol F –** White spherical crystals

^{1}H NMR (500 MHz, DMSO-d6, 0.01%, TMS, δ ppm): 3.75 (*s*, 3H; *m*-OCH3), 3.77 (*s*, 3H; *m*-OCH_3), 3.70 (*s*, 2H; CH_2), 6.52–6.69 ppm (*m*, 5H; ArH), 6.77 (*d*, 1H; *o*-ArH). 8.64 (*s*, 1H; *p*-ArOH), 8.47 (*s*, 1H; *o*-ArOH).

^{13}C NMR (500 MHz, DMSO-d6, 0.01% TMS, δ ppm): 40.61, 56.2, 110.05, 113.54, 115.67, 119.02, 121.30, 122.57, 128.56, 132.49, 144.17, 144.96, 147.73, 147.84.

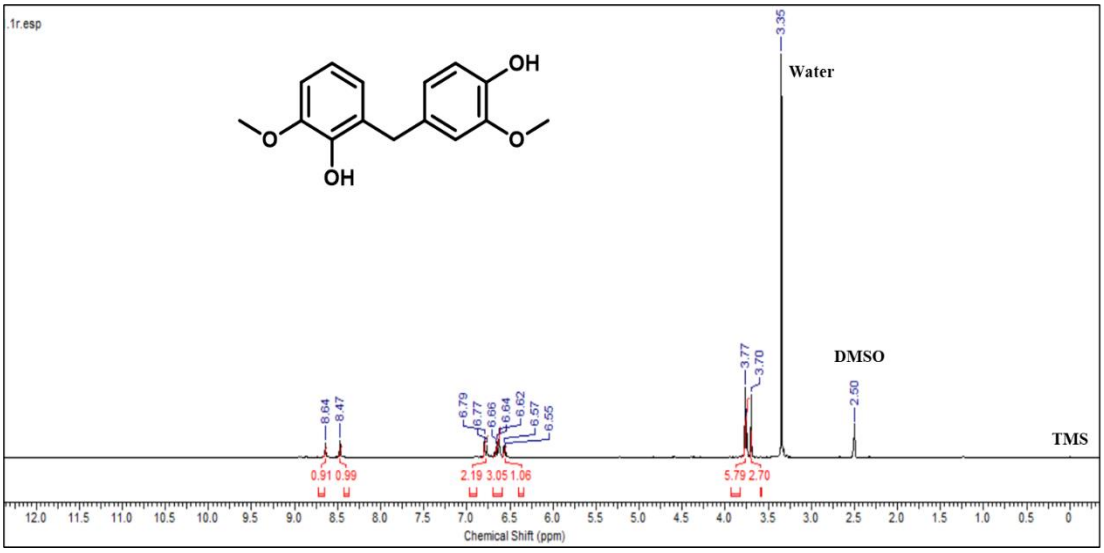

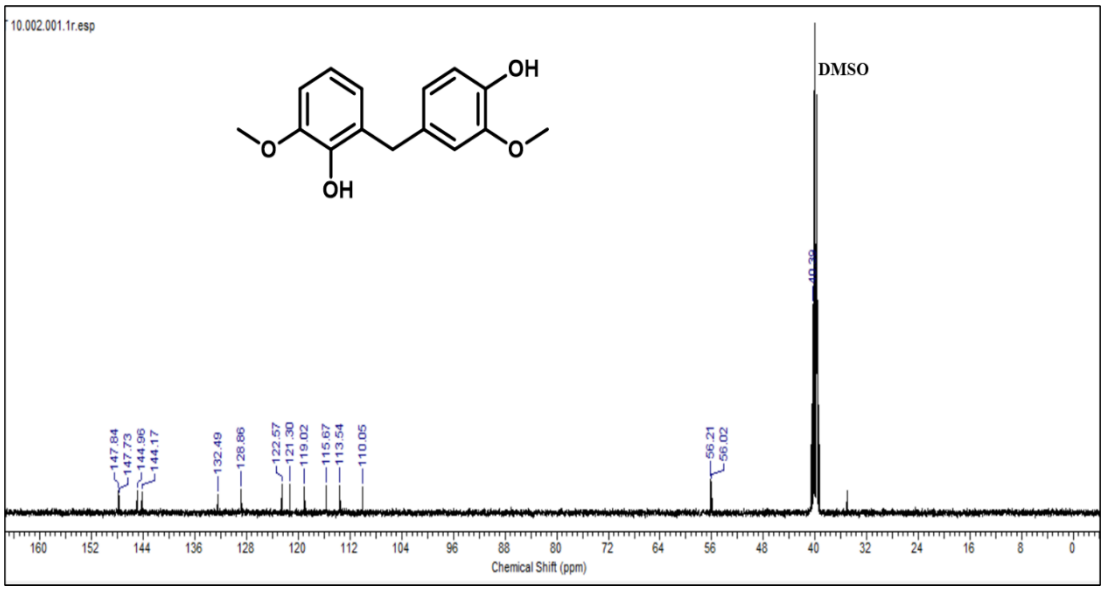

Unidentified isomers – Orange crystals

^{1}H NMR (500 MHz, DMSO-d6, 0.01%, TMS, δ ppm): 3.66 (*m*, 9H), 6.42–6.71 ppm (*m*, 6H; ArH), 8.71 (*s*, 1H; ArOH), 8.74 (*s*, 1H).

^{13}C NMR (500 MHz, DMSO-d6, 0.01% TMS, δ ppm): 37.29, 37.81, 40.64, 55.90, 55.93, 56.17, 113.09, 113.24, 114.96, 115.74, 117.81, 121.04, 121.28, 130.02, 132.25, 132.36, 132.58, 144.99, 145.01, 146.09, 147.84.

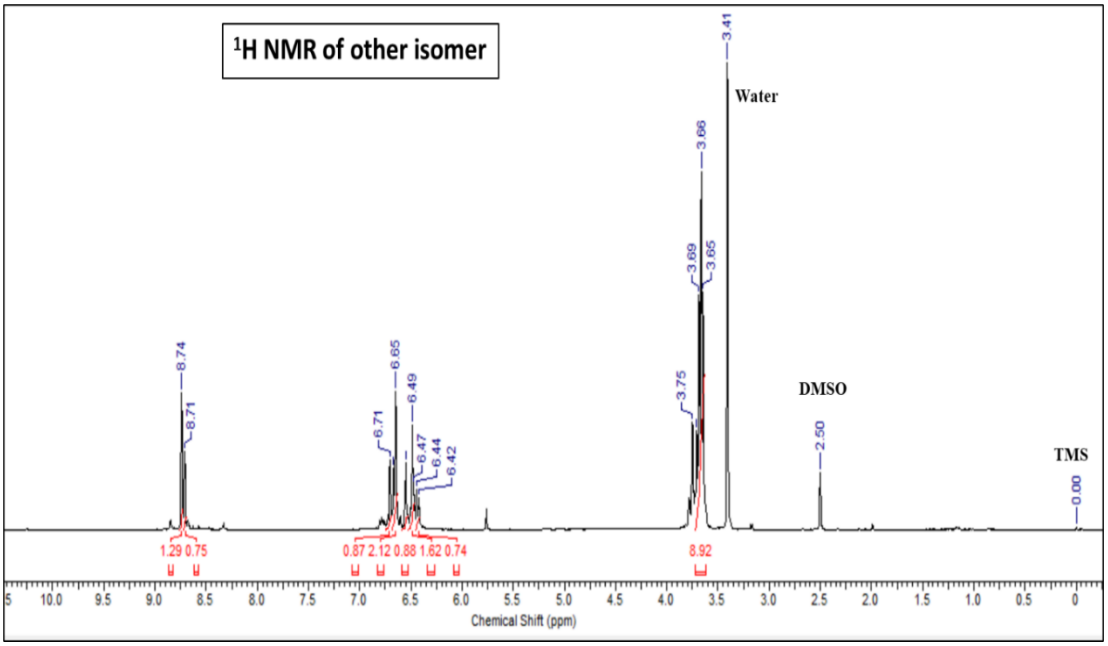

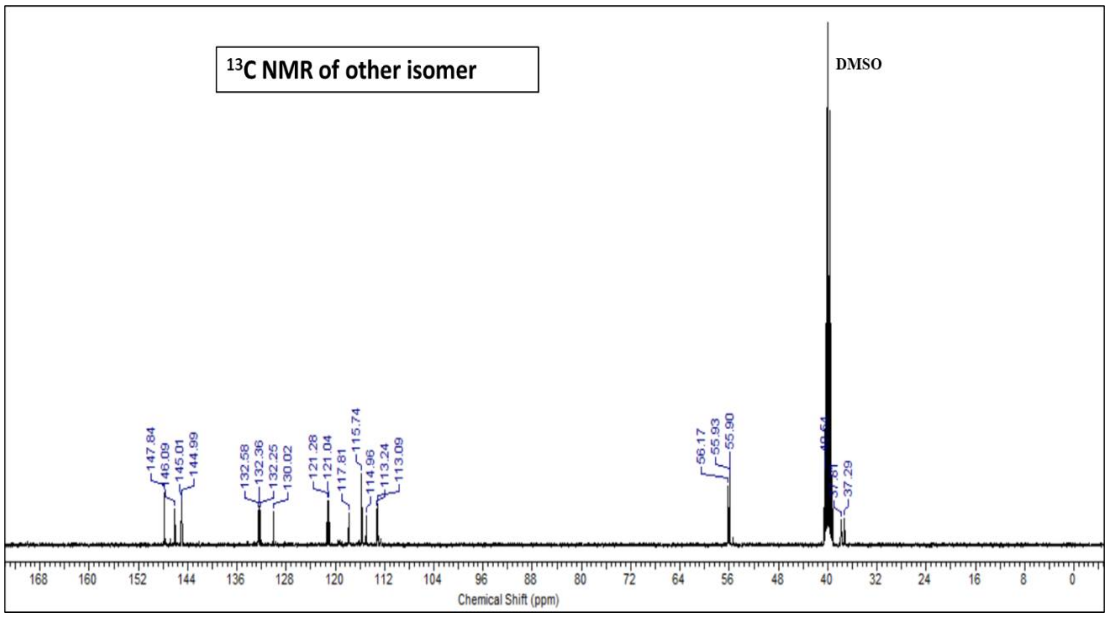

***pp'*-Bisguaiacol E** – White amorphous powder

^{1}H NMR (500 MHz, DMSO-d6, 0.01% TMS, δ ppm): 1.48 (*t*, 3H; CH_3), 3.71 (*s*, 6H; OCH_3), 3.70 (*s*, H; CH), 6.62 (*dd*, 2H; *o*-ArH), 6.68 (*dd*, 2H; *o*-ArH), 6.78 (*d*, 2H; *m*-ArH), 8.71 (*s*, 2H; *p*-ArOH).

^{13}C NMR (500 MHz, DMSO-d6, 0.01% TMS, δ ppm): 22.56, 43.72, 56.01, 112.16, 115.64, 119.68, 138.31, 144.99, 147.72.

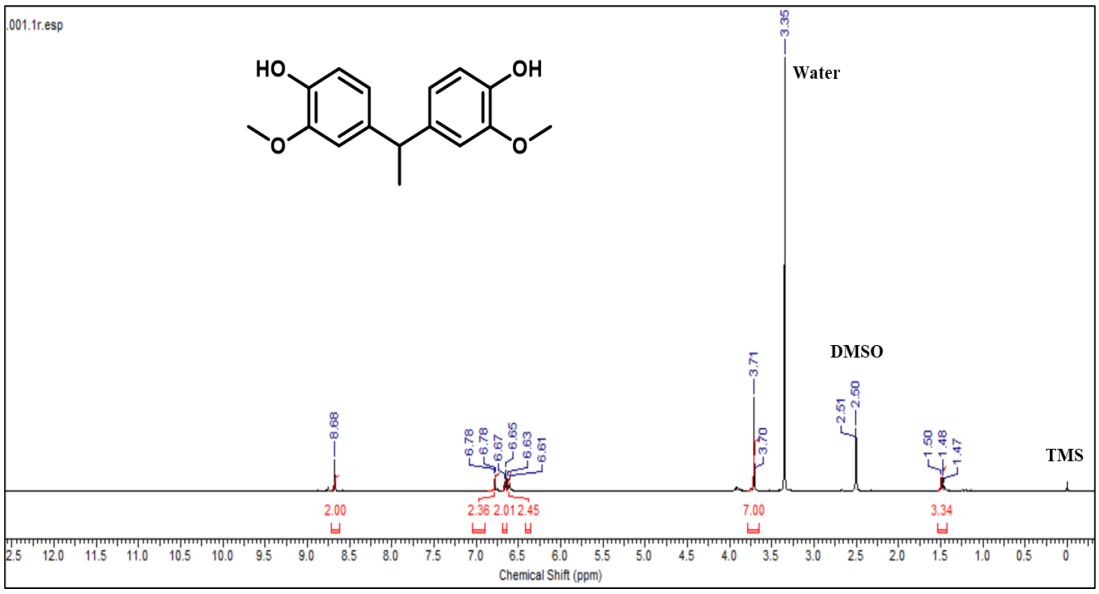

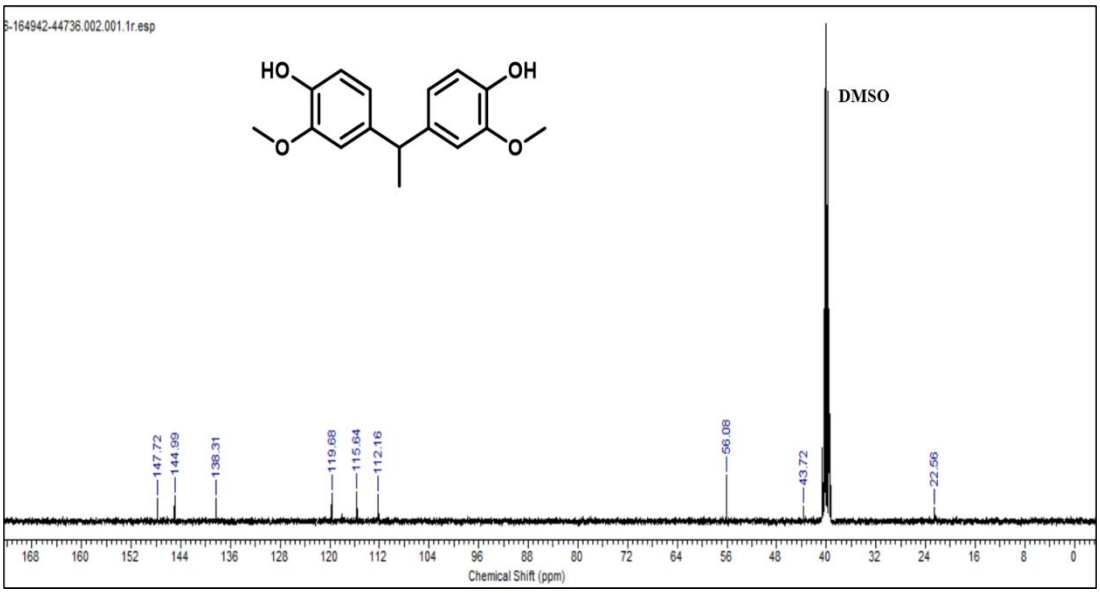

***pp'*-Bisguaiacol P – Yellow crystals**

^{1}H NMR (500 MHz, DMSO-d6, 0.01% TMS, δ ppm): 0.79 (*t*, 3H; -CH_3), 1.91 (*m*, 2H; CH_2), 3.72 (*s*, 6H; OCH_3), 3.70 (*s*, H; CH), 6.65 (*dd*, 4H; *o*-ArH), 6.80 (*d*, 2H; *m*-ArH), 8.66 (*s*, 2H; *p*-ArOH).

^{13}C NMR (500 MHz, DMSO-d6, 0.01% TMS, δ ppm): 13.29, 28.80, 52.19, 56.11, 112.36, 115.69, 120.01, 137.17, 144.96, 147.75.

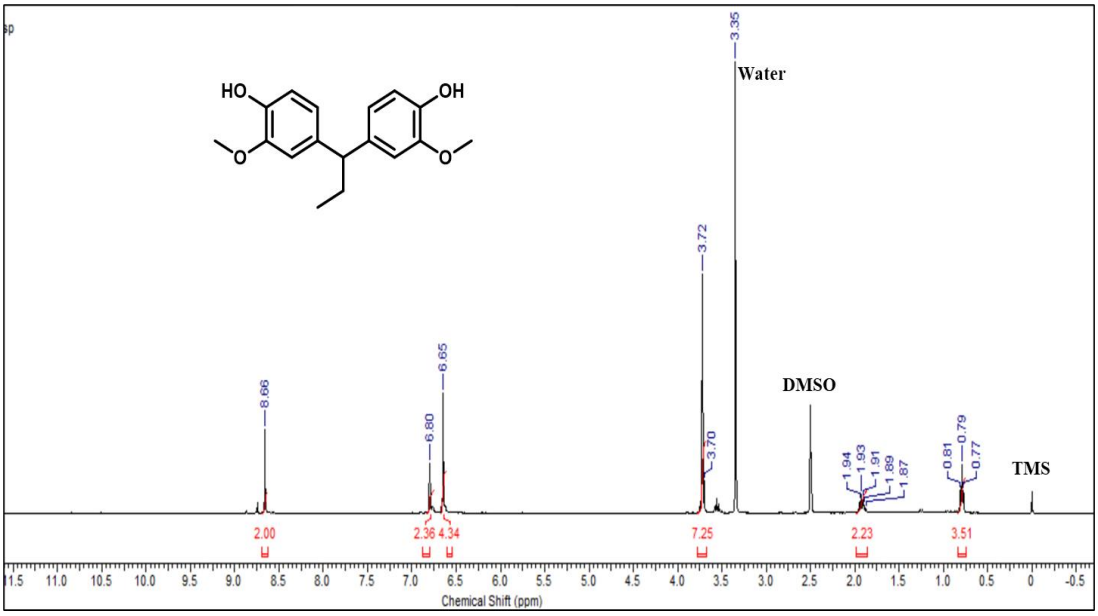

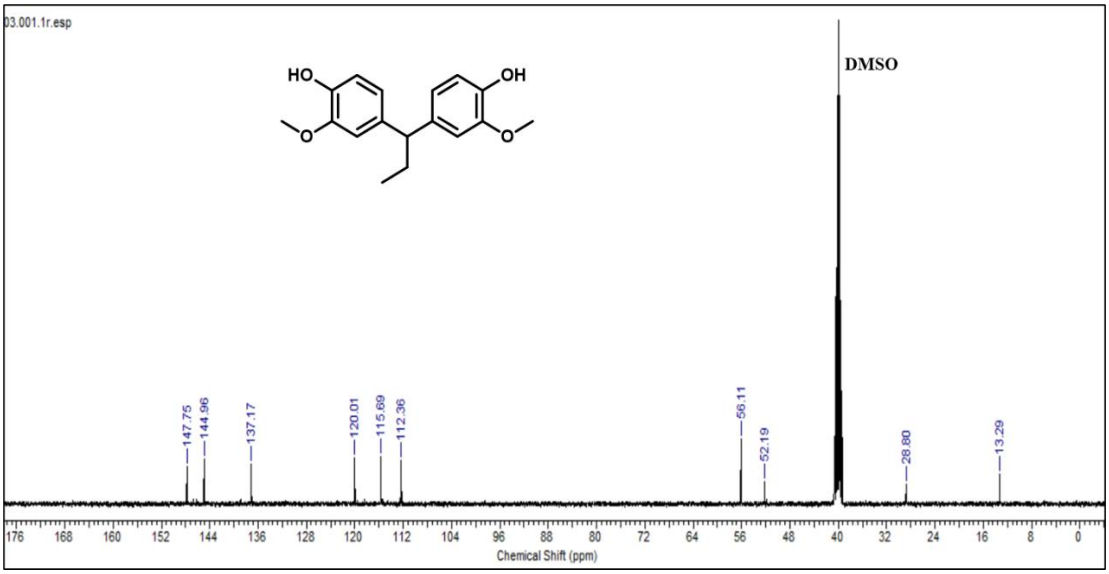

***pp'*-Bisguaiacol B – Yellow crystals**

^{1}H NMR (500 MHz, DMSO-d6, 0.01% TMS, δ ppm): 0.87 (*t*, 3H; CH_3), 1.23 (*m*, 2H; CH_2), 1.87 (*m*, 2H; CH_2), 3.72 (*s*, 6H; OCH_3), 3.70 (*s*, H; CH), 6.65 (*dd*, 4H; *o*-ArH), 6.81 (*d,* 2H; –*m*-ArH), 8.69 (*s*, 2H; *p*-ArOH).

^{13}C NMR (500 MHz, DMSO-d6, 0.01% TMS, δ ppm): 13.29, 28.79, 40.61, 52.19, 56.11, 112.36, 115.69, 120.01, 137.17, 144.96, 147.75.

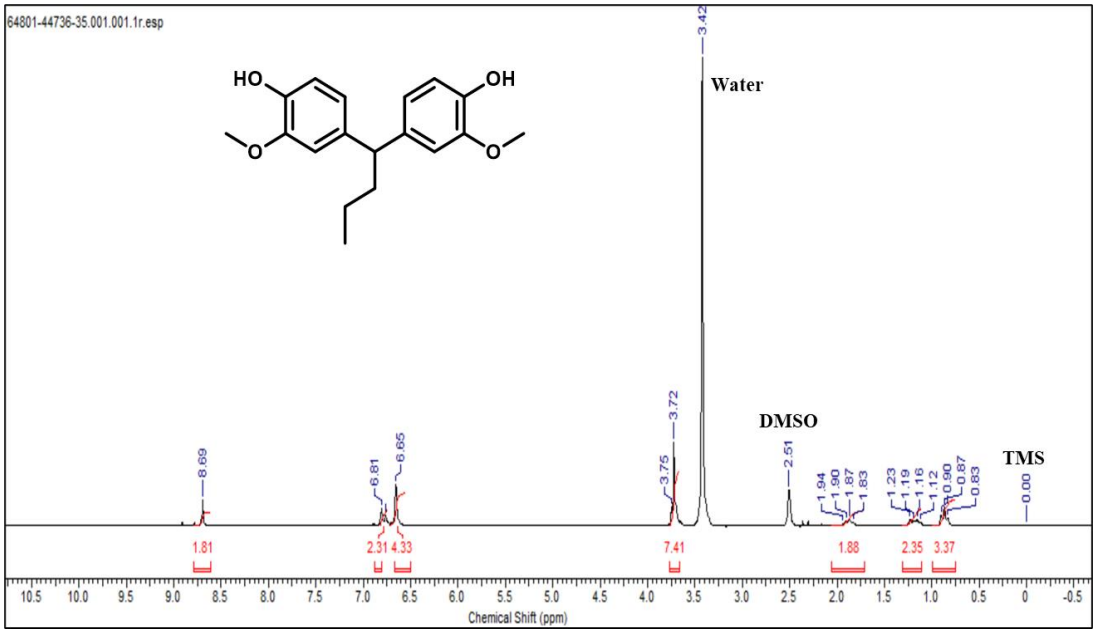

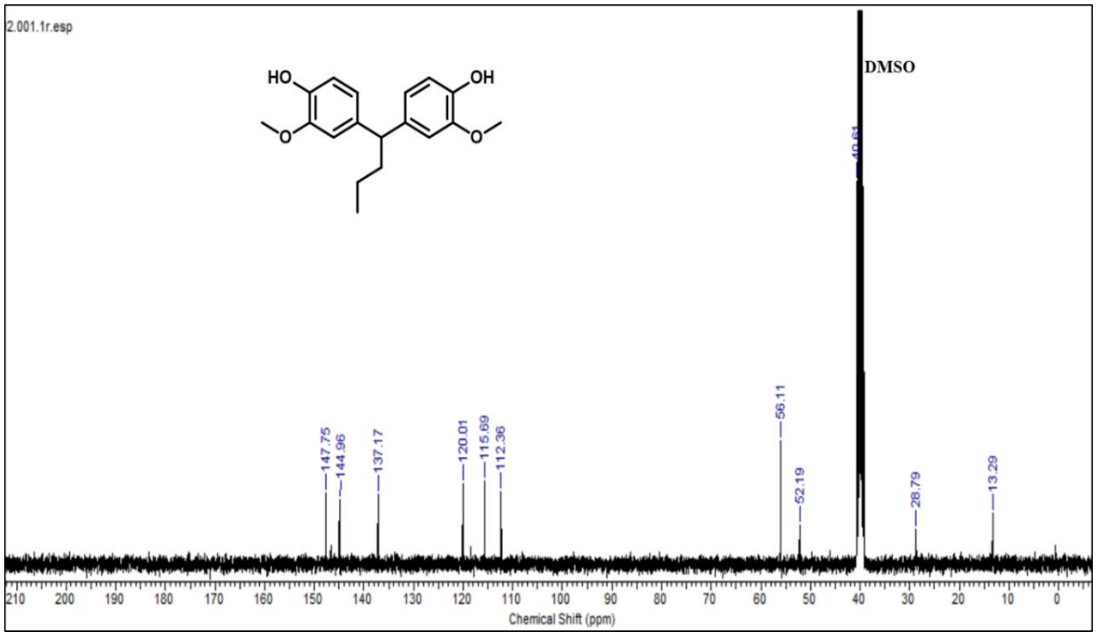

Chapter – 6

Summary & Future Scope

6.1. Summary

Forest wastes, algae, crop residues, marine organisms, household wastes are some of the potential sources of the biomass. Among the various biomass feedstocks, lignocellulose, chitin and microalgae are the most accessible for downstream processing. Utilizing lignocellulosic biomass for fuel and chemical production can help reduce global carbon dioxide emissions. However, due to the rigid and recalcitrant nature of lignocellulosic biomass, processing it is particularly challenging. Consequently, biomass is typically pre-treated using various chemical or physical methods to break down its tough polymeric structure. The pre-treated biomass can then be processed into platform molecules functionalized compounds derived from lignocellulose decomposition. These platform molecules can be further converted into a range of high-value chemicals and materials through biochemical or chemocatalytic processes. In Chapter 1, we reviewed the concepts of petrochemical and biorefinery, the types of pretreatments used for biomass deconstruction, and the production of key platform molecules and their subsequent transformation into valuable chemicals or fuels.

A catalyst is essential for accelerating a chemical reaction, or reducing the temperature or pressure required to initiate it, without being consumed in the process. Catalysis refers to the addition of a substance called a catalyst to enhance the efficiency of a reaction. In Chapter-1 we have discussed various types of catalysts, brief comparison of homogeneous *vs*. heterogeneous catalysis, mechanistic aspects of heterogeneous catalysis, brief overview of immobilisation of organic molecules on various inorganic solid supports and their structural modification to generate active sites. Due to unique structural features of immobilized organic catalysts actives sites can be easily accessible making them highly active as compared to their peer's inorganic solid oxides. With our expertise we have not only successfully designed and synthesized various immobilized organic catalysts but also explored them for transformation of multiple bio-derived platform molecules and we could achieve very good results in transformation of bio-derived platform molecules.

In Chapter-2, we have successfully designed and synthesized a versatile and robust Fe_3O_4@SiO_2-Py catalyst system for the Knoevenagel condensation of furfural with acetylacetone, achieving high yields of 3-(2-furylmethylene)-2,4-pentanedione (FMP). This innovative heterogeneous catalyst, featuring pyridine-immobilized magnetic silica (Fe_3O_4@SiO_2-Py) has proven to be an efficient and environmentally friendly solid base catalyst under optimized conditions. The resulting FMP, a C_{10} unit, can be

further converted into branched alkanes (jet fuel) through hydrodeoxygenation. The Fe_3O_4@SiO_2-Py catalyst exhibits excellent stability and recyclability, maintaining its original activity across multiple uses without degradation. Design, development and synthesis of novel catalysts for hydrodeoxygenation of FMP to a unique branched C_{10} unit is a part of our future work.

In Chapter-3, we developed a novel recyclable magnetic solid acid catalyst, [Fe_3O_4@SiO_2-Pr-Py-H][$2HSO_4^{2-}$], and utilized it for the hydroxyalkylation-alkylation of 2-methylfuran with aldehydes, yielding a wide range of furan condensation products. We have established a two-step reaction protocol involving condensation and hydrogenation for the synthesis of cyclic ethers, which are potential fuel additives from 2-methylfuran and aldehydes or ketones. It was demonstrated that these condensation products could be efficiently hydrogenated to cyclic ethers using 5% Pd/C under very mild conditions including low pressure and room temperature. Under the optimized conditions, the condensation of 2-methylfuran with various aldehydes achieved excellent yields. Additionally, several supported noble metal catalysts were screened to identify the most effective system for the selective hydrogenation of the furan ring in the condensation products. Among them, 5% Pd/C proved to be highly active and selective for furan ring hydrogenation, effectively preventing the formation of ring-opened products even at very low hydrogen pressure and room temperature. Cyclic oxygenates produced in this work can be direct fuel candidate/additive, therefore their fuel properties need to be tested.

Carbon upgrading through acid catalysed C-C bond-forming reactions of 2-methylfuran yields polyfuranic compounds that can be further hydrodeoxygenated to produce diesel fuel precursors. In Chapter-4, we developed a novel silica-supported sulfonic acid-functionalized isonicotinic acid catalyst, [SO_3H-INA@SiO_2] [Cl], as a heterogeneous solid acid for the ring-opening condensation of 2-methylfuran (as the sole carbon source) into diesel fuel precursors with C_{15} and C_{20} units. We designed a cascade process involving acid catalysed ring opening and hydroxyalkylation to form these diesel fuel precursors. Under optimized reaction conditions, [SO_3H-INA@SiO_2] [Cl] facilitated the cascade sequence, yielding condensation products such as 5,5-bis(5-methylfuran-2-yl)pentan-2-one (BMFP) and 2,4,4-tris(5-methylfuran-2-yl)pentan-1-ol (TMFP) with 99% conversion of 2-methylfuran. The [SO_3H-INA@SiO_2] [Cl] catalyst was successfully recycled for up to six consecutive runs without any loss of activity and demonstrated superior performance compared to commercially

available sulfonic acids. Detailed characterization of the catalyst, including the acid sites, was conducted and a plausible mechanistic pathway was proposed. Design, development and synthesis of novel catalysts for hydrodeoxygenation of BMFP and TMFP to a unique branched alkanes are a part of our future work.

In Chapter-5 we have presented the successful synthesis of Bisguaiacol-F and its derivatives using a bio-derived platform molecule guaiacol treated with various aldehydes in the presence of a magnetically separable catalyst. A novel and robust heterogeneous acid catalyst, $[Fe_3O_4@SiO_2\text{-}(Pr)_3\text{-}N\text{-}Bu\text{-}SO_3H]$ $[HSO_4^-]$, has demonstrated exceptional efficacy in facilitating the condensation reaction between guaiacol and aldehydes, resulting in a 99% conversion of guaiacol and complete conversion of formaldehyde, with excellent product yields. The isolated white solid products of Bisguaiacol-F and their regioisomers were meticulously characterized using NMR and melting point analysis. The superior catalytic activity of this novel magnetically separable heterogeneous catalyst is attributed to the easy access of acid sites, as the $–SO_3H$ group is attached to a long butyl chain, acting as a pendant. With its magnetic properties, the $[Fe_3O_4@SiO_2\text{-}(Pr)_3\text{-}N\text{-}Bu\text{-}SO_3H]$ $[HSO_4^-]$ catalyst can be effortlessly separated using an external magnetic field and reused multiple times for subsequent condensation reactions. This feature not only minimizes handling losses but also ensures sustained catalyst activity over multiple cycles.

6.2. Future Scope

The thesis work is focused on design, development and synthesis of immobilized organic catalysts and their exploration for conversion of couple of platform molecules to fuel, fuel additive and chemicals. There are huge number of platform molecules exist and all of them can be transformed into value added products. Therefore, design of better catalysts and development of techno-economical processes have much more room.

- There is a lot of scope for the development of more active and cheap catalysts by allowing functional group modification and considering different immobilising agents.
- The fuel precursors can be transformed into liquid alkanes through hydrodeoxygenation. For hydrodeoxygenation processes a multisite catalyst having ability to hydrogenate and dehydrate is required. Although, there are

several such type of catalysts systems has been reported but they were just conceptual and not tested on large scale. Consequently, there are much more opportunities to develop a catalytic process for various biomass transformations with scale up.

- Developing processes that utilize earth-abundant, cost-effective feedstocks such as hemicellulose, cellulose and lignin will enable the sustainable production of bulk chemicals.
- From a practical standpoint, it is crucial to develop downstream applications or markets for Bisguaiacol and its derivatives which offer a greener alternative to Bisphenol to offset their high production costs and justify the current research efforts. Currently, guaiacol have much more costly than phenol, therefore there is need to put effort on developing technology that will produce guaiacol in economical way.
- Bisguaiacol derivatives can further undergo hydrodeoxygenation to form cyclic compounds which can be potential fuel candidates. For hydrodeoxygenation processes a multisite catalyst having ability to hydrogenate and dehydrate is required. Astonishingly, hydrodeoxygenation of Bisguaiacol derivatives to cyclic compound is a very less studied area thus it is an open opportunity and worthwhile to put efforts on development of catalysts.
- Identifying suitable applications for converting furfural, 2-methylfuran, and guaiacol to value added products where their unique properties provide advantages over petroleum-based platform chemicals, is highly needed. Beyond their potential as fuels, fuel additives, and commodity chemicals, these platform molecules and their derivatives could also be explored for applications in pharmaceuticals and specialty chemicals.
- Since, all the transformations presented in this thesis are performed on heterogeneous catalysts thus there is an opportunity to develop successful continuous processes.

ABSTRACT

Name of the Student: Tarade Komal Pratap **Registration No.: 10CC20A26051**
Faculty of Study: Chemical Sciences **Year of Submission: 2024**
AcSIR academic centre/CSIR Lab: **Name of the Supervisor(s): Dr. Sanjay P. Kamble**
CSIR-National Chemical Laboratory, Pune **Dr. Chandrashekhar V. Rode**

Title of the thesis: Design of Novel, Heterogeneous Catalysts for Transformation of Bioderived Platform Molecules to Chemicals and Fuels

The thesis titled **"Design of Novel, Heterogeneous Catalysts for the Transformation of Bio-Derived Platform Molecules to Chemicals and Fuels"** is composed of seven chapters. **Chapter 1** provides a general introduction to biomass, biorefineries, bio-derived platform molecules, and a review of the literature on the conversion of these molecules into value-added chemicals and fuel precursors. This chapter also delves into the fundamentals of catalysis, including various types of catalysts, with a focus on the synthesis of heterogeneous catalysts as documented in the literature. **Chapter 2** explores the Knoevenagel condensation of furfural with acetylacetone to synthesize 3-(2-furylmethylene)-2,4-pentanedione (FMP), a precursor for jet fuel. The study identifies a novel heterogeneous catalyst, pyridine-immobilized magnetic silica (Fe_3O_4@SiO_2-Py), as an efficient, green, and solid base catalyst for this reaction. **Chapter 3** describes a two-step synthesis of saturated cyclic ethers. This process involves acid-catalyzed condensation of aldehydes with 2-methylfuran, followed by selective hydrogenation of the furan ring of the condensation products. A novel, recyclable magnetic solid acid catalyst, [Fe_3O_4@SiO_2-Pr-Py-H][$2HSO_4^{2-}$], was developed and successfully employed for the condensation of 2-methylfuran with various aldehydes and ketones. **Chapter 4** discusses the preparation of a novel silica-supported sulfonic acid-functionalized isonicotinic acid catalyst, SO_3H-INA@SiO_2. This heterogeneous solid acid catalyst was used for the solvent-free conversion of 2-methylfuran into diesel fuel precursors with C_{15} and C_{20} units via a tandem ring-opening and condensation sequence. **Chapter 5** focuses on C-C bond-forming reactions between guaiacol and various aldehydes, employing a systematically synthesized sulfonic acid-functionalized, magnetically separable heterogeneous Brønsted acid catalyst, [Fe_3O_4@SiO_2-$(Pr)_3$-N-Bu-SO_3H][HSO_4^-]. This catalyst was effectively applied in the synthesis of Bisguaiacol-F through the condensation of aqueous formaldehyde with two molecules of guaiacol, and its catalytic activity was further tested with different aldehydes to produce Bisguaiacol derivatives. **Chapter 6** presents the summary of the research and discusses the future scope of the work.

This thesis provides a comprehensive exploration of the development and application of novel heterogeneous catalysts in the transformation of bio-derived platform molecules into valuable chemicals and fuels.

List of Publications and Conference

List of Publications

1. **Komal Tarade**, Sanjay Kamble, Chandrashekhar Rode, Novel Sulfonic Acid Functionalized Silica Supported Isonicotinic Acid Catalyst for Conversion of 2-Methylfuran to Diesel Fuel Precursors, *Catalysis Letters*, **2023**, 154, 1511-1520. https://doi.org/10.1007/s10562-023-04383-2 *(Impact factor: 2.3)*

2. **Komal Tarade**, Suhas Shinde, Chandrashekhar Rode, Magnetically separable catalyst for condensation of renewable aldehydes and 2-methylfuran to saturated cyclic oxygenates, *Fuel Processing Technology*, **2020**, 197, 106191. https://doi.org/10.1016/j.fuproc.2019.106191 *(Impact factor: 7.2)*

3. **Komal Tarade**, Suhas Shinde, Sachin Sakate, Chandrashekhar Rode, Pyridine immobilized on magnetic silica as an efficient solid base catalyst for Knoevenagel condensation of furfural with acetyl acetone, *Catalysis Communications*., **2019**, 124, 81–85. https://doi.org/10.1016/j.catcom.2019.03.005 *(Impact factor: 3.7)*

4. **Komal Tarade**, Chandrashekhar Rode, Sanjay Kamble, Magnetically Separable Brønsted Acid Catalyst for Synthesis of Bisguaiacol-F, (Under review to *New Journal of Chemistry,* **2024**)

Publication Other than Thesis

1. Suhas Shinde, **Komal Tarade**, Gaurav Mitra, Chandrashekhar Rode, Integration of Heterogeneous Acid and Base Catalysis for Clean Synthesis of Jet-Fuel Precursor from Carbohydrates, Chemistry Select., 2020, *5*, 392 -400. https://doi.org/10.1002/slct.201903735 *(Impact factor: 2.109)*

Conference Presentations (Poster/Oral)

1. **Komal Tarade,** Chandrashekhar Rode "Catalytic carbon upgradation of bioderived platform molecule to transportation fuel national conference New Frontiers in Chemistry from Fundamentals to Applications (NFCFA-2019) held at BITS Pilani KK Birla, Goa 20th to 22nd December 2019.

Abstract

At present transportation fuels are largely produced from crude oil however, regrettably the sources of crude oil are tending to diminish in near future. In addition, during refining process of crude oil huge amount of CO_2 is expelled into the air that causes serious air pollution. Fortunately, these threats can be overcome by utilizing lignocellulosic biomass which is as a sustainable carbon source and green alternative to crude oil. Some important platform molecules are produced by the hydrolysis and dehydration of lignocellulosic biomass. To produce diesel-range long chain alkanes from platform molecules, it needs to undergo carbon up gradation process via acid or base catalyzed C−C bond formation followed by hydrodeoxygenation. Knoevenagel condensation reaction and hydroxyalkylation alkylation reaction are used for formation of long chain alkanes. Our novel heterogeneous pyridine immobilized magnetic silica (Fe_3O_4@SiO_2-Py) was found to be an efficient, greener and heterogeneous solid base catalyst for the Knoevenagel condensation of furfural with acetyl acetone under optimized reaction conditions. The Knoevenagel condensation product, 3-(2-furylmethylene)-2,4-pentanedione (FMP), a jet fuel precursor which was produced in high yield with good conversion of furfural at 100 oC within a period of 4h. Fe_3O_4@SiO_2-Py catalyst showed excellent stability and recyclability without losing its initial activity. By continuing this work, Lewis base Fe_3O_4@SiO_2-Py catalyst was modified to Brønsted acid [Fe_3O_4@SiO_2-Pr-Py-H][$2HSO_4^{2-}$] catalyst by sulphonation process which was then employed for the condensation of 2-methylfuran with formaldehyde to achieve very good yield and conversion at 65 ^{o}C in 3h. 5% Pd/C was found to be very active and selective catalyst for furan ring hydrogenation without formation of ring opened products under very low hydrogen pressure at room temperature with good yield.

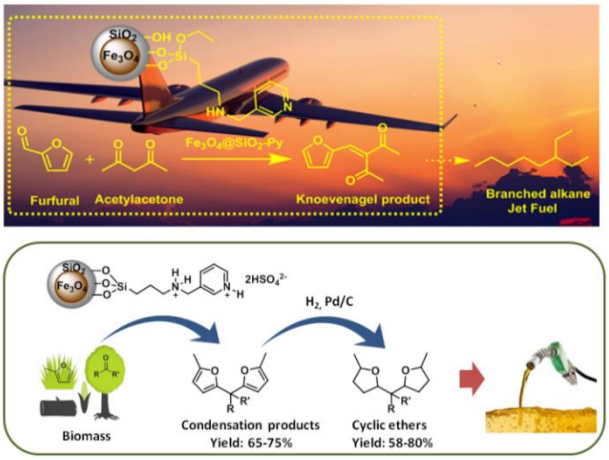

Scheme 1. Synthesis of fuel from bioderived platform molecules

2. **Komal Tarade,** Chandrashekhar Rode, Sanjay Kamble "Catalytic carbon upgradation of bioderived platform molecule to transportation fuel" NCL-RF conference held at CSIR-National Chemical Laboratory, Pune 29th to 30nd November 2022 and received **First prize** from CEPD division.

Abstract

At present, transportation fuels are predominantly derived from crude oil. However, the availability of crude oil is expected to decline in the near future. Additionally, the refining process of crude oil releases a significant amount of CO_2 into the atmosphere, contributing to severe air pollution. Fortunately, these challenges can be addressed by utilizing lignocellulosic biomass, a sustainable carbon source and a green alternative to crude oil. To produce diesel-range long-chain alkanes from platform molecules, a carbon upgrading process involving acid or base-catalyzed C−C bond formation followed by hydrodeoxygenation is required. The Knoevenagel condensation reaction and hydroxyalkylation alkylation reaction are commonly used for the formation of long-chain alkanes. Our novel heterogeneous pyridine-immobilized magnetic silica (Fe_3O_4@SiO_2-Py) has proven to be an efficient, greener, and heterogeneous solid base catalyst for the Knoevenagel condensation of furfural with acetylacetone under optimized reaction conditions. The Knoevenagel condensation product, 3-(2-furylmethylene)-2,4-pentanedione (FMP), a precursor to jet fuel, was produced in high yield with good conversion of furfural at 100°C within a period of 4 hours. The Fe_3O_4@SiO_2-Py catalyst demonstrated excellent stability and recyclability without losing its initial activity. Building on this work, the Lewis base Fe_3O_4@SiO_2-Py catalyst was modified into a Brønsted acid [Fe_3O_4@SiO_2-Pr-Py-H][$2HSO_4^{2-}$] catalyst through a sulfonation process. This modified catalyst was then employed for the condensation of 2-methylfuran with formaldehyde, achieving very good yield and conversion at 65°C in 3 hours. Additionally, 5% Pd/C was found to be a

highly active and selective catalyst for the hydrogenation of the furan ring, without forming ring-opened products, under very low hydrogen pressure at room temperature, with good yield.

3. **Komal Tarade**, Chandrashekhar Rode and Sanjay Kamble "Synthesis of Cyclic Oxygenates as Potential Fuel Precursors International Chemical Engineering Conference Energy, Environment, and Sustainability (ICECEES) held at Indian Institute of Technology, Roorkee, 15th to 17th February 2024.

Abstract

The saturated cyclic ethers produced from biomass derived aldehydes and 2-methylfuran are the potential diesel fuel candidates. The synthesis of saturated cyclic ethers is a two-step process which involves acid catalyzed condensation of aldehydes with 2-methylfuran and the subsequent selective furan ring hydrogenation of the condensation products. Here, we designed a novel recyclable magnetic solid acid catalyst such as $[Fe_3O_4@SiO_2\text{-}Pr\text{-}Py\text{-}H][2HSO_4^{2-}]$ and employed for the condensation of 2-methylfuran with formaldehyde as model substrates and reaction parameters were optimized. Under the set reaction conditions, condensation of 2-methylfuran with several other aldehydes were also successfully achieved with very good yields. Further, several supported noble metal catalysts were screened to in order to find suitable catalyst system for selective furan ring hydrogenation of condensation products. Amongst those, 5% Pd/C was found to be very active and selective for furan ring hydrogenation without formation of ring opened products under very low hydrogen pressure at room temperature. Prepared catalysts were thoroughly characterized with sophisticated techniques.

4. **Komal Tarade**, Chandrashekhar Rode, Sanjay Kamble "Catalytic carbon upgradation of bioderived platform molecule to transportation fuel" on Science Day 2024, held in at CSIR-National Chemical Laboratory, Pune.

Abstract

Currently, transportation fuels are primarily sourced from crude oil. However, crude oil reserves are anticipated to diminish in the near future. Moreover, the refining of crude oil emits substantial amounts of CO_2 into the atmosphere, significantly contributing to air pollution. These issues can be mitigated by using lignocellulosic biomass, a sustainable carbon source and an environmentally

friendly alternative to crude oil. To produce diesel-range long-chain alkanes from platform molecules, a process of carbon upgrading through acid or base-catalyzed C−C bond formation followed by hydrodeoxygenation is essential. The Knoevenagel condensation and hydroxyalkylation-alkylation reactions are key methods for forming long-chain alkanes. Our innovative heterogeneous pyridine-immobilized magnetic silica (Fe_3O_4@SiO_2-Py) has been demonstrated as an efficient, eco-friendly, and robust solid base catalyst for the Knoevenagel condensation of furfural with acetylacetone under optimized conditions. The product of this condensation, 3-(2-furylmethylene)-2,4-pentanedione (FMP), a precursor for jet fuel, was produced in high yield with excellent conversion of furfural at 100°C within 4 hours. The Fe_3O_4@SiO_2-Py catalyst exhibited remarkable stability and recyclability, maintaining its initial activity throughout multiple cycles. Building on this success, we modified the Lewis base Fe_3O_4@SiO_2-Py catalyst into a Brønsted acid catalyst, [Fe_3O_4@SiO_2-Pr-Py-H][$2HSO_4^{2-}$], via a sulfonation process. This modified catalyst was effectively used for the condensation of 2-methylfuran with formaldehyde, achieving high yield and conversion at 65°C in just 3 hours. Additionally, 5% Pd/C proved to be a highly active and selective catalyst for the hydrogenation of the furan ring, avoiding ring-opening side reactions, under low hydrogen pressure at room temperature, with excellent yield.

5. **Komal Tarade**, Chandrashekhar Rode, Sanjay Kamble “परिवहन ईंधन के लिए जैव-व्युत्पन्न अणुओं का उत्प्रेरक कार्बन उन्नयन” ‘राष्ट्रीय राजभाषा वैज्ञानिक संगोष्ठी’ held at Aagharkar Research Institute, Pune 3rd – 4th April 2024.

Abstract

वर्तमान में परिवहन ईंधन बड़े पैमाने पर कच्चे तेल से उत्पादित किया जाता है, हालांकि, अफसोस की बात है कि निकट भविष्य में कच्चे तेल के स्रोत कम होते जा रहे हैं। इसके अलावा, कच्चे तेल की परिष्कृत प्रक्रिया के दौरान भारी मात्रा में CO_2 हवा में उत्सर्जित होती है जो गंभीर वायु प्रदूषण का कारण बनती है। सौभाग्य से, लिग्नोसेल्यूलोसिक जैवद्रव्य का उपयोग करके इन खतरों को दूर किया जा सकता है जो एक टिकाऊ कार्बन स्रोत और कच्चे तेल के हरित विकल्प के रूप में है। कुछ महत्वपूर्ण अणु लिग्नोसेल्यूलोसिक जैवद्रव्य के हाइड्रोलिसिस और निर्जलीकरण द्वारा

निर्मित होते हैं। प्लेटफ़ॉर्म अणुओं से डीज़ल श्रेणी लंबी श्रृंखला वाले अल्केन्स का उत्पादन करने के लिए, इसे हाइड्रोडीऑक्सीजनेशन के बाद अम्ल या क्षार उत्प्रेरित सी-सी बंध गठन के माध्यम से कार्बन उन्नयन प्रक्रिया से गुजरना पड़ता है। लंबी श्रृंखला वाले अल्केन्स के निर्माण के लिए नोएवेनगेल संघनन प्रतिक्रिया और हाइड्रॉक्साइलकेलेशन एल्किलेशन प्रतिक्रिया का उपयोग किया जाता है। हमारा नया विषम पाइरीडीन स्थिर चुंबकीय सिलिका (Fe_3O_4@SiO_2-Py) अनुकूलित प्रतिक्रिया स्थितियों के तहत एसिटाइल एसीटोन के साथ फरफुरल के नोएवेनगेल संघनन के लिए एक कुशल, हरित और विषम ठोस आधार उत्प्रेरक पाया गया। नोएवेनगेल संघनन उत्पाद, 3-(2-फ्यूरिलमेथिलीन)-2,4-पेंटेनेडियोन (एफएमपी), एक जेट ईंधन अग्रदूत जो 4 घंटे की अवधि के भीतर 100 डिग्री सेल्सियस पर फरफुरल के अच्छे रूपांतरण के साथ उच्च उपज में उत्पादित किया गया था। Fe_3O_4@SiO_2-Py उत्प्रेरक ने अपनी प्रारंभिक गतिविधि खोए बिना उत्कृष्ट स्थिरता और पुनर्चक्रण क्षमता दिखाई। इस कार्य को जारी रखते हुए, लुईस क्षार Fe_3O_4@SiO_2-Py उत्प्रेरक को सल्फोनेशन प्रक्रिया द्वारा ब्रोंस्टेड अम्ल [Fe_3O_4@SiO_2-Pr-Py-H][$2HSO_4^{2-}$] उत्प्रेरक में संशोधित किया गया, जिसे बाद में फॉर्मेल्डिहाइड के साथ 2-मिथाइलफ्यूरन के संघनन के लिए नियोजित किया गया। 3 घंटे में 65 डिग्री सेल्सियस पर बहुत अच्छी उपज और रूपांतरण प्राप्त करने के लिए। 5% पीडी/सी को अच्छी उपज के साथ कमरे के तापमान पर बहुत कम हाइड्रोजन दबाव के तहत रिंग खोले गए उत्पादों के गठन के बिना फ्यूरान रिंग हाइड्रोजनीकरण के लिए बहुत सक्रिय और चयनात्मक उत्प्रेरक पाया गया।

Catalysis Letters
https://doi.org/10.1007/s10562-023-04383-2

Novel Sulfonic Acid Functionalized Silica Supported Isonicotinic Acid Catalyst for Conversion of 2-Methylfuran to Diesel Fuel Precursors

Komal P. Tarade[1,2] · Sanjay P. Kamble[1,2] · Chandrashekhar V. Rode[1,2]

Accepted: 4 June 2023

Abstract

Polyfuranic compounds produced after carbon up-gradation of 2-methylfuran by acid catalyzed C–C bond forming reactions when undergo hydro-deoxygenation produce diesel fuel. Herein, we prepared a simple and novel silica supported sulfonic acid functionalized isonicotinic acid SO_3H-INA@SiO_2 catalyst by treating isonicotinic acid with chlorosulphonic acid followed by heterogenization on silica. This heterogeneous solid acid catalyst was explored for the solvent free conversion of 2-methylfuran to diesel fuel precursors of C_{15} and C_{20} units via tandem ring opening followed by condensation sequence. Under optimized reaction conditions, SO_3H-INA@SiO_2 was able to convert, 2-methylfuran completely into condensation products such as 5,5-bis(5-methylfuran-2-yl)pentan-2-one **(1)** and 2,4,4-tris(5-methylfuran-2-yl)pentan-1-ol **(2)** with 19% and 67% yields, respectively. The heterogeneous SO_3H-INA@SiO_2 catalyst was successfully recycled up to six consecutive runs without loss of its activity. The SO_3H-INA@SiO_2 catalyst offered superior activity as compared to the commercially available -SO_3H functionalized resins. Superior activity of the prepared catalyst could be attributed for its higher acidity, smaller particle size and high surface area. Structure of the prepared catalyst was confirmed by FTIR and solid state NMR. Total acidity of the prepared catalyst was determined by acid–base titration.

Graphical Abstract

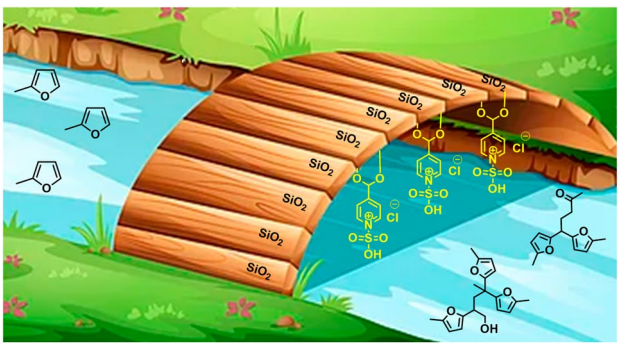

Keywords Diesel fuel · Heterogeneous catalyst · Ionic solid · Solid acid · 2-Methylfuran

✉ Sanjay P. Kamble
sp.kamble@ncl.res.in

✉ Chandrashekhar V. Rode
cv.rode@ncl.res.in; cvrode8@gmail.com

[1] Chemical Engineering and Process Development Division, CSIR-National Chemical Laboratory, Dr. Homi Bhabha Road, Pune 411008, India

[2] Academy of Scientific and Innovative Research, CSIR-HRDC Campus, Sector 19, Kamla Nehru Nagar, Ghaziabad, Uttar Pradesh 201002, India

1 Introduction

Currently, energy and chemicals consumed across the globe almost entirely rely on fossil resources. Nevertheless, these resources are exhausting much faster than expected and would be extinct in near future due to their expeditious consumption in transportation and industrial sectors. At the same time, formation of fossil-based resources requires

Published online: 10 August 2023

millions of years through natural anaerobic decomposition of buried organisms [1]. In addition to that, during refining of fossil resources huge amount of carbon dioxide (CO_2) is being continuously thrown out into the environment which not only enhances global warming but also known to inflict serious health issues to living organisms [2]. Hence, for last few decades, primary challenge in front of the scientists and technologists is to find out greener option for energy, fuels, chemicals and materials.

In recent years, biomass has emerged as one of the sustainable alternatives to fossil resources since it is a renewable source of organic carbon and available in high abundance on earth. Indeed, abundantly available lignocellulosic biomass has complex structure comprising cellulose, hemicellulose and polymeric aromatics (lignin). Cellulose (polymeric C_6 sugars) and hemicellulose (polymeric C_5 sugars) are very tightly bound with lignin thus, separation of these three components is of utmost importance. After pre-treatment of lignocellulosic biomass, a hemicellulosic part decomposes into C_5 (e.g. xylose and arabinose) and C_6 sugars (e.g. mannose, galactose and rhamnose) [1]. The C_5 sugars (xylose and arabinose) present in agricultural and forest residues can be dehydrate in presence of acid to form furfural [3]. Furfural is the most valuable industrial chemical whose current production volume is more than 200,000 tons/year [4, 5]. Furfural can be further converted into 2-methylfuran as a major product by hydrogenolysis at 250 °C [6, 7]. 2-Methylfuran is an electron rich aromatic ring which undergoes selective electrophilic substitution at the C_4 position in presence of acid catalysts [8]. 2-Methylfuran is hydrophobic in nature which allows its easy separation from water at room temperature, thus it can be used as a product extraction solvent [9]. Hydroxyalkylation-alkylation of 2-methylfuran with aldehydes/ketones/active alcohols have been well studied as these products have wide range of industrial applications [10]. These products can be processed for the production of bio-fuels via hydrodeoxygenation (HDO) reaction [11]. In this context, numerous catalytic systems were investigated for hydroxyalkylation-alkylation of 2-methylfuran which includes conc. H_2SO_4, acidic resins [8, 12, 13], sulfonic acid functionalized silica [14–19], carbocatalysts [20, 21], ionic liquids [10], supported phosphotungstic acid [22], Mo–Zr-MCM-41 [23], $AuCl_3$ [24, 25], zeolites [26], $Cu(OTf)_2$ [27], TFA-ZrO_2 [28], and molecular iodine [29].

In 2011, Corma et al. [8] reported for the first time, the tandem conversion of sylvan (aqueous 2-methylfuran) to produce diesel fuel precursor of C_{15} unit using sulfonic acid functionalized solids (e.g. Amberlyst-15, *p*TsOH) and liquid acids (e.g. conc. H_2SO_4). In 2015, the similar cascade reaction sequence was attempted by Yati et al. over Amberlyst-15, in which they found that addition of water promotes the formation of diesel precursors of C_{15} unit while without water, diesel precursors of C_{20} unit can be selectively produced [30]. However, they observed that without water, conversion of 2-methyfuran reached maximum up to 37% and addition of water leads to lowering of conversion. In 2018, Gebresillase et al. [31] reported a sulfonic acid functionalized silica such as KCC1SO_3H for selective tandem conversion of 2-methylfuran to C_{15} diesel fuel precursor by performing reaction at 80 °C for longer reaction time of 48 h.

In continuation of our recent work on new -SO_3H functionalized heterogeneous catalysts systems [18], we further developed SO_3H-INA@SiO_2 as a simple, novel and highly active heterogeneous acid catalyst and explored it for the tandem solvent free conversion of 2-methylfuran to precursors of kerosene-diesel range products (C_{15}–C_{20}) (Scheme 1). By using SO_3H-INA@SiO_2 catalyst, almost complete conversion of 2-methylfuran was achieved with high yield of diesel fuel precursors of C_{15} and C_{20} units. The reaction parameters such as effects of catalyst loading, reaction time on the conversion of 2-methylfuran have been studied in detail.

2 Experimental

2.1 Materials

Chemicals such as 2-methylfuran, 3-pyridinecarboxylic acid, conc. H_2SO_4, para-toluenesulfonic acid and chlorosulfonic acid were obtained from Sigma-Aldrich, India. Commercially available sulfonic acid functionalized resins such as Amberlyst-15, Amberlyte IR-120, Thermax resin, Dowex 50WX8 and Lanxess K11311S, were also obtained from Sigma-Aldrich, India. Solvents such as ethanol, ethyl acetate, petroleum ether and silica gel (230–400 mesh) were purchased from Chem Labs, India. Catalysts such as Sn-Mont and Zr-Mont were prepared according to the reported procedure [32, 33].

2.2 Catalyst Preparation

2.2.1 Synthesis of Ionic Solid, SO_3H-INA

To a solution of chlorosulfonic acid (1.8 mL) in ethanol (25 mL), 3-pyridine carboxylic acid (2 g) was added at room temperature under continuous stirring for 24 h. Thereafter, solvent from the resultant reaction mixture was removed on rotary evaporator to dryness to obtain a white solid (3 g).

2.2.2 Synthesis of Silica Supported Ionic Solid SO_3H-INA@SiO_2

To a stirred solution of ionic solid, SO_3H-INA (1 g) dissolved in ethanol (25 mL), silica gel (1 g, 230–400 mesh) was added portion wise and then resultant mixture was

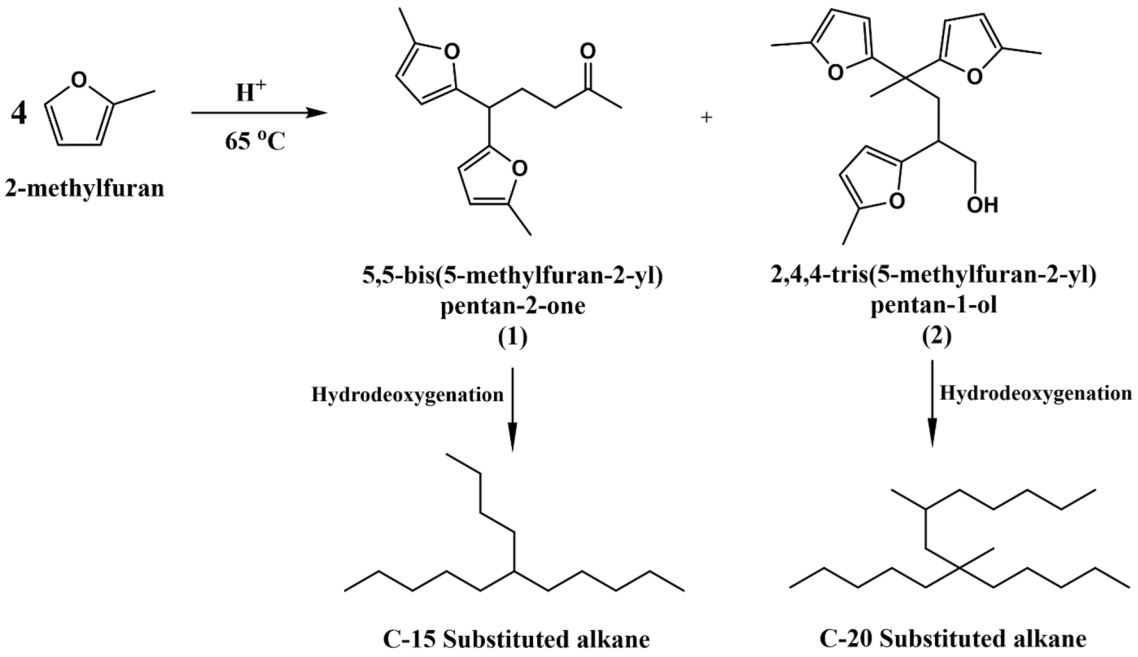

Scheme 1 Synthesis of diesel fuel precursors from 2-methylfuran

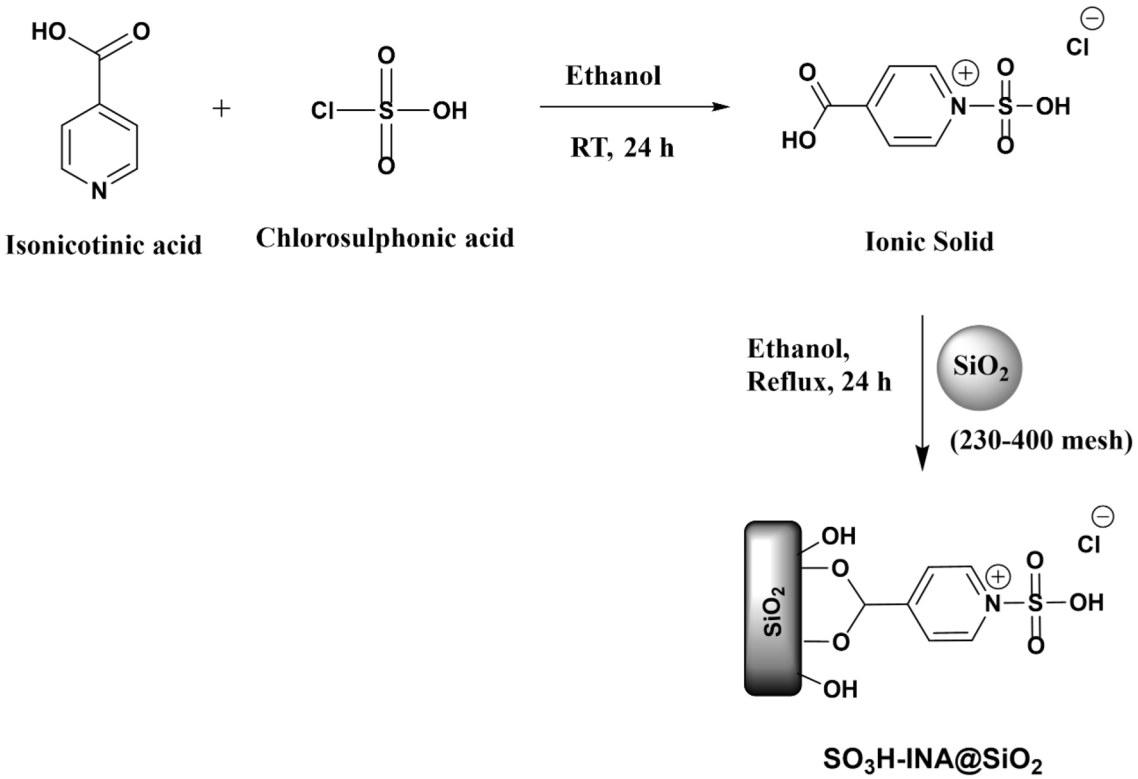

Scheme 2 Synthesis of SO_3H-INA@SiO_2

refluxed for 24 h. Thereafter, mixture was cooled to room temperature, filtered, washed with ethyl acetate (20 mL × 3) and dried well on rotary evaporator at 45 °C for 2–3 h to get white powder (Scheme 2). The surface area and particle size of SO_3H-INA@SiO_2 was observed to be 523 m^2/g and 48 µm, respectively.

2.3 Determination of Catalyst Acidity

Aqueous solution of sodium chloride (0.05 mol/g, 30 mL) was added to the SO_3H-INA@SiO_2 catalyst (0.250 g) and the resultant mixture was stirred for 1 h at room temperature under ultrasonic conditions. After centrifugation, the supernatant solution was titrated against aqueous solution of sodium hydroxide (0.05 mol/g) using phenolphthalein indicator [34, 35] giving total acidity as 0.031 mol/g. Acidity of SO_3H-INA@SiO_2 catalyst after reuse was determined to be 0.030 mol/g. Total acidity of other sulfonic acid functionalized solid acid catalysts was also estimated by similar acid–base titration method and the results are presented in Table 1.

2.4 Catalyst Test

Mixture of 2-methylfuran (1 g, 0.012 mol) and SO_3H-INA@SiO_2 (0.1 g) was stirred at 65 °C for 7 h after that the catalyst was separated by filtration and filtrate was diluted with ethyl acetate (20 mL). Dilute reaction mixture was further washed with water (20 mL × 1) and brine solution (20 mL × 1). The separated organic layer was dried over anhydrous sodium sulphate and evaporated on a rotary evaporator to get crude oil, the later was subjected to column chromatography. 5,5-bis(5-methylfuran-2-yl)pentan-2-one **(1)** was eluted by 100% petroleum ether and 2,4,4-tris(5-methylfuran-2-yl) pentan-1-ol **(2)** was eluted by ethyl acetate: petroleum ether (2:98; v/v). Eluted fractions were evaporated to remove solvents to get greenish yellow liquid of **1** and yellowish-brown liquid of **2**. After the reaction, catalyst was washed subsequently by ethyl acetate (10 mL × 1) and dried in oven at 45 °C for 3-4 h prior to reuse.

2.5 Analysis of the Reaction Products

Primary analysis of the reaction crude was performed by thin-layer chromatography using Merck 5554 aluminum-backed silica plates and the compounds were observed under UV light (254 nm) and phosphomolybdic acid stain. The conversion of reactants and selectivity of products were calculated using Agilent 7890B Gas Chromatography with

Table 1 Catalyst screening for conversion of 2-methylfuran to diesel fuel precursors

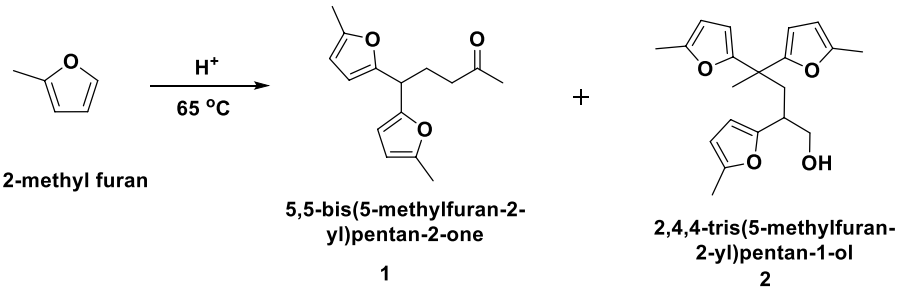

Entry	Catalyst	Acidity (mol/g)	2-Methylfuran conversion (%)[c]	Selectivity (%)[d]		
				1	**2**	Unidentified product
1[a]	Conc. H_2SO_4	–	97	65	32	03
2[b]	p-TSA	–	92	69	28	03
3	Amberlyst-15	0.019	95	68	28	04
4	Amberlyte IR-120	0.016	90	62	31	07
5	Dowex-50WX8 resin	0.018	93	70	25	05
6	Lanxess K11311S resin	0.018	96	63	32	05
7	Thermax resin	0.019	95	67	27	06
8	SO_3H-INA	0.046	99	20	72	08
9	SO_3H-INA@SiO_2	0.031	99	21	74	05
10	Zr-Mont	–	60	10	75	15
11	Sn-Mont	–	35	9	73	18

Reaction conditions: 2-methylfuran (1 g, 0.012 mol), catalyst (0.1 g), 65 °C, 7 h

[a,b]10 mol% of catalyst was used

[c,d]Conversion of 2-methylfuran and products selectivity was determined by using GC

a flame ionization detector and HP-5 column. Pure products were characterized and confirmed by ^{1}H NMR and ^{13}C NMR (500 MHz) using DMSO-d6 (0.01%, TMS) as a solvent on a 200 MHz frequency Bruker instrument (Refer Supporting Information). The products were also confirmed using QP-Ultra 2010 GCMS Shimadzu instrument, RTX-5 column, and helium as carrier gas, electrospray ionization mode, and an ionization source temperature of 200 °C.

3 Results and Discussion

3.1 Catalyst Characterization

3.1.1 FTIR Analysis

Functional groups present in isonicotinic acid, SiO_2, SO_3H-INA and SO_3H-INA@SiO_2 were observed by using FTIR analysis (Fig. 1). Characteristic band for C=O bond stretching was observed at 1700 cm^{-1} for isonicotinic acid (Fig. 1a). For SO_3H-INA, bands observed at 1090–1300, 1600, 1700 and 2700–3100 cm^{-1} were attributed to S=O, C=N, C=O and –OH (SO_3H group), respectively (Fig. 1b). In case of SiO_2, a broad band observed in the range between 950–1290 cm^{-1} could be attributed to -Si–O-Si bond stretching (Fig. 1c). In case of SO_3H-INA@SiO_2 bands observed at 1090–1300, 1600, 1700 and 2700–3100 cm^{-1} were attributed to S=O, C=N, C=O and -OH (SO_3H group), respectively (Fig. 1d). Similar FTIR pattern was observed for reused SO_3H-INA@SiO_2 suggesting that reused catalyst has retained its structural features (Fig. 1e). All the characteristic bands present in SO_3H-INA were observed in SO_3H-INA@SiO_2 which suggests that SO_3H-INA species is successfully heterogenized on SiO_2 [36].

3.1.2 TGA Analysis

A thermo gravimetric analysis of fresh and reused SO_3H-INA@SiO_2 catalysts is presented in Fig. 2. For the fresh catalyst, 7% weight loss was observed up to 100 °C due to loss of physically adsorbed water. In case of reused catalyst only 2–3% weight loss was observed up to 100 °C as this catalyst was dried at 45 °C in oven under vacuum after its recovery from the reaction mixture. After that gradual weight loss, up to 46% and 52% weight loss was observed up to 400 °C for fresh and reused catalysts, respectively which could be attributed to the thermal decomposition of SO_3H-isonicotinic acid moiety of the catalyst. It has been reported that organic groups usually tend to desorb in TGA at temperatures above 260 °C [37]. On the basis of TGA results, it can be inferred that SO_3H-INA group is successfully supported on the silica.

3.1.3 Solid State NMR

The structure of SO_3H-INA@SiO_2 catalyst was confirmed by solid state ^{13}C NMR (Fig. S.3.2). A peak observed at 162.08 ppm is attributed to carbonyl carbon of carboxylic acid. A peak at 145.63 ppm is responsible for the two chemically equivalent =CH– groups which are meta to carboxylic acid group. A peak at 144.95 ppm must be a quaternary carbon where carboxylic acid is attached. A couple of peaks noticed at 128.75 and 126.81 ppm are two =CH– ortho to carboxylic acid group.

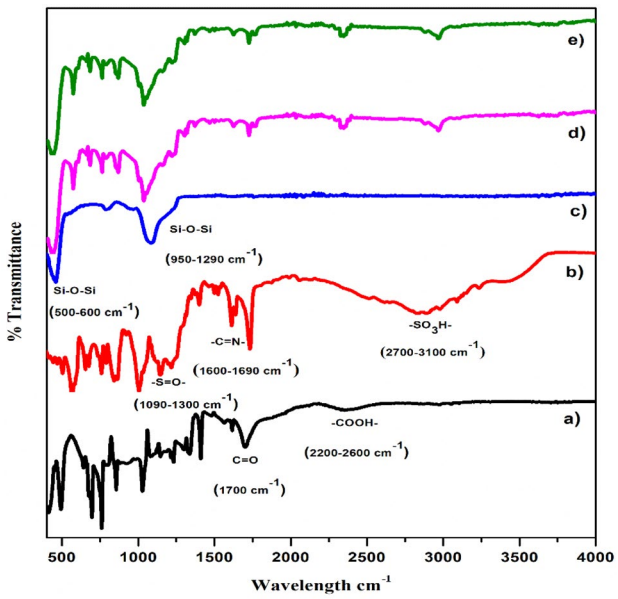

Fig. 1 FT-IR analysis of **a** isonicotinic acid, **b** SO_3H-INA, **c** SiO_2, **d** SO_3H-INA@SiO_2 and **e** SO_3H-INA@SiO_2 (reused) catalysts

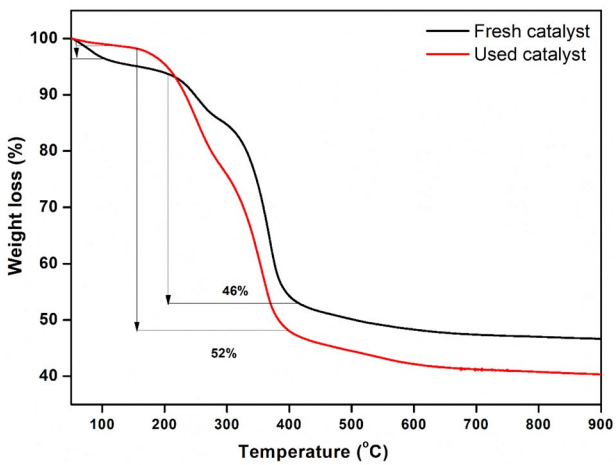

Fig. 2 TGA analysis of fresh and used SO_3H-INA@SiO_2 catalyst

3.2 Catalyst Screening for Conversion of 2-Methylfuran to Diesel Fuel Precursors

The conversion of 2-methylfuran to diesel fuel precursors (C_{15} and C_{20} unit) is aided by Brønsted acid catalysts. Therefore, several Brønsted acid catalysts were screened for self-condensation of 2-methylfuran. When aqueous solution of conc. H_2SO_4 (10 mol %) was used for the condensation reaction, 97% conversion of 2-methylfuran was noticed with 65% and 32% selectivity to products **1** and **2**, respectively (Table 1, Entry 1). The para toluene sulfonic acid (p-TSA) catalyst showed 92% conversion of 2-methylfuran with 69% selectivity to product **1** and 28% selectivity to product **2** (Table1, Entry 2). Amberlyst-15 resin offered 95% conversion of 2-methylfuran with 68% and 28% selectivity to product **1** and **2**, respectively (Table 1, Entry 3). The Amberlyte IR-120 showed somewhat less conversion (90%) of 2-methylfuran, with 62% selectivity to product **1** and 31% selectivity to product **2** (Table 1, Entry 4). Dowex-500 offered 93% conversion of 2-methylfuran with 70% and 25% selectivity to product **1** and **2**, respectively (Table 1, Entry 5). Self-Condensation reaction was further performed with Lanxess K11311S resin which showed 96% conversion of 2-methylfuran with 63% selectivity to product **1** and 32% selectivity to product **2** (Table 1, Entry 6). The Thermax resin used for this reaction offered 67% selectivity to product **1** and 27% selectivity to product **2** with 95% conversion of 2-methylfuran (Table 1, Entry 7). Astonishingly, selectivity pattern of products has been reversed when our synthesized ionic solid, [SO_3H-INA] was used which offered the highest conversion (99%) of 2-methyfuran with 20% selectivity to product **1** and 72% selectivity to product **2** (Table 1, Entry 8). Heterogeneous SO_3H-INA@SiO_2 catalyst also offered the same conversion with 21% selectivity to product **1** and 74% selectivity to product **2** (Table1, Entry 9). As compared to -SO_3H functionalized catalysts (entries 1–7), SO_3H-INA and SO_3H-INA@SiO_2 showed high selectivity towards product **2** that could be ascribed for their higher acidity. A heterogeneous Lewis–Brønsted acid catalyst such as Zr-Mont showed lower conversion (60%) of 2-methylfuran with 10%,75% and 15% selectivity to products **1**, **2** and unidentified product, respectively (Table1, Entry 10). Sn-Mont (Lewis–Brønsted acid) gave 9%, 73% and 18% selectivity to product **1**, **2** and unidentified product, respectively with 35% conversion of 2-methylfuran (Table1, Entry 11). Lewis acid sites present in Zr-Mont and Sn-Mont catalysts might have responsible for the increased formation unidentified product.

3.3 Effect of Ionic Solid SO_3H-INA (%w/w) Loading on Silica

During catalyst screening study, 50% w/w SO_3H-INA loaded on silica was used as an optimized catalyst system which offered 99% conversion of 2-methylfuran. In order to justify the selection of optimized catalyst system, lower %w/w loading of ionic solid SO_3H-INA on silica were also tested for conversion of 2-methylfuran to diesel fuel precursors (Fig. 3). With 10% w/w SO_3H-INA loaded on silica, lower conversion (65%) of 2-methylfuran was observed which was result of insufficient active sites. It was observed that as %w/w loading of ionic solid on silica increased from 20 to 50% w/w, the conversion of 2-methylfuran and yield of products **1** and **2** gradually increased. With 50% w/w SO_3H-INA loaded on silica, maximum 99% conversion of 2-methylfuran with 21% selectivity to product **1** and 74% selectivity to product **2** was observed. Therefore, for further experiments, 50% w/w SO_3H-INA loaded on silica was used as the optimized catalyst.

3.4 Effect of Reaction Time

To know the optimum reaction time for complete conversion of 2-methylfuran, reaction samples were withdrawn after every one hour and analyzed by GC. Effect of reaction time on reaction profile is presented in Fig. 4. Conversion of 2-methylfuran and selectivity to both the products increased with increase in reaction time. Maximum conversion (99%) of the 2-methylfuran was reached after 7th hour, with 21% and 74% selectivity to products **1** and **2**, respectively. Conversion of 2-methyfuran and selectivity pattern of product **1** and **2** did not vary after continuing the reaction till 8th hour.

3.5 Effect of Catalyst Amount

To find out the maximum catalyst amount needed to reach maximum conversion of 2-methylfuran, the effect of catalyst amount in the range between 5 and 15% w/w with respect to 2-methylfuran was studied (Fig. 5). With 5%w/w

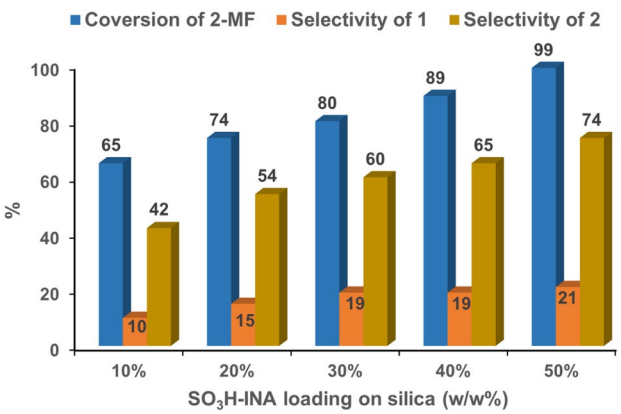

Fig. 3 Effect of Ionic solid SO_3H-INA (10–50% w/w) loading on silica on conversion of 2-methylfuran. Reaction conditions: 2-methylfuran (1 g, 0.012 mol), 10–50%w/w SO_3H-INA@SiO_2 (0.1 g), 65 °C, 7 h

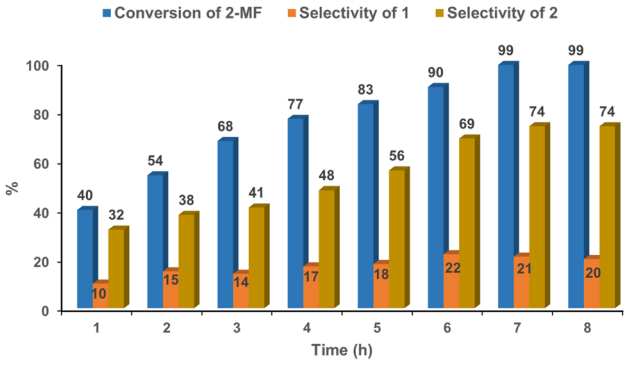

Fig. 4 Effect of reaction time on conversion of 2-methylfuran. Reaction conditions: 2-methylfuran (1 g, 0.012 mol), SO_3H-INA@SiO_2 (0.1 g), 65 °C, 1–8 h

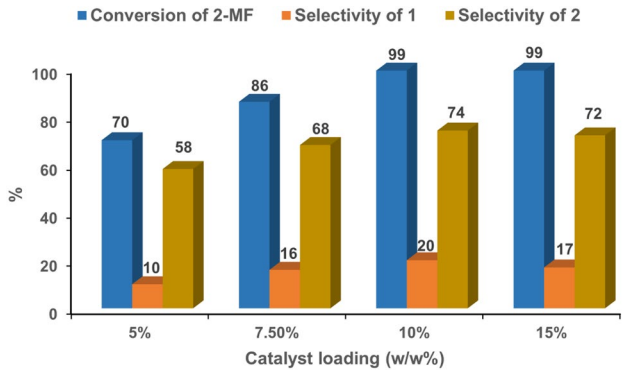

Fig. 5 Effect of catalyst amount on conversion of 2-methylfuran. Reaction conditions: 2-methylfuran (1 g, 0.012 mol), SO_3H-INA@SiO_2 (5–15% w/w), 65 °C, 7 h

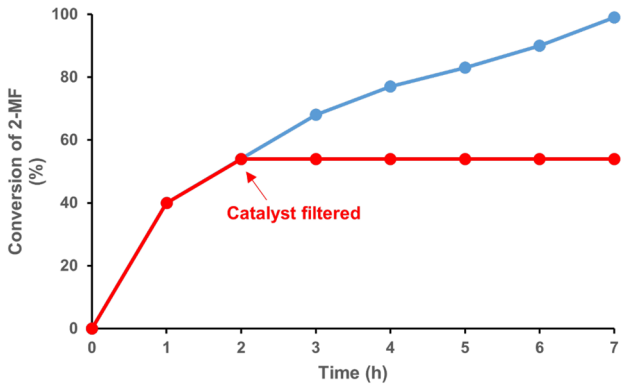

Fig. 7 Catalyst leaching test. Reaction conditions: 2-methylfuran (1 g, 0.012 mol), SO_3H-INA@SiO_2 (0.1 g), 65 °C, 7 h

of catalyst, 2-methylfuran conversion reached to 70% with 10% selectivity to product **1** and 58% selectivity to product **2**. When the amount of catalyst was increased to 10% w/w, conversion of 2-methylfuran increased to 99% with 18% and

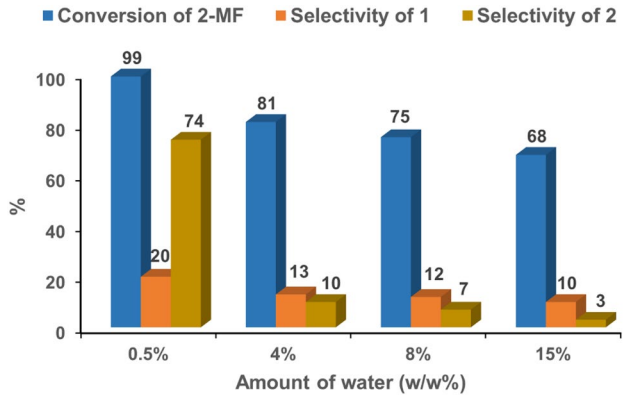

Fig. 6 Effect of water content on conversion of 2-methylfuran Reaction conditions: 2-methylfuran (1 g, 0.012 mol), SO_3H-INA@SiO_2 (0.1 g), 65 °C, 7 h

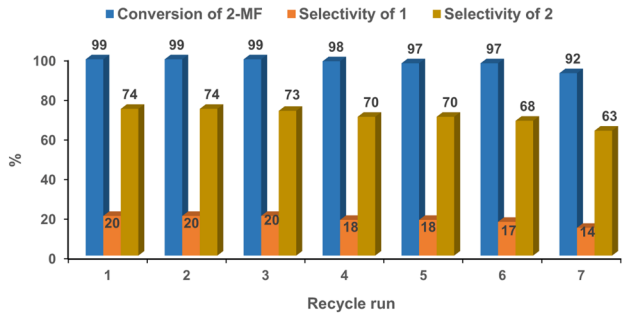

Fig. 8 Recycle study of SO_3H-INA@SiO_2. Reaction conditions: 2-methylfuran (1 g, 0.012 mol), SO_3H-INA@SiO_2 (0.1 g), 65 °C, 7 h

70% selectivity to products **1** and **2**, respectively. More than 10% w/w catalyst amount did not affect the conversion of 2-methylfuran and product distribution. From this study, it is revealed that maximum 10% w/w catalyst amount is required to reach the maximum conversion of 2-methylfuran.

3.6 Effect of Water Content

In 2015, Yati et al. [30], studied the conversion of 2-methylfuran to diesel fuel precursors with Amberlyst-15 catalyst. According to their investigation, product **1** (C_{15} unit) can be selectively formed if the reaction is performed in presence of water. On the other hand, they observed that in absence of water, product **2** can be selectively produced. Therefore, the effect of water on product distribution was also studied by adding water in the range between 0 and 15% w/w (Fig. 6). In the initial experiment without addition of water, 2-methylfuran (0.5% w/w initial moisture content) conversion was 99% with 21% selectivity to product **1** and 74% selectivity to product **2**. As extra water was added from 4 to 15%, conversion of 2-methylfuran gradually decreased to 68% and

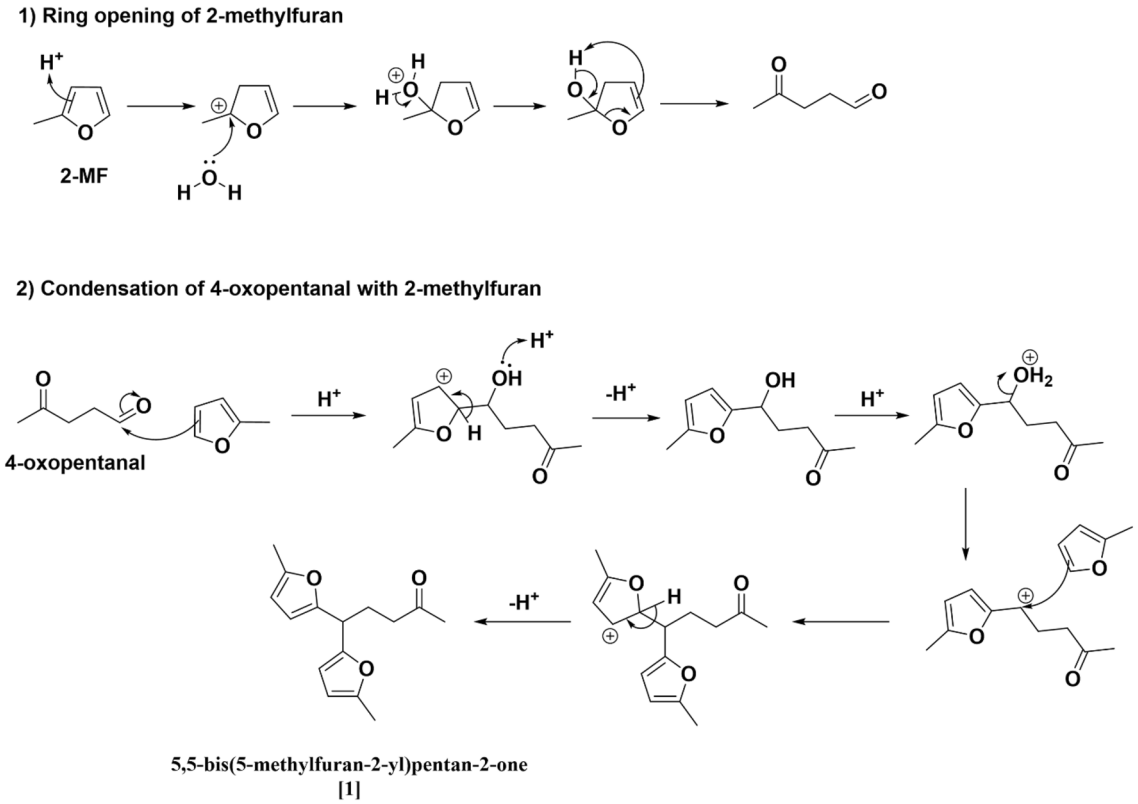

Fig. 9 Plausible reaction mechanism for condensation of 2-methylfuran to product **1**

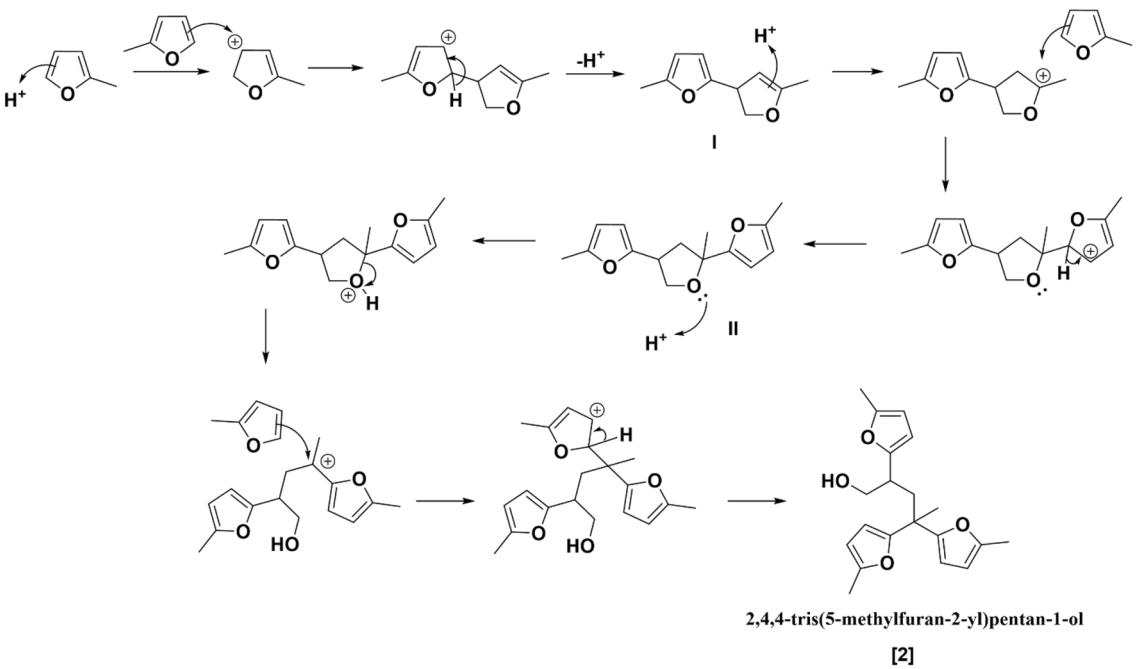

Fig. 10 Plausible reaction mechanism for condensation of 2-methylfuran to product **2**

selectivity to products **1** and **2** also significantly decreased due to enhanced formation of unidentified by-product. Addition of water to the reaction not only reduced the conversion of 2-methylfuran but also altered the selectivity pattern of both the products. After addition of water selectivity to product **1** was increased as compared to product **2** which is in agreement with the findings of Yati et al. [30].

3.7 Catalyst Leaching Test

The stability of the catalyst can be examined by leaching test experiment which was performed by following standard procedure. A reaction mixture containing 2-methylfuran (1 g, 0.012 mol) and SO_3H-INA@SiO_2 (0.1 g) was heated at 65 °C for 2 h to reach certain conversion (54%) of the 2-methylfuran. Then the reaction mixture was quickly cooled to room temperature and immediately filtered to separate the catalyst. The filtrate was then recharged into the reaction vessel and heated at 65 °C up to 7 h. It was noticed that there was no further conversion of 2-methylfuran observed after the catalyst separation which confirms that there is no leaching or loss of active sites of the catalyst during the reaction (Fig. 7).

3.8 Recycle Study of SO_3H-INA@SiO_2

The stability and reusability of the SO_3H-INA@SiO_2 catalyst was examined by performing its recycle study. For recycle experiment, after each reaction, the catalyst was separated from reaction mixture by simple filtration. The separated catalyst was subsequently washed with ethyl acetate and reused as such for the next run. The stability of SO_3H-INA@SiO_2 was evaluated by performing several recycle runs (Fig. 8). It was found that, the catalytic activity of SO_3H-INA@SiO_2 was very much consistent after being used for five times. However, during the 6th reuse, the activity of catalyst was slightly reduced, which could be attributed for partial blocking of active sites of catalyst by products deposition.

4 Plausible Reaction Pathway

Mechanistic pathway for the formation of product **1** from 2-methylfuran in presence acid catalyst is proposed in Fig. 9. In presence of an acid catalyst, the molecule of 2-methylfuran is protonated which then undergoes ring opening to form 4-oxopentanal. The protonation takes place at C_3 carbon so as to form a stable tertiary carbocation which can be further attacked by water molecule to open the ring. Then electrophilic carbonyl carbon of the aldehyde group of 4-oxapentanal is attacked by second molecule of 2-methylfuran to form a tertiary alcohol. Then tertiary alcohol gets protonated and immediately removes water leaving behind a stable secondary carbocation. The third molecule of 2-methyfuran is then added to that stable carbocation to form product **1** [30].

Formation of product **2** from 2-methylfuran in presence acid catalyst is proposed in Fig. 10. Under acidic condition, 2-methylfuran gets protonated at C_2 to form carbocation at C_3 allows nucleophilic addition of second molecule of 2-methylfuran at C_3 to form another carbocation which is stabilized by removal of a proton to form an intermediate-I. A stable tertiary carbocation formed after protonation of dihydrofuran ring to which nucleophilic addition of third molecules takes place followed by proton elimination to form intermediate-II. Tetrahydrofuran ring opening takes place after protonation which allows to form stable tertiary carbocation. Then tertiary carbocation undergoes nucleophilic addition by fourth molecule of 2-methyfuran to form the product **2**.

5 Conclusion

In summary, a simple, novel heterogeneous solid acid catalyst SO_3H-INA@SiO_2 was developed to explore solvent free conversion of bio-derived 2-methylfuran to diesel fuel precursors of C_{15} and C_{20} units. Catalytic activity of several -SO_3H functionalized acid catalysts were compared with our developed SO_3H-INA@SiO_2 catalyst, the later showed much more superior activity, due to its higher concentration of Brønsted acid sites, smaller particle size and high surface area. The SO_3H-INA@SiO_2 catalyst offered the highest conversion (99%) of 2-methylfuran with 21% selectivity to product **1** and 74% selectivity to product **2**. In addition, the heterogeneous, SO_3H-INA@SiO_2 catalyst is easily separable and reusable several times without losing its activity which is confirmed by catalyst leaching test, recycle study and acid–base titration of used catalyst. This work can inspire researchers to develop multifunctional catalysts to convert 2-methylfuran directly to diesel fuel.

6 Supporting Information Summary

Supplementary data equipped with calibration curves of reactant and products, carbon balance of condensation reaction, GC chromatogram, solid state NMR of catalyst and NMR of products.

Supplementary Information The online version contains supplementary material available at https://doi.org/10.1007/s10562-023-04383-2.

Acknowledgements Komal P. Tarade is grateful to CSIR-National Chemical Laboratory, Pune, India for providing research facilities and Academy of Scientific and Innovative Research (AcSIR), India.

References

1. Shinde SH, Hengne A, Rode CV (2020) Biomass Biofuels Biochem:1–31
2. Kirkinen J, Palosuo T, Holmgren K, Savolainen I (2008) Environ Manage 42(3):458–469
3. Mamman AS, Lee JM, Kim YC, Hwang IT, Park NJ, Hwang YK, Chang JS, Hwang JS (2008) Biofuels Bioprod Biorefin 2:438–454
4. Kottke RH (2004). Wiley Inter science, New York
5. Kamm B, Gruber PR, Kamm M (2006). Wiley-VCH, Weinheim
6. Zeitsch K (2000) vol 13. Elsevier Science, Dordrecht, pp 229–230
7. Zheng HY, Zhu YL, Teng BT, Bai ZQ, Zhang CH, Xiang HW, Li YW (2006) J Mol Catal 246:18–23
8. Corma A, Torre OD, Renz M, Villandier N (2011) Angew Chem 50:2375–2378
9. Gandini A, Belgacem MN (1997) Prog Polym Sci 22:1203–1379
10. Shinde SH, Rode CV (2017) Green Chem 19:4804
11. Balakrishnan M, Sacia ER, Bell AT (2014) Chemsuschem 7:2796
12. Li G, Li N, Wang X, Sheng X, Li S, Wang A, Cong Y, Wang X, Zhang T (2014) Energy Fuels 28:5112–5118
13. Ramírez E, Soto R, Bringué R, Iborra M, Tejero J (2020) Ind Eng Chem Res 59:20676–20685
14. VanRhijn WM, DeVos DE, Sels BF, Bossaert WD, Jacobs PA (1998) Chem Commun:317
15. Balakrishnan M, Sacia ER, Bell AT (2014) Chemsuschem 7:1078
16. Ogino I, Suzuki Y, Mukai SR (2015) ACS Catal 5:4951
17. Li H, Saravanamurugan S, Yang S, Riisager A (2015) ACS Sustain Chem Eng 3:3274
18. Tarade K, Shinde S, Rode C (2020) Fuel Process Technol 197:106191
19. Gebresillase MN, GilSeo J (2021) Appl Catal A 628:118421
20. Konwar LJ, Samikannu A, Mäki-Arvela P, Mikkola JP (2018) Catal Sci Technol 8:2449–2459
21. Li H, Deng Q, Cao X, Zheng J, Zhong Y, Zhang P, Wang J, Zeng Z, Deng S (2019) Appl Catal A 580:178–185
22. SunKwon J, Choo H, Choi JW, Jae J, Suh DJ, Lee KY, Ha JM (2019) Appl Catal A 570:238–244
23. Li T, Cheng SI, Lee JF, Jang LY (2003) J Mol Catal A Chem 198:139
24. Hashmi ASK, Schwarz L, Rubenbauer P, Blanco MC (2006) Adv Synth Catal 348:705
25. Nair V, Abhilash KG, Vidya N (2005) Org Lett 7:5857
26. Algarraa F, Corma A, Garciaa H, Primoa J (1995) Appl Catal A 128:119
27. Muthyala M, Rao VK, Kumar A (2011) Chin J Chem 29:1483
28. Zhu C, Shen T, Liu D, Wu J, Chen Y, Wang L, Guo K, Ying H, Ouyang P (2016) Green Chem 18:2165
29. Jaratjaroonphong J, Tuengpanya S, Saeeng R, Udompong S, Srisook K (2014) Eur J Med Chem 83:561
30. Yati I, Yeom M, Choi JW, Choo H, Suh DJ, Ha JM (2015) Appl Catal A Gen 495:200–205
31. Gebresillase MN, Shavi R, Seo JG (2018) Green Chem 20(22):5133–5146
32. Shinde S, Rode C (2017) Catal Commun 88:77–80
33. Shinde S, Rode C (2017) Chemsuschem 10:4090–4101
34. Suganuma S, Nakajima K, Kitano M, Yamaguchi D, Kato H, Hayashi S, Hara M (2008) J Am Chem Soc 130(38):12787
35. Thombal RS, Jadhav AR, Jadhav VH (2015) RSC Adv 5(17):12981
36. Khazaei A, Tavasoli M, Moosavi-Zara AR (2018) Res Chem Intermed 44:5893–5910
37. Ghorbani-Choghamarani A, Azadi G (2015) RSC Adv 5:9752–9758

Catalysis Communications 124 (2019) 81–85

Contents lists available at ScienceDirect

Catalysis Communications

journal homepage: www.elsevier.com/locate/catcom

Short communication

Pyridine immobilised on magnetic silica as an efficient solid base catalyst for Knoevenagel condensation of furfural with acetyl acetone

Komal Tarade, Suhas Shinde, Sachin Sakate, Chandrashekhar Rode*

Chemical Engineering and Process Development Division, CSIR-National Chemical Laboratory, Dr. Homi Bhabha Road, Pune 411008, India

ARTICLE INFO

Keywords:
Knoevenagel condensation
Furfural
Silica immobilised pyridine
Solid base
Jet fuel

ABSTRACT

Novel heterogeneous pyridine immobilised magnetic silica (Fe_3O_4@SiO_2-Py) was found to be an efficient, greener and heterogeneous solid base catalyst for the Knoevenagel condensation of furfural with acetylacetone under optimized reaction conditions. The Knoevenagel condensation product 3-(2-furylmethylene)-2,4-pentanedione (FMP), a jet fuel precursor, was produced in high yield of 85% with 94% conversion of furfural at 100 °C within a period of 4 h. Fe_3O_4@SiO_2-Py catalyst showed excellent stability and recyclability without losing its initial activity.

1. Introduction

Currently chemicals and liquid fuels are largely produced from crude oil however, the sources of crude oil will be on the verge of diminishing in near future. In addition, during crude oil refining process, huge amount of CO_2 is expelled out causing irreparable air pollution. Fortunately, these threats can be overcome by utilising lignocellulosic biomass which is as a sustainable carbon source and green alternative to crude oil [1]. Furfural is the most important platform molecule produced by the hydrolysis and dehydration of xylan contained in lignocellulosic biomass. Diesel-range long chain alkanes can be produced from furfural *via* acid or base catalyzed C–C bond formation followed by hydrodeoxygenation [2,3]. In this context, aldol, Knoevenagel condensations [4,5], Baylis – Hillman, coupling reactions [6,7], and HAA reaction [8–10] can be performed for carbon upgradation of furfural. These upgraded products are carbon-rich and can be converted into liquid hydrocarbons *via* ring-opening – dehydration – hydrodeoxygenation processes [11,12]. In particular, the Knoevenagel condensation of furfural is not studied much. For instance, Ding et al. demonstrated enzyme (lipoprotein lipase) catalyzed Knoevenagel condensation between furfural and acetyl acetone at 35 °C. However, this catalytic system required long reaction time of 48 h and gave moderate yield (76%) in dimethyl sulfoxide solvent [13]. Very recently, Appaturi et al. developed alanine functionalized MCM-41 catalyst for Knoevenagel condensation between furfural with acetyl acetone. Under the solvent-free condition and in a short reaction time (30 min) this catalyst system provided 100% selectivity to α,β-unsaturated products with 92% conversion of furfural [5]. Several organic–inorganic hybrid materials containing N-containing organic functionalities such as pyridine-functionalized porous polymers [14], DABCO based ionic liquid [15], primary amine functionalized MCM-41 [16,17] and organic polymer [18] have been found successful for the Knoevenagel condensation of active methylene compounds with aldehydes.

With this background we report a magnetically separable silica immobilised pyridine (Fe_3O_4@SiO_2-Py) (Scheme 2) as an effective solid base catalyst that shows excellent performance for the Knoevenagel condensation of furfural with acetyl acetone (Scheme 1). Fe_3O_4@SiO_2-Py catalyst showed the highest furfural conversion of 94% with 85% yield of condensation product at 100 °C in the absence of solvent. This novel catalyst showed reusability up to six times without significant decrease in activity and selectivity.

2. Experimental

2.1. Materials

Furfural, *N*,*N*-dimethylaminopyridine, furfurylamine, DBU, 4-hydroxypyridine, 3-pyridinecarbaldehyde 3-aminopropyltriethoxysilane, tetraethyl orthosilicate, $FeCl_2$ and $FeCl_3$ were purchased from Sigma-Aldrich. Sodium hydroxide, triethylamine, zinc oxide, calcium oxide and aq. ammonia (10%) were obtained from Thomas-Baker. Acetylacetone was purchased from Merk, India. Methanol, toluene, pyridine, dichloromethane, ethyl acetate petroleum ether and silica gel (230–400 mesh) were purchased from Chem Labs, India.

* Corresponding author.
E-mail address: cv.rode@ncl.res.in (C. Rode).

https://doi.org/10.1016/j.catcom.2019.03.005
Received 14 January 2019; Received in revised form 20 February 2019; Accepted 5 March 2019
Available online 05 March 2019

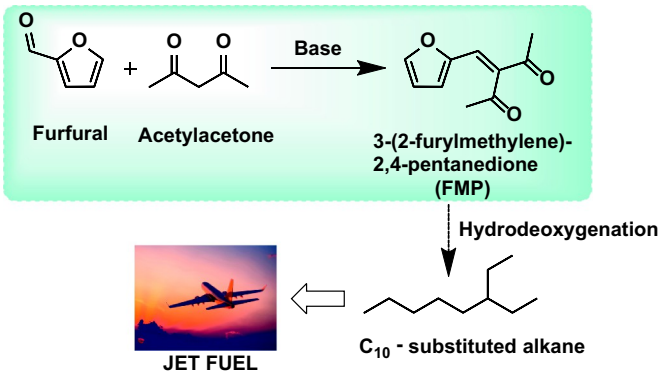

Scheme 1. Synthesis of Jet fuel precursors from furfural and acetyl acetone.

2.2. Preparation of 3-aminopropylsilica

To a solution of 3-aminopropyltriethoxysilane (3.5 g) in toluene, pyridine (1:1, 20 mL), SiO_2 (2 g, 230–400 mesh) were added. The resulting mixture was refluxed for 24 h under N_2 atmosphere after which the reaction mixture was filtered and residue was washed with toluene (20 mL × 1) and dichloromethane (20 mL × 1). The residue was dried in oven for 24 h to afford off white powder (4.8 g).

2.3. Preparation of silica-pyridine (SiO_2-Py)

Step 1(1-(pyridin-3-yl)-N-(3-(triethoxysilyl)propyl)methanimine): A mixture of 1.8 g of 3-aminopropyltriethoxysilane (AMPSi), 3-pyridinecarbaldehyde (0.877 g) and dichloromethane (25 mL) was stirred at 50 °C for 24 h and then the solvent was evaporated on rotary evaporator to afford a colorless oil (2.5 g).

Step 2 (1-(pyridin-3-yl)-N-(3-(triethoxysilyl)propyl)methanimine-silica): To a solution of 1-(pyridin-3-yl)-N-(3-(triethoxysilyl)propyl)methanimine (2.5 g) in toluene (20 mL), SiO_2 (1.7 g, 230–400 mesh) was added. The resulting mixture was refluxed for 24 h under N_2 atmosphere and then filtered to give a residue which was washed with toluene (20 mL × 1) and dichloromethane (20 mL × 1). The residue was dried in oven for 24 h to afford off white powder (4.0 g).

Step 3 (N-(pyridin-3-ylmethyl)propylamino-silica) [19]: A mixture of 1-(pyridin-3-yl)-N-(3-(triethoxysilyl)propyl)methaniminesilica (3.5 g) and methanol (25 mL) was cooled at 0 °C and $NaBH_4$ (0.619 g) was added. The resultant mixture was stirred at room temperature for 24 h then evaporated to afford off white powder (3.2 g).

2.4. Synthesis of nano-magnetite particles (Fe_3O_4)

A solution of $FeCl_2$ (5.4 g) and $FeCl_3$ (2 g) in aqueous hydrochloride acid (2 M, 25 mL) were sonicated at room temperature until the salts dissolved completely. To this solution, an aqueous ammonia solution (25%, 40 mL) was added slowly under argon atmosphere followed by 30 min stirring. The Fe_3O_4 nanoparticles were separated by an external magnet and washed with deionized water (3 × 50 mL) and ethanol (3 × 50 mL) and dried under vacuum (Scheme 2).

2.5. Synthesis of silica-coated magnetite nanoparticles (SMNP)

The synthesized Fe_3O_4 suspended in 35 mL ethanol and 6 mL deionized water was sonicated for 15 min to which, 1.5 mL of tetraethyl orthosilicate (TEOS) was added slowly and again sonicated for 10 min. Then aqueous ammonia (10%, 1.4 mL) was added slowly under stirring and the mixture was heated at 40 °C for 12 h. The iron oxide nanoparticles on a thin layer of silica (Fe_3O_4@SiO_2) were separated by an external magnet and washed three times with ethanol and dried under vacuum.

2.6. Preparation of Fe_3O_4@SiO_2-Py

To a solution of 1-(pyridin-3-yl)-N-(3-(triethoxysilyl)propyl)methanimine (2.5 g) in toluene (20 mL), Fe_3O_4@SiO_2 (10 g) was added lotwise. The resulting mixture was refluxed for 24 h under N_2 atmosphere, and then filtered to obtain the residue which was washed with toluene (20 mL × 1) and dichloromethane (20 mL × 1). Then the residue was dried in oven for 24 h to afford off white powder (4.0 g) of 1-(pyridin-3-yl)-N-(3-(triethoxysilyl)propyl)methanimine magnetic silica. Further a mixture of 1-(pyridin-3-yl)-N-(3-(triethoxysilyl)propyl)methanimine magnetic silica (4.0 g) and methanol (25 mL) was cooled at 0 °C and $NaBH_4$ (0.69 g) was added. The resultant mixture was stirred at room temperature for 24 h then evaporated to afford off white powder (3.6 g) of Fe_3O_4@SiO_2-Py (surface are of 138 m^2/g).

2.7. Catalyst test

A mixture of furfural (0.192 g, 2 mmol), acetylacetone (0.2 g, 2 mmol) and Fe_3O_4@SiO_2-Py (0.1 g) was stirred at 100 °C for 4 h after which the catalyst was separated by an external magnet and the resultant reaction mixture was diluted with ethyl acetate (20 mL × 1) and subsequently washed with water (20 mL × 1) and brine solution (20 mL × 1). Then the reaction mixture was dried over sodium sulfate and evaporated under reduced pressure. The obtained crude oil was purified by column chromatography using ethyl acetate: petroleum ether (2: 98; *v/v*) eluent to afford yellowish brown liquid. After the reaction, the catalyst was recovered with an external magnet and the reaction mass was decanted and the catalyst was subsequently washed with ethyl acetate and reused for the next run.

3. Results and discussion

3.1. Catalyst characterization

3.1.1. FTIR

Structures of organosilica catalysts were confirmed by FTIR analysis (Fig. 1). In the Fe_3O_4@SiO_2-Py catalyst, intense peaks observed between 580 cm^{-1} and 630 cm^{-1} were attributed to the stretching vibration mode associated with metal–oxygen (Fe—O) bonds in the crystalline lattice of Fe_3O_4. A band at 1647 cm^{-1} was attributed to –C = N– of pyridine moiety and the band at 3375 cm^{-1} was for assigned hydroxyl functionality. FTIR pattern of Fe_3O_4@SiO_2-Py and SiO_2-Py was almost similar except the Fe_3O_4 pattern. Aminopropylsilica showed bands at 1020 cm^{-1} and 1472 cm^{-1} for Si-O-Si and –NH_2 functionality, respectively.

3.1.2. Solid state NMR

The structure of SiO_2-Py catalyst was confirmed by solid state ^{13}C NMR (Fig. S3) in which, three well resolved lines at 10.53, 22.23, 50.38 ppm were observed,which were assigned to –CH_2– groups as a, b, (c and d) respectively. The bands at 125, 136.13, 138.24 and 148.56 ppm are assigned to –CH– groups of pyridine with carbon atoms numbered e, f, g and h, respectively.

3.1.3. XRD

To confirm the presence of Fe_3O_4 phases, XRD pattern of Fe_3O_4@SiO_2-Py was compared with the standard Fe_3O_4 (Fig. S2). A series of characteristic peaks such as (220), (311), (4 0 0), (4 2 2), (5 1 1) and (4 4 0) were observed in the Fe_3O_4@SiO_2-Py sample which are in well accordance with the inverse cubic spinel phase of Fe_3O_4 (JCPDS 85–1436).

3.1.4. TEM

Morphology and particle sizes of Fe_3O_4@SiO_2, Fe_3O_4@SiO_2-Py and Fe_3O_4@SiO_2-Py(reused) samples was investigated by using TEM analysis (Fig. S1). The results indicate that Fe_3O_4@SiO_2, Fe_3O_4@SiO_2-Py

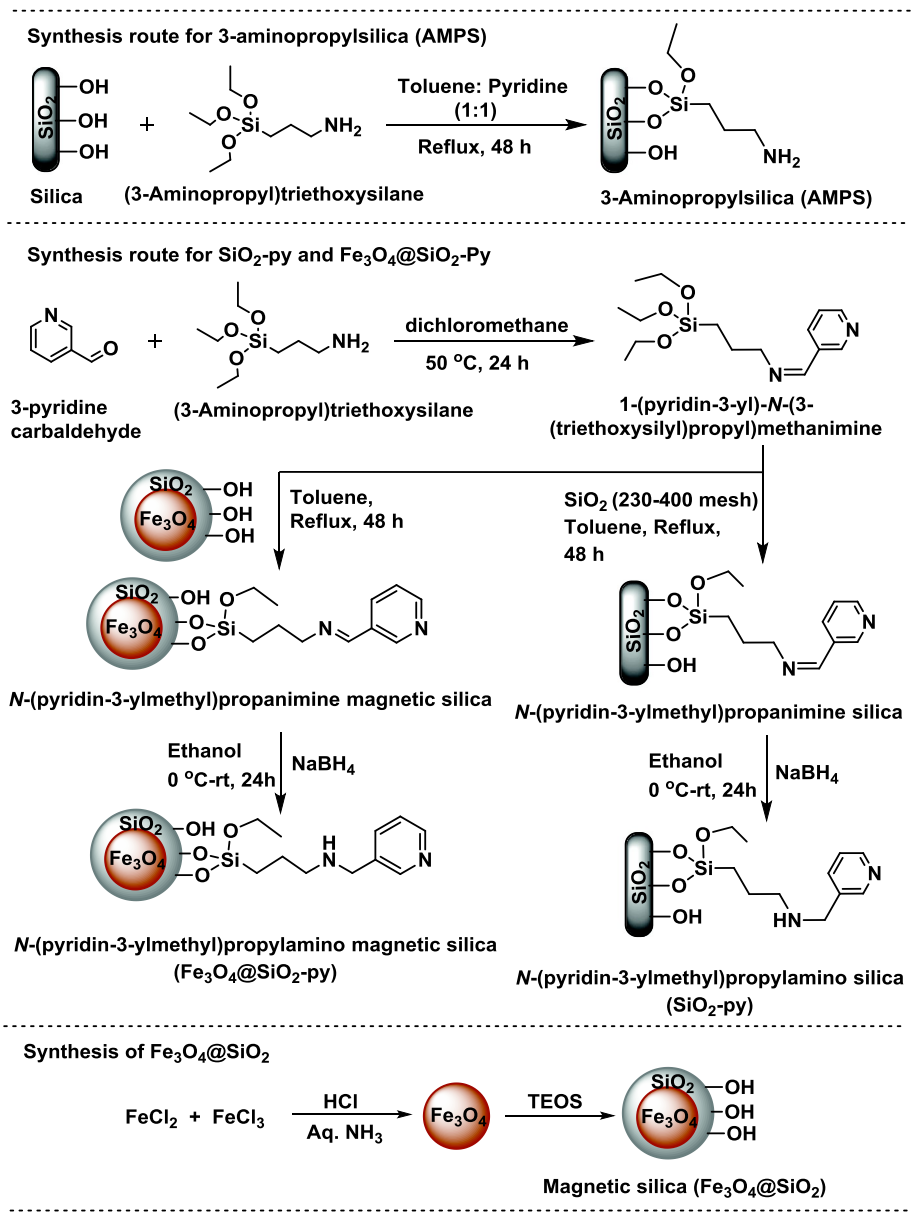

Scheme 2. Synthesis routes for 3-Aminopropylsilica, Fe_3O_4@SiO_2-Py and SiO_2-Py and Fe_3O_4@SiO_2.

and Fe_3O_4@SiO_2-Py(reused) have almost a hexagonal shape with an average particle size of 36, 40 and 41 nm, respectively. Fig. S1 clearly showed that nanoclusters of Fe_3O_4 were successfully coated with a thin layer of SiO_2 leading to core/shell structure of Fe_3O_4@SiO_2 NPs. Morphology and particle size of Fe_3O_4@SiO_2-Py sample has been retained even after its reuse which proves stability of the catalyst (Fig. S1).

3.1.5. Catalyst screening for Knoevenagel condensation of furfural with acetylacetone

The Knoevenagel condensation reaction is usually facilitated by basic catalysts. In this work, several basic catalysts were tested for the Knoevenagel condensation of furfural with acetylacetone (Table 1). Initially, furfural was treated with acetylacetone in presence of NaOH at 80 °C for 4 h to give the Knoevenagel product (FMP) in 78% yield with 95% conversion of furfural (Table 1, entry 1). Indeed, use of homogeneous base catalyst is unattractive due to downsides such as non-reusable, hazardous waste generation and it also need to be neutralized with acids which ultimately increases the process operations. Therefore, easily recoverable and environmentally compatible solid bases are usually most preferred. In this direction, we performed Knoevenagel condensation over series of solid bases. For instance, with hydrotalcite (Mg/Al = 3) at 100 °C, FMP was formed in 31% yield with only 56% conversion of furfural (Table 1, entry 2). In presence of CaO, FMP was produced in 41% yield with 67% conversion of furfural (Table 1, entry 3). With ZnO-400 catalyst, FMP obtained was in 29% yield with lower conversion (41%) of furfural (Table 1, entry 4). Although, the basic metal oxides gave 100% selectivity to FMP but the yield was low to moderate due to lower conversion of furfural. Generally, the Knoevenagel condensation is more prone over amine containing organic bases. In presence of catalytic amount of triethylamine, 79% yield of FMP was achieved with 89% conversion of furfural (Table 1, entry 5). Biomass derived furfurylamine as a catalyst showed similar activity as of triethylamine (Table 1, entry 6). Further, with *N*,*N*-dimethylaminopyridine (DMAP) the FMP was obtained in 77% yield (Table 1, entry 7). In presence of 1,8-Diazabicyclo[5.4.0]undec-7-ene (DBU) catalyst, the FMP was formed in 78% yield (Table 1, entry 8). With 4-hydroxypyridine, furfural was consumed upto 95% and 83% yield of FMP was achieved (Table 1, entry 9). Amine functionalized homogeneous

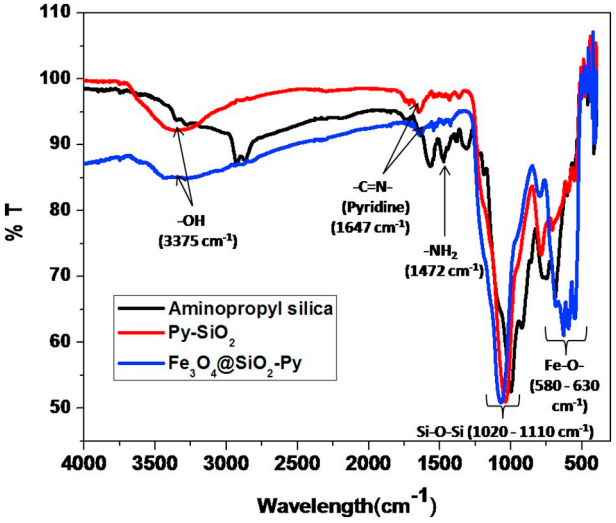

Fig. 1. FTIR of 3-Aminopropylsilica, Py-SiO_2 and Fe_3O_4@SiO_2-Py catalysts.

Table 1
Catalyst screening for Knoevenagel condensation of furfural with acetylacetone.[a]

Entry	Catalyst	Loading	T	Conv.[b]	Yield[b]	Sel.[b]
			[°C]	[%]	[%]	[%]
1	NaOH	10 mol%	80	95	78	92
2	Hydrotalcite	0.1 g	100	56	31	100
3	CaO	0.1 g	100	67	41	100
4	ZnO-400	0.1 g	100	41	29	100
5	Triethylamine	10 mol%	100	89	79	99
6	Furfurylamine	10 mol%	100	90	80	99
7	DMAP	10 mol%	100	85	77	98
8	DBU	10 mol%	100	87	78	99
9	4-Hydroxypyridine	10 mol%	100	95	83	99
10	3-Aminopropylsilica	0.1 g	100	81	76	99
11	SiO_2-Py	0.1 g	100	94	85	100
12	Fe_3O_4@SiO_2-Py	0.1 g	100	94	85	100

[a] Reaction condition: Furfural (0.196 g, 2 mmol), catalyst, acetylacetone (0.2 g, 2 mmol), 4 h.
[b] Yields are determined using HPLC.

bases gave good yield and 99% selectivity to the FMP with almost 90% conversion of furfural. Homogeneous bases are not only non-recyclable but they are soluble in organic solvents hence, they could contaminate the product. However, these catalysts can be heterogenized by anchoring functionalized organic amines on silica. For instance, 3-Aminopropylsilica was used for this reaction however a moderate yield (76%) of FMP with 99% selectivity was noticed with almost 90% conversion of furfural (Table 1, entry 10). Pyridine anchored on silica (SiO_2-Py) showed better catalytic performance than 3-Aminopropylsilica. With SiO_2-Py catalyst, 94% conversion of furfural was achieved to obtain 85% yield of FMP (Table 1, entry 11). In case of SiO_2-Py catalyst, pyridine moiety is planar and the lone pair of electrons are present perpendicular to the plane of pyridine. Hence, hydrogen from the active methylene group of acetylacetone can be easily approached. On the contrary, in 3-Aminopropylsilica, there is a distorted tetrahedral structure which creates some hinderance for the reactant as compared to pyridine. Due to these reasons SiO_2-Py showed better activity than 3-Aminopropylsilica. Fe_3O_4@SiO_2-Py catalyst showed similar activity to that of SiO_2-Py (Table 1, entry 12). Use of magnetic catalyst (Fe_3O_4@SiO_2-Py) is advantageous over SiO_2-Py because, the former can be easily separated with the help of external magnate. While, in case of SiO_2-Py, catalyst recovery is done by filtration which is associated with handling losses.

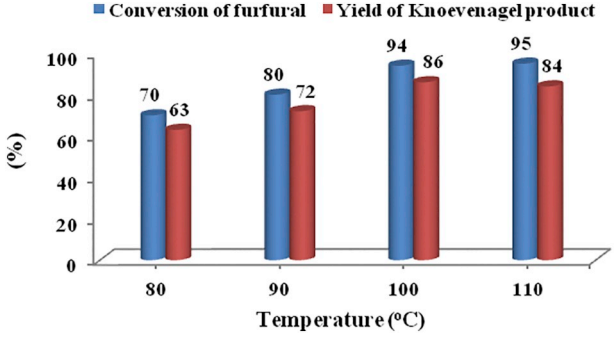

Fig. 2. Influence of temperature. Reaction conditions: Furfural (0.192 g, 2 mmol), acetyl acetone (0.2 g, 2 mmol), Fe_3O_4@SiO_2-Py (0.1 g), 4 h.

3.1.6. *Effect of temperature*

The yield of FMP increased gradually with rise in temperature from 80 to 100 °C and reached maximum (85%) at 100 °C. Further increase in temperature to 110 °C, the yield of FMP was not improved (Fig. 2).

3.1.7. *Effect of time*

Up to 85% furfural conversion 78% yield of FMP was observed within just 1.5 h. After that conversion of furfural the yield of FMP was slowly increased. At the end of 4th hour maximum conversion of furfural and yield of FMP was achieved. Extending reaction beyond 4 h did not show any improvement in the conversion and yield (Fig. 3).

3.1.8. *Effect of catalyst amount*

Influence of catalyst amount in the range of 0.05–0.150 g was investigated for this reaction (Fig. 4). With 0.05 g of Fe_3O_4@SiO_2-Py. The yield of FMP was only 61% while, increasing the catalyst amount to 0.075 g, resulted in enhancement of the yield of FMP (79%). The lower catalyst amount gave lower yield due to insufficient active site. However, with catalyst amount of 0.15 g the yield of FMP was comparable with that of 0.1 g.

3.1.9. *Recycle study*

The stability of Fe_3O_4@SiO_2-Py was evaluated by performing recycle runs (Fig. S6). It was found that the catalytic activity of Fe_3O_4@SiO_2-Py was very much consistent even after being used for six times.

4. Conclusions

We presented here a simple and robust Fe_3O_4@SiO_2-Py catalyst system for the Knoevenagel condensation of furfural with acetyl acetone to achieve high yield of FMP. The condensation product FMP is

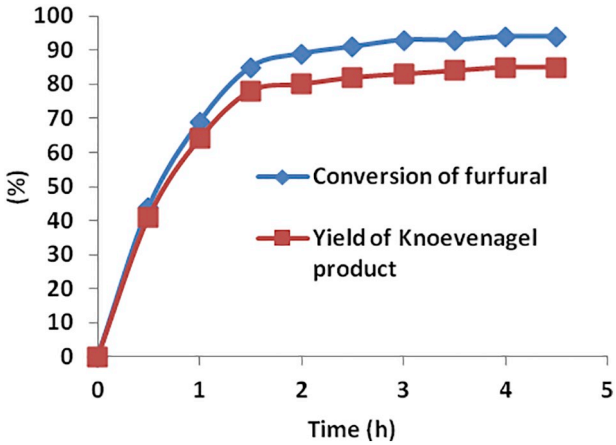

Fig. 3. Influence of time. Reaction conditions: Furfural (0.192 g, 2 mmol), acetylacetone (0.2 g, 2 mmol), Fe_3O_4@SiO_2-Py (0.1 g), 0–5 h.

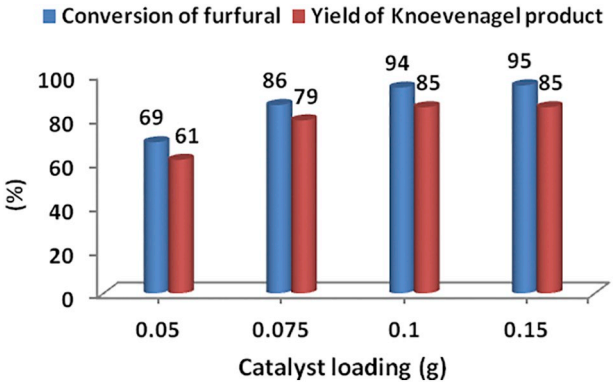

Fig. 4. Influence of catalyst amount. Reaction conditions: Furfural (0.192 g, 2 mmol), acetylacetone (0.2 g, 2 mmol), Fe_3O_4@SiO_2-Py (0.05–0.15 g), 4 h.

a unit of C_{10} and could be converted into branched alkanes (Jet fuel) through hydrodeoxygenation process. The stability of the Fe_3O_4@SiO_2-Py is confirmed by its several reuses.

Acknowledgements

S.H.S is grateful to CSIR-National Chemical Laboratory, AcSIR and CSIR.

Appendix A. Supplementary data

Supplementary data to this article can be found online at https://doi.org/10.1016/j.catcom.2019.03.005.

References

[1] J.C. Serrano-Ruiz, J.A. Dumesic, Energy Environ. Sci. 4 (2011) 83–99.
[2] J.-P. Lange, E. van der Heide, J. van Buijtenen, R. Price, ChemSusChem 5 (2012) 150–166.
[3] W. Dabelstein, A. Reglitzky, A. Schutze, K. Reders, Automotive fuels, Ullmann's Encyclopedia of Industrial Chemistry, Wiley-VCH, Weinheim, 2000.
[4] G. Liang, A. Wang, X. Zhao, N. Lei, T. Zhang, Green Chem. 18 (2016) 3430–3438.
[5] J.N. Appaturi, M. Selvaraj, S.B.A. Hamid, Microporous Mesoporous Mater. 260 (2018) 260–269.
[6] A.V. Subrahmanyam, S. Thayumanavan, G.W. Huber, ChemSusChem 3 (2010) 1158–1161.
[7] C.M. Nicklaus, A.J. Minnaard, B.L. Feringa, J.G. de Vries, ChemSusChem 6 (2013) 1631–1635.
[8] A. Corma, O. de la Torre, M. Renz, N. Villandier, Angew. Chem. Int. Ed. 50 (2011) 2375–2378.
[9] M. Balakrishnan, E.R. Sacia, A.T. Bell, ChemSusChem 7 (2014) 1078–1085.
[10] S.H. Shinde, C.V. Rode, Green Chem. 19 (2017) 4804–4810.
[11] G.W. Huber, J.N. Chheda, C.J. Barrett, J.A. Dumesic, Science 308 (2005) 1446–1450.
[12] K.S. Arias, M.J. Climent, A. Corma, S. Iborra, Energy Environ. Sci. 8 (2015) 317–331.
[13] P. Oliveira, A. Machado, A.M. Ramos, I. Fonseca, F.M.B. Fernandes, A.M.B.D. Rego, J. Vital, Microporous Mesoporous Mater. 120 (2009) 432–440.
[14] Y.L. Zhang, S. Liu, S.Y. Liu, F.J. Liu, H.Y. Zhang, Y.Y. He, F.S. Xiao, Catal. Commun. 12 (2011) 1212–1217.
[15] D.Z. Xu, Y. Liu, S. Shi, Y.M. Wang, Green Chem. 12 (2010) 514–517.
[16] J. Mondal, A. Modak, A. Bhaumik, J. Mol. Catal. A Chem. 335 (2011) 236–241.
[17] K.M. Parida, D. Rath, J. Mol. Catal. A Chem. 310 (2009) 93–100.
[18] A. Modak, J. Mondal, A. Bhaumik, Appl. Catal. A General 459 (2013) 41–51.
[19] O.C. Navarro, A. Corma, S.I. Chornet, Top. Catal. 52 (2009) 304–314.

Fuel Processing Technology 197 (2020) 106191

Contents lists available at ScienceDirect

Fuel Processing Technology

journal homepage: www.elsevier.com/locate/fuproc

Research article

Magnetically separable catalyst for condensation of renewable aldehydes and 2-methylfuran to saturated cyclic oxygenates

Komal Tarade, Suhas Shinde, Chandrashekhar Rode*

Chemical Engineering and Process Development Division, CSIR-National Chemical Laboratory, Dr. Homi Bhabha Road, Pashan, Pune 411008, India

ARTICLE INFO

Keywords:
Hydroxyalkylation-alkylation
Hydrogenation
Magnetic solid acid
Organosilica
Fuel additives

ABSTRACT

The saturated cyclic ethers produced from biomass derived aldehydes and 2-methylfuran are the potential diesel fuel candidates. The synthesis of saturated cyclic ethers is a two step process which involves acid catalyzed condensation of aldehydes with 2-methylfuran and the subsequent selective furan ring hydrogenation of the condensation products. Here, we designed a novel recyclable magnetic solid acid catalyst such as [Fe_3O_4@SiO_2-Pr-Py-H][$2HSO_4^{2-}$] and employed for the condensation of 2-methylfuran with formaldehyde as model substrates and reaction parameters were optimized. Under the set reaction conditions, condensation of 2-methylfuran with several other aldehydes were also successfully achieved with very good yields. Further, several supported noble metal catalysts were screened in order to find suitable catalyst system for selective furan ring hydrogenation of condensation products. Among those, 5% Pd/C was found to be very active and selective for furan ring hydrogenation without formation of ring opened products under very low hydrogen pressure at room temperature. Prepared catalysts were thoroughly characterized with sophisticated techniques.

1. Introduction

Owing to diminishing petroleum reserves and environmental problems such as global warming and air pollution, it is imperative to utilize biomass resources to produce fuels and chemicals [1]. A substantial growth projected in global oil consumption combined with compelling international situation of crude oil production are the key drivers for exploring alternate sustainable energy sources. Bioenergy is the largest contributor of global renewable, simultaneously providing energy security to billions and stimulates rural development [2]. Among several options, biomass is currently the largest source of carbon-based renewable energy in the world. In principle, biomass feedstock can be harnessed to meet the demands of heat, electricity, and liquid fuel. Among these, heat has been traditionally obtained to the extent of 60% from biomass mainly for cooking application in major part of the world [3]. There have been several biomass co-firing plants commissioned to produce electricity and heat [4]. However, burning of biomass is a kind of its underutilization when a practical potential of its conversion to liquid fuel like products exists [5]. Considering this fact, several countries have set a target of deriving 10–20% of transportation fuels from biomass feedstock during next decade or so [6]. The cellulose and hemicellulose are the main structural carbohydrate fractions of lignocellulosic biomass which are hydrolyzed to produce glucose and xylose followed by their dehydration to produce 5-hydroxymethylfurfural (HMF) and furfural (FUR), respectively [7,8]. Both 5-HMF and furfural are the key starting materials for production of fuel components through carbon upgradation by employing various types of C−C bond forming reactions. Hydroxyalkylation-alkylation is one such reaction involving acid catalyzed condensation of 2-methylfuran with the aldehydes, ketones or alcohols. Furan condensation reaction has been reported using several types of reagents/catalysts e.g. conc. H_2SO_4 [9], HCl [10], acidic resins [9-14], MCM-SO_3H [15], Mo-Zr-MCM-41 [16], $AuCl_3$ [17-18], Sn^{+4}-K-10 [19], zeolites [20], SiO_2-Pr-S-Pr-SO_3H [21], $Cu(OTf)_2$ [22], I_2 [23], CMH-SO_3H [24], SILC [25], TFA-ZrO_2 [26], ionic liquids [27], Sn-Mont [28] etc. The furan condensation products thus obtained can be then hydrodeoxygenated to produce hydrocarbons (Scheme 1). Corma et al. have reported the physical mixture of Pt/C and Pt/TiO_2 at 400 °C and 5 MPa hydrogen pressure for 1 h [9]. Recently, Liu et al. showed that hydrodeoxygenation of condensation products over Ir-ReO_x/SiO_2 could provide high selectivity of the desired alkanes at lower temperature of 170 °C [29]. Interestingly, Balakrishanan et al. have shown that complete hydrodeoxygenation of furan condensation products to alkanes would require 55–60% higher hydrogen compared to that hydrogen required for hydrogenation of furan condensation products to obtain cyclic ethers (furan ring saturation) which fully meet most of the specifications of diesel. Almost

* Corresponding author.
E-mail address: cv.rode@ncl.res.in (C. Rode).

https://doi.org/10.1016/j.fuproc.2019.106191
Received 31 May 2019; Received in revised form 17 August 2019; Accepted 18 August 2019

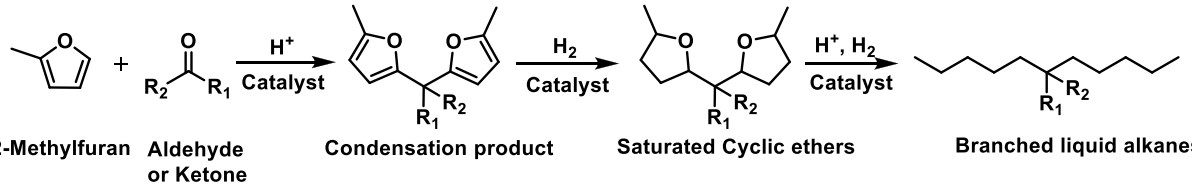

Scheme 1. General scheme for synthesis of saturated cyclic ethers and branched liquid alkanes.

complete selectivity with 95% yield of cyclic ethers, without formation of ring open products could be achieved by using Pd/IL(PF6)-SiO_2 catalyst [10]. Several Ni, Pt, Pd, Ir and Rh metal supported on different acidic supports have been designed and used for the selective production of alkanes from bio-derived platform molecules [30-39]. In this paper, we report recyclable magnetic catalyst for the hydroxyalkylation-alkylation of 2-methylfuran with aldehydes to provide a wide range of furan condensation products. It has been also demonstrated that these condensation products could be successfully hydrogenated to cyclic ethers over 5%Pd/C under very mild conditions of pressure and room temperature.

2. Experimental

2.1. Materials

Furfural, benzaldehyde, 37 wt% aqueous formaldehyde, acetone, amberlyst-15, amberlyte IR-120, 3-pyridinecarbaldehyde 3-aminopropyltriethoxysilane, tetraethyl orthosilicate, $FeCl_2$, $FeCl_3$ and palladium chloride and carbon black were purchased from Sigma-Aldrich. 2-Methylfuran was obtained from TCI. Sodium hydroxide, sulphuric acid, methanol, acetonitrile, 1,4-dioxane, ethyl acetate, petroleum ether, toluene and silica gel (100–200 mesh) were purchased from Chem Labs, India. $NaBH_4$ received from Thomas Bakers. Commercial 5% Pd/C was obtained from Aldrich chemical company. Ethanol was obtained from Changshu Hongsheng Fine Chemicals.

2.2. Catalyst preparation

2.2.1. Preparation of nano-magnetic (Fe_3O_4)

A solution of $FeCl_2$ (5.4 g) and $FeCl_3$ (2 g) in aqueous hydrochloride acid (2 M, 25 mL) was sonicated at room temperature until the salts dissolved completely. To this solution, an aqueous ammonia solution (25%, 40 mL) was added drop wise under argon atmosphere and stirred for 30 min. The Fe_3O_4 nanoparticles were separated by external magnet and washed with deionized water (3 × 50 mL) and ethanol (3 × 50 mL) and dried under vacuum.

2.2.2. Preparation of Fe_3O_4@SiO_2

Fe_3O_4 as prepared above was suspended in 35 mL ethanol and 6 mL deionized water and sonicated for 15 min to which, 1.5 mL of tetraethyl orthosilicate (TEOS) was added slowly and again sonicated for 10 min. Then aqueous ammonia (10%, 1.4 mL) was added slowly under stirring and the mixture was heated at 40 °C for 12 h. The iron oxide nanoparticles on silica (Fe_3O_4@SiO_2) were separated by an external magnet and washed three times with ethanol and dried under vacuum.

2.2.3. Preparation of [Fe_3O_4@SiO_2-Pr-Py-H][2HSO_4^{2-}]

The schematic of the catalyst preparation is shown in Scheme 2.

2.2.3.1. Step 1(1-(pyridin-3-yl)-N-(3-(triethoxysilyl)propyl)methanimine). A mixture of 1.8 g of 3-aminopropyltriethoxysilane (AMPSi), 3-pyridinecarbaldehyde (0.877 g) and dichloromethane (25 mL) was stirred at 50 °C for 24 h and then the reaction mixture was evaporated on rotary evaporator to afford colorless oil (2.5 g).

2.2.3.2. Step 2 (1-(pyridin-3-yl)-N-(3-(triethoxysilyl)propyl)methanimine-magnetic-silica). To a solution of 1-(pyridin-3-yl)-*N*-(3-(triethoxysilyl) propyl)methanimine (2.5 g) in toluene (20 mL), Fe_3O_4@SiO_2 (1.7 g, 230–400 mesh) was added lot-wise. The resulting mixture was refluxed for 24 h under N_2 atmosphere which was then cooled to room temperature and filtered. The residue thus obtained was washed with toluene (20 mL × 1) and dichloromethane (20 mL × 1) followed by its drying in an oven for 24 h to afford off white powder (4.0 g).

2.2.3.3. Step 3 (N-(pyridin-3-ylmethyl)propylaminomagnetic-silica) [39]. A mixture of 1-(pyridin-3-yl)-*N*-(3-(triethoxysilyl)propyl)methanimine-magnetic-silica (3.5 g) and methanol (25 mL) was cooled at 0 °C and $NaBH_4$ (0.619 g) was added lot-wise. The resultant mixture was stirred at room temperature for 24 h and then evaporated on rotary evaporator to afford off white powder (3.2 g).

2.2.3.4. Step 4 N-(pyridin-3-ylmethyl)propylaminomagneticacidic-silica [Fe_3O_4@SiO_2-Py-Pr-H][2HSO_4^{2-}]. *N*-(Pyridin-3-ylmethyl) propylaminomagnetic-silica (0.5 g) was treated with 15% H_2SO_4 in ethanol (5 mL) at room temperature for 24 h and dried under vacuum.

2.2.4. Preparation of supported Pd catalysts

Carbon supported catalysts with different Pd loadings were prepared according to the previously reported procedure [40]. In a typical procedure, 33 mg of $PdCl_2$ was dissolved in 50 mL aqueous hydrochloric acid and stirred for 30 min. To this, slurry of 0.99 g activated carbon in water was added slowly with constant stirring and kept it for 2 h on stirring. Then pH of the reaction mass was adjusted to 7–8 with 10 M NaOH solution and then resultant mixture was further stirred for 30 min. $NaBH_4$ (1 g) was added lot wise to the mixture and again stirred for 30 min. The resultant solid catalyst was filtered and washed several time by distilled water and dried in oven at 100 °C. Similar procedure is used for preparation of catalyst with 1–5% palladium loadings on different supports.

2.3. Determination of catalyst acidity

Sodium chloride aqueous solution (0.05 mol L^{-1}, 30 mL) was added to the [Fe_3O_4@SiO_2-Pr-Py-H][2HSO_4^{2-}] catalyst (0.250 g). The resultant mixture was stirred for 60 min at room temperature under ultrasonic conditions. After centrifugal separation, the supernatant solution was titrated by sodium hydroxide aqueous solution (0.05 mol L^{-1}) using phenolphthalein indicator [41,42]. The total acidity of [Fe_3O_4@SiO_2-Pr-Py-H][2HSO_4^{2-}] obtained was 0.027 M. Acidity of [Fe_3O_4@SiO_2-Pr-Py-H][2HSO_4^{2-}] sample after 3rd reuse determined was 0.026 M. By using similar method, acidity of other sulfonic acid functionalized solid acid catalysts were also estimated and are presented in Table 1.

2.4. Condensation of 2-methylfuran with aldehydes

A mixture of aldehyde (2 mmol), 2-methylfuran (4 mmol) and acidic catalyst (0.1 g, solid acid) or (10 mol%, liquid acid) was stirred for 3 h at 65 °C. In case of liquid acid, the reaction was neutralized by saturated solution sodium bicarbonate and resultant mixture was extracted with ethyl acetate (20 mL × 1) and subsequently washed with water

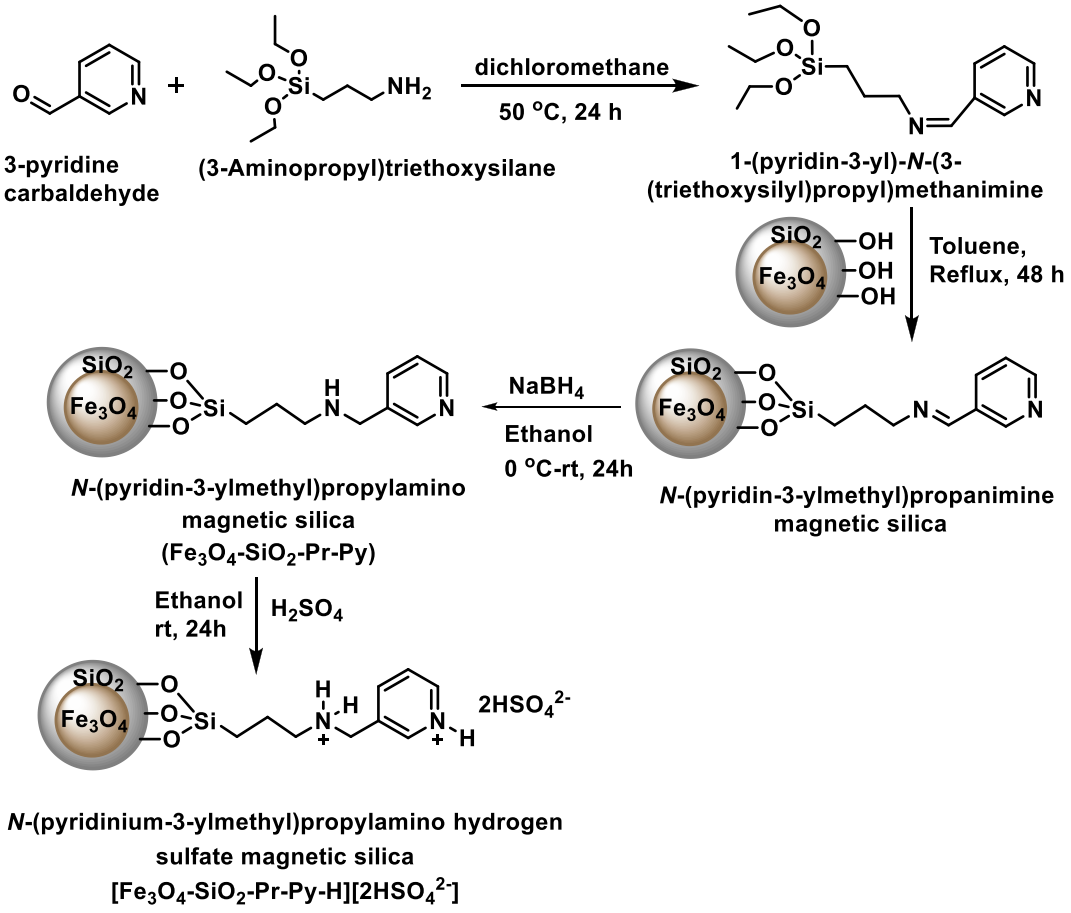

Scheme 2. Preparation of [Fe_3O_4-SiO_2-Pr-Py-H][$2HSO_4^{2-}$].

(20 mL × 1) and brine solution (20 mL × 1). In case of solid acid catalyst, the catalyst was separated by filtration or by an external magnet (for magnetic catalyst) and the filtrate was diluted with ethyl acetate (20 mL × 1) and subsequently washed with water (20 mL × 1) and brine solution (20 mL × 1). Then the reaction mixture was dried over sodium sulfate and evaporated under reduced pressure. The obtained crude oil was purified by column chromatography using petroleum ether (100 v/v) eluent.

2.5. Hydrogenation of condensation products

A mixture of the condensation product (0.2 g) dissolved in solvent (20 mL) was added to a round bottom flask containing the supported Pd catalyst (0.05 g,) and then the mixture was stirred at room temperature using hydrogen atmosphere by bladder for 10 h. Then the reaction mixture was filtered to separate the catalyst and the filtrate was evaporated under reduced pressure to obtain the product.

Table 1
Catalyst screening for condensation of formaldehyde with 2-methylfuran.[a]

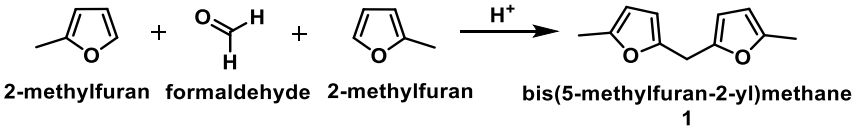

Entry	Catalyst	Acidity [mol/g]	Conv. Of 2-methyl furan [%]	Conv. of HCHO[c] [%]	Yield of 1[d] [%]	Carbon balance [%]
1[b]	H_2SO_4	–	95	92	74 (66)	74
2	Amberlyst-15	0.016	92	89	83 (74)	83
3	Amberlyte IR-120	0.014	90	87	82 (72)	82
4	Sn-Mont	–	62	60	67 (56)	67
5	Zr-Mont	–	59	58	60 (52)	60
6	[Fe_3O_4@SiO_2-Pr-Py-H] [HSO_4^{2-}]	0.027	93	90	86 (75)	86
7	SO_4^{2-}/SiO_2	0.013	71	70	74 (66)	74
8	SO_4^{2-}/Fe_3O_4@SiO_2	0.019	73	72	79 (69)	79

[a] Reaction conditions: Formaldehyde (0.162 mL, 2 mmol), 2-methylfuran (0.328 g, 4 mmol), catalyst (0.1 g), 65 °C, 3 h.
[b] 10 mol% of H_2SO_4 was used.
[c] Determined by using GC.
[d] Yields are reported by GC and values in parenthesis represent isolated yields after workup and column chromatography. Selectivity of 1 is 100% for all the catalysts.

For gram scale hydrogenation, the reaction was performed in 300 mL Parr reactor. In a typical reaction, 2.0 g of condensation product was dissolved in 140 mL of solvent and charged into the Parr reactor containing 5% Pd/C (0.610 g). The resulting mixture was stirred at 800 rpm under hydrogen pressure of 50 psig. After a period of 10 h, the reaction mixture was filtered and the filtrate was extracted with ethyl acetate (200 mL × 2) and washed with water (100 mL × 1). Then the organic layer was dried over anhydrous Na_2SO_4 and was concentrated under reduced pressure. Filtered moist catalyst was filled in the bottle, it can be reused after calcination and activation.

2.6. Analysis of the reaction products

Thin-layer chromatography was performed using Merck 5554 aluminum-backed silica plates, and the spots were observed under UV light (254 nm). The conversion of reactants and selectivity of products was calculated using GC with a flame ionization detector and a capillary column (FFAP). Pure products were characterized and confirmed by ^{1}H NMR and ^{13}C NMR (50 MHz) using $CDCl_3$ (0.01%, TMS) as a solvent on a 200 MHz frequency Bruker instrument (see Supporting Information). The products were also confirmed using QP-Ultra 2010 GCMS Shimadzu instrument, RTX-5 column, and helium as carrier gas, electrospray ionization mode, and an ionization source temperature of 200 °C.

3. Results and discussion

3.1. Catalyst characterization

3.1.1. XRD

X-ray diffraction patterns for magnetic organosilica catalyst Fe_3O_4@SiO_2, [Fe_3O_4@SiO_2-Pr-Py] and [Fe_3O_4@SiO_2-Pr-Py-H][$2HSO_4^{2-}$] before reaction and after reaction show the diffraction peaks at 2θ = 30.32°, 35.80°, 43.36°, 53.88°, 57.54° and 63.26° which corresponded to the indices (220), (311), (400), (422), (511), and (440), respectively of Fe_3O_4 (Fig. 1a). XRD patterns of all the catalysts were identical due to common Fe_3O_4@SiO_2 backbone. X-ray diffraction patterns of the prepared 1–5% Pd/C and commercial 5% Pd/C catalysts are presented in Fig. 1b. The broad diffraction peaks at 2θ = 25 and 43.5° for all of the samples exhibited a carbon structure of the support. The intensity of these peaks decreased after Pd was supported. XRD peaks of Pd supported catalysts at 2θ = 40.1, 68.1, and 82.4° were attributed to the (111), (220) and (311) planes of the face-centered cubic structure of Pd (JCPDS card no. 46-1043). The intensity of (111) peak increased with an increase in palladium loading suggesting the spherical nature of Pd nano particles. In Fig. S1, a broad peak at 2θ = 24.37° and a sharp peak at 2θ = 39.93° corresponded to (002) and (111) planes of carbon and palladium, respectively. While, the broad peak at 2θ = 44.23° corresponded to (10) plane is due to the turbostratic carbon structure.

3.1.2. FT-IR

FT-IR of magnetic organosilica catalyst [Fe_3O_4@SiO_2-Pr-Py-H][$2HSO_4^{2-}$] is shown in Fig. 2. The intense peaks between 580 cm^{-1} and 630 cm^{-1} were attributed to the stretching vibration mode associated with metal-oxygen (Fe—O) bonds in the crystalline lattice of Fe_3O_4. A band at 1635 cm^{-1} was attributed to —C═N— of pyridine moiety and the band at 3375 cm^{-1} was for hydroxyl functionality. To identify and confirm the type of acid sites present in [Fe_3O_4@SiO_2-Pr-Py-H][$2HSO_4^{2-}$], pyridine was adsorbed on the catalyst surface and the FT-IR spectrum was recorded. A band at 1446 cm^{-1} could be attributed to the Lewis acid sites of Fe_3O_4 nanoparticles which are not coated with silica and a band at 1542 cm^{-1} was assigned to Brønsted acid sites due to $-NH_2-$, Py-H and HSO_4 species.

3.1.3. HR-TEM

Morphology and particle sizes of commercial 5% Pd/C, prepared 5% Pd/C and reused 5% Pd/C (in house prepared) were compared by TEM analysis. From TEM images of these catalysts, it was observed that distribution of palladium nano particles was uniform. Average particle size of commercial and the prepared 5% Pd/C was 6.73 nm and 7.6 nm, respectively (Fig. 3a,b). In the [Fe_3O_4@SiO_2-Pr-Py-H][$2HSO_4^{2-}$] sample, almost hexagonal geometry with an average particle size of 39.39 nm was observed (Fig. 3c). TEM image clearly showed that most of the nanoclusters of Fe_3O_4 were successfully coated with a thin layer of SiO_2 leading to core/shell structure of Fe_3O_4@SiO_2NPs (Fig. 3d).

The structure of [Fe_3O_4@SiO_2-Pr-Py-H][$2HSO_4^{2-}$] catalyst was confirmed by taking solid state ^{13}C NMR of its non magnetic and not acidic counterpart SiO_2-Pr-Py. In SiO_2-Pr-Py sample three well resolved lines at 10.53, 22.23, 50.38 ppm were observed, which were assigned to

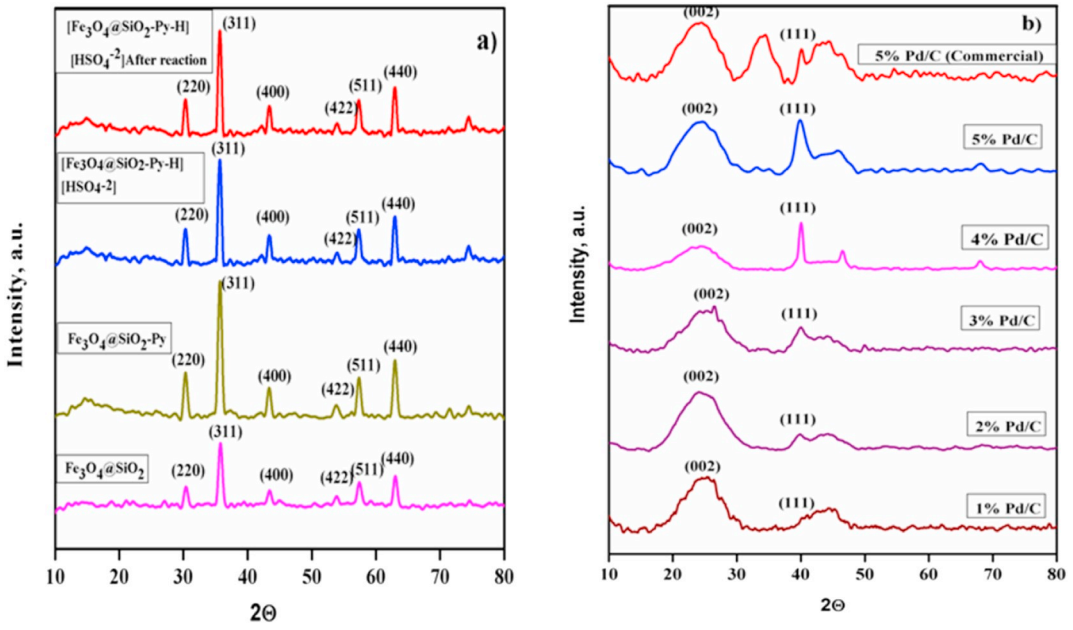

Fig. 1. a) XRD Patterns of magnetic samples and b) carbon supported 1–5 wt% palladium samples.

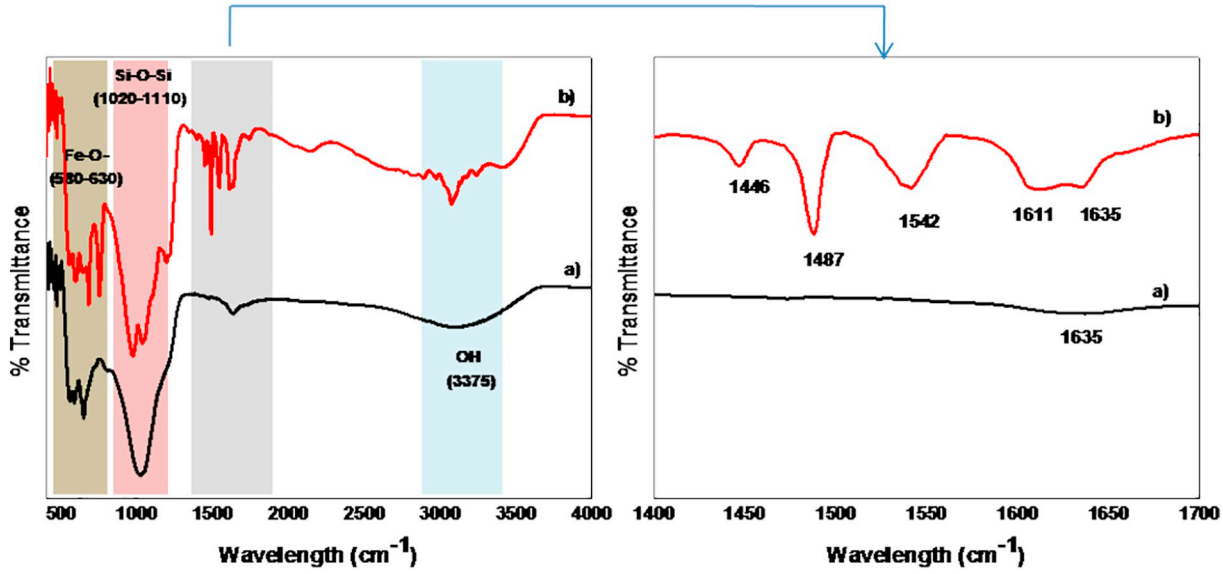

Fig. 2. a) FTIR and b) FTIR after pyridine adsorption of [Fe_3O_4@SiO_2-Pr-Py-H][$2HSO_4^{2-}$].

aliphatic $-CH_2-$ groups. The bands at 125, 136.13, 138.24 and 148.56 ppm are assigned to $-CH-$ groups of pyridine [43].

3.2. Condensation of formaldehyde with 2-methylfuran

Initially, several acid catalysts were screened for the condensation of aqueous formaldehyde with 2-methylfuran, as a model reaction and the results are summarized in Table 1. Initially, formaldehyde was reacted with 2-methylfuran in presence of H_2SO_4 (10 mol%) at 65 °C. After 3 h, 74% yield of the condensation product, **1** was observed with 92% conversion of formaldehyde (Table 1, entry 1). The use of Amberlyst-15 gave 89% conversion of formaldehyde with 83% yield of the condensation product **1** (Table 1, entry 2). Further, condensation reaction was performed over Amberlyte IR-120, to give 82% yield of **1** with 87% conversion of formaldehyde (Table 1, entry 3). Sn and Zr supported on montmorillonite catalysts gave 60 and 58% conversion of

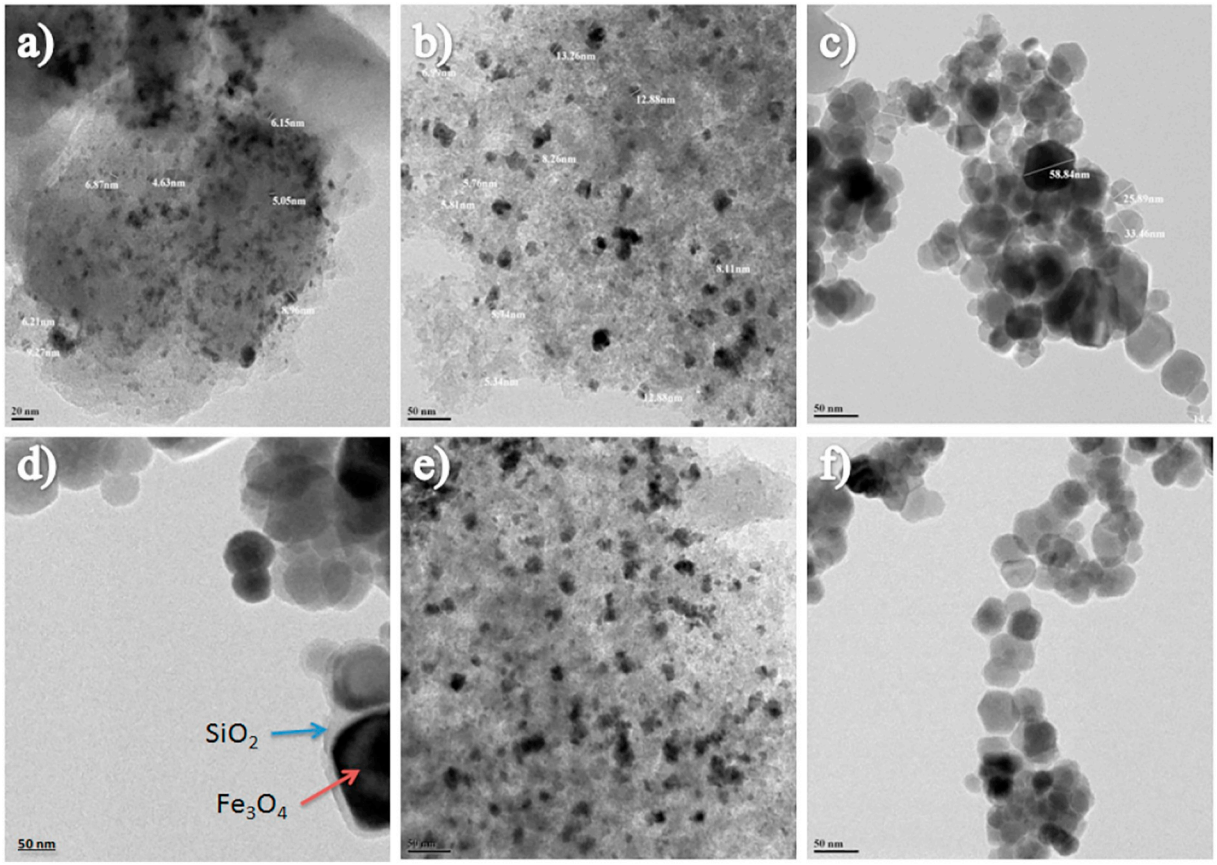

Fig. 3. HR-TEM images of 5% Pd/C (Commercial), 5% Pd/C (Prepared), 5% Pd/C (Prepared) 3rd reuse, [Fe_3O_4@SiO_2-Pr-Py-H][$2HSO_4^{2-}$] and [Fe_3O_4@SiO_2-Pr-Py-H][$2HSO_4^{2-}$] 3rd reuse.

furfural with 67 and 60% yield of **1**, respectively (Table 1, entries 4 and 5). Our novel magnetic solid acid [Fe_3O_4@SiO_2-Pr-Py-H][$2HSO_4^{2-}$] catalyst showed the highest conversion of both formaldehyde and 2-methyl furan (90 and 93%, respectively) with 86% yield of **1** (Table 1, entry 6). The rate of reaction was also maximum for this catalyst (ESI, S 2.2). Sulfated silica and sulfated magnetic silica showed almost 70% conversion of formaldehyde with > 74% yield (Table 1, entries 7 and 8). Table 1 also shows the C balance, which was highest (86%) for the best catalyst i.e. [Fe_3O_4@SiO_2-Pr-Py-H][$2HSO_4^{2-}$].

The acidity values of all the solid acid catalysts used in this work are presented in Table 1. It was observed that [Fe_3O_4@SiO_2-Pr-Py-H][$2HSO_4^{2-}$] catalyst possessed the maximum acidity of 0.027 M which contributed to its excellent activity towards the condensation reaction.

3.3. Catalyst screening for hydrogenation

Different supported noble metal catalysts were evaluated for the hydrogenation of condensation product **1**. Initially, 1% Pd/C was used for hydrogenation of condensation product **1**, to give 45% conversion and 40% yield of the ring hydrogenation product **2** (cyclic ether) along with 4.2% semi hydrogenation product **2′** (Table 2, entry 1). With increasing Pd loading from 1 to 5%, the conversion of **1** also increased gradually from 45% to 91% with an increase in the yield of cyclic ether from 40 to 87% (Table 2, entries 2–5). 5% Pd/Al_2O_3 gave 80% conversion with 74% yield of the cyclic ether (Table 2, entry 6). On the other hand, 5% Ru/C catalyst showed 47% yield of cyclic ether with 56% conversion of condensation product (Table 2, entry 7). With 5% Ru/Al_2O_3, slightly better conversion of starting material and yield of product was observed than that for 5% Ru/C catalyst (Table 2, entry 8). The lowest conversion and the product yield of 41% and 35%, respectively was obtained over 5% Pt/C catalyst (Table 2, entry 9). The commercial 5% Pd/C gave 87% conversion of condensation product with 82% yield of cyclic ether, which was comparable with that shown by the prepared 5% Pd/C catalyst (Table 2, entry 10).

3.4. Solvent Screening for the hydrogenation reaction

The activity of 5% Pd/C catalyst was studied for the ring hydrogenation of condensation product in various organic solvents at room temperature, for 10 h (Table 3). Under the optimized reaction conditions in isopropyl alcohol, a 85% yield of ring hydrogenation product **2** was achieved (Table 3, entry 1). When the reaction was carried out in methanol, a 76% yield of **2** was obtained (Table 3, entry 2) while, in presence of acetonitrile, 71% yield of **2** was achieved (Table 3, entry 3). With 1,4-dioxane, highest yield of 90% for cyclic ether **2** was obtained (Table 3, entry 4). In chloroform and dichloromethane solvents, lower yield of cyclic ether **2** was observed (Table 3, entries 5 and 6). Due to very good performance in 1,4-Dioxane, it was selected as an ideal solvent for further experiments.

Table 3
Solvent screening for hydrogenation of **1**.[a]

Entry	Solvent	Yield of **2** [%][b]
1	Isopropyl alcohol	85 (76)
2	Methanol	76 (65)
3	Acetonitrile	71 (62)
4	1,4-Dioxane	90 (81)
5	Chloroform	63 (55)
6	Dichloromethane	79 (69)

[a] Reaction conditions: Condensation product (0.2 g, 0.826 mmol), 5% Pd/C (0.035 g, 0.016 mmol), solvent (5 mL), H_2 (bladder pressure), room temperature, 10 h.
[b] Yields are reported by GC and values in parenthesis represent isolated yields after workup and column chromatography.

3.5. Substrate scope for the synthesis of cyclic ethers

Encouraged by the successful two step synthesis of cyclic ether from 2-methylfuran and formaldehyde, the scope of this protocol was further explored for the synthesis of various cyclic ethers from aldehyde or ketone and 2-methylfuran (Table 4). Furfural itself, condensed with two molecules of 2-methylfuran in the presence of [Fe_3O_4@SiO_2-Pr-Py-H][$2HSO_4^{2-}$] catalyst gave 73% yield of the condensation product **3** with 88% conversion of furfural. The resultant product was further hydrogenated over 5% Pd/C catalyst to achieve 69% yield of the ring saturated product **4** (Table 4, entry 1). Condensation product **5** was obtained in 74% yield from acetaldehyde and 2-methylfuran after 85% conversion of acetaldehyde. Subsequent hydrogenation of **5**, selectively gave product **6** in 70% yield (Table 4, entry 2). The condensation product **7** was obtained in 65% yield from the reaction of acetone and 2-methylfuran with 72% conversion of acetone. Further, hydrogenation of **7**, provided ring saturated product **8** with 58% yield (Table 4, entry 3). The condensation of benzaldehyde provided 72% yield of **9** after

Table 2
Catalyst screening for hydrogenation of condensation product.[a]

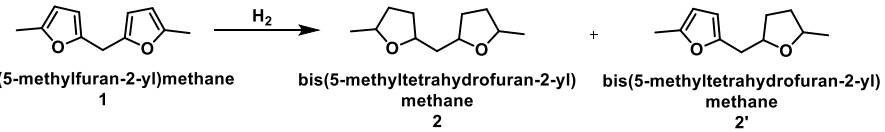

Entry	Catalyst	Conv. of **1**[b] [%]	Yield[c] [%]		Selectivity of [%]		Carbon balance [%]
			2	**2′**	**2**	**2′**	
1	1% Pd/C	45	40 (35)	4.2	88	12	44.2
2	2% Pd/C	54	49 (43)	4.8	91	09	43.8
3	3% Pd/C	66	62 (52)	3.9	94	06	65.9
4	4% Pd/C	78	73 (68)	5	93	07	82
5	5% Pd/C	91	87 (81)	4	96	05	91
6	5% Pd/Al_2O_3	80	74 (68)	6	92	08	80
7	5% Ru/C	56	47 (31)	7.5	84	16	54.5
8	5% Ru/Al_2O_3	67	55 (41)	12	82	18	67
9	5% Pt/C	41	35 (29)	6.1	85	15	41.1
10	5% Pd/C (Commercial)	87	82 (76)	5.2	94	06	87.2

[a] Reaction conditions: Condensation Product-**1** (0.2 g, 0.826 mmol), catalyst (0.050 g), 1,4-Dioxane (5 mL), room temperature, H_2 (bladder pressure), 10 h.
[b] Conversion determined by GC.
[c] Yields are reported by GC and values in parenthesis represent isolated yields after workup and column chromatography.

Table 4
Substrate screening for synthesis of cyclic ethers.

Entry	Substrate	Condensation product, **1** [yield, %]	Hydrogenation product, **2** [yield, %]
1		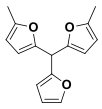 **3** 73%	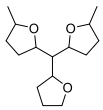 **4** 69%
2		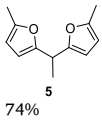 **5** 74%	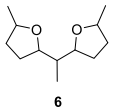 **6** 70%
3		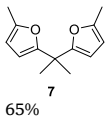 **7** 65%	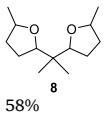 **8** 58%
4		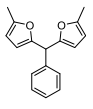 **9** 72%	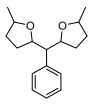 **10** 65%

Reaction conditions: Step 1- 2-methylfuan (4 mmol), aldehyde or ketone (2 mmol), [Fe_3O_4@SiO_2-Pr-Py-H][$2HSO_4^{2-}$] (0.1 g), 65 °C, 3 h. Step 2- Condensation product (0.2 g), 5% Pd/C (0.050 g), Room temperature, 1,4-Dioxane (5 mL), H_2 (bladder pressure), 10 h. Reported isolated yields after workup and column chromatography purification are reported.

80% conversion of benzaldehyde. Under optimized reaction conditions hydrogenation of **9** was performed, furan rings were successfully hydrogenated but benzene ring was left as it is and product **10** was obtained in 65% yield (Table 4, entry 4).

3.6. Plausible reaction pathway

The proposed reaction pathway for the formation of bis(5-methyltetrahydrofuran-2-yl)methane from formaldehyde and 2-methylfuran is presented in Fig. 4. Initially, the protonation of formaldehyde is catalyzed by the Brønsted acid sites of [Fe_3O_4@SiO_2-Py-H] [$2HSO_4^{2-}$] catalyst followed by its reaction with 2-methylfuran to form (5-methylfuran-2-yl)methanol, which was further reacted with the second molecule of 2-methylfuran to produce the condensation product **1**. In the next step, product **1** was a starting material for the hydrogenation over 5% Pd/C. Initially, a single furan ring of product **1** was hydrogenated and second ring was hydrogenated to produce the cyclic ether **2**.

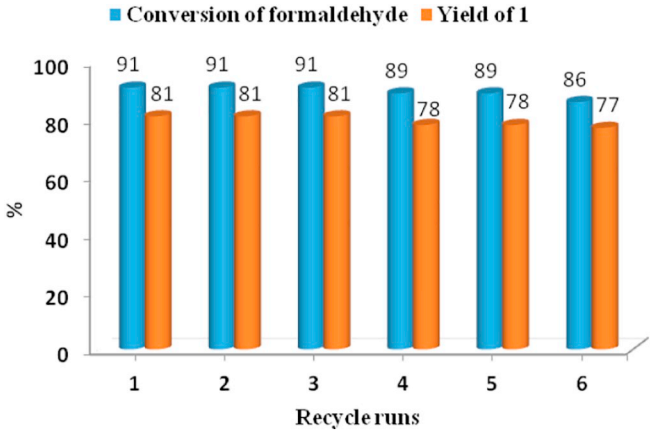

Fig. 5. Recycling of [Fe_3O_4@SiO_2-Pr-Py-H][$2HSO_4^{2-}$], Reaction Conditions: Formaldehyde (0.162 mL, 2 mmol), 2-methylfuran (0.328 g, 4 mmol), catalyst (0.1 g), 65 °C, 3 h.

3.7. Recycle study

3.7.1. Recycling of [Fe_3O_4@SiO_2-Pr-Py-H][$2HSO_4^{2-}$]

In order to know the catalyst stability, after the first reaction, external magnetic field was applied and the clear reaction crude was decanted. The separated catalyst was subsequently washed with ethyl acetate and reused for the next run. The stability of [Fe_3O_4@SiO_2-Pr-Py-H][$2HSO_4^{2-}$] was evaluated by performing several recycle runs (Fig. 5). It was found that the catalytic activity of [Fe_3O_4@SiO_2-Pr-Py-H][$2HSO_4^{2-}$] was very much consistent after being used for five times. During the 6th reuse, the activity of catalyst was slightly reduced to yield 77% of the condensation product **1** with 86% conversion of formaldehyde. This catalyst after its 3rd reuse also showed the acidity of 0.026 M which was almost the same as that of the fresh sample, confirming its stability under reaction conditions.

The XRD pattern of the spent [Fe_3O_4@SiO_2-Pr-Py-H][$2HSO_4^{2-}$] catalyst even after 3 reuses, in Fig. 1a shows the same pattern as that of the fresh catalyst confirming the excellent stability of the catalyst. The stability of the used [Fe_3O_4@SiO_2-Pr-Py-H][$2HSO_4^{2-}$] catalyst was also confirmed by FT-IR analysis. The peak positions in the used catalyst were same as those shown by the fresh catalyst [Fig. S2]. After reuse of [Fe_3O_4@SiO_2-Pr-Py-H][$2HSO_4^{2-}$] catalyst, its morphology was found to be the same as that of the fresh sample (Fig. 3f).

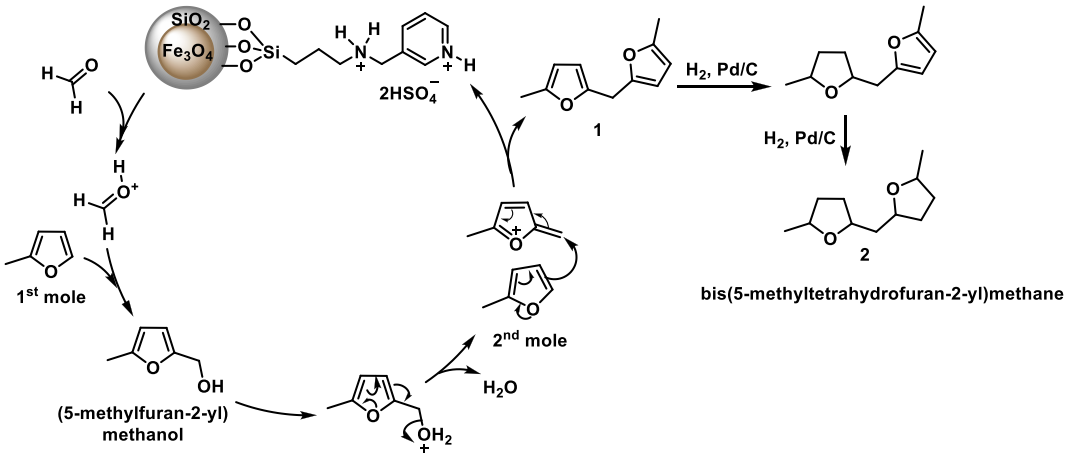

Fig. 4. Plausible reaction mechanism for condensation and hydrogenation steps.

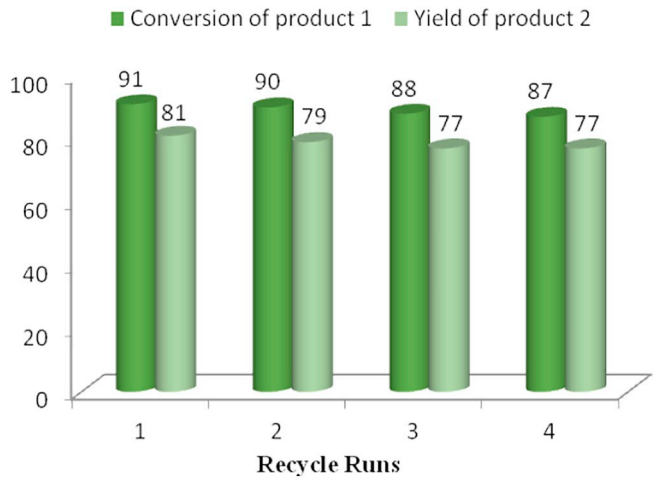

Fig. 6. Recycling of 5% Pd/C, Condensation Product-**1** (0.2 g, 0.826 mmol), catalyst (0.050 g), 1,4-Dioxane (5 mL), room temperature, H_2 (bladder pressure), 10 h.

3.7.2. Recycling of 5% Pd/C

The stability of the hydrogenation catalyst, 5% Pd/C was also evaluated by performing recycle runs (Fig. 6). After reaction with the fresh catalyst, reaction crude was filtered by simple filtration method. The recovered catalyst was further washed using distilled water and dried and then used for the subsequent run with fresh reactants. Following this procedure, it was found that the activity of 5% Pd/C catalyst was very much consistent even after being used for four times. The results indicated that the catalyst has exhibited an excellent stability upto 4th reuse. During 4th reuse, the activity was marginally decreased, may be due to the handling losses.

The XRD pattern of the spent Pd/C catalyst also did not show any change in its characteristic peak positions, confirming the robustness of catalyst even after catalyst reuse runs. A broad peak at $2\theta = 24.37^{\circ}$ and a sharp peak at $2\theta = 39.93^{\circ}$ corresponded to (002) and (111) planes of carbon and palladium, respectively [Fig. S1]. There was no any major change in morphology of 5% Pd/C was observed after its reuse (Fig. 3e), again confirming the stability of the catalyst.

4. Conclusions

A two step reaction protocol involving condensation and hydrogenation has been established for the synthesis of cyclic ethers as potential fuel additives from 2-methylfutran and aldehydes or ketones. In the first step, a newly designed acidic magnetic solid catalyst [Fe_3O_4@SiO_2-Pr-Py-H][$2HSO_4^{2-}$] showed an excellent activity for formaldehyde condensation with 2-methylfuran to give 90% conversion of formaldehyde and 75% isolated yield of the condensation product. The magnetic nature of the catalyst allowed its easy separation from reaction mixture. This catalyst was successfully explored for a wide variety of aldehydes or ketones for their condensation with 2-methylfuran. In the second step, hydrogenation of the condensation products was performed. Among the several supported catalysts, 5% Pd/C gave the highest conversion of 85% with 80% yield of saturated cyclic ether at ambient hydrogen pressure conditions in 1,4-dioxane solvent. Hydrogenation of several other condensation products was also successfully catalyzed by the prepared 5% Pd/C catalyst.

Appendix A. Supplementary data

Supplementary data to this article can be found online at https://doi.org/10.1016/j.fuproc.2019.106191.

References

[1] T. Zhao, Y. Zhang, G. Zhao, X. Chen, L. Han, W. Xiao, Impact of biomass feedstock variability on acid catalyzed alcoholysis performance, Fuel Process. Technol. 180 (2018) 14.
[2] P. Pradhan, S.M. Mahajani, A. Arora, Production and utilization of fuel pellets from biomass: a review, Fuel Process. Technol. 181 (2018) 215.
[3] IPCC, Renewable Energy Sources and Climate Change Mitigation, (2012).
[4] E. Agbor, X. Zhang, A. Kumar, Renew. Sust. Energ. Rev. 40 (2014) 930–943.
[5] A. Shrotri, H. Kobayashi, A. Fukuoka, Catalytic conversion of structural carbohydrates and lignin to chemicals, Adv. Catal. 60 (2017) 59.
[6] M. Guo, W. Song, J. Buhain, Bioenergy and biofuels: history, status and perspective, Renew. Sust. Energ. Rev. 42 (2015) 712–725.
[7] G.W. Huber, S. Iborra, A. Corma, Synthesis of transportation fuels from biomass: chemistry, catalysts and engineering, Chem. Rev. 106 (2006) 4044.
[8] D.M. Alonso, J.Q. Bond, J.A. Dumesic, Catalytic conversion of biomass to biofuels, Green Chem. 12 (2010) 1493.
[9] A. Corma, O.D. Torre, M. Renz, N. Villandier, Production of high-quality diesel from biomass waste products, Angew. Chem. Int. Ed. 50 (2011) 2375.
[10] M. Balakrishnan, E.R. Sacia, A.T. Bell, Selective hydrogenation of furan-containing condensation products as a source of biomass-derived diesel additives, ChemSusChem 7 (2014) 2796.
[11] G. Li, A.N. Li, A.S. Li, A.A. Wang, A.Y. Cong, A.X. Wanga, T. Zhang, Synthesis of renewable diesel with hydroxyacetone and 2-methylfuran, Chem. Commun. 49 (2013) 5727.
[12] W.H. Brown, W.N. French, The condensation of furan with carbonyl compounds, Can. J. Chem. 36 (1958) 537.
[13] W.H. Brown, B.J. Hutchinson, Intermediates in the cycloanhydrotetramerization of furan with aliphatic and alicyclic ketones, Can. J. Chem. 56 (1978) 617.
[14] A. Riad, Z. Mouloungui, M. Delmas, A. Gaset, New synthesis of substituted difuryl or dithienyl methanes, Synth. Commun. 19 (1989) 3169.
[15] W.M. Van Rhijn, D.E. DeVos, B.F. Sels, W.D. Bossaert, P.A. Jacobs, Sulfonic acid functionalized ordered mesoporous materials as catalysts for condensation and esterification reaction, Chem. Commun. (1998) 317.
[16] T. Li, S.I. Cheng, J.F. Lee, L.Y. Jang, MCM-41 supported Mo/Zr mixed oxides as catalysts in liquid phase condensation of 2-methylfuran with acetone, J. Mol. Catal. A Chem. 198 (2003) 139.
[17] A.S.K. Hashmi, L. Schwarz, P. Rubenbauer, M.C. Blanco, The condensation of carbonyl compounds with electron-rich arenes: mercury, thallium, gold or a proton? Adv. Synth. Catal. 348 (2006) 705.
[18] V. Nair, K.G. Abhilash, N. Vidya, Practical synthesis of triaryl- and triheteroarylmethanes by reaction of aldehydes and activated arenes promoted by Gold (III) chloride, Org. Lett. 7 (2005) 5857.
[19] Z. Wang, H. Li, W. Zhao, S. Yang, Low - temperature and solvent - free production of biomass derived diesel range C_{17} precursors via one pot cascade acylation- alkylation over Sn 4+- montmorillonite, J. Ind. and Engg. Chem 66 (2018) 325.
[20] F. Algarraa, A. Corma, H. Garciaa, J. Primoa, Acid zeolites as catalysts in organic reactions. Highly selective condensation of 2-alkylfurans with carbonylic compounds, Appl. Catal., A 128 (1995) 119.
[21] M. Balakrishnan, E.R. Sacia, A.T. Bell, Synthesis of biodiesel precursors: sulfonic acid catalysts for condensation of biomass-derived platform molecules, ChemSusChem 7 (2014) 1078.
[22] M. Muthyala, V.K. Rao, A. Kumar, $Cu(OTf)_2$ catalyzed synthesis of bis(5-methyl-2-furyl)methanes by condensation of 2-methylfuran with carbonyl compounds under solvent free conditions, Chin. J. Chem. 29 (2011) 1483.
[23] J. Jaratjaroonphong, S. Tuengpanya, R. Saeeng, S. Udompong, K. Srisook, Green synthesis and anti-inflammatory studies of a series of 1,1-bis(heteroaryl)alkane derivatives, Eur. J. Med. Chem. 83 (2014) 561.
[24] I. Ogino, Y. Suzuki, S.R. Mukai, Tuning the pore structure and surface properties of carbon-based acid catalysts for liquid-phase reactions, ACS Catal. 5 (2015) 4951.
[25] H. Li, S. Saravanamurugan, S. Yang, A. Riisager, Catalytic alkylation of 2-methylfuran with formalin using supported acidic ionic liquids, ACS Sustain. Chem. Eng. 3 (2015) 3274.
[26] C. Zhu, T. Shen, D. Liu, J. Wu, Y. Chen, L. Wang, K. Guo, H. Ying, P. Ouyang, Production of liquid hydrocarbon fuels with acetoin and platform molecules derived from lignocelluloses, Green Chem. 18 (2016) 2165.
[27] S.H. Shinde, C.V. Rode, A two-phase system for the clean and high yield synthesis of furylmethane derivatives over $–SO_3H$ functionalized ionic liquids, Green Chem. 19 (2017) 4804.
[28] S.H. Shinde, C.V. Rode, An integrated production of diesel fuel precursors from carbohydrates and 2-methylfuran over Sn-mont catalyst, ChemistrySelect 3 (2018) 4039.
[29] S. Liu, S. Dutta, W. Zheng, N.S. Gould, Z. Cheng, B. Xu, B. Saha, D.G. Vlachos, Catalytic hydrodeoxygenation of high carbon furylmethanes to renewable jet-fuel ranged alkanes over a rhenium-modified iridium catalyst, ChemSusChem 10 (2017) 3225.
[30] Y. Nakagawa, S. Liu, M. Tamura, K. Tomishige, Catalytic total hydrodeoxygenation of biomass-derived polyfunctionalized substrate to alkane, ChemSusChem 8 (2015) 1114.
[31] S. Liu, M. Tamura, Y. Nakagawa, K. Tomishige, One-pot conversion of cellulose into n-hexane over the Ir-$ReOx/SiO_2$ catalysts combined with HZSM-5, ACS Sustain. Chem & Engg 2 (2014) 1819.
[32] S. Liu, Y. Okuyama, M. Tomura, Y. Nakagawa, A. Imai, K. Tomishige, Selective transformation of hemicellulose (Xylan) into n-pentane pentanols or xylitol over a rhenium- modified iridium catalyst combined with acids, Green Chem. 18 (2016)

165.
[33] S. Liu, Y. Amada, M. Tamura, Y. Nakagawa, K. Tomshige, One- pot selective conversion of furfural into 1,5-pentanediol over a Pd-added Ir-ReOx/SiO_2 bifunctional catalyst, Green Chem. 16 (2014) 617.
[34] Y. Nakagawa, M. Tamura, K. Tomishige, Supported metal catalysts for total hydrogenation of furfural and 5-hydroxymethylfurfural, Journal of the Japan Petroleum Institute 60 (1) (2017).
[35] Y. Nakagawa, K. Takada, M. Tamura, K. Tomishige, Total hydrogenation of furfural and 5-hydroxymethylfurfural over supported Pd-Ir alloy catalyst, ACS Catal. 4 (2014) 2718.
[36] Y. Nakagawa, K. Tomishige, Total hydrogenation of furan derivatives over silica supported Ni-Pd alloy catalyst, Catal. Commun. 12 (2010) 154.
[37] S. Lui, Y. Okuyama, M. Tamura, Y. Nakagawa, A. Imai, K. Tomishige, Production of renewable hexanols from mechanocatalytically depolymerised cellulose by using Ir-ReOx/SiO_2 catalyst, ChemSusChem 8 (2015) 628.
[38] Y. Nakagawa, M. Tamura, K. Tomishige, Recent development of production technology of diesel and jet-fuel range hydrocarbons from inedible biomass, Fuel Process. Technol. 193 (2019) 404.
[39] O.C. Navarro, A. Corma, S.I. Chornet, Chemicals from biomass: aerobic oxidation of 5-hydroxymethyl-2-furaldehyde into diformylfurane catalyzed by immobilized vanadyl-pyridine complexes on polymeric and organofunctionalized mesoporous supports, Top. Catal. 52 (2009) 304.
[40] N.S. Date, N.S. Biradar, R.C. Chikate, C.V. Rode, Effect of reduction protocol of Pd catalyst on product distribution in furfural hydrogenation, ChemistrySelect 2 (2) (2017) 24.
[41] S. Suganuma, K. Nakajima, M. Kitano, D. Yamaguchi, H. Kato, S. Hayashi, M. Hara, Hydrolysis of cellulose by amorphous carbon bearing SO_3H, COOH, and OH groups, J. Am. Chem. Soc. 130 (38) (2008) 12787.
[42] R.S. Thombal, A.R. Jadhav, V.H. Jadhav, Biomass derived B-cyclodextrin-SO_3H as a solid acid catalyst for esterification of carboxylic acids with alcohols, RSC Adv. 5 (17) (2015) 12981.
[43] K. Tarade, S. Shinde, S. Sakate, C. Rode, Pyridine immobilized on magnetic silica as an efficient catalyst for Knoevenagel condensation of furfural with acetyl acetone, Catal. Commun. 124 (2019) 81.